Biodiversité et fonctionnement de l'écosystème benthique dans la Vasière Ouest Gironde

Bastien Lamarque

université de BORDEAUX

THÈSE PRÉSENTÉE

POUR OBTENIR LE GRADE DE

DOCTEUR DE

L'UNIVERSITÉ DE BORDEAUX

ÉCOLE DOCTORALE SCIENCES ET ENVIRONNEMENTS

SPÉCIALITÉ : Biogéochimie et écosystèmes

Par Bastien LAMARQUE

Biodiversité et fonctionnement de l'écosystème benthique dans la Vasière Ouest-Gironde

Sous la direction de : Antoine GREMARE
(co-encadrant : Bruno DEFLANDRE)

Soutenue le 28 janvier 2022

Membres du jury :

M. GARABETIAN, Frédéric	Professeur, Université de Bordeaux	Président
M. RIERA, Pascal	Maître de conférences HDR, Sorbonne Université	Rapporteur
M. DESROY, Nicolas	Cadre de recherche HDR, IFREMER	Rapporteur
Mme. LABRUNE, Céline	Ingénieure de recherche, CNRS	Examinateur
M. DENIS, Lionel	Professeur, Université de Lille	Examinateur
M. DE MONTAUDOUIN, Xavier	Professeur, Université de Bordeaux	Examinateur
M. GREMARE, Antoine	Professeur, Université de Bordeaux	Directeur
M. DEFLANDRE, Bruno	Maître de conférences, Université de Bordeaux	Invité

Biodiversité et fonctionnement de l'écosystème benthique dans la Vasière Ouest-Gironde

Résumé : Les grands fleuves influencent fortement certaines régions côtières (i.e., les River-dominated Ocean Margins, ou RiOMar), qui présentent de forts taux de sédimentation et auxquelles sont associés des communautés benthiques et des processus biogéochimiques dont le fonctionnement varie en fonction de la dynamique temporelle des flux particulaires et de leur interaction avec l'hydrodynamisme. La Vasière Ouest-Gironde (VOG) constitue un modèle pertinent pour ce type de systèmes puisqu'elle constitue la principale zone de dépôt primaire des particules issues de l'estuaire de la Gironde, et qu'elle est située dans un environnement hautement énergétique. Bien que sa dynamique sédimentaire ait fait l'objet de nombreux travaux, l'étude des caractéristiques (dont la matière organique associée) des sédiments superficiels, et de la macrofaune benthique y a été jusqu'à présent négligée. L'objectif de cette thèse consiste à mieux décrire la structuration spatio-temporelle de l'écosystème benthique de la VOG, via l'étude de la matière organique particulaire (MOP) sédimentée ainsi que de la composition de la macrofaune benthique et de son activité. Une comparaison a par ailleurs été effectuée avec le prodelta du Rhône qui a déjà beaucoup été étudié. Bien qu'également situé en zone tempérée, celui-ci diffère en effet de la VOG à la fois par la saisonnalité plus marquée des apports fluviaux ainsi que par la plus faible intensité de l'hydrodynamisme dans la zone réceptrice. Une campagne synoptique (juin 2018, 32 stations) et 4 campagnes saisonnières (5 stations le long d'un gradient côte-large, octobre 2016-avril 2018) ont été réalisées sur la VOG dans des conditions de débits et d'hydrodynamisme contrastées. Une large gamme de paramètres a été mesurée : (1) caractéristiques des sédiments superficiels (granulométrie, surfaces spécifiques, descripteurs quantitatifs et qualitatifs de la MOP), (2) composition de la macrofaune, et (3) traces d'activité biologique (imagerie de profils sédimentaires). Sur la base de l'analyse de la distribution spatiale de ces paramètres, les résultats obtenus confirment la subdivision de la VOG en une zone proximale et une zone distale qui avait déjà été mise en évidence par des études sédimentologiques. Ils montrent l'existence de gradients de profondeur (i.e., entre zones proximale et distale et à l'intérieur de la zone distale) marqués pour la plupart de ces paramètres. L'analyse des corrélations entre ces variations spatiales et celles de plusieurs facteurs de contrôle potentiels suggère le rôle prédominant de l'hydrodynamisme comparé à celui du débit de la Gironde et du chalutage de fond. Mes résultats montrent également l'existence de variations temporelles dont la composante saisonnière est liée à l'efflorescence printanière, et à laquelle se superpose une tendance interannuelle entre 2016 et 2018 pour la composition de la macrofaune benthique. Dans le cas de cette dernière, et pour les 3 stations déjà échantillonnées en 2010, mes résultats montrent enfin l'existence d'importants changements temporels entre 2010 et 2016-2018. Ces changements sont attribués à la succession de tempêtes exceptionnelles intervenues durant l'hiver 2013/2014, qui aurait profondément perturbé l'écosystème benthique de la VOG et initié une séquence de cicatrisation. De manière générale, une différence importante avec le prodelta du Rhône réside dans le rôle majeur joué par l'hydrodynamisme (i.e., par rapport aux apports fluviaux) dans le contrôle de la structuration spatio-temporelle des paramètres étudiés. Cette différence tend à valider la transposition aux zones tempérées de la typologie des RiOMar jusqu'ici établie sur des bases biogéochimiques et principalement à partir d'exemples tropicaux et subtropicaux.

Mots clés : RiOMar, Vasière Ouest-Gironde, Matière organique particulaire, macrofaune benthique, Bioturbation, Hydrodynamique

---

UMR CNRS 5805 EPOC
Environnements et Paléoenvironnement Océaniques et Continentaux
Allée Geoffroy Saint-Hilaire – CS50023 – 33165 Pessac Cedex - France

Biodiversity and functioning of the benthic ecosystem in the West Gironde Mud Patch

Abstract: Major rivers freshwater and sediment discharges strongly affect biodiversity and functioning of coastal marine ecosystems. They define marine regions influenced by continental inputs and high sedimentation rates (River-dominated Ocean Margins, or RiOMar), which are associated with benthic communities and biogeochemical processes whose functioning vary according to the temporal dynamics of particulate fluxes and the interaction of these latter with hydrodynamics. The West Gironde Mud Patch (WGMP) constitutes a pertinent model for this type of systems since it is the main preferential depositional area for particles from the Gironde estuary, and is located in a high-energy environment. Although its past and present sedimentary dynamics have been the subject of many studies, the analysis of the characteristics of its surface sediments in relation to organic matter, and of its biological compartment has been largely neglected. This thesis is aiming at better describing and understanding the spatio-temporal structure of the WGMP benthic ecosystem through the study of the sedimented particulate organic matter (POM) and the composition and activity of benthic macrofauna. A comparison is also achieved with the Rhône prodelta (RP)system, which has already been extensively studied. Although also characterized as a temperate area RiOMar, the RP differs from the WGMP both by the more pronounced seasonality of fluvial inputs and by the lower intensity of hydrodynamics in the receiving area. One synoptic (June 2018, 32 stations) and 4 seasonal (5 stations along an inshore-offshore gradient, October 2016-April 2018) sampling cruises were conducted in the WGMP under contrasting flow and hydrodynamics conditions. A wide range of parameters was measured: (1) surface sediment characteristics (grain size, sediment surface area, quantitative and qualitative descriptors of POM), (2) benthic macrofauna composition, and (3) biological activity traces (Sediment Profile Imaging). Based on the analysis of the spatial distribution of these parameters, my results confirm the WGMP subdivision into a proximal and a distal area, which had already been observed by sedimentological studies. They show the existence of marked gradients (i.e., between proximal and distal areas, and within the distal area) for most of the assessed parameters. The analysis of the correlation between these spatial changes and those of several controlling factors suggests the predominant role of hydrodynamics compared to Gironde estuary flow and bottom trawling. My results also show the evidence of significant temporal changes, with a seasonal component related to the spring bloom, overlaid with an inter-annual trend between 2016 and 2018 for the benthic macrofauna composition. In the latter, and for the 3 stations already sampled in 2010, my results finally point to the existence of major temporal changes between 2010 and 2016-2018. These changes are attributed to the succession of exceptionally severe storms that occurred during the 2013/2014 winter, which are suspected to have profoundly disturbed the WGMP benthic ecosystem and initiated a cicatrization sequence. Overall, an important distinction with the RP relates to the major role of hydrodynamics (i.e., compared to riverine inputs) in controlling the spatio-temporal structuration of the studied parameters. This difference tends to validate the transposition to temperate areas of the current RiOMar typology, which has been established on biogeochemical grounds and mostly based on the study of tropical and subtropical systems.

Keywords: RiOMar, West Gironde Mud Patch, Particulate organic matter, Benthic macrofauna, Bioturbation, Hydrodynamics

UMR CNRS 5805 EPOC
Environnements et Paléoenvironnement Océaniques et Continentaux
Allée Geoffroy Saint-Hilaire – CS50023 – 33165 Pessac Cedex – France

Financements

Ce travail de thèse a pu être mené à bien grâce à une bourse doctorale allouée par le Ministère français de l'Enseignement Supérieur, de la Recherche et de l'Innovation. Il a bénéficié de financements par les projets : (1) JERICO-NEXT (Programme de Recherche et d'Innovation Horizon 2020 de l'Union Européenne), (2) VOG (LEFE-CYBER et EC2CO-PNEC) et (3) MAGMA (Cluster of excellence COTE ANR-10-LABX-45, Conseil Régional de Nouvelle-Aquitaine et Office Français pour la Biodiversité). Les opérations à la mer ont été réalisées à bord du N/O "Côtes de la Manche" qui est opéré par l'Unité Mixte de Service « Flotte Océanographique Française ».

Remerciements

Je tiens tout d'abord à exprimer mes profonds remerciements à **Antoine Grémare** qui a supervisé ce travail de thèse, ainsi qu'à **Bruno Deflandre** qui l'a co-encadré.

Antoine, il m'est très difficile d'exprimer en quelques lignes ma gratitude envers vous. Merci pour la somme de connaissances en écologie benthique dont vous m'avez fait part durant ces 4 années de thèse, votre confiance, et votre rigueur scientifique. Merci également d'avoir pu vous montrer aussi disponible et de bonne humeur, aussi bien à terre qu'en mer (sauf peut-être les premiers jours de campagnes où l'on ne se croisait pas énormément), malgré vos tracas et votre emploi du temps présidentiel. **Bruno,** ce fût également un vrai plaisir de travailler avec toi. Je te suis très reconnaissant de m'avoir initié à ce domaine, autrefois obscur pour moi, qu'est la biogéochimie. Merci pour tes nombreuses connaissances partagées, des grands principes théoriques jusqu'à la technique (tout aussi importante) d'évacuation des bulles des incubations, en passant également par la dégustation de tisanes, j'ai beaucoup appris dans ce(s) domaine(s) à tes cotés. Au-delà de cet encadrement pédagogique de qualité que vous m'avez tous deux apporté, je tiens à vous remercier pour votre soutien permanent, votre disponibilité et votre écoute, qui m'auront permis d'une part de mener à bien ce travail, mais d'autre part de m'épanouir intellectuellement.

J'aimerais également remercier les membres du jury qui ont accepté de prendre du temps pour évaluer ce travail. Merci à Messieurs **Pascal Riera** et **Nicolas Desroy** qui m'ont fait l'honneur d'être rapporteurs de cette thèse. Je tiens à exprimer mes chaleureux remerciements aux autres membres examinateurs composant ce jury. Tout d'abord **Céline Labrune**, qui, en plus d'avoir directement accepté de faire partie du jury, a rendu une partie de ce travail de thèse possible via le partage de ses données de SPI relatives au prodelta du Rhône. **Lionel Denis**, qui a tout aussi rapidement accepté. Merci également pour ta participation et ta bienveillance lors des comités de suivi de thèse. Un grand merci à **Xavier de Montaudouin**, d'une part pour avoir accepté un peu à la dernière minute de faire partie du jury, mais également pour m'avoir fait découvrir le monde fabuleux de l'écologie benthique lors de mon stage de Master 1 à vos côtés. Enfin, merci à **Frédéric Garabetian** pour ta participation à ce jury de thèse, mais surtout pour ta présence (indispensable) lors des nombreuses campagnes en mer, où tes engouements pour le surf sur tabouret, Hubert Bonisseur de La Bath et le Versailles des Mers (point qui je l'espère ne deviendra pas obsessionnel maintenant que ce dernier est classé à l'UNESCO) ne pouvaient que me laisser admiratif.

Ce travail n'aurait jamais vu le jour sans l'aide et le soutien (direct ou indirect) de nombreuses personnes. Toutes ces rencontres, tant scientifiques qu'humaines, m'ont

énormément appris et enrichi au cours de ces 4 années de thèse, et je voudrais ainsi remercier tous ceux qui ont participé de près ou de loin à mon travail.

Puisque la démarche appliquée lors de ce travail débute par la collecte des échantillons, et après avoir passé un total de 80 jours en mer lors des différentes campagnes, je souhaite tout d'abord remercier la dream-team des missions (qui ne furent pas de tout repos) JERICObent et MAGMA sur le Côtes de la Manche. L'homme du sud **Sylvain Rigaud**, Bobby pour les intimes, merci pour ta bonne humeur, ton accent du soleil, et la liqueur de mélèze. En revanche non-merci pour la poutargue, ce truc devrait être illégal. **Christophe Fontanier**, merci pour ton humour brillant, tes petits pots teintés de rose (qui je pense sont piégés et ont vite tendance à décolorer sur les vêtements et le pont du bateau) et ton immense talent pour, je cite, « lixivier des kilos de boue dégoutante et parfois puante ». **Sabine Schmidt**, merci pour m'avoir initié à l'art de la découpe des carottes, niveau expert. Je te promets qu'un jour (peut-être), on retrouvera tes spatules parties trop tôt (au cas où je ne sois pas là, elles se situent aux alentours de 45°39,420'N ; 1°27,880'O). Un grand merci aux SPIonautes **Guillaume Bernard,** pour ton regard critique et ton aide précieuse sur les analyses multivariées, et **Alicia Romero-Ramirez**, dont la présence suffit à réveiller le bon fonctionnement du SPI (et l'absence conduit inexorablement à une défaillance électronique de cet engin à l'allure pourtant sympathique). Merci à **Nicolas Dubosq**, qui malgré la canicule, le froid, la tempête et les paquets de mer a su rester accroché à « sa » boite à gants pour nous offrir de superbes découpes! Cette belle équipe ne serait rien en mer sans les équipages de marins qui nous ont assisté, et que je souhaite tout autant remercier pour leur professionnalisme (certes parfois un peu effrayant) et leur bonne humeur. La liste de nom est longue, et il y en a beaucoup d'entre eux que je souhaite chaleureusement remercier, mais mon amour pour la gastronomie me pousse à dire un grand merci tout particulièrement aux cuisiniers **Bertrand**, **Xavier** et **Bruno** qui nous ont toujours régalé (et fait prendre un peu de poids). Tant qu'à rester dans le domaine maritime, je tiens également à remercier les membres d'équipage de la Planula : **Laurent**, **Anne** (promis un jour on va finir de fabriquer ton meuble), ainsi que **Philippe**, qui m'a toujours bien fait marrer.

Le traitement des échantillons a débuté par le travail conséquent de tri et d'identification de la macrofaune benthique. A ce titre je souhaite évidement remercier **Benoit Gouillieux**, pour son aide précieuse dans l'identification des crustacés et surtout des amphipodes (qui n'est toujours pas devenue ma passion) et ses dons de poissons (qui eux ont fini identifiés au four avec des oignons et des herbes). Merci également à **Nicolas Lavesque** pour le partage de son grand savoir sur les polychètes (et le reste) ! J'espère qu'un jour tu pourras gagner un blind-test. Merci encore à vous deux, et ne vous inquiétez pas ; ne pas aimer les siponcles, cet animal si attachant, ne fait pas de vous des sous-hommes.

Ce travail a également été l'occasion de réaliser tout un tas d'analyses, sur des machines aussi géniales que capricieuses. A ce titre je souhaite remercier l'ensemble des personnes qui m'ont formé et aidé tout au long de ces 4 années. Mes premières pensées vont à **Dominique Poirier**. Je pense que je me rappellerai toujours des Thugs à fond dans le labo le matin, de tes blagues, de tes visites des moindres recoins secrets du B18, et surtout de ta grande humanité.

J'espère vraiment que nos chemins se recroiseront un jour (à Tahiti ce serait bien) ! Merci également à **Marie-Ange**, pour ton aide plus que précieuse, et la quantité de boulot époustouflante que tu as réalisé à l'HPLC. De même, merci à **Martin Danilo**, même si on ne s'est pas beaucoup vu avant MAGMA-2. Du coté des arcachonnais, un grand merci à l'équipe de 2nd étage **Nathalie**, **Line** et **Laurence** pour vos aides diverses et variées, que ce soit dans les analyses pigmentaires, le CHN et ses pesées à n'en plus finir ou bien simplement le prêt et dépannage de matériel. Enfin merci à l'équipe de choc de l'atelier **Jacques**, **Christian** et **Franck** !

Je tiens également à remercier tout le reste du personnel de la Station Marine d'Arcachon, qui a contribué à rendre cette thèse plus agréable : **Hugues**, **Olivier**, **Nicolas S.**, **Michel**, **Lise**, **Antoine N.** (la planète et moi te remercions pour le tirefond de meuble qui m'a fait économiser 60km), **Cécile**, **Aurélie**, **Christelle**, **Céline** et **Vanessa**. Je m'excuse par avance auprès des gens potentiellement oubliés, cela ne veut pas dire que je ne pense pas à vous (enfin sauf durant la rédaction de ces présents remerciements...). Si vous vous sentez concernés, n'hésitez pas à rajouter votre prénom ci-contre : _ _ _ _ _ _ _ _ _ _ _ _ _ _

Merci à mes collègues (et ex-collègue) de bureau **Annabelle**, **Anais** et **Arnaud**, qui ont tant bien que mal supporté (mais je vous rassure c'est réciproque) ma personne ainsi que mes passions pour les percussions et les statuettes solaires de grands dictateurs (avouez qu'on a quand même un peu rigolé hein).

Mille mercis aux copains bordelais, les musiciens (**Terra Delia**, **Melon Balek**, **Sbonk**, même si vous êtes les mêmes personnes) et autres mélomanes (**Ugo**, **Flo**, **Caro**, **Rabo**, **Mathildo**, **RogerO**, **Chanchan**, **Pamela**, **Yann**, **Charlotte**, **Matthieu**, **DT**, **Murf**, **Rouxmout** et tous les autres que j'oublie), pour ces grands moments qui certes se sont fait plus rares pendant 4 ans, mais ont néanmoins été de grands bols d'air frais. Merci également à **Johan** pour cette incroyable colocation arcachonnaise (à défaut d'avoir eu un blaireau empaillé, j'en avais un bien vivant tous les matins dans le salon !).

Ce travail ne serait certainement pas sans le soutien, la patience et la compréhension de **Suzie**, dont la présence au quotidien a été essentielle. Merci infiniment à toi.

Enfin, je ne peux terminer ces remerciements sans une pensée particulièrement émue pour **Pascal Lebleu,** avec qui nous avons partagé de grands moments lors des campagnes en mer ou au labo. Je n'oublierai jamais ta grande gentillesse, ton humanité et ton dynamisme. Je te remercie pour tout ce que tu as fait pour nous et ces moments à tes côtés que nous n'oublierons pas. Je te remercie également pour m'avoir sauvé la vie au moins 2 fois lors des passages parfois périlleux de la passe de l'estuaire. Sans toi j'aurais certainement fini écrasé par la benne Hamon et n'aurais sans doute pas pu finir d'écrire ce manuscrit.

Table des matières

Liste des figures

Introduction

Chapitre 1 : Structuration spatiale de la matière organique particulaire et de l'activité de la macrofaune benthique dans la Vasière Ouest-Gironde

Chapitre 2: Structuration spatio-temporelle de la matière organique particulaire et de la composition de la macrofaune benthique dans la Vasière Ouest-Gironde

Chapitre 3: Structuration spatio-temporelle de l'activité de la macrofaune benthique dans la Vasière Ouest-Gironde

Liste des tableaux

Chapitre 1 : Structuration spatiale de la matière organique particulaire et de l'activité de la macrofaune benthique dans la Vasière Ouest-Gironde

Chapitre 2: Structuration spatio-temporelle de la matière organique particulaire et de la composition de la macrofaune benthique dans la Vasière Ouest-Gironde

Chapitre 3: Structuration spatio-temporelle de l'activité de la macrofaune benthique dans la Vasière Ouest-Gironde

INTRODUCTION

1. Les zones côtières

1.1. Délimitations marines

Les délimitations de la frontière marine des zones côtières varient selon les domaines scientifiques considérés (Borges 2005, Liu et al. 2010). Ainsi, d'un point de vue géologique, les zones côtières correspondent à la marge continentale, elle-même définie comme la zone de transition entre la croute continentale et la croute océanique (Kennett 1982). En océanographie, il existe plusieurs définitions de la zone côtière. Celle correspondant à l'expansion géographique la plus vaste délimite les *Large Marine Ecosystems* (LME, https://www.lmehub.net) qui s'étendent au-delà des marges continentales. Ces ensembles, définis dans une perspective de gestion des grands écosystèmes côtiers et des ressources marines exploitées, segmentent l'océan côtier en 66 régions qui s'étendent sur une surface totale de 86 145 840 km^2, soit 24 % de la surface océanique globale. Les frontières marines des zones côtières peuvent également être délimitées par des seuils bathymétriques, dont les profondeurs peuvent varier. Muller-Karger et al. (2005) ont par exemple proposé d'adopter un seuil de 2000 m, réduisant ainsi les zones côtières à une surface de 48 106 km^2. Simpson & Sharples (2012) ont quant à eux utilisé une profondeur de 500 m, conduisant à une surface totale des zones côtières égale de 33 106 km^2 (soit 9 % de la surface océanique globale). Une dernière définition, la plus communément utilisée, adopte un seuil bathymétrique de 200 m (Gattuso et al. 1998, Rabouille et al. 2001, Borges 2005, Borges et al. 2005, Cai et al. 2006, Laruelle et al. 2010, Cai 2011) selon lequel la surface des zones côtières représente seulement 7 à 8 % de la surface océanique globale. Si l'adoption de cette valeur seuil constitue un critère simple facilitant la comparaison des estimations des budgets biogéochimiques de différentes zones côtières, elle ne semble néanmoins pas pouvoir s'appliquer de manière universelle, et notamment dans les contextes polaires et subpolaires où le plateau continental peut s'étendre jusqu'à 1000 m de profondeur.

Une manière de contourner cette difficulté consiste à définir la limite des zones côtières à partir de critères physiographiques, et/ou à définir ces zones à partir de processus particuliers qui s'y déroulent. Dans cet esprit, Liu et al. (2010) ont proposé de les définir comme des régions de transition dominées par les processus résultant des interactions continent-océan. Si les dimensions exactes de ces zones varient alors en fonction de la problématique scientifique ou de l'élément chimique d'intérêt, cette définition souligne les

spécificités des zones côtières et conduit plus généralement à y intégrer le plateau et le talus continental ainsi que les mers marginales adjacentes. En pratique, ceci conduit à considérer le talus continental comme la frontière séparant l'océan côtier de l'océan ouvert (**Figure 0.1**). La surface des zones côtières ainsi définies est de 30 106 km^2, soit 8 % de la surface océanique globale.

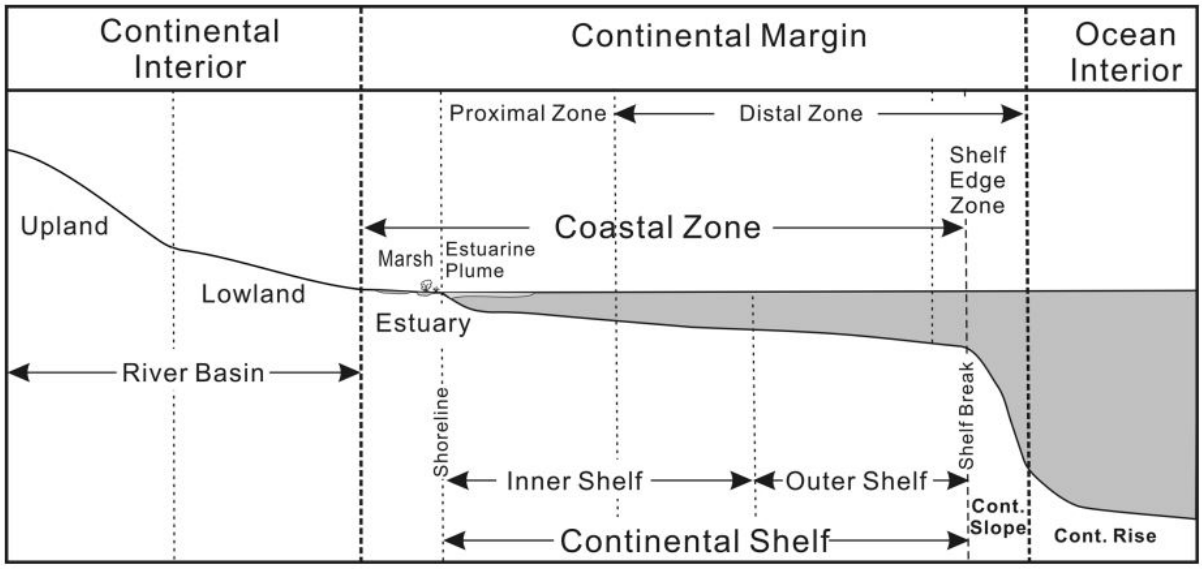

Figure 0.1. Schéma conceptuel de la coupe sagittale d'une marge continentale. Modifié par Liu et al. (2010) d'après Pernetta & Milliman (1995).

1.2. Services écosystémiques, usages et perturbations

Selon cette dernière définition, les zones côtières répondent également à la notion de « surface d'expression » (Jahnke 2010) et correspondent ainsi aux parties de l'océan hébergeant des processus physico-chimiques, biologiques et biogéochimiques influencés par le continent. Ainsi, ces zones réceptionnent de grandes quantités d'eau douce et d' éléments particulaires et dissous transportés depuis le continent via le processus de ruissellement et les fleuves. L'ensemble constitue autant d'apports susceptibles de favoriser les productions biologiques primaires et secondaires. Les remontées d'eaux profondes chargées de nutriments (upwellings) causées par les interactions entre le vent et la côte constituent un autre processus clef favorisant les productions biologiques en zone côtière. Si ces zones ne représentent que seulement environ 8 % de la surface de l'océan mondial (voir plus haut), on estime qu'elles abritent 20 % de sa production primaire (Gattuso et al. 1998) et constituent donc les espaces les plus productifs de l'océan mondial. Les zones côtières fournissent actuellement environ 43 % de la valeur estimée des services écosystémiques mondiaux (Costanza 1999), et jouent également un rôle majeur dans les grands cycles biogéochimiques,

notamment celui du carbone (Hedges & Keil 1995, Gattuso et al. 1998, Borges 2005). Elles constituent des zones d'accumulation préférentielles, où près de 80% de la préservation océanique mondiale du carbone organique s'y produirait (Smith & Hollibaugh 1993, Hedges & Keil 1995). A ce titre, les zones côtières jouent un rôle essentiel dans la régulation de l'excès de production de dioxyde de carbone résultant des activités humaines. Enfin, ces zones, et plus particulièrement leurs composantes littorales, font l'objet d'une forte exploitation touristique et culturelle (Kenchington 1993, Martínez et al. 2007). Ces quelques exemples illustrent le fait que les zones côtières abritent un ensemble de fonctions écologiques qui elles-mêmes servent de support à une large variété de services écosystémiques de toutes natures (i.e., approvisionnement, régulation et culturel ; Costanza et al. 1997). Ces services font l'objet de nombreux usages (e.g., transport, rejets, exploitation de combustibles fossiles, production d'énergies renouvelables, pêche, aquaculture, tourisme…) par les populations humaines, dont 41 % vivaient à moins de 100 km des côtes en 2002 (Martínez et al. 2007). Par ailleurs, l'intensité croissante du processus de littoralisation tend à augmenter cette densité de population (Duxbury & Dickinson 2007). Les zones côtières se situent donc au croisement de multiples enjeux socio-économiques et écologiques (Costanza et al. 1997, Costanza 1999, Burke et al. 2001, Martínez et al. 2007), et la diversité et l'intensité de leurs usages ne sont pas sans générer des perturbations significatives de leur ordonnancement et leur fonctionnement.

En écologie, une perturbation se définit comme "tout événement ponctuel qui perturbe la structure d'un écosystème, d'une communauté ou d'une population, et modifie les ressources, la disponibilité du substrat ou l'environnement physique" (Pickett & White 1985). Cette définition met en évidence la multiplicité et la complexité : (1) des facteurs de causalité des perturbations, et (2) des compartiments et processus susceptibles d'être affectés. Elle est par ailleurs suffisamment large pour suggérer que les perturbations sont omniprésentes dans les systèmes écologiques, où elles sont associées à une large gamme d'échelles spatiales et temporelles en fonction de leur nature (**Figure 0.2**). Les perturbations peuvent ainsi être caractérisées par leur fréquence d'occurrence, leur durée, leur emprise spatiale, leur intensité ainsi que l'ampleur de leurs conséquences (Holling et al. 1995, Bengtsson 2002). On distingue classiquement les perturbations selon leurs origines naturelles ou bien anthropiques. Or, ces deux types de perturbations intervenant le plus souvent

simultanément dans les écosystèmes côtiers, une question majeure en écologie consiste à déconvoluer leurs impacts respectifs (Brown et al. 2005, Ferré et al. 2008).

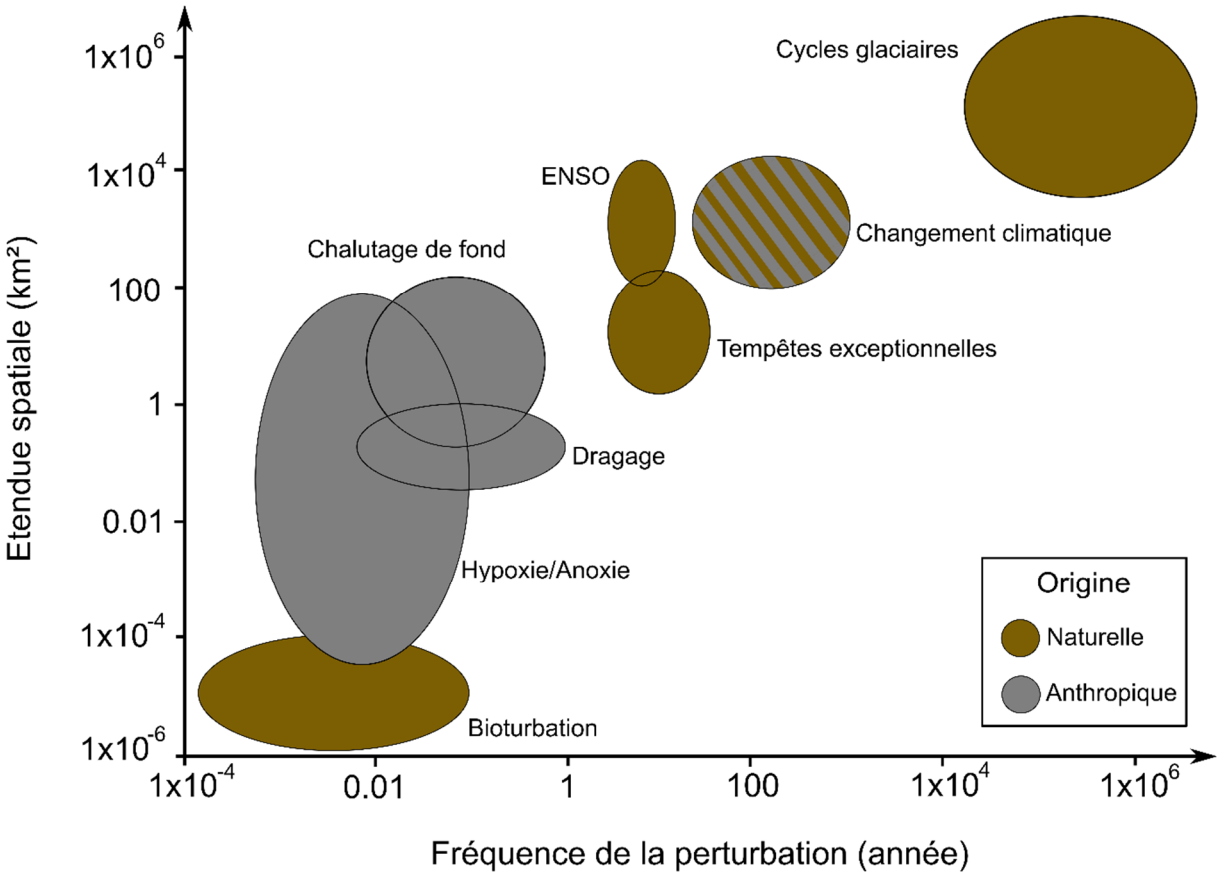

Figure 0.2. Graphique résumant la fréquence et l'emprise spatiale des principales perturbations susceptibles d'affecter les environnements marins. Modifié d'après Bigham et al. (2021), et basé sur Zajac et al. (1998), Glover et al. (2010), Harris (2014), Bigham et al. (2021) ainsi que les références y figurant.

Les zones côtières sont soumises à une large gamme de perturbations naturelles et anthropiques. En ce qui concerne les premières, il s'agit par exemple des oscillations climatiques ainsi que l'occurrence d'événements extrêmes tels que les tsunamis et les tempêtes/ouragans/cyclones (Michener et al. 1997, Kathiresan & Rajendran 2005, Nakaoka et al. 2007, Chavanich et al. 2008, Whanpetch et al. 2010, Harris 2012, 2014, Jaramillo et al. 2012). Les perturbations anthropiques affectant les zones côtières peuvent être induites par des activités ayant lieu à terre ou bien en mer (Crain et al. 2008, Halpern et al. 2008, Bowler et al. 2019). A titre d'exemple, on peut ainsi citer certaines activités terrestres telles que la déforestation ou bien l'agriculture intensive qui favorisent le lessivage des sols et augmentent par conséquent le transport de sédiments (Syvitski et al. 2005), de polluants et de nutriments

vers les eaux côtières (Vitousek et al. 1997). Cela peut engendrer des phénomènes de contamination, d'eutrophisation (Nixon et al. 1996, Desmit et al. 2018) et d'hypoxie voire d'anoxie (Diaz & Rosenberg 2008). De la même manière il est possible de prendre comme exemple certaines activités conduites en mer, telles que l'exploitation de combustibles fossiles ou de ressources vivantes, qui représentent également des sources de perturbation importantes pour les écosystèmes côtiers (Worm et al. 2006). Il est ainsi reconnu que le chalutage de fond entraine de profondes modifications des fonds marins ainsi que de la composition des communautés benthiques associées (Dayton et al. 1995, Watling & Norse 1998, Collie et al. 2000, Kaiser et al. 2002, 2006, Thrush & Dayton 2002, Gray et al. 2006, Queirós et al. 2006, Sciberras et al. 2018). Les effets du changement climatique sur les zones côtières peuvent quant à eux être considérés comme « indirectement anthropiques ». En effet, si ce changement est sans aucun doute d'origine humaine, ses effets sur les écosystèmes résultent largement de la modification des caractéristiques d'événements auparavant qualifiés de naturels (e.g., la fréquence et l'intensité des tempêtes pour ce qui concerne les zones marines côtières).

1.3. Les marges continentales influencées par les grands fleuves et leur interface eau-sédiment

L'une des caractéristiques fondamentales des zones côtières réside dans leur hétérogénéité. Celle-ci se décline suivant une large gamme d'échelles spatiales, illustrée par exemple par les différents niveaux de la classification EUNIS pour les habitats benthiques (Bajjouk et al. 2015). A une échelle plus globale, on distingue classiquement les zones des marges continentales sous l'influence des grands fleuves (i.e., eau douce et/ou sédiments d'origine terrestre), qui sont communément désignées sous l'appellation « *River-dominated Ocean Margin*s » (RiOMar ; McKee et al. 2004). Suivant leur degré de connectivité avec l'embouchure du fleuve, ainsi que leur caractère émergé/immergé, ces composantes peuvent être désignées sous les appellations de deltas, prodeltas ou bien encore vasières (Hanebuth et al. 2015). Leurs interfaces eau-sédiment constituent les principaux sites de déposition primaire des particules véhiculées par les fleuves. De manière générale, les RiOMar se différencient du reste de l'océan côtier par l'intensité des processus biologiques et biogéochimiques qui y prennent place. Les grands fleuves sont les principaux vecteurs d'introduction dans l'océan des matières dissoutes et particulaires d'origine continentale. Ces apports induisent de fortes productions biologiques qui font des RiOMar des zones de pêche

importantes (Lesueur 1992, Salen-Picard et al. 2002, Robert 2007, Ferré et al. 2008, Palanques et al. 2014, Mengual et al. 2016, 2019). D'un point de vue biogéochimique, on estime que moins de 5 % des sédiments fluviaux apportés aux zones côtières atteignent l'océan profond (Meade 1996). Ce faible pourcentage s'explique par le fait que les compartiments benthiques des RiOMar constituent des zone actives de dépôt de matériel particulaire et de transformations biogéochimiques ultérieures de la matière organique associée (McKee et al. 2004, Burdige 2005). Bien que les RiOMar ne représentent qu'une surface géographique relativement faible à l'échelle de l'océan mondial, leur caractère « biogéochimiquement dynamique » (Aller 1998) leur confère un rôle primordial dans la composante marine des grands cycles biogéochimiques. La majeure partie des matières particulaires véhiculées par les fleuves se déposant rapidement à la surface de leurs sédiments, les RiOMar constituent d'importantes zones de séquestration de la matière organique. Selon plusieurs estimations concordantes, elles abriteraient entre 40 et 50% de l'enfouissement du carbone organique particulaire intervenant sur les marges continentales (Hedges & Keil 1995, McKee et al. 2004, Burdige 2005, Blair & Aller 2012).

Si l'on ne sait encore que peu de choses sur les effets de la chronologie séquentielle des facteurs de forçage physiques (e.g., cycles de débit, événements à haute énergie liés aux courants et aux vagues) sur les processus biogéochimiques intervenant à l'interface eau-sédiment, il est cependant reconnu qu'une combinaison complexe de facteurs contrôle quand et où la matière organique particulaire (MOP) est dispersée, et comment celle-ci est transformée au sein des RiOMar (McKee et al. 2004). Ces facteurs comprennent aussi bien les débits fluviaux, la morphologie (i.e., le caractère actif ou passif) des marges et l'hydrodynamisme du milieu (qui conditionne la nature des sédiments présents), que certains processus biogéochimiques (e.g., les différentes modalités de la diagenèse précoce ainsi que son caractère stationnaire ou non) et biologiques (e.g., la bioturbation). Ceci explique que l'efficacité de préservation du carbone organique varie selon les RiOMar (McKee et al. 2004, Burdige 2005, Blair & Aller 2012) (**Figure 0.3**). Cette préservation résulte de deux processus : (1) l'enfouissement dans les sédiments des RiOMar, et (2) le transfert vers l'océan profond ; les importances relatives de ces deux processus variant selon les types de système considérés (Blair & Aller 2012).

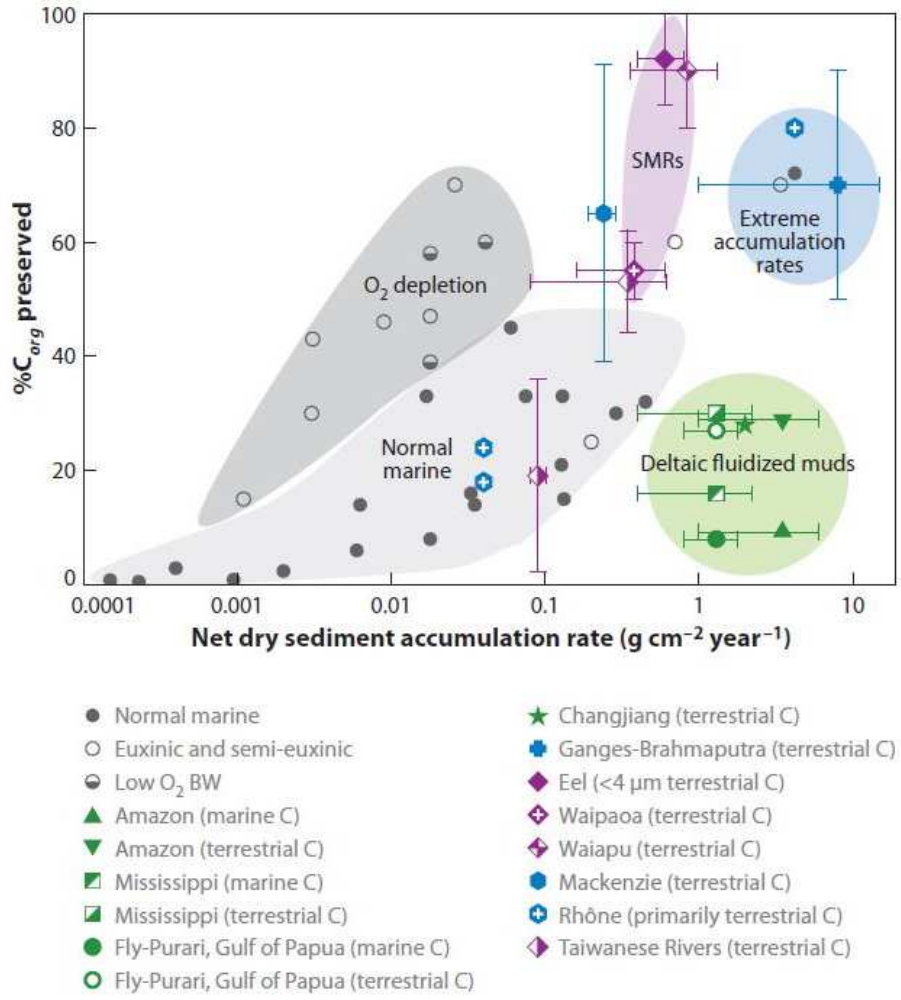

Figure 0.3. Relation liant la proportion de carbone organique préservé dans les sédiments avec le taux net d'accumulation sédimentaire au sein de différents RiOMar (d'après Blair & Aller 2012). SMRs : Small Mountainous Rivers.

La faible efficacité de préservation par enfouissement dans les vases deltaïques fluides résulte le plus souvent du remaniement physique incessant des sédiments par les courants, les marées et les vagues (Burdige 2005). Ce remaniement ré-oxygène en permanence les sédiments et favorise un mélange avec de la matière organique d'origine marine qui catalyse l'oxydation du matériel terrestre plus réfractaire (Aller 1994, Canfield 1994, Aller & Cochran 2019). Les préservations par enfouissement les plus fortes correspondent au contraire soit à des zones de fortes accumulation de sédiment, qui ont pour effet de soustraire rapidement la matière organique sédimentée aux réactions diagénétiques les plus efficaces, soit à des zones présentant naturellement de faibles concentrations en oxygène.

2. Les classifications des RiOMar

Les différences dans la structuration et le fonctionnement biogéochimique des sédiments des RiOMar ont été constatées de longue date (Rhoads et al. 1985, Aller & Aller 1986, Alongi et al. 1992, Aller & Stupakoff 1996, Wheatcroft 2006, Harmelin-Vivien et al. 2009, Akoumianaki et al. 2013, Bonifácio et al. 2014), conduisant à plusieurs essais de typologie faisant intervenir des approches différentes. En se basant principalement sur l'analyse de la distribution verticale de la macrofaune dans la colonne sédimentaire et sur des radiographies aux rayons-X de carottes sédimentaires, Rhoads et al. (1985) ont été les premiers à proposer un modèle conceptuel décrivant la réponse de la macrofaune benthique et des sédiments de surface aux apports des grands fleuves (**Figure 0.4**).

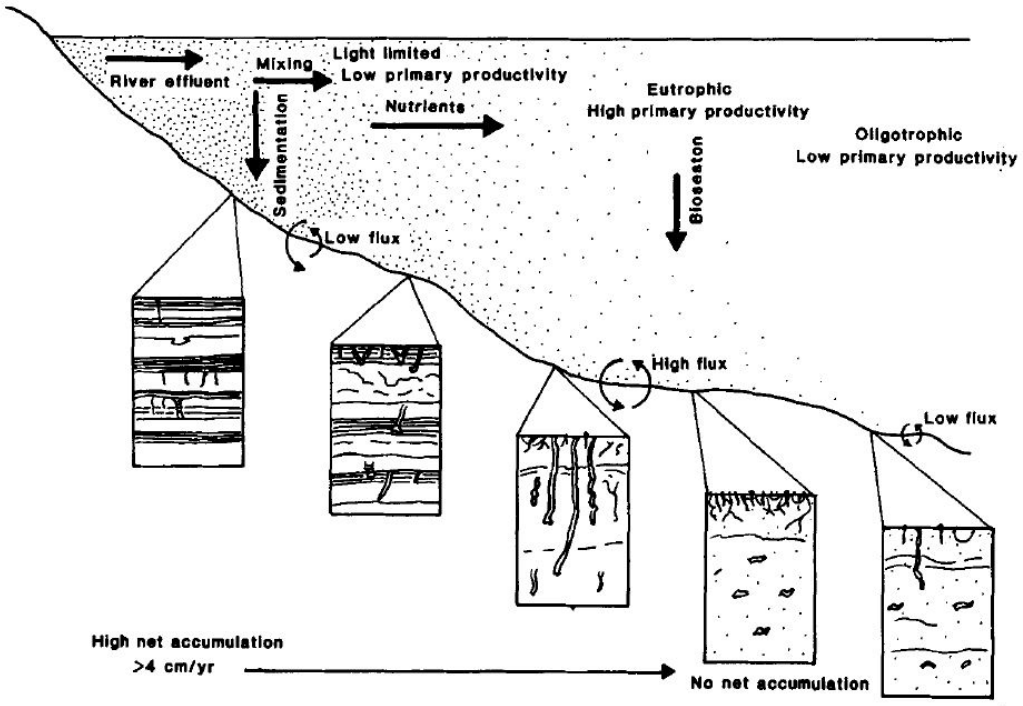

Figure 0.4. Modèle généralisé des principaux processus liés aux apports des grands fleuves ainsi que de leurs conséquences en termes de bioturbation. D'après Rhoads et al. (1985).

Selon ce modèle, dérivé de l'étude d'un seul fleuve (i.e., le Changjiang), la distribution spatiale de la macrofaune est principalement déterminée par l'interaction entre: (1) la perturbation physique induite par les apports intenses de particules continentales, et (2) la disponibilité en MOP. Dans les parties proximales des RiOMar (i.e., les plus proches de l'embouchure de la rivière), les taux de sédimentation élevés et irréguliers induisent une instabilité sédimentaire, empêchant l'établissement de communautés macrobenthiques

matures. De plus, la turbidité élevée des panaches fluviaux y limite la production primaire pélagique, ce qui se traduit par des concentrations faibles en MOP (qui présente de plus un caractère fortement réfractaire) dans les sédiments de surface. En conséquence, ces zones proximales sont caractérisées par une faible intensité de bioturbation et de faibles flux de reminéralisation du carbone organique. À l'inverse, dans les parties distales (c'est-à-dire plus profondes), une sédimentation modérée et une production primaire pélagique plus élevée favorisent l'établissement de communautés macrobenthiques matures, induisant des intensités de bioturbation et des flux de reminéralisation élevés.

Les tentatives ultérieures de classification des RiOMar se sont quant-à-elles basées sur des méta-analyses appliquées à des processus géomorphologiques et/ou biogéochimiques (McKee et al. 2004, Blair & Aller 2012). Leurs résultats ont mis en évidence l'effet majeur des régimes hydrodynamiques du milieu récepteur sur les morphologies des composantes benthiques des RiOMar (**Figure 0.5**) ainsi que sur les intensités de préservation du carbone organique particulaire (**Figure 0.3**). De fait, une des limites du modèle de Rhoads et al. (1985) réside clairement dans l'attribution de l'instabilité sédimentaire à la seule sédimentation excessive des apports particulaires fluviaux, alors que ce phénomène peut également être généré par un fort hydrodynamisme du milieu récepteur.

Ce constat a notamment conduit Blair & Aller (2012) à établir, sur des bases biogéochimiques, une distinction claire entre : (1) les systèmes à faible énergie, présentant à la fois des taux élevés de sédimentation et de préservation du carbone (qui seront appelés par la suite systèmes de type 1), et (2) les systèmes à haute énergie, présentant une oxygénation élevée des sédiments et de faibles taux de préservation du carbone (qui seront appelés par la suite systèmes de type 2).

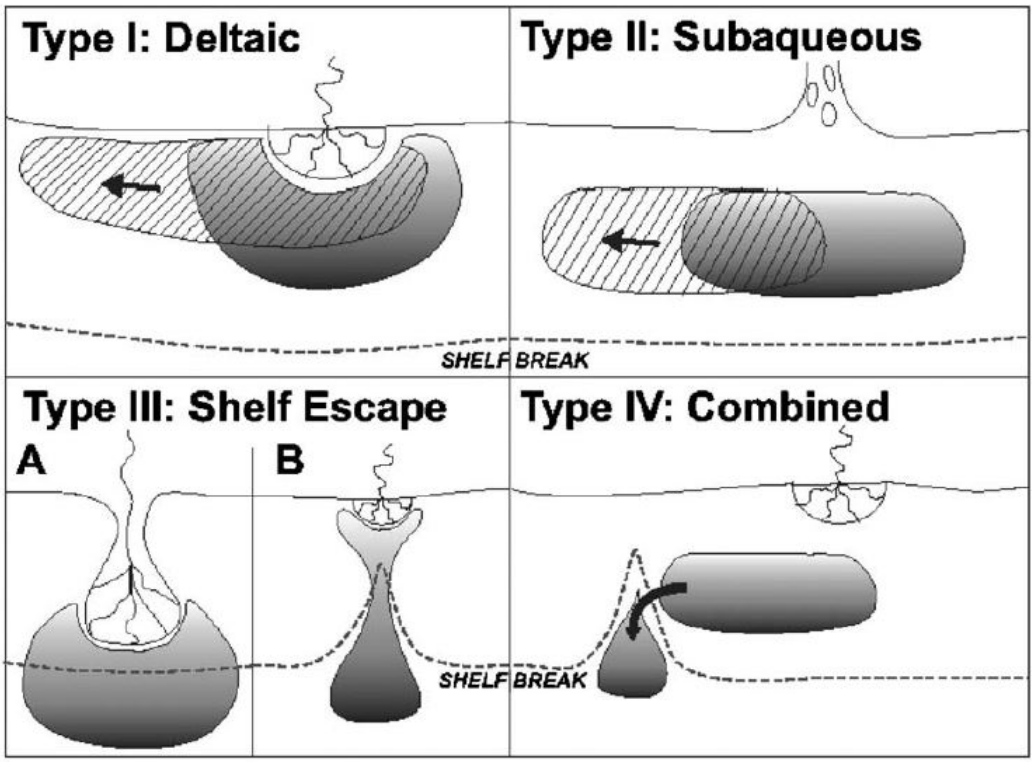

Figure 0.5. Modèle conceptuel des zones de dépôt à long terme des sédiments provenant des principaux fleuves. Les zones hachurées font référence à la délocalisation causée par un forçage majeur orienté le long de la côte. Les systèmes de type I sont associés à des fleuves deltaïques (Mississippi-Atchafalaya, Orinoco, Danube). Les systèmes de type II, à énergie plus élevée (Amazone, Yangtze, Yenisey), présentent une discontinuité entre l'embouchure du fleuve et la zone de dépôt, qui se situe plus au large où l'énergie est réduite. Les systèmes de type III sont typiquement des systèmes deltaïques où une part significative (>10%) du dépôt des sédiments a lieu après le rebord du plateau continental, soit en raison de la progradation de la zone de l'embouchure du fleuve (IIIA-Mississippi-Balize), soit en raison de la proximité de l'embouchure d'un canyon sous-marin (IIIB-Zaïre). Plusieurs fleuves (Gange-Brahmapoutre, Fleuve Jaune) présentent à la fois des systèmes deltaïques et subaquatiques (type IV) et peuvent également avoir un transport significatif de sédiments hors du plateau. D'après McKee et al. (2004).

Cette classification s'est basée sur une comparaison faisant essentiellement intervenir des systèmes tropicaux et subtropicaux ; le système constitué par le Rhône et son prodelta étant le seul grand RiOMar tempéré considéré. Ceci s'explique facilement par le fait que ce système avait alors déjà fait l'objet de nombreuses études, aussi bien biogéochimiques (Alliot et al. 2003, Darnaude et al. 2004, Tesi et al. 2007, Lansard et al. 2009, Cathalot et al. 2010, Bourgeois et al. 2011, Pastor et al. 2011a b) que biologiques (Salen-Picard et al. 2003, Hermand et al. 2008, Harmelin-Vivien et al. 2009, Labrune et al. 2012). De manière générale, les résultats de ces travaux ont montré que le système Rhône présentait deux grandes particularités : (1) de fortes variations saisonnière du régime hydrologique du fleuve qui se traduisent par une forte variabilité de la quantité et de la qualité des apports solides à l'océan,

et (2) l'hydrodynamisme relativement « faible » du milieu océanique récepteur. Ces résultats ont conduit Blair & Aller (2012) à lui conférer un statut de type 1. Dans ce contexte, il existe toujours un besoin évident de documenter la structuration spatio-temporelle d'un potentiel RiOMar tempéré de type 2.

Un deuxième point à prendre en considération réside dans le fait que, contrairement à celle initialement présentée par Rhoads et al. (1985), les classifications établies par McKee et al. (2004) puis Blair & Aller (2012) ont consisté à définir une typologie des RiOMar dans leur entièreté. Il est d'autant plus important que McKee et al. (2004) avaient eux-mêmes souligné l'intérêt de différencier des sous-environnements au sein des RiOMar et de faire intervenir l'analyse de la structuration et du fonctionnement de ces sous-environnements lors des comparaisons entre RiOMar. C'est dans cet esprit que les descriptions des variations spatio-temporelles : (1) de la macrofaune benthique et de ses traces d'activité (Salen-Picard et al. 2003, Hermand et al. 2008, Harmelin-Vivien et al. 2009, Labrune et al. 2012, Bonifácio et al. 2014), (2) des caractéristiques quantitatives et qualitatives de la MOP sédimentée (Alliot et al. 2003, Darnaude et al. 2004, Tesi et al. 2007, Bourgeois et al. 2011, Cathalot et al. 2013), et (3) de sa minéralisation dans les sédiments de surface du prodelta du Rhône (Lansard et al. 2009, Cathalot et al. 2010, Pastor et al. 2011a b, 2018) ont été réalisées. La mise en relation de ces variations a par ailleurs suggéré le rôle majeur joué par le régime hydrologique du fleuve Rhône dans le contrôle de ces compartiments/processus. Là encore, une approche similaire reste encore à conduire pour un potentiel RiOMar tempéré de type 2.

Mon travail de thèse vise à combler ces deux manques. Pour cela, il repose, d'une part, sur l'acquisition de données nouvelles au sein d'un potentiel RiOMar tempéré de type 2, et, d'autre part sur la comparaison de ces données avec celles disponibles dans la littérature relative au RiOMar Rhône (considéré comme un exemple de RiOMar de type 1).

3. La VOG en tant que potentiel RiOMar tempéré de type 2

La Vasière Ouest-Gironde (VOG) a été retenue en tant que potentiel RiOMar tempéré de type 2 du fait : (1) du caractère relativement limité des variations saisonnières des apports liquides et particulaires de la Gironde à l'océan Atlantique, et (2) du très fort hydrodynamisme du milieu récepteur de ces apports.

3.1. Description générale

La VOG est située au large de l'estuaire de la Gironde sur le plateau continental du Golfe de Gascogne (**Figure 0.6**), au sein d'un environnement meso- à macro-tidal (amplitude maximale de 4 à 5 mètres ; Jalón-Rojas et al. 2018) dont l'hydrodynamisme est dominé par les vagues de tempête (Arbouille 1987). Dans cet environnement, la nature sédimentaire est hétérogène, allant des graviers à débris coquillers jusqu'aux sables fins. Ces sédiments forment le substrat que recouvre les deux principaux champs ouverts de dépôt de particules fines. On distingue classiquement la VOG et la Vasière Sud-Gironde (VSG), qui sont localisées au large des deux chenaux de l'embouchure de l'estuaire de la Gironde par lesquels elles sont alimentées en particules fines (Allen & Castaing 1977). Ces deux entités rentrent dans la catégorie des patchs ou champs vaseux d'après la typologie des dépôts vaseux définie par Hanebuth et al. (2015). Ils constituent des patchs isolés de « faible » épaisseur et d'étendue réduite (i.e., environ 420 km^2 pour la VOG et 160 km^2 pour la VSG ; Lesueur et al. 1996), issus d'apports sédimentaires estuariens. S'ils ont été observés pour la première fois par Berthois & Le Calvez (1959), ce n'est qu'à la fin des années 1960 que leurs emprises spatiales ont été définies (Lapierre 1967, Longère & Dorel 1970, Vigneaux et al. 1972). L'épaisseur maximale de la vase déposée est d'environ 4 m pour la VOG (maximum situé entre 40 et 50 m de profondeur selon Lesueur et al., 2002) et de 2 m pour la VSG. Certains auteurs ont considéré les limites d'extension de ces deux ensembles comme stables à l'échelle décennale, voire bi-décennale (Longère & Dorel 1970). D'autres ont plus récemment envisagé l'existence de déplacements de ces limites en lien avec l'hydrodynamisme (Lesueur et al. 1991, Lesueur 1992). Lesueur (1992) mentionne également l'existence d'une zone transitoire (dont l'extension spatiale n'est pas précisément définie) de vases fluides (non consolidées) autour de ces vasières. Celles-ci seraient fréquemment présentes entre la côte et la VOG,

particulièrement durant les crues hivernales et printanières quand l'expulsion fluviatile est maximale (Castaing & Allen 1981).

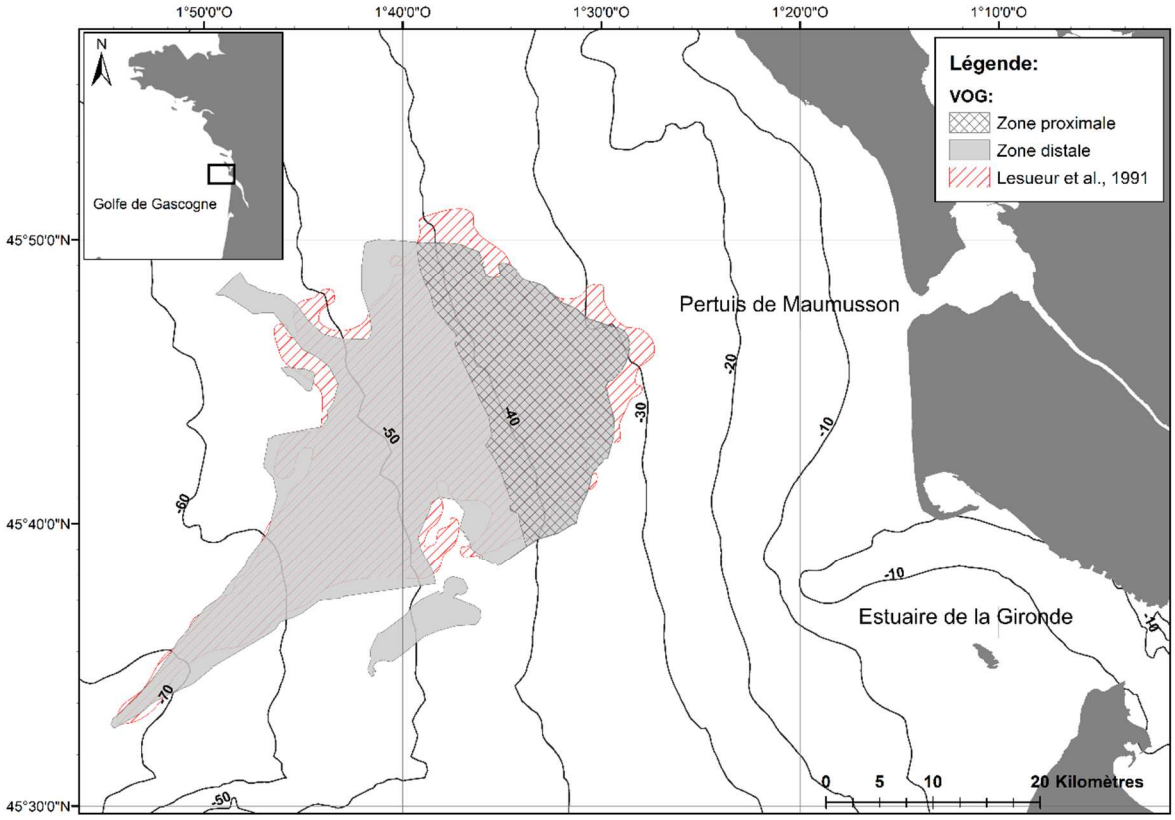

Figure 0.6. Localisation de la Vasière Ouest-Gironde (VOG) le long de la côte Atlantique, de ses zones proximale et distale, et de son emprise spatiale telle qu'estimée par Lesueur et al. (1991). La délimitation actuelle des zones proximale et distale est basée sur les mesures acoustiques réalisées lors de la campagne JERICOBENT-5-TH (Gillet & Deflandre 2018) et sur l'analyse des sédiments de surface de la campagne JERICOBENT-5 (Schmidt & Deflandre 2018).

3.2. Formation et historique

Deux théories ont successivement prévalu quant à la formation de la VOG. Selon la première, basée entre autres sur l'analyse du matériel carbonaté à la base des dépôts de la partie centrale, les vases y sont composées de dépôts paléo-lagunaires ou paléo-estuariens (Berthois & Le Calvez 1959). Cette hypothèse est étayée par des études micro-paléontologiques d'ostracodes et de foraminifères benthiques (Carbonel et al. 1972, 1975, Moyes 1974, Pujos 1976), qui attribuèrent un âge d'environ 10 000 ans à cette vasière. Elle a ensuite été affinée sur la base de datations au ^{14}C des débris coquillers issus d'une carotte longue (Feral 1970). Les résultats ainsi obtenus ont conduit à proposer une hypothèse d'évolution paléogéographique selon laquelle la VOG se serait formée dans un contexte de niveau marin bas (proche des -50 m actuels) en milieu estuarien ou lagunaire, à l'époque de

la transgression post-glaciaire. Selon la seconde théorie, la formation de la VOG résulte d'apports de particules issues de la Gironde (Castaing et al. 1971, 1979, 1982, Allen 1973, Allen & Castaing 1973, Castaing & Allen 1981). Les particules auraient d'abord été déposées sous le niveau d'action effective des vagues pendant la fin de la transgression post-glaciaire Holocène. Castaing (1981) a postulé que la sédimentation fine avait pu commencer autour de 7000 ans BP (*Before Present*) en lien avec une baisse du niveau marin. Cette hypothèse dynamique a par ailleurs été confortée par des études radio-isotopiques des dépôts superficiels (Jouanneau et al. 1989).

Les travaux de Lesueur (1992) et Lesueur et al. (1996) ont finalement invalidé la première théorie et fortement révisé la seconde. Pour cela, ces auteurs se sont appuyés sur la connaissance préalable de l'existence des apports de particules estuariennes sur le plateau continental ainsi que sur un grand nombre d'études minéralogiques, géochimiques et granulométriques (Latouche 1971, Etcheber & Relexans 1983, Jouanneau 1983, Jouanneau et al. 1983, Latouche et al. 1991, Weber et al. 1991, Lesueur & Tastet 1994, Gadel et al. 1997). La stratigraphie des dépôts vaseux a également été étudiée à l'aide de datations au ^{14}C et d'analyses palynologiques (Lesueur et al. 1996). L'ensemble a permis de montrer que le substrat clastique de la VOG date d'entre 5000 et 2000 ans BP. De plus, les coquilles présentes dans la partie basale des vases ont été datées de 500 BP pour la VOG, alors que l'étude des pollens présents indique des activités humaines de l'époque romaine (2000 BP). Selon Lesueur (1992), l'installation du corps pélitique de la VOG daterait d'environ 1500 ans . Lesueur et al. (1996) précisent par ailleurs que la formation de la VOG n'a débuté qu'après : (1) la stabilisation relative du niveau marin de l'Holocène (environ 6000 ans BP), et (2) le remplissage subséquent de l'estuaire de la Gironde, qui n'atteignit pas l'équilibre avant 2000 ans BP. L'équilibre de l'estuaire, atteint suite à son comblement, a alors induit une augmentation de l'export en particules vers le plateau continental constituant ainsi une source de matériel particulaire permettant le développement des vasières. Lesueur (1992) estime que l'installation différée des dépôts s'expliquerait par les variations des taux d'expulsion des particules par l'estuaire. L'augmentation des apports estuariens sur le plateau continental proviendrait du comblement des lits fluviaux et de l'estuaire, résultant du ralentissement de la remontée du niveau marin depuis environ 5000 ans. Du fait de la longueur de l'estuaire (une centaine de kilomètres), la propagation des apports vers l'aval s'est déroulée progressivement, ce qui aura nécessité un délai de quelques milliers d'années. D'après Allen (1973), cet « hystérésis de sédimentation fluvio-deltaïque » n'a été compensé qu'à partir de

la moitié du Moyen-âge, à partir de laquelle une plus grande partie de la charge solide véhiculée par la Gironde aurait pu être exportée en mer. Ce point semble être confirmé par les datations évoquées précédemment puisqu'une grande partie de la sédimentation fine dans la VOG date de moins de 1000 ans, voire même de moins de 500-600 ans. Les caractéristiques lithologiques de la VOG laissent également à penser que ce dépôt s'est constitué en 2 étapes (Lesueur et al. 1989, 1991, Lesueur 1992). Tout d'abord un comblement d'une paléo-dépression constituée d'un substrat sablo-graveleux par des vases et sables interlités (particules fines estuariennes mélangées à une fraction sableuse originaire des placages du substrat adjacent), à un niveau marin comparable à l'actuel. Ensuite, un développement vertical et latéral de la lentille vaseuse, qui a eu pour conséquence le recouvrement des placages sableux avoisinants, et donc l'éloignement progressif des sources adjacentes de matériel grossier du dépôt-centre de la VOG. L'étude de carottes prélevées sur la VOG suggère enfin que la sédimentation a d'abord eu lieu dans sa partie proximale (la plus proche de l'embouchure de l'estuaire de la Gironde) il y a environ 1000 ans (Lesueur 1992), puis seulement plus tard dans sa partie distale.

3.3. Alimentation en particules

L'influence des facteurs climatiques et anthropiques sur la dynamique de développement de la VOG est également à prendre en compte (Lesueur 1992). L'érosion des bassins versants aurait ainsi été accrue par une phase de refroidissement qui débuta autour du XVI^{ème} siècle et dura jusqu'à la fin du XIX^{ème} siècle (« Petit Age Glaciaire »), en lien avec une augmentation des précipitations. En parallèle, les grands défrichements intervenus en France durant la période médiévale auraient également eu pour conséquence d'accentuer le lessivage des sols mis en culture dans le bassin versant de la Gironde. Pour la période plus récente, les impacts anthropiques seraient plus importants encore, avec d'une part la rétention des particules par poldérisation des berges, mais d'autre part et surtout une expulsion accrue de particules par creusement de chenaux, endiguements et dragages, qui provoquent depuis un siècle environ d'importantes remises en suspension de particules alimentant le bouchon vaseux de la Gironde puis l'expulsion des particules de l'estuaire vers l'océan. De manière plus générale, les pratiques agricoles, les poldérisations, les constructions de digues ainsi que les dragages des chenaux de navigation de l'estuaire de la Gironde sont suspectés d'avoir entrainé une augmentation importante du flux de particules fines vers le

plateau (Lesueur et al. 1996). La diminution des débits fluviaux observée depuis plusieurs décennies (Schmidt et al. 2016, Sautour & Baron 2020) est susceptible de contrebalancer ces phénomènes et de conférer plus d'importance aux évènements météorologiques extrêmes susceptibles de créer des expulsions plus importantes.

L'export de particules depuis la Gironde vers le plateau continental a lieu à toutes les basses mers. Le plus gros de ces exports s'effectue néanmoins de manière intermittente en période de crues et pendant les marées de vive-eau. Ils prennent ainsi la forme de pulses irréguliers (Castaing 1981, Froidefond et al. 1998) contrôlés par les décharges fluviatiles et l'amplitude tidale (Castaing & Allen 1981), quand la zone de turbidité maximale est située dans la partie la plus aval de l'estuaire (Doxaran et al. 2009). Ces conditions interviendraient entre 15 et 50 jours par an (Jouanneau 1983).

La dispersion des particules estuariennes sur le plateau continental est bien documentée (Allen 1973, Castaing et al. 1979, Castaing 1981, Jouanneau 1983). Des données hydrologiques (Weber et al. 1991, Ruch et al. 1993) et satellites (Froidefond et al. 1998, Castaing et al. 1999, Constantin et al. 2018) montrent que les particules se dispersent d'abord vers le nord puis l'ouest en direction de la VOG. Les particules se déplacent de la côte vers la VOG par le biais de deux couches néphéloïdes : l'une en surface qui peut être suivie par télédétection (Castaing et al. 1979), l'autre près du fond (Castaing & Allen 1981, Weber et al. 1991, Ruch et al. 1993). Cette dernière provient de l'épanchement des eaux estuariennes turbides et va alimenter la VOG en particules fines. Deux contributions particulaires viennent se superposer au transfert des particules estuariennes vers le plateau continental du Golfe de Gascogne (Weber et al. 1991): (1) une contribution biogénique (diatomées et autres débris siliceux) identifiée dès l'embouchure de la Gironde dans les matières en suspension du panache turbide (mode granulométrique de 15-20 µm), et (2) une contribution de sables fins du plateau continental (mode de 50-60 µm) remobilisés à faible profondeur par les vagues et la houle, et qui sédimentent dans la partie proximale de la VOG.

Selon Lesueur et al. (2001), les valeurs des taux de sédimentation actuels varient entre 1 et 5,6 $mm.an^{-1}$ selon la partie de la VOG considérée. Ces taux ont récemment été recalculés par Dubosq et al. (2021) et pourraient s'élever à 9,7 $mm.an^{-1}$ dans certaines parties de la VOG. Cette sédimentation intervient selon une zonation dynamique qui se trouve reflétée dans les séquences stratigraphiques, la palynologie, les traces d'activité biologique et la radiochronographie (Jouanneau et al. 1989). Dans la zone proximale (**Figures 0.6** et **0.7**), à

partir de 30 mètres de profondeur, les dépôts récents restent transitoires du fait de la fréquence d'occurrence élevée des phénomènes de haute énergie (fortes houles et tempêtes) empêchant ainsi la préservation et la consolidation des particules fines sédimentées (Jouanneau et al. 1989). La vase de cette partie correspond à des dépôts fossiles interlités par des sédiments légèrement plus grossiers (sables) issus du plateau continental adjacent. Ces séquences sont attribuées à l'impact de fortes houles ; la plus forte granulométrie de chacune de leur partie basale résultant d'un évènement hydrodynamique de haute énergie (Lesueur & Tastet 1994). De ce fait, la fréquence d'occurrence de ces séquences décroit clairement vers le large (Jouanneau et al. 1989, Lesueur & Tastet 1994) pour n'être plus que de 1 à 5 fois par siècle dans les zones les plus profondes de la VOG (Lesueur 1992, Lesueur et al. 2002), où seuls les évènements les plus extrêmes se trouvent enregistrés dans la colonne sédimentaire (Lesueur & Tastet 1994). Ces zones (**Figures 0.6** et **0.7**) reçoivent des apports modernes de particules estuariennes (Jouanneau et al. 1989, Weber et al. 1991, Relexans et al. 1992), et la sédimentation y est plus intense que l'érosion. L'alternance de phases dynamiques et plus stables permet par ailleurs le développement d'une très forte activité de bioturbation (Jouanneau et al. 1989, Lesueur & Tastet 1994).

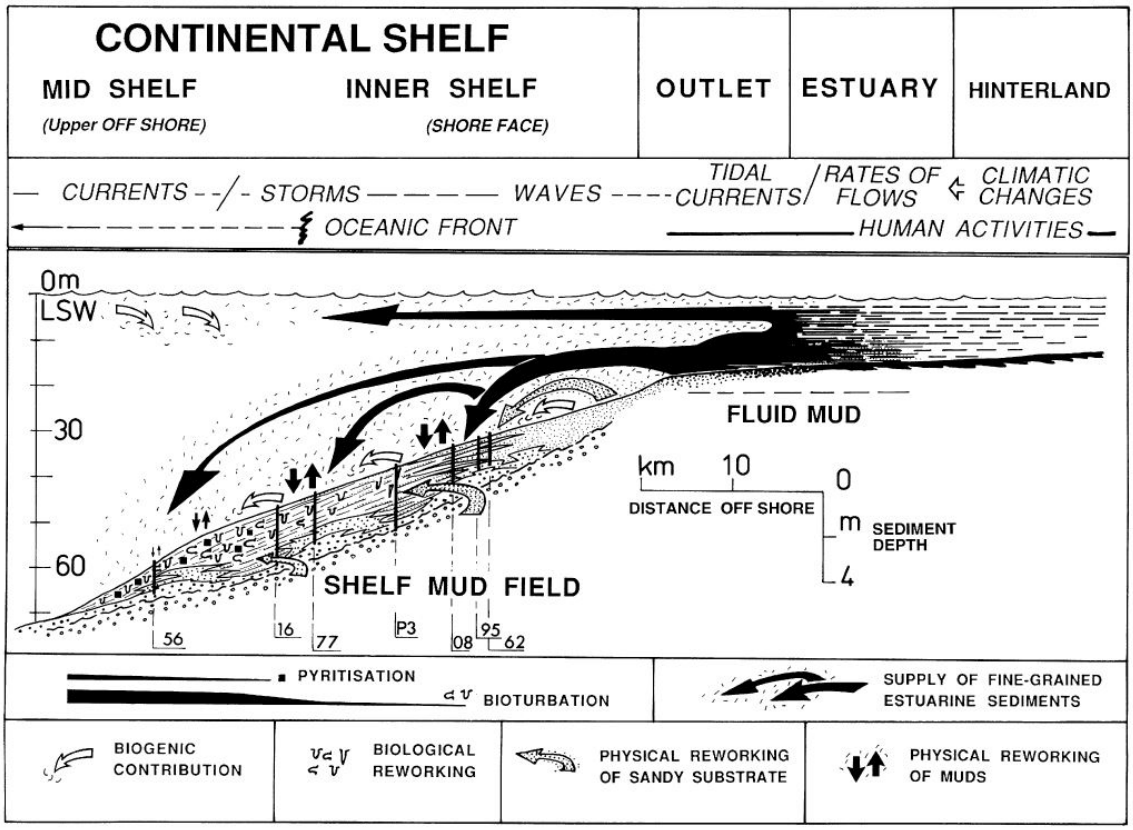

Figure 0.7. Synthèse des différents processus de dépôt responsables de la sédimentation fine sur la Vasière Ouest-Gironde. Tiré de Lesueur et al. (2002).

3.4. Bilan des connaissances

La dynamique sédimentaire passée et actuelle de la VOG a été abondamment étudiée durant la période 1980-2000 sur la base de séquences stratigraphiques, de données palynologiques, de radiographies aux rayons-X et de radiochronographies. Ces études ont attribué un rôle majeur à l'hydrodynamisme dans le contrôle de la structuration spatiale de la VOG du fait: (1) de la segmentation entre une partie proximale et une partie distale sans sédimentation persistante moderne dans la première en raison d'un fort hydrodynamisme, et (2) la diminution avec la profondeur de la fréquence d'apparition des séquences d'érosion verticale dans la colonne sédimentaire.

Les études des caractéristiques des sédiments de surface et de la matière organique qui leur est associée, ainsi que celles de la faune benthique, ont cependant été jusqu'ici largement négligées. Seules deux études se sont intéressées aux dynamiques spatiales et/ou temporelles de la matière organique et de la faune dans ce système. La première portant sur la réponse de la méiofaune à la qualité de la matière organique sédimentaire (Relexans et al. 1992), et la seconde sur la composition des communautés bactériennes et de macrofaune benthique (Massé et al. 2016). Ces deux études n'ont été conduites que sur un nombre très réduit de stations et qu'à une seule date d'échantillonnage dans le cas de Massé et al. (2016). Leurs résultats suggèrent l'existence de gradients spatiaux en lien avec la profondeur, avec entre autres des différences significatives des compositions de la macrofaune benthique aux sein des parties proximales et distales de la VOG. Néanmoins, les ampleurs des changements spatio-temporels des caractéristiques des sédiments de surface et de la composition de la macrofaune benthique, ainsi que leurs déterminismes, restent encore largement inconnus.

4. Approches méthodologiques utilisées

4.1. Les facteurs de contrôle potentiels

Plusieurs facteurs sont susceptibles d'influencer les évolutions spatio-temporelles de la structuration du compartiment benthique des RiOMar. Ces forçages sont le plus souvent associés à des phénomènes naturels tels que la sédimentation, l'hydrodynamisme du milieu récepteur ou bien le cycle saisonnier de production primaire. Des perturbations anthropiques telles que le chalutage de fond, le dragage ou le clapage de sédiments sont également

susceptibles d'intervenir. L'action de l'ensemble de ces facteurs conditionne : (1) directement la nature et la granulométrie des sédiments, ainsi que la quantité et la disponibilité de la MOP associée, et (2) indirectement la composition ainsi que les activités de bioturbation de la macrofaune benthique (Pearson & Rosenberg 1978). Etant donné le lien étroit et les rétroactions possibles entre les caractéristiques du sédiment de surface, la macrofaune benthique, et son action sur la colonne sédimentaire, il apparaissait particulièrement important dans ce travail de considérer l'ensemble de ces éléments, ainsi que les principaux facteurs susceptibles de contrôler leurs dynamiques spatio-temporelles, à savoir dans le cas de la VOG: (1) les apports particulaires de la Gironde, (2) l'hydrodynamique du milieu récepteur, et (3) le chalutage de fond. Les mesures/calculs des deux premiers éléments ont été mis en œuvre dans les chapitres 1, 2 et 3 de cette thèse alors que les estimations du chalutage de fond ne l'ont été que lors de l'étude synoptique spatiale présentée au chapitre 1.

4.1.1. Les apports de la Gironde

Les moyennes journalières des débits liquides de l'estuaire de la Gironde ont été utilisées comme proxy des apports solides de l'estuaire à la VOG après sommation des débits liquides de la Garonne (station de Tonneins) et de la Dordogne (station de Pessac-sur-Dordogne) fournis par le Ministère de l'Ecologie, du Développement Durable et de l'Energie (http://www.hydro.eaufrance.fr). Il est clair qu'il ne s'agit là que d'une estimation très imparfaite. Il était initialement prévu qu'elle soit complétée par la mise en œuvre d'un modèle hydro-sédimentaire décrivant le transfert des particules de l'estuaire au plateau continental et les taux de sédimentation sur celui-ci, ce qui n'a pu être réalisé dans le cadre de mon travail de thèse (voir également la section **Conclusions et perspectives** de ce manuscrit). Cette approche permet néanmoins d'estimer qualitativement les variations temporelles de l'importance relative des apports particulaires de la Gironde, ceux-ci se produisant principalement lors des crues (Castaing & Allen 1981, Doxaran et al. 2009). Elle ne fournit par contre aucune information sur les variations spatiales de ces mêmes apports (voir également la section **Conclusions et perspectives** de ce manuscrit).

4.1.2. L'hydrodynamisme du milieu récepteur

Les contraintes de cisaillement sur le fond ont été calculées à partir d'un modèle numérique tridimensionnel (Diaz et al. 2020) qui s'étend de l'estuaire de la Gironde au plateau continental. Ce modèle associe le modèle hydrodynamique MARS3D (Lazure & Dumas 2008) avec le modèle de vagues WAVE WATCH III® (Roland & Ardhuin 2014) et intègre des forçages hydrométéorologiques réalistes (i.e., le vent, la marée, la houle et le débit de l'estuaire de la Gironde). Les valeurs de cisaillement y sont calculées comme la résultante de leurs composantes induites par le courant et par les vagues, selon la formulation de Soulsby (Soulsby 1997). Le modèle fournit des valeurs de cisaillement sur le fond avec une résolution spatiale d'environ 0,5 km^2 sur la VOG. Les simulations réalisées ont fourni des sorties à l'échelle de l'heure qui ont ensuite été compilées quotidiennement en utilisant les $95^{ème}$ percentiles, afin de prendre en compte les événements hydrodynamiques quotidiens les plus intenses. Cet exercice a été réalisé sur la période 2010-2018. A la différence des débits, les valeurs du proxy de l'hydrodynamisme utilisées lors de ce travail comprennent donc à la fois une composante spatiale (valeurs modélisées à chaque station échantillonnée) et une composante temporelle (valeurs modélisées à chaque temps).

4.1.3. L'intensité du chalutage

Les corps vaseux que constituent les RiOMar sont enrichis en matière organique par rapport aux sédiments adjacents et constituent souvent des zones de pêche préférentielles. Ceci est le cas de la partie distale de la VOG qui est le siège d'une pêcherie utilisant des chaluts de fond (Lesueur 1992, Mengual et al. 2016, 2019, SIH Ifremer 2017), susceptibles d'induire des perturbations importantes des habitats benthiques. Les variations spatio-temporelles de l'effort de pêche correspondant ont été estimées dans et autour de la VOG pendant l'année précédant la campagne synoptique conduite en 2018 (**Chapitre 1**). J'ai utilisé pour cela les données du système d'identification automatique (AIS) recueillies et compilées par l'association Global Fishing Watch (https://globalfishingwatch.org ; Kroodsma et al. 2018) avec une résolution spatiale de $1/100^{ème}$ de degré (soit environ 1,77 km^2 dans la VOG).

4.2. Caractérisation des sédiments de surface

4.2.1. Granulométrie et surface spécifique

La caractérisation du sédiment de surface débute généralement par la détermination de sa granulométrie, le plus souvent synthétisée sous la forme de la taille médiane des grains (D_{50} ou $D_{0.5}$) lorsqu'elle présente des distributions (quasi)normales. La corrélation négative généralement trouvée entre le $D_{0.5}$ et le contenu organique du sédiment résulte en fait de la corrélation négative liant le $D_{0.5}$ et la surface des particules, cette dernière contrôlant directement le contenu organique (Premuzic et al. 1982, Mayer 1994, Hedges & Keil 1995) via le processus d'adsorption (Tiessen et al. 1984, Anderson 1988, Oades 1988). La surface spécifique est définie comme la surface totale d'un matériau par unité de masse et est généralement exprimée en $m^2.g^{-1}$. Dans le cas de particules sédimentaires fines telles que les argiles, cette surface est beaucoup plus grande que la surface géométrique des grains du fait de la présence de micro-pores d'une taille inférieure à 2 nm (Weiler & Mills 1965, Mayer 1994). Pour les sédiments vaseux, tels que ceux de la VOG, il apparait important de normaliser les concentrations des différents descripteurs quantitatifs de la MOP par la surface spécifique des sédiments analysés. Lors de ce travail, les granulométries des sédiments ont été mesurées à l'aide d'un microgranulomètre laser Master Sizer Malvern Panalytical® (**Chapitres 1, 2 et 3**) et les surfaces spécifiques à l'aide d'un Gemini VII 2390 Series Surface Area Analyzer Micromeritics® (**Chapitres 1, 2 et 3**).

4.2.2. Caractérisation de la MOP sédimentée

La MOP sédimentée interagit très fortement avec la macrofaune benthique dont elle conditionne très largement la nature, l'abondance et les fonctionnalités (Pearson & Rosenberg 1978). En retour, son devenir est fortement affecté par la présence de la macrofaune benthique via les processus de nutrition et de bioturbation (voir également ci-dessous). La MOP sédimentée consiste en un mélange hétérogène complexe d'éléments vivants (e.g., micro-organismes) ou morts et consistant alors en détritus à différents stades de dégradation (Fowler & Knauer 1986). Dans les sédiments des RiOMar, cette matière est susceptible de présenter une origine aussi bien marine que continentale. Les différentes combinaisons entre les origines des différentes composantes de la MOP et les cinétiques/états de dégradation associés déterminent les niveaux avec lesquels ces composantes peuvent être utilisées par la macrofaune benthique (Lopez & Levinton 1987). Il était par conséquent important de prendre

en compte ces différents points dans le cadre de la présente étude. J'ai pour cela utilisé : (1) des descripteurs globaux de la MOP sédimentée (e.g., les concentrations en Carbone Organique Particulaire et en acides aminés totaux (THAA) ; Medernach et al. 2001, Bonifácio et al. 2014), (2) un traceur global d'origine de la MOP sédimentée (i.e., le $\delta^{13}C$; Gearing et al. 1977, Fontugne & Jouanneau 1987, Gearing 1988, Graham et al. 2001), (3) un traceur d'origine de la matière végétale (i.e., la concentration en chlorophylle-*a* (Chl-*a*) ; Liénart et al. 2017), et (4) des traceurs des fractions labiles ou au contraire réfractaires des composantes totales ou d'origine végétale (i.e., les concentrations en acides aminés biodisponibles (EHAA ; Mayer et al. 1995, Medernach et al. 2001) et en phéophytine-*a* (Phéo-*a* ; Bianchi et al. 1988, 1991, Sun et al. 1994)). La mise en relation de certains de ces éléments permet enfin d'évaluer le niveau de labilité de la MOP sédimentée, soit dans sa globalité via le rapport EHAA/THAA (Wakeham et al. 1997, Medernach et al. 2001, Pastor et al. 2011b, Bonifácio et al. 2014), soit dans sa composante végétale via le rapport Chl-*a* / (Chl-*a* + Phéo-*a*) (Pastor et al. 2011b, Bonifácio et al. 2014). Lors de ce travail, ces paramètres ont été quantifiés à l'aide d'un ensemble de techniques (analyse élémentaire, spectrométrie de masse isotopique, spectrofluorimétrie, chromatographie liquide à haute pression). Tout ou partie des résultats ainsi obtenus a été utilisé dans les chapitres 1, 2 et 3 de ce manuscrit.

4.3. Macrofaune benthique

La macrofaune benthique constitue une composante importante de la biodiversité des fonds marins (Snelgrove 1998). Elle est le plus généralement définie comme l'ensemble des organismes de taille supérieure à 1 mm, vivant dans le sédiment ou à sa surface. Au travers de leurs fonctions de nutrition et de bioturbation (i.e., remaniement sédimentaire et bioirrigation ; Kristensen et al. 2012), ces organismes affectent profondément le devenir (i.e., resuspension, enfouissement, intégration au réseau trophique et minéralisation) de la MOP sédimentée. A ce titre, l'étude des variations spatio-temporelles de la macrofaune benthique constituait un élément fondamental de l'analyse de la structuration et du fonctionnement de la composante benthique de la VOG. Le deuxième chapitre de ce travail est plus particulièrement consacré à ce point précis, à partir d'un échantillonnage réalisé à la benne Hamon et d'un tamisage sur une maille de 1 mm.

4.4. Imagerie de profils sédimentaires

L'évaluation de la composition de la macrofaune benthique implique l'identification des espèces et leur quantification. Elle est extrêmement chronophage et ne fournit de plus que des informations indirectes sur le fonctionnement de l'écosystème. L'imagerie de profils sédimentaires a été développée à la fin des années 1960 (Rhoads & Young 1970, Rhoads & Cande 1971, Young & Rhoads 1971) afin de permettre une évaluation rapide de l'état de santé des habitats benthiques. Elle a dans ce cadre fait l'objet de nombreuses applications relatives aux évaluations de l'impact de différentes perturbations : (1) l'hypoxie/anoxie (Nilsson & Rosenberg 2000, Rosenberg et al. 2001, 2002, 2009, Rosenberg & Nilsson 2005), (2) le dragage et le chalutage benthique (Nilsson & Rosenberg 2003, Rosenberg et al. 2003, Smith et al. 2003), (3) l'aquaculture (O'Connor et al. 1989, Karakassis et al. 2002), (4) les forages pétroliers et les pollutions associées (Rumohr & Schomann 1992, Germano 1995), (5) les clapages de sédiments dragués (Wilson et al. 2009) ou bien encore (6) l'enrichissement en matière organique (Grizzle & Penniman 1991, Wildish et al. 2003, Labrune et al. 2012).

L'imagerie de profils sédimentaires consiste à collecter *in-situ* des images en deux dimensions de profils verticaux de la couche supérieure de la colonne sédimentaire, à l'aide d'un profileur de sédiments spécialement conçu pour cela (**Figure 0.8A**). Les images de profils sédimentaires ainsi collectées constituent de véritables « carottes optiques » (**Figure 0.8B** ; Germano et al. 2011) desquelles il est possible d'extraire une large variété d'informations représentatives de l'activité biologique (e.g., nombre d'organismes benthiques, nombre de tubes, nombres, surfaces et profondeurs des terriers et chambres oxyques, présence de structures de nutrition). L'imagerie sédimentaire permet également d'évaluer plusieurs paramètres complémentaires liés au fonctionnement biogéochimique des habitats benthiques, comme par exemple l'épaisseur de la discontinuité apparente du potentiel red-ox (aRPD). Un des points faibles de cette approche réside clairement dans le caractère opérateur-dépendant de ces extractions, et notamment celles faisant intervenir une interprétation de la colorimétrie comme la détermination de l'épaisseur de l'aRPD. Plusieurs procédures semi-automatiques ont été proposées pour évaluer cette dernière (Ghita et al. 2004, Teal et al. 2010, de Moura Queirós et al. 2011). Ces procédures se sont tout d'abord basées sur l'utilisation de seuils fixes (Teal et al. 2010, de Moura Queirós et al. 2011), ce qui s'est avéré insatisfaisant. Ceci a conduit Romero-Ramirez et al. (2013) à développer un logiciel spécifique (SPIArcBase) permettant (1) le calcul automatique de la profondeur/épaisseur de l'aRPD à l'aide de plusieurs algorithmes basés sur différentes méthodes de calculs, mais

également (2) de disposer rapidement des nombres, surfaces et profondeurs de chacun des types de traces d'activité biologique analysés, et (3) le stockage dans une base de données de l'ensemble des variables dérivées des images de profils sédimentaires.

Au cours de ce travail, l'imagerie de profils sédimentaires a été mise en œuvre lors de : (1) l'étude spatiale synoptique (**Chapitre 1**), et (2) l'étude des variations spatio-temporelles qui lui est spécifiquement dédiée (**Chapitre 3**). Le profileur sédimentaire utilisé (**Figure 0.8A**) est commercialisé par la société Ocean Imaging Systems et les images obtenues ont été traitées à l'aide du logiciel SPIArcBase.

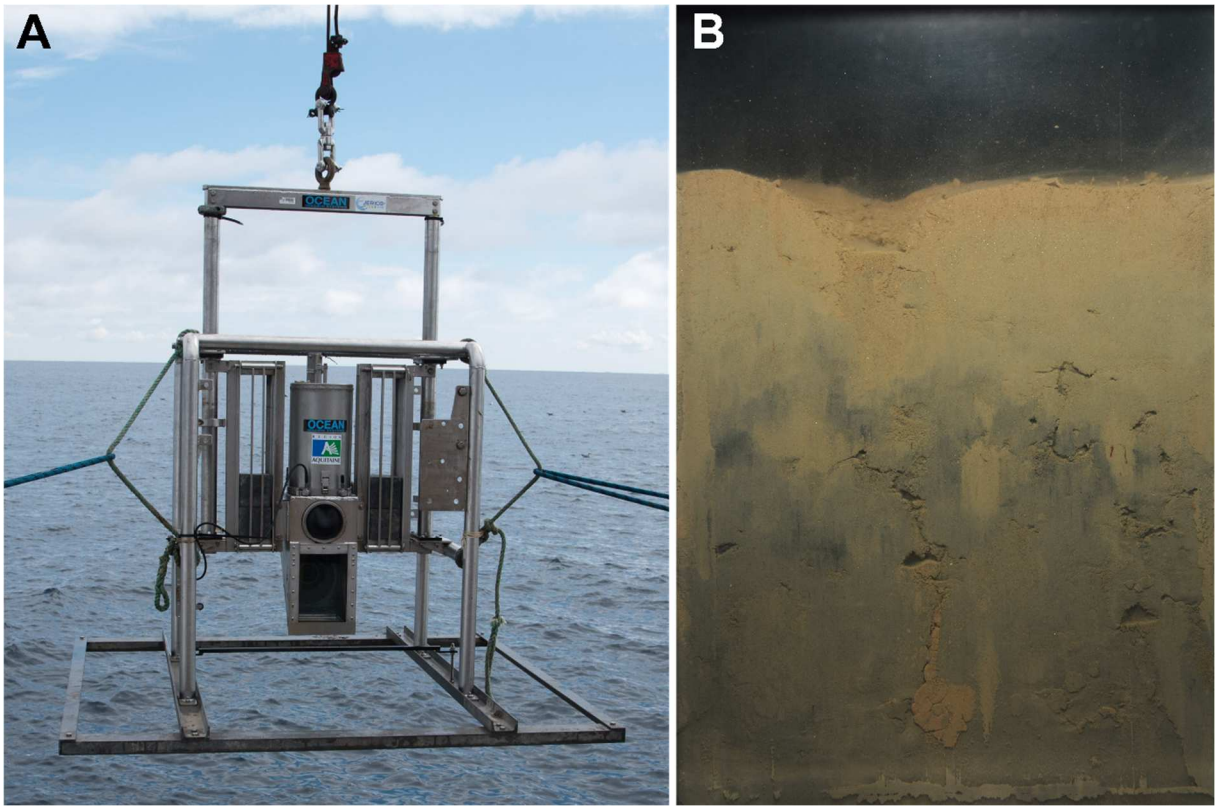

Figure 0.8. L'imageur de profils sédimentaires modèle 3941 commercialisé par la société Ocean Imaging Systems, tel que déployé durant la présente étude (**A**). Exemple d'une image de profil sédimentaire (**B**).

4.5. Traitement de données

De manière générale, les données issues de ce travail ont été traitées suivant des approches multivariées (**Figure 0.9**). Dans un premier temps, ces approches ont été de nature purement descriptive afin de définir des groupes de stations ou de couples stations*dates sur la base de trois ensembles de caractéristiques pris séparément (i.e., les caractéristiques du sédiment de surface, la composition faunistique et les paramètres dérivés des images de

profils sédimentaires). Les procédures utilisées pour cela associent : (1) des Analyses en Composantes Principales (pour les variables relatives aux caractéristiques des sédiments de surface et des images de profils sédimentaires ; Wold et al. 1987) ou des analyses de proximité non-métriques (pour les compositions faunistiques), (2) des analyses de groupements hiérarchiques à lien moyen associés à des procédures « SIMilarity PROFile » (SIMPROF, Clarke et al. 2008), et (3) des analyses « SIMilarity PERcentage » (SIMPER, Clarke 1993). Ces traitements ont été mis en œuvre dans les chapitres 1, 2 et 3. Ils ont tous été réalisés à l'aide du logiciel PRIMER® 6 (Clarke & Warwick 2001).

Dans un second temps, j'ai cherché à mettre en relation ces ensembles entre eux et également à les relier avec les facteurs de contrôle potentiels mentionnés précédemment. Dans tous les cas, les variables indépendantes potentielles ont été identifiées et leurs contributions évaluées via l'utilisation de modèles linéaires multiples basés sur les distances (DISTLM), utilisant la procédure de sélection « Best » (Anderson et al. 2008) et le critère de sélection AIC (Akaike 1973). Les résultats ainsi obtenus ont ensuite été représentés dans un espace multidimensionnel par des analyses de redondance basées elles-aussi sur les distances (dbRDA ; Anderson et al. 2008). Ces différents traitements ont également été réalisés à l'aide du logiciel PRIMER® 6 (Clarke & Warwick 2001), équipé du supplément PERMANOVA+ (Anderson et al. 2008). Dans le cas où les facteurs de contrôle potentiels étaient utilisés en tant que variables indépendantes, j'ai tout d'abord calculé les coefficients de corrélation reliant les matrices de similarité des ensembles de variables dépendantes avec celles (i.e., les matrices de similarité) issues des débits ou de l'hydrodynamisme intégrés sur des durées allant de 1 à 365 jours (**Figure 0.9**). Cette procédure visait à identifier les durées d'intégrations les plus pertinentes. Elle a été réalisé à l'aide du logiciel R version 3.6.1 (R 2019) équipé des suppléments Vegan (Oksanen et al. 2019), BBmiscn (Bischl et al. 2017) et Hmisc (Harrell 2021).

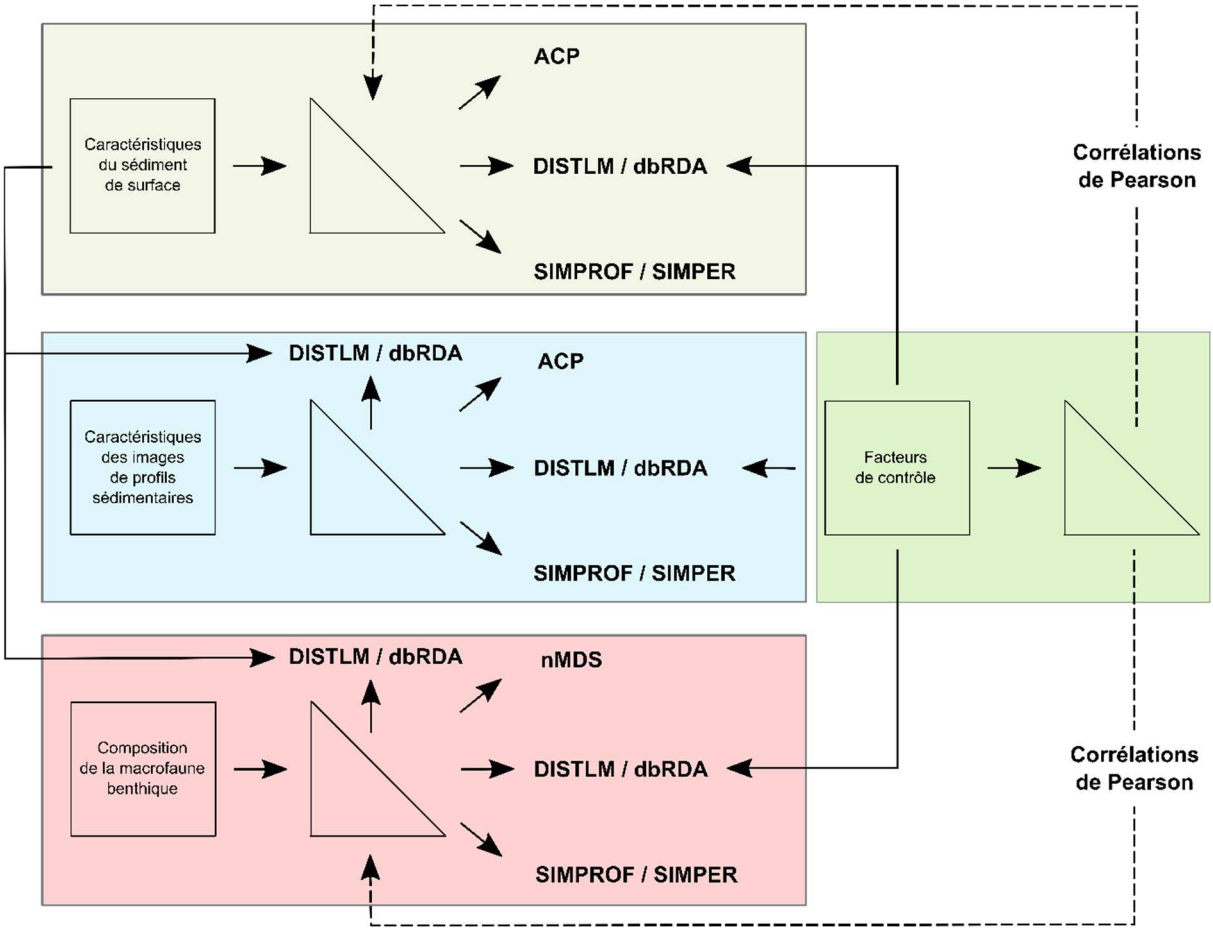

Figure 0.9. Schéma de synthèse des principales procédures d'analyses de données multivariées réalisées.

La comparaison avec le système Rhône s'est quant à elle basée sur une étude des variabilités temporelles : (1) des caractéristiques des sédiments de surface, (2) de la composition de la macrofaune benthique, et (3) des caractéristiques des images de profils sédimentaires. Pour chacun de ces jeux de données multivariés, les variabilités ont été évaluées, à chaque station, via le calcul de la moyenne des distances des différentes dates d'échantillonnage au centroïde du groupe de station*dates. Les patrons spatiaux de ces variabilités ont ensuite été comparés pour la VOG et le prodelta du Rhône.

5. Principaux objectifs et organisation de la thèse

Ce travail de thèse comporte trois objectifs majeurs, à savoir :

1) Décrire et comprendre la structuration de l'écosystème benthique de la Vasière Ouest-Gironde, à travers l'étude des variations spatio-temporelles des caractéristiques des sédiments de surface et de la matière organique particulaire associée, de la composition de la macrofaune benthique et de ses traces d'activité ; ces paramètres ayant été largement négligés durant les précédentes études de cette zone.

2) Identifier les facteurs de contrôle impliqués dans cette structuration, via la mise en relation des variables étudiées entre elles et l'utilisation de forçages naturels (i.e., régime hydrologique de l'estuaire de la Gironde et hydrodynamisme local) ou anthropiques (i.e., chalutage de fond) pour décrire les variations spatio-temporelles observées.

3) Evaluer la transposabilité de la typologie des RiOMar établie par Blair & Aller (2012) pour les zones tempérées, à partir d'une comparaison des systèmes VOG et prodelta du Rhône.

Dans ce contexte, la présentation des résultats obtenus s'organise en trois chapitres présentés sous la forme d'autant de manuscrits scientifiques qui précèdent une synthèse générale.

Chapitre 1 : Structuration spatiale de la matière organique particulaire et de l'activité de la macrofaune benthique dans la Vasière Ouest-Gironde

Ce chapitre porte sur les résultats d'une étude spatiale synoptique réalisée en juin 2018 durant laquelle un grand nombre de stations a été échantillonné dans et autour de la VOG, afin d'une part de mieux cartographier celle-ci et d'autre part de préciser l'existence de patrons spatiaux de la MOP sédimentée et des traces d'activité biologique de la macrofaune benthique. Cette étude a permis une première analyse des facteurs susceptibles de contrôler les structurations spatiales observées, par la considération d'un facteur naturel (i.e.,

l'hydrodynamisme) et d'un facteur anthropique (i.e., le chalutage de fond). Ce premier chapitre fait l'objet d'un article scientifique publié en 2021 dans la revue *Journal of Marine Science and Engineering*.

Article n°1 : B. Lamarque, B. Deflandre, A. Galindo Dalto, S. Schmidt, A. Romero-Ramirez, F. Garabetian, N. Dubosq, M. Diaz, F. Grasso, A. Sottolichio, G. Bernard, H. Gillet, M.A. Cordier, D. Poirier, P. Lebleu, H. Derriennic, M. Danilo, M. Murilo Barboza Tenório, A. Grémare (2021) **Spatial Distributions of Surface Sedimentary Organics and Sediment Profile Image Characteristics in a High-Energy Temperate Marine RiOMar: The West Gironde Mud Patch** ; Journal of Marine Science and Engineering, 9:242, doi: 10.3390/jmse9030242

Chapitre 2 : Structuration spatio-temporelle de la matière organique particulaire et de la composition de la macrofaune benthique dans la Vasière Ouest-Gironde

Ce chapitre porte sur la description et le déterminisme des variations spatio-temporelles des principales caractéristiques des sédiments de surface et de la composition de la macrofaune benthique. Il repose pour cela sur l'échantillonnage de 5 stations localisées le long d'un gradient côte-large. Ces stations ont été échantillonnées lors de 4 campagnes conduites entre 2016 et 2018 dans des conditions contrastées de débits de l'estuaire de la Gironde et d'hydrodynamisme du milieu récepteur. Cette étude a permis de préciser l'existence d'un fort gradient côte-large dans la composition de la macrofaune benthique et de confirmer l'importance de l'hydrodynamisme dans le contrôle de la structuration spatiale de la VOG. Parmi les cinq stations échantillonnées, trois d'entre elles avaient fait l'objet d'une caractérisation de la composition de la macrofaune benthique en 2010 par Massé et al. (2016). La comparaison avec ces données de référence a permis de mettre en évidence l'existence de changements temporels majeurs à « long-terme » et de suggérer qu'ils pourraient résulter du caractère particulièrement énergétique de l'hiver 2013-2014. Ce chapitre est présenté sous la forme d'un manuscrit scientifique qui sera prochainement soumis pour publication à la revue *Marine Ecology Progress Series*.

Article n°2 : B. Lamarque, B. Deflandre, S. Schmidt, G. Bernard, N. Dubosq, M. Diaz, N. Lavesque, F. Garabetian, F. Grasso, A. Sottolichio, S. Rigaud, A. Romero-Ramirez, M.A. Cordier, D. Poirier, M. Danilo, A. Grémare (à soumettre) **Spatio-temporal dynamics of surface sediments characteristics and benthic macrofauna composition in a temperate high-energy River-dominated Ocean Margin**

Chapitre 3 : Structuration spatio-temporelle de l'activité de la macrofaune benthique dans la Vasière Ouest-Gironde

Ce chapitre se situe dans la continuité directe du précédent. Il porte sur l'étude des variations spatio-temporelle des traces d'activité de la macrofaune benthique. L'étude repose sur les mêmes campagnes à la mer et présente un plan d'échantillonnage similaire à celui utilisé précédemment pour la matière organique et la macrofaune benthique. Contrairement à ceux obtenus pour la composition de la macrofaune, les résultats montrent l'absence de variations à « long-terme » pour ces caractéristiques. Ils confirment également le rôle des facteurs de contrôle potentiels identifiés lors des deux précédents chapitres. Enfin, les résultats obtenus ont permis une analyse de la capacité de l'imagerie de profils sédimentaires à être utilisée en tant que substitut à l'analyse, plus traditionnelle, de la composition de la macrofaune benthique. Il en ressort que ces approches sont beaucoup plus complémentaires que redondantes, chaque site d'étude semblant de fait constituer un cas particulier. Ce chapitre est présenté sous la forme d'un manuscrit scientifique qui sera prochainement soumis pour publication.

Article n°3 : B. Lamarque, B. Deflandre, A. Romero-Ramirez, G. Bernard, S. Schmidt, M. Diaz, N. Lavesque, F. Garabetian, F. Grasso, A. Sottolichio, N. Dubosq, S. Rigaud, M.A. Cordier, D. Poirier, M. Danilo, A. Grémare (à soumettre) **Spatio-temporal dynamics of Sediment Profile Images characteristics in a temperate high-energy River-dominated Ocean Margin**

Chapitre 4 : Synthèse et perspectives

Ce dernier chapitre constitue une synthèse générale des résultats obtenus lors de l'ensemble de ce travail de recherche. Il liste les principales conclusions relatives aux questions initialement posées et établit une liste de perspectives à partir de l'analyse des faiblesses et des extensions possibles des travaux réalisés.

Les différentes publications, relatives directement ou indirectement à la Vasière Ouest-Gironde, qui ne font pas partie intégrante de ce travail mais auxquelles j'ai été associé sont enfin présentées en Annexe.

Références

Akaike H (1973) Information theory as an extension of the maximum likelihood principle. In: *Proceedings, 2nd International Symposium on Information Theory*, Akadémiai. Csaki F, Petrov BN (eds) Budapest, p 267–281

Akoumianaki I, Papaspyrou S, Kormas KA, Nicolaidou A (2013) Environmental variation and macrofauna response in a coastal area influenced by land runoff. Estuar Coast Shelf Sci 132:34–44.

Allen GP (1973) Etude des processus sédimentaires dans l'estuaire de la Gironde. Institut de géologie du bassin d'Aquitaine.

Allen GP, Castaing P (1977) Carte de répartition des sédiments superficiels sur le plateau continental du Golfe de Gascogne. Bull l'Institut Géologie du Bassin d'Aquitaine:255–260.

Allen GP, Castaing P (1973) Suspended sediment transport from the Gironde estuary (France) onto the adjacent continental shelf. Mar Geol 14:47–53.

Aller JY, Aller RC (1986) General characteristics of benthic faunas on the Amazon inner continental shelf with comparison to the shelf off the Changjiang River, East China Sea. Cont Shelf Res 6:291–310.

Aller JY, Stupakoff I (1996) The distribution and seasonal characteristics of benthic communities on the Amazon shelf as indicators of physical processes. Cont Shelf Res 16:717–751.

Aller RC (1994) Bioturbation and remineralization of sedimentary organic matter: effects of redox oscillation. Chem Geol 114:331–345.

Aller RC (1998) Mobile deltaic and continental shelf muds as suboxic, fluidized bed reactors.

Mar Chem 61:143–155.

Aller RC, Cochran JK (2019) The critical role of bioturbation for particle dynamics, priming potential, and organic c remineralization in marine sediments: Local and basin scales. Front Earth Sci 7:157.

Alliot E, Younes WAN, Romano JC, Rebouillon P, Massé H (2003) Biogeochemical impact of a dilution plume (Rhone River) on coastal sediments: Comparison between a surface water survey (1996-2000) and sediment composition. Estuar Coast Shelf Sci 57:357–367.

Alongi DM, Christoffersen P, Tirendi F, Robertson AI (1992) The influence of freshwater and material export on sedimentary facies and benthic processes within the Fly Delta and adjacent Gulf of Papua (Papua New Guinea). Cont Shelf Res 12:287–326.

Anderson DW (1988) The effect of parent material and soil development on nutrient cycling in temperate ecosystems. Biogeochemistry 5:71–97.

Anderson M, Gorley RN, Clarke KR (2008) PERMANOVA + for PRIMER user manual.

Arbouille D (1987) La sédimentation de la plate-forme continentale Nord-Aquitaine au Quaternaire terminal : un exemple de système transgressif. Université de Bordeaux 1

Bajjouk T, Guillaumont B, Michez N, Thouin B, Croguennec C, Populus J, Louvel-Glaser J, Gaudillat V, Chevalier C, Tourolle J, Hamon D (2015) Classification EUNIS, Système d'information européen sur la nature : Traduction française des habitats benthiques des Régions Atlantique et Méditerranée. Vol. 2. Habitats subtidaux & complexes d'habitats.

Bengtsson J (2002) Disturbance and resilience in soil animal communities. Eur J Soil Biol 38:119–125.

Berthois L, Le Calvez Y (1959) Deuxieme contribution a l'etude de la sedimentation dans le Golfe de Gascogne. Rev Trav Pech marit 23:323–377.

Bianchi TS, Dawson R, Sawangwong P (1988) The effects of macrobenthic deposit-feeding on the degradation of chloropigments in sandy sediments. J Exp Mar Bio Ecol 122:243–255.

Bianchi TS, Findlay S, Fontvieille D (1991) Experimental degradation of plant materials in Hudson river sediments - I. Heterotrophic transformations of plant pigments. Biogeochemistry 12:171–187.

Bigham K, Rowden A, Leduc D, Bowden D (2021) Review and syntheses: Turbidity flows – evidence for effects on deep-sea benthic community productivity is ambiguous but the influence on diversity is clearer. Biogeosciences 18:1893–1908.

Bischl B, Lang M, Bossek J, Horn D, Richter J, Surmann D (2017) BBmisc: Miscellaneous Helper Functions for B. Bischl. R Packag version 1-1-1.

Blair NE, Aller RC (2012) The Fate of Terrestrial Organic Carbon in the Marine Environment. Ann Rev Mar Sci 4:401–423.

Bonifácio P, Bourgeois S, Labrune C, Amouroux JM, Escoubeyrou K, Buscail R, Romero-Ramirez

A, Lantoine F, Vétion G, Bichon S, Desmalades M, Rivière B, Deflandre B, Grémare A (2014) Spatiotemporal changes in surface sediment characteristics and benthic macrofauna composition off the Rhône River in relation to its hydrological regime. Estuar Coast Shelf Sci 151:196–209.

Borges A V. (2005) Do We Have Enough Pieces of the Jigsaw to Integrate CO2 Fluxes in the Coastal Ocean ? Estuaries 28:3–27.

Borges A V., Delille B, Frankignoulle M (2005) Budgeting sinks and sources of CO2 in the coastal ocean: Diversity of ecosystem counts. Geophys Res Lett 32.

Bourgeois S, Pruski AM, Sun MY, Buscail R, Lantoine F, Kerhervé P, Vétion G, Rivière B, Charles F (2011) Distribution and lability of land-derived organic matter in the surface sediments of the Rhône prodelta and the adjacent shelf (Mediterranean Sea, France): A multi proxy study. Biogeosciences 8:3107–3125.

Bowler DE, Bjorkman AD, Dornelas M, Myers-Smith IH, Navarro LM, Niamir A, Supp SR, Waldock C, Vellend M, Blowes SA, Böhning-Gaese K, Bruelheide H, Elahi R, Antão LH, Hines J, Isbell F, Jones HP, Magurran AE, Cabral JS, Winter M, Bates AE (2019) Mapping human pressures across the planet uncovers anthropogenic threat complexes. bioRxiv.

Brown EJ, Finney B, Dommisse M, Hills S (2005) Effects of commercial otter trawling on the physical environment of the southeastern Bering Sea. Cont Shelf Res 25:1281–1301.

Burdige DJ (2005) Burial of terrestrial organic matter in marine sediments: A re-assessment. Global Biogeochem Cycles 19:1–7.

Burke L, Kura Y, Kassem K, Revenga C, Spalding M, McAllister D (2001) Coastal Ecosystems. World Resources Institute, Washington, DC.

Cai WJ (2011) Estuarine and coastal ocean carbon paradox: CO2 sinks or sites of terrestrial carbon incineration? Ann Rev Mar Sci 3:123–145.

Cai WJ, Dai M, Wang Y (2006) Air-sea exchange of carbon dioxide in ocean margins: A province-based synthesis. Geophys Res Lett 33.

Canfield DE (1994) Factors influencing organic carbon preservation in marine sediments. Chem Geol 114:315–329.

Carbonel P, Moyes J, Peypouquet JP (1972) Contribution de l'étude des Ostracodes à un essai de reconstitution paléogéographique d'une lagune holocène dans la zone Ouest-Gironde (Golfe de Gascogne). Comptes Rendus l'Academie des Sci Paris 274:3500–3503.

Carbonel P, Moyes J, Peypouquet JP (1975) Utilisation des Ostracodes pour la mise en evidence et l'évolution d'une lagune holocene à l'Ouest de la Gironde, Golfe de Biscay. Bull Am Paleontol 65:445–462.

Castaing P (1981) Le transfert à l'océan des suspensions estuariennes: cas de la Gironde. Université de Bordeaux 1

Castaing P, Allen G, Houdart M, Moign Y (1979) Étude par télédétection de la dispersion en

mer des eaux estuariennes issues de la Gironde et du Pertuis de Maumusson. Oceanol Acta 2:459–468.

Castaing P, Allen GP (1981) Mechanisms controlling seaward escape of suspended sediment from the Gironde: A macrotidal estuary in France. Mar Geol 40:101–118.

Castaing P, Feral A, Klingebiel A (1971) Paléographie de l'Holocène sur le plateau continental au large de l'embouchure de la Gironde. Comptes Rendus - Sommaires des séances la Société Géologique Fr 6:325–326.

Castaing P, Froidefond JM, Lazure P, Weber O, Prud'Homme R, Jouanneau JM (1999) Relationship between hydrology and seasonal distribution of suspended sediments on the continental shelf of the Bay of Biscay. Deep Res Part II 46:1979–2001.

Castaing P, Philipps I, Weber O (1982) Répartition et dispersion des suspensions dans les eaux du plateau continental aquitain. Oceanol Acta 5:85–96.

Cathalot C, Rabouille C, Pastor L, Deflandre B, Viollier E, Buscail R, Grémare A, Treignier C, Pruski A (2010) Temporal variability of carbon recycling in coastal sediments influenced by rivers: Assessing the impact of flood inputs in the Rhône River prodelta. Biogeosciences 7:1187–1205.

Cathalot C, Rabouille C, Tisnérat-Laborde N, Toussaint F, Kerhervé P, Buscail R, Loftis K, Sun MY, Tronczynski J, Azoury S, Lansard B, Treignier C, Pastor L, Tesi T (2013) The fate of river organic carbon in coastal areas: A study in the Rhône River delta using multiple isotopic (δ13C, δ14C) and organic tracers. Geochim Cosmochim Acta 118:33–55.

Chavanich S, Viyakarn V, Sojisuporn P, Siripong A, Menasveta P (2008) Patterns of coral damage associated with the 2004 Indian Ocean tsunami at Mu Ko Similan Marine National Park, Thailand. J Nat Hist 42:177–187.

Clarke KR (1993) Non-parametric multivariate analyses of changes in community structure. Aust J Ecol 18:117–143.

Clarke KR, Somerfield PJ, Gorley RN (2008) Testing of null hypotheses in exploratory community analyses: similarity profiles and biota-environment linkage. J Exp Mar Bio Ecol 366:56–69.

Clarke KR, Warwick RM (2001) Change in Marine Communities: An Approach to Statistical Analysis and Interpretation, 2nd edition. PRIMER-E, Plymouth.

Collie JS, Hall SJ, Kaiser MJ, Poiner IR (2000) A quantitative analysis of fishing impacts on shelf-sea benthos. J Anim Ecol 69:785–798.

Constantin S, Doxaran D, Derkacheva A, Novoa S, Lavigne H (2018) Multi-temporal dynamics of suspended particulate matter in a macro-tidal river Plume (the Gironde) as observed by satellite data. Estuar Coast Shelf Sci 202:172–184.

Costanza R (1999) The ecological, economic, and social importance of the oceans. Ecol Econ 31:199–213.

Costanza R, D'Arge R, de Groot R, Farber S, Grasso M, Hannon B, Limburg K, Naeem S, O'Neill R V., Paruelo J, Raskin RG, Sutton P, van den Belt M (1997) The value of the world's ecosystem services and natural capital. Nature 387:253–260.

Crain CM, Kroeker K, Halpern BS (2008) Interactive and cumulative effects of multiple human stressors in marine systems. Ecol Lett 11:1304–1315.

Darnaude AM, Salen-Picard C, Harmelin-Vivien ML (2004) Depth variation in terrestrial particulate organic matter exploitation by marine coastal benthic communities off the Rhone River delta (NW Mediterranean). Mar Ecol Prog Ser 275:47–57.

Dayton PK, Thrush SF, Agardy MT, Hofman RJ (1995) Environmental effects of marine fishing. Aquat Conserv Mar Freshw Ecosyst 5:205–232.

Desmit X, Thieu V, Billen G, Campuzano F, Dulière V, Garnier J, Lassaletta L, Ménesguen A, Neves R, Pinto L, Silvestre M, Sobrinho JL, Lacroix G (2018) Reducing marine eutrophication may require a paradigmatic change. Sci Total Environ 635:1444–1466.

Diaz M, Grasso F, Le Hir P, Sottolichio A, Caillaud M, Thouvenin B (2020) Modeling Mud and Sand Transfers Between a Macrotidal Estuary and the Continental Shelf: Influence of the Sediment Transport Parameterization. J Geophys Res Ocean 125.

Diaz RJ, Rosenberg R (2008) Spreading dead zones and consequences for marine ecosystems. Science (80-) 321:926–929.

Doxaran D, Froidefond JM, Castaing P, Babin M (2009) Dynamics of the turbidity maximum zone in a macrotidal estuary (the Gironde, France): Observations from field and MODIS satellite data. Estuar Coast Shelf Sci 81:321–332.

Dubosq N, Schmidt S, Walsh JP, Grémare A, Gillet H, Lebleu P, Poirier D, Perello MC, Lamarque B, Deflandre B (2021) A first assessment of organic carbon burial in the West Gironde Mud Patch (Bay of Biscay). Cont Shelf Res 221.

Duxbury J, Dickinson S (2007) Principles for sustainable governance of the coastal zone: In the context of coastal disasters. Ecol Econ 63:319–330.

Etcheber H, Relexans JC (1983) Nature et répartition de la matière organique particulaire sur le plateau continental au large de l'estuaire de la Gironde. Ann l'Institut Oceanogr Paris 5:5–19.

Feral A (1970) Interprétation sédimentologique et paléogéographique des formations alluviales de l'estuaire de la Gironde et de ses dépendances marines. Université de Bordeaux

Ferré B, Durrieu de Madron X, Estournel C, Ulses C, Le Corre G (2008) Impact of natural (waves and currents) and anthropogenic (trawl) resuspension on the export of particulate matter to the open ocean. Application to the Gulf of Lion (NW Mediterranean). Cont Shelf Res 28:2071–2091.

Fontugne MR, Jouanneau JM (1987) Modulation of the particulate organic carbon flux to the

ocean by a macrotidal estuary: Evidence from measurements of carbon isotopes in organic matter from the Gironde system. Estuar Coast Shelf Sci 24:377–387.

Fowler SW, Knauer GA (1986) Role of large particles in the transport of elements and organic compounds through the oceanic water column. Prog Oceanogr 16:147–194.

Froidefond J-M, Jegou A-M, Hermida J, Lazure P, Castaing P (1998) Variabilé du panache turbide de la Gironde par télédéction. Effets des facteurs climatiques. Oceanol Acta 21:191–207.

Gadel F, Jouanneau JM, Weber O, Serve L, Comellas L (1997) Traceurs organiques dans les dépôts de la vasière Ouest-Gironde (Golfe de Gascogne). Oceanol Acta 20:687–695.

Gattuso JP, Frankignoulle M, Wollast R (1998) Carbon and carbonate metabolism in coastal aquatic ecosystems. Annu Rev Ecol Syst 29:405–434.

Gearing JN (1988) The Use of Stable Isotope Ratios for Tracing the Nearshore-Offshore Exchange of Organic Matter. In: *Coastal-Offshore Ecosystem Interactions, Volume 22*. Jansson B-O (ed) American Geophysical Union

Gearing P, Plucker FE, Parker PL (1977) Organic carbon stable isotope ratios of continental margin sediments. Mar Chem 5:251–266.

Germano JD (1995) SEDIMENT PROFILE IMAGING: A Rapid Seafloor Impact Assessment Tool for Oil Spills. Ministry of supply and services, Canada.

Germano JD, Rhoads DC, Valente RM, Carey DA, Solan M (2011) The use of sediment profile imaging (SPI) for environmental impact assessments and monitoring studies: Lessons learned from the past four decades. Oceanogr Mar Biol An Annu Rev 49:235–297.

Ghita O, Whelan PF, Kennedy R (2004) The application of image processing algorithms to the analysis of SPI images. In: *Sediment Profile Imagery Colloquium of Experts (SPICE)*. Galway

Gillet H, Deflandre B (2018) JERICOBENT-5-TH cruise, RV Thalia.

Glover AG, Gooday AJ, Bailey DM, Billett DSM, Chevaldonné P, Colaço A, Copley J, Cuvelier D, Desbruyères D, Kalogeropoulou V, Klages M, Lampadariou N, Lejeusne C, Mestre NC, Paterson GLJ, Perez T, Ruhl H, Sarrazin J, Soltwedel T, Soto EH, Thatje S, Tselepides A, Van Gaever S, Vanreusel A (2010) Temporal Change in Deep-Sea Benthic Ecosystems. A Review of the Evidence From Recent Time-Series Studies. Adv Mar Biol 58:1–95.

Graham MC, Eaves MA, Farmer JG, Dobson J, Fallick AE (2001) A study of carbon and nitrogen stable isotope and elemental ratios as potential indicators of source and fate of organic matter in sediments of the Forth Estuary, Scotland. Estuar Coast Shelf Sci 52:375–380.

Gray JS, Dayton P, Thrush S, Kaiser MJ (2006) On effects of trawling, benthos and sampling design. Mar Pollut Bull 52:840–843.

Grizzle RE, Penniman CA (1991) Effects of organic enrichment on estuarine macrofaunal benthos: a comparison of sediment profile imaging and traditional methods. Mar Ecol Prog Ser 74:249–262.

Halpern BS, Walbridge S, Selkoe KA, Kappel C V., Micheli F, D'Agrosa C, Bruno JF, Casey KS, Ebert C, Fox HE, Fujita R, Heinemann D, Lenihan HS, Madin EMP, Perry MT, Selig ER, Spalding M, Steneck R, Watson R (2008) A Global Map of Human Impact on Marine Ecosystems. Science (80-) 319:948–952.

Hanebuth TJJ, Lantzsch H, Nizou J (2015) Mud depocenters on continental shelves—appearance, initiation times, and growth dynamics. Geo-Marine Lett 35:487–503.

Harmelin-Vivien ML, Bănaru D, Dierking J, Hermand R, Letourneur Y, Salen-Picard C (2009) Linking benthic biodiversity to the functioning of coastal ecosystems subjected to river runoff (NW Mediterranean). Anim Biodivers Conserv 32:135–145.

Harrell FE (2021) Hmisc: Harrell Miscellaneous. R Packag version 4-5-0.

Harris PT (2012) On Seabed Disturbance, Marine Ecological Succession and Applications for Environmental Management: A Physical Sedimentological Perspective. Spec Publ Int Assoc Sedimentol 44:387–404.

Harris PT (2014) Shelf and deep-sea sedimentary environments and physical benthic disturbance regimes: A review and synthesis. Mar Geol 353:169–184.

Hedges JI, Keil RG (1995) Sedimentary organic matter preservation: an assessment and speculative synthesis. Mar Chem 49:81–115.

Hermand R, Salen-Picard C, Alliot E, Degiovanni C (2008) Macrofaunal density, biomass and composition of estuarine sediments and their relationship to the river plume of the Rhone River (NW Mediterranean). Estuar Coast Shelf Sci 79:367–376.

Holling CS, Schindler DW, Walker BW, Roughgarden J (1995) Biodiversity in the functioning of ecosystems: an ecological synthesis. In: *Biodiversity Loss. Economic and Ecological Issues*. Perrings C, Maler K-G, Folke C, Holling CS, Jansson B-O (eds) Cambridge University Press, Cambridge, UK, p 44–83

Jahnke RA (2010) Global Synthesis. In: *Carbon and Nutrient Fluxes in Continental Margins. Global Change - The IGBP Series*. Liu K-K, Atkinson L, Quiñones RA, Talaue-McManus L (eds) Springer Berlin Heidelberg, p 597–615

Jalón-Rojas I, Sottolichio A, Hanquiez V, Fort A, Schmidt S (2018) To what extent multidecadal changes in morphology and fluvial discharge impact tide in a convergent (turbid) tidal river. J Geophys Res Ocean 123:3241–3258.

Jaramillo E, Dugan JE, Hubbard DM, Melnick D, Manzano M, Duarte C, Campos C, Sanchez R (2012) Ecological implications of extreme events: Footprints of the 2010 earthquake along the Chilean coast. PLoS One 7.

Jouanneau JM (1983) Matières en suspension et oligo-éléments métalliques dans le système estuarien girondin: comportement et flux. Université de Bordeaux

Jouanneau JM, Berger P, Boutier B, Ewald M, Fontugne M, Heral M (1983) Extension des apports solides et liquides d'origine estuarienne dans les eaux de surface du plateau

Aquitain interne. Rev des Trav l'Institut des Pêches Marit 47:5–24.

Jouanneau JM, Weber O, Latouche C, Vernet JP, Dominik J (1989) Erosion, non-deposition and sedimentary processes through a sedimentological and radioisotopic study of surficial deposits from the 'Ouest-Gironde vasière' (Bay of Biscay). Cont Shelf Res 9:325–342.

Kaiser MJ, Clarke KR, Hinz H, Austen MCV, Somerfield PJ, Karakassis I (2006) Global analysis of response and recovery of benthic biota to fishing. Mar Ecol Prog Ser 311:1–14.

Kaiser MJ, Collie JS, Hall SJ, Jennings S, Poiner IR (2002) Modification of marine habitats by trawling activities: Prognosis and solutions. Fish Fish.

Karakassis I, Tsapakis M, Smith CJ, Rumohr H (2002) Fish farming impacts in the Mediterranean studied through sediment profiling imagery. Mar Ecol Prog Ser 227:125–133.

Kathiresan K, Rajendran N (2005) Coastal mangrove forests mitigated tsunami. Estuar Coast Shelf Sci 65:601–606.

Kenchington R (1993) Tourism in coastal and marine environments-a recreational perspective. Ocean Coast Manag 19:1–16.

Kennett J (1982) Marine geology, Prentice-H. Englewood Cliffs, New Jersey, USA.

Kristensen E, Penha-Lopes G, Delefosse M, Valdemarsen T, Quintana CO, Banta GT (2012) What is bioturbation? the need for a precise definition for fauna in aquatic sciences. Mar Ecol Prog Ser 446:285–302.

Kroodsma DA, Mayorga J, Hochberg T, Miller NA, Boerder K, Ferretti F, Wilson A, Bergman B, White TD, Block BA, Woods P, Sullivan B, Costello C, Worm B (2018) Tracking the global footprint of fisheries. Science (80-) 359:904–908.

Labrune C, Romero-Ramirez A, Amouroux JM, Duchêne JC, Desmalades M, Escoubeyrou K, Buscail R, Grémare A (2012) Comparison of ecological quality indices based on benthic macrofauna and sediment profile images: A case study along an organic enrichment gradient off the Rhône River. Ecol Indic 12:133–142.

Lansard B, Rabouille C, Denis L, Grenz C (2009) Benthic remineralization at the land-ocean interface: A case study of the Rhône River (NW Mediterranean Sea). Estuar Coast Shelf Sci 81:544–554.

Lapierre F (1967) Etude de la répartition des sédiments dans le Golfe de Gascogne. Bull l'Institut Géologie du Bassin d'Aquitaine 3:93–126.

Large Marine Ecosystems (no date)https://www.lmehub.net (accessed 18 September 2021)

Laruelle GG, Dürr HH, Slomp CP, Borges A V. (2010) Evaluation of sinks and sources of CO2 in the global coastal ocean using a spatially-explicit typology of estuaries and continental shelves. Geophys Res Lett 37.

Latouche C (1971) Les argiles des bassins alluvionnaires aquitains et des dépendances océaniques: contribution à l'étude d'un environnement. Inst géologie du bassin

d'Aquitaine.

Latouche C, Jouanneau JM, Lapaquellerie Y, Maillet N, Weber O (1991) Répartition des minéraux argileux sur le plateau continental Sud-Gascogne. Oceanol Acta Special is.

Lazure P, Dumas F (2008) An external-internal mode coupling for a 3D hydrodynamical model for applications at regional scale (MARS). Adv Water Resour 31:233–250.

Lesueur P (1992) Les vasières de la plate-forme Ouest Gironde (France) : modèle faciologique et archive sédimentaire des flux côtiers.

Lesueur P, Jouanneau JM, Boust D, Tastet JP, Weber O (2001) Sedimentation rates and fluxes in the continental shelf mud fields in the Bay of Biscay (France). Cont Shelf Res 21:1383–1401.

Lesueur P, Tastet J., Weber O, Sinko J. (1991) Modèle faciologique d'un corps sédimentaire pélitique de plate-forme la vasière Ouest-Gironde (France). Oceanol Acta 11:143–153.

Lesueur P, Tastet JP (1994) Facies, internal structures and sequences of modern Gironde-derived muds on the Aquitaine inner shelf, France. Mar Geol 120:267–290.

Lesueur P, Tastet JP, Marambat L (1996) Shelf mud fields formation within historical times: Examples from offshore the Gironde estuary, France. Cont Shelf Res 16:1849–1870.

Lesueur P, Tastet JP, Weber O (2002) Origin and morphosedimentary evolution of fine-grained modern continental shelf deposits: The Gironde mud fields (Bay of Biscay, France). Sedimentology 49:1299–1320.

Lesueur P, Weber O, Marambat L, Tastet J, Jouanneau J, Turon J (1989) Datation d'une vasière de plateforme atlantique au débouché d'un estuaire: la vasière à l'ouest de la Gironde (France) est d'âge historique (VIème siècle à nos jours). Comptes rendus l'Académie des Sci Série 2, Mécanique, Phys Chim Sci l'univers, Sci la Terre 308:935–940.

Liénart C, Savoye N, Bozec Y, Breton E, Conan P, David V, Feunteun E, Grangeré K, Kerhervé P, Lebreton B, Lefebvre S, L'Helguen S, Mousseau L, Raimbault P, Richard P, Riera P, Sauriau PG, Schaal G, Aubert F, Aubin S, Bichon S, Boinet C, Bourasseau L, Bréret M, Caparros J, Cariou T, Charlier K, Claquin P, Cornille V, Corre AM, Costes L, Crispi O, Crouvoisier M, Czamanski M, Del Amo Y, Derriennic H, Dindinaud F, Durozier M, Hanquiez V, Nowaczyk A, Devesa J, Ferreira S, Fornier M, Garcia F, Garcia N, Geslin S, Grossteffan E, Gueux A, Guillaudeau J, Guillou G, Joly O, Lachaussée N, Lafont M, Lamoureux J, Lecuyer E, Lehodey JP, Lemeille D, Leroux C, Macé E, Maria E, Pineau P, Petit F, Pujo-Pay M, Rimelin-Maury P, Sultan E (2017) Dynamics of particulate organic matter composition in coastal systems: A spatio-temporal study at multi-systems scale. Prog Oceanogr 156:221–239.

Liu K-K, Atkinson L, Quiñones RA, Talaue-McManus L (2010) Biogeochemistry of Continental Margins in a Global Context. In: *Carbon and Nutrient Fluxes in Continental Margins. Global Change - The IGBP Series*. Liu K-K, Atkinson L, Quiñones RA, Talaue-McManus L (eds) Springer Berlin Heidelberg, p 3–24

Longère P, Dorel D (1970) Etude des sédiments meubles de la vasière de la Gironde et des

régions avoisinantes. Rev des Trav l'Institut des Pêches Marit 34:233–256.

Lopez GR, Levinton JS (1987) Ecology of Deposit-Feeding Animals in Marine Sediments. Q Rev Biol 62:235–260.

Martínez ML, Intralawan A, Vázquez G, Pérez-Maqueo O, Sutton P, Landgrave R (2007) The coasts of our world: Ecological, economic and social importance. Ecol Econ 63:254–272.

Massé C, Meisterhans G, Deflandre B, Bachelet G, Bourasseau L, Bichon S, Ciutat A, Jude-Lemeilleur F, Lavesque N, Raymond N, Grémare A, Garabetian F (2016) Bacterial and macrofaunal communities in the sediments of the West Gironde Mud Patch, Bay of Biscay (France). Estuar Coast Shelf Sci 179:189–200.

Mayer LM (1994) Surface area control of organic carbon accumulation in continental shelf sediments. Geochim Cosmochim Acta 58:1271–1284.

Mayer LM, Linda L. S, Sawyer T, Plante CJ, Jumars PA, Sel RL (1995) Bioavailable amino acids in sediments: A biomimetic, kinetics based approach. Limnol Oceanogr 40:511–520.

McKee BA, Aller RC, Allison MA, Bianchi TS, Kineke GC (2004) Transport and transformation of dissolved and particulate materials on continental margins influenced by major rivers: Benthic boundary layer and seabed processes. Cont Shelf Res 24:899–926.

Meade RH (1996) Chapter 3: River-Sediment Inputs to Major Deltas. In: Sea level-rise and Coastal subsidence. US Gov.

Medernach L, Grémare A, Amoureux JM, Colomines JC, Vétion G (2001) Temporal changes in the amino acid contents of particulate organic matter sedimenting in the Bay of Banyuls-sur-Mer (northwestern Mediterranean). Mar Ecol Prog Ser 214:55–65.

Mengual B, Cayocca F, Le Hir P, Draye R, Laffargue P, Vincent B, Garlan T (2016) Influence of bottom trawling on sediment resuspension in the 'Grande-Vasière' area (Bay of Biscay, France). Ocean Dyn 66:1181–1207.

Mengual B, Le Hir P, Cayocca F, Garlan T (2019) Bottom trawling contribution to the spatio-temporal variability of sediment fluxes on the continental shelf of the Bay of Biscay (France). Mar Geol 414:77–91.

Michener WK, Blood ER, Bildstein KL, Brinson MM, Gardner LR (1997) Climate change, hurricanes and tropical storms, and rising sea level in coastal wetlands. Ecol Appl 7:770–801.

de Moura Queirós A, Hiddink JG, Johnson G, Cabral HN, Kaiser MJ (2011) Context dependence of marine ecosystem engineer invasion impacts on benthic ecosystem functioning. Biol Invasions 13:1059–1075.

Moyes J (1974) Un exemple d'étude paleoécologique et paléogéographique: La Vasière Ouest Gironde et son évolution durant l'Holocène. Bull l'Institut Géologie du Bassin d'Aquitaine 16:3–30.

Muller-Karger FE, Varela R, Thunell R, Luerssen R, Hu C, Walsh JJ (2005) The importance of

continental margins in the global carbon cycle. Geophys Res Lett 32:1–4.

Nakaoka M, Tanaka Y, Mukai H, Suzuki T, Aryuthaka C (2007) Tsunami Impacts on Biodiversity of Seagrass Communities in the Andaman Sea , Thailand : (1) Seagrass Abundance and Diversity Seagrass beds are a major component in coastal ecosystems , supporting high productivity and biodiversity (Duarte and Chiscano. Publ Seto Mar Biol Lab Spec Publ Ser 8:49–56.

Nilsson HC, Rosenberg R (2003) Effects on marine sedimentary habitats of experimental trawling analysed by sediment profile imagery. J Exp Mar Bio Ecol 285–286:453–463.

Nilsson HC, Rosenberg R (2000) Succession in marine benthic habitats and fauna. Mar Ecol 197:139–149.

Nixon SW, Ammerman JW, Atkinson LP, Berounsky VM, Billen G, Boicourt WC, Boyton WR, Church TM, Ditoro DM, Elmgren R, Garber JH, Giblin AE, Jahnke RA, Owens NJP, Pilson MEQ, Seitzinger SP (1996) The fate of nitrogen and phosphorus at the land-sea margin of the North Atlantic Ocean. Biogeochemistry 35:141–180.

O'Connor BDS, Costelloe J, Keegan BF, Rhoads DC (1989) The use of REMOTS® technology in monitoring coastal enrichment resulting from mariculture. Mar Pollut Bull 20:384–390.

Oades JM (1988) The retention of organic matter in soils. Biogeochemistry 5:35–70.

Oksanen J, Blanchet FG, Friendly M, Kindt R, Legendre P, McGlinn D, Minchin PR, O'Hara RB, Simpson GL, Solymos P, Stevens MHH, Szoecs E, Wagner H (2019) Vegan: Community Ecology Package. R Packag version 2-5-6.

Palanques A, Puig P, Guillén J, Demestre M, Martín J (2014) Effects of bottom trawling on the Ebro continental shelf sedimentary system (NW Mediterranean). Cont Shelf Res 72:83–98.

Pastor L, Cathalot C, Deflandre B, Viollier E, Soetaert K, Meysman FJR, Ulses C, Metzger E, Rabouille C (2011a) Modeling biogeochemical processes in sediments from the Rhŏne River prodelta area (NW Mediterranean Sea). Biogeosciences 8:1351–1366.

Pastor L, Deflandre B, Viollier E, Cathalot C, Metzger E, Rabouille C, Escoubeyrou K, Lloret E, Pruski AM, Vétion G, Desmalades M, Buscail R, Grémare A (2011b) Influence of the organic matter composition on benthic oxygen demand in the Rhône River prodelta (NW Mediterranean Sea). Cont Shelf Res 31:1008–1019.

Pastor L, Rabouille C, Metzger E, Thibault de Chanvalon A, Viollier E, Deflandre B (2018) Transient early diagenetic processes in Rhône prodelta sediments revealed in contrasting flood events. Cont Shelf Res 166:65–76.

Pearson TH, Rosenberg R (1978) Macrobenthos succession in relation to organic enrichment and pollution of the marine environment. Oceanogr Mar Biol Annu Rev 16:229–331.

Pernetta JC, Milliman JD (1995) Land-Ocean Interactions in the Coastal Zone: implementation plan. Oceanogr Lit Rev 9:801.

Pickett STA, White PS (1985) The Ecology of Natural Disturbance and Patch Dynamics, Academic P. San Diego.

Premuzic ET, Benkovitz CM, Gaffney JS, Walsh JJ (1982) The nature and distribution of organic matter in the surface sediments of world oceans and seas. Org Geochem 4:63–77.

Pujos M (1976) Ecologie des Foraminiferes benthiques et des Thecamoebiens de la Gironde et du plateau continental Sud-Gascogne., Application a la connaissance du quaternaire terminal de la region Ouest-Gironde. Université de Bordeaux 1

Queirós AM, Hiddink JG, Kaiser MJ, Hinz H (2006) Effects of chronic bottom trawling disturbance on benthic biomass, production and size spectra in different habitats. J Exp Mar Bio Ecol 335:91–103.

R CT (2019) R: a Language and Environment for Statistical Computing.

Rabouille C, Mackenzie FT, Ver LM (2001) Influence of the human perturbation on carbon, nitrogen, and oxygen biogeochemical cycles in the global coastal ocean. Geochim Cosmochim Acta 65:3615–3641.

Relexans JC, Lin RG, Castel J, Etcheber H, Laborde P (1992) Response of biota to sedimentary organic matter quality of the west Gironde mud patch, Bay of Biscay (France). Oceanol Acta 15:639–649.

Rhoads DC, Boesch DF, Zhican T, Fengshan X, Liqiang H, Nilsen KJ (1985) Macrobenthos and sedimentary facies on the Changjiang delta platform and adjacent continental shelf, East China Sea. Cont Shelf Res 4:189–213.

Rhoads DC, Cande S (1971) Sediment Profile Camera in situ Study of Orgainsm-Sediment Relations. Limnol Oceanogr 16:110–114.

Rhoads DC, Young DK (1970) The influences of deposit feeding benthos on bottom stability and community trophic structure. J Mar Res 28:150–178.

Robert A (2007) Effets combinés des facteurs naturels et anthropiques sur les communautés d'invertébrés benthiques des vasières à langoustine (Nephrops norvegicus) du Golfe de Gascogne. Université Européenne de Bretagne

Roland A, Ardhuin F (2014) On the developments of spectral wave models: Numerics and parameterizations for the coastal ocean. Ocean Dyn 64:833–846.

Romero-Ramirez A, Grémare A, Desmalades M, Duchêne JC (2013) Semi-automatic analysis and interpretation of sediment profile images. Environ Model Softw 47:42–54.

Rosenberg R, Agrenius S, Hellman B, Nilsson HC, Norling K (2002) Recovery of marine benthic habitats and fauna in a Swedish fjord following improved oxygen conditions. Mar Ecol Prog Ser 234:43–53.

Rosenberg R, Magnusson M, Nilsson HC (2009) Temporal and spatial changes in marine benthic habitats in relation to the EU Water Framework Directive: The use of sediment profile imagery. Mar Pollut Bull 58:565–572.

Rosenberg R, Nilsson HC (2005) Deterioration of soft-bottom benthos along the Swedish Skagerrak coast. J Sea Res 54:231–242.

Rosenberg R, Nilsson HC, Diaz RJ (2001) Response of benthic fauna and changing sediment redox profiles over a hypoxic gradient. Estuar Coast Shelf Sci 53:343–350.

Rosenberg R, Nilsson HC, Grémare A, Amouroux JM (2003) Effects of demersal trawling on marine sedimentary habitats analysed by sediment profile imagery. J Exp Mar Bio Ecol 285–286:465–477.

Ruch P, Mirmand M, Jouanneau JM, Latouche C (1993) Sediment budget and transfer of suspended sediment from the Gironde estuary to Cap Ferret Canyon. Mar Geol 111:109–119.

Rumohr H, Schomann H (1992) REMOTS sediment profiles around an exploratory drilling rig in the southern North Sea. Mar Ecol Prog Ser 91:303–311.

Salen-Picard C, Arlhac D, Alliot E (2003) Responses of a Mediterranean soft bottom community to short-term (1993-1996) hydrological changes in the Rhone river. Mar Environ Res 55:409–427.

Salen-Picard C, Darnaude AM, Arlhac D, Harmelin-Vivien ML (2002) Fluctuations of macrobenthic populations: A link between climate-driven river run-off and sole fishery yields in the Gulf of Lions. Oecologia 133:380–388.

Sautour B, Baron J (2020) L'Estuaire de la Gironde: un écosystème altéré - Entre dynamique naturelle et pressions anthropiques. Presses Universitaires de Bordeaux.

Schmidt S, Deflandre B (2018) JERICOBENT-5 cruise, RV Côtes De La Manche.

Schmidt S, Etcheber H, Sottolichio A, Castaing P (2016) Le reseau MAGEST: bilan de 10 ans de suivi haute-frequence de la qualite des eaux de l'estuaire de la Gironde. In: *Mesures haute résolution dans l'environnement marin côtier*. Schmitt F, Lefevre A (eds) Presses du CNRS

Sciberras M, Geert J, Simon H, Szostek CL, Hughes KM, Kneafsey B, Clarke LJ, Ellis N, Rijnsdorp AD, Mcconnaughey RA, Hilborn R, Collie JS, Pitcher CR, Amoroso RO, Parma AM, Suuronen P, Kaiser MJ (2018) Response of benthic fauna to experimental bottom fishing : A global meta- - analysis. 698–715.

SIH Ifremer (2017) Activité des navires de pêche -région Nouvelle-Aquitaine. 14.

Simpson JH, Sharples J (2012) Introduction to the physical and biological oceanography of shelf seas. Cambridge University Press, Cambridge, UK.

Smith CJ, Rumohr H, Karakassis I, Papadopoulou KN (2003) Analysing the impact of bottom trawls on sedimentary seabeds with sediment profile imagery. J Exp Mar Bio Ecol 285–286:479–496.

Smith S V, Hollibaugh JT (1993) Coastal Metabolism and the Oceanic Organic Carbon Balance. Rev Geophys 31:75–89.

Snelgrove PVR (1998) The biodiversity of macrofaunal organisms in marine sediments. Biodivers Conserv 7:1123–1132.

Soulsby R (1997) Dynamics of Marine Sands: A Manual for Practical Applications, Thomas Tel.

Sun MY, Aller RC, Lee C (1994) Spatial and temporal distributinos of sedimentary chloropigments as indicators of benthic processes in Long Island Sound. J Mar Res 52:149–176.

Syvitski JPM, Vörösmarty CJ, Kettner AJ, Green P (2005) Impact of Humans on the Flux of Terrestrial Sediment to the Global Coastal Ocean. Science (80-) 308:376–380.

Teal LR, Parker ER, Solan M (2010) Sediment mixed layer as a proxy for benthic ecosystem process and f.unction. Mar Ecol Prog Ser 414:27–40.

Tesi T, Miserocchi S, Goñi MA, Langone L (2007) Source, transport and fate of terrestrial organic carbon on the western Mediterranean Sea, Gulf of Lions, France. Mar Chem 105:101–117.

Thrush SF, Dayton PK (2002) Disturbance to marine benthic habitats by trawling and dredging: Implications for marine biodiversity. Annu Rev Ecol Syst 33:449–473.

Tiessen H, Stewart JWB, Hunt HW (1984) Concepts of soil organic matter transformations in relation to organo-mineral particle size fractions. Plant Soil 76:287–295.

Vigneaux M, Caralp M, Klingebiel A, Latouche C, Moyes J (1972) Sur l'origine des sédiments fins superficiels du plateau continental atlantique au large de la Gironde (France). In: *The 2nd International Ocean Development Conference*. p 372–394

Vitousek PM, Aber JD, Howarth RW, Likens GE, Matson PA, Schindler DW, Schlesinger WH, Tilman DG (1997) Human alteration of the global nitrogen cycle: Sources and consequences. Ecol Appl 7:737–750.

Wakeham SG, Lee C, Hedges JI, Hernes PJ, Peterson ML (1997) Molecular indicators of diagenetic status in marine organic matter. Geochemica Cosmochim Acta 61:5363–5369.

Watling L, Norse EA (1998) Disturbance of the seabed by mobile fishing gear: A comparison to forest clearcutting. Conserv Biol 12:1180–1197.

Weber O, Jouanneau JM, Ruch P, Mirmand M (1991) Grain-size relationship between suspended matter originating in the Gironde estuary and shelf mud-patch deposits. Mar Geol 96:159–165.

Weiler RR, Mills AA (1965) Surface properties and pore structure of marine sediments. Deep Res 12:511–529.

Whanpetch N, Nakaoka M, Mukai H, Suzuki T, Nojima S, Kawai T, Aryuthaka C (2010) Temporal changes in benthic communities of seagrass beds impacted by a tsunami in the Andaman Sea, Thailand. Estuar Coast Shelf Sci 87:246–252.

Wheatcroft RA (2006) Time-series measurements of macrobenthos abundance and sediment

bioturbation intensity on a flood-dominated shelf. Prog Oceanogr 71:88–122.

Wildish DJ, Hargrave BT, MacLeod C, Crawford C (2003) Detection of organic enrichment near finfish net-pens by sediment profile imaging at SCUBA-accessible depths. J Exp Mar Bio Ecol 285–286:403–413.

Wilson SJK, Fredette TJ, Germano JD, Blake JA, Neubert PLA, Carey DA (2009) Plan-view photos, benthic grabs, and sediment-profile images: Using complementary techniques to assess response to seafloor disturbance. Mar Pollut Bull 59:26–37.

Wold S, Esbensen K, Geladi P (1987) Principal Component Analysis. Chemom Intell Lab Syst 2:37–52.

Worm B, Barbier EB, Beaumont N, Duffy JE, Folke C, Halpern BS, Jackson JBC, Lotze HK, Micheli F, Palumbi SR, Sala E, Selkoe KA, Stachowicz JJ, Watson R (2006) Impacts of biodiversity loss on ocean ecosystem services. Science 314:787–790.

Young DK, Rhoads DC (1971) Animal-sediment relations in Cape Cod Bay, Massachusetts I. A transect study. Mar Biol 11:242–254.

Zajac RN, Whitlatch RB, Thrush SF (1998) Recolonization and succession in soft-sediment infaunal communities: The spatial scale of controlling factors. Hydrobiologia 375–376:227–240.

CHAPITRE 1

Structuration spatiale de la matière organique particulaire et de l'activité de la macrofaune benthique dans la Vasière Ouest-Gironde

Spatial Distributions of Surface Sedimentary Organics and Sediment Profile Image Characteristics in a High-Energy Temperate Marine RiOMar: The West Gironde Mud Patch

Bastien Lamarque [1], Bruno Deflandre [2], Adriana Galindo Dalto [3], Sabine Schmidt [2], Alicia Romero-Ramirez [1], Frédéric Garabetian [1], Nicolas Dubosq [2], Mélanie Diaz [2], Florent Grasso [4], Aldo Sottolichio [2], Guillaume Bernard [1], Hervé Gillet [2], Marie-Ange Cordier [2], Dominique Poirier [2], Pascal Lebleu [2,†], Hervé Derriennic [2], Martin Danilo [2], Márcio Murilo Barboza Tenório [3] and Antoine Grémare [1]

[1]UMR EPOC, Université de Bordeaux, CNRS, UMR 5805, Station Marine d'Arcachon, 2 rue du Professeur Jolyet, F33120 Arcachon, France

[2]UMR EPOC, Université de Bordeaux, CNRS, UMR 5805, Bâtiments B18/B18N, Allée Geoffroy Saint-Hilaire, F33615 Pessac CEDEX, France

[3]Departamento de Biologia Marinha, Instituto de Biologia, Universidade Federal do Rio de Janeiro,
CEP 21941-902 Rio de Janeiro, Brazil

[4]IFREMER Brest—DYNECO/DHYSED, Centre de Bretagne, CS 10070, 29280 Plouzané, France

Article publié en 2021 dans la revue *Journal of Marine Science and Engineering*

9:242, doi: 10.3390/jmse9030242

Ce manuscrit correspond à la version acceptée de l'article et présente des différences d'édition vis-à-vis de la version publiée disponible sur le site de l'éditeur.

Abstract

The spatial distributions of (1) surface sediment characteristics ($D_{0.5}$, Sediment Surface Area (SSA), Particulate Organic Carbon (POC), Chlorophyll-*a* (Chl-*a*), Phaeophytin-*a* (Phaeo-*a*), Total and Enzymatically Hydrolyzable Amino Acids (THAA, EHAA), $\delta^{13}C$) and (2) sediment profile image (apparent Redox Potential Discontinuity (aRPD), numbers and depths of biological traces) characteristics were quantified based on the sampling of 32 stations located within the West Gironde Mud Patch (Bay of Biscay, NE Atlantic) in view of (1) assessing the spatial structuration of a temperate river-dominated ocean margin located in a high-energy area, (2) disentangling the impacts of hydrodynamics and bottom trawling on this structuration, and (3) comparing the West Gironde Mud Patch with the Rhône River Prodelta (located in a low-energy area). Results support the subdivision of the West Gironde Mud Patch in a proximal and a distal part and show (1) the existence of depth gradients in surface sedimentary organics characteristics and bioturbation within the distal part; (2) no evidence for a significant effect of bottom trawling, as opposed to Bottom Shear Stress, on the West Gironde Mud Patch spatial structuration; and (3) major discrepancies between spatial structuration in the West Gironde Mud Patch and the Rhône River Prodelta, which were attributed to differences in tidal regimes, sedimentation processes, and local hydrodynamics, which is in agreement with current river-dominated ocean margin typologies.

Keywords: RiOMar; surface sediment; spatial distribution; sedimentary organics; bioturbation

1. Introduction

Continental margins are the interface between land and the open ocean, where 50 to 80% of continental Particulate Organic Carbon (POC) inputs are mineralized [1–3]. Less than 5% of these inputs are transferred to the deep ocean [4], the remaining part being buried in continental margin sediments. River-dominated ocean margins (RiOMars), defined as margins impacted by major rivers freshwater and/or sediment discharges (e.g., plumes of Amazon, Yangtze or Mississippi Rivers), are the main marine primary depositional areas of riverine particulate continental inputs [2,5]. They account for 40 to 50% of continental POC burial occurring in continental margins [2,3,6]. Burial is tightly cued by biogeochemical processes taking place at the water–sediment interface [3,5,7]. Therefore, assessments of the structuration and functioning of the benthic components of marine RiOMars are key issues to reach a comprehensive understanding of the marine contribution to global biogeochemical cycles [1,3].

Benthic macrofauna plays a major role in the biogeochemistry of the top centimeters of the sediment column through bioturbation (i.e., sediment mixing and bioirrigation [8]). This includes both changes in the spatial distribution and the temporal dynamics of electron acceptors, which influence mineralization fluxes [9–11]. Mostly based on the analysis of macrofauna vertical distribution within the sediment column and X-rays radiographies, Rhoads et al. [12] first proposed a conceptual model describing the response of macrofauna and surface sediments to the inputs of major rivers. According to this model, macrofauna spatial distribution is mainly determined by (1) physical disturbance induced by intense continental inputs, and (2) reduction in Particulate Organic Matter (POM) availability due to the limitation of primary production in turbid river plumes. In proximal (i.e., the closest to the river mouth) parts of RiOMars, high and irregular sedimentation rates induce sedimentary instability, precluding the establishment of mature macrobenthic communities. Moreover, high turbidity limits primary production and results in mainly low (and refractory) POM concentrations in surface sediments. Accordingly, RiOMar proximal areas are characterized by low bioturbation intensities and low mineralization fluxes. Conversely, in distal (i.e., deeper) parts, sedimentation is lower and primary production is higher, allowing for the establishment of mature macrobenthic communities, high bioturbation intensities, and mineralization fluxes.

Several studies have compared RiOMars based on either the characterization/quantification of geomorphological [5] or biogeochemical [3] processes. Their results highlighted the major effect of energetic regimes on RiOMar morphologies [5] and POC mineralization/burial intensities [3]. This later study drew a clear distinction between (1) low-energy systems, with both significant sedimentation rates and carbon preservation (later referred as type 1), and (2) high-energy tidal and/or wave systems with both high sediment oxygenation and low carbon preservation rates (later referred as type 2). It evidenced that the spatial distributions of the benthic components of RiOMars are cued by both riverine inputs and marine hydrodynamics. This categorization was mostly based on tropical/subtropical systems, the Rhône River being the only major (type 1) considered temperate RiOMar. Moreover, both studies considered RiOMars and their continuity with fluvial systems in their entirety, even though McKee et al. [5] underlined the interest of differencing RiOMar sub-environments and comparing RiOMar types. Thus, there is still a clear need to document the spatial structuration of a potential temperate type 2 RiOMar and to compare it with a temperate type 1 one.

Together with the bottom shear stress induced by both waves and bottom currents, bottom trawling is contributing to control sediment resuspension in coastal areas [13–20]. As such, it can deeply affect surface sediments, benthic macrofauna and bioturbation [13,21–24]. RiOMar mud fields are organically enriched as compared to surrounding sediments and often constitute preferential fishing areas [19,20]. Therefore, it is also important to unravel the role of both hydrodynamics and bottom trawling in controlling the structuration of benthic ecosystems in RiOMars.

The present study is aiming at (1) improving current knowledge regarding the spatial structuration of a potential temperate type 2 RiOMar, (2) disentangling the potential effects of hydrodynamics and bottom trawling in controlling this structuration, and (3) comparing this spatial structuration with the one of a type 1 temperate RiOMar (i.e., the Rhône River Prodelta [3]). It is based on the synoptic sampling of a large number of stations and the quantitative analysis of (1) surface sediment characteristics and (2) Sediment Profile Images (SPI).

2. Materials and Methods

2.1. The West Gironde Mud Patch

The West Gironde Mud Patch (WGMP) is a 420 km^2 sedimentary body located in the Bay of Biscay 40 km off the Mouth of the Gironde Estuary (Figure 1.1). This relict paleovalley/depression constitutes the primary depocenter (sedimentation rates between less than 1 and 5 $mm \cdot y^{-1}$ [25,26]) of fine particles originating from the Gironde Estuary, which presents an annual mean water discharge of 944 $m^3 \cdot s^{-1}$ [27] and daily discharge up to 7500 $m^3.s^{-1}$ during wintertime [28]. The WGMP is located in a macro-tidal environment with a tidal range from 1.5 to 5 m [26,29]. The continental shelf around the Mouth of the Gironde Estuary is dominated by strong swells/waves, which can reach maximal amplitudes of 15 m and time periods of 15 s during winter storms [30]. These hydrological conditions prevent the sedimentation of fine particles in the immediate vicinity of the Mouth of the Estuary. Therefore, the WGMP can a priori be considered as a potential temperate type 2 RiOMar [5].

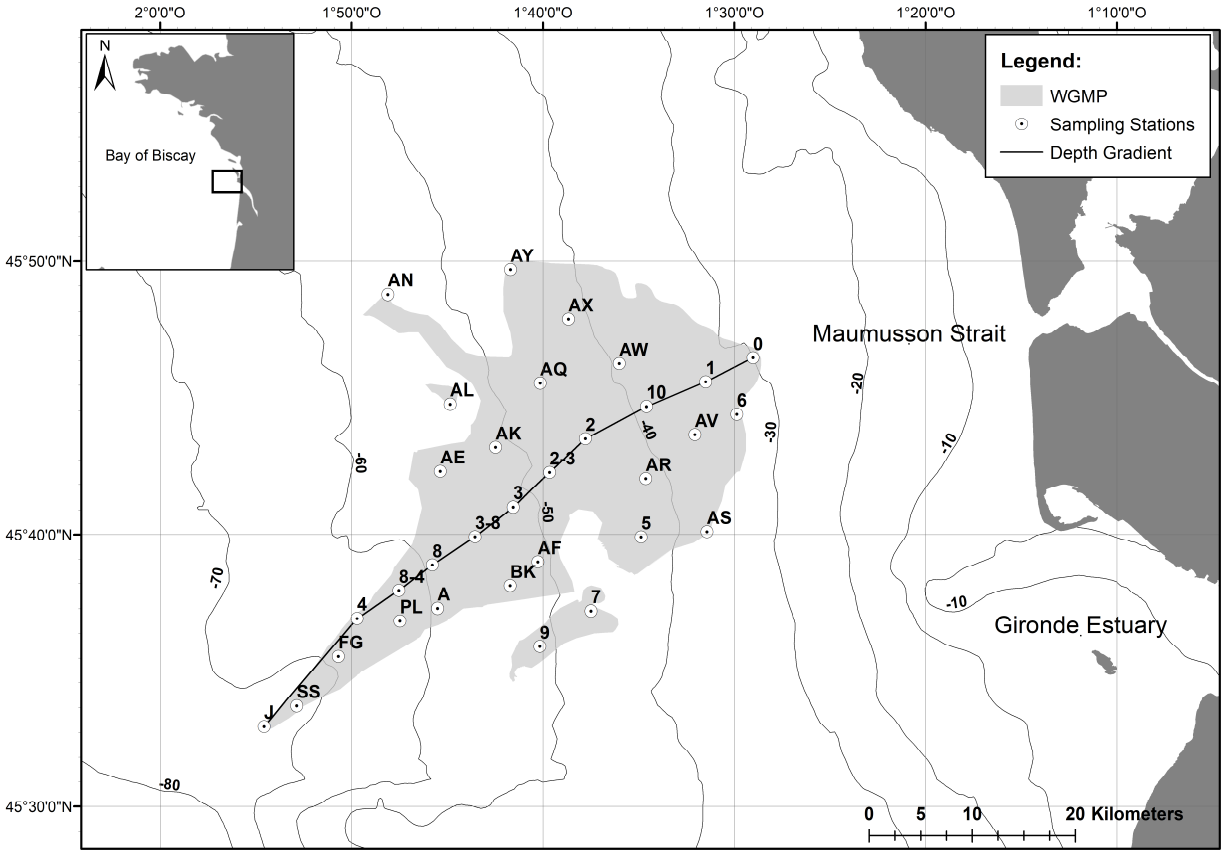

Figure 1.1. Map showing the location of the West Gironde Mud Patch along the French Atlantic coast, the locations of the 32 sampled stations, and the depth gradient sampled for X-ray radiographies and amino acids. The delimitation of the West Gironde Mud Patch (WGMP) is based on the acoustic measurements achieved during the JERICOBENT-5-TH cruise [48] and the surface sediment granulometry assessed during the present study [49].

The sedimentology of the WGMP has been extensively studied based on stratigraphic sequences, palynological data, X-rays radiographies, and radiochronographies [25,26,31–38,39–43]. Sedimentological surveys have attributed a major role to hydrodynamics in controlling the spatial structuration of the WGMP [25,26,35,38,42]. This paradigm was based on both (1) the segmentation between a proximal and a distal part with no modern persistent sedimentation in the former due to strong hydrodynamics, and (2) the decreasing frequency of occurrence of vertical erosional sequences within the sediment column with station depth. The occurrence of spatial zonation in the distal part has also been addressed [25,26,35,38,42] but without reaching a clear conclusion due to a limited number of sampled stations and to the lack of a fine quantitative assessment of bioturbation. Benthic macrofauna composition and associated biogeochemical processes have been largely neglected as well, with only two studies based on the sampling of a limited number of stations [44,45]. The WGMP is a preferential fishing area [46] where several benthic species are commercially exploited, including the Norway lobster (*Nephrops norvegicus*) and the common sole (*Solea solea*). Bottom trawls are commonly deployed in the area [46], and it has been suggested that their use may constitute a significant source of disturbance for benthic habitats [26,38,47]. Based on Vessel Monitoring System data, Mengual et al. [19,20] showed that the Benthic Trawling Effort (BTE) in the WGMP can be locally intense (up to 10 times trawled·y^{-1}) and seems to increase with depth.

2.2. Sampling of Surface Sediment and Sediment Profile Images

This study is based on samples collected during the JERICOBENT-5 cruise [49], which took place in June 2018 on board of the R/V Côtes de la Manche. Thirty-two stations located between 32.5 and 78 m depth, and allowing for a full coverage of the WGMP were sampled for both surface sediment characteristics and Sediment Profile Images (SPIs; Figure 1.1, Table A1). At each station, a sediment core (10 cm internal diameter) was collected using an Uwitec® (Mondsee, Austria) monotube-corer. The upper top centimeter (i.e., 0–1 cm depth layer) was carefully extruded and split in two subsamples immediately frozen (−20 °C) for further analyses of (1) grain size, Sediment Surface Area (SSA; [50]), Particulate Organic Carbon (POC), and OC isotopic ratio; and (2) chloropigments. Total and Enzymatically Hydrolyzable Amino Acids (THAA and EHAA) were assayed at 11 stations distributed along a depth gradient (see Figure 1.1). At these stations, a second core was collected for X-rays radiographies (SCOPIX

system; [51]). EHAA were not assayed at station J due to a technical problem. At all stations, between 4 and 8 SPIs were taken (at stations PL and J, respectively) using a sediment profile imager (Ocean Imaging Systems®, Pocasset, USA) [52] fitted with a D7100 camera (Nikon®, Tokyo, Japan).

2.3. Analysis of Surface Sediment Characteristics

Grain size was measured on duplicated aliquots of each sediment sample using a Master Sizer laser microgranulometer (Malvern Panalytical®, Malvern, UK), which allowed for the computation of median diameter ($D_{0.5}$). SSAs were measured on freeze-dried sediments, previously degassed overnight at 150 °C, using a Gemini VII 2390 Series Surface Area Analyzer (Micromeritics®, Norcross, USA) with the multi-point Brunauer–Emmett–Teller method [50]. POC was assayed using a LECO® (St. Joseph, USA) CS 200 analyzer, after 2M HCl overnight decarbonatation of previously freeze-dried sediments [53].

THAA and EHAA were analyzed on duplicates. THAA were extracted by acid hydrolysis. EHAA were extracted following the biomimetic approach proposed by Mayer et al. [54]. THAA and EHAA were analyzed by derivation to form fluorescent amino compounds with the presence of the thiol 3-mercaptopropionic acid (MPA). Fluorescent derivatives were separated by reverse-phase High-Performance Liquid Chromatography (Agilent®, Santa Clara, USA; 1260 INFINITY model) on a Phenomenex® (Torrance, USA) Kinetex 5 µm EVO C18 column using non-linear gradient of methanol–acetate buffer (pH = 7, 40 mM), and detected by fluorescence from 340 to 450 nm using an excitation wavelength of 338 nm. The EHAA/THAA ratio was used as a lability index of bulk sedimentary organics [55–57].

Chlorophyll-*a* (Chl-*a*) and Phaeophytin-*a* (Phaeo-*a*) were assayed on thawed frozen (−20 °C) sediment after overnight acetone extraction (90% final concentration) using a Perkin Elmer® LS-55 spectrofluorometer following Neveux and Lantoine [58]. Pigment data are lacking for station BK due to sample loss. All organic concentrations were normalized for SSA (i.e., expressed in terms of mass per SSA). The Chl-*a*/(Chl-*a* + Phaeo-*a*) ratio was used as a lability index of vegetal biomass [55,56].

For the analysis of OC isotopic ratio, replicated freeze-dried sediment samples were decarbonated (1M HCl) and later analyzed using a Thermo Scientific® Delta V plus IRMS

coupled with a Thermo Scientific® (Waltham, USA) Flash 2000 EA. Raw measurements were converted in usual $\delta^{13}C$ units [59].

2.4. Analysis of Sediment Profile Images

Individual SPI were analyzed for (1) apparent Redox Potential Discontinuity (aRPD) thickness, (2) numbers of biogenic structures (tubes, burrows, oxic voids, feeding pits), (3) numbers of epi- and infauna, and (4) maximal depths of oxic voids within the sediment column. For the stations presenting a surface sandy layer, the upper limit for the computation of aRPD thickness was set below the transient top coarser sediment layer. Image analyses were achieved using the SpiArcBase software [60] and mean values and standard deviations were computed for each station. In addition, all SPIs were visually inspected for the presence of potential traces of bottom trawling. This included the presence of clasts and furrows [61,62], and of a surface puzzle fabric [63].

2.5. Spatial Distribution of Bottom Shear Stress and Trawling Effort

The spatial distribution of Bottom Shear Stress (BSS) was computed from a tridimensional numerical model deployed and validated over the study area [64]. This model, stretching from the Gironde Estuary to the continental shelf, is based on the MARS3D hydrodynamic model [65] and the WAVE WATCH III® wave model [66]. Its curvilinear mesh resolution is approximately 0.5 × 0.5 km^2 over the WGMP. The model integrates realistic hydro-meteorological forcing (i.e., wind, tide, surge, and river flow). BSS was computed as the combination of current-induced and wave-induced components following Soulsby's formulation [67]. A more detailed description of the model can be found in Grasso et al. [68]. Simulations achieved during the present study provided hourly outputs over the whole year preceding the JERICOBENT-5 cruise. In order to account for intense hydrodynamic events, 95^{th} percentiles were used to characterize BSS intensities.

The spatial distribution of Bottom Trawling Effort (BTE), within and around the WGMP, was assessed based on vessel Automatic Identification System (AIS) data collected by Global Fishing Watch [69,70]. Raw (daily) BTE were available with a 1/100 degree (corresponding to 1.77 km^2 cells) spatial resolution. For each cell, daily BTE were summed over the whole year preceding the JERICOBENT-5 cruise. Summed BTE were expressed both in terms of $h.km^{-2}.y^{-1}$

and number of times trawled.y^{-1}. The conversion between these two units was achieved following Mengual et al. [19,20].

2.6. Analysis of WGMP Data

2.6.1. Sediment Characteristics and Sediment Profile Images

For both sediment (i.e., SSA, POC, Chl-*a*, Phaeo-*a*, Chl-*a*/(Chl-*a* + Phaeo-*a*) ratio and $\delta^{13}C$) and SPI (i.e., aRPD thickness; maximal oxic void depth; mean numbers of tubes, burrows, oxic voids, feeding structures, epifauna and infauna) characteristics, hierarchical clustering (Euclidean distance and average group linking) and Principal Components Analyses (PCAs) were used to define groups of stations and to assess relationships between variables. THAA, EHAA, and EHAA/THAA ratios were not included, since data were missing at some stations. Station depth, BSS, and BTE were introduced as supplementary variables in both PCAs. SIMilarity PROFile procedures (SIMPROF; [71]) were used to test for the statistical significance of differences between station groups resulting from hierarchical clustering. SIMilarity PERcentage analysis (SIMPER; [72]) was used to identify the SPI characteristics contributing the most to between-group differences. All analyses were run on normalized data using the PRIMER® 6 software package [73].

Multivariate analyses supported the distinction between a proximal and a distal part in the WGMP (see Section 4.1). Simple linear regression models were used to assess the significance of the relationships between station depth and both surface sediment and SPI characteristics in the whole WGMP and in the sole distal part to avoid confounding effects resulting from (1) the high between-station variability in the proximal part and (2) major differences in sediment and SPI characteristics between parts. The same approach was used to assess the significance of the relationships between station depths and their coordinates on the first component of both PCAs.

2.6.2. Bottom Shear Stress and Trawling Effort

BSS 95th percentiles and summed BTE were mapped using the ArcGIS Desktop® 10.6 software. The relationships between BSS 95th percentiles, summed BTE within cells containing sampled stations, and (1) station depth, (2) surface sediment characteristics, and (3) SPI characteristics were assessed using simple linear regression models at the scale of the whole

WGMP and/or its sole distal part. Multiple linear regression models were used to test for additive effects of BSS and BTE.

2.7. Comparisons with the Rhône River Prodelta

The Rhône River Prodelta (RRP) is a ca 265 km^2 [74] depositional system, located in the Gulf of Lions (North Mediterranean Sea). It is supplied with particles from the Rhône River, which presents a mean annual water discharge of 1700 $m \cdot s^{-1}$ and massive flood events (i.e., up to 11,000 $m^3 \cdot s^{-1}$; [75]). The RRP is located in an environment with micro-tidal conditions (i.e., maximal tidal range of 0.4–0.5 m) and wave mean heights of 1–1.5 m [76]. During winter storms, wave heights can exceptionally reach 3–4 m, with periods of about 6–7 s [77,78]. These conditions allow for the sedimentation of fine particles at the immediate vicinity of the river mouth. Sedimentation rates are about 40 $cm \cdot y^{-1}$ in the proximal part (i.e., 5–30 m depth) of the RRP and between 1 and 10 $cm \cdot y^{-1}$ in its distal part (30–100 m depth; [74,79,80]). According to the classifications established by McKee et al. [5] and Blair and Aller [3], the RRP therefore constitutes a low-energy (type 1) temperate RiOMar in direct continuity with the Rhône River.

WGMP results collected during the present study were compared with those originating from the Chaccra cruise (April 2007), which took place in a comparable situation in terms of river flows [56] and during which the same parameters (i.e., $D_{0.5}$, POC, chloropigments, THAA, EHAA, $\delta^{13}C$, and SPI characteristics) were measured at 7–10 stations located in the RRP [56,81,82]. Since modern sedimentation was shown to be restricted to the distal part of the WGMP (see above), the comparison was achieved between the sole WGMP distal part and the whole RRP. All organic concentrations were expressed in terms of sediment DW (eventually standardized for $D_{0.5}$), since no SSA data were available for the RRP. For the same reason, we used mean instead of maximal oxic void depth. Mean values of WGMP and RRP characteristics were compared using one-way ANOVAs.

3. Results

3.1. Surface Sediment Characteristics

Except for two stations (i.e., stations 0 and 10), all particle size distributions were unimodal. There were marked differences in surface median sediment grain size ($D_{0.5}$) among shallow stations (Figure 1.2A). $D_{0.5}$ was minimal at station AV (13.5 µm) and maximal at station 0 (64.6 µm). Conversely, deep stations featured a narrower range (i.e., between 14.9 and 24.8 µm at stations 7 and 2, respectively) of $D_{0.5}$. Sediment Surface Area (SSA) was also more dispersed at shallow stations (i.e., between 3.4 and 14.2 $m^2 \cdot gDW^{-1}$ at stations AW and AV, respectively) (Figure 1.2B) than at deep stations (i.e., between 6.1 and 9.8 $m^2 \cdot gDW^{-1}$ at stations 2 and 4, respectively).

At the scale of the whole WGMP, SSA significantly decreased with increasing $D_{0.5}$ following an exponential model ($y = 4.268 + 51.982 \times e^{-0.134x}$; n = 32, $R^2 = 0.830$, $p < 0.001$). $D_{0.5}$, all surface sediment organic concentrations and Chl-*a*/(Chl-*a* + Phaeo-*a*) ratio (Table A1) correlated significantly with station depth, which was not the case for SSA and $\delta^{13}C$ (Table A2). When considering only the distal part (see Section 4.1 for the delimitation between the proximal and distal parts), the correlations between station depth, $D_{0.5}$, Chl-*a*, and Chl-*a*/(Chl-*a* + Phaeo-*a*) were not significant (Table A2).

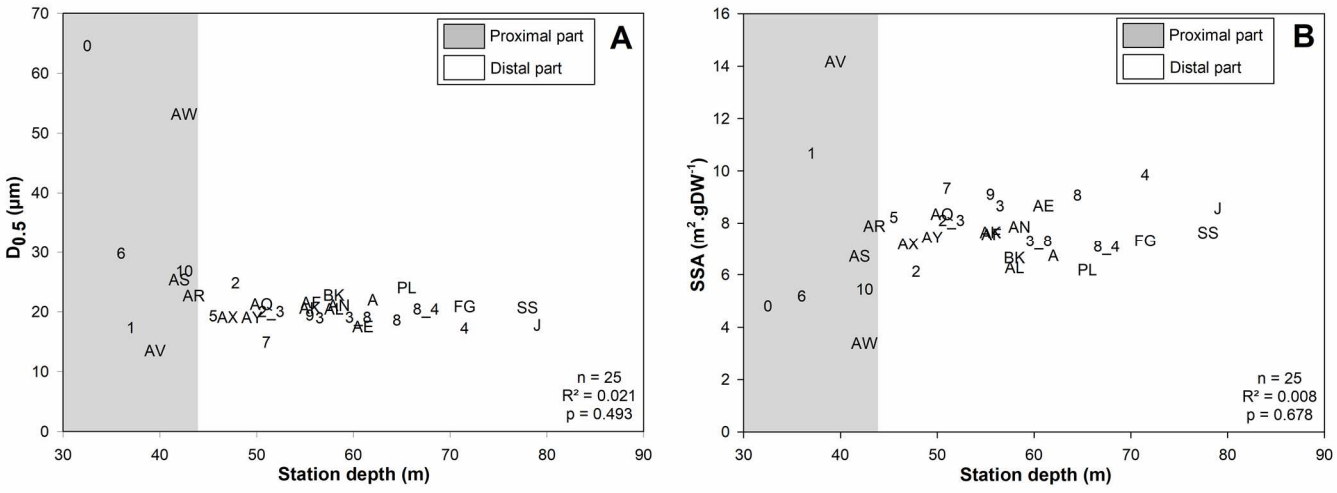

Figure 1.2. Relationships between station depth and: $D_{0.5}$ (**A**); Sediment Surface Area (SSA; (**B**)). Gray areas represent the proximal part (z < 42.5 m) of the WGMP. Station codes are the same as in Figure 1.1 and Table A1. Statistical results refer to the sole WGMP distal part.

Particulate Organic Carbon (POC) concentrations were between 0.50 and 2.06 mg.m^{-2} at stations AV and J, respectively. POC correlated positively with depth in the distal part of the West Gironde Mud Patch (WGMP; Figure 1.3A, Table A2). Total Hydrolyzable Amino Acid (THAA) concentrations were between 0.18 and 0.69 mg·m^{-2} at stations 10 and J respectively (Table A1). THAA correlated positively with station depth in both the whole WGMP and the distal part of the WGMP (Table A2). Enzymatically Hydrolyzable Amino Acids (EHAA) concentrations also correlated significantly with station depth at the scale of the whole WGMP, with values ranging from 0.047 mg·m^{-2} (station 10) to 0.109 mg.m^{-2} (stations 8–4). However, this correlation was not significant in the sole distal part. EHAA/THAA ratios ranged from 15.5 (station 8) to 26.6% (station 10) (Table A1). They did not significantly correlate with station depth when considering either the whole WGMP or its sole distal part (Table A2). Stations AN and 3_8 constituted clear outliers (i.e., featuring high ratios as regard to their depth) in the relationship linking station depth and Chl-*a*/(Chl-*a* + Phaeo-*a*) ratio (Figure 1.3B). When excluding these two stations, this relationship was significantly negative in the distal part of the WGMP (Table A2). $\delta^{13}C$ values presented a narrow variation range with values from −23.66‰ to −22.20‰ at stations 1 and 6, respectively. Variability relative to station depth was more marked in the proximal than in the distal part of the WGMP, where all $\delta^{13}C$ values were around −23‰ (Figure 1.3C).

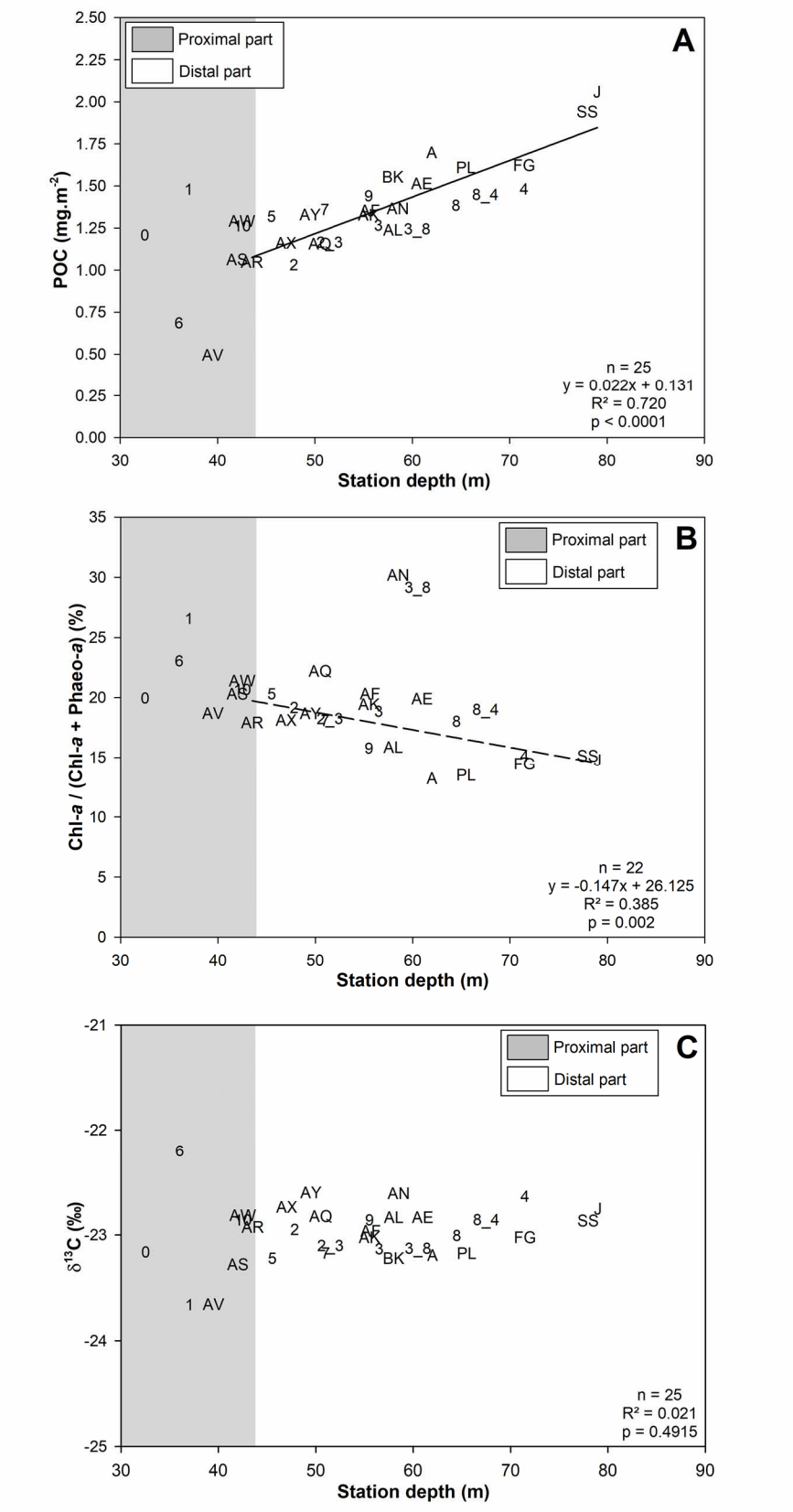

Figure 1.3. Relationships between station depth and main surface sediment characteristics: Particulate Organic Carbon concentration (POC; (**A**)); Chl-*a*/(Chl-*a*+Phaeo-*a*) ratio (**B**) and $\delta^{13}C$ (**C**). Gray areas represent the proximal part (z < 42.5 m) of the WGMP. Station codes are the same as in Figure 1.1 and Table A1. The continuous line represents the linear regression linking station depth and POC concentration within the distal part of the WGMP, and the dotted line represents the linear regression linking station depth and Chl-*a*/(Chl-*a*+Phaeo-*a*) ratio within the distal part of the WGMP (excluding stations AN and 3_8).

The first two components of the Principal Component Analysis (PCA) based on surface sediment characteristics accounted for 64.5% (i.e., 40.2% and 24.3% for the first and the second principal component, respectively) of the total variance (Figure 1.4A). The first component was defined by organic concentrations. The second component was mostly driven by the opposition between Chl-*a*/(Chl-*a* + Phaeo-*a*) ratio and $\delta^{13}C$ on one side, and SSA on the other side (Figure 1.4B).

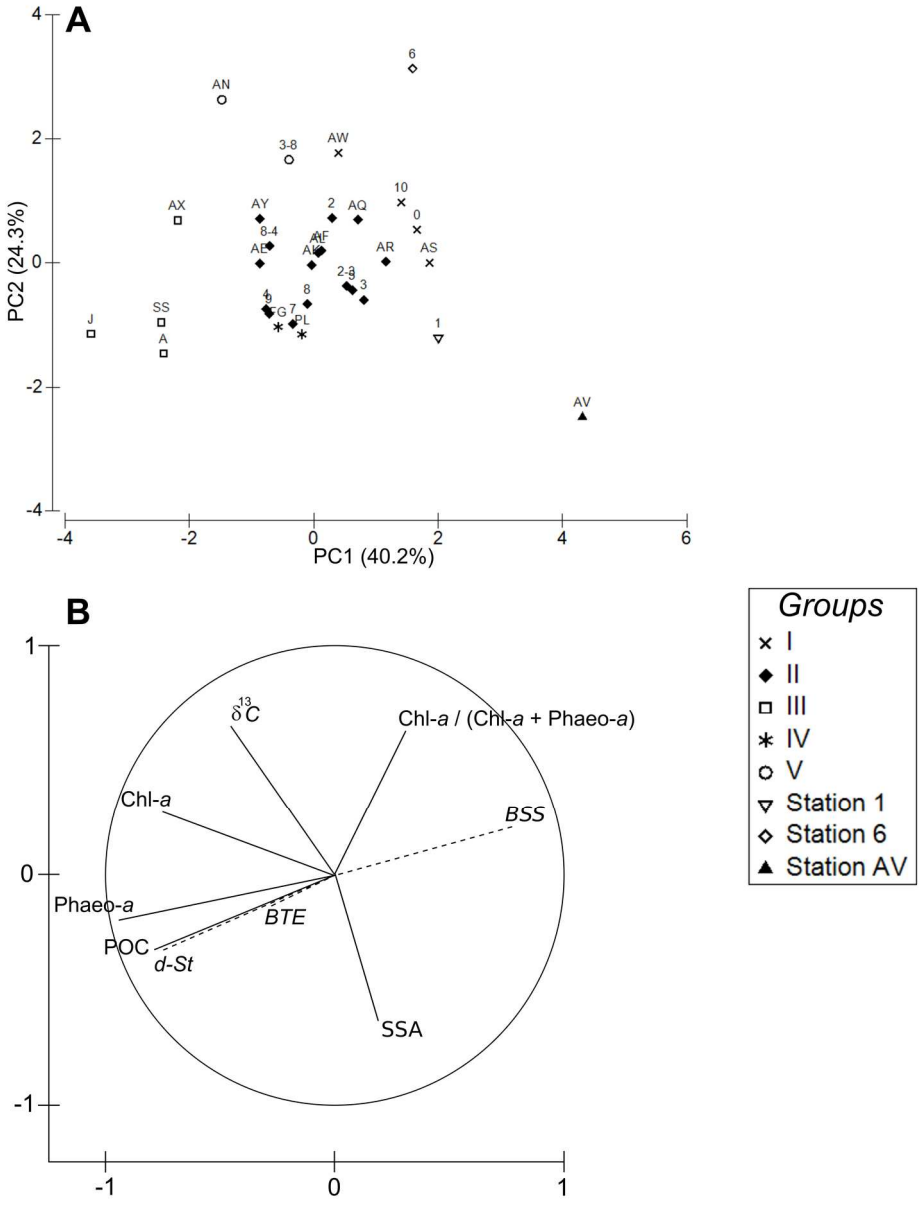

Figure 1.4. Principal component analysis based on normalized surface sediment characteristics (Sediment Surface Area (SSA), POC, Chl-*a*, Phaeo-*a*, Chl-*a*/(Chl-*a*+Phaeo-*a*) ratio and $\delta^{13}C$). Projection of stations on the first plane of the Principal Components Analysis (PCA) (**A**) and correlations of the variables with the first two components (**B**). Station depth (*d-St*), Bottom Shear Stress (*BSS*) and Bottom Trawling Effort (*BTE*) were used as supplementary variables. Group identification was achieved through the coupling of hierarchical clustering with a SIMilarity PROFile (SIMPROF) procedure. Station codes are the same as in Figure 1.1 and Table A1.

Hierarchical clustering and the associated SIMPROF procedure resulted in the identification of 5 groups and 3 “isolated” stations (Figure 1.4A). Stations of group I, together with stations 1, 6, and AV, were all shallow (i.e., from 32.5 to 42.5 m depth). Group II was mostly composed of stations from the median part of the WGMP (i.e., from 43.5 to 60.5 m depth) except for stations AE, 8, 8-4, and 4, which were deeper (i.e., 31, 64.5, 67.5, and 71.5 m, respectively). Group III was composed of deep stations (i.e., from 62 to 79 m depth) except for station AX (z = 47.0 m). Stations of group IV (i.e., FG and PL) constituted apparent outliers to this overall pattern mostly due to their low Chl-*a*/(Chl-*a* + Phaeo-*a*) ratios and $\delta^{13}C$ values compared to other deep stations. Likewise, stations of group V (i.e., AN and 3-8) differed in Chl-*a* concentrations and Chl-*a*/(Chl-*a* + Phaeo-*a*) ratios. Overall, the coordinates of stations on the first axis of the PCA correlated significantly with station depth at the scale of both the whole WGMP and its sole distal part ($n = 31$, $R^2 = 0.561$, $p < 0.001$; $n = 24$, $R^2 = 0.366$, $p = 0.002$).

3.2. X-Rays Radiographies

Examples of X-rays radiographies are shown in Figure 1.5. Stations 0 and 10 showed the presence of a ca. 6–7 cm thick surface sandy layer. Station 10 also presented traces of biological mixing within this layer. Both stations showed laminae corresponding to the denser particles deposits in the sediment column (z ≈13; 16; 17; 19 cm at station 0 and z ≈8 cm at station 10). These structures were less numerous at deeper stations. Nevertheless, some larger structures were observable: (1) at station 2–3 where a coarse layer (z≈14/15 cm) was overlaid by a finer one (11 < z < 14 cm), and (2) at station 4 where two denser (centimeter scaled) layers surrounded a finer one (10 < z < 14.5 cm). Overall, X-rays radiographies clearly showed an increase in the thickness of the bioturbated layer between stations 10 and J, whereas station 0 presented only superficial biological reworking within the surface sandy layer.

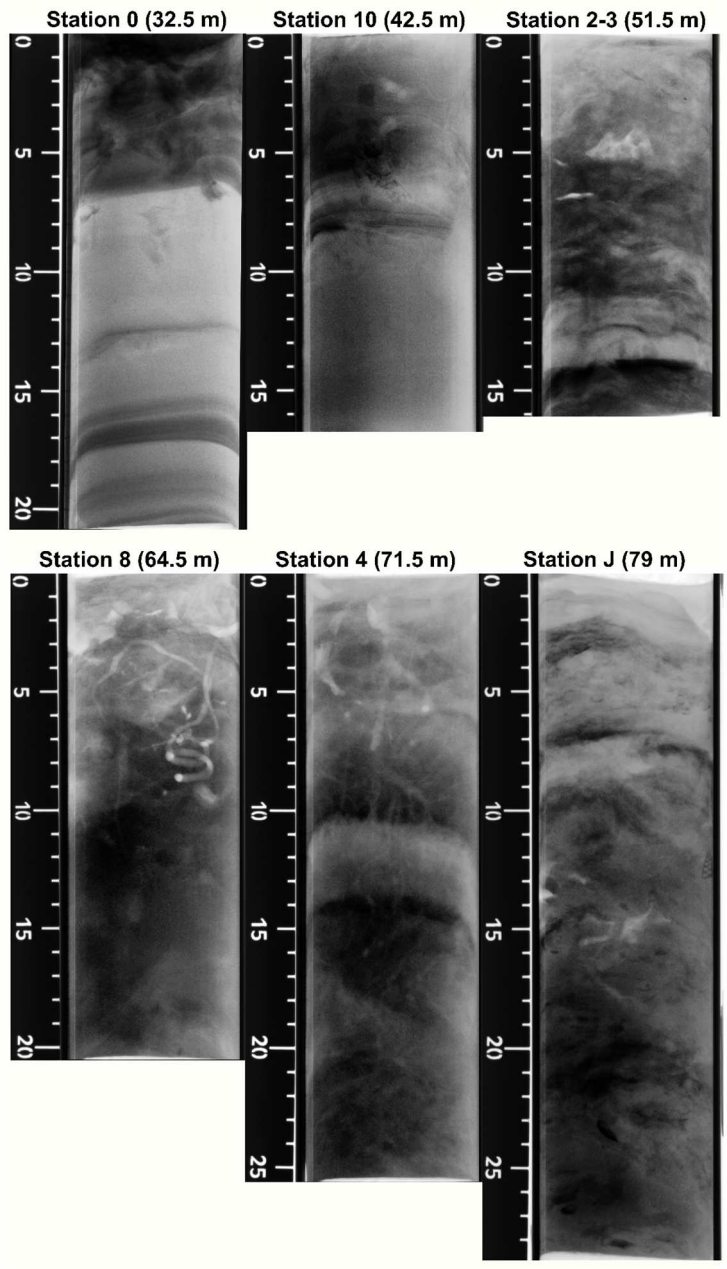

Figure 1.5. Examples of X-rays radiographies (positives; scale in cm) collected at six stations located along the sampled depth gradient (see Figure 1.1). Station codes are the same as in Figure 1.1 and Table A1.

3.3. Sediment Profile Images

Overall, 186 Sediment Profiles Images (SPI) were captured. Representative examples (Figure 1.6) show the increases in the mean values of: (1) aRPD thickness, (2) total number of biological traces (i.e., biogenic structures + epi + infauna), and (3) the thickness of the sediment layer containing biogenic structures with station depth. They also clearly show the presence of a top coarser sediment layer covering dark mud at station 0.

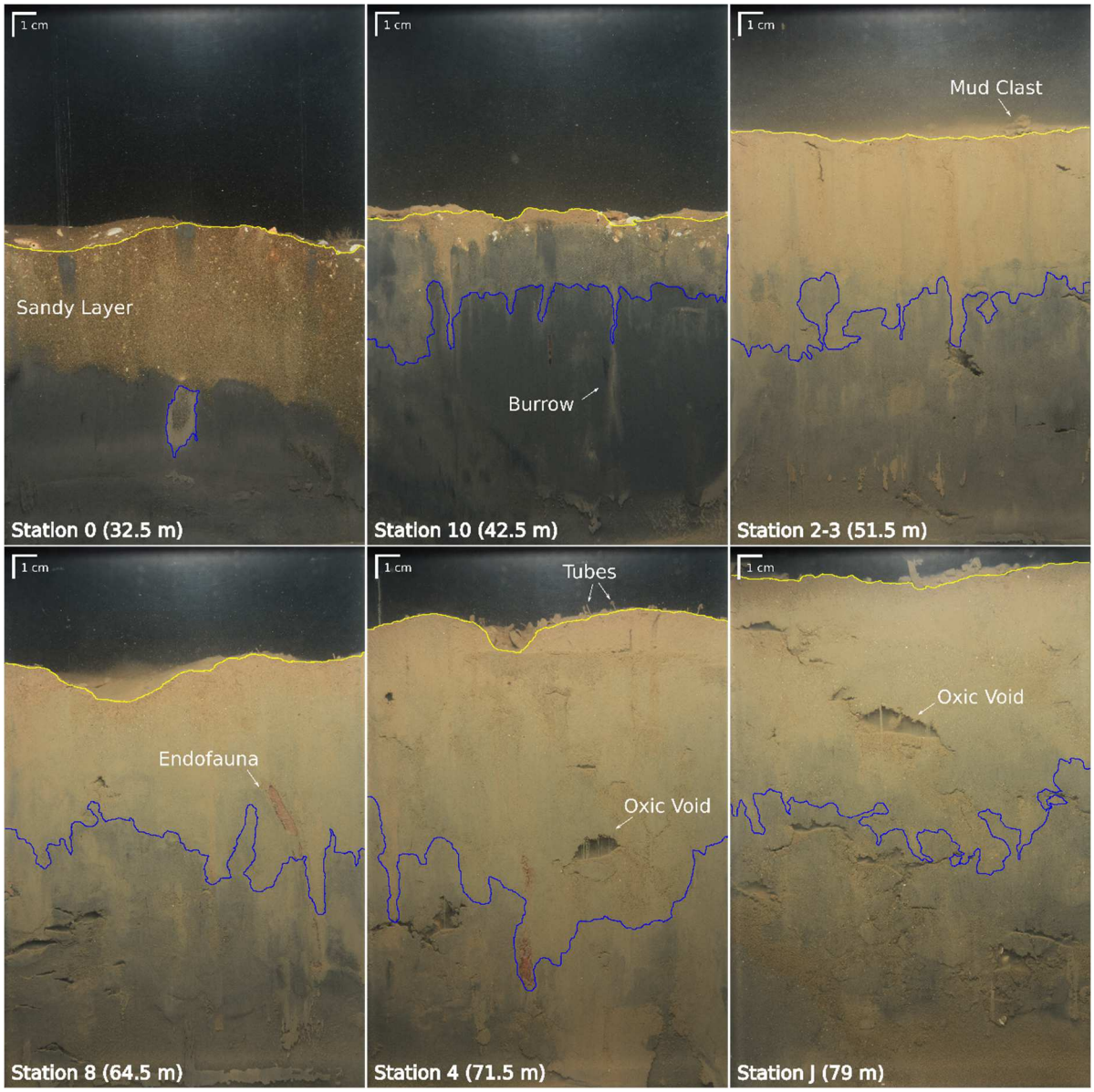

Figure 1.6. Examples of Sediment Profile Images (SPI) collected at six stations located along the depth gradient sampled for X-rays radiographies (see Figure 1.1). Yellow lines represent sediment–water interfaces and blue lines represent apparent Redox Potential Discontinuity (aRPD) thicknesses. Stations are the same as in Figure 1.5, and codes are the same as in Figure 1.1 and Table A1.

At the scale of the whole WGMP, all SPI characteristics correlated significantly with station depth except for the number of infauna (Table A2). All significant correlations were positive except for number of epifauna. Examples of such relationships are given in Figure 1.7 for mean (1) aRPD thickness, (2) total number of biological traces (i.e., biogenic structures + epi- and infauna), and (3) maximal depth of oxic voids. These three parameters presented low values and, for some of them (i.e., aRPD thickness and maximum depth of oxic void), there was a high between-station variability in the proximal part. Within the distal part, they

correlated significantly with station depth (Table A2), which was also the case of most other SPI characteristics (i.e., except for burrow and infauna numbers). All significant correlations were positive except for the number of epifauna. For both the whole WGMP and its sole distal part, the proportions of explained variance remained low (Table A2). They were higher for aRPD thickness, oxic void number and maximal depth, and tube number. This proportion was higher for the total number of biological traces than for any individual SPI characteristic.

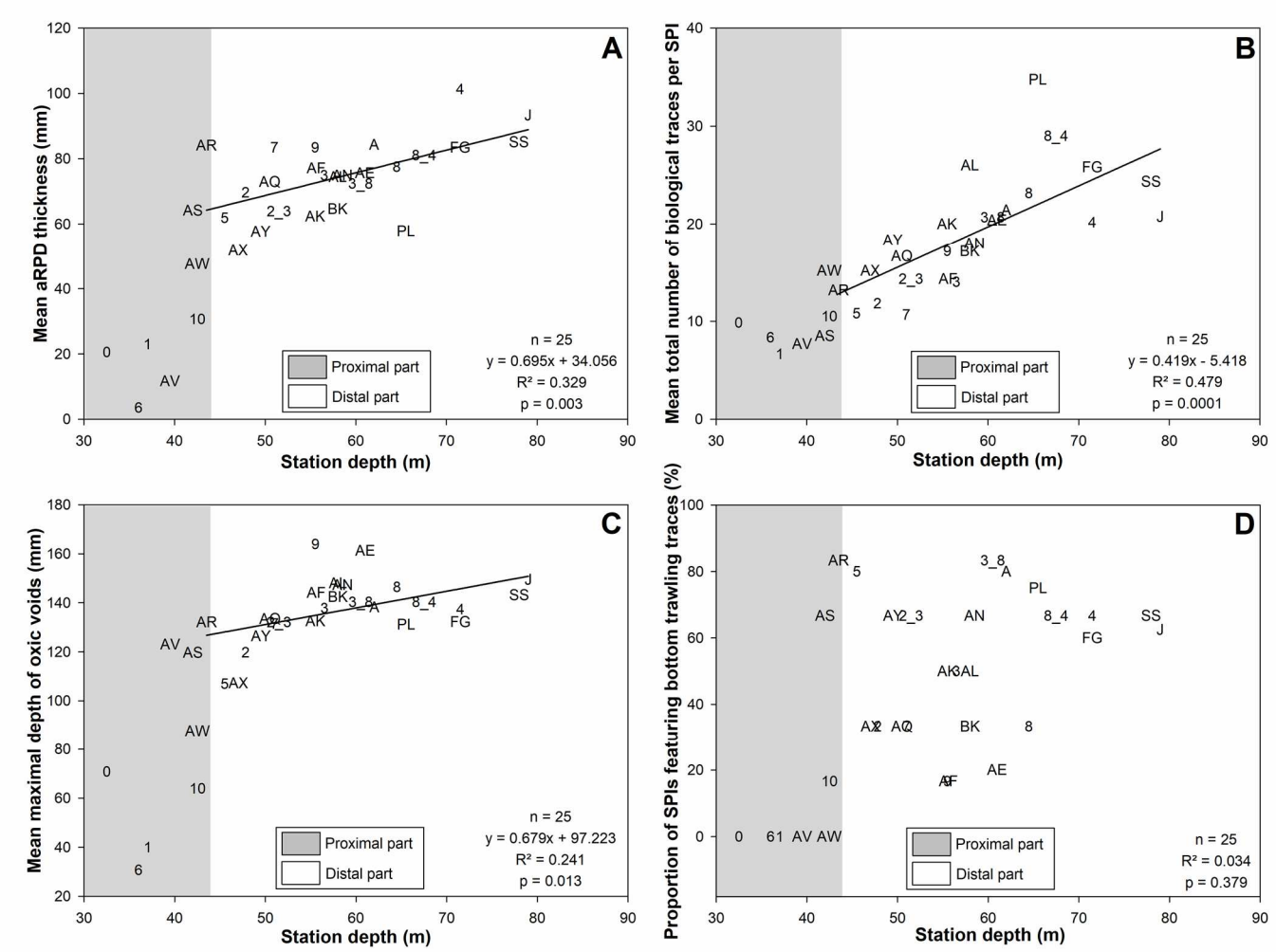

Figure 1.7. Relationships between station depth and mean main SPI characteristics: aRPD thickness (**A**), total number of biological traces per SPI (**B**), maximal depth of oxic voids (**C**), and proportion of SPIs featuring bottom trawling traces (**D**). Gray areas represent the proximal part (z < 42.5 m) of the WGMP. Station codes are the same as in Figure 1.1 and Table A1. Continuous lines represent the linear regressions linking station depth and mean SPI characteristics within the distal part of the WGMP.

The first two components of the PCA based on SPI characteristics explained 58.2% (i.e., 42.5% and 15.7% for the first and the second principal component, respectively) of the total variance (Figure 1.8A). The first component was mainly characterized by a set of co-correlated subsurface features (i.e., number and maximal depth of oxic voids, number of burrows and

aRPD thickness). The second component was mostly driven by the number of feeding pits (Figure 1.8B).

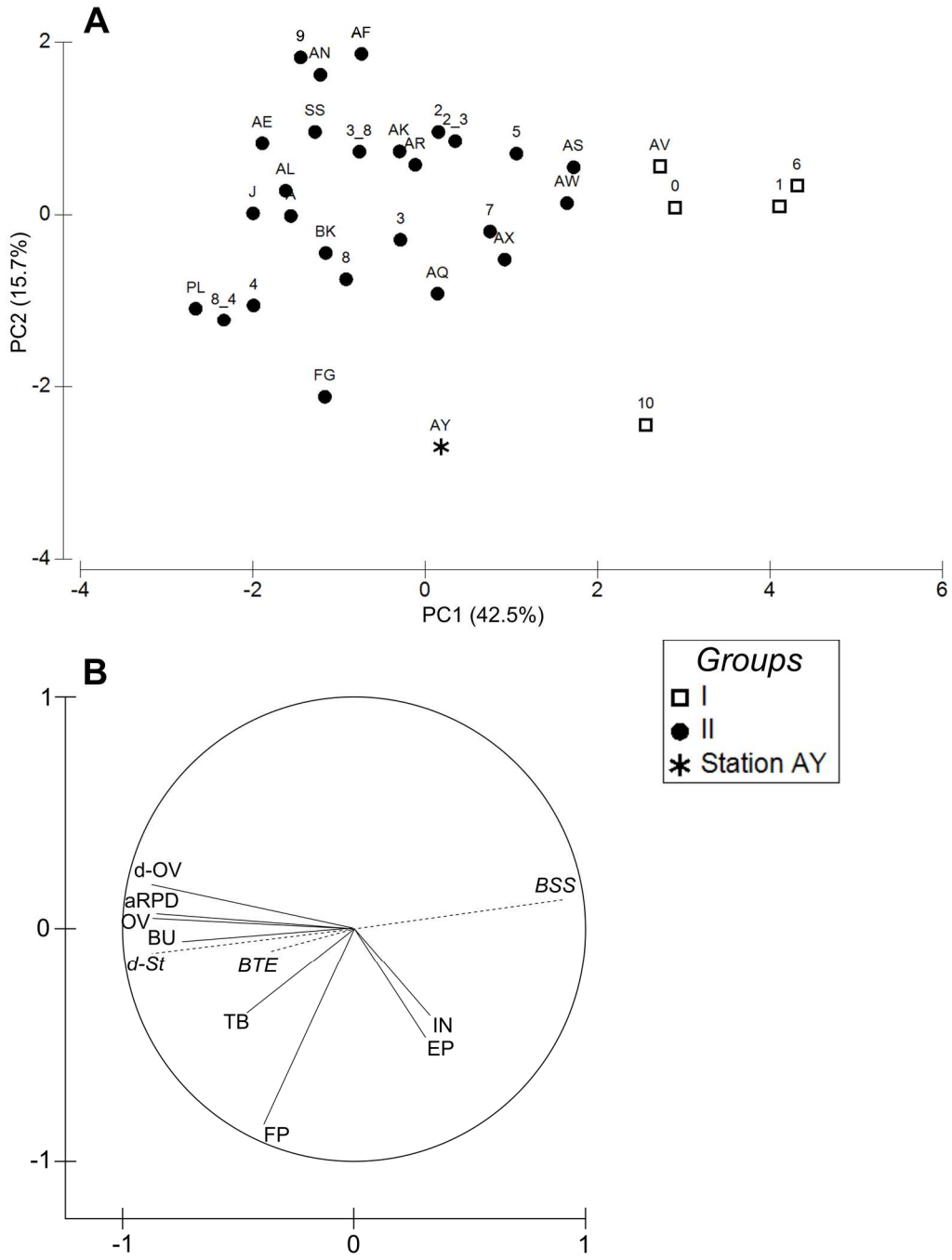

Figure 1.8. Principal component analysis based on normalized mean SPI characteristics (aRPD: aRPD thickness; BU: number of burrows; OV and d-OV: number and maximal depth of oxic voids; FP: number of feeding pits; TB: tubes; EP: epifauna and IN: infauna). Projection of stations on the first plane of the PCA (**A**), and correlations of the variables with its first two components (**B**). Station depth (*d-St*), Bottom Shear Stress (*BSS*), and Bottom Trawling Effort (*BTE*) were used as supplementary variables. Group identification was achieved through the coupling of hierarchical clustering with a SIMPROF procedure. Station codes are the same as in Figure 1.1 and Table A1.

Hierarchical clustering and the associated SIMPROF procedure resulted in the identification of three groups of stations (Figure 1.8A), one of them including only a single station. Group I was composed of five of the seven shallowest stations (i.e., stations 0, 1, 6, 10, and AV), and group II was composed of all other stations except station AY due to a high number of epifauna. The SPI characteristics accounting most for differences between groups I and II were (1) aRPD thickness (22.3%), (2) oxic void maximal depth (22.0%), (3) burrow number (14.4%), and (4) oxic void number (13.5%). The coordinates of stations on the first axis of the PCA correlated significantly with station depth at the scale of both the whole WGMP and its sole distal part (n = 32, R^2 = 0.757, p < 0.001; n = 25, R^2 = 0.601, p < 0.001; respectively).

Mud clasts were observed in 80 out of 186 SPIs, whereas furrows were recorded on only two images and surface puzzle fabrics were never observed. SPIs from five of the shallowest stations did not show any of these traces at all (Figure 1.7D). There was otherwise high among-station variability in the proportion of SPI containing such features. The proportion of SPI featuring traces indicative of bottom trawling correlated significantly with station depth at the scale of the whole WGMP, but this correlation was not significant within the sole distal part (Table A2).

3.4. Bottom Shear Stress and Bottom Trawling Effort

BSS 95th percentiles significantly decreased with station depth at the scale of the whole WGMP and of its sole distal part (Figure 1.9A,B and Table A2). Their values within cells containing sampled stations were between 0.42 at station J and 1.10 N·m^{-2} at station 0 (Figure 1.9B and Table A1). In the distal part, POC, Phaeo-*a*, and THAA correlated negatively with BSS 95th percentiles. This was also the case for six (i.e., aRPD thickness; numbers of oxic voids, feeding pits, tubes; maximal depth of oxic voids; and total number of biological traces; Table A3) of the 10 SPI characteristics assessed during the present study. Moreover, at the scale of the sole WGMP distal part, the coordinates of stations on the first axis of the PCAs based on both surface sediment and SPI characteristics correlated significantly with BSS (n = 24, R^2 = 0.348, p = 0.002; and n = 25, R^2 = 0.547, p < 0.001; respectively).

Bottom Trawling Effort (BTE) tended to be higher in the WGMP than in adjacent areas (Figure 1.9C). It was low in the shallowest part (i.e., 35 < z < 50 m) of the WGMP. Deeper, BTE was highly heterogeneous with some cells being heavily trawled between 55 and 60 m depth

(i.e., up to 39.6 h·km^{-2}·y^{-1} and 12.9 times trawled·y^{-1}; Figures 1.9C), while some others were only lightly affected. BTE within cells containing sampled stations was between 0.48 and 19.4 h·km^{-2}·y^{-1} (0.2 and 6.3 times trawled.y^{-1} for stations AN and 3-8, respectively; Figure 1.9D and Table A1). Four sampled stations (3-8, BK, PL, and FG) were located in cells featuring a BTE higher than 10 h·km^{-2}·y^{-1} (Figure 1.9D and Table A1). BTE within cells containing sampled stations correlated positively with station depth at the scale of the whole WGMP, but this correlation was not significant in the sole distal part (Table A2).

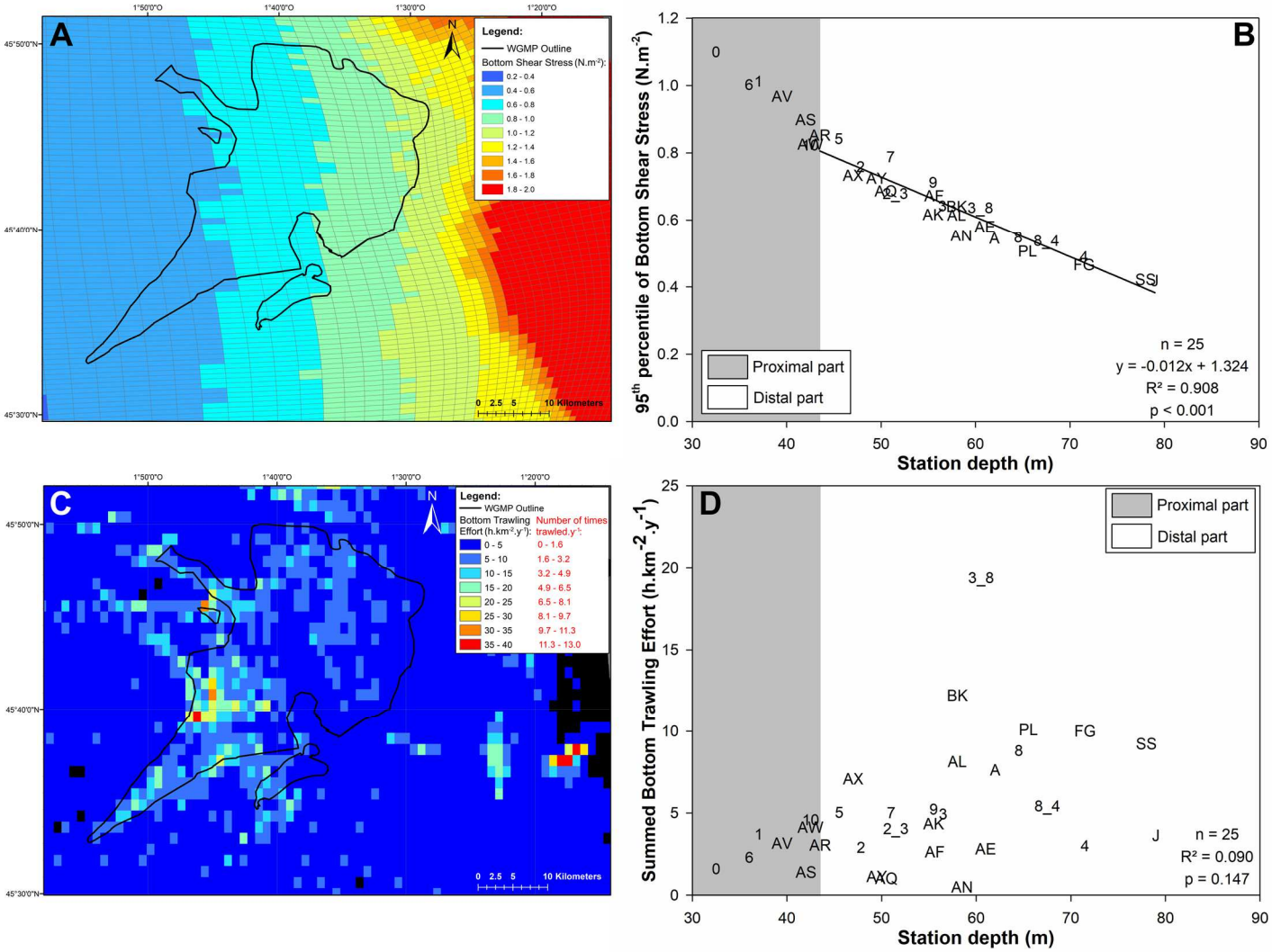

Figure 1.9. Spatial mapping of 95th percentile of Bottom Shear Stress during the year preceding the JERICOBENT-5 cruise (**A**), relationship with station depth within cells including sampled stations (**B**), summed Bottom Trawling Effort during the year preceding the JERICOBENT-5 cruise (**C**), and relationship with station depth within cells including sampled stations (**D**). Gray areas represent the proximal part (z < 42.5 m) of the WGMP. Station codes are the same as in Figure 1.1 and Table A1.

In the distal part, there was no significant correlation between BTE and any surface sediment or SPI individual characteristic (including the proportion of SPI featuring traces

indicative of bottom trawling), except for (1) $\delta^{13}C$, (2) Chl-*a*/(Chl-*a* + Phaeo-*a*), and (3) numbers of tube and total biological traces (which was largely affected by tube number; Table A3). Moreover, at the scale of the sole WGMP distal part, the coordinates of stations on the first axis of the PCAs based on both surface sediment and SPI characteristics did not correlate significantly with BTE (n = 24, R^2 = 0.003, p = 0.813; and n = 25, R^2 = 0.038, p = 0.347; respectively).

3.5. Comparison with the Rhône River Prodelta

The relationships between station depth and $D_{0.5}$, THAA, Chl-*a*/(Chl-*a* + Phaeo-*a*), and $\delta^{13}C$ in both the distal part of the WGMP and the Rhône River Prodelta (RRP) show clear differences between the two systems (Figure 1.10).

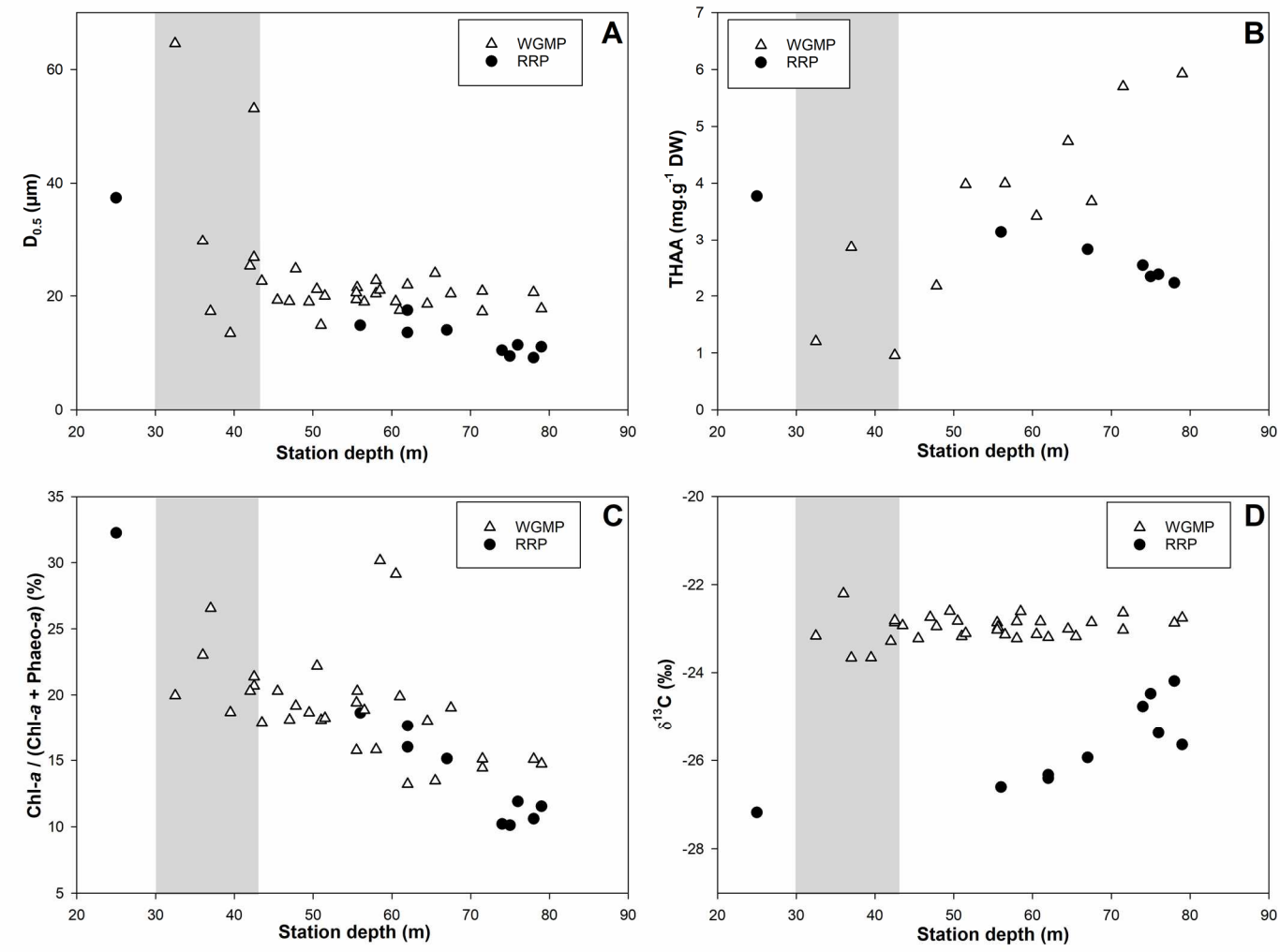

Figure 1.10. Relationships between station depth and main surface sediment characteristics in the WGMP and the Rhône River Prodelta (RRP): $D_{0.5}$ (**A**), Total Hydrolyzable Amino Acids (THAA (**B**)), Chl-*a*/(Chl-*a*+Phaeo-*a*) ratio (**C**), and $\delta^{13}C$ (**D**). Gray areas represent the proximal part of the WGMP (z < 42.5 m).

With the exception of the RRP shallowest station, surface sediments were significantly ($p < 0.001$) coarser in the distal part of the WGMP (mean $D_{0.5}$ of 20.2 µm) than in the RRP (i.e., mean $D_{0.5}$ of 12.0 µm; Figure 1.10A). Mean THAA concentrations were significantly higher in the distal part of the WGMP than in the RRP (mean values and standard deviations of 4.20 ± 1.23 mg·gDW^{-1} and 2.75 ± 0.55 mg·gDW^{-1}, respectively; p = 0.013). Moreover, changes in THAA concentrations relative to station depth showed opposite patterns in the two systems with increasing values with increasing depth in the distal part of the WGMP and decreasing values with increasing depth in the RRP (Figure 1.10B). The same result was found after standardization for $D_{0.5}$. Similar discrepancies between systems were found for POC and EHAA concentrations even though mean POC concentrations were significantly lower in the distal part of the WGMP (1.09 ± 0.24 vs. 1.39 ± 0.29%DW in the RRP; $p = 0.021$), and mean EHAA concentrations did not significantly differ between systems (0.76 ± 0.13 vs. 0.77 ± 0.19 mg·gDW^{-1}, in the distal part of the WGMP and the RRP, respectively; $p = 0.846$). Chl-*a*/(Chl-*a* + Phaeo-*a*) ratio significantly decreased with increasing station depth in both systems (Figure 1.10C) with no significant difference in their mean values ($p = 0.105$). EHAA/THAA ratios did not correlate significantly with station depth in either system ($p = 0.202$ and $p = 0.950$ in the distal part of the WGMP and the RRP, respectively). Their mean value was significantly lower in the distal part of the WGMP than in the RRP (19.8 ± 3.4% and 27.7 ± 1.5%, respectively; $p < 0.001$). The pattern of changes in $\delta^{13}C$ relative to station depth clearly differed between systems with significantly increasing values with increasing station depth in the RRP ($p = 0.005$) and no significant change in the distal part of the WGMP. Their mean value was significantly ($p < 0.001$) less negative in the WGMP (−22.9‰) than in the RRP (−25.7‰).

The relationships between station depth and (1) aRPD thickness, (2) total number of biological traces per SPI, and (3) depth of oxic voids in both the distal part of the WGMP and the RRP are shown in Figure 1.11. The two systems presented strong differences. aRPD thickness increased with station depth in both the distal part of the WGMP and in the RRP ($p = 0.003$ and $p = 0.002$, respectively; Figure 1.11A), but its mean was significantly higher in the distal part of the WGMP (74.8 ± 11.7 vs. 37.0 ± 18.1 mm in the RRP; $p < 0.001$). The mean total number of biological traces was also significantly higher in the distal part of the WGMP (Figure 1.11B; 19.1 ± 5.9 vs. 4.7 ± 2.2 per SPI in the RRP; $p < 0.001$). There were similar differences for the mean numbers of burrows, oxic voids, and tubes ($p < 0.001$ in all cases). Mean oxic void depth significantly increased with station depth in the RRP ($p = 0.022$) but not in the distal part of the WGMP ($p = 0.745$). Its mean value was also significantly higher, although to a lower

extent, in the distal part of the WGMP (Figure 1.11C; 86.7 ± 15.0 vs. 68.5 ± 29.4 mm, in the RRP; p = 0.023).

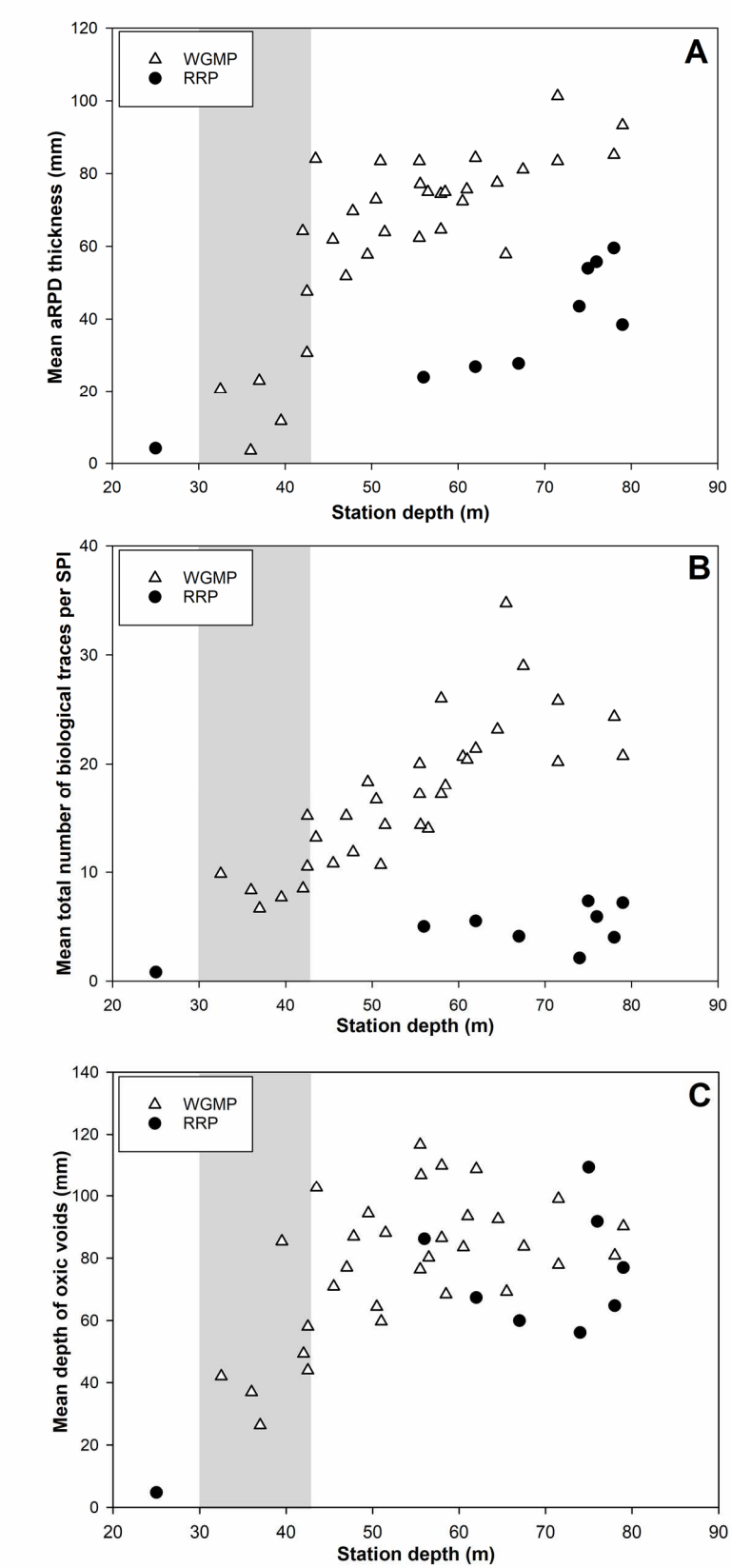

Figure 1.11. Relationships between station depth and mean main SPI characteristics in the WGMP and the RRP: aRPD thickness (A), total number of biological traces per SPI (B), and depth of oxic voids (C). Grey areas represent the proximal part of the WGMP (z < 42.5 m).

4. Discussion

4.1. Spatial Structuration

4.1.1. Subdivision between Proximal and Distal Parts

Up to now, only two studies have considered the spatial distribution of surface sediment grain size and organic contents in the West Gironde Mud Patch (WGMP; [44,45]). Both studies relied on the sampling of only three stations, and their results supported the original [26,34,40] distinction between a proximal and a distal part. Our sampling plan was based on 32 stations, which allowed showing a significant correlation between surface sediment characteristics (as summarized by the first component of the corresponding PCA) and station depth. Data analysis resulted in the identification of three main groups of stations presenting different surface sediment characteristics. Stations of groups I (together with stations 1, 6, and AV) were all shallow ($z < 42.5$ m) and tended to present coarse surface sediments and low concentrations in Particular Organic Carbon (POC) and chloropigments. A high between-station variability in $D_{0.5}$ and Sediment Surface Area (SSA) was nevertheless recorded in this group, most likely reflecting spatial differences in the transient deposition of coarse sediments [25,26,40] as observed during the present study on the Sediment Profile Images (SPIs) collected at station 0. Therefore, our results clearly support that the stations of group I, and associated isolated stations are constitutive of the proximal part of the WGMP as stated by Jouanneau et al. [35] and Lesueur et al. [26,34].

The spatial zonation of the WGMP has also been studied based on X-rays radiographies of long sediment cores [26,34,35,40,43]. Lesueur and Tastet [43] computed a crude index of bioturbation (i.e., the proportion of reworked sediment volume) based on these radiographies. They proposed to subdivide the WGMP in three parts based on the values of this index, which increased with station depth. The shallowest part could be considered as mostly representative of the proximal and the two others of the distal part (Lesueur and Tastet [43]). However, this conclusion clearly suffered from (1) the inability of X-rays radiographies to precisely assess bioturbation and (2) the use of long sediment cores, which did not allow for the preservation of the sediment–water interface. The X-rays radiographies collected during the present study were achieved on cores collected using a lightweight interface corer, which allowed for a better preservation of this interface. Results confirmed previous observations in showing (1) the occurrence of sandy layers in the top sediment column of the

three stations sampled within the proximal part (see above); (2) the presence, especially at shallow stations, of laminae attributed by Lesueur and Tastet [43] to the deposition of dense and coarse particles following high energy events; and (3) a limitation of bioturbation to the top of the sediment column at shallow stations, whereas the thickness of the mixed sediment layer was clearly higher at deep stations. During the present study, we also used Sediment Profile Imagery, which allowed for (1) an in situ 2D visualization of the sedimentary column without disturbing the sediment–water interface and (2) a multiparametric assessment of modern bioturbation through the analysis of biological traces [63]. This resulted in the identification of two main groups of stations delimited by a ca. 42.5 m depth threshold, which further supports the distinction between a proximal part where bioturbation is limited and a distal part where it is much higher (Figure 1.7A–C).

4.1.2. Spatial Structuration of the Distal Part

Previous sedimentological surveys have shown the occurrence of two major depth gradients in the distal part [26,34,35,40,43]. The first related to the frequency of occurrence of erosional surfaces and subsequent vertical decreasing granulometric sequences (see above), and the second related to bioturbation. However, these surveys did not account for modern biogeochemical processes taking place in the top of the sediment column. This issue was tackled by Relexans et al. [44] and later by Massé et al. [45] based on the analyses of surface sedimentary organics and benthic fauna composition. However, results remained largely inconclusive regarding the possible existence of spatial gradients due to limited sampling efforts.

During the present study, we sampled 25 stations within the distal part. Based on the multivariate analysis of their surface sediment characteristics, these stations were mostly distributed among two main groups, which were clearly related to station depth as confirmed by the significance of the correlations linking station depth with (1) POC, THAA, and Phaeo-*a* concentrations and (2) the coordinates of stations on the first component of the PCA based on surface sediment characteristics within the distal part of the WGMP. A significant correlation was also found for the Chl-*a*/(Chl-*a* + Phaeo-*a*) ratio when excluding two outliers. Thus, our results clearly support the occurrence of a depth gradient in surface sediment characteristics within the distal part of the WGMP. This gradient was linked to changes in

sedimentary organic characteristics and independent of changes in sediment granulometry, since all organic concentrations were normalized to SSA.

The two statistical approaches used to assess the existence of a potential depth gradient based on SPI characteristics led to apparently different conclusions. On the one hand, regression analyses showed significant correlations between most individual characteristics and station depth, and there was a significant correlation between station depth and station coordinates on the first component of the PCA based on SPI characteristics. On the other hand, the hierarchical clustering based on the whole set of SPI characteristics together with the associated SIMPROF procedure failed to identify significantly differing station subgroups. Most of the assessed individual SPI characteristics correlated significantly with station depth, and for five of them, this was indicative of an increase in bioturbation with station depth. This trend was particularly marked for (1) sediment oxidation (aRPD), (2) burrowing (oxic void number), and (3) thickness of the mixed sediment layer (oxic void maximal depth). Conversely, neither infauna nor burrow numbers did significantly correlate with station depth. For infauna, this may result from undersampling. For burrow number, this probably results from (1) large spatial extensions at highly bioturbated deep stations, which complicates the distinction between burrows and may induce an underestimation of their number; and (2) stronger difficulties in identifying burrows (i.e., oxidized structures) within sediment columns featuring thicker aRPDs at deep stations. Interestingly, the positive correlation with station depth was more pronounced for the total number of biological traces (although this last parameter included the epifauna number, which correlated negatively with station depth) than for any SPI individual characteristic. This can be interpreted as a reduction (by summation) of the lack of fit of the regression models linking station depth and individual SPI characteristics, which further supports the existence of a gradient of increasing bioturbation along the depth gradient within the distal part of the WGMP. The fact that hierarchical clustering based on SPI characteristics did not allow differentiating station subgroups is likely caused by (1) the use of normalized data, which resulted in the attribution of the same weight to all considered parameters, including those that did not correlate significantly with station depth (i.e., burrow and infauna numbers); and (2) the noise generated by the lack of fit of the regression models linking station depth and individual SPI characteristics, which differed between characteristics for a given station (as exemplified above for the total number of biological traces). Therefore, our interpretation of SPI data is that they also support the existence of a depth gradient of increasing bioturbation within the distal part.

4.1.3. Overall Conclusion

Based on a wide range of surface sediment characteristics and the use of an image analysis technique specifically designed for the top of the sediment column, our results clearly confirm the subdivision of the WGMP in a proximal and a distal part put forward by previous sedimentological surveys and support the proposed 40–45 m depth limit between these two parts [26,43]. They also show the existence of a depth gradient resulting from modern sedimentation and bioturbation processes taking place in the distal part of the WGMP.

4.2. Disentangling the Potential Effects of Hydrodynamics and Bottom Trawling

The potential impacts of hydrodynamics and bottom trawling on the spatial distributions of surface sediment and SPI characteristics were tested by the simultaneous assessments of the spatial distributions of (1) Bottom Shear Stress (BSS), (2) Bottom Trawling Effort (BTE), (3) surface sediment characteristics, and (4) SPI features. When considering the whole WGMP, the correlations between both BSS and BTE with station depth impaired the unraveling of the role of these two factors in controlling the spatial distribution of surface sediment and SPI characteristics. More generally, the correlation between environmental characteristics and fishing effort clearly constitutes a major issue when assessing the impact of benthic trawling on benthic systems [23,83,84]. During the present study, this difficulty was overcome by considering spatial changes recorded in the sole distal part where (1) BTE did not correlate significantly with station depth, (2) the ranges of $D_{0.5}$ and SSA were narrower, and (3) none of these two parameters correlated significantly with both BSS and BTE (see Queirós et al. [24] for a similar approach).

The 95th BSS percentiles recorded during the present studies were between 0.4 and 1.1 N.m^{-2}. These values can be compared with those computed in the Gulf of Lions using a similar model (i.e., a 90th percentile around 0.05 N·m^{-2} at a 30 m depth; [85]). Moreover, based on simultaneous assessments of BSS and Suspended Particulate Matter concentration, Dufois et al. [78] concluded that resuspension was induced over a critical BSS threshold of 0.35 N·m^{-2} at a 20 m deep station within the Rhône River Prodelta. Although caution should clearly be taken since sediment roughness and rheological properties were not assessed during the present study, this supports the hypothesis according to which sediment resuspension may take place over the whole WGMP [47]. Moreover, the 95th percentile value of BSS correlated negatively with station depth, which largely corresponded to the dominance of its wave-

induced component relative to its current-induced component and is also coherent with the dominant role attributed to waves in controlling the spatial structuration of the WGMP [26]. Although collected over different periods (June 2017–June 2018 vs. 2005–2013) and using different positioning systems (i.e., Automatic Identification System vs. Vessel Monitoring System), the absolute values and the spatial distribution of BTE observed during the present study were fully consistent with the one reported by Mengual et al. [19,20]. BTE was clearly higher within the distal part with a maximal average number of times trawled.y^{-1} of 12.9.

Several lines of evidence suggest that the effect of bottom trawling on the spatial distributions of both surface sediment and SPI characteristics was limited as compared to the influence of hydrodynamics. First, there were significant correlations between three (four when excluding the two above-mentioned outliers for Chl-*a*/(Chl-*a* + Phaeo-*a*)) of surface sediment characteristics and BSS, whereas only $\delta^{13}C$ (although featuring a very restricted range of variation) and Chl-*a*/(Chl-*a* + Phaeo-*a*) (when excluding the two above-mentioned outliers) correlated significantly with BTE. Second, most of the SPI individual characteristics correlated negatively with BSS, whereas the number of tubes was the only individual SPI characteristic significantly correlating with BTE. Furthermore, this last result is not supporting a strong effect of bottom trawling, since BTE is generally assumed to negatively impact benthic bioturbation [24,83,84,86–89]. Along the same line, the correlation between tube number and BTE was positive, which here again is not supporting a strong influence of bottom trawling, since according to the literature, tube-building species tend to be rare or even absent in trawled areas [61,62,90]. Third, stations coordinates of the PCAs based on both surface sediment and SPI characteristics correlated significantly with BSS, but not BTE. Fourth, the incorporation of BTE with BSS in multiple regression models did not improve the description of either the surface sediment or the SPI characteristics assessed during the present study. None of the correlations that were not significant using BSS alone as the independent variable became significant when incorporating BTE as a second independent variable. Moreover, for most characteristics correlating significantly with BSS alone (i.e., all except tube number and total number of biological traces), the incorporation of BTE resulted in poorer descriptions. Therefore, BTE did not account as well for changes in surface sediment and SPI characteristics assessed not described by changes in BSS.

Overall, the only rationale for a significant impact of bottom trawling was the sometimes high (i.e., up to ca 80%) proportion of SPI featuring trawling traces. However, these proportions were highly variable between stations and did not correlate significantly with BTE.

Moreover, the trawling traces recorded during the present study almost exclusively consisted in mud clasts with almost no furrows and no puzzle fabrics at all. This is an important point, since the direct causality linking bottom trawling and the presence of mud clasts appears still questionable [91,92]. For example, similar proportions of SPI featuring trawling traces (including mud clasts) have been reported in several areas of the Gulf of Lions experimenting different BTE [61,62,93], which further highlights the difficulty in unambiguously associating the presence of mud clasts with bottom trawling.

Based on these rationales, our overall conclusion is that the assessment of the spatial distributions of both SPI characteristics and BTE recorded during the present study does not support the hypothesis according to which bottom trawling is a key factor in controlling the spatial structuration of the WGMP. However, it should be pointed out that this conclusion may partly result from differences in spatial scales associated with the assessments of BTE (i.e., a few km^2) and SPI characteristics (i.e., typically a few m^2). BTE is known to induce spatially heterogeneous effects on benthic habitats even within experimentally heavily trawled areas [94], which led Smith et al. [95] to recommend collecting a high number of SPIs (i.e., ca. 30, which is much more than achieved during the present study) at each station to infer the impact of bottom trawling (see also [86,96], for the interest of complementary approaches). BTE was not spatially homogeneous over each of the 1.77 km^2 cells considered during the present study, which may have hampered the detection of significant correlations between BTE and both surface sediment and SPI characteristics measured over much smaller spatial scales. Differences in temporal scales associated with the assessment of BTE (i.e., one year during the present study) and the kinetics of recovery of benthic habitats may have had the same effect as well.

4.3. Comparison with the Rhône River Prodelta

4.3.1. Surface Sediment Characteristics

$\delta^{13}C$ values differed between the distal part of the WGMP and the Rhône River Prodelta (RRP) regarding both their absolute values and their changes relative to station depth. In the RRP, $\delta^{13}C$ ranged from −24.2% to −27.2‰ and significantly increased with station depth, whereas in the distal part of the WGMP, they were close to −23‰ and did not change significantly with station depth. In the RRP, these results have been interpreted as reflecting the dominance of a continental source of organic matter and its gradual mixing with marine

sources through a series of resuspension/sedimentation events occurring within the prodelta itself [74,81,97–99]. In the WGMP, $\delta^{13}C$ values around −23‰ have been reported in suspended particulate material both at the Mouth of the Gironde Estuary and in the inner part of the Bay of Biscay Continental Shelf [100]. These values were interpreted as resulting from an early mixing between (1) a continental/terrestrial source (with a mean $\delta^{13}C$ of −25.9‰), (2) estuarine sources generated by autochthonous processes due to long estuarine residence times [101,102], and (3), a marine planktonic source (with a mean $\delta^{13}C$ of −20.5‰). Such an early mixing within the Gironde Estuary is largely resulting from its macro-tidal regime [100,103]. Our own results support this interpretation and suggest the lack of subsequent significant mixing with marine sources in the WGMP itself. Overall, the discrepancies in the $\delta^{13}C$ between the two systems are indicative of major differences in the timing and the nature of the processes involved in the mixing of continental and marine sources of sedimented Particulate Organic Matter (POM).

Our results show a lack of correlation between station depth and $D_{0.5}$ and the presence of coarser sediment in the distal part of the WGMP, despite a lower water discharge and a long (i.e., 1–2 years in the Estuarine Turbidity Maximum) particle residence time in the Gironde Estuary [104,105]. There were also marked differences between systems in both sedimentary organics concentrations and their changes relative to station depth. THAA concentrations were higher in the WGMP, where they increased with station depth conversely to what was observed in the RRP. Such opposite patterns were also observed for POC and, to lesser extent, EHAA. In the RRP, spatial changes in $D_{0.5}$ and surface sediment concentrations were interpreted as resulting from (1) a particle sorting relative to size induced by the succession of sedimentation/resuspension events [106] and (2) the progressive dilution of a highly dominant continental POM source originating from the Rhône River [55,56,74,81,97–99]. The Gironde River is also the dominant source of particles fueling the WGMP [31,32,41], and successive sedimentation/resuspension events are largely responsible for the transfer of particles at depth in this system as well [26]. Therefore, the same two key driving factors are inducing major differences in the spatial structuration of the two systems. The lack of depth gradient in particle size in the distal part of the WGMP suggests that particle sorting is not predominantly controlled by particle size in the WGMP. Density may constitute an alternative sorting cue as suggested by the preferential sedimentation of denser particles following major resuspension events [43]. In coastal sediments, low-density particles are organically enriched and behave similar to smaller ones with regard to particle sorting [107]. Therefore, a density-

driven particle sorting could account for the depth gradients observed in the distal part of the WGMP; low-density (and organically enriched) particles being preferentially settled and trapped in deeper areas irrespective of their size, which would account for increasing bulk organic concentrations with station depth. At this stage, this only constitutes a working hypothesis, and it will certainly prove interesting to assess spatial changes in the proportion of low-density particles during future studies taking place in the WGMP.

EHAA/THAA ratios were lower in the distal part of the WGMP than in the RRP. This is indicative of a lower lability of sedimented POM, which may be linked to the long residence time of particles in the Gironde Estuary [104,105] and the predominance of degradation processes in its Estuarine Turbidity Maximum [101,108–110]. Conversely Chl-*a*/(Chl-*a* + Phaeo-*a*) ratios did not significantly differ between areas. These two indices showed the same pattern of change relative to station depth in both systems with (1) a significant decrease in Chl-*a*/(Chl-*a* + Phaeo-*a*) ratios and (2) no significant change in EHAA/THAA ratios. In the RRP, the discrepancy between the two indices has been attributed to the fact that the Chl-*a*/(Chl-*a* + Phaeo-*a*) ratio is representing a highly labile vegetal fraction of the sediment POM, whereas the EHAA/THAA ratio is representative of the lability of the bulk nitrogenous fraction of sedimentary organics [56,57]. This suggests that both in the WGMP and the RRP, degradation processes occurring during the transfer of deposited particles at depth are mostly affecting a highly labile fraction of POM. Since this component is contributing only to a small fraction of bulk sedimentary organics, this is also in agreement with the lack of significant changes in $\delta^{13}C$ with station depth.

Overall, the WGMP and RRP present strong similarities. Both are alimented by particles originating from major rivers. Moreover, the transfer of particles along their depth gradient is cued by sorting processes associated with the succession of sedimentation and resuspension sequences. Major differences between the two systems first refer to the tidal regime and marine hydrodynamics, which result in a much earlier mixing between continental and marine POM in the Gironde estuarine system. More specifically, this mixing is largely taking place in the RRP itself and conversely upstream the WGMP, namely in the Gironde Estuary and near its mouth. Other major differences between the two systems are linked to sedimentary organic concentrations and their patterns of change relative to station depth. We hypothesized that this may result from different particle sorting processes (i.e., mostly cued by particle size and particle density in the RRP and the WGMP, respectively) associated with

successive sedimentation/resuspension events. These differences support the distinction between type 1 and type 2 prodeltas [3,5] for temperate areas.

4.3.2. Bioturbation

In both systems, the aRPD thickness, the total number of biological traces, and the thickness of the bioturbated layer increased with station depth in accordance with the negative impact of disturbance on bioturbation described by the Pearson and Rosenberg [111] and Rhoads et al. [12] models. However, the nature of the dominant disturbance itself differs between systems. In the RRP, the shallowest stations are mostly submitted to high sedimentation rates [74,79,80,112] and associated organic matter inputs caused by river floods [56]. This results in sediment instability and organic enrichment, which largely affect benthic macrofauna composition and limit bioturbation [56]. In the distal part of the RRP, continental inputs are diluted and sediment stability is higher, which results in increasing bioturbation. In the proximal part of the WGMP, strong Bottom Shear Stress (BSS) precludes modern sedimentation [25,26]. It also largely controls the composition of resident fauna, which is largely dominated by suspension feeders (mostly the small-sized bivalve *Kurtiella bidentata* and the ophiuroid *Amphiura filiformis*; [45]) that are not efficient bioturbators under such environmental conditions.

There were also important differences in bioturbation between the distal parts of the WGMP and the RPP. These differences refer both to overall intensity and change relative to station depth. In the distal part of the WGMP, bioturbation intensity tended to increase with station depth together with decreasing BSS, which is coherent with the Rhoads et al. [12] model. Conversely, in the distal part of the RRP, there was no clear correlation between station depth and bioturbation intensity. Salen-Picard et al. [113] reported the existence of a positive impact of Rhone River floods on the abundance of subsurface feeders (i.e., potentially strong bioturbators) at a 70 m deep station with a time lag of ca. 33 months. Therefore, the lack of significant correlation between bioturbation intensity with station depth in the distal part of the RRP may result from opposite gradients in three potentially controlling factors, namely: (1) organic matter availability, which decreases with station depth; (2) the positive impact of floods on the abundance of strong bioturbators, which also decreases with station depth; and (3) sediment stability, which conversely increases with station depth. According to this hypothesis, the lack of gradient in bioturbation intensity in relation with station depth

would result from an equilibrium between organic matter availability and sediment stability and therefore conforms to the Rhoads et al. [12] model.

Differences between overall bioturbation intensities between systems are not easy to account for. According to the Rhoads et al. [12] model, bioturbation intensity results from the interaction between organic matter availability (eventually through its effect on benthic macrofauna) and physical disturbances [12]. POC sediment concentrations were quite similar in both areas, which was also true for amino acid concentrations when accounting for their bioavailability (i.e., EHAA). The comparison of benthic macrofauna abundance, biomass, and feeding types between systems is clearly complicated by the fact that they were not sampled using the same gear (i.e., an Hamon grab for Massé et al. [45] vs. a Van Veen grab for Bonifacio et al. [56]). Nevertheless, it showed no obvious difference in the nature and abundance of major potential bioturbators. During the present study, we considered the effect of hydrodynamics, sedimentation, and bottom trawling as potential sources of physical disturbances within the WGMP. Therefore, these three sources of physical disturbances could also account for differences between systems. As exemplified by differences in (1) WGMP and RRP morphologies [5], and (2) the upper depth limit allowing for modern sedimentation [25,26,114], hydrodynamics is stronger in the WGMP and therefore cannot directly account for higher bioturbation intensity in this area. Conversely, sedimentation rates are higher in the RRP; however, they decrease with depth to reach ca. 0.63 $cm.y^{-1}$ at 73 m [114,115], which is close to the sedimentation rates (i.e., between 0.15 and 0.50 $cm.y^{-1}$) recorded in the WGMP between 45 and 71 m [25,26]. Therefore, it is unlikely as well that differences in sedimentation can account for differences in bioturbation intensity between systems. Automatic Identification System (AIS) data collected by Global Fishing Watch [69,70] are available only since 2012. Therefore, we computed the spatial distribution of BTE in the Rhône River for the June 2017–June 2018. Results (available on request to B.L.) showed an overall higher (i.e., by a factor of 2.3) BTE in the RRP than in the WGMP. However, the spatial distribution of BTE clearly differed between systems. BTE was maximal in the shallowest part of the RRP and then decreased with depth so that it was not higher in the distal part of the RRP than in the WGMP. Assuming stability in BTE in the RRP between 2007 and 2017, therefore, our conclusion is that differences in the intensity of the physical disturbance caused by bottom trawling are probably not responsible for differences in bioturbation intensity between systems as well.

Overall, the identification of the cause of difference in bioturbation intensities between the WGMP and RRP distal parts will clearly require additional studies. There are

several ways forward: (1) the comparative assessment of sediment mechanical properties (Dorgan et al. [116]) in both systems, (2) the refinement of the comparison of benthic macrofauna composition through the use of the same sampling gear (see above), and (3) considering the temporal dynamics of bioturbation in both systems. Within the WGMP, Jouanneau et al. [35] indeed described the alternation of calm periods during which bioturbation is high and periods following strong storms during which bioturbation traces are destroyed. Along the same line, Bonifacio et al. [56] showed that river floods induce a quick (i.e., within 1–2 months) change in bioturbation within the RRP. Considering possible impacts of temporal dynamics may be important as well for all parameters/processes considered during the present study. This could be tackled by seasonally sampling along a depth gradient as already achieved for the RRP by Bonifacio et al. [56].

5. Conclusions

Our results first support the spatial subdivision of the West Gironde Mud Patch (WGMP) in a proximal and a distal part. They also show the existence of depth gradients in surface sedimentary organics characteristics and bioturbation within the distal part and suggest that these gradients are more related to hydrodynamics than bottom trawling. The comparison with the Rhône River Prodelta finally highlights major discrepancies. These discrepancies refer to (1) the mixing of continental and marine sources of particulate organic matter that is taking place in the Gironde Estuary versus the Rhône River Prodelta itself, and (2) opposite patterns of changes in sedimentary organic concentrations relative to depth, which may result from particle sorting processes during sedimentation/resuspension cycles mainly cued by particle size in the Rhône River Prodelta and density in the WGMP. Overall, our results support the distinction between type 1 and type 2 river-dominated ocean margins [3,5] in temperate areas.

Author Contributions: Conceptualization, B.L., B.D. and A.G.; Data curation, B.L.; Formal analysis, B.L. and A.G.; Funding acquisition, B.D. and A.G.; Investigation, B.L., B.D., S.S., N.D., G.B. and A.G.; Methodology, B.L., B.D., S.S., M.D., F.G. (Florent Grasso), A.S., H.G. and A.G.; Project administration, A.G.; Resources, B.L., B.D., A.G.D., S.S., A.R.-R., F.G. (Frédéric Garabetian), N.D., M.D., F.G. (Florent Grasso), A.S., G.B., H.G., M.-A.C., D.P., P.L., H.D., M.D.

and M.M.B.T.; Software, B.L., A.G.D., A.R.-R., M.D., F.G. (Florent Grasso) and H.G.; Validation, B.L., B.D. and A.G.; Visualization, B.L. and A.G.; Writing—original draft, B.L. and A.G.; Writing—review and editing, B.L., B.D., S.S., A.R.-R., F.G. (Frédéric Garabetian), F.G. (Florent Grasso), A.S., G.B. and A.G. All authors have read and agreed to the published version of the manuscript.

Funding: This work is part of the PhD thesis of Bastien Lamarque (Bordeaux University). Bastien Lamarque was partly supported by a doctoral grant from the French "Ministère de l'Enseignement Supérieur, de la Recherche et de l'Innovation". This work was supported by: (1) the JERICO-NEXT project (European Union's Horizon 2020 Research and Innovation program under grant agreement no. 654410), (2) the VOG project (LEFE-CYBER and EC2CO-PNEC), and (3) the MAGMA project (COTE cluster of Excellence ANR-10-LABX-45). It also benefited from additional fundings allocated by the Conseil Régional Nouvelle Aquitaine and the Agence Française de la Biodiversité. Operations at sea were funded by the French Oceanographic Fleet.

Data Availability Statement: The data presented in this study are available in SEANOE at https://doi.org/10.17882/78991, [117].

Acknowledgments: The authors wish to thank the crew of the R/V Côtes de la Manche for their help during field sampling, Céline Labrune for sharing Rhône River Prodelta SPI data, and Marie Claire Perello and Pierre Touzerie for their help in the analysis of some samples and results.

Conflicts of Interest: The authors declare no conflict of interest. The funders had no role in the design of the study; in the collection, analyses, or interpretation of data; in the writing of the manuscript, or in the decision to publish the results.

Appendix A

Table A1. Location (WGS84, degrees, and decimal minutes) and depth of the 32 sampled stations, with associated mean values (± standard deviation) of surface sediment and SPI characteristics, and Bottom Trawling Effort within cells containing stations. Station positionings are shown in Figure 1.1. $D_{0.5}$: median grain size, SSA: Sediment Surface Area, POC: Particulate Organic Carbon, Chl-*a*: Chlorophyll-*a*, Phaeo-*a*: Phaeophytin-*a*, THAA: Total Hydrolyzable Amino Acids, EHAA: Enzymatically Hydrolyzable Amino Acids, aRPD: apparent Redox Potential Discontinuity thickness, Burrows: number of burrows, OV: number of oxic voids, OV depth: maximal depth of oxic voids, Tubes: number of tubes, Feeding pits: number of feeding pits, Epifauna: number of epifauna, Infauna: number of infauna, Clasts: number of clasts, Furrows: number of furrows, BSS: 95th percentile of Bottom Shear Stress, BTE: Summed Bottom Trawling Effort.

Station	Latitude N	Longitude W	Depth (m)	$D_{0.5}$ (µm)	SSA ($m^2.gDW^{-1}$)	POC ($mg.m^{-2}$)	Chl-*a* ($µg.m^{-2}$)	Phaeo-*a* ($µg.m^{-2}$)	Chl-*a*/(Chl-*a*+Phaeo-*a*) (%)	THAA ($mg.m^{-2}$)	EHAA ($mg.m^{-2}$)	EHAA/THAA (%)	$\delta^{13}C$ (‰)	Number of SPI	aRPD (mm)	Burrows ($nb.SPI^{-1}$)	OV ($nb.SPI^{-1}$)	OV depth (mm)	Tubes ($nb.SPI^{-1}$)	Feeding pits ($nb.SPI^{-1}$)	Epifauna ($nb.SPI^{-1}$)	Infauna ($nb.SPI^{-1}$)	Clasts ($nb.SPI^{-1}$)	Furrows ($nb.SPI^{-1}$)	BSS ($N.m^{-2}$)	BTE ($h.km^{-2}.y^{-1}$)
0	45°46.465'	1°29.016'	32.5	64.6 ± 28.5	4.8 ± 0.3	1.2 ± 0.1	0.15	0.62	19.9	0.25 ± 0.01	0.05 ± 0.00	21.7 ± 1.3	-23.2 ± 0.1	6	20.6 ± 12.7	2.5 ± 1.2	2.2 ± 1.8	70.8 ± 44.7	3.5 ± 3.0	0.0 ± 0.0	0.5 ± 0.5	1.2 ± 1.2	0.0 ± 0.0	0.0 ± 0.0	1.1	1.6
1	45°45.580'	1°31.489'	37	17.3 ± 1.1	10.7 ± 0.7	1.5 ± 0.0	0.26	0.71	26.6	0.27 ± 0.04	0.05 ± 0.01	19.0 ± 0.7	-23.7	6	23.0 ± 15.0	1.2 ± 0.8	0.7 ± 0.5	39.9 ± 46.2	3.3 ± 1.9	0.0 ± 0.0	0.5 ± 0.8	1.0 ± 1.3	0.0 ± 0.0	0.0 ± 0.0	1	3.7
2	45°43.511'	1°37.773'	47.8	24.8 ± 1.4	6.1 ± 0.2	1.0 ± 0.1	0.36	1.54	19.2	0.36 ± 0.04	0.09 ± 0.00	24.5 ± 1.7	-22.9 ± 0.0	6	69.7 ± 2.2	3.8 ± 0.8	3.8 ± 2.5	119.8 ± 20.5	3.2 ± 1.6	0.0 ± 0.0	0.2 ± 0.4	0.8 ± 0.8	0.2 ± 0.4	0.0 ± 0.0	0.8	2.9
3	45°41.007'	1°41.545'	56.5	19.0 ± 0.1	8.7 ± 0.2	1.3 ± 0.0	0.28	1.2	18.8	0.46 ± 0.03	0.08 ± 0.00	17.0 ± 0.5	-23.1 ± 0.3	6	74.9 ± 9.6	3.2 ± 1.5	5.2 ± 4.9	137.8 ± 28.4	4.0 ± 2.5	0.3 ± 0.5	0.3 ± 0.5	1.0 ± 0.9	1.3 ± 2.3	0.0 ± 0.0	0.6	4.9
4	45°36.924'	1°49.712'	71.5	17.3 ± 0.6	9.8 ± 0.5	1.5 ± 0.1	0.31	1.76	15.1	0.58 ± 0.00	0.10 ± 0.01	17.0 ± 2.4	-22.6 ± 0.4	6	101.3 ± 8.8	3.0 ± 1.1	6.8 ± 2.4	137.3 ± 15.0	9.5 ± 6.1	0.7 ± 0.5	0.0 ± 0.0	0.2 ± 0.4	2.3 ± 2.3	0.0 ± 0.0	0.5	3
5	45°39.911'	1°34.866'	45.5	19.3 ± 1.9	8.2 ± 0.1	1.3 ± 0.2	0.33	1.29	20.3	n/a	n/a	n/a	-23.2 ± 0.0	5	61.9 ± 5.7	3.2 ± 0.4	3.4 ± 1.8	106.9 ± 56.4	2.6 ± 2.2	0.0 ± 0.0	0.0 ± 0.0	1.6 ± 1.3	3.2 ± 3.4	0.0 ± 0.0	0.8	5
6	45°44.412'	1°29.868'	36	29.8 ± 0.8	5.2 ± 0.3	0.7 ± 0.2	0.19	0.65	23	n/a	n/a	n/a	-22.2	6	3.5 ± 3.0	0.8 ± 1.3	0.5 ± 0.8	30.6 ± 24.0	6.3 ± 4.8	0.0 ± 0.0	0.2 ± 0.4	0.5 ± 0.5	0.0 ± 0.0	0.0 ± 0.0	1	2.3
7	45°37.189'	1°37.486'	51	14.9 ± 0.5	9.3 ± 0.3	1.4 ± 0.2	0.41	1.88	18.1	n/a	n/a	n/a	-23.2 ± 0.4	6	83.4 ± 8.4	2.3 ± 0.8	3.0 ± 2.4	131.5 ± 12.4	3.2 ± 5.0	0.2 ± 0.4	0.7 ± 0.8	1.3 ± 1.0	0.2 ± 0.4	0.0 ± 0.0	0.8	5
8	45°38.873'	1°45.777'	64.5	18.6 ± 0.2	9.1 ± 0.1	1.4 ± 0.1	0.35	1.59	18	0.52 ± 0.01	0.08 ± 0.00	15.5 ± 0.8	-23.0 ± 0.1	6	77.5 ± 11.0	2.5 ± 0.5	8.8 ± 5.9	146.4 ± 10.2	9.8 ± 5.4	0.3 ± 0.5	0.0 ± 0.0	1.7 ± 1.0	1.8 ± 3.3	0.2 ± 0.4	0.5	8.8
9	45°35.890'	1°40.157'	55.5	19.4 ± 1.4	9.1 ± 0.3	1.4 ± 0.1	0.35	1.88	15.8	n/a	n/a	n/a	-22.9 ± 0.5	6	83.4 ± 12.3	3.2 ± 1.2	11.7 ± 2.4	163.9 ± 9.7	2.0 ± 1.3	0.0 ± 0.0	0.2 ± 0.4	0.2 ± 0.4	0.3 ± 0.8	0.0 ± 0.0	0.7	5.2
10	45°44.694'	1°34.587'	42.5	26.8 ± 1.0	5.4 ± 0.8	1.3 ± 0.4	0.15	0.57	20.7	0.18 ± 0.02	0.05 ± 0.00	26.6 ± 2.0	-22.9 ± 0.5	6	30.7 ± 6.2	2.5 ± 1.0	2.7 ± 2.3	63.9 ± 38.6	1.8 ± 1.2	0.7 ± 0.8	0.2 ± 0.4	2.7 ± 2.1	0.2 ± 0.4	0.0 ± 0.0	0.8	4.6
2_3	45°42.267'	1°39.646'	51.5	20.0 ± 0.4	8.1 ± 0.1	1.2 ± 0.1	0.32	1.44	18.2	0.49 ± 0.03	0.10 ± 0.00	20.7 ± 1.2	-23.1 ± 0.0	6	63.9 ± 10.9	3.0 ± 1.4	7.0 ± 3.0	132.0 ± 20.3	2.7 ± 2.3	0.0 ± 0.0	0.0 ± 0.0	1.7 ± 1.5	0.8 ± 0.8	0.0 ± 0.0	0.7	4
3_8	45°39.919'	1°43.552'	60.5	19.1 ± 0.5	7.3 ± 0.3	1.2 ± 0.1	0.68	1.65	29.1	0.47 ± 0.03	0.11 ± 0.00	22.6 ± 1.2	-23.1 ± 0.5	6	72.4 ± 8.5	3.2 ± 1.7	8.0 ± 3.3	140.3 ± 23.3	8.5 ± 4.3	0.0 ± 0.0	0.0 ± 0.0	1.0 ± 1.1	2.3 ± 2.3	0.0 ± 0.0	0.6	19.4
8_4	45°37.929'	1°47.529'	67.5	20.4 ± 2.4	7.1 ± 1.2	1.4 ± 0.2	0.4	1.71	19	0.52 ± 0.04	0.11 ± 0.01	21.2 ± 0.3	-22.9 ± 0.0	6	81.1 ± 11.0	3.8 ± 1.0	13.0 ± 5.2	140.4 ± 12.7	10.3 ± 7.2	0.5 ± 0.5	0.0 ± 0.0	1.3 ± 1.4	2.5 ± 2.3	0.0 ± 0.0	0.5	5.4
A	45°37.284'	1°45.508'	62	22.0 ± 0.4	6.7 ± 0.2	1.7 ± 0.1	0.46	2.99	13.2	n/a	n/a	n/a	-23.2 ± 0.1	5	84.3 ± 5.3	4.4 ± 1.5	9.6 ± 3.4	138.2 ± 19.9	5.6 ± 3.3	0.2 ± 0.4	0.0 ± 0.0	1.6 ± 1.3	2.2 ± 2.3	0.2 ± 0.4	0.5	7.6
AE	45°42.305'	1°45.361'	61	17.5 ± 1.3	8.7 ± 1.3	1.5 ± 0.1	0.44	1.77	19.9	n/a	n/a	n/a	-22.8 ± 0.4	5	75.6 ± 14.6	3.8 ± 1.1	10.8 ± 3.9	161.3 ± 8.8	5.2 ± 3.7	0.2 ± 0.4	0.0 ± 0.0	0.4 ± 0.9	0.2 ± 0.4	0.0 ± 0.0	0.6	2.8
AF	45°38.984'	1°40.254'	55.6	21.5 ± 0.1	7.6 ± 0.1	1.4 ± 0.1	0.35	1.37	20.3	n/a	n/a	n/a	-23.0 ± 0.2	6	77.1 ± 9.6	3.0 ± 0.6	10.0 ± 7.1	144.1 ± 37.9	1.2 ± 0.4	0.0 ± 0.0	0.2 ± 0.4	0.0 ± 0.0	0.3 ± 0.8	0.0 ± 0.0	0.7	2.6
AK	45°43.191'	1°42.472'	55.5	20.6 ± 0.0	7.6 ± 0.6	1.3 ± 0.0	0.37	1.54	19.4	n/a	n/a	n/a	-23.0 ± 0.3	4	62.3 ± 26.2	3.3 ± 1.0	11.3 ± 5.7	132.5 ± 23.4	3.8 ± 1.9	0.0 ± 0.0	0.0 ± 0.0	1.8 ± 1.0	1.3 ± 1.9	0.0 ± 0.0	0.6	4.3
AL	45°44.774'	1°44.853'	58	20.4 ± 1.7	6.3 ± 0.5	1.2 ± 0.2	0.27	1.44	15.8	n/a	n/a	n/a	-22.8 ± 0.5	6	74.4 ± 12.1	2.7 ± 1.0	9.8 ± 4.3	148.0 ± 12.6	13.2 ± 11.9	0.2 ± 0.4	0.0 ± 0.0	0.2 ± 0.4	0.7 ± 0.8	0.0 ± 0.0	0.6	8.1
AN	45°48.792'	1°48.100'	58.5	21.0 ± 1.8	7.8 ± 0.3	1.4 ± 0.0	0.78	1.8	30.2	n/a	n/a	n/a	-22.6 ± 0.1	6	74.9 ± 14.5	3.5 ± 2.4	10.7 ± 2.1	147.2 ± 24.8	3.5 ± 2.2	0.0 ± 0.0	0.0 ± 0.0	0.3 ± 0.5	2.8 ± 2.9	0.0 ± 0.0	0.6	0.5
AQ	45°45.532'	1°40.140'	50.5	21.2 ± 0.3	8.3 ± 0.1	1.2 ± 0.1	0.33	1.15	22.2	n/a	n/a	n/a	-22.8 ± 0.4	6	72.9 ± 14	2.5 ± 0.8	8.7 ± 3.1	133.4 ± 34.7	3.0 ± 4.0	0.3 ± 0.8	1.0 ± 0.6	1.2 ± 0.8	0.7 ± 1.2	0.0 ± 0.0	0.7	1
AR	45°42.034'	1°34.628'	43.5	22.6 ± 1.4	7.9 ± 0.3	1.0 ± 0.1	0.23	1.05	17.9	n/a	n/a	n/a	-22.9 ± 0.1	6	84.1 ± 9.2	2.5 ± 1.4	6.0 ± 2.9	132.1 ± 47.1	3.7 ± 2.7	0.2 ± 0.4	0.3 ± 0.5	0.5 ± 0.5	2.8 ± 2.6	0.0 ± 0.0	0.9	3
AS	45°40.103'	1°31.427'	42	25.3 ± 8.0	6.7 ± 0.4	1.1 ± 0.0	0.2	0.79	20.3	n/a	n/a	n/a	-23.3 ± 0.1	6	64.1 ± 9.5	2.0 ± 0.6	2.7 ± 3.2	119.6 ± 25.8	1.8 ± 1.3	0.0 ± 0.0	0.3 ± 0.5	1.7 ± 1.2	1.3 ± 1.5	0.0 ± 0.0	0.9	1.4
AV	45°43.660'	1°32.057'	39.5	13.4 ± 1.7	14.2 ± 1.2	0.5 ± 0.0	0.08	0.36	18.7	n/a	n/a	n/a	-23.7 ± 0.0	6	11.7 ± 14.5	1.8 ± 1.9	0.3 ± 0.8	123.0 ± 0.0	4.0 ± 2.8	0.0 ± 0.0	0.2 ± 0.4	1.3 ± 2.1	0.0 ± 0.0	0.0 ± 0.0	1	3.1
AW	45°46.252'	1°36.005'	42.5	53.1 ± 11.8	3.4 ± 0.6	1.3 ± 0.7	0.28	1.03	21.4	n/a	n/a	n/a	-22.8 ± 0.4	6	47.6 ± 9.3	2.0 ± 1.3	4.0 ± 3.7	87.6 ± 40.8	8.2 ± 4.0	0.0 ± 0.0	0.7 ± 0.5	0.3 ± 0.5	0.0 ± 0.0	0.0 ± 0.0	0.8	4.1
AX	45°47.892'	1°38.657'	47	19.1 ± 0.7	7.2 ± 0.6	1.2 ± 0.1	0.64	2.89	18.1	n/a	n/a	n/a	-22.7 ± 0.1	6	51.8 ± 3.9	3.0 ± 1.8	5.0 ± 3.0	107.2 ± 30.3	5.3 ± 5.0	0.2 ± 0.4	0.8 ± 1.2	0.8 ± 0.8	0.5 ± 0.8	0.0 ± 0.0	0.7	7.1
AY	45°49.688'	1°41.691'	49.5	19.0 ± 0.5	7.4 ± 0.1	1.3 ± 0.0	0.41	1.79	18.6	n/a	n/a	n/a	-22.6 ± 0.2	6	57.7 ± 11.9	3.8 ± 1.8	5.8 ± 3.3	126.4 ± 26.0	5.3 ± 4.0	0.5 ± 0.5	2.0 ± 1.4	0.8 ± 1.3	0.8 ± 1.0	0.0 ± 0.0	0.7	1.1
BK	45°38.109'	1°41.705'	58	22.7 ± 0.2	6.6 ± 0.0	1.6 ± 0.1	n/a	n/a	n/a	n/a	n/a	n/a	-23.2 ± 0.1	6	64.6 ± 8.4	3.7 ± 1.6	7.3 ± 2.9	142.3 ± 26.7	5.2 ± 4.1	0.5 ± 0.5	0.2 ± 0.4	0.3 ± 0.5	0.3 ± 0.5	0.0 ± 0.0	0.6	12.2
FG	45°35.524'	1°50.689'	71.5	20.9 ± 0.0	7.3 ± 0.1	1.6 ± 0.1	0.28	1.64	14.4	n/a	n/a	n/a	-23.0 ± 0.1	5	83.4 ± 15.1	2.4 ± 0.9	8.4 ± 3.3	132.2 ± 6.9	12.8 ± 7.2	0.6 ± 0.5	0.4 ± 0.9	1.2 ± 0.8	1.4 ± 1.7	0.0 ± 0.0	0.5	10
J	45°32.950'	1°54.563'	79	17.8 ± 0.5	8.6 ± 0.3	2.1 ± 0.3	0.53	3.08	14.7	n/a	n/a	n/a	-22.8 ± 0.1	8	93.3 ± 17.6	3.5 ± 0.8	10.1 ± 3.9	149.5 ± 25.4	6.1 ± 5.1	0.4 ± 0.7	0.0 ± 0.0	0.6 ± 0.7	1.4 ± 2.0	0.0 ± 0.0	0.4	3.6
PL	45°36.826'	1°47.471'	65.5	24.0 ± 0.2	6.2 ± 0.2	1.6 ± 0.1	0.22	1.44	13.5	n/a	n/a	n/a	-23.2 ± 0.0	4	57.8 ± 13.2	4.0 ± 1.8	18.0 ± 2.2	131.1 ± 19.3	11.5 ± 3.9	0.5 ± 1.0	0.0 ± 0.0	0.8 ± 1.5	6.8 ± 6.4	0.0 ± 0.0	0.5	10.1
SS	45°33.696'	1°52.863'	78	20.7 ± 0.1	7.6 ± 0.4	1.9 ± 0.2	0.44	2.46	15.1	0.69 ± 0.05	n/a	n/a	-22.9 ± 0.3	6	85.2 ± 14.4	2.3 ± 1.6	11.2 ± 5.8	143.1 ± 18.9	10.3 ± 7.3	0.0 ± 0.0	0.0 ± 0.0	0.5 ± 0.8	4.8 ± 5.0	0.0 ± 0.0	0.4	9.2

Table A2. Determination coefficients (R^2), associated probability levels (p), slopes and intercepts of the simple linear regression models linking station depth and assessed parameters within: (1) the whole WGMP and (2) its sole distal part. Bold types are indicative of significant ($p < 0.05$) correlations and underlined types correspond to simple linear regression models without the outliers constituted by stations AN and 3_8.

		Whole WGMP					Distal area				
		n	**R^2**	**p**	**Slope**	**Intercept**	**n**	**R^2**	**p**	**Slope**	**Intercept**
Surface sediment characteristics	$D_{0.5}$	**32**	**0.182**	**0.015**	**-0.358**	**42.362**	25	0.021	0.493		
	SSA	32	0.013	0.533			25	0.008	0.678		
	POC	**32**	**0.578**	**<0.001**	**0.019**	**0.290**	**25**	**0.720**	**<0.001**	**0.022**	**0.131**
	Chl-*a*	**31**	**0.207**	**0.010**	**0.006**	**0.040**	24 22	0.008 0.011	0.682 0.638		
	Phaeo-*a*	**31**	**0.485**	**<0.001**	**0.039**	**-0.580**	**24** **22**	**0.185** **0.187**	**0.036** **0.044**	**0.024** **0.024**	**0.350** **0.347**
	Chl-*a* / (Chl-*a* + Phaeo-*a*)	**31**	**0.190**	**0.014**	**-0.144**	**26.990**	24 **22**	0.107 **0.385**	0.118 **0.002**	**-0.147**	**26.125**
	THAA	**11**	**0.873**	**<0.001**	**0.010**	**-0.113**	**8**	**0.850**	**0.001**	**0.009**	**-0.028**
	EHAA	**10**	**0.638**	**0.006**	**0.001**	**0.006**	7	0.089	0.515		
	EHAA / THAA	10	0.218	0.174			7	0.301	0.202		
	$\delta^{13}C$	32	0.041	0.267			25	0.021	0.492		
SPI characteristics	aRPD thickness	**32**	**0.598**	**<0.001**	**1.531**	**-18.413**	**25**	**0.329**	**0.003**	**0.695**	
	Number of burrows	**32**	**0.255**	**0.003**	**0.034**	**1.034**	25	<0.001	0.903		
	Number of oxic voids	**32**	**0.578**	**<0.001**	**0.262**	**-7.139**	**25**	**0.303**	**0.004**	**0.193**	**-2.743**
	Maximal depth of oxic voids	**32**	**0.498**	**<0.001**	**1.892**	**21.080**	**25**	**0.241**	**0.013**	**0.679**	**97.223**
	Number of feeding pits	**32**	**0.194**	**0.012**	**0.009**	**-0.260**	**25**	**0.168**	**0.042**	**0.009**	**-0.319**
	Number of tubes	**32**	**0.351**	**<0.001**	**0.169**	**-3.512**	**25**	**0.433**	**<0.001**	**0.244**	**-8.228**
	Number of epifauna	**32**	**0.133**	**0.040**	**-0.013**	**0.961**	**25**	**0.174**	**0.038**	**-0.020**	**-0.020**
	Number of infauna	32	0.053	0.204			25	0.022	0.475		
	Total number of biological traces	**32**	**0.654**	**<0.001**	**0.449**	**-7.325**	**25**	**0.479**	**<0.001**	**0.419**	**-5.418**
BSS	BSS 95th percentile	**32**	**0.926**	**<0.001**	**-0.014**	**1.469**	**25**	**0.908**	**<0.001**	**-0.012**	**1.324**
Trawling	Summed Bottom Trawling Effort	**32**	**0.180**	**0.016**	**0.138**	**-2.267**	25	0.090	0.147		
	Proportion of SPI featuring bottom trawling traces	**32**	**0.295**	**0.001**	**1.261**	**-24.374**	25	0.034	0.379		

Table A3. Determination coefficients (R^2), associated probability levels (p), slopes, and intercepts of the simple linear regression models linking 95th percentile of Bottom Shear Stress (BSS) and one-year summed Bottom Trawling Effort (BTE) within cells containing sampled stations, and assessed parameters within the distal part of the WGMP. Adjusted determination coefficients (R^2) and associated probability levels (p) of the multiple linear regression models linking the combination of BSS and BSS with assessed parameters within the distal part of the WGMP. Bold types are indicative of significant ($p < 0.05$) correlations and underlined types correspond to simple linear regression models without the outliers constituted by stations AN and 3_8.

		BSS					**BTE**					**BSS + BTE**	
		n	**R^2**	**p**	**Slope**	**Intercept**	**n**	**R^2**	**p**	**Slope**	**Intercept**	**Adjusted R^2**	**p**
Surface sediment characteristics	$D_{0.5}$	25	<0.001	0.890			25	0.007	0.686			<0.001	0.897
	SSA	25	<0.001	0.902			25	0.119	0.091			0.040	0.238
	POC	**25**	**0.603**	**<0.001**	**-1.591**	**2.399**	25	0.039	0.343			**0.567**	**0.001**
	Chl-*a*	24	0.020	0.514			24	0.019	0.518			<0.001	0.720
		22	0.012	0.634			22	0.005	0.765				
	Phaeo-*a*	**24**	**0.175**	**0.042**	**-1.878**	**2.939**	24	0.016	0.557			0.100	0.132
		22	0.177	0.052			22	0.061	0.266				
	Chl-*a* / (Chl-*a* + Phaeo-*a*)	24	0.070	0.210			24	<0.001	0.971			<0.001	0.433
		22	**0.357**	**0.003**	**11.392**	**10.376**	**22**	**0.420**	**0.001**	**-0.006**	**0.205**		
	THAA	**8**	**0.899**	**<0.001**	**-0.838**	**1.004**	8	0.025	0.708			**0.862**	**0.003**
	EHAA	7	0.052	0.624			7	0.076	0.547			<0.001	0.765
	EHAA / THAA	7	0.443	0.103			7	0.028	0.719			0.215	0.274
	$\delta^{13}C$	25	0.039	0.344			**25**	**0.272**	**0.008**	**-0.024**	**-22.806**	**0.325**	**0.005**
SPI characteristics	aRPD thickness	**25**	**0.181**	**0.034**	**-41.196**	**100.531**	25	0.010	0.635			0.153	0.062
	Number of burrows	25	0.014	0.571			25	0.003	0.793			<0.001	0.785
	Number of oxic voids	**25**	**0.402**	**<0.001**	**-17.711**	**19.618**	25	0.024	0.456			**0.347**	**0.003**
	Maximal depth of oxic voids	**25**	**0.219**	**0.018**	**-51.777**	**169.396**	25	0.001	0.858			0.154	0.061
	Number of feeding pits	**25**	**0.166**	**0.043**	**-0.741**	**0.692**	25	0.002	0.824			0.009	0.132
	Number of tubes	**25**	**0.428**	**<0.001**	**-19.387**	**18.187**	**25**	**0.283**	**0.006**	**0.456**	**3.378**	**0.539**	**<0.001**
	Number of epifauna	25	0.148	0.057			25	0.088	0.149			<0.001	0.708
	Number of infauna	25	0.012	0.602			25	0.012	0.610			0.120	0.094
	Total number of biological traces	**25**	**0.567**	**<0.001**	**-36.452**	**41.931**	**24**	**0.159**	**0.048**	**0.558**	**15.841**	**0.583**	**<0.001**
Trawling	Proportion of SPI featuring bottom trawling traces	25	0.030	0.407			25	0.052	0.273			<0.001	0.466

References

1. Aller, R.C. Mobile deltaic and continental shelf muds as suboxic, fluidized bed reactors. *Mar. Chem.* **1998**, *61*, 143–155, doi:10.1016/S0304-4203(98)00024-3.
2. Burdige, D.J. Burial of terrestrial organic matter in marine sediments: A re-assessment. *Glob. Biogeochem. Cycles* **2005**, *19*, 1–7, doi:10.1029/2004GB002368.
3. Blair, N.E.; Aller, R.C. The fate of terrestrial organic carbon in the marine environment. *Ann. Rev. Mar. Sci.* **2012**, *4*, 401–423, doi:10.1146/annurev-marine-120709-142717.
4. Meade, R.H. River-sediment inputs to major deltas. In *Sea Level-Rise and Coastal Subsidence. Coastal Systems and Continental Margins*; Miliman, J.D., Haq, B.U.; Springer: Dordrecht, The Netherlands, 1996; Volume 2, pp. 63–85, doi:10.1007/978-94-015-8719-8_4.
5. McKee, B.A.; Aller, R.C.; Allison, M.A.; Bianchi, T.S.; Kineke, G.C. Transport and transformation of dissolved and particulate materials on continental margins influenced by major rivers: Benthic boundary layer and seabed processes. *Cont. Shelf Res.* **2004**, *24*, 899–926, doi:10.1016/j.csr.2004.02.009.
6. Hedges, J.I.; Keil, R.G. Sedimentary organic matter preservation: An assessment and speculative synthesis. *Mar. Chem.* **1995**, *49*, 81–115, doi:10.1016/0304-4203(95)00008-F.
7. Burdige, D.J. Estuarine and coastal sediments—Coupled biogeochemical cycling. In *Treatise on Estuarine and Coastal Science*; Wolanski, E., McLusky, D., Eds.; Academic Press: Cambridge, MA, USA, 2012; Volume 5, pp. 279–316, doi:10.1016/B978-0-12-374711-2.00511-8.
8. Kristensen, E.; Penha-Lopes, G.; Delefosse, M.; Valdemarsen, T.; Quintana, C.O.; Banta, G.T. What is bioturbation? The need for a precise definition for fauna in aquatic sciences. *Mar. Ecol. Prog. Ser.* **2012**, *446*, 285–302, doi:10.3354/meps09506.
9. Aller, R.C. The effects of macrobenthos on chemical properties of marine sediment and overlying water. In *Animal-Sediment Relations*; McCall, P.L., Tevesz, M.J.S., Eds.; Springer: Boston, MA, USA, 1982; Volume 100, pp. 53–102, doi:10.1007/978-1-4757-1317-6_2.
10. Kristensen, E. Organic matter diagenesis at the oxic/anoxic interface in coastal marine sediments, with emphasis on the role of burrowing animals. *Hydrobiologia* **2000**, *426*, 1–24, doi:10.1023/A:1003980226194.
11. Kristensen, E.; Kostka, J.E. Macrofaunal burrows and irrigation in marine sediment: Microbiological and biogeochemical interactions. In *Interactions Between Macro- and Microorganisms in Marine Sediments*; Kristensen, E., Haese, R.R., Kostka; J.E., Eds.; American Geophysical Union: Washington, DC, USA, 2013; pp. 125–157, doi:10.1029/CE060p0125.
12. Rhoads, D.C.; Boesch, D.F.; Zhican, T.; Fengshan, X.; Liqiang, H.; Nilsen, K.J. Macrobenthos and sedimentary facies on the Changjiang delta platform and adjacent continental shelf, East China Sea. *Cont. Shelf Res.* **1985**, *4*, 189–213, doi:10.1016/0278-4343(85)90029-9.

13. Watling, L.; Norse, E.A. Disturbance of the seabed by mobile fishing gear: A comparison to forest clearcutting. *Conserv. Biol.* **1998**, *12*, 1180–1197, doi:10.1046/j.1523-1739.1998.0120061180.x.
14. Durrieu De Madron, X.; Ferré, B.; Le Corre, G.; Grenz, C.; Conan, P.; Pujo-Pay, M.; Buscail, R.; Bodiot, O. Trawling-induced resuspension and dispersal of muddy sediments and dissolved elements in the Gulf of Lion (NW Mediterranean). *Cont. Shelf Res.* **2005**, *25*, 2387–2409, doi:10.1016/j.csr.2005.08.002.
15. Ferré, B.; Durrieu de Madron, X.; Estournel, C.; Ulses, C.; Le Corre, G. Impact of natural (waves and currents) and anthropogenic (trawl) resuspension on the export of particulate matter to the open ocean. Application to the Gulf of Lion (NW Mediterranean). *Cont. Shelf Res.* **2008**, *28*, 2071–2091, doi:10.1016/j.csr.2008.02.002.
16. Palanques, A.; Guillén, J.; Puig, P. Impact of bottom trawling on water turbidity and muddy sediment of an unfished continental shelf. *Limnol. Oceanogr.* **2001**, *46*, 1100–1110, doi:10.4319/lo.2001.46.5.1100.
17. Palanques, A.; Puig, P.; Guillén, J.; Demestre, M.; Martín, J. Effects of bottom trawling on the Ebro continental shelf sedimentary system (NW Mediterranean). *Cont. Shelf Res.* **2014**, *72*, 83–98, doi:10.1016/j.csr.2013.10.008.
18. Oberle, F.K.J.; Storlazzi, C.D.; Hanebuth, T.J.J. What a drag: Quantifying the global impact of chronic bottom trawling on continental shelf sediment. *J. Mar. Syst.* **2016**, *159*, 109–119, doi:10.1016/j.jmarsys.2015.12.007.
19. Mengual, B.; Cayocca, F.; Le Hir, P.; Draye, R.; Laffargue, P.; Vincent, B.; Garlan, T. Influence of bottom trawling on sediment resuspension in the 'Grande-Vasière' area (Bay of Biscay, France). *Ocean Dyn.* **2016**, *66*, 1181–1207, doi:10.1007/s10236-016-0974-7.
20. Mengual, B.; Le Hir, P.; Cayocca, F.; Garlan, T. Bottom trawling contribution to the spatio-temporal variability of sediment fluxes on the continental shelf of the Bay of Biscay (France). *Mar. Geol.* **2019**, *414*, 77–91, doi:10.1016/j.margeo.2019.05.009.
21. Thrush, S.F.; Dayton, P.K. Disturbance to marine benthic habitats by trawling and dredging: Implications for marine biodiversity. *Annu. Rev. Ecol. Syst.* **2002**, *33*, 449–473, doi:10.1146/annurev.ecolsys.33.010802.150515.
22. Thrush, S.F.; Gray, J.S.; Hewitt, J.E.; Ugland, K.I. Predicting the effects of habitat homogenization on marine biodiversity. *Ecol. Appl.* **2006**, *16*, 1636–1642, doi:10.1890/1051-0761(2006)016[1636:PTEOHH]2.0.CO;2.
23. Kaiser, M.J.; Collie, J.S.; Hall, S.J.; Jennings, S.; Poiner, I.R. Modification of marine habitats by trawling activities: Prognosis and solutions. *Fish Fish.* **2002**, *3*, 114–136, doi:10.1046/j.1467-2979.2002.00079.x.
24. Queirós, A.M.; Hiddink, J.G.; Kaiser, M.J.; Hinz, H. Effects of chronic bottom trawling disturbance on benthic biomass, production and size spectra in different habitats. *J. Exp. Mar. Bio. Ecol.* **2006**, *335*, 91–103, doi:10.1016/j.jembe.2006.03.001.
25. Lesueur, P.; Jouanneau, J.M.; Boust, D.; Tastet, J.P.; Weber, O. Sedimentation rates and fluxes in the continental shelf mud fields in the Bay of Biscay (France). *Cont. Shelf Res.* **2001**, *21*, 1383–1401, doi:10.1016/S0278-4343(01)00004-8.

26. Lesueur, P.; Tastet, J.P.; Weber, O. Origin and morphosedimentary evolution of fine-grained modern continental shelf deposits: The Gironde mud fields (Bay of Biscay, France). *Sedimentology* **2002**, *49*, 1299–1320, doi:10.1046/j.1365-3091.2002.00498.x.
27. Doxaran, D.; Froidefond, J.M.; Castaing, P.; Babin, M. Dynamics of the turbidity maximum zone in a macrotidal estuary (the Gironde, France): Observations from field and MODIS satellite data. *Estuar. Coast. Shelf Sci.* **2009**, *81*, 321–332, doi:10.1016/j.ecss.2008.11.013.
28. Constantin, S.; Doxaran, D.; Derkacheva, A.; Novoa, S.; Lavigne, H. Multi-temporal dynamics of suspended particulate matter in a macro-tidal river Plume (the Gironde) as observed by satellite data. *Estuar. Coast. Shelf Sci.* **2018**, *202*, 172–184, doi:10.1016/j.ecss.2018.01.004.
29. Etcheber, H.; Schmidt, S.; Sottolichio, A.; Maneux, E.; Chabaux, G.; Escalier, J.M.; Wennekes, H.; Derriennic, H.; Schmeltz, M.; Quéméner, L.; et al. Monitoring water quality in estuarine environments: Lessons from the MAGEST monitoring program in the Gironde fluvial-estuarine system. *Hydrol. Earth Syst. Sci.* **2011**, *15*, 831–840, doi:10.5194/hess-15-831-2011.
30. Cirac, P.; Berne, S.; Castaing, P.; Weber, O. Processus de mise en place et d'évolution de la couverture sédimentaire superficielle de la plate-forme nord-aquitaine. *Oceanol. Acta* **2000**, *23*, 663–686, doi:10.1016/s0399-1784(00)00110-9.
31. Castaing, P.; Allen, G.P. Mechanisms controlling seaward escape of suspended sediment from the Gironde: A macrotidal estuary in France. *Mar. Geol.* **1981**, *40*, 101–118, doi:10.1016/0025-3227(81)90045-1.
32. Castaing, P.; Allen, G.; Houdart, M.; Moign, Y. Étude par télédétection de la dispersion en mer des eaux estuariennes issues de la Gironde et du Pertuis de Maumusson. *Oceanol. Acta* **1979**, *2*, 459–469.
33. Castaing, P.; Philipps, I.; Weber, O. Répartition et dispersion des suspensions dans les eaux du plateau continental aquitain. *Oceanol. Acta* **1982**, *5*, 85–96.
34. Longère, P.; Dorel, D. Etude des sédiments meubles de la vasière de la Gironde et des régions avoisinantes. *Rev. des Trav. l'Institut des Pêches Marit.* **1970**, *34*, 233–256.
35. Jouanneau, J.M.; Weber, O.; Latouche, C.; Vernet, J.P.; Dominik, J. Erosion, non-deposition and sedimentary processes through a sedimentological and radioisotopic study of surficial deposits from the "Ouest-Gironde vasière" (Bay of Biscay). *Cont. Shelf Res.* **1989**, *9*, 325–342, doi:10.1016/0278-4343(89)90037-X.
36. Weber, O.; Jouanneau, J.M.; Ruch, P.; Mirmand, M. Grain-size relationship between suspended matter originating in the Gironde estuary and shelf mud-patch deposits. *Mar. Geol.* **1991**, *96*, 159–165, doi:10.1016/0025-3227(91)90213-N.
37. Lesueur, P.; Tastet, J.P. Les Vasières de plate-forme du Golfe de Gascogne (France). *Actes du III^{e} Colloque International « Océanographie du Golfe de Gascogne »* **1993**, 181–184.
38. Lesueur, P.; Tastet, J.P. Facies, internal structures and sequences of modern Gironde-derived muds on the Aquitaine inner shelf, France. *Mar. Geol.* **1994**, *120*, 267–290, doi:10.1016/0025-3227(94)90062-0.

39. Gadel, F.; Jouanneau, J.M.; Weber, O.; Serve, L.; Comellas, L. Traceurs organiques dans les dépôts de la vasière Ouest-Gironde (Golfe de Gascogne). *Oceanol. Acta* **1997**, *20*, 687–695.
40. Parra, M.; Castaing, P.; Jouanneau, J.M.; Grousset, F.; Latouche, C. Nd-Sr isotopic composition of present-day sediments from the Gironde Estuary, its draining basins and the WestGironde mud patch (SW France). *Cont. Shelf Res.* **1998**, *19*, 135–150, doi:10.1016/S0278-4343(98)00083-1.
41. Lesueur, P.; Weber, O.; Marambat, L.; Tastet, J.P.; Jouanneau, J.M.; Turon, J.L. Datation d'une vasière de plateforme atlantique au débouché d'un estuaire: La vasière à l'ouest de la Gironde (France) est d'âge historique (VIème siècle à nos jours). *Comptes rendus l'Académie des Sci. Série 2* **1989**, *308*, 935–940.
42. Lesueur, P.; Tastet, J.P.; Weber, O.; Sinko, J.A. Modèle faciologique d'un corps sédimentaire pélitique de plate-forme la vasière Ouest-Gironde (France). *Oceanol. Acta* **1991**, *11*, 143–153**.**
43. Lesueur, P.; Tastet, J.P.; Marambat, L. Shelf mud fields formation within historical times: Examples from offshore the Gironde estuary, France. *Cont. Shelf Res.* **1996**, *16*, 1849–1870, doi:10.1016/0278-4343(96)00013-1.
44. Relexans, J.C.; Lin, R.G.; Castel, J.; Etcheber, H.; Laborde, P. Response of biota to sedimentary organic matter quality of the west Gironde mud patch, Bay of Biscay (France). *Oceanol. Acta* **1992**, *15*, 639–649.
45. Massé, C.; Meisterhans, G.; Deflandre, B.; Bachelet, G.; Bourasseau, L.; Bichon, S.; Ciutat, A.; Jude-Lemeilleur, F.; Lavesque, N.; Raymond, N.; et al. Bacterial and macrofaunal communities in the sediments of the West Gironde Mud Patch, Bay of Biscay (France*). Estuar. Coast. Shelf Sci.* **2016**, *179*, 189–200, doi:10.1016/j.ecss.2016.01.011.
46. Système d'Informations Halieutiques Ifremer. Activité des navires de pêche région Nouvelle-Aquitaine. 2017.
47. Lesueur, P. Les Vasières de la Plate-Forme Ouest Gironde (France) : Modèle Faciologique Et Archive Sédimentaire Des Flux Côtiers **1992**. Ph.D. Thesis, Université Bordeaux 1, Talence, France, 19 October 1992.
48. Gillet, H.; Deflandre, B. JERICOBENT-5-TH cruise, RV Thalia **2018**. https://doi.org/10.17600/18000425.
49. Schmidt, S.; Deflandre, B. JERICOBENT-5 cruise, RV Côtes De La Manche **2018**. https://doi.org/10.17600/18000471.
50. Mayer, L.M. Surface area control of organic carbon accumulation in continental shelf sediments*. Geochemica Cosmochim. Acta* **1994**, *58*, 1271–1284.
51. Migeon, S.; Weber, O.; Faugeres, J.C.; Saint-Paul, J. SCOPIX: A new X-ray imaging system for core analysis. *Geo-Marine Lett.* **1999**, *18*, 251–255, doi:10.1007/s003670050076.
52. Rhoads, D.C.; Germano, J.D. Characterization of organism-sediment relations using sediment profile imaging: An efficient method of remote ecological monitoring of the seafloor (Remots System). *Mar. Ecol. Prog. Ser.* **1982**, *8*, 115–128.
53. Etcheber, H.; Relexans, J.C.; Beliard, M.; Weber, O.; Buscail, R.; Heussner, S. Distribution and quality of sedimentary organic matter on the Aquitanian margin (Bay

of Biscay). *Deep. Res. Part II* **1999**, *46*, 2249–2288, doi:10.1016/S0967-0645(99)00062-4.

54. Mayer, L.M.; Schick, L.L.; Sawyer, T.; Plante, C.J.; Jumars, P.A.; Self, R.L. Bioavailable amino acids in sediments: A biomimetic, kinetics based approach. *Limnol. Oceanogr.* **1995**, *40*, 511–520, doi:10.4319/lo.1995.40.3.0511.
55. Pastor, L.; Deflandre, B.; Viollier, E.; Cathalot, C.; Metzger, E.; Rabouille, C.; Escoubeyrou, K.; Lloret, E.; Pruski, A.M.; Vétion, G.; et al. Influence of the organic matter composition on benthic oxygen demand in the Rhône River prodelta (NW Mediterranean Sea). *Cont. Shelf Res.* **2011**, *31*, 1008–1019, doi:10.1016/j.csr.2011.03.007.
56. Bonifácio, P.; Bourgeois, S.; Labrune, C.; Amouroux, J.M.; Escoubeyrou, K.; Buscail, R.; Romero-Ramirez, A.; Lantoine, F.; Vétion, G.; Bichon, S.; et al. Spatiotemporal changes in surface sediment characteristics and benthic macrofauna composition off the Rhône River in relation to its hydrological regime. *Estuar. Coast. Shelf Sci.* **2014**, *151*, 196–209, doi:10.1016/j.ecss.2014.10.011.
57. Wakeham, S.G.; Lee, C.; Hedges, J.I.; Hernes, P.J.; Peterson, M.L. Molecular indicators of diagenetic status in marine organic matter. *Geochemica Cosmochim. Acta* **1997**, *61*, 5363–5369, doi:10.5833/jjgs.33.70.
58. Neveux, J.; Lantoine, F. Spectrofluorometric assay of chlorophylls and phaeopigments using the least squares approximation technique. *Deep. Res. Part I* **1993**, *40*, 1747–1765, doi:10.1016/0967-0637(93)90030-7.
59. Coplen, T.B. Guidelines and recommended terms for expression of stable- isotope-ratio and gas-ratio measurement results. *Rapid Commun. Mass Spectrom* **2011**, *25*, 2538–2560, doi:10.1002/rcm.5129.
60. Romero-Ramirez, A.; Grémare, A.; Desmalades, M.; Duchêne, J.C. Semi-automatic analysis and interpretation of sediment profile images. *Environ. Model. Softw.* **2013**, *47*, 42–54, doi:10.1016/j.envsoft.2013.04.008.
61. Rosenberg, R.; Grémare, A.; Amouroux, J.M.; Nilsson, H.C. Benthic habitats in the northwest Mediterranean characterised by sedimentary organics, benthic macrofauna and sediment profile images. *Estuar. Coast. Shelf Sci.* **2003**, *57*, 297–311, doi:10.1016/S0272-7714(02)00356-6.
62. Rosenberg, R.; Nilsson, H.C.; Grémare, A.; Amouroux, J.M. Effects of demersal trawling on marine sedimentary habitats analysed by sediment profile imagery. *J. Exp. Mar. Bio. Ecol.* **2003**, *285–286*, 465–477, doi:10.1016/S0022-0981(02)00577-4.
63. Germano, J.D.; Rhoads, D.C.; Valente, R.M.; Carey, D.A.; Solan, M. The use of sediment profile imaging (SPI) for environmental impact assessments and monitoring studies: Lessons learned from the past four decades. *Oceanogr. Mar. Biol. An Annu. Rev.* **2011**, *49*, 235–298, doi:10.1201/b11009-7.
64. Diaz, M.; Grasso, F.; Le Hir, P.; Sottolichio, A.; Caillaud, M.; Thouvenin, B. Modeling mud and sand transfers between a macrotidal estuary and the continental shelf: Influence of the sediment transport parameterization. *J. Geophys. Res. Oceans* **2020**, *125*, e2019JC015643, doi:10.1029/2019JC015643.

65. Lazure, P.; Dumas, F. An external-internal mode coupling for a 3D hydrodynamical model for applications at regional scale (MARS). *Adv. Water Resour.* **2008**, *31*, 233–250, doi:10.1016/j.advwatres.2007.06.010.
66. Roland, A.; Ardhuin, F. On the developments of spectral wave models: Numerics and parameterizations for the coastal ocean. *Ocean Dyn.* **2014**, *64*, 833–846, doi:10.1007/s10236-014-0711-z.
67. Soulsby, R. Dynamics of Marine Sands: A Manual for Practical Applications; Inst of Civil Engineers Pub: London, UK, 1997.
68. Grasso, F.; Verney, R.; Le Hir, P.; Thouvenin, B.; Schulz, E.; Kervella, Y.; Khojasteh Pour Fard, I.; Lemoine, J.P.; Dumas, F.; Garnier, V. Suspended sediment dynamics in the macrotidal seine estuary (France)—Part 1: Numerical modeling of turbidity maximum dynamics. *J. Geophys. Res. Oceans.* **2008**, *123*, 558–577, doi:10.1002/2017JC013185.
69. Global Fishing Watch. Available online: https://globalfishingwatch.org (accessed on 13 March 2019).
70. Kroodsma, D.A.; Mayorga, J.; Hochberg, T.; Miller, N.A.; Boerder, K.; Ferretti, F.; Wilson, A.; Bergman, B.; White, T.D.; Block, B.A.; et al. Tracking the global footprint of fisheries. *Science* **2018**, *359*, 904–908, doi:10.1126/science.aao5646.
71. Clarke, K.R.; Somerfield, P.J.; Gorley, R.N. Testing of null hypotheses in exploratory community analyses: Similarity profiles and biota-environment linkage. *J. Exp. Mar. Bio. Ecol.* **2008**, *366*, 56–69, doi:10.1016/j.jembe.2008.07.009.
72. Clarke, K.R. Non-parametric multivariate analyses of changes in community structure. *Aust. J. Ecol.* **1993**, *18*, 117–143, doi:10.12691/marine-1-1-6.
73. Clarke, K.R.; Warwick, R.M. *Change in Marine Communities: An Approach to Statistical Analysis and Interpretation*, 2nd ed.; PRIMER-E: Plymouth, UK, 2001.
74. Lansard, B.; Rabouille, C.; Denis, L.; Grenz, C. Benthic remineralization at the land-ocean interface: A case study of the Rhône River (NW Mediterranean Sea). *Estuar. Coast. Shelf Sci.* **2009**, *81*, 544–554, doi:10.1016/j.ecss.2008.11.025.
75. Antonelli, C.; Eyrolle, F.; Rolland, B.; Provansal, M.; Sabatier, F. Suspended sediment and 137Cs fluxes during the exceptional December 2003 flood in the Rhone River, southeast France. *Geomorphology* **2008**, *95*, 350–360, doi:10.1016/j.geomorph.2007.06.007.
76. Touzani, A.; Giresse, P. The Rhone River prodelta: Short-term (100–103 year) sedimentation patterns and human impact. *J. Coast. Res.* **2002**, *18*, 102–117.
77. Marion, C.; Dufois, F.; Arnaud, M.; Vella, C. In situ record of sedimentary processes near the Rhône River mouth during winter events (Gulf of Lions, Mediterranean Sea). *Cont. Shelf Res.* **2010**, *30*, 1095–1107, doi:10.1016/j.csr.2010.02.015.
78. Dufois, F.; Verney, R.; Le Hir, P.; Dumas, F.; Charmasson, S. Impact of winter storms on sediment erosion in the Rhone River prodelta and fate of sediment in the Gulf of Lions (North Western Mediterranean Sea). *Cont. Shelf Res.* **2014**, *72*, 57–72, doi:10.1016/j.csr.2013.11.004.
79. Calmet, D.; Fernandez, J. Caesium distribution in northwest Mediterranean seawater, suspended particles and sediments. *Cont. Shelf Res.* **1990**, *10*, 895–913.

80. Charmasson, S.; Radakovitch, O.; Arnaud, M.; Bouisset, P.; Pruchon, A.S. Long-core profiles of 137Cs, 134Cs, 60Co and 210Pb in sediment near the Rhone River (northwestern Meiterranean Sea). *Estuaries* **1998**, *21*, 367–378, doi:10.2307/1352836.
81. Bourgeois, S.; Pruski, A.M.; Sun, M.Y.; Buscail, R.; Lantoine, F.; Kerhervé, P.; Vétion, G.; Rivière, B.; Charles, F. Distribution and lability of land-derived organic matter in the surface sediments of the Rhône prodelta and the adjacent shelf (Mediterranean Sea, France): A multi proxy study. *Biogeosciences* **2011**, *8*, 3107–3125, doi:10.5194/bg-8-3107-2011.
82. Labrune, C.; Romero-Ramirez, A.; Amouroux, J.M.; Duchêne, J.C.; Desmalades, M.; Escoubeyrou, K.; Buscail, R.; Grémare, A. Comparison of ecological quality indices based on benthic macrofauna and sediment profile images: A case study along an organic enrichment gradient off the Rhône River. *Ecol. Indic.* **2012**, *12*, 133–142, doi:10.1016/j.ecolind.2011.04.028.
83. Kaiser, M.J.; Clarke, K.R.; Hinz, H.; Austen, M.C.V.; Somerfield, P.J.; Karakassis, I. Global analysis of response and recovery of benthic biota to fishing. *Mar. Ecol. Prog. Ser.* **2006**, *311*, 1–14, doi:10.3354/meps311001.
84. Sciberras, M.; Geert, J.; Simon, H.; Szostek, C.L.; Hughes, K.M.; Kneafsey, B.; Clarke, L.J.; Ellis, N.; Rijnsdorp, A.D.; McConnaughey, R.A.; et al. Response of benthic fauna to experimental bottom fishing : A global meta-analysis. Fish Fish. **2018**, *19*, 698–715, doi:10.1111/faf.12283.
85. Dufois, F.; Garreau, P.; Le Hir, P.; Forget, P. Wave-and current-induced bottom shear stress distribution in the Gulf of Lions. *Cont. Shelf Res.* **2008**, *28*, 1920–1934, doi:10.1016/j.csr.2008.03.028.
86. Kaiser, M.J.; Spencer, B.E. The effects of beam-trawl disturbance on infaunal communities in different habitats. *J. Anim. Ecol.* **1996**, *65*, 348–358, doi:10.2307/5881.
87. Smith, C.J.; Banks, A.C.; Papadopoulou, K.N. Improving the quantitative estimation of trawling impacts from sidescan-sonar and underwater-video imagery. *ICES J. Mar. Sci.* **2007**, *64*, 1692–1701, doi:10.1093/icesjms/fsm165.
88. Olsgard, F.; Schaanning, M.T.; Widdicombe, S.; Kendall, M.A.; Austen, M.C. Effects of bottom trawling on ecosystem functioning. *J. Exp. Mar. Bio. Ecol.* **2008**, *366*, 123–133, doi:10.1016/j.jembe.2008.07.036.
89. De Juan, S.; Demestre, M.; Sánchez, P. Exploring the degree of trawling disturbance by the analysis of benthic communities ranging from a heavily exploited fishing ground to an undisturbed area in the NW Mediterranean. *Sci. Mar.* **2011**, *75*, 507–516, doi:10.3989/scimar.2011.75n3507.
90. Widdicombe, S.; Austen, M.C. The interaction between physical disturbance and organic enrichment: An important element in structuring benthic communities. *Limnol. Oceanogr.* **2001**, *46*, 1720–1733, doi:10.4319/lo.2001.46.7.1720.
91. Selby, I.; Evans, N.C. Origins of mud clasts and suspensions on the seabed in Hong Kong. *Cont. Shelf Res.* **1997**, *17*, 57–78, doi:10.1016/0278-4343(96)00018-0.
92. Fettweis, M.; Du Four, I.; Zeelmaekers, E.; Baeteman, C.; Francken, F.; Houziaux, J.-S.; Mathys, M.; Nechad, B.; Pison, V.; Vandenberghe, N.; et al. *Mud Origin, Characterisation and Human Activities (MOCHA): Final Report*; Belgian Science Policy Office: Brussels, Belgium, 2007**.**

93. Grémare, A. (Université de Bordeaux, Talence, France). **Personal communication, 2020.**
94. Nilsson, H.C.; Rosenberg, R. Effects on marine sedimentary habitats of experimental trawling analysed by sediment profile imagery. *J. Exp. Mar. Bio. Ecol.* **2003**, *285–286*, 453–463, doi:10.1016/S0022-0981(02)00543-9.
95. Smith, C.J.; Rumohr, H.; Karakassis, I.; Papadopoulou, K.N. Analysing the impact of bottom trawls on sedimentary seabeds with sediment profile imagery. *J. Exp. Mar. Bio. Ecol.* **2003**, *285–286*, 479–496, doi:10.1016/S0022-0981(02)00545-2.
96. Tiano, J.C.; Van Der Reijden, K.J.; O'Flynn, S.; Beauchard, O.; Van Der Ree, S.; Van Der Wees, J.; Ysebaert, T.; Soetaert, K. Experimental bottom trawling finds resilience in large-bodied infauna but vulnerability for epifauna and juveniles in the Frisian Front. *Mar. Environ. Res.* **2020**, *159*, 104964, doi:10.1016/j.marenvres.2020.104964.
97. Darnaude, A.M.; Salen-Picard, C.; Harmelin-Vivien, M.L. Depth variation in terrestrial particulate organic matter exploitation by marine coastal benthic communities off the Rhone River delta (NW Mediterranean). *Mar. Ecol. Prog. Ser.* **2004**, *275*, 47–57, doi:10.3354/meps275047.
98. Tesi, T.; Miserocchi, S.; Goñi, M.A.; Langone, L. Source, transport and fate of terrestrial organic carbon on the western Mediterranean Sea, Gulf of Lions, France. *Mar. Chem.* **2007**, *105*, 101–117, doi:10.1016/j.marchem.2007.01.005.
99. Cathalot, C.; Rabouille, C.; Tisnérat-Laborde, N.; Toussaint, F.; Kerhervé, P.; Buscail, R.; Loftis, K.; Sun, M.Y.; Tronczynski, J.; Azoury, S.; et al. The fate of river organic carbon in coastal areas: A study in the Rhône River delta using multiple isotopic (δ13C, δ14C) and organic tracers. *Geochim. Cosmochim. Acta* **2013**, *118*, 33–55, doi:10.1016/j.gca.2013.05.001.
100. Fontugne, M.R.; Jouanneau, J.M. Modulation of the particulate organic carbon flux to the ocean by a macrotidal estuary: Evidence from measurements of carbon isotopes in organic matter from the Gironde system. *Estuar. Coast. Shelf Sci.* **1987**, *24*, 377–387, doi:10.1016/0272-7714(87)90057-6.
101. Middelburg, J.J.; Herman, P.M.J. Organic matter processing in tidal estuaries. *Mar. Chem.* **2007**, *106*, 127–147, doi:10.1016/j.marchem.2006.02.007.
102. Savoye, N.; David, V.; Morisseau, F.; Etcheber, H.; Abril, G.; Billy, I.; Charlier, K.; Oggian, G.; Derriennic, H.; Sautour, B. Origin and composition of particulate organic matter in a macrotidal turbid estuary: The Gironde Estuary, France. *Estuar. Coast. Shelf Sci.* **2012**, *108*, 16–28, doi:10.1016/j.ecss.2011.12.005.
103. Sottolichio, A.; Castaing, P. A synthesis on seasonal dynamics of highly-concentrated structures in the Gironde estuary. *Earth Planet. Sci.* **1999**, *329*, 795–800.
104. Jouanneau, J.M.; Latouche, C. *The Gironde Estuary*; Publisher: Schweizerbart Science Publishers, Stuttgart, Germany, 1981.
105. Etcheber, H.; Taillez, A.; Abril, G.; Garnier, J.; Servais, P.; Moatar, F.; Commarieu, M.V. Particulate organic carbon in the estuarine turbidity maxima of the Gironde, Loire and Seine estuaries: Origin and lability. *Hydrobiologia* **2007**, *588*, 245–259, doi:10.1007/s10750-007-0667-9.

106. Ulses, C.; Estournel, C.; Durrieu de Madron, X.; Palanques, A. Suspended sediment transport in the Gulf of Lions (NW Mediterranean): Impact of extreme storms and floods. *Cont. Shelf Res.* **2008**, *28*, 2048–2070, doi:10.1016/j.csr.2008.01.015.
107. Mayer, L.M.; Jumars, P.A.; Taghon, G.L.; Macko, S.A.; Trumbore, S. Low-density particles as potential nitrogenous foods for benthos. *J. Mar. Res.* **1993**, *51*, 373–389, doi:10.1357/0022240933223738.
108. Abril, G.; Etcheber, H.; Le Hir, P.; Bassoullet, P.; Boutier, B.; Frankignoulle, M. Oxic/anoxic oscillations and organic carbon mineralization in an estuarine maximum turbidity zone (The Gironde, France). *Limnol. Oceanogr.* **1999**, *44*, 1304–1315, doi:10.4319/lo.1999.44.5.1304.
109. Abril, G.; Nogueira, M.; Etcheber, H.; Cabeçadas, G.; Lemaire, E.; Brogueira, M.J. Behaviour of organic carbon in nine contrasting European estuaries. *Estuar. Coast. Shelf Sci.* **2002**, *54*, 241–262, doi:10.1006/ecss.2001.0844.
110. Lemaire, E.; Abril, G.; De Wit, R.; Etcheber, H. Effect of turbidity on phytoplanktonic pigments degradation in the Gironde Estuary. *Comptes Rendus Geosci.* **2002**, *334*, 251–258, doi:10.1016/S1631-0713(02)01747-9.
111. Pearson, T.H.; Rosenberg, R. Macrobenthos succession in relation to organic enrichment and pollution of the marine environment. *Oceanogr. Mar. Biol. Annu. Rev.* **1978**, *16*, 229–331.
112. Miralles, J.; Arnaud, M.; Radakovitch, O.; Marion, C.; Cagnat, X. Radionuclide deposition in the Rhône River Prodelta (NW Mediterranean sea) in response to the December 2003 extreme flood. *Mar. Geol.* **2006**, *234*, 179–189, doi:10.1016/j.margeo.2006.09.004.
113. Salen-Picard, C.; Darnaude, A.M.; Arlhac, D.; Harmelin-Vivien, M.L. Fluctuations of macrobenthic populations: A link between climate-driven river run-off and sole fishery yields in the Gulf of Lions. *Oecologia* **2002**, *133*, 380–388, doi:10.1007/s00442-002-1032-3.
114. Miralles, J.; Radakovitch, O.; Aloisi, J.C. 210Pb sedimentation rates from the Northwestern Mediterranean margin. *Mar. Geol.* **2005**, *216*, 155–167, doi:10.1016/j.margeo.2005.02.020.
115. Zuo, Z.; Eisma, D.; Berger, G.W. Determination of sediment accumulation and mixing rates in the Gulf of Lions, Mediterranean Sea. *Oceanol. Acta* **1991**, *14*, 253–262.
116. Dorgan, K.M.; Jumars, P.A.; Johnson, B.D.; Boudreau, B.P. Macrofaunal burrowing: The medium is the message. *Oceanogr. Mar. Biol.* **2006**, *44*, 85–121.
117. Lamarque, B.; Deflandre, B.; Galindo Dalto, A.; Schmidt, S.; Romero-Ramirez, A.; Garabetian, F.; Dubosq, N.; Diaz, M.; Grasso, F.; Sottolichio, A.; et al. Spatial Distributions of Surface Sedimentary Organics and Sediment Profile Image Characteristics in a High-Energy Temperate Marine RiOMar: The West Gironde Mud Patch; SEANOE. 2021. Available online: http://b2find.eudat.eu/dataset/e591e5d7-3dbc-57bc-9588-532deed0a3c2 (accessed on 1 February 2021).

CHAPITRE 2

Structuration spatio-temporelle de la matière organique particulaire et de la composition de la macrofaune benthique dans la Vasière Ouest-Gironde

Spatio-temporal Dynamics of Surface Sediment Characteristics and Benthic Macrofauna Composition in a Temperate High-energy River-dominated Ocean Margin

Bastien Lamarque[1], Bruno Deflandre[2], Sabine Schmidt[2], Guillaume Bernard[1], Nicolas Dubosq[2], Mélanie Diaz[2], Nicolas Lavesque[1], Frédéric Garabetian[1], Florent Grasso[3], Aldo Sottolichio[2], Sylvain Rigaud[4], Alicia Romero-Ramirez[1], Marie-Ange Cordier[2], Dominique Poirier[2], Martin Danilo[2] and Antoine Grémare[1]

[1]UMR EPOC, Université de Bordeaux, CNRS, UMR 5805, Station Marine d'Arcachon, 2 rue du Professeur Jolyet, F33120 Arcachon, France

[2]UMR EPOC, Université de Bordeaux, CNRS, UMR 5805, Bâtiments B18/B18N, Allée Geoffroy Saint-Hilaire, F33615 Pessac CEDEX, France

[3]Departamento de Biologia Marinha, Instituto de Biologia, Universidade Federal do Rio de Janeiro, CEP 21941-902 Rio de Janeiro, Brazil

[4]IFREMER Brest—DYNECO/DHYSED, Centre de Bretagne, CS 10070, 29280 Plouzané, France

Abstract

The benthic compartment of River-dominated Ocean Margins (RiOMar) is largely affected by sedimentary processes, as well as natural and anthropogenic disturbances. Recent works confirmed the major importance of riverine inputs and hydrodynamics in the spatial structuration of low- and high-energy temperate RiOMar, respectively. Differences in the nature of these structuring factors could also affect the temporal dynamics of these two systems. The present study is aiming at: (1) quantifying spatio-temporal changes in surface sediment and benthic macrofauna within the West Gironde Mud Patch (WGMP; high-energy system) over two different time scales, (2) identifying the main environmental factors controlling those changes, and (3) achieving a comparison with the Rhône River Prodelta (RRP; low-energy system) in view of further characterizing the benthic component functioning of these two temperate RiOMar. For this purpose, surface sediment characteristics (grain size, quantitative and qualitative descriptors of particulate organic matter) and benthic macrofauna compositions were assessed based on four seasonal sampling of five stations located along a depth gradient within the WGMP. Results highlight the existence of spatial patterns for both surface sediment and benthic macrofauna, which are cued by hydrodynamics. These variables present classical seasonal changes, but benthic macrofauna compositions also show pluri-annual changes corresponding to a cicatrization process following a major disturbance caused by a series of severe storms. This underliness the major role of hydrodynamics in also controlling long-term temporal changes in WGMP benthic macrofauna compositions. Finally, the comparison with the RRP highlights major discrepancies in the main processes (i.e., hydrodynamics versus river hydrological regime) involved in the control of the surface sediment characteristics and benthic macrofauna compositions between the two systems, and thus further supports the current RiOMar typologies.

Keywords: RiOMar; West Gironde Mud Patch; North-East Atlantic shelf; Particulate organic matter; Benthic macrofauna; Spatio-temporal variations; Hydrodynamics; Storms

1. Introduction

Continental margins are key areas for the marine component of major biogeochemical cycles, accounting for the mineralization of 50 to 80% of continental Particulate Organic Carbon (POC) inputs (Aller 1998, Burdige 2005, Blair & Aller 2012). Those of the continental margins impacted by major river freshwater and sediment discharges are defined as River-dominated Ocean Margins (RiOMar). These areas provide a large variety of ecosystem services including provisioning (e.g. fisheries), regulating (e.g. carbon mineralization/burial) and supporting (e.g. nutrients cycling, habitats) services (Aller 1998, Levin et al. 2001, Lansard et al. 2009). RiOMar account for 40 to 50% of continental POC burial occurring in continental margins (Hedges & Keil 1995, Burdige 2005, Blair & Aller 2012). Their benthic components constitute the main marine primary depositional areas of riverine particulate inputs (McKee et al. 2004, Burdige 2005). Benthic biological compartments (e.g. macrofauna) and biogeochemical fluxes (e.g., mineralization) are herein largely affected by a large variety of natural and anthropogenic disturbances (Rhoads et al. 1985, Aller 1998, Lotze et al. 2006, Worm et al. 2006, Tesi et al. 2007, Ulses et al. 2008, Lansard et al. 2009).

The impact of both sediment discharges and associated organic matter inputs on the structuration of benthic macrofauna communities and biogeochemical functioning of the sediment-water interface has been documented for a large variety of RiOMar (Rhoads et al. 1985, Aller & Aller 1986, Alongi et al. 1992, Aller & Stupakoff 1996, Wheatcroft 2006, Harmelin-Vivien et al. 2009, Akoumianaki et al. 2013, Bonifácio et al. 2014). Mostly based on the analysis of macrofauna vertical distribution in the sediment column and X-ray radiographies, Rhoads et al. (1985) first proposed a conceptual model describing the response of benthic macrofauna and surface sediments to the inputs of major rivers. According to this model, macrofauna spatial distribution is mainly determined by the interaction between: (1) the physical disturbance induced by intense continental particles inputs, and (2) Particulate Organic Matter (POM) availability. In proximal (i.e., the closest to the river mouth) parts of RiOMar, high and irregular sedimentation rates induce sedimentary instability, precluding the establishment of mature macrobenthic communities. Moreover, high turbidity of river plumes limits primary production in the water column, resulting in mainly low (and refractory) POM concentrations in surface sediments. Accordingly, RiOMar proximal areas are characterized by low bioturbation intensities and low mineralization fluxes. Conversely, in distal (i.e., deeper)

parts, moderated sedimentation and enhanced primary production in the water column allow for the establishment of mature macrobenthic communities, high bioturbation intensities and mineralization fluxes.

Later RiOMar classification attempts have been based on meta analyses (mostly achieved on tropical and subtropical systems) of geomorphological and biogeochemical processes (McKee et al. 2004, Blair & Aller 2012). Results highlighted the major effect of hydrodynamics regimes on RiOMar morphologies and POC mineralization/burial intensities. One of the clear limitations of the Rhoads et al. (1985) model is the attribution of sediment instability to the sole sedimentation of riverine particulate inputs, whereas it may also largely depend on local hydrodynamics. This led Blair & Aller (2012) to draw a clear distinction between: (1) low-energy systems, with both high sedimentation rates and carbon preservation (later referred as type 1), and (2) high-energy tidal and/or wave systems with both high sediment oxygenation and low carbon preservation rates (later referred as type 2). Lamarque et al. (2021) recently assessed the main environmental factors responsible for the spatial structuration of temperate type 1 and type 2 systems based on the comparison between spatial surveys conducted within the Rhone River Prodelta (RRP; type 1, French Mediterranean coast) and the West Gironde Mud Patch (WGMP; type 2, French Atlantic coast). Their results confirmed the major importance of riverine inputs and local hydrodynamics in the spatial structuration of type 1 and type 2 temperate RiOMar, respectively.

Such a difference in the nature of their main structuring factors could as well affect the spatio-temporal dynamics of the two systems. Seasonal changes in both surface sediment characteristics and benthic macrofauna composition along a depth gradient have already been addressed within the RRP by Bonifácio et al. (2014). Results showed that temporal changes were larger at the most proximal station in relation with changes in river flow. Larger changes were observed after a prolonged low flow period, which allowed for the development of a mature macrobenthic community (otherwise precluded due to high sedimentation rates and POM riverine inputs). Conversely, temporal changes in benthic surface sediment characteristics and benthic macrofauna composition within the WGMP have been largely neglected so far. The only available quantitative benthic macrofauna composition data have been collected during July 2010 at only 3 stations (Massé et al. 2016). Consequently, the controlling factors and the magnitude of spatio-temporal changes in surface sediment

characteristics and benthic macrofauna composition within the WGMP (taken as an example of temperate type 2 RiOMar) are still largely unknown.

The present study is aiming at filling this gap by: (1) quantifying spatio-temporal changes in surface sediment characteristics and benthic macrofauna composition within the WGMP over both short (2016-2018) and long (2010-2018) time scales, (2) identifying the main environmental factors potentially controlling these changes, and (3) achieving a comparison with the RRP in view of further characterizing the benthic components of temperate type 1 and type 2 RiOMar.

2. Materials and Methods

2.1. Sampling area

The West Gironde Mud Patch (WGMP) is a 420 km^2 sedimentary body located on the Bay of Biscay 40 km off the Mouth of the Gironde Estuary, between ca. 30 and 75 m depth (Figure 2.1A). This relict paleovalley/depression is the primary depocenter (sedimentation rates between less than 1 and 10 $mm.y^{-1}$; Dubosq et al. 2021) of fine particles originating from the Gironde Estuary, which has an annual mean water flow of 944 $m^3.s^{-1}$ (Doxaran et al. 2009) with daily flows up to 7,500 $m^3.s^{-1}$ during winter floods (Constantin et al. 2018). The WGMP is located in a macro-tidal environment with a tidal range from 1.5 to 5 m (Jalón-Rojas et al. 2018). The continental shelf off the Mouth of the Gironde Estuary is periodically submitted to strong swells/waves, which can reach maximal amplitudes of 15 m and periods of 15 s during winter storms (Cirac et al. 2000, Masselink et al. 2016). These hydrological conditions prevent the sedimentation of fine particles in the immediate vicinity of the Gironde mouth (Jouanneau et al. 1989).

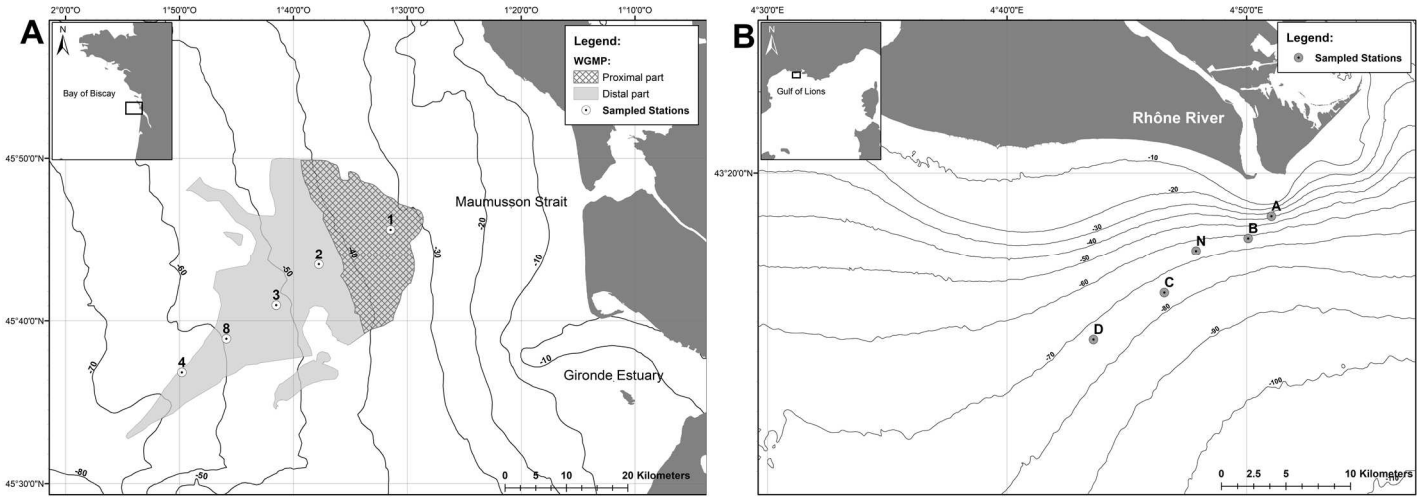

Figure 2.1. Map showing the delimitation of: (**A**) the West Gironde Mud Patch (WGMP) along the French Atlantic Coast together with the locations of the 5 sampled stations. Stations 1, 3 and 4 were also sampled in July 2010 (corresponding to stations E, C and W in Massé et al. 2016, respectively); and (**B**) the Rhône River Prodelta in the Gulf of Lions (NW Mediterranean) together with the locations of the 5 sampled stations (Bonifácio et al. 2014).

The sedimentology of the WGMP has been extensively studied based on stratigraphic sequences, palynological data, X-ray radiographies and radiochronographies (Longère & Dorel 1970, Castaing et al. 1979, 1982, Castaing & Allen 1981, Lesueur et al. 2001, 2002, Jouanneau et al. 1989, Lesueur et al. 1989, 1991, 1996, Weber et al. 1991, Lesueur & Tastet 1993, 1994, Gadel et al. 1997, Parra et al. 1998). These surveys have attributed a major role to hydrodynamics in controlling the spatial structuration of the WGMP. This paradigm was based on both: (1) the segmentation between a proximal and a distal part with no modern persistent sedimentation in the former due to strong hydrodynamics, and (2) the decreasing frequency of occurrence of vertical erosional sequences within the sediment column with station depth (Jouanneau et al. 1989, Lesueur et al. 1991, 2001, 2002, Lesueur & Tastet 1994). It was recently further validated by a synoptic survey of the spatial distributions of surface sediment characteristics and biological activity traces (Lamarque et al. 2021).

2.2. Sampling of surface sediment and benthic macrofauna

Five stations located within the WGMP along a depth gradient (Figure 2.1A, Table 2.I) were sampled for surface sediment characteristics and benthic macrofauna during four cruises, which took place on board of the R/V Côtes de la Manche in October-November 2016 (hereafter October 2016, JERICObent-1; Deflandre 2016), August 2017 (JERICObent-2; Deflandre 2017), January-February 2018 (hereafter February 2018; JERICObent-3; Deflandre

2018a) and April-May 2018 (hereafter April 2018; JERICObent-4; (Deflandre 2018b). Only 4 stations were sampled in February 2018 due to bad meteorological conditions. During each cruise, 4 sediment cores (10 cm internal diameter) were collected at each station using an Oktopus GmbH® multiple corer. The upper top 0.5 cm was sliced and immediately frozen (-20°C) on board prior further analyses. A single core was used to assess sediment grain size, Sediment Surface Area (SSA; Mayer 1994), Particulate Organic Carbon (POC) and $\delta^{13}C$. The remaining 3 cores were used to assess chloropigment and amino acid contents. Benthic macrofauna was sampled using a 0.25 m² Hamon grab (3 replicates), sieved on a 1 mm mesh and fixed with 4% formalin.

2.3. Gironde Estuary water flows

Daily water flows of the Gironde Estuary were calculated by summing the flows of its two main tributaries, the Garonne and Dordogne Rivers, measured at Tonneins and Pessac-sur-Dordogne, respectively. Data were provided by the French Ministère de l'Ecologie, du Développement Durable et de l'Energie (http://www.hydro.eaufrance.fr).

Table 2.I. Location (WGS84, degrees, and decimal minutes) and depth of the 5 stations (1, 2, 3, 8, 4) sampled in the West Gironde Mud Patch (WGMP) during the present study and of the 5 stations (A, B, N, C, D) sampled in the Rhône River Prodelta (RRP) by Bonifácio et al. (2014).

System	Station	Latitude (N)	Longitude (W)	Depth (m)
WGMP	1	45°45.580'	1°31.489'	37
	2	45°43.511'	1°37.773'	47.8
	3	45°41.007'	1°41.545'	56.5
	8	45°38.873'	1°45.777'	64.5
	4	45°36.924'	1°49.712'	71.5
RRP	A	43°18.690'	04°51.042'	24
	B	43°18.013'	04°50.068'	54
	N	43°17.626'	04°47.896'	67
	C	43°16.343'	04°46.565'	76
	D	43°14.917'	04°43.613'	74

2.4. Bottom Shear Stress

At each of the 5 sampled stations (Figure 2.1, Table 2.I), daily values of Bottom Shear Stress (BSS) were computed from a tridimensional numerical model (Diaz et al. 2020). This model, stretching from the Gironde Estuary to the continental shelf, is based on the MARS3D hydrodynamic model (Lazure & Dumas 2008) and the WAVE WATCH III® wave model (Roland & Ardhuin 2014). Its curvilinear mesh resolution is ca. 0.5x0.5 km^2 over the WGMP. The model integrates realistic hydro-meteorological forcing (i.e. wind, tide, surge and river flow). BSS were computed as the combination of their current-induced and wave-induced components following Soulsby's formulation (Soulsby 1997). A more detailed description of the model can be found in Grasso et al. (2018). Simulations achieved during the present study provided hourly outputs from 2010 to 2018 that were daily compiled, and 95^{th} percentiles were used to characterize BSS intensities to account for intense hydrodynamic events. Since BSS correlates negatively with station depth (Lamarque et al. 2021), their temporal changes were presented only for the station 3.

2.5. Analysis of surface sediment characteristics

Grain size was measured on aliquots of unreplicated sediment samples using a Malvern® Master Sizer laser microgranulometer. Almost all distributions were unimodal and therefore characterized through their median diameter ($D_{0.5}$). SSA was measured on freeze-dried sediment samples, previously degassed overnight at 150°C, using a Gemini® VII Surface Area Analyzer (Micromeritics® 2390a model) with the multi-point Brunauer-Emmett-Teller method (Mayer 1994). POC was assayed using a LECO® CS 200 analyzer, after 2M HCl overnight decarbonation (Etcheber et al. 1999) of previously freeze-dried unreplicated sediment samples. POC concentrations were normalized for SSA (i.e., expressed in terms of mass per SSA) since these two parameters were assessed on the same sediment core at each combination of stations*dates.

Total and Enzymatically Hydrolysable Amino Acids (THAA and EHAA) were analyzed on triplicates for each of the 3 sampled cores. THAA were extracted through acid hydrolysis (6M HCl, 100°C, 24h). EHAA were extracted following the biomimetic approach proposed by Mayer et al. (1995). THAA and EHAA were derivatized to form fluorescent amino compounds, which were separated by reverse phase High-Performance Liquid Chromatography (Agilent® 1260 INFINITY) on a Phenomenex® Kinetex 5µm EVO C18 column and detected using a 338 nm

excitation wavelength. Concentrations were expressed in terms of mass per mass of sediment dry wet since SSA were not measured on the same sediment cores.

Chlorophyll-*a* (Chl-*a*) and Phaeophytin-*a* (Phaeo-*a*) were assayed on unreplicated thawed frozen (-20°C) sediment samples after overnight acetone extraction (90% final concentration) using a Perkin Elmer® LS-55 spectrofluorometer following Neveux & Lantoine (1993). Concentrations were expressed in terms of mass per mass of sediment dry wet since SSA was not measured on the same sediment cores.

The Chl-*a*/(Chl-*a* + Phaeo-*a*) ratio was used as a lability index of vegetal biomass (Pastor et al. 2011, Bonifácio et al. 2014) and the EHAA/THAA ratio was used as a lability index of bulk sedimentary organics (Wakeham et al. 1997, Medernach et al. 2001, Grémare et al. 2005, Pastor et al. 2011, Bonifácio et al. 2014).

For the analysis of OC isotopic ratio, duplicated freeze-dried sediment samples were decarbonated (1M HCl) and later analyzed using a Thermo Scientific® Delta V plus IRMS coupled with a Thermo Scientific® Flash 2000 EA. Raw measurements were converted in usual $\delta^{13}C$ units (Coplen 2011).

2.6. Analysis of benthic macrofauna

Macrofauna was sorted, identified to the lowest tractable taxonomic level and counted. Species richness was computed on pooled replicates for each combination of stations and dates. Biomasses (Ash-Free Dry Weights, AFDW) were measured for each individual taxon as ignition loss (450°C, 4 h) except for Ophiuridae taxa for which an allometric regression was used to account for arm loss: AFDW = 0.0111 x (disk diameter)$^{2.5268}$ (where AFDW and disk diameter are expressed in g and mm, respectively; N. Lavesque, personal communication). Abundances and biomasses were then standardized per m^2.

2.7. Data analysis

To identify the most pertinent time scales for assessing the structuring role of river flow and hydrodynamics on spatio-temporal changes in surface sediment characteristics (i.e., mean: SSA, POC/SSA, Chl-*a*, Phaeo-*a*, Chl-*a*/(Chl-*a*+Phaeo-*a*) ratio, THAA, EHAA, EHAA/THAA ratio and $\delta^{13}C$) and macrofauna community composition, the Pearson correlation coefficients

linking their similarity matrices (Euclidean and Bray-Curtis distances, respectively) with both River flow and BSS were computed. This was achieved using R version 3.6.1 (R Core Team, 2019) with the additional packages vegan (Oksanen et al. 2019), BBmisc (Bischl et al. 2017) and Hmisc (Harrell 2021) for River flow and BSS integrated over 1 to 365 days before each of the 4 cruises.

For the same surface sediment characteristics (same variables as described above), hierarchical clustering (Euclidean distance and average group linking) and Principal Components Analysis (PCA) were used to define groups of stations*sampling dates and to assess relationships between variables. A SIMilarity PROFile procedure (SIMPROF, Clarke et al. 2008) was used to test for the statistical significance of between-group differences. SIMilarity PERcentage analysis (SIMPER, Clarke 1993) was used to identify the sediment characteristics contributing most to those differences. A DISTance-based Linear Model (DISTLM) was established to assess the potential contributions of river flow and BSS to spatio-temporal changes in surface sediment characteristics. This model was built using the Best selection procedure (Anderson et al. 2008) and the AIC selection criterion (Akaike 1973). It was represented in a multidimensional space through a distance-based Redundancy Analysis (dbRDA; Anderson et al. 2008). All surface sediment analyses were performed on normalized data and River flow and BSS were summed over both a 100 (i.e., seasonal) and 365 (i.e., annual) days periods (later $Flow_{100}$, $Flow_{365}$, BSS_{100} and BSS_{365}) based on results of the above-described correlation analysis. Station depth, Annual Julian Days (i.e., AJD: the number of days since the beginning of the sampling year), and Cumulated Julian Days (i.e., CJD: the number of days since the first day of the October 2016 cruise) were introduced as supplementary variables. The same approach was used for benthic macrofauna abundances. However, in this case and because of the use of the Bray-Curtis similarity, a Non-metric Multidimensional Scaling (nMDS) was achieved instead of a PCA. Moreover, an intermediate DISTLM/dbRDA was achieved using macrofauna composition as response variable and normalized surface sediment characteristics as predictor variables. POC, Phaeo-*a* and EHAA were excluded from the DISTLM procedure due to their correlation with other sediment characteristics.

A long-term comparison with macrofauna abundance data collected in July 2010 at stations 1, 3 and 4 (i.e., station E, C and W in Massé et al. 2016) was achieved through hierarchical clustering (Bray-Curtis distance and average group linking) and nMDS together with the SIMPROF and SIMPER procedures. To avoid possible inconsistencies in taxa

identification, these analyses were conducted at the genus level (square-root transformed data).

All multivariate analyses were computed using the PRIMER® 6 software package (Clarke & Warwick 2001) with the PERMANOVA+ add-on (Anderson et al. 2008).

Intra-station temporal variabilities in sediment surface characteristics and benthic macrofauna composition were compared in the WGMP (4 cruises during the 2016-2018 sampling period) and the Rhône River Prodelta (4 cruises during the 2007-2011 sampling period; Figure 2.1B; Table 2.I; Bonifácio et al. 2014) based on the information contained in dissimilarity matrices computed using: (1) $D_{0.5}$, POC, Chl-*a*, Phaeo-*a*, Chl-*a*/(Chl-*a*+Phaeo-*a*) ratio, THAA, EHAA and EHAA/THAA ratio (i.e., all the surface sediment characteristics measured during both studies), and (2) benthic macrofauna abundances. The sums of squared distances from individual points (i.e., station*sampling date) to their group (i.e., station) centroids were computed for each station (following Anderson 2001 and Anderson et al. 2008) and used as an indices of intra-station temporal variability after standardization for the number of sampling dates. Variables contributing most to intra-station temporal variabilities were also identified.

3. Results

3.1. Water flows and Bottom Shear Stress over the 2010-2018 period

Water flows presented a clear seasonal pattern with winter floods (peaks up to 5 590 $m^3.s^{-1}$ on January 23 2018) and low water period during summer and fall (Figure 2.2A). Over the whole 2010-2018 period, major events were clearly constituted by the January 2018 and to a slightly lower extent, the January 2014 floods. Between October 2016 and April 2018, there were clear inter-annual differences in water flows during the high-flow period as indicated by the moderate values recorded during the 2016-2017 as opposed to 2017-2018 winter. The July 2010 cruise (Massé et al. 2016) was achieved immediately after the end of a high-flow period. The October 2016 and August 2017 cruises were achieved during low-flow periods (112 and 67 days after the end of the preceding high-flow period, respectively). Conversely, both the February 2018 and the April 2018 cruise took place during a high-flow period, respectively 5 and 87 days after the January 2018 flood.

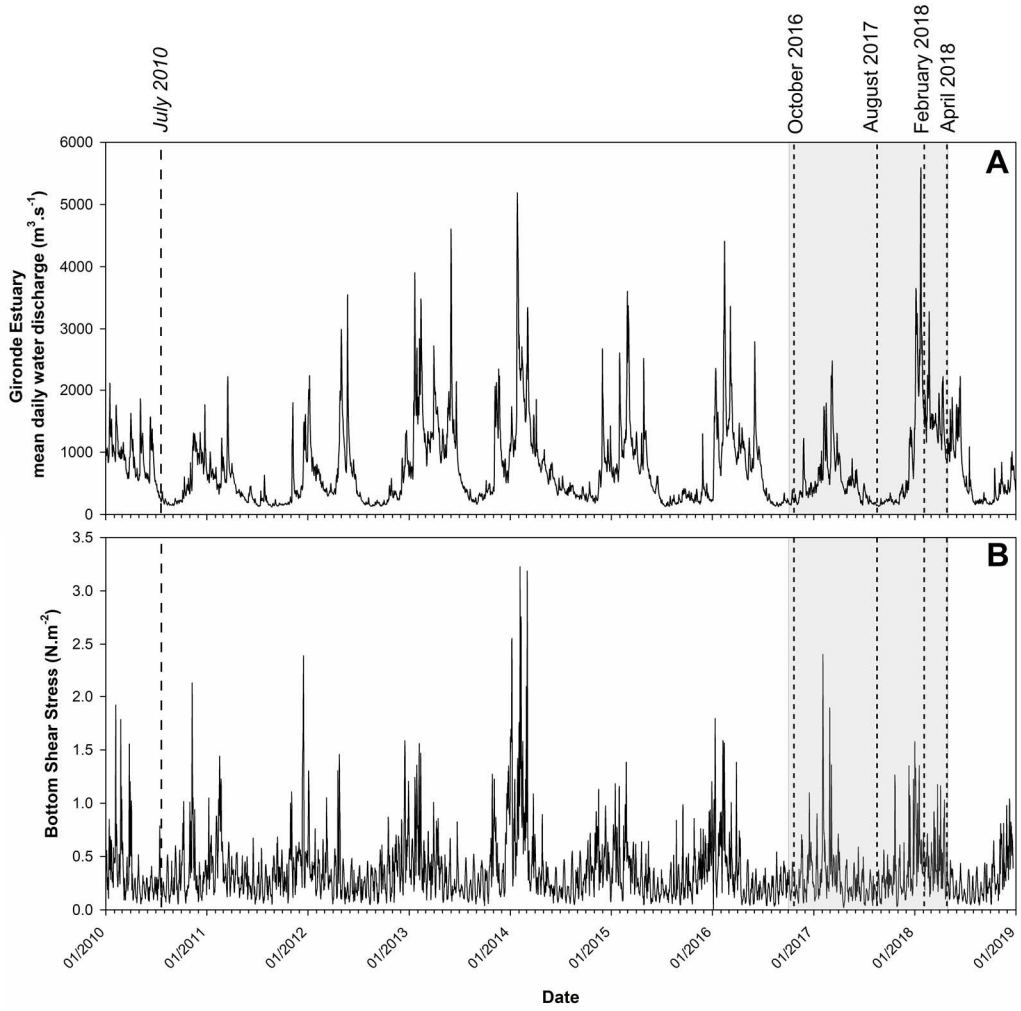

Figure 2.2. Temporal changes in Gironde Estuary mean daily water flows (**A**) and in the 95th percentile of Bottom Shear Stress at station 3 (**B**) during the 2010-2018 period. The short-dashed lines indicate the four cruises achieved between 2016 and 2018 (grey area) and the long-dashed line indicates the July 2010 cruise (Massé et al., 2016).

Bottom Shear Stress (BSS) also showed a clear seasonal cycle with a succession of peaks induced by winter storms and conversely low values during summer and fall (Figure 2.2B). Over the whole 2010-2018 period, the major event was the succession of peaks (i.e., up to 3.23 N.m^{-2}) induced by the repetition of strong storms during the 2013-2014 winter. The July 2010 cruise (Massé et al. 2016) was achieved immediately after a low-BSS period. Between 2016 and 2018, there were slight differences between temporal changes in water flows and BSS since: (1) high-BSS periods generally preceded high-flow periods, and (2) highest BSS (up to 2.40 N.m^{-2} on February 3 2017) were recorded during 2016-2017 conversely to highest water flows, which were recorded in 2018. Nevertheless, both the October 2016 and August 2017 cruises were conducted during low-BSS periods (i.e., <0.5 N.m^{-2}) as opposed to the February 2018 and the April 2018 cruises, which both took place during the 2017-2018 high-BSS period.

3.2. Short-term (2016-2018) spatio-temporal changes in surface sediment characteristics

Median grain sizes ($D_{0.5}$) of surface sediments were usually coarser (60, 76 and 92 µm in October 2016, August 2017 and February 2018, respectively) and much more variable (16 µm in April 2018) at the most proximal station 1 compared to other stations (Table 2.II, Figure 2.3A). At all other sampled stations, $D_{0.5}$ were homogeneous (mean values around 20 µm) and temporally stable. Spatio-temporal changes in $\delta^{13}C$ values were limited (i.e. between −25.12 and −23.01 ‰) with the exception of station 1 in October 2016 (−18.11 ‰, Table 2.II, Figure 2.3B). Particulate Organic Carbon (POC) concentrations showed a clear increase along the depth gradient (i.e., from stations 1 to 4), with a maximal value of 1.79 $mg.m^{-2}$ SSA at station 4 during April 2018 (Table 2.II, Figure 2.3C). The only exception to this pattern was recorded in February 2018 with a maximal value of 1.58 $mg.m^{-2}$ SSA at station 3. At station 4, POC was higher in April 2018 than during the 3 other cruises (mean value of 1.44 $mg.m^{-2}$ SSA). Total Hydrolysable Amino Acid concentrations (THAA) also showed a clear increase along the depth gradient (Table 2.II, Figure 2.3D). THAA ranged from 0.51 $mg.gDW^{-1}$ (station 1 in August 2017) to 4.65 $mg.gDW^{-1}$ (stations 3 and 4 in April 2018). Temporal changes in THAA were lower at station 4 (variation coefficient of 5.4 % versus a mean of 22.0 % at the 4 other stations). Chlorophyll-*a* concentrations (Chl-*a*) at station 1 were low (i.e., between 0.23 and 0.66 $µg.gDW^{-1}$ in August 2017 and April 2018, respectively) during all cruises, (Table 2.II, Figure 2.3E). At all stations but station 1, Chl-*a* concentrations were much higher in April 2018 (with a maximal value of 5.86 $µg.gDW^{-1}$ at station 4) than during the 3 other cruises (mean value of 1.09 ± 0.37 $µg.gDW^{-1}$ for stations 2, 3, 8 and 4).

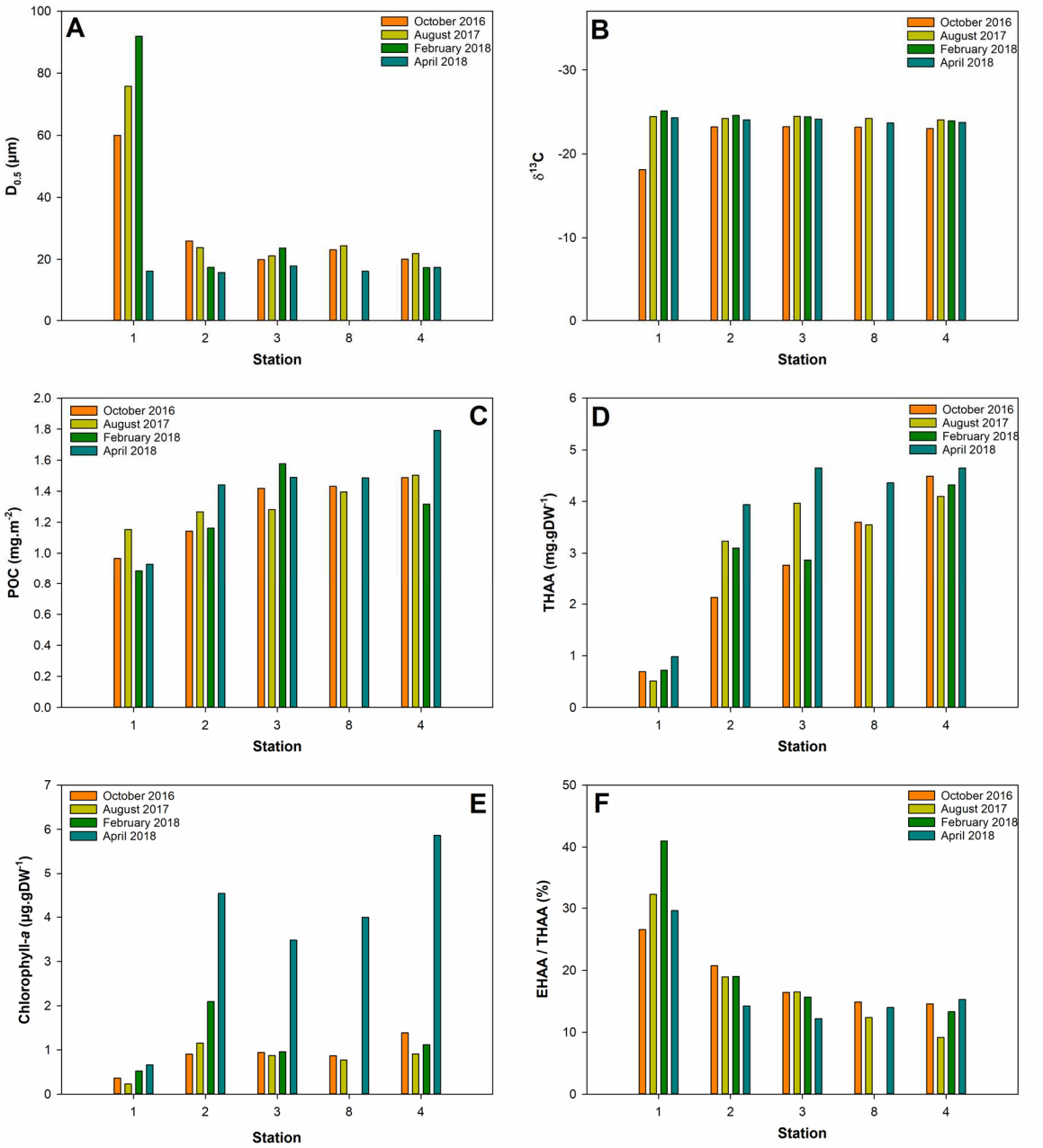

Figure 2.3. Spatio-temporal changes in the (mean) values of surface sediment characteristics between 2016 and 2018: Median grain size ($D_{0.5}$; **A**), $\delta^{13}C$ (**B**), Particulate Organic Carbon concentration normalized by SSA (POC; **C**), Total Hydrolysable Amino Acids concentration (THAA; **D**), Chlorophyll-*a* concentration (**E**), and Enzymatically/Total Hydrolysable Amino Acids ratio (EHAA/THAA; **F**). Stations are ordered according to their depth.

Enzymatically/Total Hydrolysable Amino Acids ratio (EHAA/THAA) presented a clear decrease along the depth gradient (Table 2.II, Figure 2.3F). EHAA/THAA was maximal (41.0 %) at station 1 in February 2018 and minimal (9.1 %) at station 4 in August 2017. Temporal changes were higher at stations 4 and 1 (variation coefficient of 21.0 and 19.2 %, respectively) than at the 3 other stations (mean variation coefficient of 12.7 %).

Table 2.II. Mean values (± standard deviations for replicated measures) of surface sediment and benthic macrofauna characteristics. $D_{0.5}$: median grain size, SSA: Sediment Surface Area, POC: Particulate Organic Carbon, Chl-*a*: Chlorophyll-*a*, Phaeo-*a*: Phaeophytin-*a*, THAA: Total Hydrolyzable Amino Acids, EHAA: Enzymatically Hydrolyzable Amino Acids, SR: Species Richness and J': Pielou's evenness.

Cruise	Station	$D_{0.5}$ (µm)	SSA ($m^2.gDW^{-1}$)	POC ($mg.m^{-2}$)	Chl-*a* ($\mu g.gDW^{-1}$)	Phaeo-*a* ($\mu g.gDW^{-1}$)	Chl-*a*/(Chl-*a*+Phaeo-*a*) (%)	THAA ($mg.gDW^{-1}$)	EHAA ($mg.gDW^{-1}$)	EHAA/THAA (%)	$\delta^{13}C$ (‰)	Abundance ($ind.m^{-2}$)	Biomass ($mgAFDW.m^{-2}$)	SR ($taxa.0.75m^{-2}$)	J'
October 2016	1	60.0	5.0	0.97	0.36 ± 0.10	2.95 ± 0.27	10.9 ± 2.0	0.69 ± 0.06	0.18 ± 0.05	26.5 ± 4.5	-18.11 ± 0.41	544.0 ± 198.9	1969.2 ± 2260.5	38	0.73
	2	26.0	6.1	1.14	0.90 ± 0.36	8.27 ± 1.05	10.0 ± 4.6	2.13 ± 0.13	0.44 ± 0.06	20.7 ± 1.8	-23.20 ± 0.05	410.7 ± 112.0	4473.4 ± 4494.1	30	0.69
	3	20.0	8.1	1.42	0.94 ± 0.02	8.39 ± 1.11	10.2 ± 1.3	2.77 ± 0.10	0.45 ± 0.02	16.4 ± 1.1	-23.23 ± 0.13	141.3 ± 68.2	474.2 ± 433.1	16	0.89
	8	23.1	7.5	1.43	0.87 ± 0.35	6.75 ± 0.37	11.3 ± 4.2	3.60 ± 0.23	0.53 ± 0.07	14.9 ± 2.6	-23.16 ± 0.08	228.0 ± 28.0	1922.4 ± 890.6	27	0.88
	4	20.1	10.3	1.49	1.39 ± 0.47	9.59 ± 1.69	13.0 ± 5.8	4.49 ± 0.27	0.65 ± 0.12	14.6 ± 3.2	-23.01 ± 0.03	92.0 ± 42.3	796.2 ± 418.2	18	0.92
August 2017	1	75.8	2.5	1.15	0.23 ± 0.09	1.46 ± 0.46	13.4 ± 2.5	0.51 ± 0.18	0.16 ± 0.04	32.2 ± 3.8	-24.44 ± 0.35	784.0 ± 360.6	958.1 ± 552.5	43	0.67
	2	23.8	7.3	1.27	1.15 ± 0.20	6.65 ± 0.88	14.9 ± 2.7	3.23 ± 0.29	0.61 ± 0.02	18.9 ± 1.4	-24.22 ± 0.55	294.7 ± 109.3	1405.8 ± 259.1	26	0.68
	3	21.2	8.4	1.28	0.87 ± 0.05	6.07 ± 1.64	13.1 ± 3.2	3.97 ± 0.07	0.66 ± 0.10	16.5 ± 2.2	-24.46 ± 0.10	218.7 ± 154.6	754.9 ± 189.9	24	0.67
	8	24.4	7.6	1.40	0.77 ± 0.29	5.25 ± 0.57	12.7 ± 4.0	3.55 ± 0.10	0.44 ± 0.01	12.3 ± 0.5	-24.22 ± 0.19	89.3 ± 43.1	1081.0 ± 1147.4	18	0.92
	4	21.9	9.3	1.50	0.91 ± 0.18	6.90 ± 1.28	12.0 ± 4.0	4.10 ± 0.19	0.38 ± 0.02	9.1 ± 0.5	-24.03 ± 0.38	176.0 ± 60.4	2569.4 ± 1698.6	27	0.92
February 2018	1	92.0	1.9	0.89	0.52 ± 0.37	2.53 ± 1.58	16.4 ± 1.8	0.72 ± 0.32	0.29 ± 0.12	41.0 ± 2.0	-25.12 ± 0.23	840.0 ± 342.0	1625.4 ± 541.0	32	0.62
	2	17.5	14.2	1.16	2.09 ± 0.72	9.61 ± 2.47	17.6 ± 1.5	3.10 ± 0.16	0.59 ± 0.14	19.0 ± 4.2	-24.58 ± 0.48	269.3 ± 217.0	1149.6 ± 1093.7	35	0.81
	3	23.7	6.2	1.58	0.96 ± 0.19	6.22 ± 0.63	13.3 ± 1.3	2.87 ± 0.43	0.45 ± 0.06	15.7 ± 0.3	-24.41 ± 0.01	174.7 ± 130.1	1113.3 ± 1190.6	27	0.85
	4	17.4	12.6	1.32	1.12 ± 0.17	9.51 ± 1.86	10.6 ± 1.0	4.32 ± 0.43	0.57 ± 0.07	13.3 ± 3.0	-23.91 ± 0.10	162.7 ± 112.4	1313.4 ± 1035.7	22	0.88
April 2018	1	16.3	12.9	0.93	0.66 ± 0.05	3.67 ± 0.38	15.2 ± 0.5	0.98 ± 0.51	0.26 ± 0.04	29.6 ± 11.0	-24.29 ± 0.002	821.3 ± 615.5	1271.2 ± 175.0	35	0.62
	2	15.8	11.0	1.44	4.54 ± 1.96	18.16 ± 8.17	20.1 ± 0.6	3.94 ± 0.67	0.56 ± 0.07	14.2 ± 1.4	-24.05 ± 0.05	314.7 ± 32.6	1569.5 ± 1071.7	25	0.67
	3	17.9	7.7	1.49	3.48 ± 1.98	15.57 ± 8.18	18.1 ± 0.6	4.65 ± 1.44	0.56 ± 0.11	12.2 ± 1.2	-24.11 ± 0.20	134.7 ± 50.0	306.8 ± 354.9	25	0.84
	8	16.2	10.0	1.48	3.99 ± 1.66	18.37 ± 6.26	17.6 ± 2.1	4.36 ± 0.26	0.61 ± 0.03	14.0 ± 0.9	-23.69 ± 0.18	388.0 ± 69.4	1522.5 ± 1301.5	28	0.62
	4	17.4	8.9	1.79	5.86 ± 0.85	29.35 ± 2.83	16.6 ± 1.3	4.65 ± 0.49	0.72 ± 0.20	15.3 ± 2.8	-23.74 ± 0.31	882.7 ± 202.6	4985.9 ± 5475.4	33	0.45

The Pearson correlation coefficients values between summed river flows and the similarity matrices based on either surface sediment characteristics or benthic macrofauna composition are shown in Figure 2.4A. They first increased with summation period durations, became significant for a 53 days summation period and reached a maximal value of 0.34 for summation periods between 156 and 222 days. They then decreased constantly down to a value of 0.01 for a summation period of 365 days. Moreover, the correlation coefficients of benthic macrofauna composition similarity matrix with summed river flows remained insignificant over the whole range of tested summation periods.

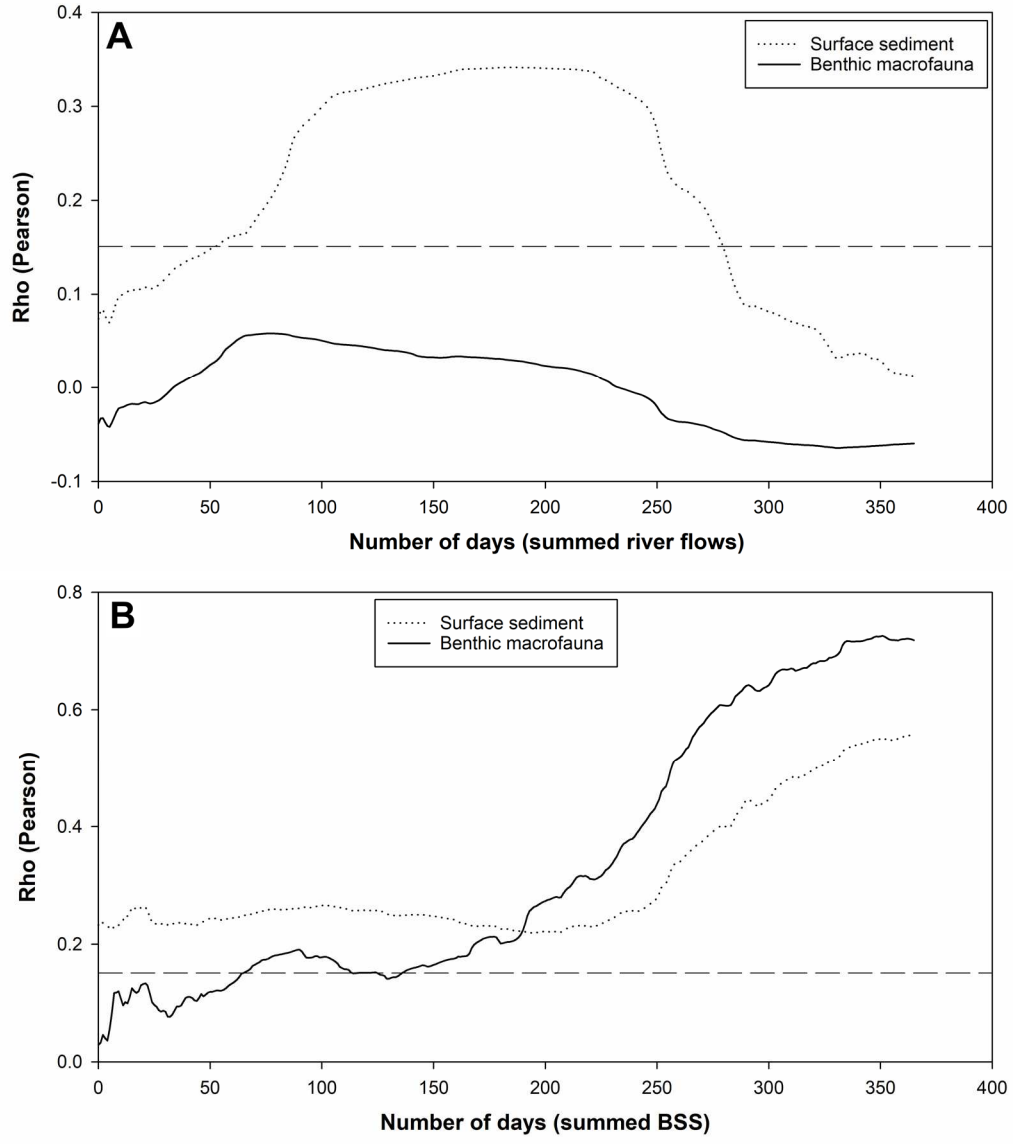

Figure 2.4. Changes in the Pearson correlation coefficient linking the similarity matrices based on either surface sediment characteristics or benthic macrofauna composition (all data collected between 2016 and 2018) with river flows (**A**) and BSS (**B**) summed over 1 to 365 days periods. Dotted lines represent the 0.05 significance threshold.

Conversely, the Pearson correlation coefficients linking the same matrices with summed BSS increased with the duration of the summation period for BSS (Figure 2.4B). In both cases, maximal correlation coefficients were recorded around 1-year summation period (i.e., 0.56 and 0.73 at 365 and 351 days, respectively). However, the patterns of changes with increasing summation periods clearly differed. Correlation coefficients for the surface sediment characteristics similarity matrix were always significant and almost constant for summation periods between 1 to ca. 250 days. Conversely, the benthic macrofauna composition similarity matrix did not significantly correlate with BSS for summation periods less than 65 days. It then presented a relative maximum (0.19 for a 90 days summation period) before almost constantly increasing for summation periods longer than 130 days.

The first two components of the Principal Component Analysis (PCA) based on surface sediment characteristics accounted for 72.8 % (i.e., 55.4 % and 17.4 % for the first and the second principal component, respectively) of the total variance (Figure 2.5A). Hierarchical clustering and the associated SIMPROF procedure resulted in the identification of 3 groups and 2 “isolated” stations*dates (Figure 2.5A). “Isolated” stations*dates consisted of station 2 in February 2018 and station 4 in April 2018. Group I was exclusively composed of stations 1 (all sampling dates). Group II was composed of all remaining stations*dates except for the April 2018 cruise. All the stations sampled during this cruise clustered into group III, except stations 1 (Group I) and 4 (isolated). The first principal component was mostly defined by the opposition between the quantitative and qualitative characteristics of surface sedimentary organics with THAA, EHAA, POC, Chl-*a*, Phaeo-*a* and POC concentrations on one side and the EHAA/THAA ratio on the other. The second component was mostly defined by the Chl-*a*/(Chl-*a*+Phaeo-*a*) ratio (Figure 2.5B). The average dissimilarity between groups I and II was 25.0 %, with EHAA/THAA ratio contributing for 20 %, $\delta^{13}C$ for 16.9 %, THAA for 16.3 %, and EHAA for 14.9 %. The average dissimilarity between groups II and III was 13.5 %, with Chl-*a*/(Chl-*a*+Phaeo-*a*) ratio (37.3 %), Chl-*a* (27.1 %) and Phaeo-*a* (16.5 %) contributing most. Station 2*February 2018 differed from group II (average dissimilarity of 10.8 %) due to higher SSA (contributing for 33.9 %), Chl-*a*/(Chl-*a*+Phaeo-*a*) ratio (contributing for 33.7 %) and lower POC (contributing for 10.7 %). Station 4*April 2018 differed from group III (average dissimilarity of 8.2 %) due to higher Phaeo-*a* (contributing for 38.0 %), POC (contributing for 22.5 %) and Chl-*a* (contributing for 17.5 %) concentrations.

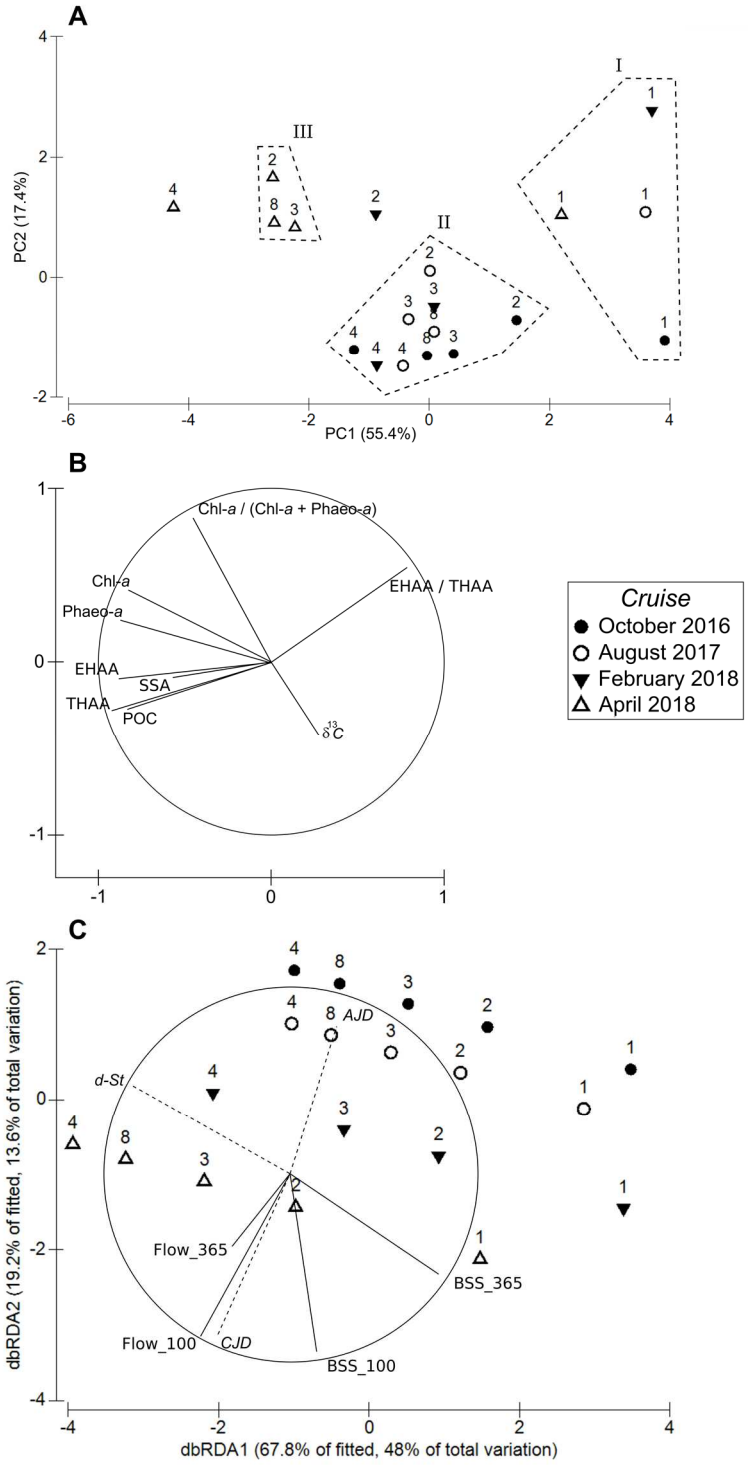

Figure 2.5. Multivariate analyses of surface sediment characteristics recorded between 2016 and 2018. Projection of stations*dates on the first plane of a Principal Component Analysis (**A**). Figures refer to stations and symbols to cruises. Dotted lines indicate groups of samples issued from the hierarchical clustering as identified through the SIMPROF procedure. Correlations of the variables with the first two principal components (**B**). Distance-based Redundancy Analysis based on summed BSS and river flows (**C**). Station depth (*d-St*), Annual Julian Days (*AJD*) and Cumulated Julian Days (*CJD*) were used as supplementary variables. SSA: Sediment Surface Area; POC: Particulate Organic Carbon; Chl-*a*: Chlorophyll-*a*; Phaeo-*a*: Phaeophytin-*a*; THAA; Total Hydrolysable Amino Acids; EHAA: Enzymatically Hydrolysable Amino Acids; BSS_100 and BSS_365: summed Bottom Shear Stress over 100 and 365 days; Flow_100 and Flow_365: summed river flow over 100 and 365 days.

The parsimonious DISTance-based Linear Model (DISTLM) included BSS_{100}, BSS_{365}, $Flow_{100}$ and $Flow_{365}$ as independent variables. It explained 70.7 % of the initial variance of surface sediment characteristics. Its representation through the first plane of the distance-based Redundancy Analysis (dbRDA) accounted for 61.6 % of this initial variance and clearly showed two main orientations (Figure 2.5C). The first one, mainly along the first component of the dbRDA, corresponded to the positioning of the stations along the depth gradient and was mainly cued by the BSS_{365}. The second one, mainly along the second component of the dbRDA, separated the 4 cruises and was mainly cued by the $Flow_{100}$ and to a lesser extent the BSS_{100}. When used as supplementary variables, cumulated and annual julian days correlated significantly ($p < 0.05$) with this second orientation. This correlation was slightly higher for cumulated julian days ($r = 0.934$ versus $r = 0.822$).

3.3. Short-term (2016-2018) spatio-temporal changes in benthic macrofauna composition

Overall, 6391 specimens belonging to 146 taxa were collected and identified (123 taxa after pooling species at the *Ampelisca*, *Glycera* and *Nephtys* genus) during the 4 cruises. Molluscs (mainly abundant at stations 1 and 2) represented 34 % of total macrofauna abundance, followed by polychaetes (27.8 %), echinoderms (22 %) and crustaceans (13.4 %). Species richness was higher at station 1, with a maximum of 43 taxa in August 2017 (Table 2.II, Figure 2.6A). Species richness did not show any clear spatio-temporal pattern. It tended to decrease from stations 1 to 3, where a minimal value of 16 taxa was recorded in October 2016, and seemed to increase from stations 3 to 4 in August 2017 and April 2018. Equitability tended to be lower at stations 1 and 2 than at stations 3, 8 and 4 (Table 2.II). It was temporally more stable at stations 1 and 2 than at stations 8 and 4, whose variability resulted from low values in April 2018 caused by exceptionally high abundances of two species (see below). Mean macrobenthic abundances were between 882.7 (station 4*April 2018) and 89.3 (station 8*August 2017) individuals per m^2 (Table 2.II, Figure 2.6B). Abundances were higher at station 1 and tended to decrease with depth. Only stations 8*April 2018 and 4*April 2018 differed from this general pattern with especially high values due to high densities of *Ampelisca spp.* (182.7 and 593.3 individuals per m^2 at station 8 and 4 respectively) and *Hyala vitrea* (93.3 and 100.0 individuals per m^2 at stations 8 and 4 respectively). Changes in mean macrobenthic biomasses did not show any clear spatio-temporal pattern (Table 2.II, Figure 2.6C) and were characterized by the occurrence of 3 outliers featuring high values. The high biomass recorded

for station 2*October 2016 resulted from the presence of both a single individual of *Asterias rubens* (2019.0 mgAFDW) and a high biomass of numerous individuals (i.e., 57.3 per m²) of *Abra alba* (910.6 mg.m^{-2} AFDW). The high biomasses recorded for station 4*August 2017 and station 4*April 2018 both resulted from the presence of a single individual of *Cereus pedunculatus* in August 2017 (747.0 mgAFDW) and of *Nephrops norvegicus* in April 2018 (2379.2 mgAFDW).

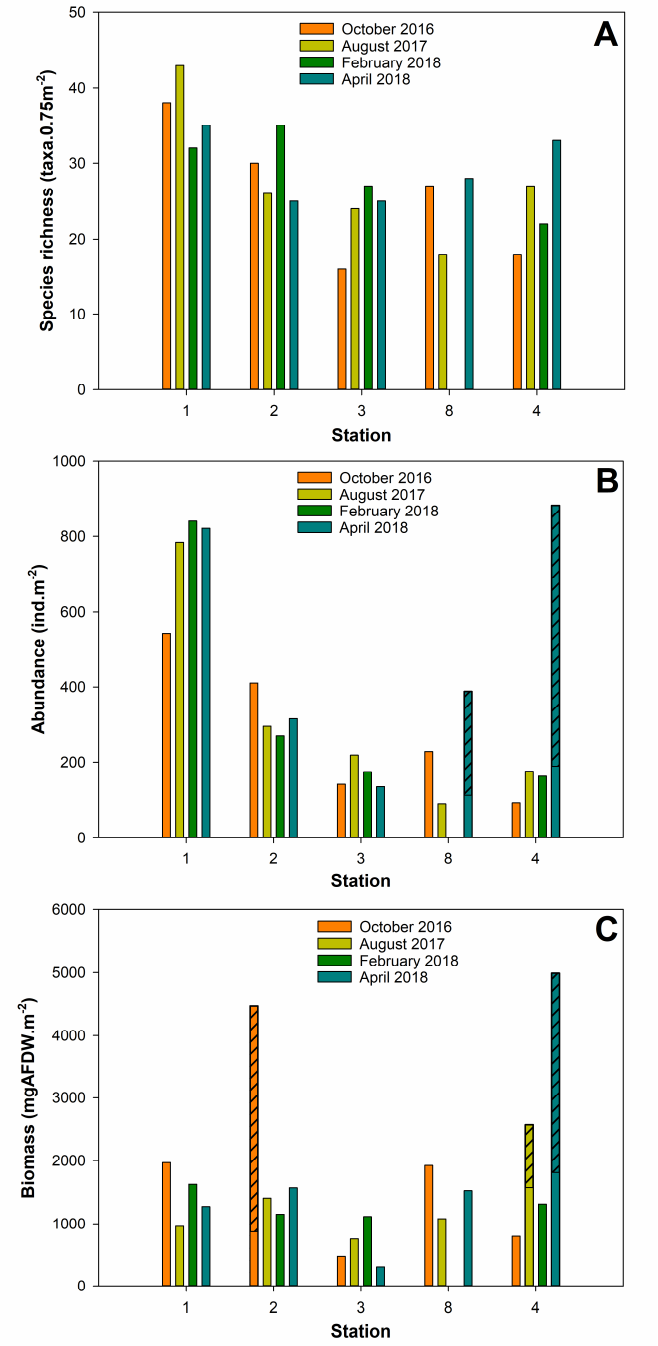

Figure 2.6. Spatio-temporal changes in the (mean) values of benthic macrofauna characteristics between 2016 and 2018: species richness (**A**), abundance (**B**), and biomass (**C**). Hatching corresponds to the exceptional presence of: (1) numerous individuals of a single taxon for abundance barplot and (2), high biomass of a single taxon for biomass barplot. Stations are ordered according to their depth.

The non-metric Multidimensional Scaling (nMDS) based on macrofauna abundance data collected between 2016 and 2018 is shown in Figure 2.7A. The horizontal dimension of the reduced space displayed correctly the order of stations along the depth gradient, reflecting the progressive change in benthic macrofauna composition with depth. For all stations, the vertical dimension of the reduced space mostly separated sampling cruises. The dispersion of the different cruises for each station suggests that between-cruises changes in benthic macrofauna composition were larger at deep (stations 3, 4 and 8) than at shallow (i.e., 1 and 2) stations. The hierarchical clustering further confirmed this pattern with the identification of 5 groups: (I) station 1 in February and April 2018, (II) station 2 during all sampling periods, (III) station 3 in February and April 2018, (IV) stations 8 and 4 in October 2016, and (V) stations 8 and 4 in August 2017, February 2018 and April 2018. Between-groups, between isolated stations*dates, and isolated stations versus groups dissimilarities resulted from low contributions of high numbers of taxa. Contributions to spatial changes were determined through the assessments of species contributions to between-clusters dissimilarities. Average dissimilarity between groups I and II (i.e., between stations 1 and 2) was 48.9 % with *Kurtiella bidentata* (16.3 %), *Nucula nitidosa* (6.0 %), *Cylichna cylindracea* (4.4 %) and *Venus casina* (4.1 %) contributing most, and being more abundant in stations of group I. Average dissimilarity between groups II and III (i.e., between stations 2 and 3) was 54.2 % with *Amphiura filiformis* (8.7 %), *K. bidentata* (6.3 %), *A. alba* (5.7 %) and *Ophiura ophiura* (5.6 %) contributing most, and being more abundant in stations of group II. Average dissimilarity between groups III and IV (i.e., between stations 3 and 8 and 4) was 54.6 % with *A. filiformis* (10.5 %, more abundant in group III), *Spiophanes afer* (5.8 %, more abundant in group IV), *Ancistrosyllis groenlandica* (5.7 %, more abundant in group III) and *Ampharete lindstroemi* (5.1 %, more abundant in group IV) contributing most. Average dissimilarity between groups III and V was 53.0 % with *Ampelisca spp.* (9.8 %, more abundant in group V), *A. filiformis* (9.7 %, more abundant in group III), *Mediomastus sp.* (4.4 %, more abundant in group V) and *Hyala vitrea* (4.1 %, more abundant in group V) contributing most. Contributions to temporal changes were determined through the assessments of species contributions to dissimilarities between (1) isolated stations*dates corresponding to the same station, (2) isolated stations*dates and groups containing the same station, and (3) dissimilarities between groups containing the same stations (i.e., groups IV and V). Here again, dissimilarities were due to low contributions of numerous taxa. Average dissimilarity between station 1*October 2016 and others stations 1*sampling dates was 42.0 % with *K. bidentata* (8.4 %, less abundant in October 2016), *A. alba* (7.5 %, more abundant in October 2016), *A. filiformis* (6.9 %, less

abundant in October 2016), and *V. Casina* (3.8 %, absent in October 2016) contributing most. Average dissimilarity between station 3*October 2016 and station 3*August 2017 was 48.2 %, with *A. filiformis* (13.4 %), *A. lindstroemi* (8.4 %), *Varicorbula gibba* (7.5 %) and *S. afer* (6.2 %) contributing most. With the exception of *A. filiformis*, all these taxa were more abundant in October 2016. Average dissimilarity between station 3*August 2017 and group III (the other sampling dates of stations 3) was 43.7 %, with *A. filiformis* (11.3 %, more abundant in August 2017), *Ampelisca spp.* (8.1 %, absent in August 2017), *K. bidentata* (7.2 %, more abundant in August 2017) and *A. groenlandica* (6.9 %, absent in August 2017) contributing most. Average dissimilarity between groups IV (stations 8 and 4 sampled in October 2016) and V (other stations 8 and 4 sampling dates) was 51.8 % with *Ampelisca spp.* (12.5 %), *Mediomastus sp.* (7.0 %), *H. vitrea* (4.8 %) and *S. afer* (4.7 %) contributing most. With the exception of *S. afer*, these taxa were more abundant at stations of group V.

The parsimonious DISTLM involving surface sediment characteristics as predictory variables included THAA and Chl-*a* concentrations. It explained 42.0 % of the initial variance of benthic macrofauna composition. Its representation through the first plane of a dbRDA also accounted for 42.0 % of this initial variance and clearly showed two main orientations (Figure 2.7B). The first one, mainly along the first component of the dbRDA, corresponded to the positioning of the stations along the depth gradient and was mainly cued by THAA concentrations. The second one, mainly along the second component of the dbRDA, separated stations (except station 1) sampled during April 2018 cruise from all other stations*dates, and was mainly cued by Chl-*a* concentrations. When used as supplementary variables, cumulated julian days correlated significantly with this second orientation ($r = 0.560$, $p < 0.05$) but not annual julian days ($r = 0.393$, $p = 0.07$). The parsimonious DISTLM involving BSS and river flows included BSS_{365}, $Flow_{100}$ and $Flow_{365}$ as independent variables. It explained 53.5 % of the initial variance of benthic macrofauna composition. Its representation through the first plane of a dbRDA accounted for 49.9 % of this initial variance and here again showed two main orientations (Figure 2.7C). The first one, along the first component of the dbRDA, corresponded to the positioning of the stations along the depth gradient and was mainly cued by BSS_{365}. The second one, along the second component of the dbRDA, separated the 4 cruises, and was mainly cued by $Flow_{100}$. The contribution of $Flow_{365}$ was poorly described by the first plane of the dbRDA. When used as supplementary variables, cumulated and annual julian days correlated significantly ($p < 0.05$) with this second orientation. This correlation was slightly higher for cumulated julian days ($r = 0.992$ versus $r = 0.820$).

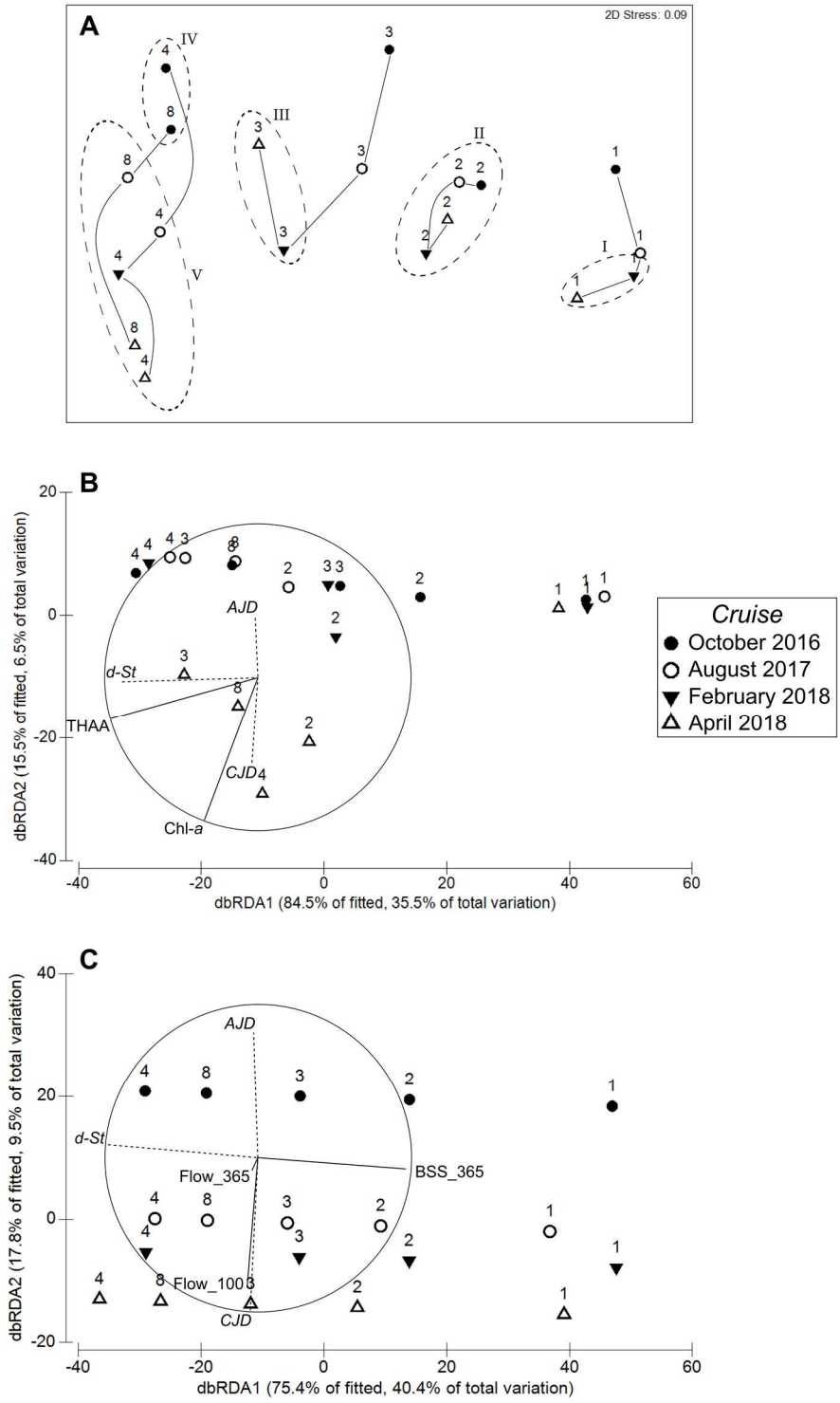

Figure 2.7. Multivariate analyses of benthic macrofauna compositions (all data collected between 2016 and 2018). Non-metric Multidimensional Scaling of macrofauna composition data for stations*dates during 2016-2018 cruises (**A**). Figures refer to stations and symbols to cruises. Solid lines represent trajectories of stations over time and dotted lines indicate groups of samples issued from the hierarchical clustering as identified through the SIMPROF procedure. Distance-based Redundancy Analysis based on surface sediment characteristics (**B**). Distance-based Redundancy Analysis based on summed BSS and river flows (**C**). Station depth (*d-St*), Annual Julian Days (*AJD*) and Cumulated Julian Days (*CJD*) were used as supplementary variables. Chl-*a*: Chlorophyll-*a*; THAA; Total Hydrolysable Amino Acids; BSS_365: summed Bottom Shear Stress over 365 days; Flow_100 and Flow_365: summed river flow over 100 and 365 days.

3.4. Long-term spatio-temporal changes (2010/2016-2018) in benthic macrofauna composition

The long-term comparison of univariate benthic macrofauna descriptors highlighted major differences between the July 2010 cruise (Massé et al. 2016) and the 4 cruises of the 2016-2018 period. Species richness values were in the same order of magnitude in July 2010 (32, 22 and 21 taxa at stations 1, 3 and 4, respectively) and in 2016-2018 (means of 37, 23 and 25 taxa at stations 1, 3 and 4, respectively). Conversely, abundances were much higher at station 1 in July 2010 than during all 2016-2018 cruises (1628.0 vs 747.3 ± 137.5 ind.m^{-2}, respectively). Abundances were also higher at station 3 (328.0 vs 167.4 ± 38.5 ind.m^{-2}, respectively), but tended to be equivalent at station 4 (118.7 in July 2010 vs 155.0 ± 43.4 ind.m^{-2} during 2016-2018 cruises) when excluding the rarely present individuals identified in April 2018 (see section 3.3). Biomasses were higher as well at stations 1 and 3 in July 2010 (4696.0 and 3495.7 mgAFDW.m^{-2}, respectively) than during the 2016-2018 cruises (means of 1456.0 ± 437.5 and 662.3 ± 353.0 mgAFDW.m^{-2}, respectively). They also tended to be equivalent at station 4 between July 2010 (1901.9 mgAFDW.m^{-2}) and 2016-2018 cruises (1374.2 ± 436.1 mgAFDW.m^{-2}) when excluding the large and rarely present individuals identified at station 4 during August 2017 and April 2018 (see section 3.3).

The representation of stations*dates through the non-metric Multidimensional Scaling (nMDS) based on macrofauna abundance data from the 2010 and 2016-2018 cruises is shown in Figure 2.8. The horizontal dimension clearly accounted for the positioning of stations along the depth gradient, whereas the vertical dimension separated sampling dates and more specifically July 2010 (Massé et al. 2016) from all the 2016-2018 cruises. Hierarchical clustering confirmed this pattern with the identification of 5 clusters. The first four were almost identical to those of the analysis conducted on the sole 2016-2018 data (see above) and group V was only constituted by stations 3 and 4*July 2010. The positioning of stations*dates along the horizontal dimension were similar in 2010 and 2016-2018 as opposed to their positioning along the second dimension, which showed important differences in benthic macrofauna composition between the 2010 and 2016-2018 cruises and suggested that these differences were larger at stations 3 and 4 than at station 1. Average dissimilarity between station 1*July 2010 and stations 1 from 2016-2018 cruises was 43.6 % with *Kurtiella* (14.7 %), *Owenia* (4.7 %), *Gammarus* (4.1 %) and *Ampelisca* (4.0 %) genus contributing most. All genus were more abundant in July 2010 than in 2016-2018. Average dissimilarity between station 3*July 2010 and stations 3 from 2016-2018 cruises was 67.3 % with *Gammarus* (12.6 %), *Scalibregma* (12.3

%), *Nepthys* (6.0 %) and *Terebellides* (6.0 %) genus contributing most and being more abundant in July 2010 as well. Average dissimilarity between station 4*July 2010 and stations 4 from 2016-2018 cruises was 69.6 % with *Gammarus* (10.0 %), *Ampelisca* (8.6 %), *Hyala* (7.2 %) and *Lumbrineris* (5.3 %) genus contributing most. *Gammarus* and *Lumbrineris* genus were absent during 2016-2018, whereas *Hyala* and *Ampelisca* were less abundant in 2010.

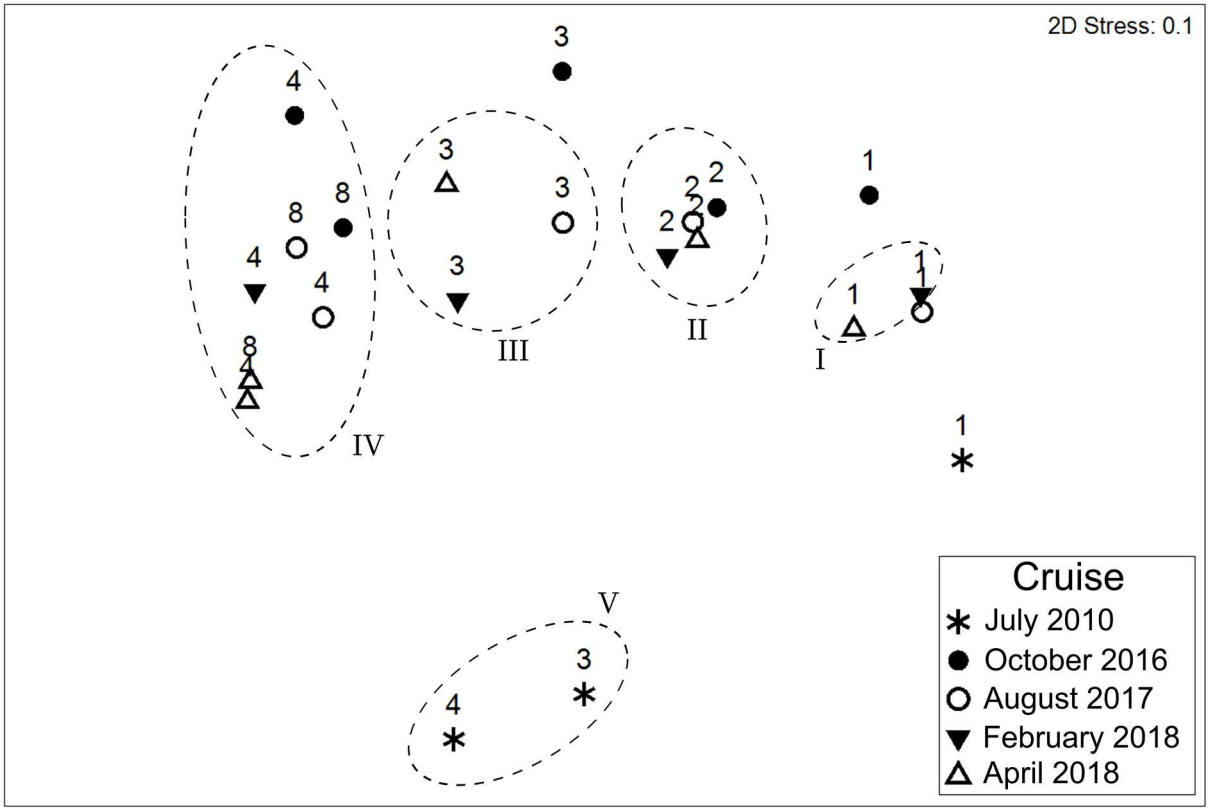

Figure 2.8. Non-metric Multidimensional Scaling of macrofauna composition data for stations*dates during both the 2010 and 2016-2018 cruises. Figures refer to stations and symbols to cruises. Dotted lines indicate the groups of samples issued from the hierarchical clustering as identified through the SIMPROF procedure.

3.5. Comparison of short-term spatio-temporal changes in surface sediment characteristics and benthic macrofauna compositions within the WGMP and the RRP

The relationships between station depth and short-term intra-station temporal variabilities in surface sediment characteristics and benthic macrofauna composition both largely differed in the West Gironde Mud Patch (WGMP) and the Rhône River Prodelta (RRP; Figure 2.9). In both cases and although caution should clearly be taken when comparing absolute values of WGMP and RRP data, the highest intra-station variabilities were associated with the RRP shallowest station. Short-term intra-station temporal variabilities in RRP surface sediment characteristics clearly decreased with station depth. They were mostly due to

important temporal changes in EHAA, $D_{0.5}$, EHAA/THAA ratio and Chl-*a* at the shallowest station (i.e., station A). At the three deepest stations, short-term temporal variabilities were low and mostly resulted from limited changes in EHAA/THAA ratios and Phaeo-*a*. Conversely, short-term intra-station temporal variabilities in surface sediment characteristics in the WGMP did not show any clear pattern relative to station depth. These variabilities resulted mostly from changes in $D_{0.5}$ and POC at the shallowest station (i.e., station 1), whereas they were mostly cued by Chl-*a*, Phaeo-*a* and the Chl-*a*/(Chl-*a*+Phaeo-*a*) ratio at all the other stations. Short-term temporal variabilities in benthic macrofauna composition was much higher at the shallowest station (i.e., station A) than at the 4 other sampled stations. The polychaete *Sternaspis scutata* largely contributed to this variability at all stations with higher abundances during July 2011.

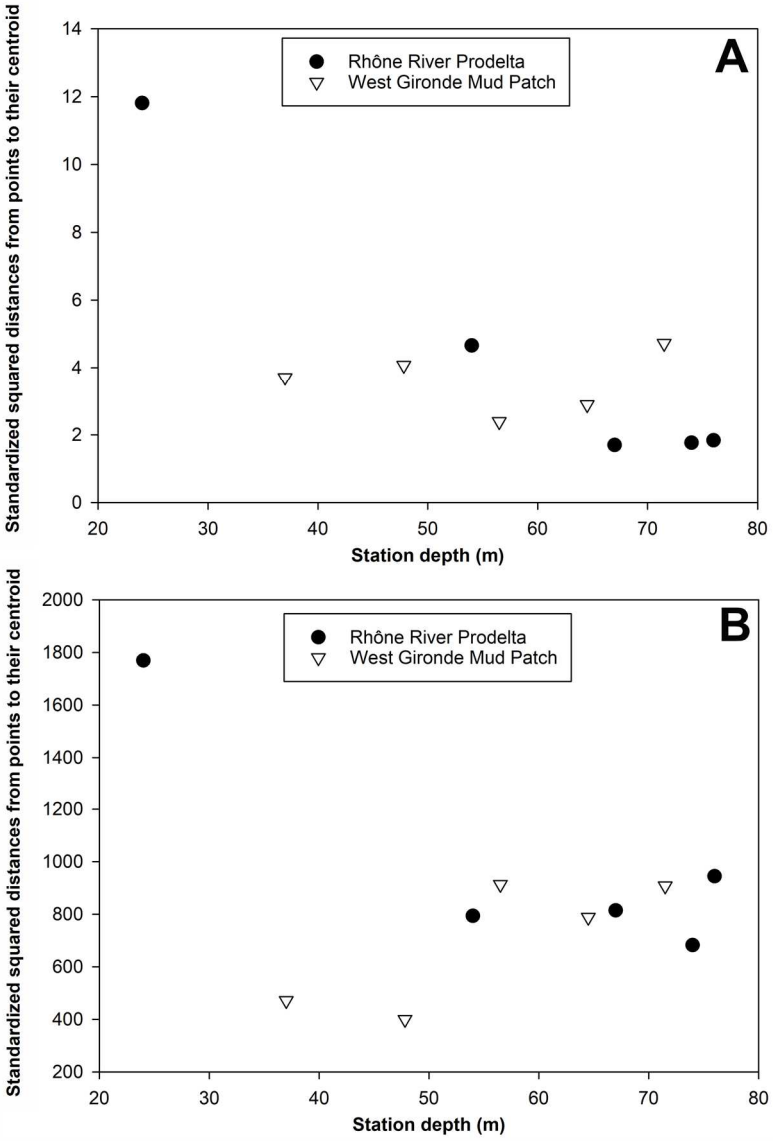

Figure 2.9. Relationship between station depth and intra-station short-term temporal variabilities in sediment surface characteristics (**A**) and benthic macrofauna composition (**B**) in both the WGMP (data collected between 2016 and 2018) and the RRP (data collected between 2007 and 2011; Bonifácio et al. 2014). See text for further details.

In the WGMP, short-term intra-station temporal variabilities were lower at the two shallowest stations, mainly resulting from limited changes in the abundances of *Amphiura filiformis* (echinoderm), *Kurtiella bidentata* (crustacean) and *Abra alba* (crustacean). They were higher at the three other sampled stations. At station 3, this was mainly due to changes in the abundance of *Amphiura filiformis* (echinoderm), *Ancistrosyllis groenlandica* (polychaete) and *Varicorbula gibba* (mollusca). At stations 8 and 4, this mainly resulted from strong increases in the abundance of *Ampelisca spp.* (crustacea) and *Hyala vitrea* (mollusca) during April 2018.

4. Discussion

4.1. WGMP short-term (2016-2018) spatio-temporal changes

4.1.1. Surface sediment characteristics

Based on the assessment of: (1) the frequency of occurrence of erosional surfaces within the sediment column (Lesueur et al. 1991, 1996, Lesueur & Tastet 1994) and (2) bioturbation intensities (Jouanneau et al. 1989, Lesueur & Tastet 1994), early sedimentological surveys have shown that spatial changes within the West Gironde Mud Patch (WGMP) mostly take place along the depth gradient with a subdivision between a proximal and a distal part (Lesueur & Tastet 1994, Lesueur et al. 2002). Relexans et al. (1992) and Massé et al. (2016) achieved preliminary assessments of changes in surface sediment characteristics based on the sampling of a limited number of stations (i.e., 3) along this gradient. Their studies were recently deepened by the use of sediment profile imaging and the assessments of a comprehensive qualitative and quantitative set of surface sedimentary organics characteristics at a much larger number (i.e., 32) of stations sampled during the same cruise (Lamarque et al. 2021). Results clearly supported the correlation between station depth and spatial changes in WGMP surface sediment characteristics.

The present results clearly show the higher importance of spatial relative to short-term temporal changes in surface sediment. Station 1 was the only station located in the proximal part. It presented coarse surface sediments during three cruises (i.e., October 2016, August 2017 and February 2018) but not during the last one (April 2018). Such temporal changes have been attributed to the transient deposition of coarse sediments during high-energy events

(Lesueur et al. 2001, 2002) although it should be pointed out that a strong spatial heterogeneity in surface sediment granulometry at 7 simultaneously sampled stations located within the WGMP proximal part was also reported (Lamarque et al. 2021). This clearly highlights the difficulty in unambiguously unravelling spatial and temporal changes. Along the same line, the surface sediment collected at station 1 in April 2018 tended to be slightly coarser than deep old muds (BL and ND, personal observations), which may be indicative of transient sedimentation of fine particles as well. All other sampled stations were located in the distal part. They showed significantly different surface sediment characteristics as compared to station 1. They presented restricted spatial changes in surface sediment granulometry, but conversely a clear increase in organics contents (i.e., POC and THAA) as well as a clear decrease in their EHAA/THAA ratio with depth. Moreover, their surface $\delta^{13}C$ did not show any clear spatial pattern. These results support previous conclusions based on a snapshot synoptic sampling (Lamarque et al. 2021): (1) the subdivision of the WGMP in a proximal and a distal part, (2) the existence of depth gradients for both qualitative and quantitative characteristics of surface sedimentary organics within the distal part, and (3) the mixing of continental and marine sources of particulate organic matter before its sedimentation in the WGMP. Early sedimentological surveys have attributed the spatial zonation of the WGMP to hydrodynamics (Jouanneau et al. 1989, Lesueur et al. 1991, 2001, 2002, Lesueur & Tastet 1994). A recent study showed that the role of hydrodynamics, mostly through wave-induced Bottom Shear Stress, was dominant with no evidence of a significant impact of bottom trawling (Lamarque et al. 2021). The results of the DISTLM/dbRDA analysis achieved in the present study further support the predominant role of hydrodynamics as the driving factor of the spatial structuration of surface sediment characteristics in the WGMP. They also suggest a lack of significant impact of the Gironde Estuary flow. Caution should nevertheless clearly be taken in interpreting these results due to: (1) co-correlations between station depth, BSS and surface sediment characteristics, and (2) the use of river flows (which do not include a spatial component during each individual cruise) as a proxy of (particle) inputs to the WGMP.

At all stations, surface sediments showed higher chloro-pigment concentrations and Chl-*a*/(Chl-*a*+Phaeo-*a*) ratio in April 2018 than during the three other cruises. A similar pattern has been reported by Relexans et al. (1992) for two stations sampled in the distal part. The seasonality of primary production in this part of the Bay of Biscay is characterized by the occurrence of a spring phytoplankton bloom (Herbland et al. 1998, Labry et al. 2002). Both

fluorescence profiles and satellite image analyses (Copernicus Sentinel data 2018, processed by ESA; Chl-*a* concentrations computed using SNAP software, data available on request to B. Lamarque) indeed confirmed that the period immediately preceding the April 2018 cruise was characterized by high chlorophyll concentrations (i.e., ca. 10 $mg.m^{-3}$) off the mouth of the Gironde Estuary. Our interpretation is thus that the high chloropigment concentrations recorded in the surface sediment in April 2018 likely result from the sedimentation of this bloom. The importance of the seasonal component in driving short-term temporal changes in surface sediment characteristics is further supported by the results of the DISTLM/dbRDA analysis, showing that temporal changes correlate better with $Flow_{100}$ and to a lesser extent BSS_{100} rather than $Flow_{365}$ and BSS_{365}. This seasonal component clearly dominated short-term temporal changes at the 4 stations located in the distal part but not at station 1, which is located in the proximal part where short-term temporal changes in surface sediment characteristics largely result from transient sedimentation following hydrodynamic events (Lesueur et al. 2001, see also above).

4.1.2. Benthic macrofauna

Before the present study, the only WGMP benthic macrofauna quantitative data have been collected at 3 stations sampled on a single occasion (i.e., July 2010; Massé et al. 2016). Our results thus constitute the first comprehensive data set allowing for a sound assessment of spatio-temporal changes in benthic macrofauna composition in this area. As for surface sediment characteristics (see above), they clearly show the higher importance of spatial relative to short-term temporal changes.

Overall, all stations tended to present significantly different macrofauna compositions, except for stations 8 and 4 (Figure 2.7). As evidenced by their representations in the nMDS plan, the composition changed gradually in relation with depth. This supports and complements the pattern observed in July 2010 by Massé et al. (2016), which was strongly dominated by differences in benthic macrofauna composition between the proximal (i.e., station 1) and the distal (i.e., stations 3 and 4) parts of the WGMP. During the present study, stations 1 and 2 were dominated by *Amphiura filiformis* and *Kurtiella bidentata*, which is consistent with the presence of the *A. filiformis-K. bidentata-Abra nitida* community in cohesive muddy sands off wave exposed coast (Hiscock 1984, Picton et al. 1994). This clearly corresponds to the A5.351 ("*Amphiura filiformis*, *Kurtiella bidentata* and *Abra nitida* in

circalittoral sandy mud") habitat of the EUNIS classification (Bajjouk et al. 2015). Deeper stations featured higher equitability and therefore could not be as easily associated with a specific EUNIS habitat. They nevertheless were all strongly bioturbated (Lamarque et al. 2021 and unpubl. data) and characterized by the presence of: (1) a large variety of polychaetes, (2) seapens (*Cavernularia pusilla* and *Veretillum cynomorium*) and (3) *Nephrops norvegicus* (GB, personal observation based on sediment trawling). In this sense, they can be related with the A5.361 ("Seapens and burrowing megafauna in circalittoral fine mud") habitat of the EUNIS classification (Bajjouk et al. 2015).

Benthic macrofauna abundances presented a strong decreasing trend along the depth gradient (if omitting the exceptional presence of numerous individuals of *Ampelisca spp.* and *Hyala vitrea* at stations 8 and 4 in April 2018), which is conform to the trend observed by Massé et al. (2016). Such a decreasing pattern is not fully consistent with the results of surveys achieved in the marine environments of other rivers (e.g., Amazon, Changjiang, Fly, Spercheios and Rhône), where increasing trends in benthic macrofauna abundances with the distance to the river mouth have been most often observed (Rhoads et al. 1985, Aller & Aller 1986, Alongi et al. 1992, Akoumianaki et al. 2013, Bonifácio et al. 2014). These last results were usually interpreted as being conform to the Rhoads et al. (1985) model, according to which the maturity and the abundance of benthic macrofauna communities at the immediate vicinity of river mouths are limited by the sediment instability induced by riverine inputs. During the present study, we attempted to unravel the effects of riverine inputs and hydrodynamics (as respectively approached by river flows and BSS integrated over two different periods) on the spatiotemporal structuration of benthic macrofauna through the use of DISTLM/dbRDA. Spatial changes in benthic macrofauna composition correlated best with BSS_{365} and not significantly with river flows. As for surface sediment characteristics (see the section above), caution should be taken in interpreting these results. Nevertheless, they suggest that estuarine inputs probably do not constitute the main factor controlling sediment instability in the WGMP. This conclusion is further supported by the lack of modern sedimentation in the proximal part and by the frequent presence of vertical erosion sequences within its sediments (Lesueur & Tastet 1994, Lesueur et al. 2001, 2002). As a consequence, the present results support the approaches relying on hydrodynamics proposed by McKee et al. (2004) and then Blair & Aller (2012) for the classification of marine RiOMar. Within the frame of these classifications, the WGMP would correspond to a type 2/high energy "bypassed" (*sensu* McKee et al. 2004) system where the impact of hydrodynamics is dominant relative to the one

of riverine inputs. The WGMP presents the additional complexity of being composed of two different parts: the proximal one, which is composed of consolidated relict muds deposited ca. 1000 years BP (Lesueur et al. 2002) and the distal part, which is the active depocenter (Dubosq et al. 2021). This discrepancy also corresponds to different surface sediment characteristics (Figure 2.5, Lamarque et al. 2021) and thus to different habitats for macrofauna, which may also contribute to differences in benthic macrofauna compositions although these compositions correlated less with individual sediment characteristics than with BSS.

Overall, short-term temporal changes in benthic macrofauna composition tended to be higher at deep stations and lower at the two shallowest stations. Here again, those changes correlated better with environmental parameters than with surface sediment characteristics with some evidence that short-term temporal changes in benthic macrofauna compositions include both a seasonal component and an interannual trend. There are several rationales for the occurrence of seasonal changes in benthic macrofauna composition. First, the reduced space of the nMDS, individual station trajectories tended to "close" when they were defined based on Annual Julian Days (which can be considered as indicative of within year/seasonal variability). Second, temporal changes in benthic macrofauna compositions correlated best with Flow100, which reflects the correlation between changes in seasonally integrated river flows and benthic macrofauna composition. Third, Annual Julian Days correlated significantly with the second component of the dBRDA, which was indicative of benthic macrofauna temporal changes. There is some indirect evidence for an inter-annual component to short-term temporal changes in benthic macrofauna composition as well since: (1) a common inter-annual trend was clearly observable at stations 1, 8 and 4, and (2) the second component of the dBRDA correlated slightly better with Cumulated Julian Days (indicative of inter-annual/cumulated changes but also significantly correlated with Annual Julian Days due to the sampling sequence) than with Annual Julian days (indicative of within year/seasonal changes only).

4.2. Long-term comparison (2010/2016-2018) of benthic macrofauna compositions in the WGMP

The existence of an inter-annual component to temporal changes in benthic macrofauna composition becomes even more obvious when 2016-2018 data were compared

to those collected in July 2010 (Massé et al. 2016). At the three considered stations, differences in benthic macrofauna compositions between 2010 and 2016-2018 were indeed much larger than differences observed during 2016-2018. At all stations, differences in benthic macrofauna composition relative to July 2010 were maximal in October 2016 and, for most of them, changes occurring during the 2016-2018 period tended to reduce those differences, which is coherent with an ongoing cicatrization process following a major disturbance (Rosenberg & Pearson 1978) that would have taken place between July 2010 and October 2016.

Sediment characteristics are commonly considered to control the composition of benthic macrofauna (Thrush 1991, Snelgrove & Butman 1994). The comparison of those characteristics in July 2010 and the 2016-2018 period is complicated by the limited number of common parameters that were assessed both by Massé et al. (2016) and in the present study. Based on $D_{0.5}$, POC, Chl-*a*, Phaeo-*a* and Chl-*a*/(Chl-*a*+Phaeo-*a*) concentrations/values, there is nevertheless no evidence of changes in surface sediment characteristics between these two periods (data not shown available on request to B. Lamarque). Hence, changes in surface sediment characteristics were unlikely responsible for the long-term changes observed in the benthic macrofauna composition. In the WGMP, hydrodynamics is clearly a key factor structuring the spatial distributions of benthic macrofauna composition and activity (Lamarque et al. 2021, see also above). Disturbances of the sediments during strong hydrodynamic events have already been documented based on the analysis of vertical erosional sequences (following resuspension induced by storms) within sediment columns (Lesueur et al. 1991, 2002, Lesueur & Tastet 1994). It has been estimated that such disturbances occur every ca. 22 years at 35m depth, and only every ca. 80 years at 64m depth (Lesueur et al. 2002). The analysis of the 2010-2018 BSS time series showed higher values during the 2013-2014 winter. During this particular winter, the WGMP experienced significant wave heights and a total storm duration higher (i.e., 40 and 300%, respectively) than the overall means of the 1948-2015 period. Overall, the 2013-2014 winter has been the most energetic one during the 1948-2015 period along most of the European Atlantic coast (Masselink et al. 2016). Storm-induced physical disturbance during this uncommon winter could have affected both the sediment and benthic macrofauna of the whole WGMP. The duration of successional recovery of benthic macrofauna increases with the spatial scale of the disturbance (Zajac et al. 1998). Cárcamo et al. (2017) have for example shown that, following a major physical disturbance, benthic macrofauna compositions in Concepcion Bay

were still not restored to their initial state 3 years after a tsunami. Moreover, the fact that the WGMP consists in an isolated habitat (i.e., surrounded by sand, and well separated from other mud patches), which can be entirely physically disturbed also contribute to extend the duration of the cicatrization period by reducing potential for source populations to supply colonists including both mobile adults and pelagic larvae (Probert 1984, Zajac et al. 1998). These elements are fully consistent with the occurrence of a cicatrization process lasting several years in the WGMP after a major disturbance.

Based on these rationale, our current interpretation of long-term temporal changes in benthic macrofauna composition is therefore that: (1) the repetition of strong storms during the 2013-2014 winter has induced strong physical disturbances of benthic habitats and consequently strong changes in benthic macrofauna composition over the whole WGMP, and (2) since then temporal changes in benthic macrofauna composition consist in an ongoing (pluri-annual) cicatrization process superimposed to a seasonal dynamics (Cárcamo et al. 2017). The increase in long-term temporal changes in benthic macrofauna composition with depth seems, however, counter-intuitive since the intensity of physical disturbance during strong storms is clearly higher at shallower stations. In “normal” conditions (i.e., not during extreme events), shallower stations are also clearly experiencing tougher hydrodynamical conditions than deeper ones. In addition, the frequency of severe storms impacting the sediment column and thus potentially benthic macrofauna composition (Rees et al. 1977, Glémarec 1978, Dobbs & Vozarik 1983) also decreases with depth (Lesueur et al. 2002). This may result in faster recovery at shallower stations as postulated by Collie et al. (2000) and later tested by Dernie et al. (2003) for less physically stable habitats such as sandy bottoms. One can thus assume that resident benthic macrofauna are less resilient to physical disturbance at deeper than at shallower stations, thereby accounting for the larger observed impact at depth. This hypothesis should now be further tested through an extension of the observation period of the WGMP.

4.3. Comparison between the West Gironde Mud Patch and the Rhône River Prodelta

Differences in the spatial zonation of surface sediment characteristics and biological activity traces in the WGMP and the Rhône River Prodelta (RRP) have already been assessed by Lamarque et al. (2021). As for benthic macrofauna composition, the comparison of the present study with the results of Bonifácio et al. (2014) highlights the existence of depth

gradients in benthic macrofauna composition within these two systems. However, these gradients largely differ regarding univariate indices with decreasing abundances with depth in the WGMP, and conversely higher values at intermediate depth in the RRP except during July 2011 (see also above). Overall, this suggests that the RRP is more conforming to the Rhoads et al. (1985) model (i.e., disturbance of benthic macrofauna through sediment instability) than the WGMP.

Short-term intra-station temporal variabilities in surface sediment characteristics differed between the two systems as well with a much higher value at the immediate vicinity of the Rhone River Mouth than in the proximal area of the WGMP. In the shallowest area of the RRP, the short-term temporal variability in surface sediment characteristics is mainly resulting from high sedimentation taking place during floods (Cathalot et al. 2010, Bonifácio et al. 2014, Pastor et al. 2018). Mostly during autumn and winter, part of these deposits are resuspended initiating a series of resuspension/depositions which result in the displacement of fine particles offshore (Ulses et al. 2008, Marion et al. 2010). During this transfer, particles are sorted relative to their size and the most labile particulate organic matter components are degraded (Bonifácio et al. 2014), which contribute to reduce the magnitude of short-term temporal changes in surface sediment characteristics in deeper areas. Conversely, the magnitude of intra-station short-term temporal changes in surface sediment characteristics tended to be constant all over the WGMP. In the proximal part, the magnitude of these changes is mostly linked to $D_{0.5}$ and associated parameters, whereas in the distal part, it mostly results from elevated pigment concentrations and ratios in April 2018. Such an absence of clear seasonal change in the biochemical characteristics of WGMP surface sedimentary organics has already been reported by Relexans et al. (1992), who characterized it, with the exception of pigment concentrations, as a “monotonous” area featuring limited seasonal temporal changes in its surface sediment characteristics. As opposed to the RRP, the WGMP is not directly connected to the mouth of the Gironde Estuary. Consequently, dilution effects are affecting the whole WGMP, whereas they clearly increase with the distance to the river mouth (and depth) in the RRP (Tesi et al. 2007, Lansard et al. 2009, Bourgeois et al. 2011, Cathalot et al. 2013). Moreover, due to strong hydrodynamics, the fine particles originating from the Gironde Estuary do not settle in the proximal part of the WGMP (Lesueur et al. 2001), whereas conversely, high sedimentation rates are taking place at the immediate vicinity of the Rhône River Mouth (Zuo et al. 1991, Miralles et al. 2005). Overall, in the proximal part of the WGMP, this contributes to reduce the magnitude of short-term temporal changes in surface

sediment characteristics possibly induced by seasonal changes in the hydrodynamic regime of the Gironde Estuary.

The magnitude of short-term intra-station temporal variabilities in benthic macrofauna composition showed opposite spatial patterns in the RRP and the WGMP. In both cases, there were differences between shallower and deeper stations. In the RRP, the magnitude of short-term temporal changes was much higher at the immediate vicinity of the Rhône River due to the shift between high and low sedimentation rates during high and low flow periods, respectively (Bonifácio et al. 2014). Here again, this pattern largely conforms to the Rhoads et al. (1985) model, which attributes a major role to sedimentation in controlling benthic macrofauna in RiOMar. Conversely, the magnitude of short-term intra-station temporal changes in benthic macrofauna composition within the WGMP tended to be lower at the two shallowest stations than at the three deepest one, which was put in relation with a better tolerance of benthic macrofauna to wave-induced disturbance in the proximal part of the WGMP (see above). Here again, this pinpoints to differences in the relative roles of riverine inputs and hydrodynamics in controlling spatio-temporal changes within the two systems.

5. Conclusions

The present assessment of short-term (i.e., over the 2016-2018 period) spatio-temporal changes in the West Gironde Mud Patch (WGMP) surface sediment characteristics confirms the existence of a spatial structuration relative to depth. This structuration is cued by hydrodynamics as previously highlighted (Lamarque et al. 2021). The present results also demonstrated the presence of a benthic macrofauna spatial gradient characterized by gradual changes in composition according to depth. Here again, the control of this spatial structuration is linked to hydrodynamics integrated over a 1-year period suggesting the major influence of main annual events such as winter storms.

Both surface sediment characteristics and benthic macrofauna presented short-term (i.e., seasonal) changes best described by the Gironde Estuary flow, and to a lesser extent Bottom Shear Stress, integrated over 100 days. Benthic macrofauna compositions also presented long-term (i.e. pluri-annual) changes superimposed over this seasonal dynamics. Moreover, the marked shift observed in benthic macrofauna compositions between 2010 and 2016-2018 suggests the occurrence of a major disturbance between these two periods, which

may have been initiated by an exceptional series of severe storms during the 2013-2014 winter. This highlights the major role of hydrodynamic events in controlling long-term temporal changes in WGMP benthic macrofauna composition.

The comparison between the WGMP and Rhone River Prodelta (RRP) showed major differences in the control of temporal changes in both surface sediment characteristics and benthic macrofauna composition within their proximal parts. In the RRP, these are cued by changes in sedimentation rates in relation with the hydrological regime of the Rhône River, whereas in the WGMP it results from strong hydrodynamics. Another major difference is that, through extreme events, hydrodynamics is clearly affecting both sediment characteristics and benthic macrofauna composition over the whole WGMP. This further supports the characterization of the RRP as a temperate type 1 (i.e. low-energy system with high sedimentation rates) and of the WGMP as temperate type 2 (i.e., high-energy system) RiOMar, respectively and highlights the different mechanisms involved in the control of their surface sediment characteristics and benthic macrofauna composition.

Acknowledgements: This work is part of the PhD thesis of Bastien Lamarque (Bordeaux University). Bastien Lamarque was partly supported by a doctoral grant from the French “Ministère de l’Enseignement Supérieur, de la Recherche et de l’Innovation”. This work was supported by: (1) the JERICO-NEXT project (European Union’s Horizon 2020 Research and Innovation program under grant agreement no. 654410), (2) the VOG project (LEFE-CYBER and EC2CO-PNEC), and (3) the MAGMA project (COTE cluster of Excellence ANR-10-LABX-45). It also benefited from additional fundings allocated by the Conseil Régional Nouvelle-Aquitaine and the Office Français de la Biodiversité. Operations at sea were funded by the French Oceanographic Fleet. The authors wish to thank the crew of the R/V Côtes de la Manche for their help during field sampling, Christophe Fontanier, Marie Claire Perello, Pascal Lebleu and Hervé Derriennic for their help during sampling and sample analysis.

References

Akaike H (1973) Information theory as an extension of the maximum likelihood principle. In: Proceedings, 2nd International Symposium on Information Theory, Akadémiai. Csaki F, Petrov BN (eds) Budapest, p 267–281

Akoumianaki I, Papaspyrou S, Kormas KA, Nicolaidou A (2013) Environmental variation and macrofauna response in a coastal area influenced by land runoff. Estuar Coast Shelf Sci 132:34–44.

Aller JY, Aller RC (1986) General characteristics of benthic faunas on the Amazon inner continental shelf with comparison to the shelf off the Changjiang River, East China Sea. Cont Shelf Res 6:291–310.

Aller JY, Stupakoff I (1996) The distribution and seasonal characteristics of benthic communities on the Amazon shelf as indicators of physical processes. Cont Shelf Res 16:717–751.

Aller RC (1998) Mobile deltaic and continental shelf muds as suboxic, fluidized bed reactors. Mar Chem 61:143–155.

Alongi DM, Christoffersen P, Tirendi F, Robertson AI (1992) The influence of freshwater and material export on sedimentary facies and benthic processes within the Fly Delta and adjacent Gulf of Papua (Papua New Guinea). Cont Shelf Res 12:287–326.

Anderson M, Gorley RN, Clarke KR (2008) PERMANOVA + for PRIMER user manual.

Anderson MJ (2001) A new method for non-parametric multivariate analysis of variance. Austral Ecol 26:32–46.

Bajjouk T, Guillaumont B, Michez N, Thouin B, Croguennec C, Populus J, Louvel-Glaser J, Gaudillat V, Chevalier C, Tourolle J, Hamon D (2015) Classification EUNIS, Système d'information européen sur la nature : Traduction française des habitats benthiques des Régions Atlantique et Méditerranée. Vol. 2. Habitats subtidaux & complexes d'habitats.

Bischl B, Lang M, Bossek J, Horn D, Richter J, Surmann D (2017) BBmisc: Miscellaneous Helper Functions for B. Bischl. R Packag version 1-1-1.

Blair NE, Aller RC (2012) The Fate of Terrestrial Organic Carbon in the Marine Environment. Ann Rev Mar Sci 4:401–423.

Bonifácio P, Bourgeois S, Labrune C, Amouroux JM, Escoubeyrou K, Buscail R, Romero-Ramirez A, Lantoine F, Vétion G, Bichon S, Desmalades M, Rivière B, Deflandre B, Grémare A (2014) Spatiotemporal changes in surface sediment characteristics and benthic macrofauna composition off the Rhône River in relation to its hydrological regime. Estuar Coast Shelf Sci 151:196–209.

Bourgeois S, Pruski AM, Sun MY, Buscail R, Lantoine F, Kerhervé P, Vétion G, Rivière B, Charles F (2011) Distribution and lability of land-derived organic matter in the surface sediments of the Rhône prodelta and the adjacent shelf (Mediterranean Sea, France): A multi proxy study. Biogeosciences 8:3107–3125.

Burdige DJ (2005) Burial of terrestrial organic matter in marine sediments: A re-assessment. Global Biogeochem Cycles 19:1–7.

Cárcamo PJ, Hernández-Miranda E, Veas R, Quiñones RA (2017) Macrofaunal community structure in Bahía Concepción (Chile) before and after the 8.8 Mw Maule mega-earthquake and tsunami. Mar Environ Res 130:233–247.

Castaing P, Allen G, Houdart M, Moign Y (1979) Étude par télédétection de la dispersion en mer des eaux estuariennes issues de la Gironde et du Pertuis de Maumusson. Oceanol Acta 2:459–468.

Castaing P, Allen GP (1981) Mechanisms controlling seaward escape of suspended sediment from the Gironde: A macrotidal estuary in France. Mar Geol 40:101–118.

Castaing P, Philipps I, Weber O (1982) Répartition et dispersion des suspensions dans les eaux du plateau continental aquitain. Oceanol Acta 5:85–96.

Cathalot C, Rabouille C, Pastor L, Deflandre B, Viollier E, Buscail R, Grémare A, Treignier C, Pruski A (2010) Temporal variability of carbon recycling in coastal sediments influenced by rivers: Assessing the impact of flood inputs in the Rhône River prodelta. Biogeosciences 7:1187–1205.

Cathalot C, Rabouille C, Tisnérat-Laborde N, Toussaint F, Kerhervé P, Buscail R, Loftis K, Sun MY, Tronczynski J, Azoury S, Lansard B, Treignier C, Pastor L, Tesi T (2013) The fate of river organic carbon in coastal areas: A study in the Rhône River delta using multiple isotopic (δ13C, δ14C) and organic tracers. Geochim Cosmochim Acta 118:33–55.

Cirac P, Berne S, Castaing P, Weber O (2000) Processus de mise en place et d'évolution de la couverture sédimentaire superficielle de la plate-forme nord-aquitaine. Oceanol Acta 23:663–686.

Clarke KR (1993) Non-parametric multivariate analyses of changes in community structure. Aust J Ecol 18:117–143.

Clarke KR, Somerfield PJ, Gorley RN (2008) Testing of null hypotheses in exploratory community analyses: similarity profiles and biota-environment linkage. J Exp Mar Bio Ecol 366:56–69.

Clarke KR, Warwick RM (2001) Change in Marine Communities: An Approach to Statistical Analysis and Interpretation, 2nd edition. PRIMER-E, Plymouth.

Collie JS, Hall SJ, Kaiser MJ, Poiner IR (2000) A quantitative analysis of fishing impacts on shelf-sea benthos. J Anim Ecol 69:785–798.

Constantin S, Doxaran D, Derkacheva A, Novoa S, Lavigne H (2018) Multi-temporal dynamics of suspended particulate matter in a macro-tidal river Plume (the Gironde) as observed by satellite data. Estuar Coast Shelf Sci 202:172–184.

Coplen TB (2011) Guidelines and recommended terms for expression of stable- isotope-ratio and gas-ratio measurement results. Rapid Commun Mass Spectrom 25:2538–2560.

Deflandre B (2016) JERICOBENT-1 cruise, RV Côtes De La Manche.

Deflandre B (2017) JERICOBENT-2 cruise, RV Côtes De La Manche.

Deflandre B (2018a) JERICOBENT-3 cruise, RV Côtes De La Manche.

Deflandre B (2018b) JERICOBENT-4 cruise, RV Côtes De La Manche.

Dernie KM, Kaiser MJ, Warwick RM (2003) Recovery rates of benthic communities following physical disturbance. J Anim Ecol 72:1043–1056.

Diaz M, Grasso F, Le Hir P, Sottolichio A, Caillaud M, Thouvenin B (2020) Modeling Mud and Sand Transfers Between a Macrotidal Estuary and the Continental Shelf: Influence of the Sediment Transport Parameterization. J Geophys Res Ocean 125.

Dobbs FC, Vozarik JM (1983) Immediate effects of a storm on coastal infauna. Mar Ecol Prog Ser 11:273–279.

Doxaran D, Froidefond JM, Castaing P, Babin M (2009) Dynamics of the turbidity maximum zone in a macrotidal estuary (the Gironde, France): Observations from field and MODIS satellite data. Estuar Coast Shelf Sci 81:321–332.

Dubosq N, Schmidt S, Walsh JP, Grémare A, Gillet H, Lebleu P, Poirier D, Perello MC, Lamarque B, Deflandre B (2021) A first assessment of organic carbon burial in the West Gironde Mud Patch (Bay of Biscay). Cont Shelf Res 221.

Etcheber H, Relexans JC, Beliard M, Weber O, Buscail R, Heussner S (1999) Distribution and quality of sedimentary organic matter on the Aquitanian margin (Bay of Biscay). Deep Res Part II 46:2249–2288.

Gadel F, Jouanneau JM, Weber O, Serve L, Comellas L (1997) Traceurs organiques dans les dépôts de la vasière Ouest-Gironde (Golfe de Gascogne). Oceanol Acta 20:687–695.

Glémarec M (1978) Problèmes d'écologie dynamique et de succession en baie de Concarneau. Vie Milieu:1–20.

Grasso F, Verney R, Le Hir P, Thouvenin B, Schulz E, Kervella Y, Khojasteh Pour Fard I, Lemoine JP, Dumas F, Garnier V (2018) Suspended Sediment Dynamics in the Macrotidal Seine Estuary (France): 1. Numerical Modeling of Turbidity Maximum Dynamics. J Geophys Res Ocean 123:558–577.

Grémare A, Gutiérrez D, Anschutz P, Amouroux JM, Deflandre B, Vétion G (2005) Spatio-temporal changes in totally and enzymatically hydrolyzable amino acids of superficial sediments from three contrasted areas. Prog Oceanogr 65:89–111.

Harmelin-Vivien ML, Bănaru D, Dierking J, Hermand R, Letourneur Y, Salen-Picard C (2009) Linking benthic biodiversity to the functioning of coastal ecosystems subjected to river runoff (NW Mediterranean). Anim Biodivers Conserv 32:135–145.

Harrell FE (2021) Hmisc: Harrell Miscellaneous. R Packag version 4-5-0.

Hedges JI, Keil RG (1995) Sedimentary organic matter preservation: an assessment and speculative synthesis. Mar Chem 49:81–115.

Herbland A, Delmas D, Laborde P, Sautour B, Artigas F (1998) Phytoplankton spring bloom of the Gironde plume waters in the Bay of Biscay: Early phosphorus limitation and food-web consequences. Oceanol Acta 21:279–291.

Hiscock K (1984) Rocky shore surveys of the Isles of Scilly. March 27th to April 1st and July 7th to 15th 1983. Peterbrgh Nat Conserv Counc CSD Rep 509.

Jalón-Rojas I, Sottolichio A, Hanquiez V, Fort A, Schmidt S (2018) To what extent multidecadal changes in morphology and fluvial discharge impact tide in a convergent (turbid) tidal river. J Geophys Res Ocean 123:3241–3258.

Jouanneau JM, Weber O, Latouche C, Vernet JP, Dominik J (1989) Erosion, non-deposition and sedimentary processes through a sedimentological and radioisotopic study of surficial deposits from the 'Ouest-Gironde vasière' (Bay of Biscay). Cont Shelf Res 9:325–342.

Labry C, Herbland A, Delmas D (2002) The role of phosphorus on planktonic production of the Gironde plume waters in the Bay of Biscay. J Plankton Res 24:97–117.

Lamarque B, Deflandre B, Dalto AG, Schmidt S, Romero-Ramirez A, Garabetian F, Dubosq N, Diaz M, Grasso F, Sottolichio A, Bernard G, Gillet H, Cordier MA, Poirier D, Lebleu P, Derriennic H, Danilo M, Tenório MMB, Grémare A (2021) Spatial distributions of surface sedimentary organics and sediment profile image characteristics in a high-energy temperate marine riomar: The west gironde mud patch. J Mar Sci Eng 9:242.

Lansard B, Rabouille C, Denis L, Grenz C (2009) Benthic remineralization at the land-ocean interface: A case study of the Rhône River (NW Mediterranean Sea). Estuar Coast Shelf Sci 81:544–554.

Lazure P, Dumas F (2008) An external-internal mode coupling for a 3D hydrodynamical model for applications at regional scale (MARS). Adv Water Resour 31:233–250.

Lesueur P, Jouanneau JM, Boust D, Tastet JP, Weber O (2001) Sedimentation rates and fluxes in the continental shelf mud fields in the Bay of Biscay (France). Cont Shelf Res 21:1383–1401.

Lesueur P, Tastet J., Weber O, Sinko J. (1991) Modèle faciologique d'un corps sédimentaire pélitique de plate-forme la vasière Ouest-Gironde (France). Oceanol Acta 11:143–153.

Lesueur P, Tastet JP (1994) Facies, internal structures and sequences of modern Gironde-derived muds on the Aquitaine inner shelf, France. Mar Geol 120:267–290.

Lesueur P, Tastet JP (1993) Les Vasières de plate-forme du Golfe de Gascogne (France). Océanographie du Golf Gascogne:181–184.

Lesueur P, Tastet JP, Marambat L (1996) Shelf mud fields formation within historical times: Examples from offshore the Gironde estuary, France. Cont Shelf Res 16:1849–1870.

Lesueur P, Tastet JP, Weber O (2002) Origin and morphosedimentary evolution of fine-grained modern continental shelf deposits: The Gironde mud fields (Bay of Biscay, France). Sedimentology 49:1299–1320.

Lesueur P, Weber O, Marambat L, Tastet J, Jouanneau J, Turon J (1989) Datation d'une vasière de plateforme atlantique au débouché d'un estuaire: la vasière à l'ouest de la Gironde (France) est d'âge historique (VIème siècle à nos jours). Comptes rendus l'Académie des Sci Série 2, Mécanique, Phys Chim Sci l'univers, Sci la Terre 308:935–940.

Levin LA, Boesch DF, Covich A, Dahm C, Erséus C, Ewel KC, Kneib RT, Moldenke A, Palmer MA, Snelgrove P, Strayer D, Weslawski JM (2001) The function of marine critical transition zones and the importance of sediment biodiversity. Ecosystems 4:430–451.

Longère P, Dorel D (1970) Etude des sédiments meubles de la vasière de la Gironde et des régions avoisinantes. Rev des Trav l'Institut des Pêches Marit 34:233–256.

Lotze HK, Lenihan HS, Bourque BJ, Bradbury RH, Cooke RG, Kay MC, Kidwell SM, Kirby MX, Peterson CH, Jackson JBC (2006) Depletion, Degradation, and Recovery Potential of Estuaries and Coastal Seas. Science 312:1806–1809.

Marion C, Dufois F, Arnaud M, Vella C (2010) In situ record of sedimentary processes near the Rhône River mouth during winter events (Gulf of Lions, Mediterranean Sea). Cont Shelf Res 30:1095–1107.

Massé C, Meisterhans G, Deflandre B, Bachelet G, Bourasseau L, Bichon S, Ciutat A, Jude-Lemeilleur F, Lavesque N, Raymond N, Grémare A, Garabetian F (2016) Bacterial and macrofaunal communities in the sediments of the West Gironde Mud Patch, Bay of Biscay (France). Estuar Coast Shelf Sci 179:189–200.

Masselink G, Castelle B, Scott T, Dodet G, Suanez S, Jackson D, Floc'h F (2016) Extreme wave activity during 2013/2014 winter and morphological impacts along the Atlantic coast of Europe. Geophys Res Lett 43:2135–2143.

Mayer LM (1994) Surface area control of organic carbon accumulation in continental shelf sediments. Geochim Cosmochim Acta 58:1271–1284.

Mayer LM, Linda L. S, Sawyer T, Plante CJ, Jumars PA, Sel RL (1995) Bioavailable amino acids in sediments: A biomimetic, kinetics based approach. Limnol Oceanogr 40:511–520.

McKee BA, Aller RC, Allison MA, Bianchi TS, Kineke GC (2004) Transport and transformation of dissolved and particulate materials on continental margins influenced by major rivers: Benthic boundary layer and seabed processes. Cont Shelf Res 24:899–926.

Medernach L, Grémare A, Amoureux JM, Colomines JC, Vétion G (2001) Temporal changes in the amino acid contents of particulate organic matter sedimenting in the Bay of Banyuls-sur-Mer (northwestern Mediterranean). Mar Ecol Prog Ser 214:55–65.

Miralles J, Radakovitch O, Aloisi JC (2005) 210Pb sedimentation rates from the Northwestern Mediterranean margin. Mar Geol 216:155–167.

Neveux J, Lantoine F (1993) Spectrofluorometric assay of chlorophylls and phaeopigments using the least squares approximation technique. Deep Res Part I 40:1747–1765.

Oksanen J, Blanchet FG, Friendly M, Kindt R, Legendre P, McGlinn D, Minchin PR, O'Hara RB, Simpson GL, Solymos P, Stevens MHH, Szoecs E, Wagner H (2019) Vegan: Community Ecology Package. R Packag version 2-5-6.

Parra M, Castaing P, Jouanneau JM, Grousset F, Latouche C (1998) Nd-Sr isotopic composition of present-day sediments from the Gironde Estuary, its draining basins and the WestGironde mud patch (SW France). Cont Shelf Res 19:135–150.

Pastor L, Deflandre B, Viollier E, Cathalot C, Metzger E, Rabouille C, Escoubeyrou K, Lloret E, Pruski AM, Vétion G, Desmalades M, Buscail R, Grémare A (2011) Influence of the organic matter composition on benthic oxygen demand in the Rhône River prodelta (NW Mediterranean Sea). Cont Shelf Res 31:1008–1019.

Pastor L, Rabouille C, Metzger E, Thibault de Chanvalon A, Viollier E, Deflandre B (2018) Transient early diagenetic processes in Rhône prodelta sediments revealed in contrasting flood events. Cont Shelf Res 166:65–76.

Picton BE, Emblow CS, Morrow CC, Sides EM, Costello MJ (1994) Marine communities of the Mulroy Bay and Lough Swill area, north-west Ireland, with an assessment of their nature conservation importance. Environ Sci Unit, Trinity Coll (f Surv Report).

Probert PK (1984) Disturbance, sediment stability, and trophic structure of soft-bottom communities. J Mar Res 42:893–921.

Rees EIS, Nicholaidou A, Laskaridou P (1977) The Effects of Storms on the Dynamics of Shallow Water Benthic Associations. Biol Benthic Org:465–474.

Relexans JC, Lin RG, Castel J, Etcheber H, Laborde P (1992) Response of biota to sedimentary organic matter quality of the west Gironde mud patch, Bay of Biscay (France). Oceanol Acta 15:639–649.

Rhoads DC, Boesch DF, Zhican T, Fengshan X, Liqiang H, Nilsen KJ (1985) Macrobenthos and sedimentary facies on the Changjiang delta platform and adjacent continental shelf, East China Sea. Cont Shelf Res 4:189–213.

Roland A, Ardhuin F (2014) On the developments of spectral wave models: Numerics and parameterizations for the coastal ocean. Ocean Dyn 64:833–846.

Rosenberg R, Pearson TH (1978) Macrobenthos succession in relation to organic enrichment and pollution of the marine environment. Oceanogr Mar Biol Annu Rev 16:229–331.

Snelgrove PVR, Butman CA (1994) Animal Sediment Relationships Revisited – Cause Versus Effect. Oceanogr Mar Biol an Annu Rev 32:111–177.

Soulsby R (1997) Dynamics of Marine Sands: A Manual for Practical Applications, Thomas Tel.

Tesi T, Miserocchi S, Goñi MA, Langone L (2007) Source, transport and fate of terrestrial organic carbon on the western Mediterranean Sea, Gulf of Lions, France. Mar Chem 105:101–117.

Thrush SF (1991) Spatial patterns in soft-bottom communities. Trends Ecol Evol 6:75–79.

Ulses C, Estournel C, Durrieu de Madron X, Palanques A (2008) Suspended sediment transport in the Gulf of Lions (NW Mediterranean): Impact of extreme storms and floods. Cont Shelf Res 28:2048–2070.

Wakeham SG, Lee C, Hedges JI, Hernes PJ, Peterson ML (1997) Molecular indicators of diagenetic status in marine organic matter. Geochemica Cosmochim Acta 61:5363–5369.

Weber O, Jouanneau JM, Ruch P, Mirmand M (1991) Grain-size relationship between suspended matter originating in the Gironde estuary and shelf mud-patch deposits. Mar Geol 96:159–165.

Wheatcroft RA (2006) Time-series measurements of macrobenthos abundance and sediment bioturbation intensity on a flood-dominated shelf. Prog Oceanogr 71:88–122.

Worm B, Barbier EB, Beaumont N, Duffy JE, Folke C, Halpern BS, Jackson JBC, Lotze HK, Micheli F, Palumbi SR, Sala E, Selkoe KA, Stachowicz JJ, Watson R (2006) Impacts of biodiversity loss on ocean ecosystem services. Science 314:787–790.

Zajac RN, Whitlatch RB, Thrush SF (1998) Recolonization and succession in soft-sediment infaunal communities: The spatial scale of controlling factors. Hydrobiologia 375–376:227–240.

Zuo Z, Eisma D, Berger GW (1991) Determination of sediment accumulation and mixing rates in the Gulf of Lions, Mediterranean Sea. Oceanol Acta 14:253–26

CHAPITRE 3

Structuration spatio-temporelle de l'activité de la macrofaune benthique dans la Vasière Ouest-Gironde

Spatio-temporal dynamics of Sediment Profile Images characteristics in a temperate high-energy River-dominated Ocean Margin

Bastien Lamarque[1], Bruno Deflandre[2], Sabine Schmidt[2], Guillaume Bernard[1], Nicolas Dubosq[2], Mélanie Diaz[2], Nicolas Lavesque[1], Frédéric Garabetian[1], Florent Grasso[3], Aldo Sottolichio[2], Sylvain Rigaud[4], Alicia Romero-Ramirez[1], Marie-Ange Cordier[2], Dominique Poirier[2], Martin Danilo[2] and Antoine Grémare[1]

[1]UMR EPOC, Université de Bordeaux, CNRS, UMR 5805, Station Marine d'Arcachon, 2 rue du Professeur Jolyet, F33120 Arcachon, France

[2]UMR EPOC, Université de Bordeaux, CNRS, UMR 5805, Bâtiments B18/B18N, Allée Geoffroy Saint-Hilaire, F33615 Pessac CEDEX, France

[3]Departamento de Biologia Marinha, Instituto de Biologia, Universidade Federal do Rio de Janeiro, CEP 21941-902 Rio de Janeiro, Brazil

[4]IFREMER Brest—DYNECO/DHYSED, Centre de Bretagne, CS 10070, 29280 Plouzané, France

Abstract

The benthic compartment of River-dominated Ocean Margins (RiOMar) is largely affected by sedimentary processes, as well as natural and anthropogenic disturbances. Recent works confirmed the major importance of riverine inputs and hydrodynamics in the spatial structuration of temperate RiOMar located in low- and high-energy environments, respectively. Differences in the nature of these structuring factors could also affect the temporal dynamics of these two systems. The present study is aiming at: (1) quantifying spatio-temporal changes in Sediment Profile Images (SPI) characteristics within the West Gironde Mud Patch (WGMP; high-energy system) and identifying the main environmental factors controlling these changes based on the same methodology already used for surface sediment characteristics and benthic macrofauna composition, (2) achieving a comparison with the Rhône River Prodelta (RRP; low-energy system) in view of further characterizing benthic functionings in these two temperate RiOMar, and (3) evaluate the use of Sediment Profile Imagery as a surrogate of benthic macrofauna composition by identifying the set of SPI characteristics best describing spatio-temporal changes in benthic macrofauna composition in both systems. For this purpose, SPI characteristics were assessed at five stations located along a depth gradient within the WGMP and during six seasonally-contrasted sampling periods. Results support the existence of a spatial pattern cued by hydrodynamics, as already described based on a one-shot synoptic survey. SPI characteristics present seasonal changes. However, and conversely to benthic macrofauna compositions (Lamarque et al. in prep.), they do not show any significant pluri-annual changes. The comparison with the RRP highlights major discrepancies in the mechanisms involved in the control of biological activity in the two systems, which further supports current RiOMar typologies. The present study also underlines the inability of any set of SPI characteristics to fully describe changes in benthic macrofauna composition in the two considered systems.

Keywords: RiOMar; West Gironde Mud Patch; North-East Atlantic shelf; Sediment Profile Imagery; Bioturbation; Benthic macrofauna; Spatio-temporal variations; Hydrodynamics

1. Introduction

River-dominated Ocean Margins (RiOMars) are the parts of continental margins impacted by major rivers freshwater and/or sediment discharges. They constitute the main marine primary depositional areas of riverine particulate continental inputs (McKee et al. 2004, Burdige 2005). RiOMars provide a large variety of ecosystem services (Aller 1998, Levin et al. 2001, Lansard et al. 2009). They account for 40 to 50% of continental Particulate Organic Carbon (POC) burial occurring in continental margins (Hedges & Keil 1995, Burdige 2005, Blair & Aller 2012). The assessment of the functioning of their benthic compartment is therefore essential to reach a comprehensive understanding of the marine contribution to global biogeochemical cycles (Aller 1998, Blair & Aller 2012). Mostly based on geomorphological and biogeochemical processes occurring in tropical and subtropical RiOMars, two studies have attempted to classify these particular areas (McKee et al. 2004, Blair & Aller 2012). Their results highlighted the major effect of hydrodynamics regimes on RiOMar morphologies and POC mineralization/burial intensities. Blair & Aller (2012) drew a distinction between: (1) low-energy systems, with both high sedimentation rates and carbon preservation (later referred as type 1), and (2) high-energy tidal and/or wave systems with both high sediment oxygenation and low carbon preservation rates (later referred as type 2).

The validity of this distinction was recently established by Lamarque et al. (2021 and in prep.) based on a comparison between the West Gironde Mud Patch (WGMP; taken as a representative example of high-energy system) and the Rhône River Prodelta (RRP; taken has an example of low-energy system). The work by Lamarque et al. (in prep) involved the comparison of spatio-temporal changes in surface sediment characteristics and benthic macrofauna composition. It was based on a restricted number of stations (i.e., 5 in both systems) and of sampling dates (4 for both the WGMP and the RRP). Results highlighted the major role of hydrodynamics in controlling the spatial structuration of the WGMP, which was mostly related to depth and characterized by the subdivision between a proximal and a distal part. Temporal changes in the WGMP were both short- and long-term and larger at deep stations. They were interpreted as resulting from a seasonal dynamics superimposed to a cicatrization process following major physical disturbances caused by severe storms. This was not the case in the RRP where temporal changes were higher at the shallowest station in relation with changes in the hydrological regime of the Rhône River (see also Bonifácio et al.

2014). The work by Lamarque et al. (2021) consisted in a comparison of the spatial structuration of the two systems based on the simultaneous sampling of a much higher number of stations (32 in the WGMP and 7-10 in the RRP, respectively). Here again, it involved the assessments of surface sediment characteristics. The number of stations was however only poorly compatible with the assessment of benthic macrofauna composition, which involves the time-consuming identification of species and their quantification and provides only indirect information on ecosystem functioning.

Sediment Profile Imaging (Germano et al. 2011 and references therein) was introduced by Rhoads & Young (1970) with the aim of quickly assessing the health of benthic habitats by taking a picture of a vertical section of the upper part of the sediment column including the water-sediment interface. This method provides *in-situ* information about various processes such as bioturbation, trophic stratification, biogenic irrigation, or interspecies competition as manifested in small-scale spatial relationships (Wilson et al. 2009). Since, this method has been used for assessing the health of benthic habitats submitted to a large variety of disturbances such as aquaculture (Karakassis et al. 2002, Mulsow et al. 2006), bottom trawling (Nilsson & Rosenberg 2003, Rosenberg et al. 2003b, Smith et al. 2003), dredging disposal (Wilson et al. 2009), sewage effluent and organic enrichment (Makra et al. 2001, Wildish et al. 2003, Labrune et al. 2012) or oil spills and drilling (Rumohr & Schomann 1992, Germano 1995). Several studies have compared the conclusion derived from the use of Sediment Profile Imaging and benthic macrofauna composition (Nilsson & Rosenberg 1997, 2000, Karakassis et al. 2002, Rosenberg et al. 2003a). Their results showed that both methods are able to detect disturbances and distinguish benthic communities between the different successional stages issued from the Rosenberg & Pearson (1978) model especially when environmental gradients are well marked and/or disturbances are pronounced (Karakassis et al. 2002). Results were much less conclusive in the presence of weaker environmental gradients and/or disturbances partly due to the choice of the variables describing Sediment Profile Images (SPI; O'Reilly et al. 2006).

In the WGMP, spatial changes in benthic macrofauna composition were higher than short-term temporal changes and mostly related to depth (Lamarque et al. in prep.). Lamarque et al. (2021) used Sediment Profile Imaging to characterize spatial changes occurring in WGMP sediments. Their results were fully coherent with those derived from the analysis of benthic macrofauna composition (Lamarque et al. in prep). However, the ability of

SPI to account for the weaker temporal changes in benthic macrofauna composition still remains questionable due to the lower magnitude of these changes. The present study is aiming at filling this gap by: (1) quantifying spatio-temporal changes in Sediment Profile Images characteristics within the WGMP, identifying the main environmental factors potentially controlling these changes and comparing these items with those already put forward based on benthic macrofauna composition (Lamarque et al. in prep.), (2) comparing the differences between the WGMP and the RRP based on the assessments of benthic macrofauna composition and SPI characteristics, and (3) identifying the set of SPI characteristics best describing spatio-temporal changes in benthic macrofauna composition in both systems.

2. Materials & Methods

2.1. The West Gironde Mud Patch

The West Gironde Mud Patch (WGMP) is a 420 km^2 sedimentary body located in the Bay of Biscay 40 km off the Mouth of the Gironde Estuary, between ca. 30 and 75m depth (Figure 3.1A). This relict paleovalley/depression is the primary depocenter (sedimentation rates between less than 1 and 10 $mm.y^{-1}$; Dubosq et al. 2021) of fine particles originating from the Gironde Estuary (annual mean water flow of 944 $m^3.s^{-1}$ (Doxaran et al. 2009) with daily flows up to 7,500 $m^3.s^{-1}$ during winter floods (Constantin et al. 2018)). The WGMP is located in a macro-tidal environment with a tidal range from 1.5 to 5 m (Jalón-Rojas et al. 2018). The continental shelf off the Mouth of the Gironde Estuary is dominated by strong swells/waves, which can reach maximal amplitudes of 15 m and time periods of 15 s during winter storms (Cirac et al. 2000, Masselink et al. 2016). These hydrodynamics conditions prevent the sedimentation of fine particles in the immediate vicinity of the Mouth of the Estuary (Jouanneau et al. 1989). The sedimentology of the WGMP has been extensively studied based on stratigraphic sequences, palynological data, X-rays radiographies and radiochronographies (Longère & Dorel 1970, Castaing et al. 1979, 1982, Castaing & Allen 1981, Jouanneau et al. 1989, Lesueur et al. 1989, 1991, 1996, 2001, 2002, Weber et al. 1991, Lesueur & Tastet 1993, 1994, Gadel et al. 1997, Parra et al. 1998). Sedimentological surveys have attributed a major role to hydrodynamics in controlling the spatial structuration of the WGMP. This paradigm

was based on both: (1) the segmentation between a proximal and a distal part with no modern persistent sedimentation in the former due to strong hydrodynamics, and (2) the decreasing frequency of occurrence of vertical erosional sequences within the sediment column with station depth (Jouanneau et al. 1989, Lesueur et al. 1991, 2001, 2002, Lesueur & Tastet 1994). This was recently further validated, based on: (1) a synoptic survey of the spatial distributions of surface sediment characteristics and biological activity traces (Lamarque et al. 2021), and (2) the assessment of both short-term and long-term (i.e., decadal) changes in surface sediment characteristics and benthic macrofauna composition (Lamarque et al. in prep.).

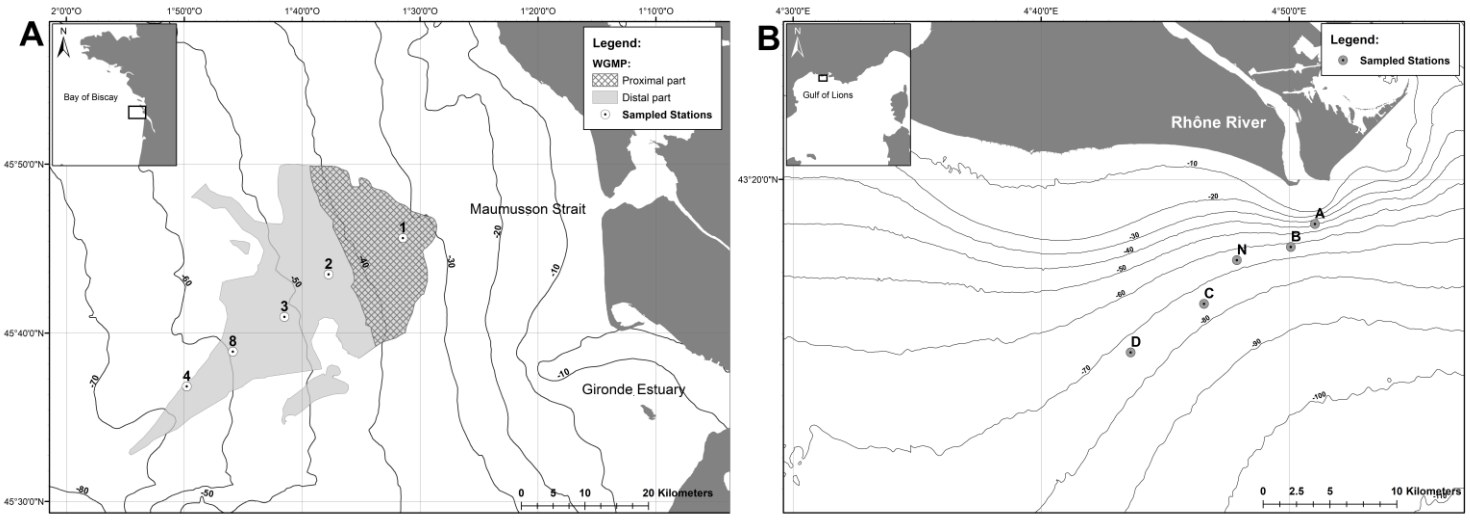

Figure 3.1. Map showing the delimitation of: (**A**) the West Gironde Mud Patch (WGMP) along the French Atlantic Coast together with the locations of the 5 stations sampled for SPI. Stations 1, 3 and 4 were also sampled in July 2010 (corresponding to stations E, C and W in Massé et al. 2016, respectively); and (**B**) the Rhône River Prodelta in the Gulf of Lions (NW Mediterranean) together with the locations of the 5 stations sampled for SPI (Labrune et al. 2012, Bonifacio et al. 2014).

2.2. Collection and processing of Sediment Profile Images in the WGMP

Our sampling strategy deployed in the WGMP was based on the same 5 stations and the 4 sampling dates used by Lamarque et al. (in prep.) for benthic macrofauna samplings. The 5 stations were located within the WGMP along a depth gradient (Figure 3.1A, Table 3.I) and the 4 cruises took place on board of the R/V Côtes de la Manche in October-November 2016 (hereafter October 2016, JERICObent-1; Deflandre 2016), August 2017 (JERICObent-2; Deflandre 2017), January-February 2018 (hereafter February 2018; JERICObent-3; Deflandre 2018), April-May 2018 (hereafter April 2018; JERICObent-4; Deflandre 2018b). An additional cruise took place in June 2018 (JERICObent-5; Schmidt & Deflandre 2018). Only 4 stations were sampled in February 2018 due to bad meteorological conditions. Moreover, 3 stations (i.e., 1,

3 and 4) had been also previously sampled in July 2010 but not processed (Massé et al. 2016). At all stations, between 6 (all stations in June 2018) and 16 (station 2 in February 2018) Sediment Profile Images (SPI) were collected using an Ocean Imaging Systems® Sediment Profile Imager fitted with a Nikon® D7100 camera.

Individual SPI were analyzed for (1) apparent Redox Potential Discontinuity (aRPD) thickness, (2) numbers of biogenic structures (i.e., tubes, burrows, oxic voids, feeding structures), (3) numbers of epi- and infauna, and (4) mean depths of oxic voids within the sediment column. For station 1, presenting a surface sandy layer, the upper limit for the computation of aRPD thickness was set below the transient top coarser sediment layer. Numbers of both infauna and epifauna were summed and expressed as "fauna". Image analyses were achieved using the SpiArcBase software (Romero-Ramirez et al. 2013) and mean values and standard deviations were computed for each combination of stations and sampling dates.

Table 3.I. Location (WGS84, degrees, and decimal minutes) and depth of the 5 stations (1, 2, 3, 8, 4) sampled in the WGMP during the present study and of the 5 stations sampled in the RRP (A, B, N, C, D) by Labrune et al (2012) and Bonifacio et al (2014).

System	Station	Latitude (N)	Longitude (W)	Depth (m)
WGMP	1	45°45.580'	1°31.489'	37
	2	45°43.511'	1°37.773'	47.8
	3	45°41.007'	1°41.545'	56.5
	8	45°38.873'	1°45.777'	64.5
	4	45°36.924'	1°49.712'	71.5
RRP	A	43°18.690'	04°51.042'	24
	B	43°18.013'	04°50.068'	54
	N	43°17.626'	04°47.896'	67
	C	43°16.343'	04°46.565'	76
	D	43°14.917'	04°43.613'	74

2.3. Water flow, Bottom Shear Stress and surface sediment characteristics in the WGMP

Daily water flows of the Gironde Estuary were estimated by summing the flows from the Garonne and Dordogne Rivers, measured at Tonneins and Pessac-sur-Dordogne, respectively as achieved by Lamarque et al. (in prep.). Data were provided by the French Ministère de l'Ecologie, du Développement Durable et de l'Energie (http://www.hydro.eaufrance.fr). At each sampled station, daily values of Bottom Shear Stress (BSS) were computed from the tridimensional numerical model (Diaz et al. 2020) already used by Lamarque et al. (in prep.) for the same purpose. For each combination of stations and sampling dates, the values of surface sediment characteristics (i.e. $D_{0.5}$, SSA, POC, Chl-*a*, Phaeo-a, Chl-*a*/(Chl-*a*+Phaeo-*a*) ratio, THAA, EHAA, EHAA/THAA ratio and $\delta^{13}C$) were taken from Lamarque et al. (2021 and in prep.).

2.4. Data analysis

2.4.1. Analysis of WGMP data

Two-way PERMANOVA (Anderson 2001, Anderson et al. 2008) achieved on measurements at station 1, 3 and 4 were first used to assess the significance of spatio-temporal (i.e. between combinations of stations and sampling dates) changes in main SPI characteristics (i.e., all individual characteristics but feeding structures plus the total number of biological traces and the number of subsurface (burrows + oxic voids) structures). A hierarchical clustering (Euclidean distance and average group linking) and a Principal Components Analysis (PCA) were then used to define groups of stations and to assess the relationships between mean SPI characteristics (i.e., aRPD thickness, mean depth of oxic void, number of tubes, number of burrows, number of oxic voids and number of fauna). A SIMilarity PROFile procedure (SIMPROF; Clarke et al. 2008) was used to test for the statistical significance of differences between station groups resulting from hierarchical clustering. Two DISTance-based Linear Model (DISTLM; Anderson et al. 2008) were established to assess the contributions of potential explanatory variables to spatio-temporal changes in SPI characteristics. The first one was conducted using the surface sediment characteristics (i.e. SSA, Chl-*a*, Chl-*a*/(Chl-*a*+Phaeo-*a*) ratio, THAA, EHAA/THAA ratio and $\delta^{13}C$) measured during the 5 JERICO-bent cruises (Lamarque et al. 2021 and in prep.). POC, Phaeo-*a* and EHAA were excluded from this procedure due to their correlation with other sediment characteristics. The

second DISTLM was conducted using river flows and Bottom Shear Stress summed over both 100 and 365 days periods preceding each cruise (later designed as $Flow_{100}$, $Flow_{365}$, BSS_{100} and BSS_{365}) as already achieved by Lamarque et al. (in prep.) for both surface sediment characteristics and benthic macrofauna composition during the 4 first JERICObent cruises. The significance of the correlation between the similarity matrices based on benthic macrofauna composition and SPI characteristics was assessed using a Mantel test (Mantel 1967). A third DISTLM was conducted to account for spatio-temporal changes in benthic macrofauna composition based on SPI characteristics. These procedures were based on macrofauna data collected at the same stations during October 2016, August 2017, February and April 2018 (Lamarque et al. in prep.). All models were built using the Best selection procedure (Anderson et al. 2008) and the AIC selection criterion (Akaike 1973). Each DISTLM was represented in a multidimensional space through a distance-based Redundancy Analysis (dbRDA; Anderson et al. 2008). All analyses were run on normalized datasets (except for PERMANOVA conducted on individual SPI characteristics) using the PRIMER® 6 software package (Clarke & Warwick 2001) with the PERMANOVA+ add-on (Anderson et al. 2008) except for the Mantel test which was achieved using R version 3.6.1 (R Core Team 2019) with the additional package ade4 (Dray & Dufour 2007).

2.4.2. Comparison between the West Gironde Mud Patch and the Rhône River Prodelta

SPI characteristics collected in the WGMP were compared with those derived from SPI previously collected during 3 cruises, which took place in the Rhône River Prodelta (RRP) in April 2007, May 2008 and July 2011. Five stations located on a depth gradient were sampled during each cruise (Figure 3.1B; Table 3.I). Station A was located in the delta front; station B in the prodelta and stations N, C and D in the distal zone (*sensu* Bonifácio et al. 2014). Collected SPI were processed by Labrune et al. (2012) and then Bonifácio et al. (2014) using the SPIArcBase software (Romero-Ramirez et al. 2013). We used the raw data produced by these authors during the present study since the same characteristics as listed above for the WGMP were available. Patterns in intra-station temporal variability were compared in the WGMP (4 cruises during the 2016-2018 sampling period) and the RRP (3 cruises during the 2007-2011 sampling period; Labrune et al. 2012, Bonifácio et al. 2014) based on the information contained in the dissimilarity matrices (i.e., one for each system) computed using 6 SPI characteristics (i.e., aRPD thickness, number of burrows, number and mean depth of oxic

voids, number of tubes, and number of fauna). The sums of squared distances from individual points (i.e., station*sampling date) to their group (i.e., station) centroids were computed for each station following Anderson (2001) and Anderson et al. (2008) and used as indices of intra-station temporal variability after standardization for the number of sampling dates. As for the WGMP, the significance of the correlation between the similarity matrices based on benthic macrofauna composition and SPI characteristics in the RRP was assessed using a Mantel test (Mantel 1967) and a DISTLM was conducted to account for spatio-temporal changes in benthic macrofauna composition based on SPI characteristics. The model and its representation were built as described above for the WGMP.

3. Results

3.1. Temporal changes in water flows and Bottom Shear Stress in the WGMP

Water flows presented a clear seasonal pattern with a high-flood period during winter and spring (with flooding peaks up to 5 590 $m^3.s^{-1}$ on January 23 2018) and a low flow period during summer and fall (Figure 3.2A). Over the whole 2010-2018 time period, major events were constituted by the January 2018 and to a lower extent, the January 2014 floods. Between October 2016 and June 2018, there were clear inter-annual differences in water flows during the high-flow period as indicated by the moderate values recorded during 2016-2017 as opposed to 2017-2018. The October 2016 and August 2017 cruises were achieved during low-flow periods. Conversely, the February, April and June 2018 cruises took place during a high-flow period, respectively 5, 87 and 136 days after the major January 2018 flood.

Bottom Shear Stress (BSS) also showed a clear seasonal cycle with a succession of peaks induced by winter storms and conversely low values during summer and fall (Figure 3.2B). Over the whole 2010-2018 time period, the major event was the succession of peaks (i.e., up to 3.23 $N.m^{-2}$) during the 2013-2014 winter. Between 2016 and 2018, there were slight differences between temporal changes in water flows and BSS since: (1) high-BSS periods generally preceded high-flow periods, and (2) highest BSS (up to 2.40 $N.m^{-2}$ on February 3 2017) were recorded during 2016-2017 conversely to highest water flows which were

recorded in 2018 (see above). Nevertheless, the October 2016, August 2017 and June 2018 cruises were conducted during low-BSS periods (i.e., < 0.5 $N.m^{-2}$) as opposed to the February 2018 and the April 2018 cruises, which both took place during the 2018 high-BSS period.

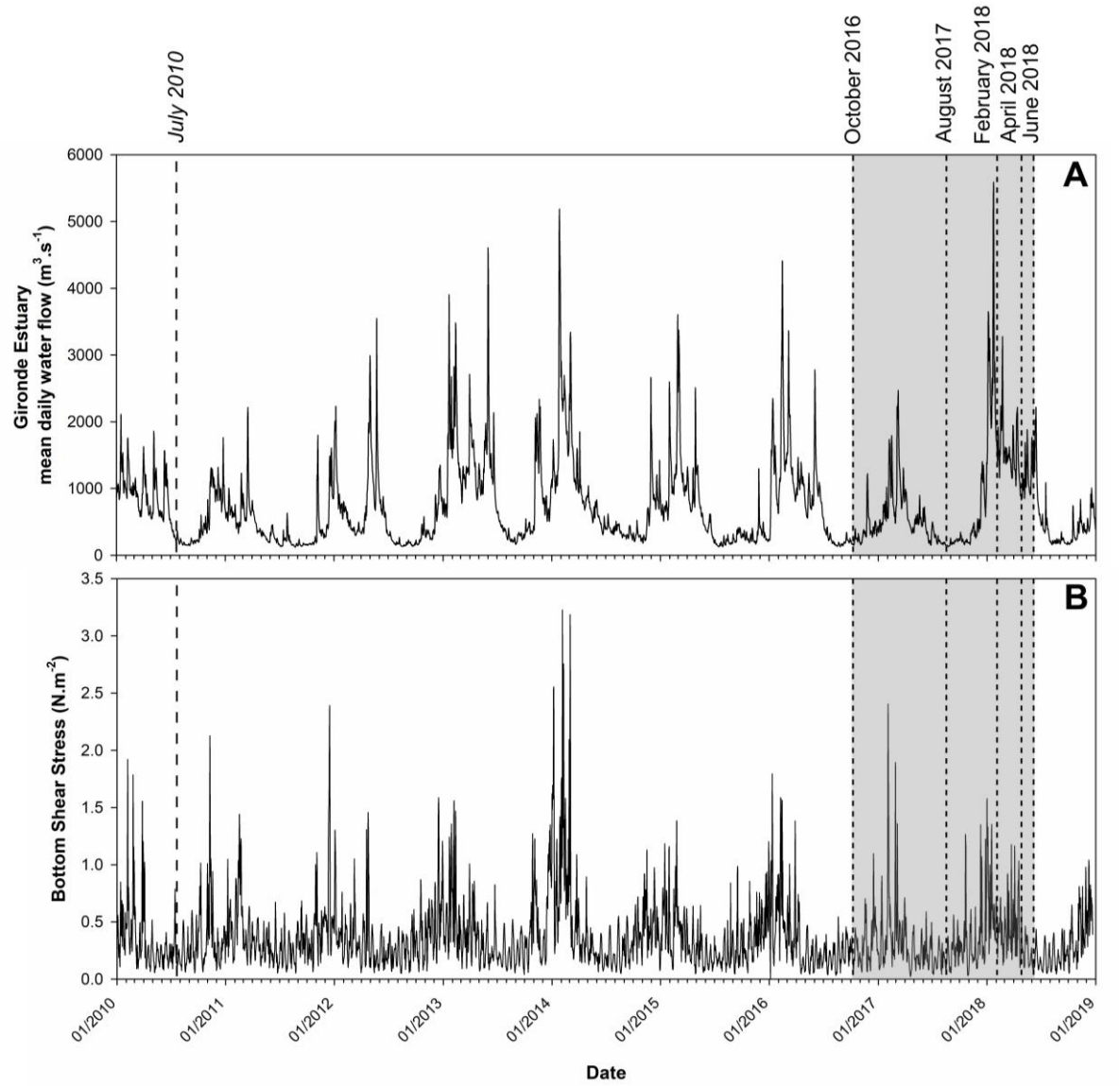

Figure 3.2. Temporal changes in Gironde Estuary mean daily water flow (**A**) and in the 95th percentile of Bottom Shear Stress at station 3 (**B**) during the 2010-2018 period. Short-dashed lines indicate the five cruises achieved in the WGMP between 2016 and 2018 (grey area) and the long-dashed line indicates the July 2010 cruise (Massé et al. 2016).

3.2. Spatio-temporal changes in WGMP SPI

Overall, 301 Sediment Profiles Images (SPI) were sampled. Representative examples collected at stations 1, 3 and 4 during July 2010, October 2016 and April 2018 are shown in Figure 3.3.

Only 12 feeding structures were identified. This parameter was thus excluded from further analyses due to its low representativity. Mean values of SPI characteristics per pair of stations and sampling dates together with their standard deviations are shown in Table 3.II. The p values of corresponding PERMANOVA are given in Table 3.III. There was a significant effect of the interaction between stations and sampling dates for all characteristics but oxic void mean depth. Differences between stations were significant for all characteristics except for burrow number. Differences between sampling dates were significant as well except for oxic void number.SPI^{-1} and mean depth.

The mean apparent Redox Potential Discontinuity (aRPD) thickness was lower at station 1 where it ranged from 7.8 to 23.0 mm in February 2018 and June 2018, respectively (Figure 3.4A; Table 3.II). It then tended to increase from station 2 to station 4, where it reached a maximal value of 107.4 mm in August 2017. Temporal changes were less clear and relatively more important at station 1 and 4 (variation coefficients of 40.9 and 16.8%, respectively), accounting for the significant interaction between station and sampling date. Except for station 1, the mean aRPD thickness tended to be lower in October 2016 and February 2018 than during the 4 other sampling dates.

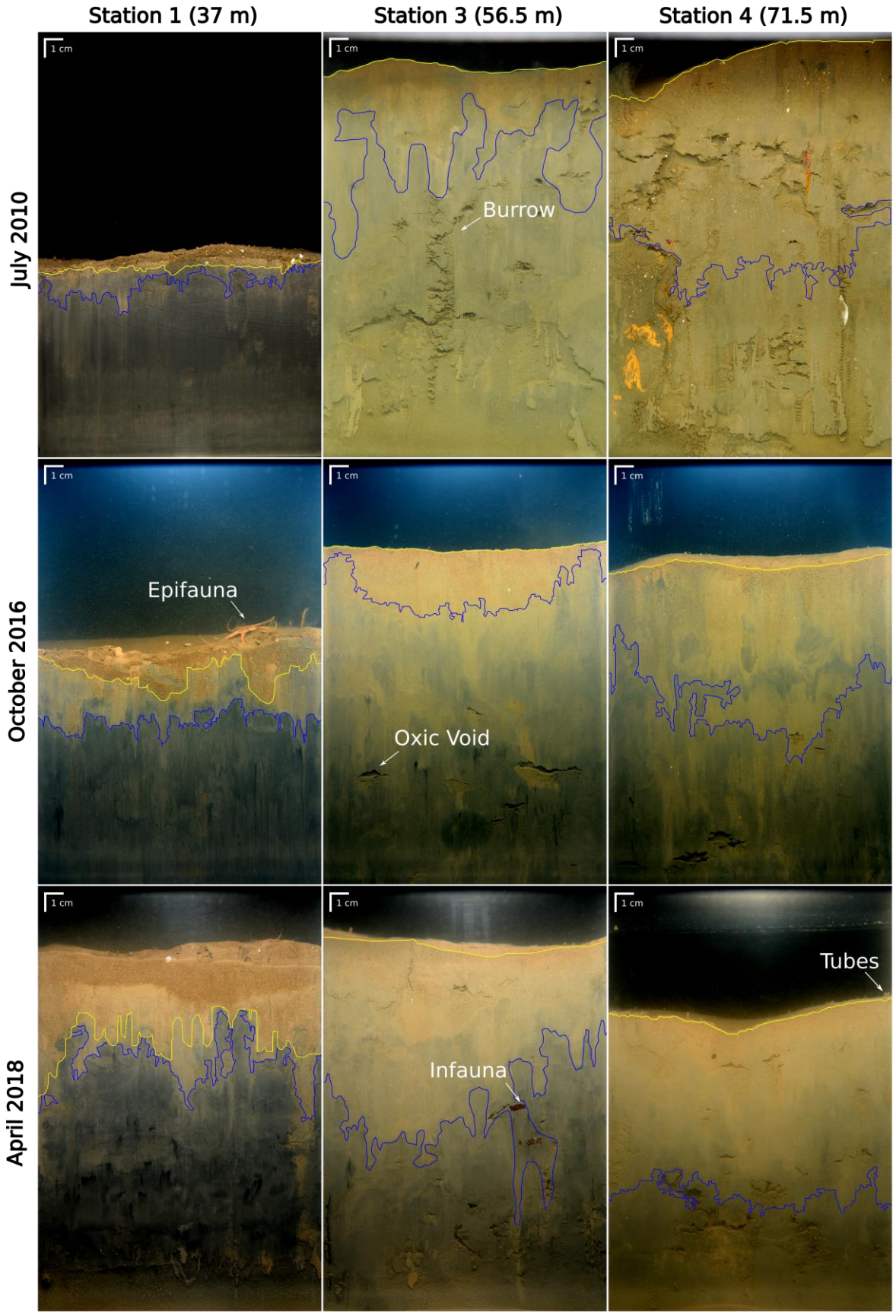

Figure 3.3. Examples of Sediment Profile Images (SPI) collected at stations 1, 3 and 4 during July 2010, October 2016 and April 2018. Yellow lines represent sediment– water interfaces and blue lines represent apparent Redox Potential Discontinuity (aRPD) thicknesses. Station codes are the same as in Figure 3.1A and Table 3.I. Similar examples for the RRP can be found in Bonifacio et al. (2014).

There was no significant effect of the interaction between stations and sampling dates nor of sampling dates alone on the mean depth of oxic voids. Conversely, these characteristics significantly differed between stations with lower values at station 1 ranging from 12.4 to 56.2 mm in February 2018 and October 2016, respectively (Tables 3.II and 3.III, Figure 3.4B).

Table 3.II. Mean values (± standard deviation) of SPI characteristics. aRPD: apparent Redox Potential Discontinuity thickness, Burrows: number of burrows per SPI, OV: number of oxic voids per SPI, OV depth: mean depth of oxic voids, Tubes: number of tubes per SPI, Feeding structures: number of feeding structures per SPI, Fauna: summed numbers of infauna and epifauna per SPI, Subsurface structures: summed numbers of burrows and oxic voids per SPI, Total number: Total number of biological traces per SPI.

Cruise	Station	Number of sampled SPI	aRPD (mm)	Burrows (nb.SPI^{-1})	OV (nb.SPI^{-1})	OV depth (mm)	Tubes (nb.SPI^{-1})	Feeding structures (nb.SPI^{-1})	Fauna (nb.SPI^{-1})	Subsurface structures (nb.SPI^{-1})	Total number (nb.SPI^{-1})
July 2010	1	9	12.3 ± 3.0	4.7 ± 1.9	0.1 ± 0.3	24.042	2.9 ± 1.8	0.0 ± 0.0	0.1 ± 0.3	4.8 ± 2.0	7.8 ± 2.6
	3	10	77.5 ± 17.7	5.6 ± 1.7	6.0 ± 4.5	78.8 ± 24.3	0.2 ± 0.6	0.1 ± 0.3	0.7 ± 0.7	11.6 ± 5.7	12.6 ± 5.9
	4	9	93.6 ± 18.0	5.6 ± 1.9	6.0 ± 3.4	71.6 ± 36.7	0.2 ± 0.4	0.0 ± 0.0	0.9 ± 1.2	11.6 ± 4.2	12.7 ± 5.2
October 2016	1	10	19.4 ± 10.3	3.9 ± 1.8	0.4 ± 1.0	56.2 ± 3.0	8.3 ± 3.8	0.0 ± 0.0	2.3 ± 1.3	4.3 ± 1.9	14.9 ± 4.1
	2	11	52.7 ± 7.0	4.6 ± 2.3	1.1 ± 2.1	81.2 ± 30.5	2.8 ± 2.1	0.1 ± 0.3	2.5 ± 1.5	5.7 ± 2.1	11.1 ± 3.7
	3	14	58.6 ± 13.9	4.8 ± 1.8	5.1 ± 2.2	111.1 ± 15.3	4.9 ± 3.3	0.1 ± 0.3	0.9 ± 1.5	9.9 ± 2.7	15.6 ± 5.7
	8	11	60.9 ± 11.9	5.1 ± 1.1	4.1 ± 1.9	92.9 ± 27.4	2.5 ± 3.1	0.0 ± 0.0	0.8 ± 0.9	9.2 ± 1.7	12.5 ± 2.8
	4	11	73.9 ± 12.0	4.5 ± 2.0	3.2 ± 2.9	104.6 ± 38.0	3.8 ± 3.1	0.0 ± 0.0	0.5 ± 1.3	7.7 ± 3.4	12.1 ± 4.1
August 2017	1	14	12.0 ± 5.6	7.1 ± 3.4	0.6 ± 0.9	34.4 ± 33.3	4.2 ± 8.3	0.0 ± 0.0	3.4 ± 2.6	7.7 ± 4.0	15.4 ± 10.4
	2	12	53.7 ± 7.8	8.0 ± 4.5	1.8 ± 1.2	92.3 ± 30.7	2.0 ± 2.9	0.0 ± 0.0	4.3 ± 3.1	9.8 ± 4.5	16.1 ± 6.5
	3	11	71.7 ± 12.6	5.4 ± 2.2	4.6 ± 2.7	92.6 ± 23.4	0.5 ± 0.9	0.0 ± 0.0	0.6 ± 0.7	10.0 ± 3.4	11.2 ± 3.4
	8	15	78.4 ± 10.1	3.6 ± 2.7	3.3 ± 3.0	103.5 ± 46.7	2.1 ± 2.9	0.0 ± 0.0	0.3 ± 0.5	6.9 ± 3.5	9.4 ± 3.8
	4	10	107.4 ± 17.9	2.7 ± 1.1	3.0 ± 1.7	67.7 ± 18.4	0.6 ± 0.8	0.0 ± 0.0	0.5 ± 0.7	5.7 ± 2.0	6.8 ± 2.7
February 2018	1	15	7.8 ± 6.6	3.9 ± 2.3	0.1 ± 0.3	12.42	1.2 ± 1.4	0.0 ± 0.0	0.8 ± 1.1	3.9 ± 2.3	5.9 ± 2.3
	2	16	52.4 ± 12.7	5.3 ± 1.8	3.1 ± 1.7	95.3 ± 39.2	0.2 ± 0.4	0.0 ± 0.0	1.2 ± 1.1	8.4 ± 2.9	9.8 ± 3.5
	3	13	59.4 ± 11.5	4.3 ± 2.1	3.2 ± 2.2	102.9 ± 33.0	0.5 ± 1.0	0.0 ± 0.0	0.4 ± 0.5	7.5 ± 3.1	8.3 ± 3.4
	4	14	69.2 ± 13.6	4.1 ± 2.0	5.8 ± 2.6	108.2 ± 34.5	1.8 ± 2.7	0.1 ± 0.3	0.1 ± 0.3	9.9 ± 2.8	11.9 ± 4.5
April 2018	1	13	10.4 ± 4.3	8.1 ± 2.9	0.3 ± 0.5	39.6 ± 22.8	1.1 ± 1.4	0.0 ± 0.0	2.1 ± 1.4	8.4 ± 3.0	11.5 ± 4.0
	2	14	69.3 ± 12.3	8.5 ± 1.8	3.0 ± 2.4	67.1 ± 36.4	2.6 ± 2.5	0.0 ± 0.0	2.5 ± 1.6	11.5 ± 2.4	16.6 ± 3.4
	3	12	75.7 ± 16.0	8.9 ± 3.4	4.3 ± 1.6	83.0 ± 24.9	3.6 ± 5.5	0.0 ± 0.0	0.8 ± 1.1	13.3 ± 3.9	17.7 ± 6.3
	8	13	76.8 ± 31.5	8.4 ± 3.2	4.9 ± 3.1	68.9 ± 26.7	12 ± 12.2	0.0 ± 0.0	0.8 ± 0.8	13.3 ± 5.3	26.2 ± 14.1
	4	14	91.5 ± 17.3	8.1 ± 2.0	6.9 ± 3.3	82.9 ± 27.0	13.1 ± 5.4	0.0 ± 0.0	0.4 ± 0.7	15.0 ± 4.2	28.4 ± 8.2
June 2018	1	6	23.0 ± 15.0	1.2 ± 0.8	0.7 ± 0.5	35.7 ± 47.5	3.3 ± 1.9	0.0 ± 0.0	1.5 ± 2.0	1.8 ± 1.0	6.7 ± 1.2
	2	6	69.7 ± 2.2	3.8 ± 0.8	3.8 ± 2.5	86.4 ± 14.8	3.2 ± 1.6	0.0 ± 0.0	1.0 ± 0.9	7.7 ± 2.0	11.8 ± 3.0
	3	6	74.9 ± 9.6	3.2 ± 1.5	5.2 ± 4.9	90.8 ± 16.6	4.0 ± 2.5	0.3 ± 0.5	1.3 ± 1.0	8.3 ± 5.5	14.0 ± 7.0
	8	6	77.5 ± 11.0	2.5 ± 0.5	8.8 ± 5.9	96.8 ± 24.1	9.8 ± 5.4	0.3 ± 0.5	1.7 ± 1.0	11.3 ± 5.8	23.2 ± 9.1
	4	6	101.3 ± 8.8	3.0 ± 1.1	6.8 ± 2.4	101.2 ± 17.1	9.5 ± 6.1	0.7 ± 0.5	0.2 ± 0.4	9.8 ± 3.0	20.2 ± 7.9

The spatio-temporal pattern of the mean number of oxic voids per SPI was rather similar to the one of the mean aRPD thickness with low values at station 1 and then a trend toward an increase along the depth gradient (Tables 3.II and 3.III, Figure 3.4C). Temporal changes were not significant and not consistent among stations with maximal values at station 3 in July 2010 (6.0 oxic voids.SPI^{-1}) and at station 8 in June 2018 (8.3 oxic voids.SPI^{-1}), which accounted for the significance of the interaction between stations and sampling dates.

There was a significant effect of the interaction between stations and sampling dates and of sampling dates alone, but conversely no significant effect of stations alone on the mean number of burrows per SPI (Tables 3.II and 3.III, Figure 3.4D). At all 5 sampled stations, values were maximal in April 2018 (e.g., 8.9 burrows.SPI^{-1} at station 3) and conversely minimal in June 2018 (e.g., between 1.2 and 3.8 burrow.SPI^{-1} at stations 1 and 4, respectively). The significance of the interaction between stations and sampling dates mainly resulted from the high values recorded at stations 1 and 2, but not at the 3 other stations, during August 2017.

Table 3.III. Probability levels of two-way (sampling date x station) PERMANOVA conducted on individual SPI characteristics. Bold types are indicative of significant ($p < 0.05$) differences.

	Sampling date	**Station**	**Sampling date x Station**
aRPD thickness	**< 0.001**	**< 0.001**	**< 0.001**
Number of burrows	**< 0.001**	0.226	**0.001**
Number of oxic voids	0.066	**< 0.001**	**0.004**
Mean depth of oxic voids	0.087	**< 0.001**	0.721
Number of tubes	**< 0.001**	**0.001**	**< 0.001**
Number of fauna	**0.002**	**< 0.001**	**< 0.001**
Total number of biological traces	**< 0.001**	**< 0.001**	**< 0.001**
Number of subsurface structures	**< 0.001**	**< 0.001**	**< 0.001**

There was a significant effect of the interaction between stations and sampling dates, and sampling dates or station alones on the mean number of fauna per SPI (Tables 3.II and 3.III, Figure 3.4E). For most sampling dates, values were higher at stations 1 and 2, especially in August 2017 (maximal value of 4.3 ind.SPI^{-1} at station 2) and then tended to decrease along the depth gradient (Table 3.II; Figure 3.4E). The only exception was July 2010, during which

values were much lower (i.e., between 0.1 and 0.9 ind.SPI^{-1} at stations 1 and 4, respectively) and increased with depth.

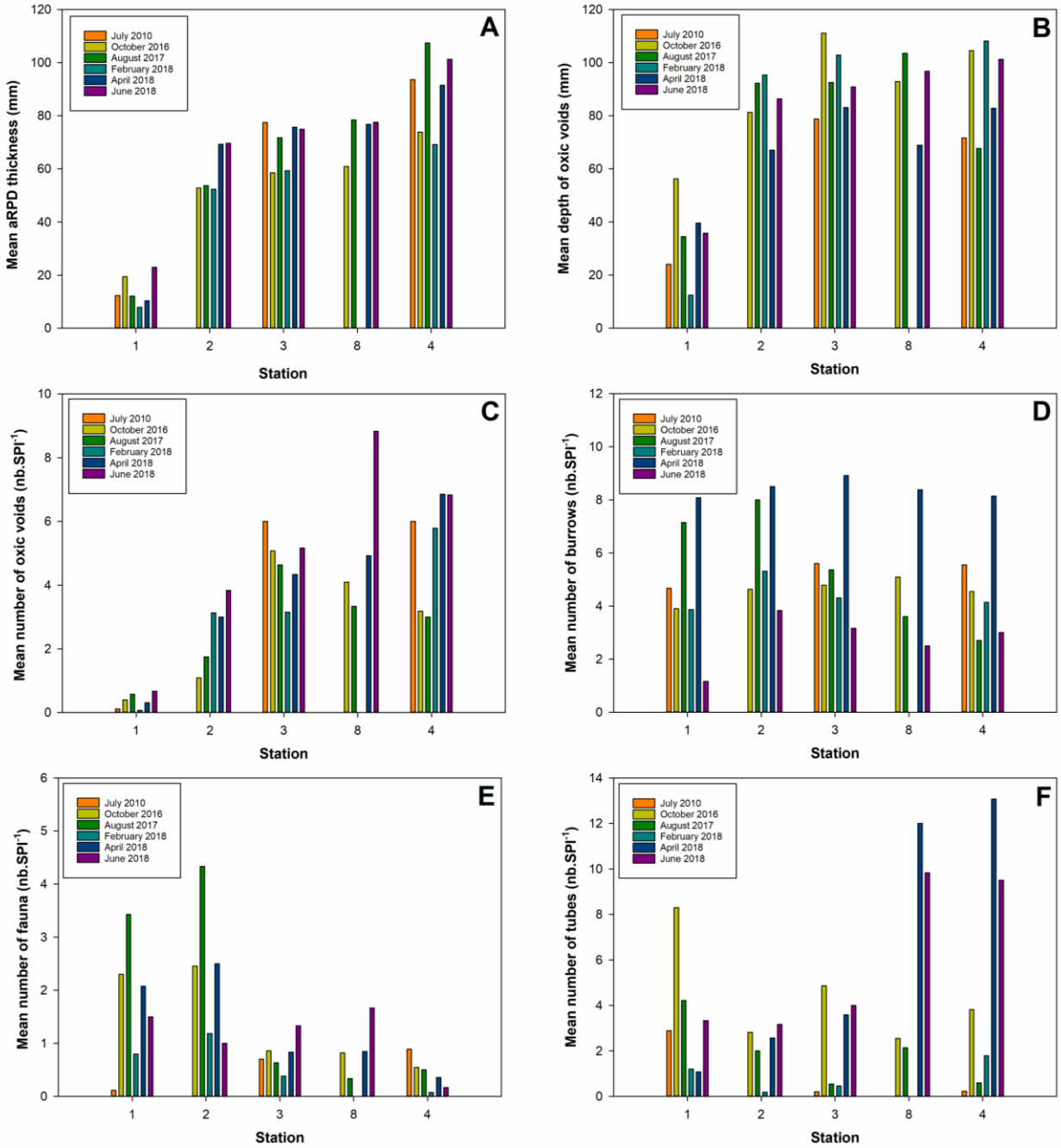

Figure 3.4. Spatio-temporal changes in the mean values of main SPI characteristics: aRPD thickness (**A**), depth of oxic voids (**B**), number of oxic voids per SPI (**C**), number of burrows per SPI (**D**), number of fauna per SPI (**E**) and number of tubes per SPI (**F**). Standard deviations are given in Table 3.II.

There was a significant effect of the interaction between stations and sampling dates, and sampling dates or station alones on the mean number of tubes per SPI (Tables 3.II and 3.III, Figure 3.4F). In July 2010, values were maximal at station 1 (2.9 tubes.SPI^{-1}) and much lower at stations 3 and 4 (0.2 tubes.SPI^{-1} at both stations). The same spatial pattern was

observed in August 2017 and values were also higher (8.3 tubes.SPI^{-1}) at station 1 in October 2016. Conversely, both the April and June 2018 sampling dates presented an opposed spatial pattern, with lower values at stations 1 and 2 (e.g. 1.1 and 2.6 tubes.SPI^{-1} in April 2018, respectively), and higher ones at stations 8 and 4 (e.g. 12.0 and 13.1 tubes.SPI^{-1} in April 2018, respectively).

There was a significant effect of the interaction between stations and sampling dates, and sampling dates or station alone on the mean total number of biological traces (Tables 3.II and 3.III, Figure 3.5A). Values presented different spatial changes depending on sampling dates. They tended to increase along the depth gradient in July 2010, April and June 2018, with maximal values in April 2018 at stations 8 and 4 (i.e., 26.2 and 28.4 traces.SPI^{-1}, respectively). Values recorded during February 2018 also tended to slightly increase with depth, but were also lower. Conversely to this general pattern, values tended to decrease with depth in August 2017.

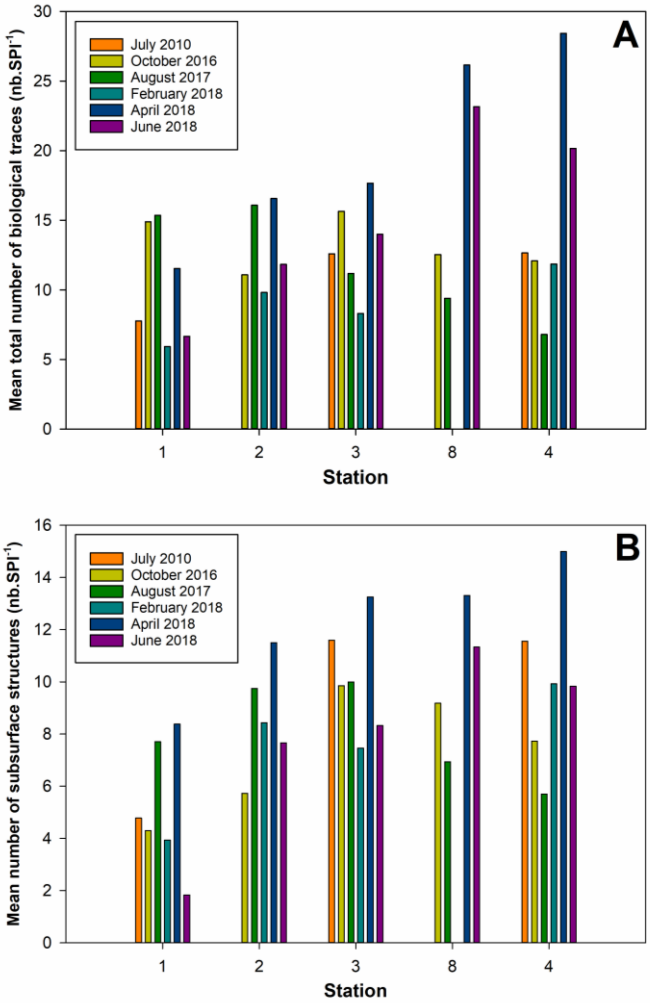

Figure 3.5. Spatio-temporal changes in the mean values of Sediment Profile Images characteristics: total number of biological traces per SPI (**A**) and number of subsurface structures per SPI (**B**). Standard deviations are given in Table 3.II.

There was also a significant effect of the interaction between stations and sampling dates, sampling dates alone and station alone on the mean number of subsurface structures per SPI (Tables 3.II and 3.III, Figure 3.5B); which tended to increase with depth for all sampling dates except August 2017. For each cruise, values were minimal at station 1 (between 1.8 and 8.4 structures.SPI^{-1} in June 2018 and April 2018, respectively). Values of the July 2010 and April 2018 cruises were maximal at stations 3 and 4 with a maximum of 15 structures.SPI^{-1} at station 4 in April 2018.

The first two components of the PCA based on SPI characteristics explained 67.5% (i.e., 46.3% and 21.2% for the first and the second principal component, respectively) of the total variance of SPI characteristics (Figure 3.6A). The first component was mainly characterized by a set of co-correlated subsurface features (i.e., number and mean depth of oxic voids, and aRPD thickness), whereas the second component was mostly driven by the number of burrows and to a lesser extent the numbers of tubes and fauna (Figure 3.6B).

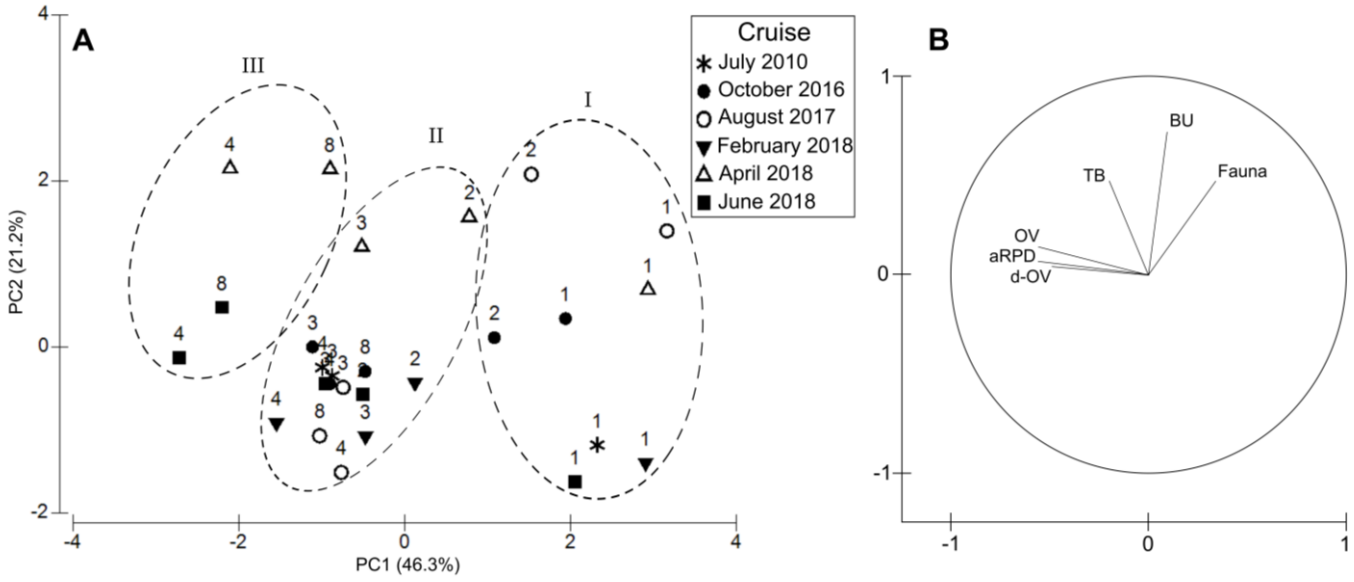

Figure 3.6. Multivariate analyses of Sediment Profile Image characteristics recorded in 2010 and between 2016 and 2018. Projection of stations*dates on the first plane of a Principal Component Analysis (**A**). Figures refer to stations and symbols to cruises. Dotted lines indicate groups of samples issued from the hierarchical clustering as identified through the SIMPROF procedure. Correlations of the variables with the first two principal components (**B**). aRPD: apparent Redox Potential Discontinuity thickness; BU: number of burrows per SPI; OV and d-OV: mean number per SPI and mean depth of oxic voids; TB: mean number of tubes per SPI and Fauna: mean summed numbers of infauna and epifauna per SPI.

Hierarchical clustering and the associated SIMPROF procedure resulted in the identification of 3 groups of stations (Figure 3.6A). Group I was composed of all the sampling dates of station 1, and of the October 2016 and August 2017 samplings of station 2. Group II was composed of all other pairs of stations and sampling dates except the April 2018 and June 2018 samplings of stations 8 and 4, which were constitutive of group III. There was no evidence that the overall SPI characteristics measured in 2010 at stations 1, 3 and 4 differed from those measured during the 5 other sampling dates.

The parsimonious DISTLM involving surface sediment characteristics as predictors included THAA and Chl-*a* concentrations, the Chl-*a*/(Chl-*a*+Phaeo-*a*) ratio and $\delta^{13}C$ as independent variables. It explained 59 % of the initial variance of SPI characteristics. Its representation through the first plane of a dbRDA accounted for 53.1 % of this initial variance and clearly showed two main orientations (Figure 3.7A).

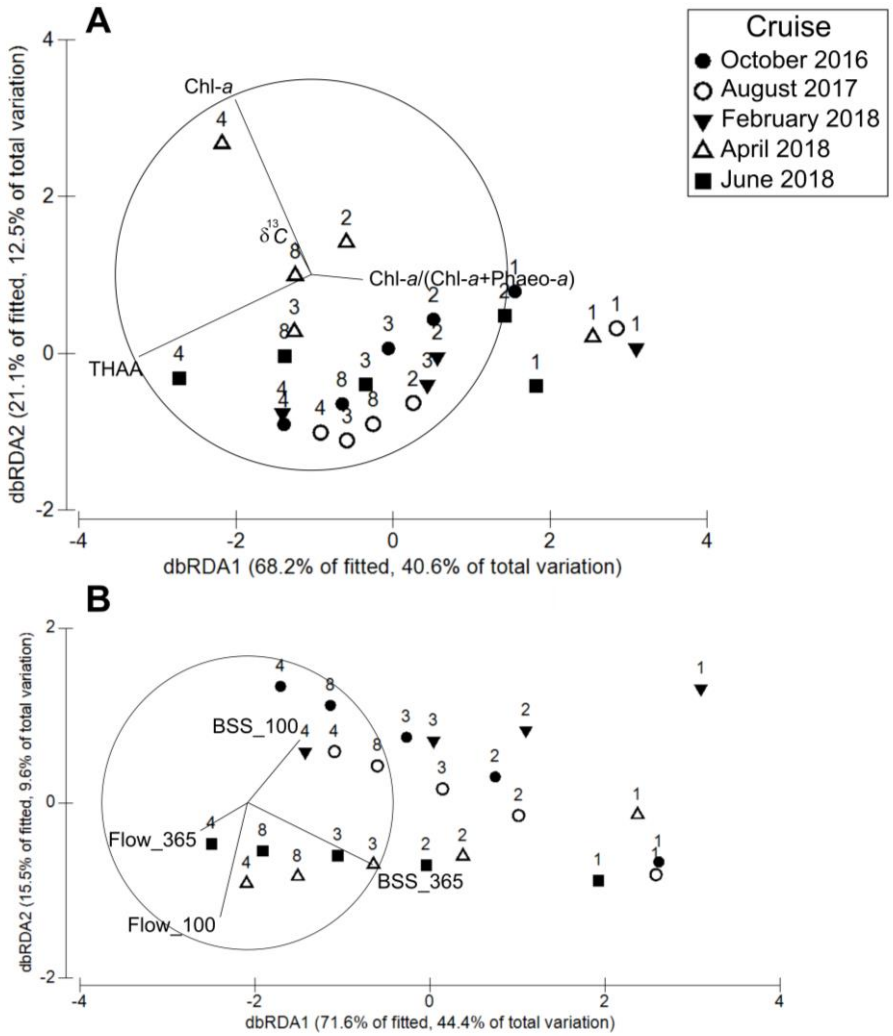

Figure 3.7. Distance-based Redundancy Analysis based on surface sediment characteristics (**A**) and summed BSS and river flows (**B**). Chl-*a*: Chlorophyll-*a*; THAA; Total Hydrolysable Amino Acids; BSS_100 and BSS_365: summed Bottom Shear Stress over 100 and 365 days; Flow_100 and Flow_365: summed river flow over 100 and 365 days.

The first one, mainly along the first component of the dbRDA, corresponded to the positioning of the stations along the depth gradient and was mainly characterized by the opposition between THAA concentrations and Chl-*a*/(Chl-*a*+Phaeo-*a*) ratios. The second one, mainly along the second component of the dbRDA, separated the April 2018 sampling of stations 2, 8 and 4 from those of all other pairs of stations and sampling dates. It was mainly associated with Chl-*a* concentrations and to a much lesser extent $\delta^{13}C$.

The parsimonious DISTLM involving BSS and river flows included BSS_{100}, BSS_{365}, $Flow_{100}$ and $Flow_{365}$ as independent variables. It explained 62 % of the initial variance of SPI characteristics. Its representation through the first plane of a dbRDA accounted for 54.0 % of this initial variance and here again showed two main orientations (Figure 3.7B). The first one, along the first component of the dbRDA, corresponded to the positioning of the stations along the depth gradient. It was mainly associated with BSS_{365}. The second one, along the second component of the dbRDA, mostly separated the April and June 2018 sampling dates from the 3 other ones. It was mainly characterized by the opposition between BSS_{100} and $Flow_{100}$.

3.3. Comparison between the WGMP and the RRP

3.3.1 Differences in the magnitudes of short-term temporal changes in SPI characteristics

The relationships between station depth and intra-station short-term temporal variabilities in SPI characteristics differed in the West Gironde Mud Patch (WGMP) and the Rhône River Prodelta (RRP; Figure 3.8). In both cases, high intra-station variabilities were associated with the two deepest stations. However, the intra-station temporal variabilities of the shallower (i.e., until ca. 60m depth) stations tended to be much lower in the WGMP that in the RRP.

In the WGMP, the high intra-station short-term temporal variabilities observed at the two deepest stations mostly resulted from the higher numbers of tubes (and to a lesser extent burrows) recorded during April 2018. In the RRP, the high intra-station short-term temporal variability observed at the shallowest station mostly resulted from changes in the number of tubes and aRPD thickness, which showed higher values in July 2011. Conversely, the high intra-station short-term temporal variabilities at the two deepest stations resulted from changes in

a larger number of SPI characteristics (i.e., aRPD thickness, numbers of burrows, oxic-voids and fauna) between all three sampling dates.

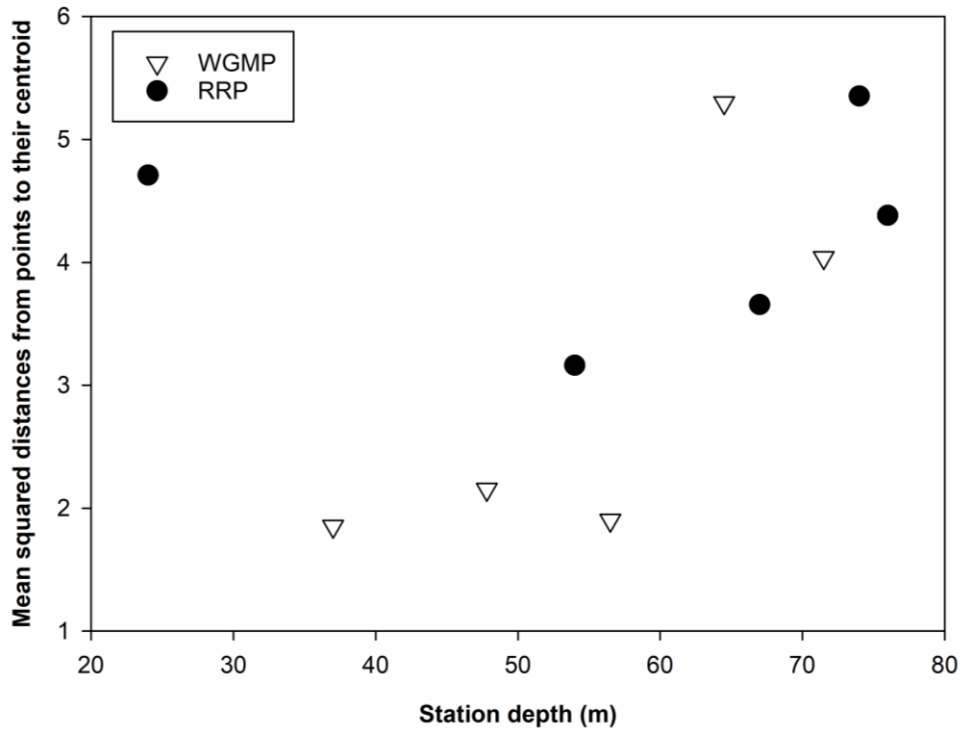

Figure 3.8. Relationship linking station depth and intra-station temporal variabilities in Sediment Profile Images characteristics in both the West Gironde Mud Patch (WGMP) and the Rhône River Prodelta (RRP).

In both systems, the magnitudes of short-term temporal changes in benthic macrofauna composition and SPI characteristics did not correlate significantly ($n = 4$, $r = 0.46$, $p = 0.43$ and $n = 3$, $r = 0.22$, $p = 0.73$ in the WGMP and the RRP, respectively).

3.3.2 Ability of SPI characteristics to account for spatio-temporal changes in benthic macrofauna composition

Similarity matrices based on benthic macrofauna composition and SPI characteristics correlated significantly both in the WGMP and in the RRP ($r = 0.59$, $p < 0.001$ and $r = 0.39$, $p = 0.002$ in the WGMP and the RRP, respectively).

The parsimonious DISTLM established to assess the contributions of SPI characteristics to spatio-temporal changes in benthic macrofauna composition within the WGMP included

the mean aRPD thickness, the mean numbers of fauna and tubes per SPI, and the mean depth of oxic voids as independent variables (Figure 3.9A). It explained 54 % of the variance of benthic macrofauna composition. The representation of the model through the first plane of a dbRDA accounted for 47.5 % of this initial variance. Spatial changes in benthic macrofauna composition were mainly associated with mean aRPD thickness and the mean depth of oxic void, whereas temporal changes at station 8 and 4 were mostly characterized by the high values of the mean numbers of tubes during April 2018.

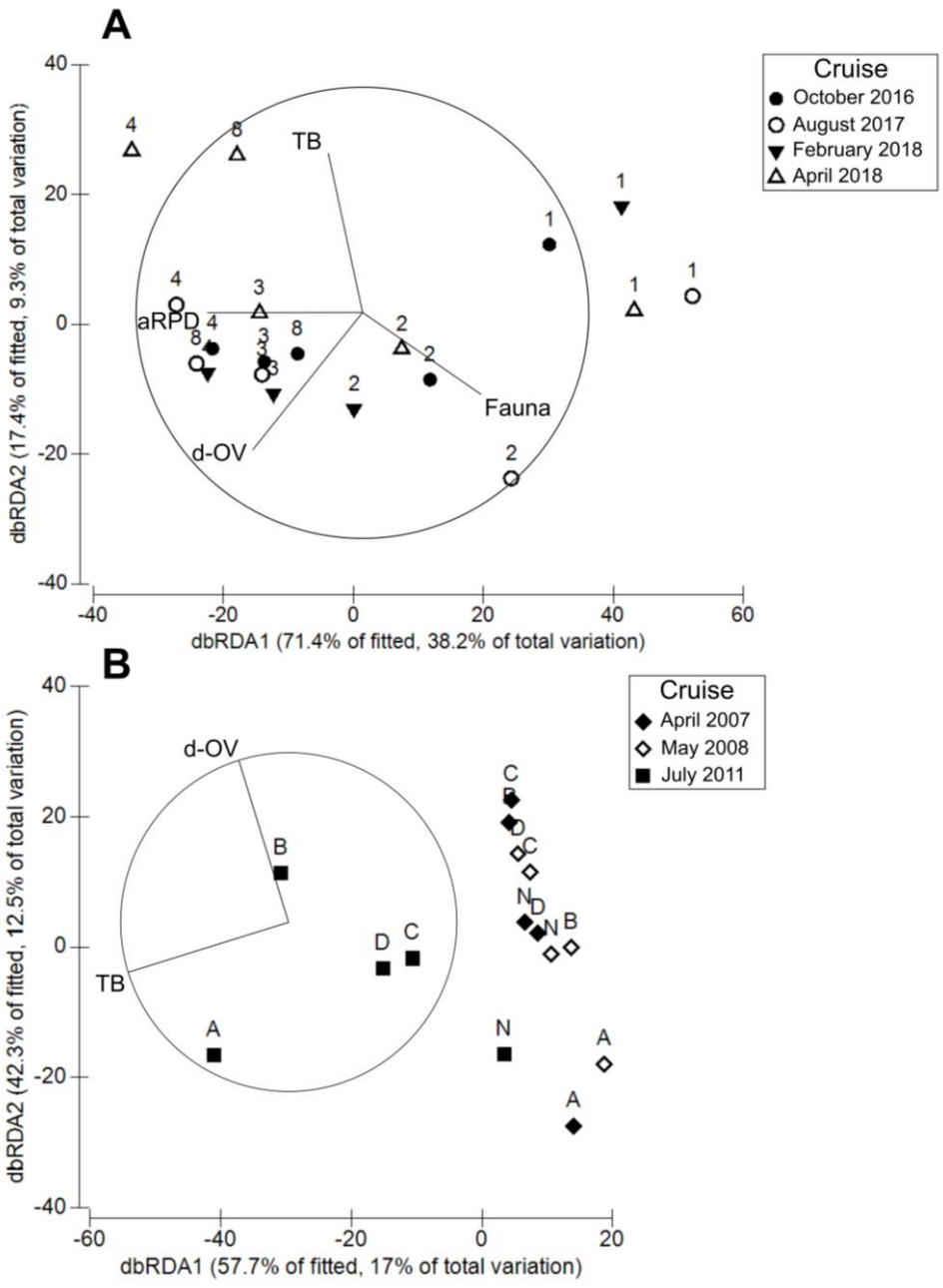

Figure 3.9. Distance-based Redundancy Analysis based on benthic macrofauna compositions and SPI characteristics as explanatory variables for (**A**) the WGMP and (**B**) the RRP. aRPD: apparent Redox Potential Discontinuity thickness; d-OV: mean depth of oxic voids; TB: mean number of tubes per SPI and Fauna: mean summed numbers of infauna and epifauna per SPI.

The model established for the RRP included the mean number of fauna per SPI and the mean depth of oxic voids as independent variables (Figure 3.9B). It explained only 29.5 % of the variance of benthic macrofauna composition. The representation of the model through the first plane of a dbRDA also accounted for 29.5 % of this initial variance. The general spatial pattern of benthic macrofauna composition seemed mainly associated with the mean depth of oxic voids, whereas the temporal changes in benthic macrofauna composition, observed in July 2011, seemed mainly associated with the mean number of tubes per SPI.

4. Discussion

4.1. West Gironde Mud Patch: spatio-temporal changes in SPI characteristics

Before the present study, the only West Gironde Mud Patch (WGMP) Sediment Profile Images (SPI) data had been collected during July 2010 (3 stations, Massé et al. 2016) and June 2018 (32 stations, Lamarque et al. 2021). Our results thus constitute the first comprehensive data set allowing for a sound assessment of spatio-temporal changes in WGMP SPI characteristics. As highlighted by the assessment of spatio-temporal changes in benthic macrofauna composition by Lamarque et al. (in prep.), changes in SPI characteristics clearly show the higher importance of spatial relative to short-term (i.e., during the 2016-2018 time period) temporal changes.

Our results support previous observations relative to the spatial structuration of the WGMP in showing a segmentation between a proximal and a distal area and the occurrence of marked depth gradients, as already observed for both surface sediment and SPI characteristics in June 2018 (Lamarque et al. 2021) and both surface sediment characteristics and benthic macrofauna composition during 4 sampling dates (Lamarque et al. in prep.). However, and as opposed to benthic macrofauna composition, SPI characteristics were unable to differentiate stations 2, 3 and 8/4 despite the significant correlation between SPI characteristics and benthic macrofauna composition matrices. Such an inability of Sediment Profile Imaging to detect slight changes in benthic macrofauna composition has already been reported by O'Reilly et al. (2006) (see section 4.3 for more details). Our results also support previous conclusions relative to the nature of the environmental factors driving the spatial structuration of the WGMP. They indeed reinforce the importance of hydrodynamics (i.e.,

Bottom Shear Stress integrated over a 365 days time period). In this sense they support previous observations achieved on : (1) both SPI and surface sediment characteristics during a one-shot synoptic survey (Lamarque et al. 2021), and, (2) surface sediment characteristics and benthic macrofauna composition based on a similar sampling design as the one used during the present study (Lamarque et al. in prep.).

There were differences in the temporal changes in WGMP benthic macrofauna composition and SPI characteristics as well. Lamarque et al. (in prep.) showed that benthic macrofauna composition presented a short-term (i.e. between 2016 and 2018) superimposed over a long-term (i.e. between 2010 and 2016-2018) temporal dynamics. These authors observed a major shift in benthic macrofauna composition between 2010 and 2016 likely due to an exceptional succession of severe storms during the 2013-2014 winter. During the present study, the only evidences of short-term temporal changes were recorded in spring (i.e., April and June) 2018, during which stations from the distal area (i.e., stations 2 and 3 during April and stations, 8 and 4 during both April and June) differed by: (1) the number and depth of subsurface structures (i.e., aRPD, burrows and oxic voids), and (2) the number of tubes. These changes were best described using either Chlorophyll-*a* concentrations or both Bottom Shear Stress and River Flow integrated over a 100 days period. These 3 parameters are all associated with an infra-annual (seasonal) time scale. This suggests that some observed changes (e.g. burrow and oxic void numbers) may result from the sedimentation of the spring phytoplankton bloom, which increases the availability of fresh/labile organic matter at the sediment-water interface and enhances bioturbation (Gerino et al. 1998). Along the same line, the increase in tube numbers was probably tightly related with the boom of several *Ampelisca* species (including *A. armoricana* and *A. brevicornis*) observed by Lamarque et al. (in prep.) at stations 8 and 4 during April 2018, which could be related to the current knowledge regarding the timing of their reproduction in Atlantic and English Channel waters (Dauvin 1988a b).

Conversely to benthic macrofauna composition (Lamarque et al. in prep.), SPI characteristics did not show any significant long-term temporal change nor cicatrization dynamics. Long-term temporal changes in benthic macrofauna were higher at deep stations, which were considered as representative of the “Seapens and burrowing megafauna in circalittoral fine mud” EUNIS habitat (Lamarque et al. in prep., Bajjouk et al. 2015) and characterized by the presence of deep-burrowing bioturbators such as *Nephrops norvegicus*. Deep-burrowing species tend to be preserved from physical disturbances such as bottom

trawling (Tiano et al. 2020) and storms (Posey et al. 1996). As stated above, the long term shift in WGMP benthic macrofauna composition is currently attributed to the physical disturbance resulting from the repetition of exceptionally strong storms during the 2013/2014 winter (Lamarque et al. in prep.). These events may have had a limited effect on major bioturbation contributors, which would account for the lack of long-term changes in SPI characteristics. Moreover, Lamarque et al. (in prep.) used a Hamon grab to quantitatively collect benthic macrofauna. Overall, benthic grabs are known to undersample deep-burrowing species (Kendall & Widdicombe 1999, Wilson et al. 2009), which may also account for the discrepancy between observed long term temporal changes in benthic macrofauna composition and SPI characteristics. Anyhow, the absence of long-term temporal changes in SPI characteristics as opposed to benthic macrofauna composition certainly accounts for the observed lack of any interannual component in short-term temporal changes, which were considered as indicative of a cicatrization process affecting benthic macrofauna composition by Lamarque et al. (in prep.).

4.2. Comparison between the West Gironde Mud Patch and the Rhône River Prodelta

Lamarque et al. (2021) compared spatial changes in SPI characteristics in the WGMP and the Rhône River Prodelta (RRP) based on one-shot synoptic samplings. These authors highlighted discrepancies between the two systems, with a mean aRPD thickness and a mean total number of biological traces, which tended to be higher in the WGMP. They hypothesized that this resulted from the occurrence of long calm periods allowing for the complete development of mature communities enhancing bioturbation and associated biological activity traces, which were periodically destroyed following major energetic events (Lesueur & Tastet 1994, Lesueur et al. 2002). Along the same line, Bonifácio et al. (2014) showed that changes in the hydrological regime of the Rhône River induces rapid changes in SPI characteristics. The study of their temporal changes is therefore essential to reach a better understanding of the dynamics of bioturbation and of its control by benthic macrofauna composition within the two systems.

Lamarque et al. (in prep.) showed that the magnitude of short-term temporal changes in benthic macrofauna composition within the two systems presented opposite spatial patterns, with higher values in the shallowest part of the RRP, and conversely increasing values

with station depth in the WGMP, which was here again coherent with the difference in the nature of the major controlling processes, namely: (1) the hydrological regime of the Rhône River, and (2) hydrodynamics in the WGMP. Our results show no significant correlation between the magnitude of short-term temporal changes in benthic macrofauna composition and SPI characteristics in either system. As for benthic macrofauna composition, short-term intra-station temporal variability in SPI characteristics was also higher at the two deepest WGMP stations mainly due to the strong increase during April 2018 in: (1) the number of tubes, and (2) the number of subsurface structures. The only discrepancy was related to the low short-term temporal variability in SPI characteristics observed at station 3. This was linked to the species mostly responsible for changes in benthic macrofauna composition, namely: *Amphiura filiformis* at station 3 during August 2017, and (2) *Ampelisca* spp. at the two deepest WGMP stations during April 2018. Conversely, to *A. filiformis*, the tube-dweller *Ampelisca spp.* is indeed producing a biogenic structure, which is included in the assessment of biological traces/activity. Overall, in the WGMP, the distribution of short-term changes in SPI characteristics with depth is thus in full agreement with the one of benthic macrofauna composition, both being mainly controlled by local hydrodynamics and life cycle seasonality (Lamarque et al. in prep.).

There was a good agreement between the magnitudes of short-term temporal changes in benthic macrofauna composition and SPI characteristics in the RRP. In the delta front (station A), largest changes in both benthic macrofauna composition and SPI characteristics were observed in July 2011, which was preceded by an extended period of reduced water flow and characterized by “the establishment of a more mature benthic macrofauna community including both tube-dwelling and deep-burrowing macrofauna” (Bonifácio et al. 2014). Observed changes in benthic macrofauna composition were thus likely responsible for the large number of tubes observed at station A in July 2011 (i.e., 4.0 vs a mean of 0.3 tubes.SPI^{-1} for the other cruises; data not shown above). Bonifácio et al. (2014) suggested that the effect of river floods in the delta front is negative and almost immediate, which could partly account for the relative homogeneity in both benthic macrofauna composition and SPI characteristics observed at station A during the 3 (or 2 in the case of SPI characteristics) other cruises.

In the prodelta (station B) and the distal zone (stations N, C and D) of the RRP, the relationship linking the magnitudes of short-term temporal changes in benthic macrofauna

compositions and SPI characteristics is much more difficult to interpret. In the distal zone, large short-term temporal changes in SPI characteristics were also observed in July 2011 but they did not coincide with strong short-term temporal changes in benthic macrofauna compositions (Lamarque et al. in prep., Bonifácio et al. 2014). Several rationales can be put forward to account for such a discrepancy. First, the creation of subsurface structures, which showed higher numbers in July 2011 within the distal zone (i.e., means of 6.0 vs 2.8 subsurface structures.SPI^{-1} for the other cruises) usually results from the activity of a limited number of equilibrium species, which do not necessarily constitute a dominant component of sampled communities in terms of abundances (Rosenberg & Pearson 1978) and therefore are not the main contributors to changes in benthic macrofauna composition. Moreover, they are not necessarily fully satisfactorily sampled using grabs (see above for the WGMP), which complicates the assessment of the interactions between benthic macrofauna compositions and SPI characteristics in the distal zone. Second, there is a significant time lag between changes in Rhône River flows and in the abundances of equilibrium species in the distal zone, (up to 1-2 years for the polychaete *Sternaspis scutata*; Salen-Picard et al. 2003). The time duration between the May 2008 and July 2011 cruises (i.e., 38 months) indeed exceeded this delay, which may have hampered the observation of the lagged effect of the strong winter 2008 flood on benthic macrofauna composition in the distal zone. Moreover, the discrepancy between the responses of benthic macrofauna composition and SPI characteristics in July 2011 may also result from differences in the durations of the integration of environmental signals, which could be longer for SPI characteristics due to low hydrodynamics.

Overall, the environmental factors controlling the magnitudes of short-term temporal changes in both systems are largely compatible with those involved in the control of temporal changes in benthic macrofauna composition (Lamarque et al. in prep.). In the WGMP, the control of changes in SPI characteristics results from an interplay between the intensity of hydrodynamics and seasonal biological cycles. In the delta front of the RRP, temporal changes in SPI characteristics are tightly related to changes in the hydrological regime of the Rhône River. The strong and almost immediate effect of floods largely induces the quasi-absence of biological traces, whereas conversely low flow periods allow for the emergence of these traces. In the distal zone of the RRP, there is a discrepancy between the magnitudes of short-term temporal changes in benthic macrofauna composition and SPI characteristics. This is nevertheless not incompatible with a similar control by the hydrological regime of the Rhône River given: (1) the low abundances and possible under-representation of major bioturbators,

(2) the complexity of the processes linking changes in river flow and the temporal dynamic of equilibrium species (including main bioturbators), and (3) possible differences in the integration durations of environmental signals by benthic macrofauna compositions and SPI characteristics.

4.3. Sediment Profile Imaging as surrogate of benthic macrofauna

Several studies have simultaneously sampled benthic macrofauna and SPI characteristics to assess the redundancy/complementarity of the two approaches. Results are still controversial, with some studies showing a good agreement (Nilsson & Rosenberg 1997, 2000, Karakassis et al. 2002, Rosenberg et al. 2003a) and others (O'Reilly et al. 2006, Wilson et al. 2009, Labrune et al. 2012) leading to more controversial results depending on: (1) the magnitude of the considered disturbance, (2) sampling designs, and (3) data processing procedures.

O'Reilly et al. (2006) reported that Sediment Profile Imaging does not allow for fully distinguishing the intermediate stages of a secondary succession model along a weak environmental gradient in Galway Bay. They also concluded that this technology can only map the impact of a strong disturbance gradient but is only of limited use for predicting less important changes in benthic macrofauna species composition. Our own results support this conclusion since the multivariate analysis based on SPI characteristics proved much less efficient in differentiating WGMP stations as compared to the one based on benthic macrofauna composition. Moreover, during the present study we reported low determination coefficients between the benthic macrofauna and SPI characteristics measured between 2016 and 2018 in the WGMP and between 2007 and 2011 in the RRP. This discrepancy was further supported by the occurrence of long-term (i.e., 2010-2018) changes in benthic macrofauna composition but not in SPI characteristics within the WGMP.

O'Reilly et al. (2006) partly attributed the discrepancy between benthic macrofauna and SPI to the procedure (including the list of SPI characteristics) used to summarize the information contained in SPI and used a BIOENV procedure (Clarke & Ainsworth 1993) to identify the set of SPI characteristics generating the highest correlation with the benthic macrofauna similarity matrix before coding and combining these variables within a new synthetic index. In the present study, we adopted a similar approach but used more powerful

data analysis procedures (i.e., DISTLM and dbRDA) and applied them simultaneously to two different systems. Our results showed that, even after optimization, the proportions of benthic macrofauna composition variance explained by SPI characteristics remained low both in the WGMP (54%) and the RRP (29.5%). They also showed major differences in SPI characteristics best explaining short-term spatio-temporal changes in benthic macrofauna composition within the two systems. Moreover, and except for aRPD thickness, all these characteristics differed from those identified by O'Reilly et al. (2006) in Galway Bay.

Our overall conclusion is thus that both in the WGMP and in the RRP, Sediment Profile Imaging probably does not constitute a fully suitable surrogate for benthic macrofauna composition. It should probably rather be considered as a complementary source of information on benthic macrofauna activities and their interactions with sediments (Rhoads & Germano 1982). Sediment Profile Imaging allows for example to take into account the vertical distribution of fauna, or the presence of large and deep burrowing species through their effect on sediment structure, whereas these species tend to be undersampled with grabs (Wilson et al. 2009). It also allows to assess parameters indicative of the biogeochemical functioning of benthic habitats, such as aRPD thickness and sulfide chemistry (Wilson & Vopel 2012, Statham et al. 2019, Simone & Grant 2020). Should Sediment Profile Imaging nevertheless be used as a surrogate for benthic macrofauna composition, this would clearly require preliminary surveys aiming at determining the set of SPI characteristics best describing spatio-temporal changes in benthic macrofauna composition within each considered system since this approach is not transposable between systems.

5. Conclusions

The present study was aiming at: (1) quantifying spatio-temporal changes in Sediment Profile Image (SPI) characteristics within the West Gironde Mud Patch (WGMP) and identifying main potential controlling environmental factors, (2) achieving a comparison with the Rhône River Prodelta (RRP), and (3) assessing the potential of Sediment Profile Imaging as a surrogate to the assessment of benthic macrofauna composition.

Results show the existence of a spatial structuration of SPI characteristics relative to depth in the WGMP, which is likely controlled by hydrodynamics. In this sense, they support

the conclusions of previous studies based on; (1) a one-shot synoptic assessment of SPI characteristics (Lamarque et al. 2021), and (2) the assessments of spatio-temporal changes in both surface sediment characteristics and benthic macrofauna composition (Lamarque et al. in prep.). As opposed to benthic macrofauna composition, SPI characteristics in the WGMP do not show any significant long-term (i.e., 2010/2016-2018) temporal changes. They conversely present short-term (seasonal) temporal changes, which are compatible with those in benthic macrofauna composition and mainly associated with the spring phytoplanktonic bloom.

The comparison between the WGMP and the RRP show major differences in the control of temporal changes in SPI characteristics. In the WGMP, the distribution of the magnitude of short-term changes in SPI characteristics with depth is in good agreement with the one of benthic macrofauna composition, both being mainly controlled by local hydrodynamics and life cycle seasonality. In the RRP delta front, there is also a tight agreement between short-term temporal changes in benthic macrofauna composition and SPI characteristics, which are both cued by the strong and rapid effects of changes in the hydrological regimes of the Rhône River. In the distal zone, there is conversely a discrepancy between the magnitudes of short-term temporal changes in benthic macrofauna composition and SPI characteristics, which is partly resulting from the complexity of the processes linking changes in river flow and the temporal dynamics of equilibrium species including main potential bioturbators.

Our results also underlines that the use of Sediment Profile Imagery as a surrogate for benthic macrofauna composition is showing clear limitations by showing the inability of any set of SPI characteristics to fully describe changes in benthic macrofauna composition in both the WGMP and the RRP.

Acknowledgements: This work is part of the PhD thesis of Bastien Lamarque (Bordeaux University). Bastien Lamarque was partly supported by a doctoral grant from the French “Ministère de l’Enseignement Supérieur, de la Recherche et de l’Innovation”. This work was supported by: (1) the JERICO-NEXT project (European Union’s Horizon 2020 Research and Innovation program under grant agreement no. 654410), (2) the VOG project (LEFE-CYBER and EC2CO-PNEC), and (3) the MAGMA project (COTE cluster of Excellence ANR-10-LABX-45). It also benefited from additional fundings allocated by the Conseil Régional Nouvelle-Aquitaine

and the Office Français de la Biodiversité. Operations at sea were funded by the French Oceanographic Fleet. The authors wish to thank the crew of the R/V Côtes de la Manche for their help during field sampling, Christophe Fontanier, Marie Claire Perello, Pascal Lebleu and Hervé Derriennic for their help during sampling and sample analysis.

References

Akaike H (1973) Information theory as an extension of the maximum likelihood principle. In: Proceedings, 2nd International Symposium on Information Theory, Akadémiai. Csaki F, Petrov BN (eds) Budapest, p 267–281

Aller RC (1998) Mobile deltaic and continental shelf muds as suboxic, fluidized bed reactors. Mar Chem 61:143–155.

Anderson M, Gorley RN, Clarke KR (2008) PERMANOVA + for PRIMER user manual.

Anderson MJ (2001) A new method for non-parametric multivariate analysis of variance. Austral Ecol 26:32–46.

Bajjouk T, Guillaumont B, Michez N, Thouin B, Croguennec C, Populus J, Louvel-Glaser J, Gaudillat V, Chevalier C, Tourolle J, Hamon D (2015) Classification EUNIS, Système d'information européen sur la nature : Traduction française des habitats benthiques des Régions Atlantique et Méditerranée. Vol. 2. Habitats subtidaux & complexes d'habitats.

Blair NE, Aller RC (2012) The Fate of Terrestrial Organic Carbon in the Marine Environment. Ann Rev Mar Sci 4:401–423.

Bonifácio P, Bourgeois S, Labrune C, Amouroux JM, Escoubeyrou K, Buscail R, Romero-Ramirez A, Lantoine F, Vétion G, Bichon S, Desmalades M, Rivière B, Deflandre B, Grémare A (2014) Spatiotemporal changes in surface sediment characteristics and benthic macrofauna composition off the Rhône River in relation to its hydrological regime. Estuar Coast Shelf Sci 151:196–209.

Burdige DJ (2005) Burial of terrestrial organic matter in marine sediments: A re-assessment. Global Biogeochem Cycles 19:1–7.

Castaing P, Allen G, Houdart M, Moign Y (1979) Étude par télédétection de la dispersion en mer des eaux estuariennes issues de la Gironde et du Pertuis de Maumusson. Oceanol Acta 2:459–468.

Castaing P, Allen GP (1981) Mechanisms controlling seaward escape of suspended sediment from the Gironde: A macrotidal estuary in France. Mar Geol 40:101–118.

Castaing P, Philipps I, Weber O (1982) Répartition et dispersion des suspensions dans les eaux du plateau continental aquitain. Oceanol Acta 5:85–96.

Cirac P, Berne S, Castaing P, Weber O (2000) Processus de mise en place et d'évolution de la couverture sédimentaire superficielle de la plate-forme nord-aquitaine. Oceanol Acta 23:663–686.

Clarke KR, Ainsworth M (1993) A method of linking multivariate community structure to environmental variables. Mar Ecol Prog Ser 92:205–219.

Clarke KR, Somerfield PJ, Gorley RN (2008) Testing of null hypotheses in exploratory community analyses: similarity profiles and biota-environment linkage. J Exp Mar Bio Ecol 366:56–69.

Clarke KR, Warwick RM (2001) Change in Marine Communities: An Approach to Statistical Analysis and Interpretation, 2nd edition. PRIMER-E, Plymouth.

Constantin S, Doxaran D, Derkacheva A, Novoa S, Lavigne H (2018) Multi-temporal dynamics of suspended particulate matter in a macro-tidal river Plume (the Gironde) as observed by satellite data. Estuar Coast Shelf Sci 202:172–184.

Dauvin JC (1988a) Biologie, dynamique, et production de populations de crustacés amphipodes de la Manche occidentale. 2. Ampelisca brevicornis (Costa). J Exp Mar Bio Ecol 119:213–233.

Dauvin JC (1988b) Life cycle, dynamics, and productivity of Crustacea-Amphipoda from the western English Channel. 4. Ampelisca armoricana Bellan-Santini et Dauvin. J Exp Mar Bio Ecol 123:235–252.

Deflandre B (2016) JERICOBENT-1 cruise, RV Côtes De La Manche.

Deflandre B (2017) JERICOBENT-2 cruise, RV Côtes De La Manche.

Deflandre B (2018a) JERICOBENT-3 cruise, RV Côtes De La Manche.

Deflandre B (2018b) JERICOBENT-4 cruise, RV Côtes De La Manche.

Diaz M, Grasso F, Le Hir P, Sottolichio A, Caillaud M, Thouvenin B (2020) Modeling Mud and Sand Transfers Between a Macrotidal Estuary and the Continental Shelf: Influence of the Sediment Transport Parameterization. J Geophys Res Ocean 125.

Doxaran D, Froidefond JM, Castaing P, Babin M (2009) Dynamics of the turbidity maximum zone in a macrotidal estuary (the Gironde, France): Observations from field and MODIS satellite data. Estuar Coast Shelf Sci 81:321–332.

Dray S, Dufour AB (2007) The Ade4 Package: Implementing the Duality Diagram for Ecologists. J Stat Softw 22:1–20.

Dubosq N, Schmidt S, Walsh JP, Grémare A, Gillet H, Lebleu P, Poirier D, Perello MC, Lamarque B, Deflandre B (2021) A first assessment of organic carbon burial in the West Gironde Mud Patch (Bay of Biscay). Cont Shelf Res 221.

Gadel F, Jouanneau JM, Weber O, Serve L, Comellas L (1997) Traceurs organiques dans les dépôts de la vasière Ouest-Gironde (Golfe de Gascogne). Oceanol Acta 20:687–695.

Gerino M, Aller RC, Lee C, Cochran JK, Aller JY, Green MA, Hirschberg D (1998) Comparison of different tracers and methods used to quantify bioturbation during a spring bloom: 234-thorium, luminophores and chlorophyll a. Estuar Coast Shelf Sci 46:531–547.

Germano JD (1995) SEDIMENT PROFILE IMAGING: A Rapid Seafloor Impact Assessment Tool for Oil Spills. Ministry of supply and services, Canada.

Germano JD, Rhoads DC, Valente RM, Carey DA, Solan M (2011) The use of sediment profile imaging (SPI) for environmental impact assessments and monitoring studies: Lessons learned from the past four decades. Oceanogr Mar Biol An Annu Rev 49:235–297.

Hedges JI, Keil RG (1995) Sedimentary organic matter preservation: an assessment and speculative synthesis. Mar Chem 49:81–115.

Jalón-Rojas I, Sottolichio A, Hanquiez V, Fort A, Schmidt S (2018) To what extent multidecadal changes in morphology and fluvial discharge impact tide in a convergent (turbid) tidal river. J Geophys Res Ocean 123:3241–3258.

Jouanneau JM, Weber O, Latouche C, Vernet JP, Dominik J (1989) Erosion, non-deposition and sedimentary processes through a sedimentological and radioisotopic study of surficial deposits from the 'Ouest-Gironde vasière' (Bay of Biscay). Cont Shelf Res 9:325–342.

Karakassis I, Tsapakis M, Smith CJ, Rumohr H (2002) Fish farming impacts in the Mediterranean studied through sediment profiling imagery. Mar Ecol Prog Ser 227:125–133.

Kendall MA, Widdicombe S (1999) Small scale patterns in the structure of macrofaunal assemblages of shallow soft sediments. J Exp Mar Bio Ecol 237:127–140.

Labrune C, Romero-Ramirez A, Amouroux JM, Duchêne JC, Desmalades M, Escoubeyrou K, Buscail R, Grémare A (2012) Comparison of ecological quality indices based on benthic macrofauna and sediment profile images: A case study along an organic enrichment gradient off the Rhône River. Ecol Indic 12:133–142.

Lamarque B, Deflandre B, Dalto AG, Schmidt S, Romero-Ramirez A, Garabetian F, Dubosq N, Diaz M, Grasso F, Sottolichio A, Bernard G, Gillet H, Cordier MA, Poirier D, Lebleu P, Derriennic H, Danilo M, Tenório MMB, Grémare A (2021) Spatial distributions of surface sedimentary organics and sediment profile image characteristics in a high-energy temperate marine riomar: The west gironde mud patch. J Mar Sci Eng 9:242.

Lamarque B, Deflandre B, Schmidt S, Bernard G, Dubosq N, Diaz M, Lavesque N, Garabetian F, Grasso F, Sottolichio A, Rigaud S, Romero-Ramirez A, Cordier MA, Poirier D, Danilo M, Grémare A (no date) Spatio-temporal dynamics of surface sediments characteristics and benthic macrofauna composition in a temperate high-energy River-dominated Ocean Margin (in prep.).

Lansard B, Rabouille C, Denis L, Grenz C (2009) Benthic remineralization at the land-ocean interface: A case study of the Rhône River (NW Mediterranean Sea). Estuar Coast Shelf Sci 81:544–554.

Lesueur P, Jouanneau JM, Boust D, Tastet JP, Weber O (2001) Sedimentation rates and fluxes in the continental shelf mud fields in the Bay of Biscay (France). Cont Shelf Res 21:1383–1401.

Lesueur P, Tastet J., Weber O, Sinko J. (1991) Modèle faciologique d'un corps sédimentaire pélitique de plate-forme la vasière Ouest-Gironde (France). Oceanol Acta 11:143–153.

Lesueur P, Tastet JP (1994) Facies, internal structures and sequences of modern Gironde-derived muds on the Aquitaine inner shelf, France. Mar Geol 120:267–290.

Lesueur P, Tastet JP (1993) Les Vasières de plate-forme du Golfe de Gascogne (France). Océanographie du Golf Gascogne:181–184.

Lesueur P, Tastet JP, Marambat L (1996) Shelf mud fields formation within historical times: Examples from offshore the Gironde estuary, France. Cont Shelf Res 16:1849–1870.

Lesueur P, Tastet JP, Weber O (2002) Origin and morphosedimentary evolution of fine-grained modern continental shelf deposits: The Gironde mud fields (Bay of Biscay, France). Sedimentology 49:1299–1320.

Lesueur P, Weber O, Marambat L, Tastet J, Jouanneau J, Turon J (1989) Datation d'une vasière de plateforme atlantique au débouché d'un estuaire: la vasière à l'ouest de la Gironde (France) est d'âge historique (VIème siècle à nos jours). Comptes rendus l'Académie des Sci Série 2, Mécanique, Phys Chim Sci l'univers, Sci la Terre 308:935–940.

Levin LA, Boesch DF, Covich A, Dahm C, Erséus C, Ewel KC, Kneib RT, Moldenke A, Palmer MA, Snelgrove P, Strayer D, Weslawski JM (2001) The function of marine critical transition zones and the importance of sediment biodiversity. Ecosystems 4:430–451.

Longère P, Dorel D (1970) Etude des sédiments meubles de la vasière de la Gironde et des régions avoisinantes. Rev des Trav l'Institut des Pêches Marit 34:233–256.

Makra A, Thessalou-Legaki M, Costelloe J, Nicolaidou A, Keegan BF (2001) Mapping the pollution gradient of the Saronikos Gulf Benthos prior to the operation of the Athens sewage treatment plant, Greece. Mar Pollut Bull 42:1417–1419.

Mantel N (1967) The Detection of Disease and a Generalized Regression Approach. Cancer Res 27:209–220.

Massé C, Meisterhans G, Deflandre B, Bachelet G, Bourasseau L, Bichon S, Ciutat A, Jude-Lemeilleur F, Lavesque N, Raymond N, Grémare A, Garabetian F (2016) Bacterial and macrofaunal communities in the sediments of the West Gironde Mud Patch, Bay of Biscay (France). Estuar Coast Shelf Sci 179:189–200.

Masselink G, Castelle B, Scott T, Dodet G, Suanez S, Jackson D, Floc'h F (2016) Extreme wave activity during 2013/2014 winter and morphological impacts along the Atlantic coast of Europe. Geophys Res Lett 43:2135–2143.

McKee BA, Aller RC, Allison MA, Bianchi TS, Kineke GC (2004) Transport and transformation of dissolved and particulate materials on continental margins influenced by major rivers: Benthic boundary layer and seabed processes. Cont Shelf Res 24:899–926.

Mulsow S, Krieger Y, Kennedy R (2006) Sediment profile imaging (SPI) and micro-electrode technologies in impact assessment studies: Example from two fjords in Southern Chile used for fish farming. J Mar Syst 62:152–163.

Nilsson HC, Rosenberg R (1997) Benthic habitat quality assessment of an oxygen stressed fjord by surface and sediment profile images. J Mar Syst 11:249–264.

Nilsson HC, Rosenberg R (2003) Effects on marine sedimentary habitats of experimental trawling analysed by sediment profile imagery. J Exp Mar Bio Ecol 285–286:453–463.

Nilsson HC, Rosenberg R (2000) Succession in marine benthic habitats and fauna. Mar Ecol 197:139–149.

O'Reilly R, Kennedy R, Patterson A, Keegan BF (2006) Ground truthing sediment profile imagery with traditional benthic survey data along an established disturbance gradient. J Mar Syst 62:189–203.

Parra M, Castaing P, Jouanneau JM, Grousset F, Latouche C (1998) Nd-Sr isotopic composition of present-day sediments from the Gironde Estuary, its draining basins and the WestGironde mud patch (SW France). Cont Shelf Res 19:135–150.

Posey M, Lindberg W, Alphin T, Vose F (1996) Influence of storm disturbance on an offshore benthic community. Bull Mar Sci 59:523–529.

R CT (2019) R: a Language and Environment for Statistical Computing.

Rhoads DC, Germano JD (1982) Characterization of Organism-Sediment. 8.

Rhoads DC, Young DK (1970) The influences of deposit feeding benthos on bottom stability and community trophic structure. J Mar Res 28:150–178.

Romero-Ramirez A, Grémare A, Desmalades M, Duchêne JC (2013) Semi-automatic analysis and interpretation of sediment profile images. Environ Model Softw 47:42–54.

Rosenberg R, Grémare A, Amouroux JM, Nilsson HC (2003a) Benthic habitats in the northwest Mediterranean characterised by sedimentary organics, benthic macrofauna and sediment profile images. Estuar Coast Shelf Sci 57:297–311.

Rosenberg R, Nilsson HC, Grémare A, Amouroux JM (2003b) Effects of demersal trawling on marine sedimentary habitats analysed by sediment profile imagery. J Exp Mar Bio Ecol 285–286:465–477.

Rosenberg R, Pearson TH (1978) Macrobenthos succession in relation to organic enrichment and pollution of the marine environment. Oceanogr Mar Biol Annu Rev 16:229–331.

Rumohr H, Schomann H (1992) REMOTS sediment profiles around an exploratory drilling rig in the southern North Sea. Mar Ecol Prog Ser 91:303–311.

Salen-Picard C, Arlhac D, Alliot E (2003) Responses of a Mediterranean soft bottom community to short-term (1993-1996) hydrological changes in the Rhone river. Mar Environ Res 55:409–427.

Schmidt S, Deflandre B (2018) JERICOBENT-5 cruise, RV Côtes De La Manche.

Simone M, Grant J (2020) Visually-based alternatives to sediment environmental monitoring. Mar Pollut Bull 158:111367.

Smith CJ, Rumohr H, Karakassis I, Papadopoulou KN (2003) Analysing the impact of bottom trawls on sedimentary seabeds with sediment profile imagery. J Exp Mar Bio Ecol 285–286:479–496.

Statham PJ, Homoky WB, Parker ER, Klar JK, Silburn B, Poulton SW, Kröger S, Pearce RB, Harris EL (2019) Extending the applications of sediment profile imaging to geochemical interpretations using colour. Cont Shelf Res 185:16–22.

Tiano JC, Reijden KJ Van Der, Flynn SO, Beauchard O, Ree S Van Der, Wees J Van Der, Ysebaert T, Soetaert K (2020) Experimental bottom trawling finds resilience in large-bodied infauna but vulnerability for epifauna and juveniles in the Frisian Front. Mar Environ Res 159:104964.

Weber O, Jouanneau JM, Ruch P, Mirmand M (1991) Grain-size relationship between suspended matter originating in the Gironde estuary and shelf mud-patch deposits. Mar Geol 96:159–165.

Wildish DJ, Hargrave BT, MacLeod C, Crawford C (2003) Detection of organic enrichment near finfish net-pens by sediment profile imaging at SCUBA-accessible depths. J Exp Mar Bio Ecol 285–286:403–413.

Wilson PS, Vopel K (2012) Estimating the in situ distribution of acid volatile sulfides from sediment profile images. Limnol Oceanogr Methods 10:1070–1077.

Wilson SJK, Fredette TJ, Germano JD, Blake JA, Neubert PLA, Carey DA (2009) Plan-view photos, benthic grabs, and sediment-profile images: Using complementary techniques to assess response to seafloor disturbance. Mar Pollut Bull 59:26–37

CHAPITRE 4

Conclusions et perspectives

1. Rappel des objectifs

Pour rappel, les principaux objectifs de ce travail de thèse consistaient à :

1) Décrire et comprendre la structuration de l'écosystème benthique de la Vasière Ouest-Gironde, à travers l'étude des variations spatio-temporelles des caractéristiques des sédiments de surface et de la matière organique particulaire associée, de la composition de la macrofaune benthique et de ses traces d'activité ; ces paramètres ayant été largement négligés durant les précédentes études de cette zone.

2) Identifier les facteurs de contrôle impliqués dans cette structuration, via la mise en relation des variables étudiées entre elles et l'utilisation de forçages naturels (i.e., régime hydrologique de l'estuaire de la Gironde et hydrodynamisme local) ou anthropiques (i.e., chalutage de fond) pour décrire les variations spatio-temporelles observées.

3) Evaluer la transposabilité de la typologie des RiOMar établie par Blair & Aller (2012) pour les zones tempérées, à partir d'une comparaison des systèmes VOG et prodelta du Rhône.

2. Principales conclusions

2.1. Structuration spatiale

2.1.1. Caractéristiques des sédiments de surface

Sur la base de l'analyse: (1) de la granulométrie des sédiments de surface, (2) de la fréquence d'apparition des surfaces d'érosion dans la colonne sédimentaire (Lesueur et al. 1991, 1996, 2002, Lesueur & Tastet 1994), et (3) d'évaluations qualitatives de l'intensité de la bioturbation (Jouanneau et al. 1989, Lesueur & Tastet 1994), les études sédimentologiques

précédemment conduites au sein de la Vasière Ouest-Gironde (VOG) avaient déjà montré l'existence d'une subdivision entre une partie proximale et une partie distale délimitées par un seuil bathymétrique compris entre 40 et 45 m (Lesueur & Tastet 1994, Lesueur et al. 2002). Je me suis personnellement intéressé à l'étude de processus plus récents, ce qui a impliqué l'analyse d'une gamme de paramètres beaucoup plus large (i.e., la caractérisation des contenus organiques des sédiments de surface, la composition de la macrofaune benthique, et l'imagerie de profils sédimentaires pour analyser les traces d'activités biologiques récentes dans la partie supérieure de la colonne sédimentaire). Mes résultats confirment clairement la subdivision de la VOG en une partie proximale et une partie distale et soutiennent la limite de profondeur initialement proposée pour délimiter ces deux parties. Ces deux zones présentent des caractéristiques contrastées, avec une granulométrie des sédiments superficiels plus grossière dans la partie proximale (**Chapitres 1 et 2**) du fait du placage transitoire de sédiments adjacents sableux qui sont remobilisés durant les évènements de haute-énergie (Lesueur et al. 2001, 2002). Les concentrations en Matière Organique Particulaire (MOP) des sédiments de surface y sont plus faibles, en lien avec cette différence granulométrique, mais la MOP y est par contre plus labile (**Chapitres 1 et 2**). Enfin, la partie proximale de la VOG abrite une communauté macrobenthique qui lui est propre (**Chapitre 2**). Cette communauté est caractérisée par des abondances et une richesse spécifique élevée. Elle est principalement composée d'organismes à faible potentiel de bioturbation (**Chapitre 3**).

Des études sédimentologiques anciennes ont montré l'existence de deux gradients de profondeur dans la partie distale de la VOG (Jouanneau et al. 1989, Lesueur et al. 1991, 1996, 2002, Lesueur & Tastet 1994). Le premier est lié à la fréquence d'apparition des surfaces d'érosion et des séquences verticales de granulométrie décroissante qui leur sont associées ; le second aux traces de bioturbation mises en évidence par la radiographie à rayons-X. Ces travaux ont ignoré les processus actuels se déroulant dans la partie supérieure de la colonne sédimentaire. Ces derniers n'ont été ultérieurement que très partiellement abordés par Relexans et al. (1992) puis Massé et al. (2016) à partir d'analyses globales de la MOP des sédiments de surface et de la composition de la (micro-, méio- et macro-) faune benthique. Les résultats ainsi obtenus n'ont néanmoins pas permis de conclure quant à l'existence d'éventuels gradients spatiaux pour ces paramètres en raison d'un effort d'échantillonnage limité à trois stations dont seulement deux en partie distale. Lors de mon travail de thèse, de nombreux résultats ont été acquis lors de la campagne d'échantillonnage synoptique de la VOG (i.e., 32 stations ; **Chapitre 1**), ainsi que lors de l'échantillonnage de cinq stations

localisées le long d'un gradient de profondeur au cours de quatre autres campagnes effectuées durant des conditions de débits de la Gironde et d'hydrodynamisme contrastées (**Chapitres 2 et 3**). Ces résultats m'ont permis de démontrer : (1) l'homogénéité de la composition de la MOP dans l'ensemble de la partie distale, et (2) l'existence de gradients spatiaux nets pour la concentration en MOP, la composition de la macrofaune benthique et les traces d'activités biologiques révélées par l'imagerie de profils sédimentaires. Les processus susceptibles d'expliquer les patrons ainsi observés sont discutés ci-dessous.

Le $\delta^{13}C$ est un marqueur d'origine de la MOP (Gearing et al. 1977, Fontugne & Jouanneau 1987, Gearing 1988, Graham et al. 2001). Au large des grands fleuves, ce traceur montre habituellement des valeurs croissantes depuis la côte vers le large ; ce qui traduit la modification des contributions relatives des sources continentales et marines (Fontugne & Jouanneau 1987, Goñi et al. 1998, Blair et al. 2003, 2004, Gordon & Goñi 2003, Bourgeois et al. 2011, Cathalot et al. 2013). Ceci n'est pas le cas dans la VOG pour laquelle ce rapport ne varie pas significativement avec la profondeur dans les sédiments de surface (**Chapitres 1 et 2**). Les raisons de cet état de fait sont probablement à rechercher dans les modalités du mélange entre les sources de MOP continentales et marines qui alimentent la VOG. Du fait du fort marnage et de l'hydrodynamisme local, un mélange précoce entre la MOP continentale et marine intervient en effet très rapidement dans l'estuaire de la Gironde et à proximité de son embouchure (Fontugne & Jouanneau 1987). Ce mélange, intervenant en amont des processus prenant place dans la VOG elle-même, explique que les sédiments de cette dernière soient alimentés par de la MOP présentant une composition « homogène ».

Une autre spécificité des résultats obtenus lors de mon travail réside dans l'augmentation des concentrations en carbone organique particulaire (COP) le long du gradient de profondeur, ce qui est contradictoire avec la dilution d'apports continentaux massifs généralement observée aux débouchés des (grands) fleuves (Goñi et al. 1998, Alliot et al. 2003, Blair et al. 2003, Gordon & Goñi 2003, Bourgeois et al. 2011). De manière générale, dans les marges continentales sous l'influence des grands fleuves, le mouvement des particules sédimentaires vers le large résulte le plus souvent de cycles de sédimentation/resuspension successifs qui s'accompagnent d'une dégradation de la MOP sédimentée (Gordon et al. 2001, Tesi et al. 2007, Bonifácio et al. 2014) ; phénomène que l'on observe également dans la VOG. A chacun de ces cycles est associé un tri particulaire dont le déterminisme est lié aux caractéristiques physiques des particules qui conditionnent leur sédimentation. Le paramètre le plus souvent invoqué à ce sujet est le rapport surface/volume

qui est inversement proportionnel au rayon équivalent des particules (Mayer 1994a b, Hedges & Keil 1995, Keil et al. 1997, 1998). Dans le cas de la VOG, ce paramètre semble néanmoins largement inopérant du fait de la constance de la taille médiane des grains des sédiments superficiels et de leur surface spécifique pour l'ensemble des stations situées dans la partie distale (**Chapitres 1 et 2**). Cette dernière observation est cohérente avec le fait que la VOG se trouve géographiquement déconnectée de l'estuaire de la Gironde et que les particules qui l'alimentent ont déjà très largement fait l'objet d'un tri conditionné par leur taille. La densité est le deuxième facteur le plus susceptible d'affecter la flottabilité des particules, ce qui m'a amené à formuler l'hypothèse selon laquelle le tri particulaire intervenant dans la parte distale de la VOG serait contrôlé par la densité et non par la taille des particules. Selon cette hypothèse, les particules les moins denses (et potentiellement les plus enrichies en matière organique ; Mayer et al. 1993) seraient peu à peu charriées vers la partie la plus profonde de la VOG, ce qui rendrait compte tout à la fois de l'augmentation de la quantité et de la diminution de la labilité de la MOP sédimentée avec la profondeur dans la partie distale de la VOG.

2.1.2. Macrofaune benthique

Au début de mon travail, les seules données quantitatives relatives à la macrofaune benthique de la VOG avaient été recueillies à trois stations échantillonnées à une seule reprise (Massé et al. 2016). Les données issues de mon travail constituent donc le premier ensemble permettant une réelle évaluation des changements spatio-temporels de la composition de la macrofaune benthique au sein de la VOG (**Chapitre 2**). Mes résultats montrent que (si l'on omet la présence exceptionnelle de nombreux individus d'*Ampelisca spp*. et de *Hyala vitrea* aux stations 8 et 4 en avril 2018) l'abondance du macrobenthos présente une forte tendance décroissante le long du gradient de profondeur. Ce résultat conforte la tendance déjà (qualitativement) observée par Massé et al. (2016). Un tel schéma n'est pas en totale cohérence avec les résultats d'études réalisées dans des marges continentales sous l'influence d'autres fleuves (e.g., l'Amazone, le Changjiang, le Fly, le Spercheios et le Rhône) pour lesquelles des tendances à l'augmentation des abondances de la macrofaune benthique avec la distance à l'embouchure du fleuve ont été le plus souvent observées (Rhoads et al. 1985, Aller & Aller 1986, Alongi et al. 1992, Akoumianaki et al. 2013, Bonifácio et al. 2014). Ces tendances ont été interprétées comme étant conformes au modèle de Rhoads et al. (1985),

selon lequel le degré de maturité des communautés et l'abondance de la macrofaune benthique à proximité immédiate des embouchures des fleuves sont limités par l'instabilité sédimentaire induite par de forts taux de sédimentation.

Globalement, les cinq stations échantillonnées le long du gradient de profondeur présentent des compositions de macrofaune benthique significativement différentes entre elles, à l'exception des stations 8 et 4. Là encore, ce résultat est en bon accord avec les observations préliminaires effectuées en juillet 2010 par Massé et al. (2016) qui montraient des différences de composition de la macrofaune benthique entre les parties proximale (i.e., la station 1) et distale (i.e., les stations 3 et 4). La partie proximale de la VOG est largement dominée par *Amphiura filiformis* et *Kurtiella bidentata*, qui composent avec *Abra alba* une communauté couramment retrouvée dans les fonds sablo-vaseux côtiers exposés aux vagues (Hiscock 1984, Picton et al. 1994). La macrofaune benthique des stations les plus profondes (i.e., 8 et 4) présente quant à elle une équitabilité plus élevée et ne peut pas être associée aussi aisément à un habitat ou une communauté spécifique. Ces stations présentent de fortes intensités de bioturbation (**Chapitres 1 et 3**) et une grande diversité d'espèces de polychètes. De plus, une campagne récemment réalisée a permis de signaler la présence de Pennatulacea (*Cavernularia pusilla* et *Veretillum cynomorium*) et de *Nephrops norvegicus* (G. Bernard, communication personnelle) à ces stations. En ce sens, la macrofaune benthique de la partie profonde de la VOG peut donc probablement être mise en relation avec la communauté A5.361 ("Pennatules et mégafaune fouisseuse des vases fines circalittorales") de la classification EUNIS (Bajjouk et al. 2015). L'installation dans la partie distale de la VOG de cette communauté, que l'on peut qualifier de plus « mature » (selon le modèle de succession de Pearson & Rosenberg 1978), est tout à fait cohérente au regard des conditions d'hydrodynamisme plus faibles qui y règnent, ainsi que de la rareté des évènements tempétueux extrêmes ayant un impact sur la colonne sédimentaire, et donc potentiellement sur la macrofaune benthique (Lesueur & Tastet 1994, Lesueur et al. 2002).

2.1.3. Traces d'activité de la macrofaune benthique et bioturbation

La plupart des caractéristiques des images de profils sédimentaires évaluées durant ce travail de thèse sont fortement corrélées avec la profondeur des stations (**Chapitres 1 et 3**). Plus spécifiquement, les valeurs de cinq d'entre elles augmentent avec la profondeur. Cette tendance est particulièrement marquée pour (1) l'oxydation du sédiment (via l'évolution de

la profondeur de la discontinuité apparente du potentiel red-ox, ou aRPD), (2) le remaniement sédimentaire (notamment via l'évolution du nombre de chambres oxyques), et (3) l'épaisseur de la couche sédimentaire remaniée (via l'évolution de la profondeur maximale de ces mêmes chambres oxyques). Contrairement à la composition de la macrofaune benthique, les caractéristiques des images de profils sédimentaires ne permettent pas de clairement différencier les stations 2, 3 et 8/4, et ce malgré la corrélation significative entre ces mêmes caractéristiques et la composition de la macrofaune. De manière plus générale, l'augmentation apparente des traces d'activité et donc, indirectement, de l'intensité de la bioturbation révélée par l'analyse des caractéristiques des images de profils sédimentaires, apparait largement cohérente avec la présence de communautés macrobenthiques plus matures aux profondeurs les plus fortes (Pearson & Rosenberg 1978, Nilsson & Rosenberg 2000).

2.2. Dynamique temporelle

Si les résultats de mon travail montrent clairement la prédominance des changements spatiaux, les changements temporels sont néanmoins également très significatifs au sein de la VOG. Ils peuvent être subdivisés en une composante « court terme » (i.e., intervenant sur la période 2016-2018) et, pour la composition de la macrofaune benthique, une composante « long terme » (i.e., intervenant entre 2010 et la période 2016-2018).

2.2.1. Caractéristiques des sédiments de surface

Dans la partie proximale de la VOG, les sédiments superficiels présentent une forte variabilité granulométrique selon les campagnes d'échantillonnage conduites entre 2016 et 2018 (**Chapitre 2**). De tels changements sont classiquement attribués à des dépôts (placages) transitoires de sédiments adjacents plus grossiers lors d'événements à haute énergie (Lesueur et al. 2001, 2002). Il est de ce point de vue également important de souligner l'existence d'une forte hétérogénéité spatiale (i.e., inter-stations) de la granulométrie des sédiments superficiels de cette même partie proximale, telle que mise en évidence par l'échantillonnage de sept stations localisées dans cette zone durant l'étude synoptique réalisée dans le cadre de ce travail (**Chapitre 1**). Ceci illustre bien la difficulté d'ordre général à évaluer sans aucune ambiguïté les importances relatives des variabilités spatiales et temporelles à partir de l'échantillonnage conduit lors de la présente étude.

A l'ensemble des stations situées dans la partie distale de la VOG, les sédiments de surface ont présenté des concentrations en pigments chlorophylliens et un rapport Chl-*a*/(Chl-*a*+Phéo-*a*) plus élevés en avril 2018 que lors des trois autres campagnes de la période 2016-2018 (**Chapitre 2**), ce qui traduit un apport de matériel organique végétal plus frais en période printanière. Un schéma similaire avait déjà été rapporté par Relexans et al. (1992) pour deux stations échantillonnées en partie distale de la VOG. Des analyses de profils de fluorescence réalisés dans la colonne d'eau durant la campagne d'avril 2018, ainsi que des données issues d'images satellites (**Chapitre 2**) confirment que la période précédant immédiatement cette campagne s'est caractérisée par de fortes concentrations de l'eau de surface en chlorophylle-*a* (i.e., jusqu'à environ 10 $mg.m^{-3}$) au large de l'embouchure de l'estuaire de la Gironde. Les fortes concentrations en pigments chlorophylliens enregistrées dans le sédiment de surface de la VOG en avril 2018 résultent donc très probablement de la sédimentation d'un bloom phytoplanctonique, qui intervient classiquement en fin d'hiver/début de printemps dans cette zone du Golfe de Gascogne (Herbland et al. 1998, Labry et al. 2002). Ces fortes concentrations ne s'accompagnent pas d'augmentations aussi massives des contenus en COP et en acides aminés totaux (THAA). Cet enrichissement en MOP végétale ne s'observe pas non plus sur le traceur d'origine que constitue le $\delta^{13}C$. Au final, cette fraction végétale fraîche ne représente probablement qu'une faible proportion de la MOP sédimentée. Les caractéristiques des sédiments de surface de la VOG semblent donc suivre une dynamique saisonnière fortement influencée par des processus pélagiques printaniers d'une part, mais également par l'occurrence de houles plus énergétiques en hiver qui impactent la granulométrie du sédiment de surface dans la partie proximale.

2.2.2. Macrofaune benthique

Mes résultats montrent que la composition de la macrofaune benthique présente des variations temporelles significatives dont l'amplitude a tendance à augmenter avec la profondeur (**Chapitre 2**).

La composante « court terme » de ces variations semble correspondre à des variations saisonnières avec des abondances largement supérieures en avril 2018 aux deux stations les plus profondes, du fait d'un nombre très élevé d'amphipodes *Ampelisca spp.*, dont la reproduction dans les eaux de l'Atlantique et de la Manche a classiquement lieu au printemps (Dauvin 1988a b). L'existence de cette contribution saisonnière à la variabilité « court terme »

se trouve par ailleurs confirmée par le fait que : (1) les trajectoires des stations dans l'espace réduit de la nMDS ont tendance à se "rapprocher/fermer" lorsqu'elles sont définies en fonction des jours juliens de l'année, et (2) les changements temporels dans la composition de la macrofaune benthique sont le mieux corrélés avec les débits fluviaux intégrés sur 100 jours, et les concentrations en chlorophylle-*a*.

Mon travail a également permis de mettre en évidence l'existence d'une composante interannuelle dans les changements temporels de la composition de la macrofaune benthique, qui se superpose à la composante saisonnière pendant la période 2016-2018. Cette composante comprend tout d'abord des variations à « long terme » mises en évidence par la comparaison des données de la période 2016-2018 avec celles de juillet 2010 (Massé et al. 2016). Aux trois stations pour lesquelles cette comparaison est possible, les différences de composition entre 2010 et 2016-2018 sont beaucoup plus importantes que les différences observées pendant la période 2016-2018. A ces trois stations, les différences de composition par rapport à juillet 2010 sont maximales en octobre 2016. Ces différences ont ensuite tendance à se réduire au cours de la période 2016-2018 (i.e., sur le « court terme »), ce qui est cohérent avec un processus de cicatrisation (Pearson & Rosenberg 1978) induit par une perturbation qui aurait eu lieu entre juillet 2010 et octobre 2016.

La nature exacte d'une telle perturbation ne peut à ce jour qu'être suspectée. Le rôle majeur attribué à l'hydrodynamisme dans le contrôle des caractéristiques sédimentaires ainsi que des variations spatiales et temporelles à « court terme » de la composition des communautés benthiques de la VOG (voir ci-dessus) suggère néanmoins la possibilité de l'impact d'un événement hydrodynamique majeur. Ceci m'a conduit à proposer l'hypothèse de l'occurrence d'une perturbation majeure résultant de la succession de tempêtes ayant affecté le Golfe de Gascogne durant l'hiver 2013/2014 (i.e., le plus énergétique enregistré sur la période 1948-2015 le long de la côte atlantique française ; Masselink et al. 2016). Au cours de cet hiver exceptionnel, des hauteurs significatives de houle 40 % supérieures et une durée totale de tempête trois fois plus élevées que les moyennes globales de la période 1948-2015 ont été relevées. La perturbation physique induite par la houle pourrait dès lors avoir affecté la macrofaune benthique sur l'ensemble de la VOG. Dans ce contexte, la cicatrisation progressive de la composition de la macrofaune vers son état observé en 2010 pourrait sembler lente (i.e., plus de huit ans). Elle reste néanmoins cohérente avec le fait que cette durée est connue pour augmenter avec l'échelle spatiale impactée et l'intensité de la perturbation subie, et ce jusqu'à atteindre plusieurs années (Zajac et al. 1998, Cárcamo et al.

2017). De plus, l'isolement géographique de la VOG (car celle-ci est entourée de sédiments grossiers et bien séparée des autres patchs vaseux du Golfe de Gascogne) contribue probablement à augmenter la durée de cette cicatrisation, en réduisant le potentiel des populations sources à fournir des organismes susceptibles de (re)coloniser la zone (Probert 1984, Zajac et al. 1998). L'augmentation de la magnitude des variations temporelles à « long terme » de la composition de la macrofaune benthique avec la profondeur peut également sembler contre-intuitive puisque l'intensité de la perturbation physique induite par la houle diminue avec la profondeur. Dans des conditions "normales" (i.e., en dehors des événements extrêmes), les stations peu profondes de la VOG subissent clairement des conditions hydrodynamiques bien plus énergétiques que les stations plus profondes. La fréquence d'occurrence des tempêtes exceptionnelles, ayant un impact sur la colonne sédimentaire et donc potentiellement sur la macrofaune benthique (Rees et al. 1977, Glémarec 1978, Dobbs & Vozarik 1983), diminue de plus avec la profondeur (Lesueur et al. 2002). Il peut donc en résulter un impact moindre et/ou une cicatrisation plus rapide aux stations les moins profondes, les espèces présentes y étant adaptées à des conditions d'hydrodynamisme plus intenses. A l'inverse, il est fort probable que la macrofaune benthique occupant la partie la plus profonde de la VOG soit moins adaptée/résistante/résiliente aux perturbations physiques, ce qui explique à la fois l'impact observé plus important et la cicatrisation plus lente aux stations de la partie distale.

2.2.3. Traces d'activité de la macrofaune benthique

Les seules évidences de changements temporels à « court terme » dans les traces d'activité de la macrofaune (telle que mise en évidence par l'analyse des caractéristiques des images de profils sédimentaires) ont été enregistrées au printemps (i.e., en avril et juin) 2018 durant lequel les stations de la partie distale ont différé des autres dates d'échantillonnage par le nombre et la profondeur des structures de subsurface ainsi que par le nombre de tubes (**Chapitre 3**). Ces changements sont le mieux mis en corrélation avec trois paramètres (i.e., la chlorophylle-*a*, les débits de la Gironde et le cisaillement sur le fond intégrés sur 100 jours) associés à une échelle de temps infra-annuelle (saisonnière). Ceci suggère que certains changements observés (e.g., ceux relatifs aux nombres de terriers et de chambres oxyques) résultent très probablement de la sédimentation du bloom phytoplanctonique printanier qui, en augmentant la disponibilité en matière organique fraîche/labile à l'interface eau-sédiment,

est susceptible de favoriser la bioturbation (Gerino et al. 1998). De la même manière, l'augmentation du nombre de tubes est probablement étroitement liée à l'augmentation printanière des abondances d'amphipodes du genre *Ampelisca* (**Chapitre 2**), dont certaines des espèces présentes (i.e., *A. armoricana* et *A. brevicornis*) sont connues pour construire des tubes.

A la différence de la composition de la macrofaune benthique, les caractéristiques des images de profils sédimentaires n'ont pas montré de changements temporels significatifs à « long terme ». Comme exposé ci-dessus, les changements temporels de la composition de la macrofaune benthique sont plus importants dans les stations profondes, qui sont caractérisées par la présence de forts bioturbateurs vivant profondément enfouis dans le sédiment (e.g., *Nephrops norvegicus, Callianassa subterranea*) et qui ont donc tendance à être mieux préservés des perturbations physiques telles que les tempêtes (Posey et al. 1996). La répétition de tempêtes exceptionnellement fortes durant l'hiver 2013/2014, suspectée d'avoir fortement impacté la composition de la macrofaune (voir ci-dessus), a par conséquent pu exercer un effet plus limité sur les espèces principalement responsables de la bioturbation, ce qui expliquerait cette absence de changements significatifs à « long terme » des caractéristiques des images de profils sédimentaires. De plus, l'utilisation de la benne de Hamon pour l'échantillonnage de la macrofaune s'accompagne probablement d'un sous-échantillonnage des espèces à fort potentiel de bioturbation (Kendall & Widdicombe 1999, Wilson et al. 2009), ce qui peut également contribuer à expliquer la divergence entre les changements temporels à « long terme » observés dans la composition de la macrofaune benthique et ses traces d'activité dans le sédiment.

2.3. Le rôle prépondérant de l'hydrodynamisme

Mon travail a reposé sur l'analyse d'une large gamme de caractéristiques des sédiments superficiels ainsi que de la composition et de l'activité de la macrofaune benthique de la VOG. Ces paramètres ont ensuite été mis en relation avec des forçages environnementaux potentiels de nature, soit naturelle (i.e., débits de la Gironde et cisaillement au fond dû à l'hydrodynamisme), soit anthropique (chalutage de fond).

Les débits liquides de l'estuaire de la Gironde ont été utilisés comme proxy des apports solides de l'estuaire à la VOG. Bien que ce paramètre ne constitue clairement qu'une estimation très indirecte des apports solides, et que ses variations ne comprennent

notamment pas de composante spatiale, cette approche permet néanmoins d'approcher les variations temporelles des apports de la Gironde. Les meilleurs ajustements des modèles de régressions linéaires multiples basés sur les distances (DISTLM) montrent que les débits journaliers intégrés sur une durée de 100 jours expliquent une part significative de la variabilité (majoritairement temporelle) des caractéristiques des sédiments de surface et des images de profils sédimentaires ainsi que de la composition de la macrofaune benthique (**Chapitres 2** et **3**). La pertinence de l'impact indirect des débits liquides (et de l'impact direct des apports particulaires) sur la dynamique temporelle ne peut pas, à ce jour, être affirmée de manière absolument certaine. Néanmoins, les résultats acquis permettent, de par la sélection de la période d'intégration de 100 jours, de confirmer l'existence d'une composante infra-annuelle (assimilée à une composante saisonnière) impliquée dans le contrôle de la dynamique temporelle de la VOG.

La mise en relation des données relatives aux caractéristiques des sédiments de surface et des images de profils sédimentaires avec l'effort de pêche au chalut benthique ne montre par contre pas d'impact évident de cette pression sur les paramètres étudiés (**Chapitre 1**). Bien que la VOG constitue une zone de pêche privilégiée (Lesueur 1992, Mengual et al. 2016, 2019, SIH Ifremer 2017) pour des espèces benthiques comme la langoustine (*Nephrops norvegicus*) et la sole commune (*Solea solea*), l'activité de pêche aux engins trainants semble y être cantonnée à des zones extrêmement localisées. Il convient néanmoins de noter que l'effort de pêche ne peut probablement pas être considéré comme homogène au sein des cellules du maillage utilisé pour sa quantification, ce qui peut avoir contribué à l'absence de détection de corrélations significatives entre celui-ci et les caractéristiques des sédiments de surface et des images de profils sédimentaires, qui sont mesurées sur des échelles spatiales beaucoup plus petites. De possibles différences dans les échelles temporelles associées à l'évaluation de l'effort de pêche (intégré sur un an) et à la cinétique de cicatrisation des habitats benthiques (telle que mise en évidence par les images de profils sédimentaires) sont par ailleurs susceptibles d'avoir eu un effet similaire.

Mes résultats mettent clairement en lumière le rôle prépondérant des conditions hydrodynamiques sur la structuration spatiale et la dynamique temporelle des sédiments superficiels et de la macrofaune benthique de la VOG. Ils confirment l'importance de ce forçage dans la subdivision de la VOG en une partie proximale et une partie distale (**Chapitres 1, 2 et 3**). En ce sens, ils confortent très largement les conclusions issues d'études sédimentologiques plus anciennes (Jouanneau et al. 1989, Lesueur et al. 1991, 1996, 2002,

Lesueur & Tastet 1994). Ils montrent également la présence de gradients de profondeur marqués dans : (1) les caractéristiques des sédiments de surface (**Chapitres 1 et 2**), (2) la composition de la macrofaune benthique (**Chapitre 2**) et (3) de ses traces d'activité (**Chapitres 1 et 3**). Ces gradients sont le mieux mis en corrélation avec l'intensité du cisaillement au fond intégrée sur une année ce qui conforte l'existence d'une structuration spatiale de l'ensemble de la VOG principalement induite par l'hydrodynamisme. Ce forçage impacte d'une part le fonctionnement sédimentaire, via : (1) le contrôle de l'emprise spatiale de la VOG, (2) les apports transitoires de sédiment grossier adjacent dans sa partie proximale, et (3) la restriction de la sédimentation moderne dans sa partie distale. De ce fait, l'hydrodynamisme impacte également la composition, la quantité et la distribution de la matière organique particulaire sédimentée. L'hydrodynamisme contrôle d'autre part la composition des communautés macrobenthiques le long du gradient côte-large, en diminuant l'instabilité sédimentaire générée par la houle avec la profondeur, permettant ainsi l'établissement de communautés matures dans la partie la plus profonde de la VOG ; ce qui s'accompagne d'une augmentation de l'intensité de la bioturbation. La mise en évidence de changements à long terme majeurs couplés à une cinétique attribuée à un processus de cicatrisation sur la période 2016-2018 (**Chapitre 2**) permet enfin de suggérer le rôle majeur des événements hydrodynamiques extrêmes dans le contrôle des changements temporels de la composition de la macrofaune benthique.

2.4. Différences dans les principaux facteurs de structuration de la VOG et du prodelta du Rhône

De manière générale, la VOG et le Prodelta du Rhône (PR) présentent de fortes similitudes dans leur fonctionnement sédimentaire. Tous deux sont alimentés par des particules provenant de grands fleuves. De plus, le transfert de ces particules sédimentées le long du gradient de profondeur est gouverné par des processus de tri associés à la succession de séquences de sédimentation et de remise en suspension.

Une première différence majeure entre ces deux systèmes concerne le régime des marées et l'hydrodynamisme local, qui se traduisent par un mélange beaucoup plus précoce des sources de MOP continentales et marines dans le système estuarien de la Gironde, alors que ce mélange a lieu en grande partie dans le PR lui-même une fois les particules

sédimentées (**Chapitre 1**). Contrairement au PR, la VOG n'est pas directement reliée à l'embouchure de l'estuaire de la Gironde. Par conséquent, les effets de dilution affectent l'ensemble de la VOG, alors qu'ils augmentent clairement avec la distance à l'embouchure (et la profondeur) dans le PR (Tesi et al. 2007, Lansard et al. 2009, Bourgeois et al. 2011, Cathalot et al. 2013).

Une deuxième différence entre les deux systèmes est liée aux évolutions des concentrations en MOP le long du gradient de profondeur, croissantes dans la VOG et décroissantes dans le PR (**Chapitre 1**). La principale hypothèse avancée pour expliquer ces patrons d'évolution inversés est que les processus de tri particulaire qui interviennent dans ces deux systèmes sont régis par des paramètres différents : la taille des particules dans le PR, et leur densité dans la VOG (voir **2.1.1**). De plus, en raison d'un fort hydrodynamisme, les particules fines provenant de l'estuaire de la Gironde ne sédimentent pas dans la partie proximale de la VOG (Lesueur et al. 2001). A l'inverse, une forte sédimentation a lieu à proximité immédiate de l'embouchure du Rhône (Zuo et al. 1991, Miralles et al. 2005).

Les données relatives à la composition de la macrofaune benthique mettent également en évidence l'existence de gradients de profondeur au sein de ces deux systèmes (**Chapitre 2**). Les variations des indices univariés caractérisant la macrofaune diffèrent néanmoins largement entre les deux systèmes avec des abondances décroissantes avec la profondeur dans la VOG contre des valeurs généralement plus élevées à une profondeur intermédiaire dans le PR (hors été 2011). Dans le PR ces observations sont conformes au modèle de Rhoads et al. (1985) selon lequel, dans la partie la plus proche de l'embouchure, la structuration de la communauté benthique est contrôlée par l'instabilité sédimentaire générée par de forts taux de sédimentation résultant d'apports fluviaux massifs. Le patron spatial observé dans la VOG est quant à lui lié à l'hydrodynamisme plus important dans la partie proximale qui empêche l'installation de communautés macrobenthiques matures (caractérisées par des abondances plus faibles) dans cette zone et les cantonne aux parties plus profondes (voir **2.1.2**). Les deux forçages ainsi identifiés sont probablement largement impliqués dans le contrôle des caractéristiques des images de profils sédimentaires. Dans la VOG et le PR, l'épaisseur de l'aRPD, le nombre total de traces biologiques, et l'épaisseur de la couche bioturbée augmentent avec la profondeur (**Chapitre 1**), conformément à l'impact négatif exercé par les perturbations sur la bioturbation (Pearson & Rosenberg 1978, Rhoads et al. 1985). Dans les stations les moins profondes du PR, l'instabilité sédimentaire liée aux taux de sédimentation élevés limite fortement la bioturbation. Dans la partie distale du PR, la stabilité des sédiments

est plus élevée ce qui induit une augmentation des traces d'activité biologique dans la colonne sédimentaire. Comme expliqué précédemment, la forte contrainte de cisaillement au fond dans la partie proximale de la VOG contrôle en grande partie la composition de la macrofaune qui y est dominée par des suspensivores épibenthiques (principalement par le bivalve de petite taille *Kurtiella bidentata* et par l'ophiure *Amphiura filiformis*) qui ne sont pas reconnus comme des organismes à fort potentiel de bioturbation. Le long du gradient de profondeur, l'effet conjoint de l'augmentation de la stabilité sédimentaire et des concentrations en MOP permet le développement de communautés macrobenthiques matures caractérisées par la présence de forts bioturbateurs générant d'importantes traces d'activité dans la colonne sédimentaire (voir **2.1.3**).

L'étude de la variabilité temporelle permet de conforter l'existence de ces deux forçages environnementaux distincts, propres à chacun des deux systèmes. Les changements temporels des caractéristiques des sédiments de surface diffèrent fortement entre les deux systèmes (**Chapitre 2**), avec une variabilité beaucoup plus élevée à proximité immédiate de l'embouchure du Rhône que dans la zone proximale de la VOG. Ceci résulte principalement de la forte sédimentation dans le PR qui a lieu pendant les crues (Cathalot et al. 2010, Bonifácio et al. 2014). Essentiellement en automne et en hiver, une partie de ces dépôts est remaniée, initiant une série de remises en suspension/dépositions qui entraînent le déplacement des particules fines vers le large (Ulses et al. 2008, Marion et al. 2010). Au cours de ce transfert, les composants les plus labiles de la MOP sont dégradés (Bonifácio et al. 2014) ce qui contribue à réduire l'ampleur des changements temporels des caractéristiques des sédiments de surface dans les zones plus profondes du PR. A l'inverse, l'intensité des changements temporels dans les caractéristiques des sédiments superficiels de la VOG ne varie pas avec la profondeur. Ceci traduit un équilibre entre plusieurs processus, à savoir : (1) dans la partie proximale, des changements principalement liés à la granulométrie dus aux placages de sédiment grossier adjacent par les fortes houles, et (2) des concentrations en pigments chlorophylliens particulièrement élevées au printemps dans la partie distale (voir **2.2.1**). L'amplitude des changements temporels de la composition de la macrofaune benthique est également beaucoup plus élevée à proximité immédiate de l'embouchure du Rhône (**Chapitre 2**), en raison de la forte variabilité des taux de sédimentation, élevés lors des crues et faibles pendant les périodes d'étiage. Pendant ces dernières, on assiste ainsi à une « extension » des communautés habituellement présentes plus en profondeur vers l'embouchure (Bonifácio et al. 2014). Là encore, ce schéma est conforme au modèle de Rhoads et al. (1985), qui attribue

un rôle majeur à la sédimentation dans le contrôle de la composition de la macrofaune benthique au sein des RiOMar. Dans la VOG, l'intensité des changements dans la composition de la macrofaune benthique a tendance à être plus faible aux deux stations les moins profondes, ce que l'on peut mettre en relation avec une meilleure résistance/résilience à la fréquence élevée des perturbations induites par l'hydrodynamisme (voir **2.2.2**). Là encore, mes résultats mettent donc en évidence des différences importantes dans les rôles relatifs des apports fluviaux et de l'hydrodynamisme dans le contrôle des changements spatio-temporels dans les deux systèmes.

Comme avancé plus haut, les changements spatio-temporels des caractéristiques des images de profils sédimentaires dans la VOG résultent très probablement d'une interaction entre l'intensité de l'hydrodynamisme et les cycles biologiques saisonniers de certaines espèces (voir **2.2.3**). Dans la partie la moins profonde du PR, les changements temporels dans les traces d'activité biologique sont, comme la composition de la macrofaune benthique, étroitement liés aux changements du régime hydrologique du Rhône (**Chapitre 3**). L'effet, fort et quasi immédiat, des crues induit la quasi-absence de traces d'activité, alors qu'à l'inverse, les périodes d'étiage permettent l'émergence de communautés benthiques matures et donc l'augmentation des traces d'activité associées. Une discordance entre les variations, avec la profondeur, de l'intensité des changements temporels de la composition de la macrofaune benthique et de ses traces d'activité a cependant été observée dans la partie plus profonde du PR. Ce résultat est susceptible d'être expliqué par: (1) les faibles abondances et le possible sous-échantillonnage des principaux bioturbateurs, (2) la complexité des processus liant les changements de débit du fleuve et la dynamique de population des espèces (y compris celles des principaux bioturbateurs), et (3) les différences possibles dans les durées d'intégration des signaux environnementaux par les compositions de la macrofaune benthique et les caractéristiques des images de profils sédimentaires.

De manière générale, l'ensemble des différences entre la VOG et le PR, observées au cours des différents chapitres de ce manuscrit, mettent en évidence le rôle structurant des apports particulaires continentaux dans les RiOMar situées dans des environnements dits à faible énergie comme le PR (type 1), et l'impact prépondérant de l'hydrodynamisme dans celles situées au sein d'environnements plus énergétiques comme la VOG (type 2). En ce sens, la comparaison conduite durant mon travail de thèse conforte la transposabilité, pour la zone tempérée, de la classification des RiOMar précédemment établie sur la base d'environnements majoritairement tropicaux (Blair & Aller 2012).

3. Limites du travail réalisé et perspectives d'amélioration

Mon travail repose sur l'analyse d'une grande quantité de paramètres dont l'échantillonnage a été réalisé lors de campagnes en mer conduites dans une zone réputée particulièrement difficile : le Golfe de Gascogne. En ce sens, je reste tout à la fois : (1) satisfait de l'échantillonnage réalisé (étude spatiale synoptique de 32 stations et échantillonnage à 4 reprises d'un gradient côte-large de 5 stations), et (2) conscient de certaines limites d'interprétation qui résultent de cet échantillonnage. Je discute ci-dessous de certaines des limites du travail réalisé ainsi que des perspectives d'amélioration qui en découlent directement.

3.1. Amélioration de l'échantillonnage de certains paramètres

De manière générale, la mise en corrélation de deux paramètres suppose que tous deux soient suffisamment bien échantillonnés pour bien rendre compte de cette corrélation. Lors de la présente étude, cette hypothèse n'a, très probablement, pas été parfaitement remplie pour les caractéristiques des images de profils sédimentaires et la composition de la macrofaune benthique. Smith et al. (2003) ont par exemple suggéré la prise d'une trentaine d'images de profils sédimentaires (contre seulement une dizaine lors de la présente étude) pour mettre en évidence les effets du chalutage de fond ce qui peut avoir contribué à sous-estimer le rôle de cette activité dans la structuration spatiale de la VOG (**Chapitre 1**). De même, l'utilisation de la benne Hamon (et des bennes de manière plus générale) est connue pour sous-échantillonner certaines espèces vivant en profondeur dans la colonne sédimentaire (Kendall & Widdicombe 1999, Wilson et al. 2009) dont celles à fort potentiel de bioturbation. Cette sous-représentation d'espèces contribuant fortement à la production de traces d'activités biologiques visibles sur les images de profils sédimentaires peut contribuer à expliquer la divergence entre les changements temporels à « long terme » observés dans la composition de la macrofaune benthique et dans l'intensité des traces d'activité biologique (voir **2.2.3** et **Chapitre 3**). Afin de mieux évaluer la biodiversité de la macrofaune benthique dans la VOG et de compléter la caractérisation des communautés, tout en palliant au sous-échantillonnage de certaines espèces, un échantillonnage qualitatif complémentaire utilisant d'autres engins (i.e., drague et chalut à perche) s'avérerait très certainement profitable. Ceci a d'ailleurs récemment (avril et octobre 2021) été réalisé dans la VOG dans le cadre du projet

MAGMA, et a permis l'identification d'espèces jusqu'à présent sous-échantillonnées ou absentes lors de mon propre travail (e.g., *Nephrops norvegicus* (Crustacé), *Goneplax rhomboides* (Crustacé), *Cavernularia pusilla* (Cnidaires), *Veretillum cynomorium* (Cnidaire) *et Aphrodita aculeata* (Polychète)). Dans cette même logique d'amélioration, l'acquisition de séquences d'images de la surface du fond pourrait également apporter des informations complémentaires sur la composition de la (méga)faune ainsi que sur l'intensité de la bioturbation (via par exemple les dénombrements des ouvertures de terriers et/ou des structures de nutrition). Ceci pourrait être réalisé à l'aide d'une plateforme fixe (e.g., dispositif de type Plan View fixé à la structure de l'imageur de profils sédimentaires et permettant d'acquérir des images du fond avant que l'imageur ne s'y pose ; voir Carey et al. 2015, 2019 pour des exemples d'utilisation) ou mobile (e.g., Remotely Operated underwater Vehicle ou ROV).

3.2. Amélioration de l'appréhension des dynamiques temporelles par la mise en place d'un suivi

L'analyse des compositions de la macrofaune benthique a montré l'existence de changements importants entre 2010 et 2016. L'analyse portant sur la période 2016-2018 a par ailleurs montré une tendance à un « retour » vers les compositions observées en 2010 (voir **2.2.2** et **Chapitre 2**). L'ensemble, mis en relation avec une analyse rétrospective des épisodes de tempêtes intervenus durant ces 67 dernières années sur la côte atlantique (Masselink et al. 2016) m'a amené à proposer que ces changements pourraient résulter : (1) d'une perturbation majeure induite par la série de tempêtes exceptionnelles de l'hiver 2013/2014, et (2) d'un processus de cicatrisation toujours en cours. A ce stade, il est clair que cette hypothèse revêt toujours un caractère prospectif d'autant plus important que je ne disposais pas de données relatives à la composition de la macrofaune benthique immédiatement avant et après cette série de tempêtes. Dans une moindre mesure, l'existence du processus de cicatrisation est soutenue par les résultats issus d'une série de seulement 4 campagnes qui se sont déroulées sur plusieurs années durant lesquelles ce processus s'est superposé à une dynamique saisonnière. Afin de conforter l'hypothèse de l'existence de ce processus, il serait par conséquent utile d'instaurer un suivi régulier de la composition de la macrofaune benthique et des principales variables environnementales. Un tel suivi permettrait notamment de confirmer ou d'infirmer la réalité du processus de cicatrisation et

d'augmenter la probabilité de documenter les effets d'un événement hydrodynamique extrême. Là encore cette démarche a déjà débuté dans le cadre du projet MAGMA qui a permis d'échantillonner, pour les mêmes paramètres et à deux reprises, les 5 stations principales étudiées dans le cadre de mon travail. A plus long terme, la mise en place d'un suivi annuel (sur une durée de 6 ans) de la station 3 (z = 56,5 m) est actuellement proposée dans le cadre d'un projet déposé en réponse à l'appel d'offres du PPR « Océan et Climat ».

3.3. Amélioration de l'identification des facteurs de contrôle

3.3.1. Prise en compte des hétérogénéités spatiales

L'une des caractéristiques de mon travail a consisté à considérer un grand nombre de paramètres associés à des compartiments/processus différents. Ces entités ont été appréhendées à différentes échelles spatiales, et pour certaines également temporelles. Ainsi, les intensités de cisaillement ont été dérivées d'un modèle hydrodynamique dont la maille était d'environ 0,5 km^2. Les caractéristiques images de profils sédimentaires ont été évaluées à l'aide d'une dizaine de photographies, soit une couverture d'environ 2 mètres linéaires de sédiment. La composition de la macrofaune benthique a quant à elle été étudiée à l'aide de 3 prélèvement réalisés à la benne Hamon, soit une surface totale de 0,75 m^2. Enfin, les caractéristiques des sédiments superficiels ont été déterminées à partir de l'analyse de 3 carottes sédimentaires de 0,008 m^2 chacune. La mise en corrélation de paramètres associés à des échelles spatiales différentes suppose que le paramètre mesuré à la plus petite échelle spatiale présente les mêmes valeurs sur la plus grande échelle spatiale considérée pour un autre paramètre, et inversement (hypothèse d'homogénéité). Cette hypothèse est de fait implicite dans la quasi-totalité des études d'écologie benthique mettant en corrélation des variables environnementales et biologiques. Il est possible de l'appréhender, pour certains paramètres au moins (e.g., les caractéristiques sédimentaires), à partir de plans d'échantillonnage spécifiques permettant d'évaluer les niveaux de variabilité associés à une gamme d'échelles spatiales emboitées (Mouret et al. 2016). Il serait très certainement intéressant d'envisager une telle démarche pour la VOG afin de mieux cerner, par des approches de ré-échantillonnage aléatoire par exemple, le niveau d'incertitude associé à la détermination des différents facteurs de contrôle ; et ce même si la mise en œuvre d'une telle action dans le Golfe de Gascogne s'avérera très certainement lourde. Il convient par ailleurs de souligner que la prise en compte de la variabilité spatiale à l'échelle associée à chacun des

paramètres considérés permettrait également de mieux cerner la composante temporelle des changements de ce paramètre.

3.3.2. Amélioration de la quantification des apports particulaires de l'estuaire de la Gironde

Les importances relatives des apports particulaires en provenance de la Gironde et des contraintes hydrodynamiques (i.e., cisaillement sur le fond) ont été déterminées à partir de mises en corrélation des variations de ces paramètres avec celles des variations spatiales (**Chapitre 1**) ou spatio-temporelles (**Chapitres 2 et 3**) des caractéristiques sédimentaires, et/ou de la composition de la macrofaune benthique, et/ou des caractéristiques des images de profils sédimentaires. Les valeurs de cisaillement sur le fond ont été dérivées du modèle hydrodynamique MARS3D (Lazure & Dumas 2008) couplé au modèle de vagues WAVE WATCH III® (Roland & Ardhuin 2014), et disposent de composantes spatiales et temporelles explicites. Il était à l'origine prévu que les variations spatio-temporelles des apports en particules issues de la Gironde aux sédiments de surface soient calculées par l'adjonction d'un module hydro-sédimentaire à ce modèle. Si ce modèle couplé a effectivement été développé (Diaz et al. 2020), son état d'avancement s'est avéré insuffisant pour évaluer les variations spatio-temporelles des taux de sédimentation sur le plateau continental et donc sur la VOG. Ces taux ont par conséquent été approchés via les mesures des débits liquides de la Gironde. Ceci présente plusieurs inconvénients dont certains sont majeurs : (1) les débits liquides ne rendent pas forcément bien compte des débits solides, (2) l'export des particules depuis l'estuaire n'est pas seulement fonction des débits liquides mais résulte de leurs interactions avec plusieurs facteurs additionnels tels que le marnage et le régime de marée ainsi que la direction et la force du vent (Castaing & Allen 1981, Doxaran et al. 2009), et (3) les variations des débits liquides ne comportent par nature qu'une dimension temporelle et n'intègrent donc pas de composante spatiale sur la VOG. Pour l'ensemble de ces raisons, l'impact de la sédimentation des particules issues de l'estuaire de la Gironde sur la structuration spatio-temporelle de la VOG a peut-être été sous-estimé dans le cadre de ce travail. Une priorité consiste maintenant à achever la calibration et la validation du modèle hydro-sédimentaire développé par Diaz et al. (2020) de manière à accéder à des évaluations pertinentes des variations spatio-temporelles des taux de sédimentation sur l'ensemble de la VOG ; données qui permettront de s'affranchir de l'utilisation des débits liquides en tant que proxy de l'apport

en particules estuariennes et ainsi d'affiner l'estimation de l'impact de la sédimentation des particules en provenance de la Gironde sur la structuration spatio-temporelle de la VOG.

3.3.3. Confirmation du rôle de la densité dans les processus de tri particulaire

L'origine des gradients spatiaux observés pour les caractéristiques quantitatives et qualitatives de la MOP dans la VOG a été en grande partie attribuée à l'effet de la densité des particules elles-mêmes (voir **2.1.1** et **Chapitre 1**). Cependant durant ce travail de thèse, aucune mesure de densité n'a été effectuée. Afin de confirmer le rôle attribué à ce paramètre, il serait clairement intéressant d'analyser la densité des particules des sédiments superficiels, ainsi que d'évaluer les concentrations en carbone organique de différentes fractions de densité, en mettant par exemple en œuvre l'un des protocoles proposés par Mayer et al. (1993) ou Keil et al. (1998).

4. Autres perspectives d'utilisation des données acquises

Mon travail de thèse ouvre plusieurs possibilités de recherches qui sont principalement liées à l'adoption d'autres angles de traitement de données déjà acquises mais non nécessairement prises en compte au cours des études constitutives de ce manuscrit.

La première de ces perspectives consisterait à améliorer la comparaison entre la VOG et le prodelta du Rhône en prenant en compte les processus biogéochimiques qui ont fait l'objet de plusieurs études dans ce dernier (Lansard et al. 2009, Cathalot et al. 2010, Pastor et al. 2011a b, 2018). Ceci permettrait notamment de compléter avantageusement l'étude de la transposabilité de la classification des RiOMar établie par Blair & Aller (2012) sur la base de processus biogéochimiques mesurés principalement dans des RiOMar tropicaux et subtropicaux. Ce point devait initialement faire partie de mon travail de thèse. Il a été laissé de côté pour des raisons de contraintes temporelles. Les flux d'oxygène (dissous et totaux), et de sels nutritifs ont néanmoins été mesurés lors de l'ensemble des campagnes réalisées dans la VOG depuis 2010. Ces données sont disponibles et il conviendra de les traiter rapidement afin de décrire les variations spatio-temporelles de ces différents flux, ainsi que leurs relations avec : (1) la composition de la macrofaune benthique, (2) la bioturbation, et (3) les différents forçages externes que sont l'hydrodynamisme, les apports de l'estuaire de la Gironde, et le

chalutage. Ce premier travail, auquel je serai partie prenante, sera réalisé en étroite collaboration avec Mr Nicolas Dubosq dont la thèse en cours porte sur le fonctionnement biogéochimique actuel et passé de l'écosystème benthique de la VOG et qui prend en compte les processus de reminéralisation, de recyclage et de stockage du carbone organique et des éléments associés (azote, manganèse, fer, phosphore et soufre).

En continuité directe avec ce premier point, il serait également intéressant d'étendre la comparaison entre la VOG et le prodelta du Rhône à d'autres RiOMar tempérés, afin d'encore mieux conforter la transposabilité de la typologie établie par Blair & Aller (2012). De plus, une méta-analyse similaire pourrait être réalisée sur la base de la structuration spatio-temporelle de la composition de la macrofaune benthique et de son activité dans la colonne sédimentaire, afin de définir des modèles de structuration pour ces deux paramètres selon les forçages structurants propres aux différents types de RiOMar (i.e., les apports particulaires continentaux dans les RiOMar de type 1 et l'impact de l'hydrodynamisme dans les RiOMar de type 2). Ceci permettrait, d'une part, de compléter le modèle déjà établi par Rhoads et al. (1985) pour une perturbation uniquement liée à de forts taux de sédimentation, et ouvre d'autre part la possibilité de mieux prendre en compte l'interaction entre l'hydrodynamisme et les apports continentaux dans des systèmes actuellement considérés comme de type 2 (tels que l'Amazone en zone tropicale).

Une autre perspective pour des recherches futures consiste à exploiter les données relatives à la composition de la macrofaune benthique et aux caractéristiques des images de profils sédimentaires obtenues lors de mon travail aux fins d'évaluation de la qualité écologique des habitats benthiques. Ces données peuvent en effet servir de base aux calculs de nombreux indices biologiques benthiques (Dauvin et al. 2007, Blanchet et al. 2008, Pinto et al. 2009). Un tel travail permettrait notamment de tester la validité d'indices biotiques dérivés de la composition de la macrofaune benthique avec un indice dérivé des caractéristiques de profils sédimentaires à l'instar de ce qui a déjà été réalisé pour le prodelta du Rhône (Labrune et al. 2012). De ce point de vue, la VOG pourrait constituer un bon modèle pour la mise en œuvre de la Directive Cadre Stratégie Milieu Marin dans un système du large. Elle présente en effet deux sous-ensembles contrastés (i.e., ses parties proximale et distale), est soumise à des évènements énergétiques extrêmes à périodicité interannuelle et constitue également en tant que pêcherie une zone d'intérêt socio-économique. L'extension d'une telle approche dans le temps est déjà amorcée avec le projet MAGMA (« The West Gironde Mud Patch: an integrated model for the application of the Marine Strategy Framework Directive to

marine offshore systems ») qui a permis le ré-échantillonnage, à deux reprises (avril et octobre 2021), des 5 stations étudiées entre 2016 et 2018. Je serai personnellement étroitement associé à l'analyse des échantillons ainsi obtenus qui prolongeront la série temporelle ayant servi de base à mon travail de thèse. A plus long terme, la mise en place d'un suivi annuel de la station 3 pour une durée de 6 ans est actuellement proposée dans le cadre du projet « RiOMar » récemment présenté à l'appel d'offres *«* Un océan de solutions *»* du PPR *«* Océan et Climat » (voir **3.2**).

Il convient enfin de souligner que la mise en place d'un suivi de la VOG sur le long terme pourrait également s'avérer pertinente dans un contexte d'analyse de l'impact du changement global. Le cinquième rapport d'évaluation du GIEC (IPCC 2014) conclut en effet que le changement climatique pourrait affecter l'intensité, la fréquence et la durée des événements extrêmes tels que les tempêtes. Pour ce qui concerne plus précisément le Golfe de Gascogne, le nombre de vagues supérieures à 5 m a effectivement tendance à augmenter significativement le long de la côte basque entre 1993 et 2012 (Borja et al. 2013). D'autres travaux montrent au contraire que la hauteur des vagues tend à diminuer au large de Biscarosse, bien que cette tendance ne fasse pas l'objet d'un consensus clair en dessous de 55° de latitude dans l'Atlantique nord, et varie significativement d'une étude à l'autre (Dupuis et al. 2006). De plus, la fréquence et la durée des tempêtes semblent montrer une tendance à la diminution, bien que l'intensité de ces dernières semble à l'inverse augmenter entre 1948 et 2013 (Cid et al. 2016). Il existe au contraire une tendance claire à la diminution des débits liquides de la Gironde entre 1949 et 2014 (Schmidt et al. 2016). Les débits conditionnent la localisation de la zone de turbidité maximale (bouchon vaseux), qui lors des crues est déplacée en aval de l'estuaire, favorisant ainsi l'expulsion de matières en suspension vers le plateau continental (Castaing & Allen 1981, Doxaran et al. 2009). Toute future diminution des débits est par conséquent susceptible d'engendrer un accroissement de la durée de présence du bouchon vaseux dans la zone amont de l'estuaire et donc de diminuer les exports de particules vers la VOG. Mon travail a fortement suggéré le rôle prépondérant de l'hydrodynamisme par rapport au régime hydrologique de l'estuaire de la Gironde. Il s'inscrit dans un contexte hydrodynamique et hydrologique particulier dont on sait qu'il va changer dans les prochaines années. Il serait donc particulièrement intéressant de déterminer si ces futurs changements vont modifier ou non les importances relatives de l'hydrodynamisme du milieu récepteur et des apports particulaires en provenance de la Gironde dans le contrôle de la structuration et de la dynamique spatio-temporelles de la VOG.

Références

Akoumianaki I, Papaspyrou S, Kormas KA, Nicolaidou A (2013) Environmental variation and macrofauna response in a coastal area influenced by land runoff. Estuar Coast Shelf Sci 132:34–44.

Aller JY, Aller RC (1986) General characteristics of benthic faunas on the Amazon inner continental shelf with comparison to the shelf off the Changjiang River, East China Sea. Cont Shelf Res 6:291–310.

Alliot E, Younes WAN, Romano JC, Rebouillon P, Massé H (2003) Biogeochemical impact of a dilution plume (Rhone River) on coastal sediments: Comparison between a surface water survey (1996-2000) and sediment composition. Estuar Coast Shelf Sci 57:357–367.

Alongi DM, Christoffersen P, Tirendi F, Robertson AI (1992) The influence of freshwater and material export on sedimentary facies and benthic processes within the Fly Delta and adjacent Gulf of Papua (Papua New Guinea). Cont Shelf Res 12:287–326.

Bajjouk T, Guillaumont B, Michez N, Thouin B, Croguennec C, Populus J, Louvel-Glaser J, Gaudillat V, Chevalier C, Tourolle J, Hamon D (2015) Classification EUNIS, Système d'information européen sur la nature : Traduction française des habitats benthiques des Régions Atlantique et Méditerranée. Vol. 2. Habitats subtidaux & complexes d'habitats.

Blair NE, Aller RC (2012) The Fate of Terrestrial Organic Carbon in the Marine Environment. Ann Rev Mar Sci 4:401–423.

Blair NE, Leithold EL, Aller RC (2004) From bedrock to burial: the evolution of particulate organic carbon across coupled watershed-continental margin systems. Mar Chem 92:141–156.

Blair NE, Leithold EL, Ford ST, Peeler KA, Holmes JC, Perkey DW (2003) The persistence of memory: The fate of ancient sedimentary organic carbon in a modern sedimentary system. Geochim Cosmochim Acta 67:63–73.

Blanchet H, Lavesque N, Ruellet T, Dauvin JC, Sauriau PG, Desroy N, Desclaux C, Leconte M, Bachelet G, Janson AL, Bessineton C, Duhamel S, Jourde J, Mayot S, Simon S, de Montaudouin X (2008) Use of biotic indices in semi-enclosed coastal ecosystems and transitional waters habitats-Implications for the implementation of the European Water Framework Directive. Ecol Indic 8:360–372.

Bonifácio P, Bourgeois S, Labrune C, Amouroux JM, Escoubeyrou K, Buscail R, Romero-Ramirez A, Lantoine F, Vétion G, Bichon S, Desmalades M, Rivière B, Deflandre B, Grémare A (2014) Spatiotemporal changes in surface sediment characteristics and benthic macrofauna composition off the Rhône River in relation to its hydrological regime. Estuar Coast Shelf Sci 151:196–209.

Borja Á, Fontán A, Muxika I (2013) Interactions between climatic variables and human pressures upon a macroalgae population: Implications for management. Ocean Coast

Manag 76:85–95.

Bourgeois S, Pruski AM, Sun MY, Buscail R, Lantoine F, Kerhervé P, Vétion G, Rivière B, Charles F (2011) Distribution and lability of land-derived organic matter in the surface sediments of the Rhône prodelta and the adjacent shelf (Mediterranean Sea, France): A multi proxy study. Biogeosciences 8:3107–3125.

Cárcamo PJ, Hernández-Miranda E, Veas R, Quiñones RA (2017) Macrofaunal community structure in Bahía Concepción (Chile) before and after the 8.8 Mw Maule mega-earthquake and tsunami. Mar Environ Res 130:233–247.

Carey DA, Doolittle DF, Smith K (2019) Forward scouting: Use of sediment profile imagery in conjunction with multibeam echosounder mapping for offshore wind cable routes and site characterization. Proc Annu Offshore Technol Conf 2019-May.

Carey DA, Hayn M, Germano JD, Little DI, Bullimore B (2015) Marine habitat mapping of the Milford Haven Waterway, Wales, UK: Comparison of facies mapping and EUNIS classification for monitoring sediment habitats in an industrialized estuary. J Sea Res 100:99–119.

Castaing P, Allen GP (1981) Mechanisms controlling seaward escape of suspended sediment from the Gironde: A macrotidal estuary in France. Mar Geol 40:101–118.

Cathalot C, Rabouille C, Pastor L, Deflandre B, Viollier E, Buscail R, Grémare A, Treignier C, Pruski A (2010) Temporal variability of carbon recycling in coastal sediments influenced by rivers: Assessing the impact of flood inputs in the Rhône River prodelta. Biogeosciences 7:1187–1205.

Cathalot C, Rabouille C, Tisnérat-Laborde N, Toussaint F, Kerhervé P, Buscail R, Loftis K, Sun MY, Tronczynski J, Azoury S, Lansard B, Treignier C, Pastor L, Tesi T (2013) The fate of river organic carbon in coastal areas: A study in the Rhône River delta using multiple isotopic (δ13C, δ14C) and organic tracers. Geochim Cosmochim Acta 118:33–55.

Cid A, Menéndez M, Castanedo S, Abascal AJ, Méndez FJ, Medina R (2016) Long-term changes in the frequency, intensity and duration of extreme storm surge events in southern Europe. Clim Dyn 46:1503–1516.

Dauvin JC (1988a) Biologie, dynamique, et production de populations de crustacés amphipodes de la Manche occidentale. 2. Ampelisca brevicornis (Costa). J Exp Mar Bio Ecol 119:213–233.

Dauvin JC (1988b) Life cycle, dynamics, and productivity of Crustacea-Amphipoda from the western English Channel. 4. Ampelisca armoricana Bellan-Santini et Dauvin. J Exp Mar Bio Ecol 123:235–252.

Dauvin JC, Ruellet T, Desroy N, Janson AL (2007) The ecological quality status of the Bay of Seine and the Seine estuary: Use of biotic indices. Mar Pollut Bull 55:241–257.

Diaz M, Grasso F, Le Hir P, Sottolichio A, Caillaud M, Thouvenin B (2020) Modeling Mud and Sand Transfers Between a Macrotidal Estuary and the Continental Shelf: Influence of the

Sediment Transport Parameterization. J Geophys Res Ocean 125.

Dobbs FC, Vozarik JM (1983) Immediate effects of a storm on coastal infauna. Mar Ecol Prog Ser 11:273–279.

Doxaran D, Froidefond JM, Castaing P, Babin M (2009) Dynamics of the turbidity maximum zone in a macrotidal estuary (the Gironde, France): Observations from field and MODIS satellite data. Estuar Coast Shelf Sci 81:321–332.

Dupuis H, Michel D, Sottolichio A (2006) Wave climate evolution in the Bay of Biscay over two decades. J Mar Syst 63:105–114.

Fontugne MR, Jouanneau JM (1987) Modulation of the particulate organic carbon flux to the ocean by a macrotidal estuary: Evidence from measurements of carbon isotopes in organic matter from the Gironde system. Estuar Coast Shelf Sci 24:377–387.

Gearing JN (1988) The Use of Stable Isotope Ratios for Tracing the Nearshore-Offshore Exchange of Organic Matter. In: *Coastal-Offshore Ecosystem Interactions, Volume 22*. Jansson B-O (ed) American Geophysical Union

Gearing P, Plucker FE, Parker PL (1977) Organic carbon stable isotope ratios of continental margin sediments. Mar Chem 5:251–266.

Gerino M, Aller RC, Lee C, Cochran JK, Aller JY, Green MA, Hirschberg D (1998) Comparison of different tracers and methods used to quantify bioturbation during a spring bloom: 234-thorium, luminophores and chlorophyll a. Estuar Coast Shelf Sci 46:531–547.

Glémarec M (1978) Problèmes d'écologie dynamique et de succession en baie de Concarneau. Vie Milieu:1–20.

Goñi MA, Ruttenberg KC, Eglinton TI (1998) A reassessment of the sources and importance of land-derived organic matter in surface sediments from the Gulf of Mexico. Geochim Cosmochim Acta 62:3055–3075.

Gordon ES, Goñi MA (2003) Sources and distribution of terrigenous organic matter delivered by the Atchafalaya River to sediments in the northern Gulf of Mexico. Geochim Cosmochim Acta 67:2359–2375.

Gordon ES, Goñi MA, Roberts QN, Kineke GC, Allison MA (2001) Organic matter distribution and accumulation on the inner Louisiana shelf west of the Atchafalaya River. Cont Shelf Res 21:1691–1721.

Graham MC, Eaves MA, Farmer JG, Dobson J, Fallick AE (2001) A study of carbon and nitrogen stable isotope and elemental ratios as potential indicators of source and fate of organic matter in sediments of the Forth Estuary, Scotland. Estuar Coast Shelf Sci 52:375–380.

Hedges JI, Keil RG (1995) Sedimentary organic matter preservation: an assessment and speculative synthesis. Mar Chem 49:81–115.

Herbland A, Delmas D, Laborde P, Sautour B, Artigas F (1998) Phytoplankton spring bloom of the Gironde plume waters in the Bay of Biscay: Early phosphorus limitation and food-web

consequences. Oceanol Acta 21:279–291.

Hiscock K (1984) Rocky shore surveys of the Isles of Scilly. March 27th to April 1st and July 7th to 15th 1983. Peterbrgh Nat Conserv Counc CSD Rep 509.

IPCC (2014) Climate change 2014: synthesis report. Contribution of Working Groups I, II and III to the fifth assessment report of the Intergovernmental Panel on Climate Change. Core Wrinting Team, Pachauri RK, Meyer LA (eds) IPCC, Geneva, Switzerland.

Jouanneau JM, Weber O, Latouche C, Vernet JP, Dominik J (1989) Erosion, non-deposition and sedimentary processes through a sedimentological and radioisotopic study of surficial deposits from the 'Ouest-Gironde vasière' (Bay of Biscay). Cont Shelf Res 9:325–342.

Keil RG, Tsamakis E, Giddings JC, Hedges JI (1998) Biochemical distributions (amino acids, neutral sugars, and lignin phenols) among size-classes of modern marine sediments from the Washington coast. Geochim Cosmochim Acta 62:1347–1364.

Keil RG, Tsamakis E, Wolf N, Hedges JI, Goñi M (1997) Relationships between organic carbon preservation and mineral surface area in Amazon Fan (Holes 932A and 942A). Proc Ocean Drill Program, 155 Sci Results.

Kendall MA, Widdicombe S (1999) Small scale patterns in the structure of macrofaunal assemblages of shallow soft sediments. J Exp Mar Bio Ecol 237:127–140.

Labrune C, Romero-Ramirez A, Amouroux JM, Duchêne JC, Desmalades M, Escoubeyrou K, Buscail R, Grémare A (2012) Comparison of ecological quality indices based on benthic macrofauna and sediment profile images: A case study along an organic enrichment gradient off the Rhône River. Ecol Indic 12:133–142.

Labry C, Herbland A, Delmas D (2002) The role of phosphorus on planktonic production of the Gironde plume waters in the Bay of Biscay. J Plankton Res 24:97–117.

Lansard B, Rabouille C, Denis L, Grenz C (2009) Benthic remineralization at the land-ocean interface: A case study of the Rhône River (NW Mediterranean Sea). Estuar Coast Shelf Sci 81:544–554.

Lazure P, Dumas F (2008) An external-internal mode coupling for a 3D hydrodynamical model for applications at regional scale (MARS). Adv Water Resour 31:233–250.

Lesueur P (1992) Les vasières de la plate-forme Ouest Gironde (France) : modèle faciologique et archive sédimentaire des flux côtiers.

Lesueur P, Jouanneau JM, Boust D, Tastet JP, Weber O (2001) Sedimentation rates and fluxes in the continental shelf mud fields in the Bay of Biscay (France). Cont Shelf Res 21:1383–1401.

Lesueur P, Tastet J., Weber O, Sinko J. (1991) Modèle faciologique d'un corps sédimentaire pélitique de plate-forme la vasière Ouest-Gironde (France). Oceanol Acta 11:143–153.

Lesueur P, Tastet JP (1994) Facies, internal structures and sequences of modern Gironde-derived muds on the Aquitaine inner shelf, France. Mar Geol 120:267–290.

Lesueur P, Tastet JP, Marambat L (1996) Shelf mud fields formation within historical times: Examples from offshore the Gironde estuary, France. Cont Shelf Res 16:1849–1870.

Lesueur P, Tastet JP, Weber O (2002) Origin and morphosedimentary evolution of fine-grained modern continental shelf deposits: The Gironde mud fields (Bay of Biscay, France). Sedimentology 49:1299–1320.

Marion C, Dufois F, Arnaud M, Vella C (2010) In situ record of sedimentary processes near the Rhône River mouth during winter events (Gulf of Lions, Mediterranean Sea). Cont Shelf Res 30:1095–1107.

Massé C, Meisterhans G, Deflandre B, Bachelet G, Bourasseau L, Bichon S, Ciutat A, Jude-Lemeilleur F, Lavesque N, Raymond N, Grémare A, Garabetian F (2016) Bacterial and macrofaunal communities in the sediments of the West Gironde Mud Patch, Bay of Biscay (France). Estuar Coast Shelf Sci 179:189–200.

Masselink G, Castelle B, Scott T, Dodet G, Suanez S, Jackson D, Floc'h F (2016) Extreme wave activity during 2013/2014 winter and morphological impacts along the Atlantic coast of Europe. Geophys Res Lett 43:2135–2143.

Mayer LM (1994a) Relationships between mineral surfaces and organic carbon concentrations in soils and sediments. Chem Geol 114:347–363.

Mayer LM (1994b) Surface area control of organic carbon accumulation in continental shelf sediments. Geochim Cosmochim Acta 58:1271–1284.

Mayer LM, Jumars PA, Taghon GL, Macko SA, Trumbore S (1993) Low-density particles as potential nitrogenous foods for benthos. J Mar Res 51:373–389.

Mengual B, Cayocca F, Le Hir P, Draye R, Laffargue P, Vincent B, Garlan T (2016) Influence of bottom trawling on sediment resuspension in the 'Grande-Vasière' area (Bay of Biscay, France). Ocean Dyn 66:1181–1207.

Mengual B, Le Hir P, Cayocca F, Garlan T (2019) Bottom trawling contribution to the spatio-temporal variability of sediment fluxes on the continental shelf of the Bay of Biscay (France). Mar Geol 414:77–91.

Miralles J, Radakovitch O, Aloisi JC (2005) 210Pb sedimentation rates from the Northwestern Mediterranean margin. Mar Geol 216:155–167.

Mouret A, Anschutz P, Deflandre B, Deborde J, Canton M, Poirier D, Grémare A, Howa H (2016) Spatial heterogeneity of benthic biogeochemistry in two contrasted marine environments (Arcachon Bay and Bay of Biscay, SW France). Estuar Coast Shelf Sci 179:51–65.

Nilsson HC, Rosenberg R (2000) Succession in marine benthic habitats and fauna. Mar Ecol 197:139–149.

Pastor L, Cathalot C, Deflandre B, Viollier E, Soetaert K, Meysman FJR, Ulses C, Metzger E, Rabouille C (2011a) Modeling biogeochemical processes in sediments from the Rhŏne

River prodelta area (NW Mediterranean Sea). Biogeosciences 8:1351–1366.

Pastor L, Deflandre B, Viollier E, Cathalot C, Metzger E, Rabouille C, Escoubeyrou K, Lloret E, Pruski AM, Vétion G, Desmalades M, Buscail R, Grémare A (2011b) Influence of the organic matter composition on benthic oxygen demand in the Rhône River prodelta (NW Mediterranean Sea). Cont Shelf Res 31:1008–1019.

Pastor L, Rabouille C, Metzger E, Thibault de Chanvalon A, Viollier E, Deflandre B (2018) Transient early diagenetic processes in Rhône prodelta sediments revealed in contrasting flood events. Cont Shelf Res 166:65–76.

Pearson TH, Rosenberg R (1978) Macrobenthos succession in relation to organic enrichment and pollution of the marine environment. Oceanogr Mar Biol Annu Rev 16:229–331.

Picton BE, Emblow CS, Morrow CC, Sides EM, Costello MJ (1994) Marine communities of the Mulroy Bay and Lough Swill area, north-west Ireland, with an assessment of their nature conservation importance. Environ Sci Unit, Trinity Coll (f Surv Report).

Pinto R, Patrício J, Baeta A, Fath BD, Neto JM, Marques JC (2009) Review and evaluation of estuarine biotic indices to assess benthic condition. Ecol Indic 9:1–25.

Posey M, Lindberg W, Alphin T, Vose F (1996) Influence of storm disturbance on an offshore benthic community. Bull Mar Sci 59:523–529.

Probert PK (1984) Disturbance, sediment stability, and trophic structure of soft-bottom communities. J Mar Res 42:893–921.

Rees EIS, Nicholaidou A, Laskaridou P (1977) The Effects of Storms on the Dynamics of Shallow Water Benthic Associations. Biol Benthic Org:465–474.

Relexans JC, Lin RG, Castel J, Etcheber H, Laborde P (1992) Response of biota to sedimentary organic matter quality of the west Gironde mud patch, Bay of Biscay (France). Oceanol Acta 15:639–649.

Rhoads DC, Boesch DF, Zhican T, Fengshan X, Liqiang H, Nilsen KJ (1985) Macrobenthos and sedimentary facies on the Changjiang delta platform and adjacent continental shelf, East China Sea. Cont Shelf Res 4:189–213.

Roland A, Ardhuin F (2014) On the developments of spectral wave models: Numerics and parameterizations for the coastal ocean. Ocean Dyn 64:833–846.

Schmidt S, Etcheber H, Sottolichio A, Castaing P (2016) Le reseau MAGEST: bilan de 10 ans de suivi haute-frequence de la qualite des eaux de l'estuaire de la Gironde. In: *Mesures haute résolution dans l'environnement marin côtier*. Schmitt F, Lefevre A (eds) Presses du CNRS

SIH Ifremer (2017) Activité des navires de pêche -région Nouvelle-Aquitaine. 14.

Smith CJ, Rumohr H, Karakassis I, Papadopoulou KN (2003) Analysing the impact of bottom trawls on sedimentary seabeds with sediment profile imagery. J Exp Mar Bio Ecol 285–286:479–496.

Tesi T, Miserocchi S, Goñi MA, Langone L (2007) Source, transport and fate of terrestrial organic carbon on the western Mediterranean Sea, Gulf of Lions, France. Mar Chem 105:101–117.

Ulses C, Estournel C, Durrieu de Madron X, Palanques A (2008) Suspended sediment transport in the Gulf of Lions (NW Mediterranean): Impact of extreme storms and floods. Cont Shelf Res 28:2048–2070.

Wilson SJK, Fredette TJ, Germano JD, Blake JA, Neubert PLA, Carey DA (2009) Plan-view photos, benthic grabs, and sediment-profile images: Using complementary techniques to assess response to seafloor disturbance. Mar Pollut Bull 59:26–37.

Zajac RN, Whitlatch RB, Thrush SF (1998) Recolonization and succession in soft-sediment infaunal communities: The spatial scale of controlling factors. Hydrobiologia 375–376:227–240.

Zuo Z, Eisma D, Berger GW (1991) Determination of sediment accumulation and mixing rates in the Gulf of Lions, Mediterranean Sea. Oceanol Acta 14:253–262.

Annexes

Annexe 1.

New insights in the biogeographical distributions of two Spionidae (Annelida) from the NE Atlantic and Mediterranean French coasts

Jérôme Jourde[1,5*], Nicolas Lavesque[2,7], Céline Labrune[3,10], Jean-Michel Amouroux[3,12], Paulo Bonifácio[3,11], Suzie Humbert[2,8], Bastien Lamarque[2,9], Pierre-Guy Sauriau[1,6] & Karin Meißner[4,13]

[1]La Rochelle Université, CNRS, UMR 7266 LIENSs, 2 rue Olympe de Gouges 17000 La Rochelle, France

[2]Université de Bordeaux, CNRS, UMR 5805 EPOC, Station Marine d'Arcachon, 2 rue du Professeur Jolyet, 33120 Arcachon, France

[3]Sorbonne Université, CNRS, UMR LECOB 8222, Laboratoire d'Ecogéochimie des Environnements Benthiques, Observatoire Océanologique de Banyuls, Avenue Pierre Fabre, 66650 Banyuls-sur-Mer, France

[4]Senckenberg Forschungsinstitute und Naturmuseen (SFN), Deutsches Zentrum für Marine Biodiversitätsforschung, Biozentrum Grindel, Martin-Luther-King-Platz 3, D-20146 Hamburg, Germany

[5]jjourde@univ-lr.fr

[6]pierre-guy.sauriau@univ-lr.fr

[7]nicolas.lavesque@u-bordeaux.fr

[8]suzie.humbert@u-bordeaux.fr

[9]bastien.lamarque@u-bordeaux.fr

[10]labrune@obs-banyuls.fr

[11]bonif@me.com

[12]phaxas.amouroux@gmail.com

[13]karin.meissner@senckenberg.de

[*]Corresponding author

Article publié en 2020 dans la revue *Zoosymposia*

https://doi.org/10.11646/zoosymposia.19.1.18

Abstract

We report the first occurrences of *Spiophanes afer* Meißner, 2005 and *Prionospio cristaventralis* Delgado-Blas, Díaz- Díaz & Viéitez, 2018 from French marine waters (from the southern part of the Bay of Biscay in NE Atlantic, and the Gulf of Lion in the Mediterranean Sea). Morphological characters of *S. afer* include the presence of an occipital antenna, dorsal ciliated organs extending to chaetigers 13–15, neuropodial hooks from chaetiger 15, ventrolateral intersegmental pouches from chaetigers 14–15, chaetal spreaders of "2+3 type", and conspicuous dark brown pigmentation on parapodia of chaetigers 9–13. *Prionospio cristaventralis* has four pairs of branchiae (1st and 4th pinnate, 2nd and 3rd apinnate), ventral crests from chaetigers 11–12, high dorsal crests on chaetigers 10–11, and very large notopodial prechaetal lamellae on anterior chaetigers. Both records represent northern extensions of their known distributions. However, the presence of *S. afer* on French coasts may have been overlooked for several decades. The validity of the recently proposed *Spiophanes adriaticus* is questioned.

Keywords: polychaetes, *Spiophanes adriaticus*, *Spiophanes afer*, *Prionospio cristaventralis*, Bay of Biscay, Gulf of Lion

Introduction

Spionidae (Annelida: Polychaeta) is a large taxon currently including 38 genera and 590 valid species worldwide (Read & Fauchald 2019). They inhabit both fresh and marine waters with silty, sandy and rocky bottoms, from shallow to deep waters, and from clean to polluted environments (Blake *et al*. 2017, Martinez & Adarraga 2019). In the Bay of Biscay and Mediterranean waters, new species are regularly recorded as progress is made in the systematics and biogeography of Spionidae (Aguirrezabalaga & Ceberio 2005; Meißner 2005; Çinar *et al.* 2015; Lavesque *et al.* 2015; Radashevsky *et al.* 2016; Surugiu 2016; Bogantes *et al.* 2018; Delgado-Blas *et al.* 2018; Delgado-Blas *et al.* 2019; Radashevsky *et al.* 2019).

Among spionids, species of *Spiophanes* and *Prionospio* are regularly found in samples from French coastal marine waters. The genera *Prionospio* Malmgren, 1867 and *Spiophanes* Grube, 1860 comprise 104 and 31 species, respectively, of which nine and five have been reported from French waters (RESOMAR 2019; OBIS 2019): *P. caspersi* Laubier, 1962, *P. cirrifera* Wirén, 1883, *P. dubia* Day, 1961, *P. elhersi* Fauvel, 1928, *P. fallax* Söderström, 1920, *P. multibranchiata* Berkeley, 1927, *P. saldanha* Day, 1961, *P. sexoculata* Augener, 1918, *P. steenstrupi* Malmgren, 1867, and *S. bombyx* (Claparède, 1870), *S. kroyeri* Grube, 1860, *S. duplex* (Chamberlin, 1919), *S. reyssi* Laubier, 1964 and *S. viriosus* Meißner & Hutchings, 2003. However, in recent surveys along the French coast of the Bay of Biscay two additional spionid species hitherto not reported from the French Atlantic were collected: *Prionospio cristaventralis* Delgado-Blas, Díaz-Díaz & Viéitez, 2018 and *Spiophanes afer* Meißner, 2005. *Prionospio cristaventralis* was originally described from the Spanish Atlantic coast of the Bay of Biscay (Delgado-Blas *et al.* 2018), while *S. afer was* described from waters adjacent to the African continent (Mediterranean Sea and South Atlantic Ocean) with the type locality in the Spanish Mediterranean Sea between Cape San Antonio and the Port of Valencia (Meißner, 2005) (Fig. 1). The latter had never been recorded in Atlantic waters further north than on the continental shelf off Aveiro, Portugal (Gil 2011; Ravara & Moreira 2013, Delgado-Blas *et al.* 2019). Furthermore, NE Atlantic reports of *S. afer* are very rare, with records in the 1st and 2nd part of the SEPLAT 7 campaigns in 1981 and 1983 (Gil 2011), and in 1995 and 1996 (Ravara & Moreira 2013). Prior to our study, *S. afer* had also not been reported from the French Mediterranean coast.

In this study we analyse the geographical distributions of both species, and provide complementary morphological information.

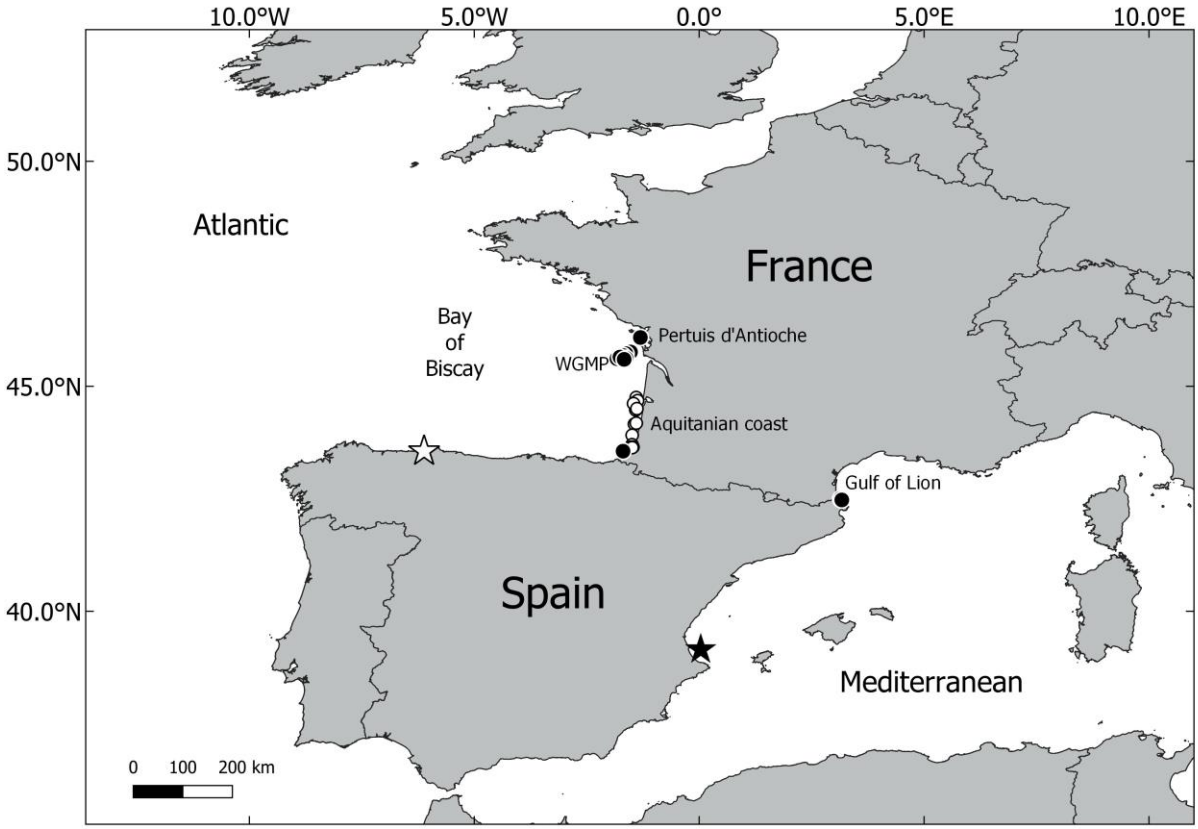

FIGURE 1. *Spiophanes afer* (black dots) and *Prionospio cristaventralis* (white dots) distributions along French coasts (WGMP: West Gironde Mud Patch). Black and white stars indicate the respective type localities.

Material and methods

Samples examined in the course of the present study were collected during several benthic ecology projects. OBIONE is an annual monitoring project implemented since 2011 on a subtidal SOMLIT (*i.e.*, French Coastal Monitoring Network, Liénart *et al.* 2018) station located between Ré and Oléron islands (Pertuis d'Antioche) at 40 m water depth on muddy sands (Fig. 1, Table 1). The JERICO project was implemented from 2016 to 2018 at the West Gironde Mud Patch (WGMP), a 420 km² clay-silt sedimentary area, 25 km off the mouth of the Gironde Estuary in the Bay of Biscay (Deflandre 2016, Massé *et al.* 2016) (Fig. 1). The RT E (French transmission system operator: https://www.rte-france.com/en) is a biosedimentary study carried out in May 2018 on sandy sediments, from 20 to 120 m water depth, along the Aquitanian coast (southern Bay of Biscay). The REDIT, RNMCB and IBIS projects were implemented between 2009 and 2018 in the Gulf of Lion (French Catalan coast, NW Mediterranean).

TABLE 1. Sampling stations from where *Spiophanes afer* (*S.a.*) and *Prionospio cristaventralis* (*P.c.*) were collected. Coordinates are in WGS84. (HMS: Heterogeneous muddy sand).

	Station	Y (N)	X (E)	Species	Years	Abundances	Depth (m)	Sediment
Gulf of Lion	26	42.4987°	3.1465°	*S.a.*	2017	2	31	Sandy Mud
	183	42.5083°	3.1518°	*S.a*	2018	2	40	Sandy Mud
	Em_30	42.4839°	3.1467°	*S.a.*	2017	1	31	HMS
	y30	42.5053°	3.1452°	*S.a.*	2010	1	30	HMS
	z40	42.4738°	3.1699°	*S.a.*	2010	3	40	Sandy Mud
Pertuis d'Antioche	SoMIIt	46.0842°	-1.3083°	*S.a.*	2011-18	5	40	Muddy Sand
WGMP	1	45.7617°	-1.5278°	*S.a.*	2016-18	1	40	Mud
	2	45.7244°	-1.6292°	*S.a.*	2016-18	1	47	Mud
	3	45.6825°	-1.6917°	*S.a.*	2016-18	1	56	Mud
	4	45.6139°	-1.8297°	*S.a.*	2016-18	1	69	Mud
	7	45.6208°	-1.6253°	*S.a.*	2016	1	53	Mud
	8	45.6483°	-1.7633°	*S.a.*	2016-18	1	61	Mud
	9	45.5981°	-1.6689°	*S.a.*	2016	1	55	Mud
Aquitanian coast	P40	43.5572°	-1.6936°	*S.a.*	2018	1	112	Fine Sand
	P07	44.7500°	-1.4014°	*P.c.*	2018	1	35	Medium Sand
	P09	44.6433°	-1.4192°	*P.c.*	2018	5	47	Medium Sand
	P10	44.5981°	-1.4272°	*P.c.*	2018	1	55	Fine Sand
	P12	44.4736°	-1.4103°	*P.c.*	2018	1	51	Coarse Sand
	P13	44.6806°	-1.3708°	*P.c.*	2018	1	35	Medium Sand
	P14	44.6156°	-1.4608°	*P.c.*	2018	3	59	Medium Sand
	P15	44.5033°	-1.3856°	*P.c.*	2018	1	46	Coarse Sand
	P19	44.1597°	-1.4414°	*P.c.*	2018	1	47	Fine Sand
	P21	44.1808°	-1.3994°	*P.c.*	2018	3	39	Fine Sand
	P23	43.9119°	-1.4911°	*P.c.*	2018	1	48	Fine Sand
	P25	43.7014°	-1.4942°	*P.c.*	2018	1	40	Fine Sand
	P29	43.6494°	-1.4733°	*P.c.*	2018	1	19	Fine Sand
	P30	43.6458°	-1.5183°	*P.c.*	2018	1	46	Fine Sand
	P33	43.6369°	-1.4914°	*P.c.*	2018	1	29	Fine Sand

Sampling gear included a Smith-McIntyre grab (Pertuis d'Antioche), a Hamon grab (WGMP and Aquitanian coast), and a van Veen grab (Gulf of Lion), sampling 0.1 m² (Pertuis d'Antioche, Gulf of Lion) or 0.25 m² (WGMP and Aquitanian coast). All samples were washed through a 1 mm-mesh sieve and preserved with a 10% formalin/marine water solution on board. They were subsequently washed again through a 0.5 mm-mesh sieve. Extracted macrofauna was preserved in 70% ethanol. For identification a Leica M205C stereomicroscope equipped with a Leica MC190 HD camera and an Olympus BH2 light microscope wereused. Following Meißner (2005) we define body width in *Spiophanes* as the distance between the distalmost points of both parapodial rami from chaetiger 4 (chaetae and postchaetal lobes disregarded) seen from above. Some specimens were stained with a dark solution of methyl

green in ethanol. Specimens were dipped into the solution for five minutes, allowed to destain in ethanol for a few seconds, then observed in water. Specimens of *P. cristaventralis* used for scanning electron microscopy (SEM) were critical point dried, gold coated, then examined and photographed with a Hitachi TM3030. Part of the studied material is deposited at the Muséum National d'Histoire Naturelle, Paris (MNHN) and the Senckenberg Museum, Frankfurt (SMF).

Results

This study focused on the examination of twenty-two specimens of both *S. afer* and *P. cristaventralis* (Table 1). While, *S. afer* was collected from all localities, *P. cristaventralis* was sampled only in the Aquitanian coast. Further descriptions of both species are provided in the systematic account section. In addition, among the nine *Spiophanes* specimens from the French Mediterranean coast off Banyuls sur-Mer, four sampled in 2010 and previously identified as *Spiophanes viriosus* Meißner & Hutchings, 2003 were re-examined and eventually attributed to *S. afer*.

Systematic account

Spionidae Grube, 1850

***Spiophanes* Grube, 1860**

***Spiophanes afer* Meißner, 2005**
(Fig. 2)

***Type locality*.** Between Cape San Antonio and Port of Valencia, Mediterranean Spanish coast (Fig.1).

Material examined. Non-type material: NE Atlantic Ocean, Bay of Biscay, Pertuis d'Antioche, 40 m, 3 specimens (September 2011, MNHN-IA- PNT 100; 2016, MNHN-IA- PNT 101 and 2018, SMF 28059), West Gironde (WGMP) and Aquitanian coast, 40–69 m, 3 specimens (2016, MNHN-IA- PNT 110; March, MNHNIA- PNT 111; and August 2017, MNHN-IA- PNT 112); Mediterranean Sea, off Banyuls-sur-Mer, 30–40 m, 9 specimens (2010, MNHN-

IA- PNT 106, MNHN-IA- PNT 107, MNHN-IA- PNT 108, MNHN-IA- PNT 109; 2017, MNHN-IA-PNT 102, MNHN-IA- PNT 103, MNHN-IA- PNT 105; and 2018 SMF 28060, MNHN-IAPNT 104).

***Description of material collected in the course of the present study*.** All specimens incomplete, 6.4–30 mm long for 22–60 chaetigers, 0.7–1.2 mm wide. Colour in alcohol pale white (West Gironde and Pertuis d'Antioche) to grey/brown (Banyuls sur Mer), except for dark pigmentation on parapodia of chaetigers 9–13 (Fig. 2A). Prostomium broad anteriorly, bell-shaped, with blunt, short anterolateral projections (Fig. 2A). Palps lost. Occipital antenna present. Up to four eye spots, rarely absent (see remarks). Dorsal ciliated organs as two straight ciliated bands along dorsum, extending usually to chaetigers 13–15 (Fig. 2A; see remarks).

Chaetal spreader of "2+3 type" with undulate glandular opening well developed in chaetigers 5–7 (Fig. 2B); opening of glandular organ absent on chaetiger 8, as lateral vertical slits on chaetigers 9 14. Ventrolateral intersegmental pouches present from chaetigers 14–15, fully developed from chaetigers 15–16. Dorsal ciliated crests distinct from chaetigers 17–19, moderately to well developed.

Neuropodium of chaetiger 1 usually with one stout, crook-like chaeta (see remarks) and numerous simple capillaries; notochaetae much longer than neurochaetae, almost twice as long as those of chaetiger 2 (Fig. 2C). Capillaries on chaetiger 2 twice as long as on chaetigers 3–4. From chaetiger 15, with quadridentate non-hooded neuropodial hooks, initially numbering 6–8 (4–7 in Mediterranean specimens). Bacillary chaetae as thin hirsute bristles with brush-like tip, sometimes exposed on chaetigers 5–7. Ventral sabre chaetae from chaetiger 4.

Pygidium unknown.

Tube. Tube coated with sand (Fig. 2D), sometimes with up to two dark, complex chitinous ring-like structures inside, divided into two parts linked by a transparent membrane, the bigger part nail-shaped with two lateral wings, the second x-shaped (Fig. 2D, E).

Pigmentation. These observations are based on specimens fixed in formalin solution then preserved in 70% ethanol. Dark pigment on chaetigers 9–13 (Fig. 2A, B), most intense anterior to the parapodia and around the opening of the glandular organ, entirely encompassing parapodium on chaetigers 10 11; pigmented area smaller on chaetiger 9 compared to 10–13. Among our specimens, slight variations were observed: in specimens from the Pertuis Charentais, dark pigmentation of chaetigers 9–13 was more intense than in other localities; West Gironde and Aquitanian specimens were almost completely unpigmented (apart from chaetigers 9–13), while those of Pertuis d'Antioche showed variable

patterns of blots of light brown pigment on anterior segments including the peristomium (Fig. 2C).

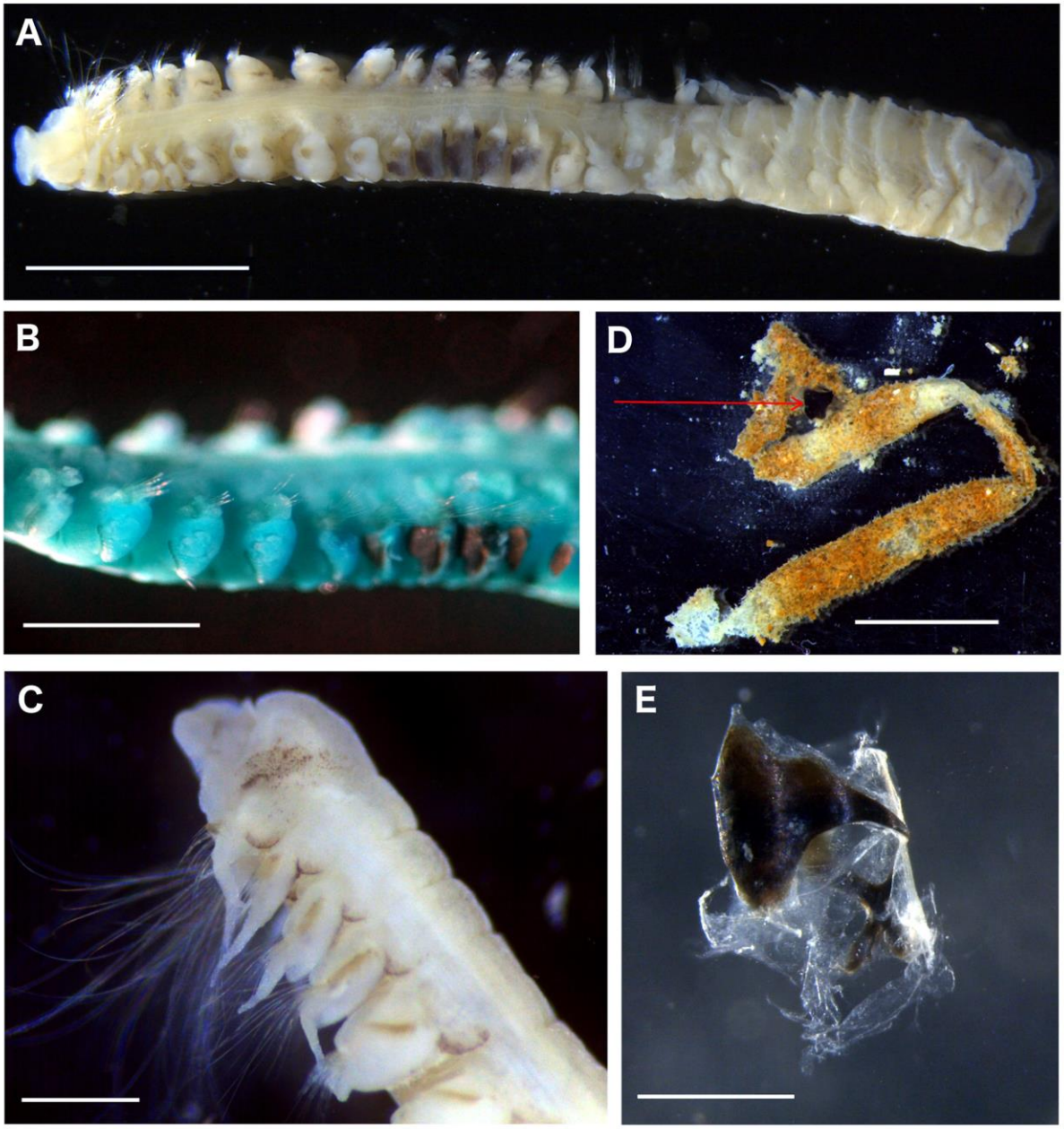

FIGURE 2. *Spiophanes afer*, MNHN-IA-PNT 101 (A, C, D, E), MNHN-IA-PNT 100 (B). A. Anterior fragment, dorsal view, B. Segments 4–13, lateral view, note chaetal spreader of "2+3 type" in chaetigers 5, 6 & 7 and dark brown pigment in chaetigers 9–13; blue colour due to staining with methyl green. C. Anterior region, ventro-lateral view, D. Tube, chitinous ring arrowed, E. Detail of chitinous ring. Scales: A=2 mm, B, E=1 mm, C=500 µm, D=5 mm.

Methyl green staining pattern. No particular pattern.

Remarks. To date, three valid species of *Spiophanes* are known, presenting the following combination of morphological characters: presence of an occipital antenna, glandular organs in chaetigers 5–7 with "2+3" chaetal spreader type, and obvious dark pigment on chaetigers 9–13. These species are *S. afer* from seas around Africa, *S. kimballi* Meißner, 2005 from off California, USA, and *S. viriosus* Meißner & Hutchings, 2003 from

Eastern Australia. The species are easily distinguished by the extension of the dorsal ciliated organs which reach chaetigers 13–15 in *S. afer*, chaetigers 17–18 in *S. viriosus,* and chaetigers 11–13 in *S. kimballi* (Meißner, 2005), this latter exhibiting a distinctive shape. Also, in *S. afer*, ventrolateral intersegmental pouches begin from chaetiger 14 and are first fully developed between chaetigers 15–16. In contrast, they are fully developed from between chaetigers 14–15 in *S. viriosus*, whereas in *S. kimballi* pouches were only observed in reproductive specimens (Meißner, 2005). In addition, to our knowledge, both *S. kimballi* and *S. viriosus* have never been recorded far from their original distribution areas.

Recently a fourth species presenting the same above-mentioned character combination has been described from the Adriatic Sea: *Spiophanes adriaticus* D'Alessandro, Castriota, Maggio, Nasi, Carletti, Auriemma & Romeo 2019 (D'Alessandro *et al.* 2019). However, we are not entirely convinced that *S. adriaticus* is a new species. Based on the type of chaetal spreader ("2+3" with undulate opening in chaetigers 5–7), D'Alessandro *et al*. (2019) acknowledged morphological similarities between *S. adriaticus* and *S. afer* and discussed characters in disagreement between the two species. Accordingly, the first morphological difference is the presence of eyes in adult specimens in *S. adriaticus* whereas they were reported to be only rarely present in juvenile *S. afer* and absent in adult specimens. It has to be considered that the description of *S. adriaticus* is based exclusively on recently collected material preserved in 96% ethanol whereas the description of *S. afer* was undertaken based on material from museum collections collected decades ago and fixed in formalin. Formalin and ethanol preserve pigmentation in a different way, and pigment is well maintained in freshly preserved ethanol material (see *e.g*. figure 13 page 229 in Meißner *et al.* 2014 and page 396 in Meißner & Götting 2015). A second distinctive morphological feature is the length of the dorsal ciliated organs running to about chaetigers 13–15 in *S. afer* and to about chaetigers 11–12 in *S. adriaticus*. However, the illustrations supposedly documenting this in *S. adriaticus* are difficult to interpret and suggest that dorsal ciliated organs could reach chaetiger 13. The third differential character listed by the authors is the shape of parapodia, without detailing the differences. Based on the illustrations provided, such differences are not obvious to us. A fourth distinction is that dorsal ciliated crests are described as usually distinct from chaetigers 18–19 in *S. afer*, and from chaetigers 14–17 in *S. adriaticus*. The crests are usually not well preserved in every specimen and the differentiation between the first presence and their appearance as distinct crest is not clear-cut and might be biased. We do not think that this character is the most reliable but it could of course be an indication of species-level differences. We think the examination of a greater number of specimens from

different locations, differently preserved, collected in different seasons, and belonging to different age classes is required before defining stable differential characters. D'Alessandro *et al.* (2019) presented results of morphological examination of 20 specimens collected at two different locations in the Adriatic Sea, but did not conclusively assess ontogenetic variability of various morphological characters. In any case, we are missing comparative studies of morphologically similar species from the publication by D'Alessandro *et al*. (2019). Also, the deposition of type material in museum collections is compulsory but official registration numbers were not provided by the authors. D'Alessandro *et al*. (2019) also retrieved molecular information from their Adriatic specimens but the publication is missing sequence information (*e.g.* GenBank accession numbers). More importantly, the presented phylogenetic analysis of *Spiophanes* species undertaken by D'Alessandro *et al*. (2019) includes only species distantly related to *S. adriaticus/S. afer* (based on our judgement of their morphology), and hence neither supports nor rejects the hypothesis of *S. adriaticus* being a formerly unknown *Spiophanes* species. Thus, the separation of *S. afer* and *S. adriaticus* is not well resolved yet, and we reject a formal acceptance of this species and urge the authors to provide registration numbers for type material.

All our specimens are in good agreement with the original description of *S. afer* and only the presence of eye spots was observed to vary.

The main variation observed between our specimens consists in differences in the extension of the dorsal ciliary band: Mediterranean individuals have dorsal ciliary bands mainly extending to chaetiger 13 (instead of chaetiger 15 for Pertuis d'Antioche individuals, or intermediate for West Gironde and Aquitania individuals). However, within localities the dorsal ciliary band extension also varied (to chaetigers 9–14 in Banyuls-sur- Mer, to chaetigers 11–14 in West Gironde). Intraindividual variation was also observed on a specimen showing asymmetric bands: one extending to chaetiger 13 and the other to chaetiger 14 (MNHN-IA-PNT 105). Other observed variations were: no eye spot on one specimen (MNHN-IA-PNT 101), three eye spots on two specimens (MNHN-IA-PNT 100 and MNHN-IA-PNT-105), and two crook-like chaetae on chaetiger 1 neuropodium of one specimen (MNHN-IA-PNT 111). Mediterranean individuals are generally darker and initially have 4–7 neuropodial hooks (6–8 in the Atlantic).

As previously noted, the occurrence of eye spots is likely linked to preservation method. The dorsal ciliary band extension and initial number of neuropodial hooks are likely to be linked to the development stage and, consequently, to body size (Meißner 2005). Accordingly, our Mediterranean specimens were smaller, measuring 0.8–1 mm wide vs. 1–1.2

mm wide for the Atlantic specimens. However, these characters vary within and among our populations.

The dark chitinous rings found in the tubes of Atlantic specimens have also been reported by D'Alessandro *et al.* (2019). Following these authors, they could have a support function.

Habitat. From intertidal to depths up to 60 m (Meißner, 2005). Between 40 and 112 m, usually in muddy sediments, sometimes on fine sand (*e.g.*, on the Aquitanian coast, this study).

Distribution. Mediterranean Sea: off Spain, off Israel, off France (this study); South Atlantic Ocean: off Namibia; North Atlantic Ocean: Bay of Biscay (this study); Indian Ocean: off South Africa;

Prionospio* Malmgren, 1867 *sensu stricto

***Prionospio cristaventralis* Delgado-Blas, Díaz-Díaz & Viéitez, 2018**
(Fig. 3, 4)

Type locality. Between Cabo Vidio and Cabo de Peñas, Asturias, Spain (Fig. 1).

Material examined. Non-type material: Atlantic, Bay of Biscay, station P21, 39 m, 3 specimens (May 2018, MNHN-IA- PNT 113); Atlantic, Bay of Biscay, station P14, 59 m, 3 specimens (May 2018, MNHNIA- PNT 114), mounted for SEM; SMF 25 327, Atlantic, Bay of Biscay, station P09, 47 m, 5 specimens (May 2018).

Description. Complete specimen, 22.6 mm long (about 65 chaetigers), 0.9 mm wide. Pale white in alcohol (Fig. 3A). Prostomium bottle-shaped, broadly rounded (Fig. 3A, D), dorsoventrally flattened on anterior margin (Fig. 4A, C); long, narrow caruncle extending to end of chaetiger 2, sinusoidal at posterior end (Fig. 3D); nuchal organs U-shaped. Two pairs of black subdermal eyes in trapezoidal arrangement; those of anterior pair small round, those on posterior pair large crescent shaped (Fig. 3A).

Four pairs of long branchiae on chaetigers 2–5 (Figs 3A, C, D; 4A, B), first pair slightly longer than fourth, both with long, slender, dense digitiform pinnules on posterior stem faces and very long, naked, smooth distally pointed tips. Pairs 2 and 3 apinnate, shorter than pinnate pairs, but slightly longer than notopodial lamellae.

Notopodial postchaetal lamellae joining dorsally forming dorsal crests (Fig. 4B) from chaetigers 9 to 19, highest on chaetigers 10–11.

Anterior neuropodial prechaetal lamellae connected through poor-developed ventral crests from chaetigers 9 to 14, forming central U-shaped short depressions (Fig. 4D); subsequent chaetigers without ventral crests.

Neuropodial sabre chaetae from chaetiger 10, one per fascicle, stout, distinctly curved, basally smooth, heavily granulated medially and distally, with sheaths. Neuropodial hooded hooks from chaetiger 15, up to 10 per fascicle. Hooks with five pairs of small teeth above large main tooth, and short, small secondary hoods (Fig. 4E).

Pygidium with two short bulbous cirri (Figs. 3B, 4F).

Methyl green staining pattern. Peristomium and posterior dorsal part of prostomium deeply stained, as notopodial lamellae of chaetigers 1–5 and neuropodial lamellae of chaetiger 1, anterior part of caruncle and posterior part of prostomium pigmented (Fig. 3C, D).

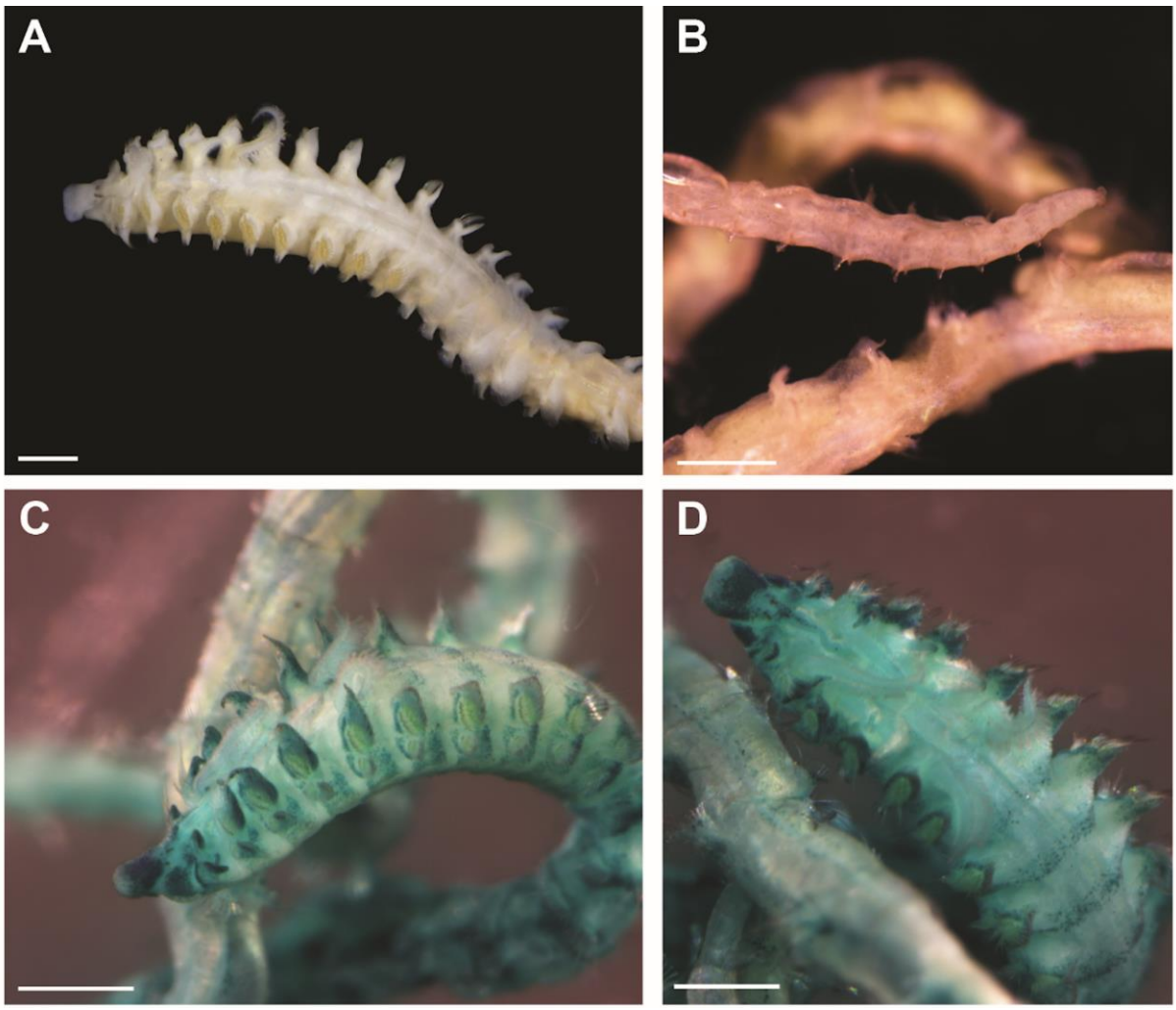

FIGURE 3. *Prionospio cristaventralis*, MNHN-IA-PNT-113. A. Anterior part; B. Pygidium; C. Anterior part, lateral view (Methyl green staining applied); D. Anterior part, dorsal view (Methyl green staining applied). Scales A–D=0.5 mm.

***Remarks*.** The specimens of *P. cristaventalis* from French coast mostly fit in the type description but present a few variations: neuropodial postchaetal lamellae on chaetiger 1 slightly larger than notopodial one (much larger in Spanish specimens), notopodial postchaetal lamellae with pointed tips on chaetigers on chaetigers 2–5 (2–3 in Spanish specimens), dorsal crest begins on chaetiger 9 (10 in Spanish specimens), ventral crest poorly developed (well-developed in Spanish specimens), and sheath on sabre chaetae (absent in Spanish specimens).

***Habitat*.** Shallow waters from 24 to 34 m (Delgado-Blas et al., 2018), in fine to coarse sand from 20 to 60 m (this study).

***Distribution*.** Atlantic Ocean. Cantabrian Sea, Asturias, Spain (Delgado-Blas et al., 2018), Aquitanian coast, Bay of Biscay, France (this study, Fig. 1).

Discussion

Prionospio cristaventralis was recently described from museum specimens collected in the South Bay of Biscay in 1998 (Delgado-Blas *et al*. 2018) and there is no other information on its geographic distribution to date. These specimens were initially identified as *P. fallax* Söderström*, 1920* or *P. caspersi* Laubier, 1962 (Delgado- Blas *et al.* 2018). Accordingly, specimens of these two species from South Western Europe, especially in the Bay of Biscay, should be re-examined and specimens collected *de novo* will require careful identifications. The Spanish type locality and the Aquitanian coast are quite close to each other, but the benthic communities of the latter area are still poorly known. However, the seasonal fluctuations in water circulation south to the Bay of Biscay, with eastward drift in autumn/winter and westward drift in spring/summer (Charria *et al*. 2013) may lead to connectivity between northern Spanish and southwestern French coasts, suggesting that the species may be naturally present on the Aquitanian coast.

Spiophanes afer was described from its type locality in the Mediterranean Sea near Valencia, but additional records from various localities around the African continent outlined a rather large distribution range (*e.g.* off Israel, Mozambique, South Africa, Namibia, and Angola) (Meißner 2005; Gil 2011; Moritz 2012). In the Mediterranean the species was reported from the Spanish coast (Meißner 2005; same records confirmed by Delgado-Blas *et al*. 2019), the Adriatic Sea (Mikac 2015), the Aegean Sea off Turkey (Dagli *et al*. 2011; Çinar *et al.* 2014), and Israel (Meißner 2005). Some specimens in our local collection (initially

misidentified as *S. viriosus*) were collected off Banyuls-sur Mer in 2010, and thus represent the first confirmed occurrence of *S. afer* on the French Mediterranean coast. The northern-most records in the Atlantic came from Portugal, off Sines (1980s, Gil 2011) and from off Aveiro (1995–1996, Ravara & Moreira 2013). Considering this, our recent sample of *S. afer* from Pertuis d'Antioche makes it the northern-most record from the NE Atlantic. Moreover, its arrival in the area seems recent since the only *Spiophanes* species known from there to date was *S. bombyx* (de Montaudouin & Sauriau 2000). This latter species has a very different morphology and is unlikely to be confused with *S. afer*.

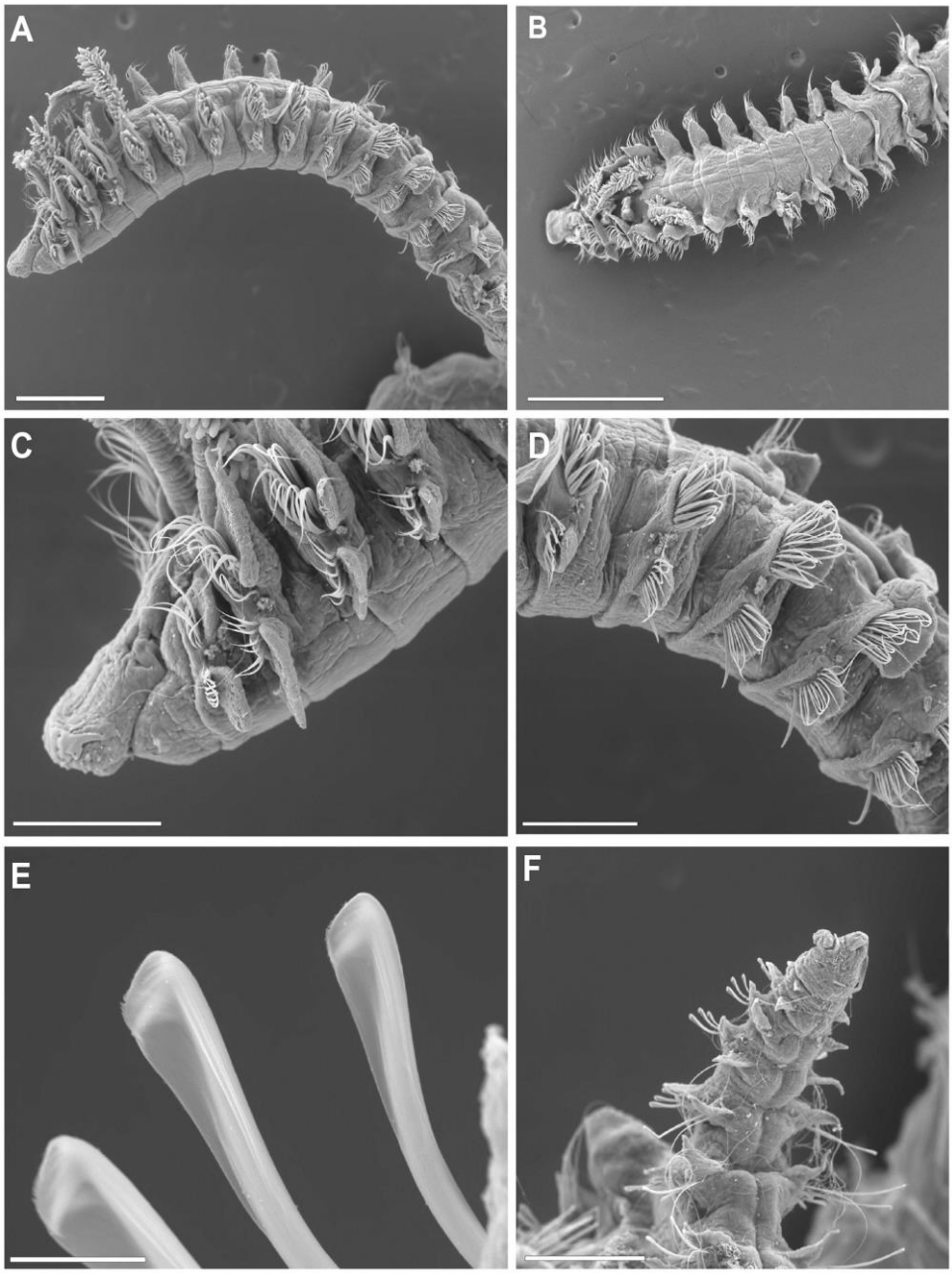

FIGURE 4. *Prionospio cristaventralis* SEM, MNHN-IA-PNT-114. A. Anterior region, lateral view B. Anterior region, dorsal view; C. Anterior region, lateral view; D. Chaetigers 9 to 13, lateral view; E. Neuropodial hooded hooks from far posterior; F. Pygidium, dorsal view. Scales: A, C, F=500 µm, B=1 mm, C=125 µm, D=250 µm, E=15 µm.

Also, it has been suggested that most records of *S. kroyeri* from the Western Mediterranean, including the Adriatic, and South European Atlantic refer to *S. afer* (Gil 2011; Mikac 2014). *Spiophanes kroyeri*, being an Arctic species, is unlikely to occur in Southern Europe (Meißner 2005). In French marine waters, *S. kroyeri* has been reported from the Bay of Biscay in the Atlantic (Glémarec 1969; Amoureux 1971; Lagardère 1972) and from Cerbère to Saint Raphael (RESOMAR 2019) in the Mediterranean. However, some specimens of *Spiophanes* from the Bay of Biscay (not *S. bombyx*) show "0+1 type" chaetal spreaders on chaetigers 5–7 and lack pigmentation on chaetigers 9 13. Despite resembling *S. kroyeri*, we suggest they more likely belong to a different, undescribed species (Jourde and Lavesque, unpublished data). *Spiophanes duplex*, described from Southern California, was also reported from the French Mediterranean during 1969–1972 and then in 2009, together with *S. viriosus* (OBIS, 2019; RESOMAR, 2019) and has not been recorded since then. In 2012, *S. afer* was reported between Italy and Spain, including Corsica (OBIS 2019), suggesting that the previous reports of *Spiophanes* in the Mediterranean Sea may also refer to this species. Therefore, despite the fact that we are reporting *S. afer* as present on the French Mediterranean coast at least since 2010, the literature and databases strongly suggest that it has been present in the area for a longer period of time.

In summary, the present state of knowledge on the spatio-temporal distribution of the species of *Spiophanes*, and particularly *S. afer,* does not allow an assessment of its real distribution in Europe. Further investigations will require that museum and private collections be checked, and new morphological and molecular analyses on fresh material (or preserved in a compatible way for DNA extraction) be carried out. In particular, acquisition of DNA sequences of *S. afer* from its type locality is needed to clarify the status of *S. adriaticus*.

Acknowledgments

The authors would like to thank those involved in sampling campaigns on board the RV "Côtes de la Manche" (JERICO-Next-H2020 and VOG CNRS LEFE-EC2CO programs, Bruno Deflandre, SGC CDM Fred (2016) JERICOBENT, https://doi.org/10.18142/284), RV "L'Estran" (La Rochelle Université) and "JIF Surveyor" (Jifmar Offshore Services, Bayonne), RV "Tethys II" (REDIT 2010, http://dx.doi.org/10.17600/10450130) funded by "Agence de l'Eau Corse-Méditerranée" (convention n°2010 0871) and the "Agence des Aires Marines Protégées" (Marché N° 2009-AAMP-16; Lot N°9; ASCONIT/GIS Posidonie), and RV "Nereis II" (RNMCB funded by Conseil Départemental des Pyrénées Orientales and IBIS). We thank Tarik Meziane (MNHN Paris) for

providing accession numbers in the difficult context of Covid-19 confinement. We are grateful to Pauline Cajéri, Jérôme Davignon and Jean-Damien Bergeron (CREOCEAN), Etienne Serres, Damien Saffroy and Aude Laurens (RT E) who kindly gave us worms collected in the southern Bay of Biscay, and to Fabien Aubert (Cohabys/ADERA) for his help on figure preparation. We are also grateful to the editor handling our manuscript and to Daniel Martin and an anonymous reviewer, who helped to improve an earlier version of the manuscript.

References

Aguirrezabalaga, F. & Ceberio, A. (2005) Spionidae (Polychaeta) from the Capbreton Canyon (Bay of Biscay, NE Atlantic) with description of a new genus and three new species. *Marine Biology Research*, 1, 267–280. https://doi.org/10.1080/17451000500262066

Amoureux, L. (1971) Annélides Polychètes capturés au large de la côte d'Arcachon. Inventaire taxonomique. *Bulletin de la Société Linnéenne de Bordeaux*, 1, 147–164.

Augener, H. (1918) Polychaeta. *Beitrage zur Kenntnis der Meeresfauna Westafrikas*, 2 (2), 67–625.

Blake, J.A., Maciolek, N.J. & Meißner, K. (2017) *Spionidae Grube, 1850. A Natural History of the Phyla of the Animal Kingdom, Annelida: Polychaeta*. A. Schmidt-Rhaesa. Berlin, Boston: De Gruyter, pp. 1–109.

Berkeley, E. (1927) Polychaetous annelids from the Nanaimo district. Part 3. Leodicidae to Spionidae. *Contributions to Canadian Biology and Fisheries*, 3 (17), 407–422. https://doi.org/10.1139/f26-017

Bogantes, V.E., Halanych, K.M. & Meißner, K. (2018) Diversity and phylogenetic relationships of North Atlantic *Laonice* Malmgren, 1867 (Spionidae, Annelida) including the description of a novel species. *Marine Biodiversity*, 48, 737–749. https://doi.org/10.1007/s12526-018-0859-8

Chamberlin, R.V. (1919) New polychaetous annelids from Laguna Beach, California. *Pomona College Journal of Entomology and Zoology*, 11 (1), 1–23.

Charria, G., Lazure, P., Le Cann, B., Serpette, A., Reverdin, G., Louazel, S., Batifoulier, F., Dumas, F., Pichon, A. & Morel, Y. (2013) Surface layer circulation derived from Lagrangian drifters in the Bay of Biscay. *Journal of Marine Systems*, 109–110, Supplement, 60–76. https://doi.org/10.1016/j.jmarsys.2011.09.015

Çinar, M.E., Dağli, E. & Şahin, G.K. (2014) Checklist of Annelida from the coasts of Turkey. *Turkish Journal of Zoology*, 38, 734–764. https://doi.org/10.3906/zoo-1405-72

Çinar, M.E., Dağli, E., Çağlar, S. & Albayrak, S. (2015) Polychaetes from the northern part of the Sea of Marmara with the description of a new species of *Polydora* (Annelida: Polychaeta: Spionidae). *Mediterranean Marine Science*, 16 (3), 524–532. https://doi.org/10.12681/mms.1226

Claparède, E. (1870) Les Annélides Chétopodes du Golfe de Naples. Supplément. *Mémoires de la Société de physique et d'histoire naturelle de Genève*, 20 (2), 365–542.

D'Alessandro, M., Castriota, L., Maggio, T., Nasi, F., Carletti, M., Auriemma, R., Romeo, T. & Del Negro, P. (2019) *Spiophanes adriaticus*, a new species from the Mediterranean Sea. *Journal of the Marine Biological Association of the United Kingdom* 100, 45–54. https://doi.org/10.1017/S0025315419001061

Day, J.H. (1961) The Polychaete Fauna of South Africa. Part 6. Sedentary species dredged off Cape coasts with a few new records from the shore. *Journal of the Linnean Society of London,* 44 (299), 463–560. https://doi.org/10.1111/j.1096-3642.1961.tb01623.x

Dagli, E., Cinar, M.E. & Ergen Z. (2011) Spionidae (Annelida: Polychaeta) from the Aegean Sea (eastern Mediterranean). *Italian Journal of Zoology* 78, 49–64. https://doi.org/10.1080/11250003.2011.567828

Deflandre, B. (2016) JERICOBENT.

de Montaudouin, X. & Sauriau, P.-G. (2000) Contribution to a synopsis of marine species richness in the Pertuis Charentais Sea with new insights in soft-bottom macrofauna of the Marennes-Oléron Bay. *Cahiers de Biologie Marine*, 41 (2), 181–222.

Delgado-Blas, V.H., Díaz-Díaz, O. & Viéitez J.M. (2018) *Prionospio* from the coast of the Iberian Peninsula, with the description of two new species (Annelida, Spionidae). *ZooKeys,* 810, 1–18. https://doi.org/10.3897/zookeys.810.26910

Delgado-Blas, V.H., Díaz-Díaz, O. & Viéitez J.M. (2019) On the diversity of the genus *Spiophanes* Grube, 1860(Annelida: Spionidae) in the Spanish peninsular coast, with descriptions of two new species. *Cahiers de Biologie Marine*, 60, 335–351.

Fauvel, P. (1928) Annélides polychètes nouvelles du Maroc. *Bulletin de la Société Zoologique de France,* 53 (1), 9–13.

Gil, J. (2011) *The European fauna of Annelida Polychaeta*. Unpublished PhD Thesis, Universidade de Lisboa, Lisbon, 1554 pp.

Glémarec, M. (1969) *Les peuplements benthiques du plateau continental Nord-Gascogne*. Thèse de Doctorat d'Etat *es* Sciences Naturelles. Université de Paris VI, Paris, 167 pp.

Grube, A.E. (1860) Beschreibung neuer oder wenig bekannter Anneliden. *Fünfter Beitrag. Archiv für Naturgeschichte, Berlin*. 26 (1), 71–118. https://doi.org/10.5962/bhl.title.11291

Lagardère, F. (1972) Les fonds de pêche de la côte ouest de l'île d'Oléron. Cartographie bionomique. III—Les peuplements benthiques. *Tethys*, 3 (3), 507–538.

Laubier, L. (1962) Quelques Annélides Polychètes de la Lagune de Venise description de *Prionospio caspersi* n. sp. *Vie et Milieu*, 13 (1), 123–159.

Laubier, L. (1964) Un Spionidien des vases bathyales de Banyuls-sur-Mer, Spiophanes kroyeri reyssi ssp. n. *Bulletin de la Société Zoologique de France*, 89 (4), 562–577.

Lavesque, N., Bonifácio, P., Meißner, K., Blanchet, H., Gouillieux, B., Dubois, S. & Bachelet, G. (2015) New records of *Spio symphyta* and *Spio martinensis* ('Polychaeta': Canalipalpata: Spionidae) from Arcachon Bay (France), NE Atlantic. *Marine Biodiversity*, 45 (1), 77–86. https://doi.org/10.1007/s12526-014-0230-7

Liénart, C., Savoye, N., Bozec, Y., Breton, E., Conan, P., David, V., Feunteun, E., Grangeré, K., Kerhervé, P., Lebreton, B., Lefebvre, S., L'Helguen, S., Mousseau, L., Raimbault, P., Richard, P., Riera, P., Sauriau, P.-G., Schaal, G., Aubert, F., Aubin, S., Bichon, S., Boinet, C.,

Bourasseau, L., Bréret, M., Caparros, J., Cariou, T., Charlier, K., Claquin, P., Cornille, V., Corre, A.-M., Costes, L., Crispi, O., Crouvoisier, M., Czamanski, M., Del Amo, Y., Derriennic, H., Dindinaud, F., Durozier, M., Hanquiez, V., Nowaczyk, A., Devesa, J., Ferreira, S., Fornier, M., Garcia, F., Garcia, N., Geslin, S., Grossteffan, E., Gueux, A., Guillaudeau, J., Guillou, G., Joly, O., Lachaussée, N., Lafont, M., Lamoureux, J., Lecuyer, E., Lehodey, J.-P., Lemeille, D., Leroux, C., Macé, E., Maria, E., Pineau, P., Petit, F., Pujo-Pay, M., Rimelin-Maury, P. & Sultan, E. (2017) Dynamics of particulate organic matter composition in coastal systems: A spatio-temporal study at multi-systems scale. *Progress in Oceanography*, 156, 221–239. https://doi.org/10.1016/j.pocean.2017.03.001

Malmgren, A.J. (1867) *Annulata Polychaeta Spetsbergiæ, Groenlandiæ, Islandiæ et Scandinaviæ*. Hactenus Cognita. Ex Officina Frenckelliana, Helsingforslæ, 127 pp. https://doi.org/10.5962/bhl.title.13358

Massé, C., Meisterhans, G., Deflandre, B., Bachelet, G., Bourasseau, L., Bichon, S., Ciutat, A., Jude-Lemeilleur, F., Lavesque, N., Raymond, N., Grémare, A. & Garabetian, F. (2016) Bacterial and macrofaunal communities in the sediments of the West Gironde Mud Patch, Bay of Biscay (France). *Estuarine, Coastal and Shelf Science,* 179, 189–200. https://doi.org/10.1016/j.ecss.2016.01.011

Martínez, J. & Adarraga, I. (2019) First records of two species of Spionidae (Annelida) from Bay of Biscay and European coasts. *Cahiers de Biologie Marine*, 60, 369–379.

Meißner, K. (2005) Revision of the genus *Spiophanes* (Polychaeta, Spionidae); with new synonymies, new records and descriptions of new species. *Mitteilungen aus dem Museum für Naturkunde in Berlin, Zoologische Reihe,* 81 (1), 3–66. https://doi.org/10.1002/mmnz.200310001

Meißner, K. & Hutchings, P.A. (2003) Spiophanes species (polychaeta: Spionidae) from eastern Australia: with descriptions of new species, new records and an emended generic diagnosis. *Records of the Australian Museum*, 55 (2), 117–140. https://doi.org/10.3853/j.0067-1975.55.2003.1379

Meißner, K., Bick, A., Guggolz, T. & Götting, M. (2014) Spionidae (Polychaeta: Canalipalpata: Spionida) from seamounts in the NE Atlantic. *Zootaxa*, 3786 (3), 201–245. https://doi.org/10.11646/zootaxa.3786.3.1

Mikac, B. (2015) A sea of worms: polychaete checklist of the Adriatic Sea. *Zootaxa*, 3943 (1), 1–172. https://doi.org/10.11646/zootaxa.3943.1.1

Moritz, D. (2012) *Composition and distribution of the macrozoobenthic communities on the shelf off Angola*. Master Thesis Marine Biology, University of Rostock, 49 pp. OBIS (2019) Ocean Biogeographic Information System. Intergovernmental Oceanographic Commission of UNESCO. Available from: www.iobis.org (accessed 18 September 2019)

Radashevsky, V.I., Pankova, V.V., Neretina, T.V., Stupnikova, A.N. & Tzetlin, A.B. (2016) Molecular analysis of the *Pygospio elegans* group of species (Annelida: Spionidae). *Zootaxa*, 4083 (2), 239–250. https://doi.org/10.11646/zootaxa.4083.2.4

Radashevsky, V.I., Pankova, V.V., Malyar, V.V., Neretina, T.V., Wilson, R.S., Worsfold, T.M., Diez, M., Harris, L., Hourdez, S., Labrune, C., Houbin, C., Kind, B., Kuhlenkamp, R., Nygren, A., Bonifacio, P. & Bachelet, G. (2019) Molecular analysis and new records of the invasive polychaete *Boccardia proboscidea* (Annelida: Spionidae). *Mediterranean Marine Science*, 20 (2), 393–408. https://doi.org/10.12681/mms.20363

Ravara, A. & Moreira M.H. (2013) Polychaeta (Annelida) from the continental shelf off Aveiro (NW Portugal): Species composition and community structure. Check List, 9 (3), 533–539. https://doi.org/10.15560/9.3.533

Read, G. & Fauchald, K. (Ed.) (2019) World Polychaeta database. Spionidae Grube, 1850. Available from: http://marinespecies.org/aphia.php?p=taxdetails&id=913 (accessed 2 September 2019)

RESOMAR (2019) French marine stations and observatories network Database. Available from: http://resomar.cnrs.fr/bases/index.php (accessed 18 September 2019)

Söderström, A. (1920) *Studien über die Polychätenfamilie Spionidae*. Uppsala University, pp. 1–286. Surugiu, V. (2016) On the taxonomic status of the European *Scolelepis (Scolelepis) squamata* (Polychaeta: Spionidae), with description of a new species from southern Europe. *Zootaxa*, 4161 (2), 151–176. https://doi.org/10.11646/zootaxa.4161.2.1

Wirén, A. (1883) Chaetopoder från Sibiriska Ishafvet och Berings Haf Insamlade under Vega Expeditionen 1878–1879. *Vega- Expeditionens Vetenskapliga Iakttagelser bearbetade af deltagare i resan och andra forskare: Stockholm, F&G Beijers Förlag,* 2, 383–428.

Annexe 2.

The Spaghetti Project: the final identification guide to European Terebellidae (*sensu lato*) (Annelida, Terebelliformia)

Nicolas LAVESQUE[1*], Pat HUTCHINGS[2], Mario H. LONDOÑO-MESA[3], João M. M. NOGUEIRA[4], Guillemine DAFFE[5], Arne NYGREN[6], Hugues BLANCHET[7], Paulo BONIFÁCIO[8], Caroline BROUDIN[9], Jean-Claude DAUVIN[10], Gabin DROUAL[11], Benoit GOUILLIEUX[12], Jacques GRALL[13], Benjamin GUYONNET[14], Céline HOUBIN[15], Suzie HUMBERT[16], Anne-Laure JANSON[17], Jérôme JOURDE[18], Céline LABRUNE[19], Bastien LAMARQUE[20], Lise LATRY[21], Vincent LE GARREC[22], Corine PELAPRAT[23], Jean-Philippe PEZY[24], Pierre-Guy SAURIAU[25], Xavier DE MONTAUDOUIN[26]

[1,7,12,16,20, 21,26] CNRS, Univ. Bordeaux, EPOC, UMR 5805, Station Marine d'Arcachon, Arcachon, France

[2] Australian Museum Research Institute, Australian Museum, Sydney, Australia; Department of Biological Sciences, Macquarie University, Australia

[3] Grupo LimnoBasE y Biotamar, Instituto de Biología Facultad de Ciencias Exactas y Naturales, Universidad de Antioquia, Medellín, Colombia.

[4] Laboratório de Poliquetologia, Departamento de Zoologia, Instituto de Biociências, Universidade de São Paulo, Brazil

[5] CNRS, Université de Bordeaux, Observatoire Aquitain des Sciences de l'Univers, UMS 2567 POREA, Pessac, France

[6] Sjöfartmuseet Akvariet, Göteborg, Sweden; Institutionen för marina vetenskaper, Göteborgs Universitet, Göteborg, Sweden

[8] Independent researcher, Brest, France

[9, 15] Sorbonne Université, CNRS, Station Biologique de Roscoff, 29680 Roscoff, France

[10,24] Normandie Univ, UNICAEN, UNIROUEN, Laboratoire Morphodynamique Continentale et Côtière, CNRS UMR 6143 M2C, Caen, France

[11] Ifremer, DYNECO-LEBCO, Plouzané, France; Ifremer, EMH, Nantes, France

[13, 22] Univ Brest, CNRS, IRD, OSU-IUEM, Plouzané, France

[14] TBM Environnement, Auray, France

[17] OFB, CNRS, MNHN, UMS 2006 Patrimoine Naturel, Station Marine de Dinard, Dinard, France

[18,25] CNRS, La Rochelle Université, Littoral Environnement et Sociétés, UMR 7266 LIENSs, La Rochelle, France

[19] CNRS, Sorbonne Université, Laboratoire d'Ecogéochimie des Environnements Benthiques, LECOB, Banyuls, France

[23] Benthos Identification, 33840 Escaudes, France; Stareso, Calvi, France

[1]Email: nicolas.lavesque@u-bordeaux.fr*

[2]Email: Pat.Hutchings@austmus.gov.au

[3]Email: hernan.londono@udea.edu.co

[4]Email: nogueira@ib.usp.br

[5]Email: guillemine.daffe@u-bordeaux.fr

[6]Email: maskmedmera@gmail.com

[7]Email: hugues.blanchet@u-bordeaux.fr

[8]Email: bonif@me.com

[9]Email: broudin@sb-roscoff.fr

[10]Email: jean-claude.dauvin@unicaen.fr

[11]Email: Gabin.Droual@ifremer.fr

[12]Email: benoit.gouillieux@u-bordeaux.fr

[13]Email: jacques.grall@univ-brest.fr

[14]Email: b.guyonnet@tbm-environnement.com

[15]Email: houbin@sb-roscoff.fr

[16]Email: suzie.humbert@u-bordeaux.fr

[17]Email: anne-laure.janson@mnhn.fr

[18]*Email: jjourde@univ-lr.fr*
[19]*Email: celine.labrune@obs-banyuls.fr*
[20]*Email: bastien.lamarque@u-bordeaux.fr*
[21]*Email: lise.latry@u-bordeaux.fr*
[22]*Email: Vincent.Legarrec@univ-brest.fr*
[23]*Email: benthid@gmail.com*
[24]*Email: jean-philippe.pezy@unicaen.fr*
[25]*Email: pierre-guy.sauriau@univ-lr.fr*
[26]*Email : xavier.de-montaudouin@u-bordeaux.fr*

[1]*urn:lsid:zoobank.org:author:3E6771E7-1A94-4FD2-8E7B-36AD6ED8B446*
[2]*urn:lsid:zoobank.org:author:E83A37D3-33D8-4999-ACA6-8DFECAF05D11*
[3]*urn:lsid:zoobank.org:author:198696D8-8FB2-4F03-AFEB-0E0773CB6669*
[4]*urn:lsid:zoobank.org:author:C40C8C12-619D-4EC2-8998-253708120D3F*
[5]*urn:lsid:zoobank.org:author:BC283B5F-3757-4941-BEED-4004C685091*
[6]*urn:lsid:zoobank.org:author:46801B86-2D81-4702-A1D1-65E1C6C40FC1*
[8]*urn:lsid:zoobank.org:author:19882300-C635-4CF2-A7CE-98EE01C87120*
[10]*urn:lsid:zoobank.org:author:12B3072A-421D-47A0-82BE-10125016C8D9*
[12]*urn:lsid:zoobank.org:author:D0BE2D38-05DC-4DE0-BEE2-D458ED5C3299*
[13]*urn:lsid:zoobank.org:author:74F9A220-94E5-4C80-B375-0FD4C894F804*
[15]*urn:lsid:zoobank.org:author:41D368C7-3084-4E8A-B6EF-24E184D4752E*
[16]*urn:lsid:zoobank.org:author:4354F19C-8567-4713-8E3B-492B4025EF26*
[18]*urn:lsid:zoobank.org:author:746DEE71-E146-4355-B164-D55D9A971044*
[19]*urn:lsid:zoobank.org:author:9200C8BA-E199-46B8-8727-BCF01DBC383A*
[20]*urn:lsid:zoobank.org:author:BE414235-3305-483C-8ED2-53AF7F68482A*
[22]*urn:lsid:zoobank.org:author:299DA6A8-98CF-49F7-B809-A32CB991613D*
[25]*urn:lsid:zoobank.org:author:C5012CB5-D12A-468F-9536-E0C08F9A91E6*

Article accepté en 2021 dans la revue *European Journal of Taxonomy*

Abstract

This paper is the conclusion of the “Spaghetti project” aiming to revise French species of Terebellidae *sensu lato (s.l.)* belonging to the five families: Polycirridae, Telothelepodidae Terebellidae *sensu stricto (s.s.)*, Thelepodidae and Trichobranchidae. During this project, 41 species were observed, 31 of them new for science: eight species of Polycirridae, eleven species of Terebellidae *s.s.*, three species of Thelepodidae and nine species of Trichobranchidae. We provide a comprehensive key for all European species of terebellids with a focus on the important diagnostic characters for each family. Finally, we discuss issues on taxonomy, biodiversity and cryptic species of polychaetes in European waters, based on results obtained during this project.

Keywords. Taxonomy, terebellids, spaghetti worms, cryptic species, identification key.

Introduction

This is the concluding paper of the series devoted to the "Spaghetti project" which aims to revise the French species of Terebellidae *sensu lato* (*s.l.*), referring to the original taxa previously considered as subfamilies of the family Terebellidae Johnston, 1846, namely Polycirrinae Malmgren, 1866 (now referred to Polycirridae), Terebellinae Johnston, 1846 (now referred to Terebellidae *sensu stricto* (*s.s.*)) and Thelepodidae Hessle, 1917, together with the closely related family Trichobranchidae Malmgren, 1866 and the recently described family Telothelepodidae Nogueira, Fitzhugh & Hutchings, 2013 (Johnston 1846; Malmgren 1866; Hessle 1917; Nogueira *et al.* 2013; Hutchings *et al.* 2021a).

These tubiculous polychaetes are characterised by the presence of numerous grooved buccal tentacles used for selective deposit feeding, rendering these animals the name of "Spaghetti worms" (Hutchings *et al.* 2021b). These tentacles are of prostomial origin and not retractable into the mouth. They are generally smooth, except for in some polycirrids where they are papillose. Most of the terebellids are sedentary worms found in all marine environments, from the intertidal to the abyss and are common worldwide, distributed from polar to tropical regions (Hutchings *et al.* 2021b). The five families belonging to Terebellidae (*s.l.*) can be separated from each other by the morphology of the upper lip, the shape and number of branchiae, the glandular areas of ventral segments, the neuropodia and the arrangement of the uncini of anterior segments (i.e. in single or double rows) (Hutchings *et al.* 2021b).

The "Spaghetti Project" was initiated when NL realized that the taxonomy of these worms in France, but also in Europe, was poorly documented. Indeed, the lack of accurate literature and the absence of useful and up-to-date keys of identification for this part of the world has led to their misidentifications for decades. In 2016, after observations of several specimens of Terebelliformia during a national workshop (at Arcachon conducted by Mario Londoño-Mesa) and a national taxonomic course (at Caen conducted by Pat Hutchings), we realized that many of the species required in-depth investigations. This collaborative project involved all benthic taxonomists at all French marine stations (RESOMAR network) who sent us fresh material as well as specimens stored in local collections. The first part of the project, devoted to the Trichobranchidae, allowed us to describe nine new species along the French coasts (Lavesque *et al.* 2019a). The second paper, focused on Telothelepodidae and Thelepodidae, described three new species (Lavesque *et al.* 2020a) and the third one on Polycirridae described eight new species (Lavesque *et al.* 2020b). Finally, the fourth paper

dealt with the Terebellidae *sensu stricto* (*s.s.*) and included the description of nine species (Lavesque *et al.* 2021). With the previous descriptions of *Lomia ramzega* Lavesque, Bonifácio, Londoño-Mesa, Le Garrec & Grall, 2017a from Brittany and *Pista colini* Labrune, Lavesque, Bonifácio & Hutchings, 2019 from the Gulf of Lion (Lavesque *et al.* 2017; Labrune *et al.* 2019), a total of 31 new species have been described from French waters in the past five years, combining both morphological and molecular data. This "Spaghetti project" is thus an excellent example of what can be done by working in a network, with limited funding but enthusiastic people.

The main objectives of this last paper are (1) to provide a comprehensive key for all European species of terebellids (*s.l.*) with a focus on important diagnostic characters for each family and (2) to discuss the main results obtained during this project.

Abbreviations

AM Australian Museum, Sydney, Australia
CH Chaetiger
CEMUA Colección Estuarina y Marina, Universidad de Antioquiain Medellin, Colombia
GNM Göteborg Natural History Museum, Sweden
KGB Department of Hydrobiology Moscow Lomonosov State University, Russia
LACM Natural History Museum of Los Angeles County, Los Angeles, USA
MG Methyl green
MNHB Museum der Naturkunde für Humboldt Universität zu Berlin, Germany
MNHN Muséum National d'Histoire Naturelle, Paris, France
MZDAUT Museum of the Department of Zoology, Aristoteleion University of Thessaloniki, Greece
NHMUK Natural History Museum, London, UK
NMSE National Museum of Scotland, Edinburgh
NMW-Z National Museum Wales, Cardiff
NTNU Norwegian University of Science and Technology, University Museum, Trondheim, Norway
PMR Natural History Museum Rijeka, Croatia
SEM Scanning Electron Microscope
SG Segment
SMF Senckenberg Museum Frankfurt, Germany
SMNH Swedish Museum of Natural History, Stockholm, Sweden
USNM National Museum of Natural History, Smithsonian Institution, Washington, USA
UZMO Universitetet i Oslo, Zoologisk Museum, Norway
ZIN Zoological Institute of Russian Academy of Science, St. Petersburg, Russia
ZMUB Zoological Museum, University of Bergen, Norway

ZMUU Zoologiska Museet Uppsala Universitets, Sweden

Material and methods

During the Spaghetti Project, morphological observations were conducted on specimens stored in the MNHN collection and specimens collected during different research programs and specific samplings along the French coasts (see previous papers).

Specimens were fixed in 4% formaldehyde in filtered seawater solution, washed and then, transferred to 70% ethanol for preservation. Methyl green, which can be washed out, was used to reveal the abundant glandular areas and to highlight the ornamentation of these areas, which are difficult to observe otherwise. For the molecular studies, several parapodia were removed from several fresh specimens, or from specimens fixed in 96% ethanol.

Preserved specimens were examined under a Nikon SMZ25 stereomicroscope and a Nikon Eclipse *Ci* microscope, and photographed with a Nikon DS-Ri 2 digital camera. Dehydrated specimens used for examination by scanning electron microscopy (SEM) were prepared by critical point drying, coated with gold and examined and photographed with JEOL JSM 6480LA at Macquarie University, Sydney and Hitachi TM3030 at Arcachon Marine Station.

Morphological terminology follows Nogueira *et al.* (2010) and Hutchings *et al.* (2021a), especially concerning the anterior end and the general structure of the uncini (Fig. 1), Glasby & Hutchings (2014) for the types of uncini present in *Polycirrus* species and Parapar *et al.* (2020a, b) for those found in *Terebellides* species.

Authorities of each species are given in the different keys and cited in the references.

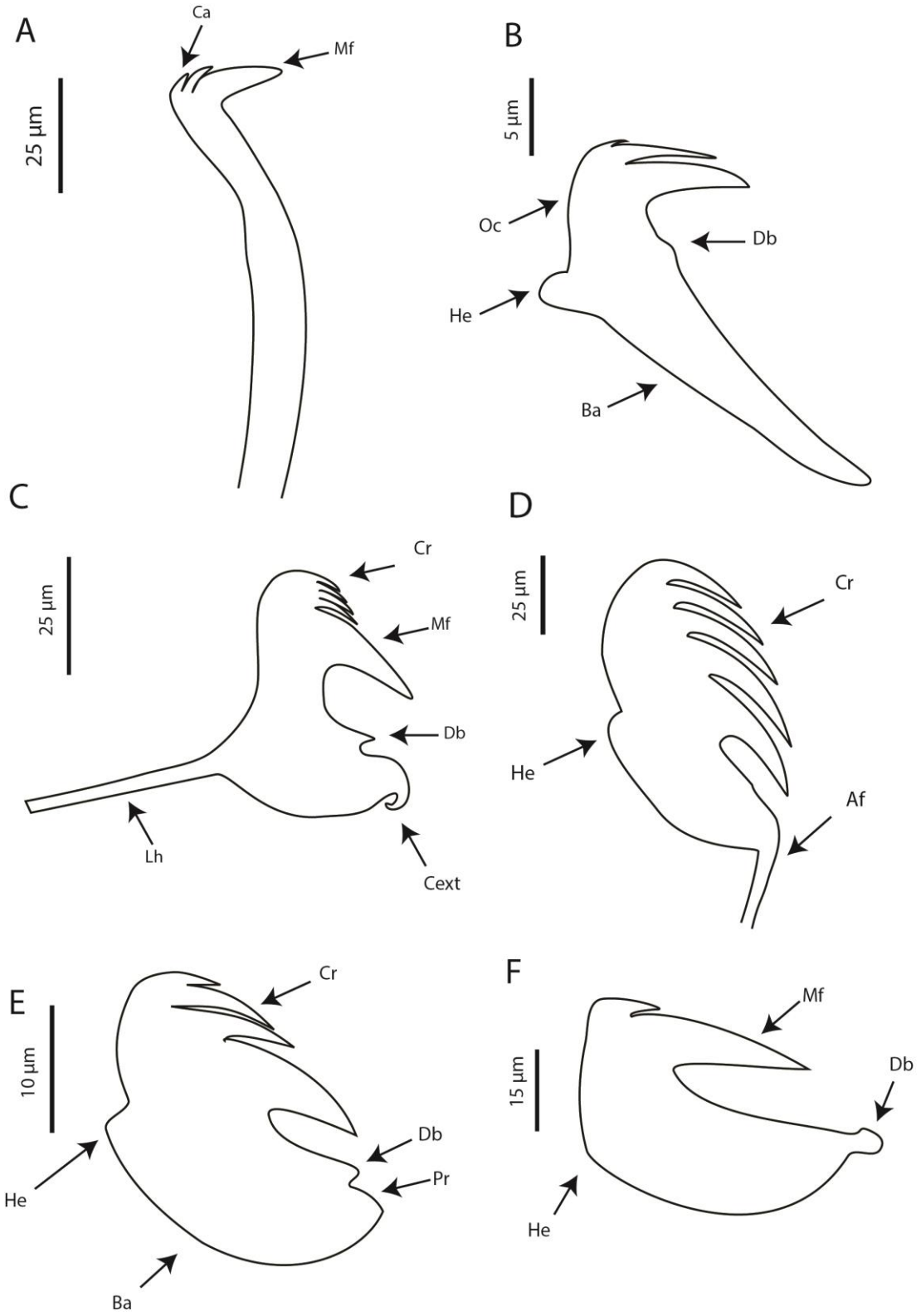

Fig. 1. Schematic illustrations of different uncini morphologies, in lateral view (following Nogueira *et al.* 2010). **A.** *Terebellides* sp., SG IX (SMA-BR-Terebellides-KER1). **B.** *Polycirrus catalanensis*, SG XX (holotype MNHN-IA-TYPE 2007). **C.** *Pista sauriaui*, SG V (paratype MNHN-IA-TYPE 2036). **D.** *Lomia ramzega*, SG XII (paratype MNHN-IA-TYPE 1791). **E.** *Streblosoma cabiochi*, SG VI (holotype MNHN-IA- type 2000). **F.** *Thelepus japonicus*, SG XVII - MNHN-IA-PNT 117). Abbreviations: Af, anterior filament; Ba, base; Ca, capitium; Cext, coma-shape extension; Cr, crest; Db, dorsal button; He, heel; Lh, long handle; Mf, main fang; Oc, occipitium; Pr, prow.

Results

Phylum Annelida Lamarck, 1809

Class Polychaeta Grube, 1850

Order Terebellida Rouse & Fauchald, 1997

Key to the families of Terebellidae *sensu lato*

1A. Notopodia, if present, elongate, roughly cylindrical, distally bilobed; branchiae absent; ventrum of anterior segments with paired glandular pads (Fig. 2B, D)…… **Polycirridae**
1B. Notopodia always present, short, conical, distally bi- or single lobed; branchiae usually present; development and shape of ventral glandular areas of anterior segments variable between families, but never as paired mid-ventral pads…… **2**

2A. Thoracic uncini acicular (Figs 1A, 7D)…….. **Trichobranchidae**
2B. Thoracic uncini avicular (Fig. 1B–F)…… **3**

3A. Neuropodia with uncini in double rows on some segments (Fig. 6E); branchiae, if present, cirriform, arborescent or spiralled……. **Terebellidae *sensu stricto***
3B. Neuropodia with uncini in single rows throughout; branchiae rarely absent, always cirriform …… **4**

4A. Upper lip expanded, distinctly longer than wide (Figs 3F, 4A); neuropodia poorly developed throughout, as nearly sessile ridges and distinctly low pinnules on thoracic and abdominal segments, respectively …….. **Telothelepodidae**
4B. Upper lip short, hood-like, about as wide as long, frequently circular (Figs 3D–E, 4B–C); well-developed neuropodia throughout, as fleshy ridges and elongate pinnules on thoracic and abdominal segments, respectively …….. **Thelepodidae**

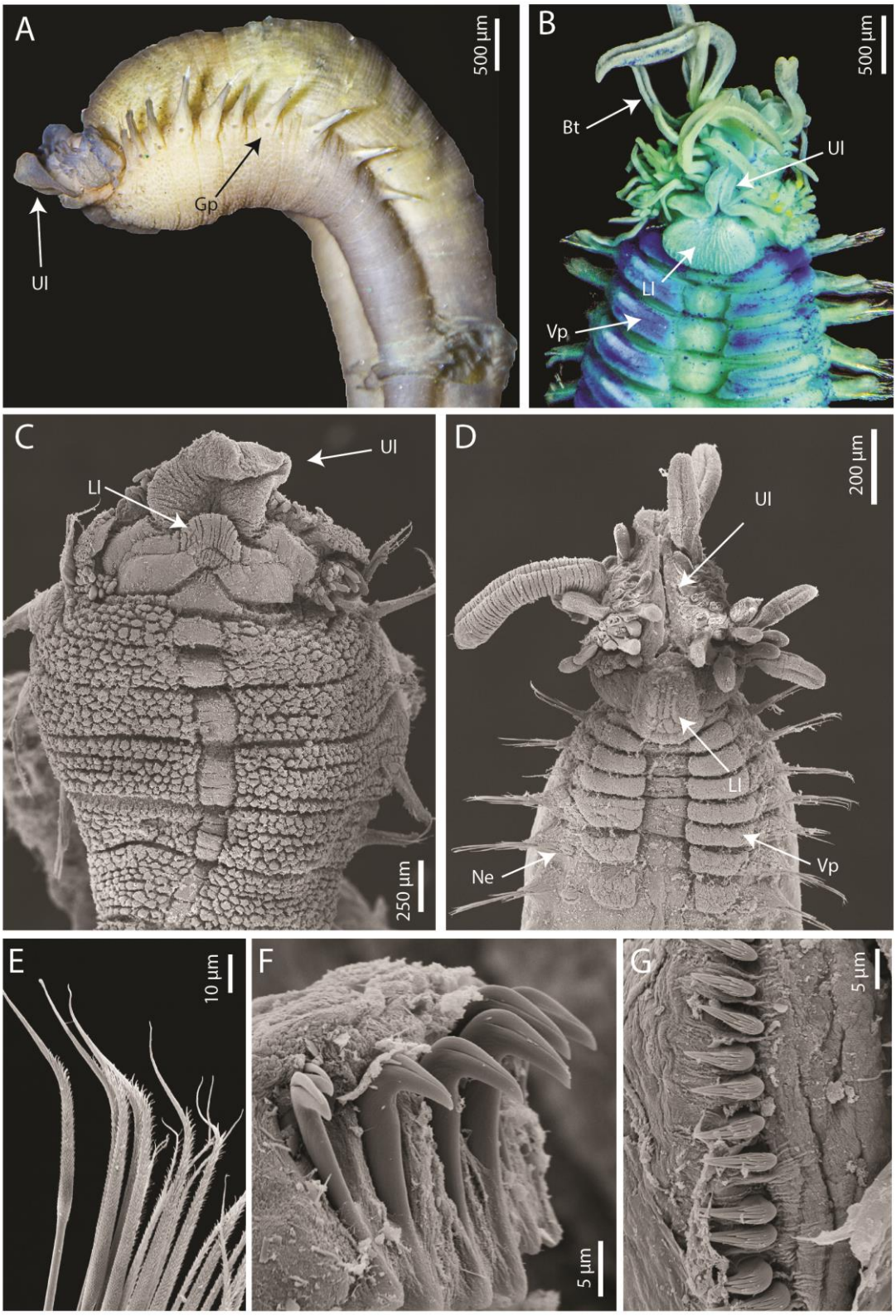

Fig. 2. Diversity of Polycirridae. **A.** *Amaeana gremarei*, anterior end, lateral view (MNHN-IA-Type 2006). **B.** *Polycirrus gujanensis*, anterior end, ventral view (MNHN-IA-Type 2013). **C.** *Amaeana gremarei*, anterior end, ventral view (AM W.53111). **D.** *Polycirrus idex*, anterior end, ventral view (AM W.53127). **E.** *Polycirrus glasbyi*, notochaetae SG V (AM W.53118). **F.** *Polycirrus catalanensis*, abdominal uncini (AM W.53113). **G.** *Polycirrus glasbyi*, thoracic uncini (AM W.53118). Abbreviations: Bt, buccal tentacles; Gp, genital papilla; Ll, lower lip; Ne, neuropodia; Ul, upper lip; Vp, ventral pads.

Polycirridae Malmgren, 1866

Figs 1B, 2

Diagnosis (after Hutchings *et al.* 2021a; most important diagnostic characters highlighted in bold). Transverse prostomium attached to dorsal surface of upper lip; basal part usually as thick horse-shoe shaped crest, eye spots absent; distal part either as another thick crest, with flaring distal lobes, with or without mid-dorsal process, or extending along upper lip until near anterior margin of lip; prostomium frequently extending ventrally, terminating laterally to mouth (Fig. 2A–D). Buccal tentacles of two types at least, short ones thin, uniformly cylindrical, long tentacles stouter, expanded at tips at variable degrees, distally spatulate (Fig. 2B, D) or more specialised. Peristomium forming lips; lips expanded, upper lip large, frequently circular and convoluted, folded into three lobes; swollen lower lip, only mid-ventral or cushion-like across ventrum, sometimes extending posteriorly for a few segments (Fig. 2A–D). Segment I reduced, frequently only visible ventrally, sometimes completely hidden. Segment II distinctly narrower than following segments, constricting body posteriorly to "lips head"; **SG II usually with rectangular or pentagonal mid-ventral shield at beginning of mid-ventral groove**, sometimes extending anteriorly through SG I until near posterior margin of lower lip (Fig. 2C). Anterior segments highly glandular ventrally, frequently papillose or tessellated, **with paired ventro-lateral pads** separated from each other within pairs by mid-ventral groove extending from SG II–IV to posterior body (Fig. 2A–D). **Branchiae absent**. Notopodia, if present, from SG III (Fig. 2A–D), extending for variable number of segments, usually few; bilobed, elongate notopodia, post-chaetal lobes sometimes longer, notochaetae originating between lobes along all extension of notopodia, separating lobes from base on ventral side of notopodia (Fig. 2A–D); notochaetae winged (Fig. 2E) and/or pinnate, wings of variable width. **Neuropodia, if present, located posteriorly to notopodia, frequently from posterior thoracic segments or only on abdomen; neurochaetae as acicular spines or avicular uncini, of two types, and arranged in a single row** (Figs 1C; 2F, G). Nephridial and genital papillae usually present, at anterior bases of all notopodia, or only at anteriormost notopodia (Fig. 2A). Pygidium smooth or with rounded ventral papilla.

This family was previously considered as a subfamily of Terebellidae (Polycirrinae Malmgren, 1866), but was recently raised to familial level after a comprehensive phylogenetic analysis showed the monophyly of this group (Nogueira *et al.* 2013). Polycirridae is represented by six genera (*Amaeana* Hartman, 1959; *Biremis* Polloni, Rowe & Teal, 1973;

Enoplobranchus Verrill, 1879; *Hauchiella* Levinsen, 1893; *Lysilla* Malmgren, 1866 and *Polycirrus* Grube, 1850), distinguished from each other by the presence/absence of noto- and neuropodia, and if present, the type of neurochaetae (Grube 1850; Malmgren 1866; Verrill 1879; Levinsen 1893; Hartman 1959; Polloni et al. 1973). Only *Amaeana* (Fig. 2A, C), *Hauchiella*, *Lysilla* and *Polycirrus* (Fig. 2B, D–G) are represented in European waters (Lavesque *et al.* 2020b) (Table 1).

Main morphological characters of European species

Parapodia. The parapodia of the members of this family are extremely important to separate the different genera. The genus *Hauchiella* is characterised by the absence of parapodia and *Lysilla* by the absence of neuropodia only. The neuropodia of members of *Amaeana* are characterised by the presence of spines, while those of *Polycirrus* bear avicular uncini (Figs 1B, 2F–G). Within the genus *Polycirrus*, the number and location of segments with notopodia and/or neuropodia are of important taxonomic value. Particularly, some species have uncini present only on abdominal segments, i.e. on segments without notopodia, and others have uncini starting before the end of the thorax, on segments bearing also notopodia.

Shape of the lips. As for other terebellids, polycirrids have a peristomium with well-defined upper and lower lips. The upper lip is large and can be trilobed (Fig. 2B) or with a single medial lobe (Fig. 2D). Generally, the upper lip is trilobed but the lobes differ in size and shape and lateral lobes can be reduced or well developed. The shape and the size of the lower lip is also highly variable between species. This lip can be rectangular, squared, rounded or subtriangular, swollen or not, longer than wide or wider than long (Fig. 2B–D).

Notochaetae. Two types of notochaetae can be present: winged chaetae as for *P. glasbyi* (Fig. 2E) and/or pinnate as for *P. plumosus*. The winged notochaetae have wings of different width which are often conspicuous under light microscope but appear hirsute under SEM (Fig. 2E).

Uncini shape and denticulation. In *Polycirrus* two types of uncini are present: Type 1 with a short occipitum (back) and a straight to slightly convex base (Fig. 1B); and Type 2 with a long occipitum and a concave base (Glasby & Hutchings 2014). To date, all described European species have Type 1 uncini. The denticulation of uncini is also helpful in separating

species, with the presence (as for *P. catalanensis*) (Fig. 2 F) or the absence (as for *P. arenivorus*) of a main tooth above the main fang, and the number of rows of secondary teeth.

Key to European species of Polycirridae (after Lavesque *et al.* 2020b)

1A. Parapodia absent (no chaetae)…… ***Hauchiella tribullata*** **McIntosh, 1869 (McIntosh, 1869)**

1B. Parapodia present…… **2**

2A (1B). Only notopodia present…….. **3 (*Lysilla*)**
2B. Notopodia and neuropodia present…….. **4**

3A (2A). Notochaetae with smooth tips, 6 pairs of thoracic papillae…….. ***L. loveni*** **Malmgren, 1866 (Malmgren 1866)**

3B. Notochaetae with plumose tips, 9 pairs of thoracic papillae…… ***L. nivea*** **Langerhans, 1884 (Langerhans 1884)**

4A (2B). Neuropodia with spines…… **5 (*Amaeana*)**
4B. Neuropodia with avicular uncini…… **6 (*Polycirrus*)**

5A (4A). Upper lip without lobe, lower lip rounded, long achaetous region…… ***A. gremarei*** **Lavesque, Hutchings, Daffe & Londoño-Mesa, 2020 (Lavesque *et al.* 2020b)**
5B. Upper lip with trilobed, lower lip rectangular, short achaetous region…… ***A. trilobata*** **(Sars, 1863) (Sars 1863)**

6A (4B). With 28 or more segments with notochaetae……**7**
6B. With 22 or fewer segments with notochaetae……**8**

7A (6A). With 29 segments with notopodia, neuropodia from SG XII, lower lip longer than wide, uncini without a main tooth above the main fang…… ***P. arenivorus*** **(Caullery, 1915) (Caullery 1915)**
7B. With 46 segments with notopodia, neuropodia from SG XIV, lower lip longer than wide, uncini with a main tooth above the main fang…….. ***P. aurantiacus*** **Grube, 1860 (Grube 1860)**
7C. With 28 segments with notopodia, neuropodia from SG XV, lower lip wider than long, uncini with a main tooth above the main fang..... ***P. gujanensis*** **Lavesque, Hutchings, Daffe & Londoño-Mesa, 2020 (Lavesque *et al.* 2020b)**

8A (6B). Neuropodia beginning before SG VIII……**9**
8B. Neuropodia beginning between SG IX and SG XII……**10**
8C. Neuropodia beginning after SG XIII……**14**

9A (8A). Upper lip trilobed, lower lip wider than long, uncini with 2 rows of teeth above the main tooth…… ***P. asturiensis*** **Cepeda & Lattig, 2016 (Cepeda & Lattig 2016)**
9B. Upper lip with single medial lobe, lower lip longer than wide, uncini with 1 row of teeth above the main tooth…… ***Polycirrus idex*** **Lavesque, Hutchings, Daffe & Londoño-Mesa, 2020b (Lavesque *et al.* 2020b)**

10A (8B). Uncini without a main tooth about the main fang…. ***P. norvegicus*** **Wollebaek, 1912 (Wollebaek 1912)**
10B. Uncini with a main tooth about the main fang……**11**

11A (10B). Lower lip subtriangular, pointed towards mouth……**12**
11B. Lower lip oval or oblong……**13**

12A (11A). With 12 or 13 segments with notopodia, lower lip longer than wide…….. ***P. denticulatus*** **Saint-Joseph, 1894 (Saint-Joseph 1894)**
12B. With 16 segments with notopodia, lower lip wider than long…….. ***P. elisabethae*** **McIntosh, 1915 (McIntosh 1915)**

13A (11B). With 18 or more segments with notopodia, lower lip oval, ventro-lateral pads not separated by a large mid-ventral groove…… ***P. glasbyi*** **Lavesque, Hutchings, Daffe & Londoño-Mesa, 2020 (Lavesque *et al.* 2020b)**
13B. Fewer than 18 segments with notopodia, lower lip oblong, ventro-lateral pads separated by a large midventral groove…….. ***P. readi*** **Lavesque, Hutchings, Daffe & Londoño-Mesa, 2020 (Lavesque *et al.* 2020b)**

14A (8C). With 16 or more segments with notopodia……**15**
14B. Fewer than 16 segments with notopodia……**17**

15A (14A). Neuropodia beginning from SG XIV–XVI…… **16**
15B. Neuropodia beginning from SG XVIII–XX…… ***P. plumosus*** **(Wollebaek, 1912) (Wollebaek 1912)**

16A (15A). Upper lip elongated, uncini with a main tooth above the main fang, ventro-lateral pads well developed …… ***P. nogueirai*** **Lavesque, Hutchings, Daffe & Londoño-Mesa, 2020 (Lavesque *et al.* 2020b)**
16B. Upper lip semicircular, uncini without a main tooth above the main fang, ventro-lateral pads poorly defined…… ***P. arcticus*** **Sars, 1865 (Sars 1865)**

17A (14B). Neuropodia beginning from SG XIV, uncini with four teeth above the main fang arranged in single vertical series; lower lip large, shield-like, wider than long……. ***P. latidens*** **Eliason, 1962 (Eliason 1962)**
17B. Neuropodia beginning from SG XV or after, secondary teeth of uncini not as above…… **18**

18A (17B). Upper lip trilobed, lower lip subtriangular pointed toward mouth……. ***P. medusa*** **Grube, 1850 (Grube 1850)**
18B. Upper lip with a single median lobe, lower lip not subtriangular……**19**

19A (18B). Upper lip with thick medial lobe, uncini with two small lateral teeth above the main tooth, lower lip rectangular longer than wide…… ***P. catalanensis*** **Lavesque, Hutchings, Daffe & Londoño-Mesa, 2020 (Lavesque *et al.* 2020b)**
19B. Upper lip with elongated triangular medial lobe, uncini with two rows of teeth above the main tooth, lower lip oval and wider than long…….. ***P. pennarbedae*** **Lavesque, Hutchings, Daffe & Londoño-Mesa, 2020 (Lavesque *et al.* 2020b)**

Table 1. European species of Terebellidae s.l., by family, with authorities, if species are type species of the genus, type locality and collections where type specimens are lodged. In red, doubtful records in Europe, probably representing misidentification.

Family	Species	Authority	Type species	Type locality	Type specimens collection
Polycirridae	*Amaeana gremarei*	Lavesque, Hutchings, Daffe & Londoño-Mesa, 2020		Gulf of Lion, France	MNHN /AM
	Amaeana trilobata	(Sars, 1863)	yes	Lofoten Islands, Norway	UZMO
	Hauchiella tribullata	(McIntosh, 1869)	yes	England, UK	NHMUK
	Lysilla loveni	Malmgren, 1866	yes	Bohuslän, Sweden	Probably lost or never designated
	Lysilla nivea	Langerhans, 1884		Madeira, Portugal	Cannot be traced
	Polycirrus arcticus	Sars, 1865		Barents Sea, Spitsbergen	UZMO
	Polycirrus arenivorus	(Caullery, 1915)		Normandy, France	Cannot be traced
	Polycirrus asturiensis	Cepeda & Lattig, 2016		Asturias, Spain	MNCN
	Polycirrus aurantiacus	Grube, 1860		Adriatic Sea, Croatia	MNHB
	Polycirrus catalanensis	Lavesque, Hutchings, Daffe & Londoño-Mesa, 2020		Gulf of Lion, France	MNHN /AM
	Polycirrus denticulatus	Saint-Joseph, 1894		Normandy France	MNHN, doubtful
	Polycirrus elisabethae	McIntosh, 1915		Scotland, UK	NHMUK
	Polycirrus fedorovi	Jirkov & Leontovich in Jirkov, 2001		Arctic Ocean	KGB
	Polycirrus glasbyi	Lavesque, Hutchings, Daffe & Londoño-Mesa, 2020		Arcachon Bay, France	MNHN /AM
	Polycirrus gujanensis	Lavesque, Hutchings, Daffe & Londoño-Mesa, 2020		Arcachon Bay, France	MNHN /AM
	Polycirrus idex	Lavesque, Hutchings, Daffe & Londoño-Mesa, 2020		Corsica Cape, France	MNHN /AM
	Polycirrus latidens	Eliason, 1962		Skagerrak, North Sea	ZMUU / GNM
	Polycirrus medusa	Grube, 1850	yes	Mediterranean Sea, France	MNHN
	Polycirrus nogueirai	Lavesque, Hutchings, Daffe & Londoño-Mesa, 2020		Arcachon Bay, France	MNHN /AM
	Polycirrus norvegicus	Wollebaek, 1912		Drøbak, Norway	UZMO

	Polycirrus pennarbedae	Lavesque, Hutchings, Daffe & Londoño-Mesa, 2020		Southern Brittany, France	MNHN /AM
	Polycirrus plumosus	(Wollebaek, 1912)		Norway	UZMO
	Polycirrus readi	Lavesque, Hutchings, Daffe & Londoño-Mesa, 2020		Corsica Cape, France	MNHN /AM
Telothelepodidae	*Parathelepus collaris*	(Southern, 1914)	yes	Clew Bay, Ireland	Not designated in original description
Terebellidae	*Amphitrite affinis*	Malmgren, 1866		Saguenay Fjord, Canada	SMNH
	Amphitrite cirrata	Müller, 1776	yes	Not stated, but probably Norway or Denmark	Probably lost or never designated
	Amphitrite edwardsii	(Quatrefages, 1866)		Normandy, France	Lost
	Amphitrite fauveli	Jirkov, Ravara & Cunha, 2018		Capbreton Canyon, Spain	NHMUK
	Amphitrite figulus	(Dalyell, 1853)		Scotland, UK	Cannot be traced
	Amphitrite grayi	Malmgren, 1866		Bohuslän, Sweden	SMNH
	Amphitrite groenlandica	Malmgren, 1866		Greenland	SMNH
	Amphitrite rubra	Risso, 1826		Mediterranean Sea, France	Cannot be traced
	Amphitrite rzhavskyi	Jirkov, 2020		Melilla, Morocco	MNCN
	Amphitrite variabilis	(Risso, 1826)		Mediterranean Sea, France	Cannot be traced
	Amphitritides gracilis	(Grube, 1860)	yes	Scilly Isles, UK	MNHB
	Amphitritides kuehlmanni	Arvanitidis & Koukouras, 1995		Euboia Gulf, Greece	MZDAUT
	Artacama proboscidea	Malmgren, 1866	yes	Spitzbergen, Norway	Probably lost or never designated
	Axionice maculata	(Dalyell, 1853)		Scotland, UK	Cannot be traced
	Axionice flexuosa	(Grube, 1860)	yes	Greenland	MNHB
	Baffinia hesslei	(Annenkova, 1924)	yes	Barents Sea	ZIN
	Eupolymnia gili	Lavesque, Daffe, Londoño-Mesa & Hutchings, 2021		Normandy, France	MNHN /AM
	Eupolymnia lacazei	Lavesque, Daffe, Londoño-Mesa & Hutchings, 2021		Gulf of Lion, France	MNHN /AM
	Eupolymnia meissnerae	Lavesque, Daffe, Londoño-Mesa & Hutchings, 2021		Bay of Brest, France	MNHN /AM
	Eupolymnia nebulosa	(Montagu, 1819)		Devon, England, UK	Cannot be traced

	Eupolymnia nesidensis	(Delle Chiaje, 1828)	yes	Gulf of Naples, Italy	Cannot be traced
	Lanassa nordenskioldi	Malmgren, 1866	yes	Spitzbergen, Norway	Probably lost or never designated
	Lanassa venusta	(Malm, 1874)		Sweden	GNM
	Lanice conchilega	(Pallas, 1766)	yes	Netherlands	Probably lost or never designated
	Lanice kellyslateri	Lavesque, Daffe, Londoño-Mesa & Hutchings, 2021		Arcachon Bay, France	MNHN /AM
	Laphania boecki	Malmgren, 1866	yes	Finmark, Norway	SMNH
	Leaena ebranchiata	(M. Sars, 1865)	yes	Norway	UZMO
	Loimia medusa	(Savigny, 1822)	yes	Red Sea	LACM
	Loimia ramzega	Lavesque, Bonifácio, Londoño-Mesa, Le Garrec & Grall, 2017		Northern Brittany, France	MNHN / NMW-Z / CEMUA
	Nicolea venustula	(Montagu, 1819)		Devon, England, UK	Cannot be traced
	Nicolea zostericola	(Örsted, 1844)	yes	Denmark	Probably lost or never designated
	Paramphitrite birulai	Ssolowiew, 1899	yes	White Sea	ZMUB
	Paramphitrite dragovabeci	Lavesque, Daffe, Londoño-Mesa & Hutchings, 2021		Bay of Brest, France	MNHN
	Phisidia aurea	Southward, 1956		Ireland	NHMUK
	Phisidia oculata	(Langerhans, 1880)	yes	Madeira, Portugal	Cannot be traced
	Pista adriatica	Mikac & Hutchings, 2017		Istrian Peninsula, Croatia	AM
	Pista bansei	Saphronova, 1988		NW Pacific	ZIN
	Pista colini	Labrune, Lavesque, Bonifácio & Hutchings, 2019		Gulf of Lion, France	MNHN /AM
	Pista cretacea	(Grube, 1860)		Cres Island, Croatia	Cannot be traced
	Pista cristata	(Müller, 1776)	yes	Kristiansand Fjord, Norway	Probably lost or never designated
	Pista labruneae	Lavesque, Daffe, Londoño-Mesa & Hutchings, 2021		Gulf of Lion, France	MNHN /AM
	Pista mediterranea	Gaillande, 1970		Mediterranean Sea, France	MNHN / USNM
	Pista miosseci	Lavesque, Daffe, Londoño-Mesa & Hutchings, 2021		Bay of Brest, France	MNHN /AM

	Pista mirabilis	McIntosh, 1885		Rio de la Plata, Argentina	Not stated in original description
	Pista sauriaui	Lavesque, Daffe, Londoño-Mesa & Hutchings, 2021		Bay of Brest, France	MNHN /AM
	Pista wui	Saphronova, 1988		Pacific Ocean	Cannot be traced
	Pistella lornensis	(Pearson, 1969)	yes	Scotland, UK	NHMUK
	Pistella rovignensis	Mikac & Hutchings, 2017		Istrian peninsula, Croatia	AM
	Proclea graffii	(Langerhans, 1884)	yes	Madeira, Portugal	Cannot be traced
	Proclea malmgreni	(Ssolowiew, 1899)		White Sea	Probably lost
	Stschapovella tatjanae	Levenstein, 1957		Arctic Ocean, Bering Sea	Cannot be traced
	Terebella banksyi	Lavesque, Daffe, Londoño-Mesa & Hutchings, 2021		Arcachon Bay, France	MNHN /AM
	Terebella lapidaria	Linnaeus, 1767	yes	Mediterranean Sea	Cannot be traced
Thelepodidae	*Euthelepus setubalensis*	McIntosh, 1885	yes	Setúbal, Portugal	NHMUK
	Streblosoma bairdi	(Malmgren, 1866)	yes	Sweden	Probably lost
	Streblosoma cabiochi	Lavesque, Londoño-Mesa, Daffe & Hutchings, 2020		Northern Brittany, France	MNHN /AM
	Streblosoma hutchingsae	Lezzi & Giangrande, 2019		Torre Inserraglio, Italy	MNCN
	Streblosoma intestinale	M. Sars in G.O. Sars, 1872		Oslo Fjord, Norway	UZMO
	Streblosoma lindsayae	Lavesque, Londoño-Mesa, Daffe & Hutchings, 2020		Bay of Biscay, France	MNHN
	Streblosoma nogueirai	Lezzi & Giangrande, 2019		Torre Guaceto, Italy	MNCN
	Streblosoma pseudocomatus	Lezzi & Giangrande, 2019		Mar Grande of Taranto, Italy,	MNCN
	Thelepus cincinnatus	(Fabricius, 1780)	yes	Greenland	Probably lost
	Thelepus corsicanus	Lavesque, Londoño-Mesa, Daffe & Hutchings, 2020		Corsica Cape, France	MNHN /AM
	Thelepus davehalli	Jirkov, 2018		Faroe Islands	KGB / MNCN
	Thelepus japonicus	Marenzeller, 1884		Japan	Cannot be traced
	Thelepus marthae	Jirkov, 2018		Norwegian Sea	KGB / MNCN / ZIN
	Thelepus nucleolata	(Claparède, 1869)		Gulf of Naples, Italy	Cannot be traced
	Thelepus parapari	Jirkov, 2018		Almería, Spain	KGB / MNCN
	Thelepus setosus	(Quatrefages, 1866)		Normandy, France	MNHN

	Thelepus triserialis	(Grube, 1855)		Mediterranean Sea	Cannot be traced
Trichobranchidae	*Octobranchus floriceps*	Kingston & Mackie, 1980		Northern North Sea	NHMUK / NMSE
	Octobranchus lingulatus	(Grube, 1863)	yes	Adriatic Sea, Croatia	MNHB
	Terebellides atlantis	Williams, 1984		New England, USA	AM / USNM
	Terebellides bakkeni	Parapar, Capa, Nygren & Moreira, 2020		Lofoten Islands, Norway	ZMBN / NTNU
	Terebellides bigeniculatus	Parapar, Moreira & Helgason, 2011		Iceland	NMSE / NHMUK / MNCN
	Terebellides bonifi	Lavesque, Hutchings, Daffe, Nygren & Londoño-Mesa, 2019		Gulf of Lion, France	MNHN
	Terebellides ceneresi	Lavesque, Hutchings, Daffe, Nygren & Londoño-Mesa, 2019		Bay of Biscay, France	MNHN
	Terebellides europaea	Lavesque, Hutchings, Daffe, Nygren & Londoño-Mesa, 2019		Bay of Brest, France	MNHN
	Terebellides gentili	Lavesque, Hutchings, Daffe, Nygren & Londoño-Mesa, 2019		Northern Brittany, France	MNHN /AM
	Terebellides gracilis	Malm, 1874		Norway	GNM
	Terebellides gralli	Lavesque, Hutchings, Daffe, Nygren & Londoño-Mesa, 2019		Bay of Brest, France	MNHN /AM
	Terebellides kongsrudi	Parapar, Capa, Nygren & Moreira, 2020		Skagerrak	GNM / ZMBN / NTNU
	Terebellides lilasae	Lavesque, Hutchings, Daffe, Nygren & Londoño-Mesa, 2019		Bay of Biscay, France	MNHN /AM
	Terebellides mediterranea	Parapar, Mikac & Fiege, 2013		North Adriatic Sea	PMR / MNCN
	Terebellides norvegica	Parapar, Capa, Nygren & Moreira, 2020		Roagland, Norway	ZMBN /NTNU / GNM
	Terebellides parapari	Lavesque, Hutchings, Daffe, Nygren & Londoño-Mesa, 2019		Bay of Biscay, France	MNHN /AM
	Terebellides resomari	Lavesque, Hutchings, Daffe, Nygren & Londoño-Mesa, 2019		North Sea, France	MNHN /AM
	Terebellides ronningae	Parapar, Capa, Nygren & Moreira, 2020		Norway	ZMBN
	Terebellides scotica	Parapar, Capa, Nygren & Moreira, 2020		Scotland, UK	ZMBN
	Terebellides shetlandica	Parapar, Moreira & O'Reilly, 2016		between Shetland Islands and Norway	NMSE /NHMUK / MNCN

	Terebellides stroemii	Sars, 1835	yes	Bergensfjord, Norway	UZMO
	Trichobranchus demontaudouini	Lavesque, Hutchings, Daffe, Nygren & Londoño-Mesa, 2019		Bay of Biscay, France	MNHN
	Trichobranchus glacialis	Malmgren, 1866	yes	Norway	Probably lost
	Trichobranchus roseus	(Malm, 1874)		Sweden	GNM

Telothelepodidae Nogueira, Fitzhugh & Hutchings, 2013

Figs 3–4

Diagnosis (after Nogueira *et al*. 2018; Hutchings *et al.* 2021a, most important diagnostic characters highlighted in bold). Transverse prostomium attached to dorsal surface of upper lip; basal part as thick crest, eyespots frequently present in one pair of dorso-lateral clusters, each with several rows of eyespots (Fig. 3A); distal part at base of upper lip, frequently **with low or erect mid-dorsal tongue-like process**, fused to upper lip at variable degrees, with free distal lobe(s), or free from the base. Buccal tentacles of two types, short ones thin, uniformly cylindrical, long tentacles stouter and expanded at tips, slightly spatulate (Figs 3A–B, F; 4A). Peristomium forming lips and continuing dorsally at least for short extension, with dorso-lateral nuchal organs at margin with prostomium; lips expanded, **upper lip distinctly elongate and narrow, undulated to convoluted**; swollen lower lip extending across ventrum, cushion-like or segment-like, frequently deeply grooved (Figs 3A–B; 4A). Either SG I or SG II reduced, not forming complete ring in many species. Anterior segments glandular ventrally, smooth, discrete shields absent and frequently with glandular regions poorly developed in comparison to other families of Terebellidae *s.l.*; mid-ventral groove frequently extending from anterior segments. **Two pairs of cirriform branchiae on SG II–III,** each pair with simple thin, curled and relatively short filaments progressively tapering to tips (Figs 3A; 4A), originating from raised crests on anterior margins of SG II and III, or from specialised, apparently glandular, dorso-lateral cushion-like pads occupying from anterior margins to level of posterior bases of notopodia of those segments. Notopodia beginning from SG II or III, usually SG III, extending for at least 15 segments; notopodia as short cones, notochaetae originating from central core on top, distal lobes absent; notochaetae winged, sometimes with bulbous head and alimbate tips (bayonet-like chaetae), at least in anterior row of anterior thoracic segments. **Neuropodia beginning posteriorly to notopodia, usually around SG VIII–XII**; neuropodia in conjunction with **notopodia as sessile tori, as distinctly low pinnules after notopodia terminate; neurochaetae in single row, as avicular uncini** about as long as high, with short triangular heel directed posteriorly, wide and slightly curved base, and dorsal button near mid-length of uncini, but closer to anterior margin (Fig. 4E). Nephridial and genital papillae, if conspicuous, on SG V–VII, posterior to bases of notopodia.

This recent family was described by Nogueira *et al.* (2013) after conducting a comprehensive phylogenetic analysis. The members of this family were previously considered

as Thelepodidae but differ in having a narrow and elongate upper lip, poorly developed neuropodia and anterior segments less glandular ventrally than in other thelepodids. In European waters, this family is represented by a single species, *Parathelepus collaris* (Figs 3A–B, 4A, E; Table 1), characterised by an expanded, tongue-like upper lip, by neuropodia poorly developed and beginning from SG XI.

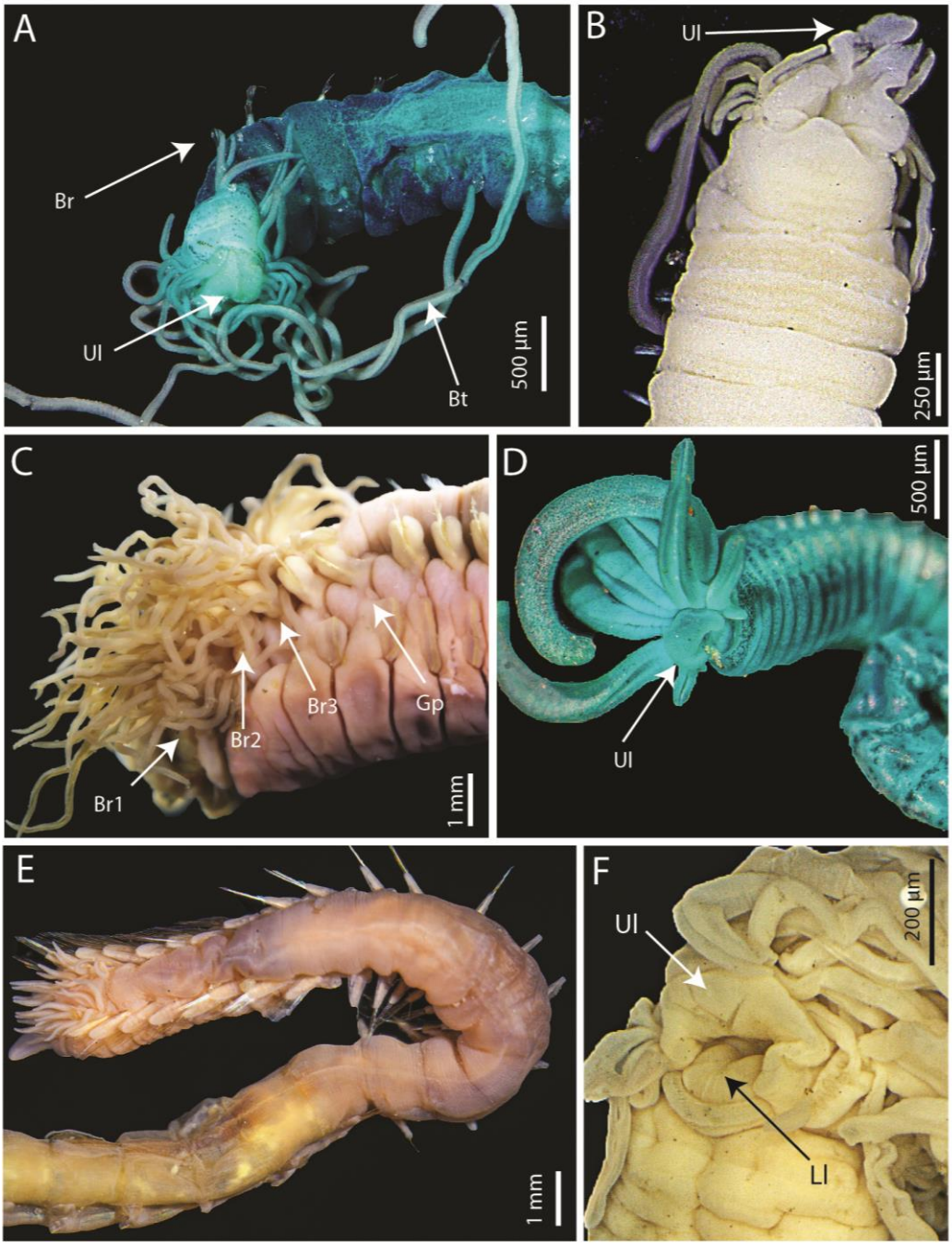

Fig. 3. Diversity of Telothelepodidae and Thelepodidae. **A.** *Parathelepus collaris*, anterior end, frontal view (AM W.53063). **B.** *Parathelepus collaris*, anterior end, ventral view (NHMUK ANEA 1983.1696). **C.** *Thelepus japonicus*, anterior end, lateral view (AM W.53073). **D.** *Thelepus corsicanus*, anterior end, frontal view (AM W.53068). **E.** *Streblosoma cabiochi*, anterior end, dorsal view (MNHN-IA-Type 2000). **F.** *Thelepus japonicus*, anterior end, ventral view (MNHN-IA-PNT 117). Abbreviations: Br, Branchiae; Bt, Buccal tentacles; Gp, genital papillae; Ll, Lower lip; Ul, Upper lip.

Thelepodidae Hessle, 1917

Figs 1F, 3–4

Diagnosis (after Hutchings *et al.* 2021a, most important diagnostic characters highlighted in bold). Transverse prostomium attached to dorsal surface of upper lip; basal part as thick crest, eyespots frequently present, in short lateral rows, or extending transversely across basal part of prostomium, usually progressively more spaced towards dorsal mid-line, with mid-dorsal gap or not; distal part at base of upper lip short, from nearly indistinct to shelf-like. Buccal tentacles all uniformly thin and cylindrical, to slightly spatulate distally (Figs 3D, F; 4B). Peristomium forming lips, sometimes also complete annulation, with dorso-lateral nuchal organs as ciliated grooves; lips expanded, relatively short upper lip, hood-like, about as long as wide; swollen, button-like, mid-ventral lower lip (Figs 3D, F; 4B, C). Segment 1 usually present all around, frequently with ventral lobe marginal to mouth (Figs 3D, F; 4B–C); **SG II typically with anterior margin as protruding crest**, at least ventrally (Figs 3D–E; 4B, C); lobes on following anterior segments sometimes present. Anterior segments highly glandular ventrally, smooth to highly corrugated between neuropodia within pairs, discrete shields absent (Figs 3D F; 4B); mid-ventral groove frequently extending from anterior segments with notopodia. **Two to three pairs of branchiae**, on SG II–III or II–IV, each pair with **simple thin, curled and relatively short filaments** progressively tapering to tips (Figs 3C, E; 4C), leaving mid-dorsal gap or not between filaments within pairs; branchial filaments originating directly from the body wall or from specialised dorso-lateral cushion-like pads. **Notopodia beginning on SG II–III**, usually extending to mid-body, at least, sometimes until near posterior end; cylindrical to rectangular, distally bilobed notopodia, notochaetae originating between lobes; most taxa with winged notochaetae only, with wings of variable width (Fig. 4D), distally serrated notochaetae sometimes also present; bayonet-like and pinnate chaetae both absent. Neuropodia beginning posteriorly to notopodia, on SG IV–VI, typically on SG V; neuropodia in conjunction with notopodia *as fleshy, swollen ridges, as raised rectangular to cylindrical pinnules after notopodia terminate*; neurochaetae as avicular uncini frequently longer than high, with short triangular heel directed posteriorly, distinctly **curved and wide base**, and dorsal button near anterior margin of uncini, or within anterior third of distance between anterior margin of uncini and base of main fang (Fig. 4F). Nephridial and genital papillae usually present, on SG IV–VII, posterior to bases of notopodia or between parapodial lobes (Fig. 3C).

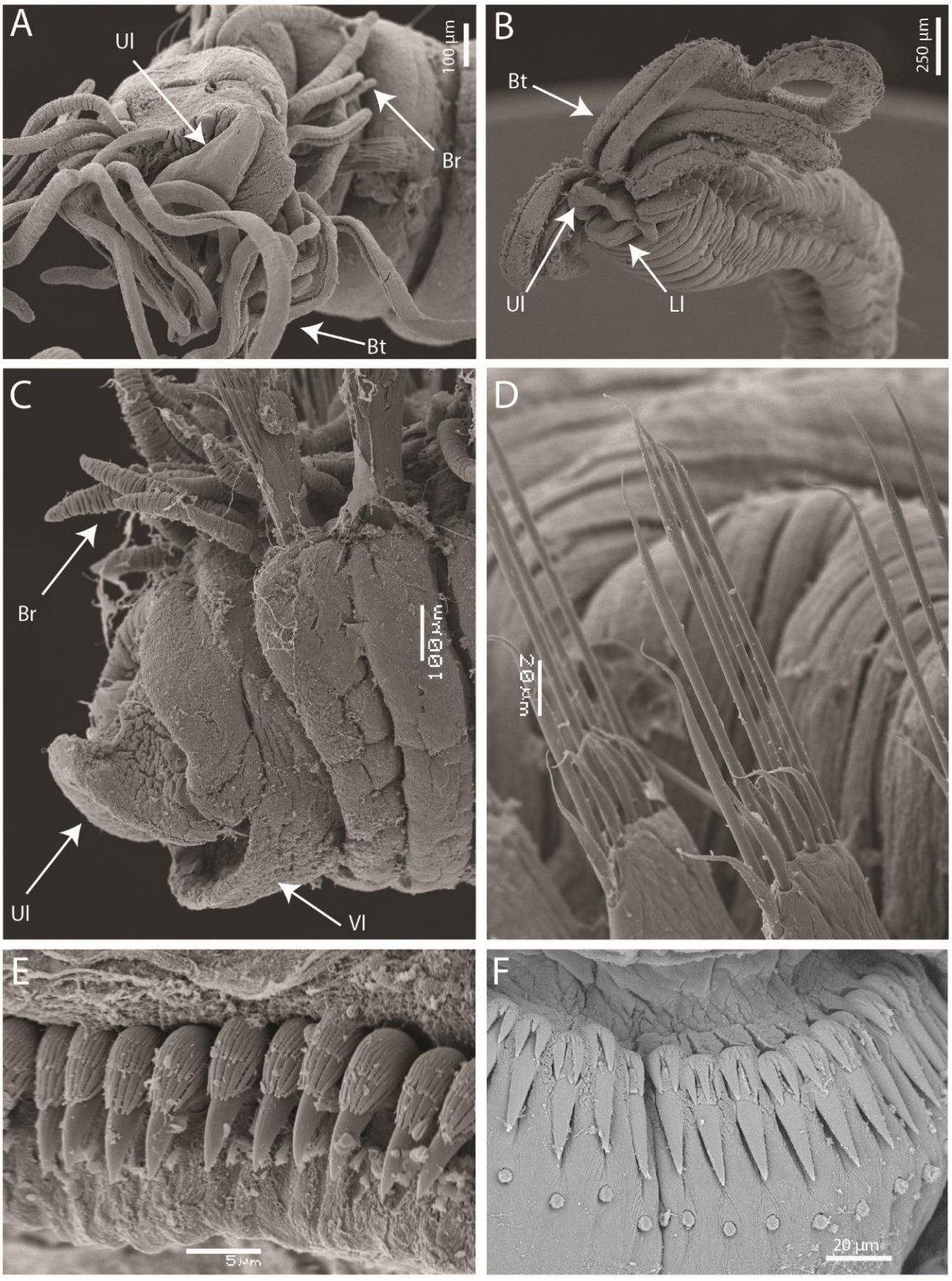

Fig. 4. Diversity of Telothelepodidae and Thelepodidae, SEM. **A.** *Parathelepus collaris*, anterior end, frontal view (AM W.53063). **B.** *Thelepus corsicanus*, anterior end, latero-frontal view (AM W.53069). **C.** *Streblosoma cabiochi*, anterior end, lateral view (AM W.53066). **D.** *Thelepus corsicanus*, thoracic notochaetae (AM W.53069). **E.** *Parathelepus collaris*, abdominal uncini, (AM W.53063). **F.** *Thelepus japonicus*, abdominal uncini, SG48. (SMA-NL-Thele08). Abbreviations: Br, Branchiae; Bt, Buccal tentacles; Ll, Lower lip; Vl, Ventral lobe of SG I.

A comprehensive phylogenetic analysis conducted by Nogueira *et al.* (2013) permitted the elevation of the previous Thelepodinae subfamily to Thelepodidae family level, as they represented a separate clade from other terebellids. This family is represented in European waters by three genera *Euthelepus* McIntosh, 1885 (a single species), *Streblosoma* Sars, 1872 (seven species) and *Thelepus* Leuckart, 1849 (nine species) (Table 1) (Leuckart 1849; Sars 1872; McIntosh 1885). Among these species, *Thelepus japonicus* Marenzeller, 1884, native from Japan, is considered as a non-indigeneous species in French waters, probably introduced with oyster transfers (Marenzeller 1884; Lavesque *et al.* 2020a) (Fig. 3C).

Main morphological characters of European species

Branchiae. Both in *Thelepus* and *Streblosoma* genera, the number of pairs of branchiae varies between two (e.g. *Streblosoma lindsayae* or *Thelepus nucleolata*) and three (e.g. *Streblosoma hutchingsae* or *Thelepus setosus*). Branchiae in Thelepodidae are always cirriform (Figs 3C, E; 4C) but the number of branchial filaments varies among the species with for example 5–10 filaments on the second and third pairs of branchiae for *Streblosoma cabiochi* (Fig. 3E) and only three or less filaments for *Streblosoma intestinale*. Finally, the size of the medial dorsal gap separating the pairs of branchiae is a good diagnostic character. This gap is for example inconspicuous for *T. parapari* and wide for *Thelepus cincinnatus* (Nogueira 2019).

Presence of eyespots. The eyespots are very useful in differentiating species of *Streblosoma* and *Thelepus* for which they can be absent (e.g. *Thelepus davehalli* or *S. hutchingsae*) or present (e.g. *Thelepus corsicanus* or *Streblosoma nogueirai*). Also, the arrangement of the eyespots, if in a continuous line, or leaving a medial gap is of taxonomic importance (Nogueira *et al.* 2010).

Start and extension of notopodia. The segment with the first appearance of notopodia permits the discrimination between the genus *Streblosoma,* for which notopodia begin on the second segment, and *Euthelepus* and *Thelepus* for which it begins on the third segment. These notopodia also extend for a variable number of segments, sometimes present only on the anterior half of the body (e.g. *T. corsicanus*) or present until the end of the body (*T. japonicus*).

Shape of neuropodia and uncini. In most of the species, the uncini start on SGV which could correspond to CH3 (as in *Thelepus*) or CH4 (as in *Streblosoma*). The uncini are arranged habitually in single rows but some have uncini forming loops (C-shaped arrangement) from

mid thorax onwards. This last character is found for example in *S. nogueirai*. Between species, the uncini differ in the development of the prow (e.g. well developed in *T. triserialis*), the shape of the base (e.g. strongly curved in *S. cabiochi*), the position of the dorsal button (e.g. far from anterior margin in *S. bairdi* or in a terminal position for *T. japonicus* (Fig. 1F) and number of secondary of teeth.

Crest and lateral lobes. The presence of lateral lobes on SG II–IV allows the separation of the genus *Euthelepus* from other genera of the family. The presence of lateral crests on SG II (= thick anterior margin) is an important character within the *Streblosoma* genus. For example, *S. cabiochi* has a very low crest on SG II (Fig. 4C) while *S. bairdi* has a protruding crest (Nogueira 2019).

Key to European species of Thelopodidae (after Lavesque *et al.* (2020a))

1A. Notopodia from SG II (i.e. first branchiferous segment), start of uncini from CH4…….. **2 (*Streblosoma*)**
1B. Notopodia from SG III (i.e. second branchiferous segment), start of uncini from CH3……. **8**

2A (1A). Two pairs of branchiae……..……***Streblosoma lindsayae*** **Lavesque, Londoño-Mesa, Daffe & Hutchings, 2020 (Lavesque *et al.* 2020a)**

2B. Three pairs of branchiae…….…… **3**

3A (2B). Uncini arranged in C-shaped loops from mid thorax……..…..**4**
3B. Uncini always in straight rows……..……..……**6**

4A (3A). Notopodia not extending to posterior body……..……**5**
4B. Notopodia until posterior body…… ***Streblosoma pseudocomatus*** **Lezzi & Giangrande, 2019 (Lezzi & Giangrande 2019)**

5A (4A). Eyespots absent…….. ***Streblosoma hutchingsae*** **Lezzi & Giangrande, 2019 (Lezzi & Giangrande 2019)**

5B. Eyespots present…… ***Streblosoma nogueirai*** **Lezzi & Giangrande, 2019 (Lezzi & Giangrande 2019)**

6A (3B). Branchiae on SG III and SG IV with 3 or less filaments on each side…….. ***Streblosoma intestinale*** **M. Sars in G.O. Sars, 1872 (Sars 1872)**
6B. Branchiae on SG III and SG IV with 5–10 filaments on each side…….. **7**

7A (6B). Absence of prostomial process, presence of lateral crest on SG II, absence of branchial cushion…… ***Streblosoma cabiochi*** **Lavesque, Londoño-Mesa, Daffe & Hutchings, 2020 (Lavesque *et al.* 2020a)**

7B. Presence of prostomial process, absence of lateral crest on SG II, presence of branchial cushion…….. ***Streblosoma bairdi*** **(Malmgren, 1866) (Malmgren 1866)**

8A (1B). Lateral lobes on SG II–IV…… ***Euthelepus setubalensis*** **McIntosh, 1885 (McIntosh 1885)**
8B. Lateral lobes on SG I only…….. **9 (*Thelepus*)**

9A (8B). Two pairs of branchiae…… **10**
9B. Three pairs of branchiae…….. **15**

10A (9A). Uncini in a single row throughout……..…**11**
10B. Uncini in loops from SG XIV….. ***Thelepus nucleolata*** **(Claparède, 1870) (Clarapède 1870)**

11A (10A). Notopodia present on 50–66% of body length…….. **12**
11B. Notopodia present on at least 90% of body length……..…**13**

12A (11A). Eyespots absent…… ***Thelepus davehalli*** **Jirkov, 2018**
12B. Eyespots present…….. ***Thelepus corsicanus*** **Lavesque, Londoño-Mesa, Daffe & Hutchings, 2020 (Lavesque *et al.* 2020a)**

13A (11B). Uncini of CH 1 with one tooth above main fang……**14**
13B. Uncini of CH 1 with two teeth above main fang… ***Thelepus parapari*** **Jirkov, 2018 (Jirkov 2018)**

14A (13A). Eyespots present…… ***Thelepus cincinnatus*** **(Fabricius, 1780) (Fabricius 1780)**
14B. Eyespots absent…….. ***Thelepus marthae*** **Jirkov, 2018 (Jirkov 2018)**

15A (9B). Prow of uncini well developed; notch between the prow and dorsal button of the uncini well marked…… ***Thelepus triserialis*** **(Grube, 1855) (Grube 1855)**
15B. Prow of uncini poorly developed; notch between the prow and dorsal button of the uncini poorly marked…… **16**

16A (15B). Notopodia present on about 60% of the body length…… ***Thelepus setosus*** **(Quatrefages, 1866) (Quatrefages 1866)**

16B. Notopodia present until end of the body length…… ***Thelepus japonicus*** **Marenzeller, 1884 (Marenzeller 1884)**

Terebellidae Johnston, 1846 (*sensu stricto*)

Figs 1C–D, 5–6

Diagnosis (after Hutchings *et al.* 2021a, most important diagnostic characters highlighted in bold). Transverse prostomium attached to dorsal surface of upper lip; basal part as thick crest, eyespots frequently present (Fig. 5B), in short rows at each lateral sides, or extending transversely across basal part of prostomium. Buccal tentacles all usually uniformly cylindrical. Peristomium usually forming lips only; lips expanded, relatively short upper lip, hood-like, about as long as wide; swollen, usually button-like and mid-ventral lower lip. Segment I terminating laterally to ventro-laterally, partially fused to expanded lower lip, or developed, forming lobes of variable extension and position. Lobes on anterior segments frequently present, of variable length, sometimes extending to SGV–VII (Figs 5B–D; 6A–D). Anterior segments highly glandular ventrally, with discrete, smooth to corrugated, rectangular to trapezoidal mid-ventral shields extending from anterior segments until termination of notopodia, or near it; mid-ventral groove extending from termination of mid-ventral shields. **Two to three pairs of branchiae usually present** (Figs 5A–D; 6A–D), but three genera have a single pair and several are abranchiate; branchial filaments originating all together from single point on body wall, on either side of branchiferous segments, unbranched, or, more frequently, originating from conspicuous main stalk on either side of pair, branching from one to several levels, in plumose (spiraled), dichotomous, pectinate or arborescent arrangement. Notopodia beginning on SGII–V, SGIV in most genera, usually extending to mid-body, around SGXX, but sometimes present on fewer segments or extending more posteriorly for variable extension, rarely until near posterior end; first pairs of notopodia inserted dorso-laterally, progressively more laterally, then vertically aligned; cylindrical to rectangular notopodia.

Notochaetae originating from central core on top, distal lobes absent; notochaetae distally winged, wings of variable length and width, or serrate, sometimes with wings at midlength, basally to a serrated blade; some more specialised types of notochaetae may be present (Fig. 5E–G). Neuropodia beginning posteriorly to notopodia, on SGV–IX, usually on SGV; neuropodia in conjunction with notopodia as low, sessile ridges, sometimes continuing posteriorly until pygidium, but most taxa with rectangular to cylindrical or foliaceous neuropodial pinnules after notopodia terminate; neurochaetae as avicular uncini usually as long as high, with short triangular heel directed posteriorly, slightly curved and wide base, and dorsal button (Figs 1C–D; 6E–F); **uncini arranged in double rows** (Fig. 6E) from around SGXI usually until termination of notopodia, but several genera with double rows.

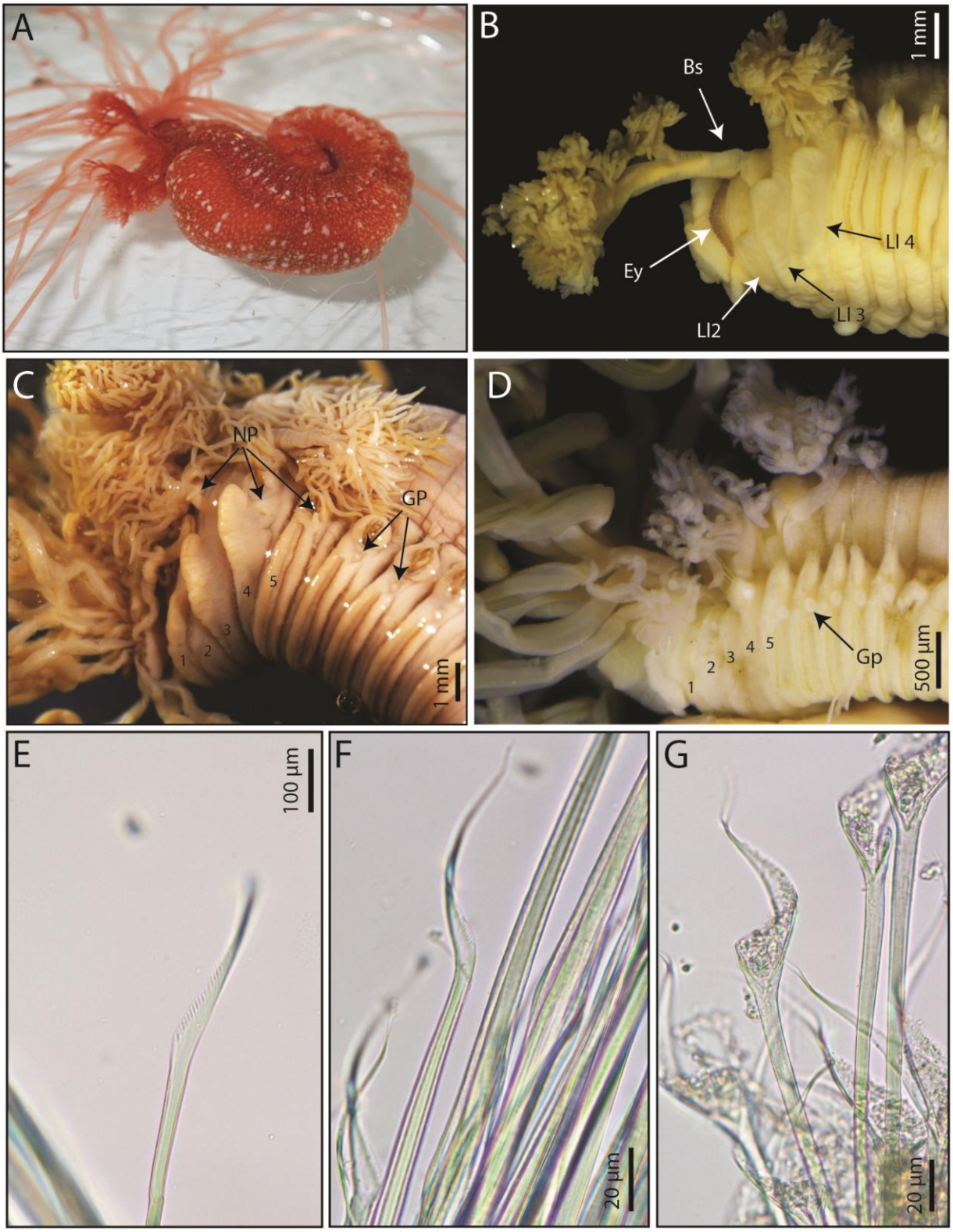

Fig. 5. Diversity of Terebellidae (*s.s.*) **A.** *Eupolymnia lacazei*, live specimen (paratype MNHN-IA-TYPE 2023). B. *Eupolymnia gili*, anterior end, lateral view (holotype MNHN-IA-TYPE 2020). **C.** *Amphitrite edwardsii*, anterior end, lateral view (MNHN-IA-PNT 126). **D.** *Terebella banksyi*, anterior end, lateral view (holotype MNHN-IA-TYPE 2037). **E.** *Paramphitrite dragovabeci*, Notochaeta, SG XI (paratype MNHN-IA-TYPE 2030). **F.** *Terebella* cf. *lapidaria,* Notochaetae, SG IX (MNHN-IA-PNT 131). **G.** *Terebella lapidaria,* notochaetae, posterior segments (MNHN-IA-PNT 131). Abbreviations: Bs, branchial stem ; Ey, eyes ; Gp, genital papillae; Ll, lateral lobes; Np, nephridial papillae. Numbers referring to segments.

In European waters, the Terebellidae *s.s.* are represented by 19 genera and 44 species (Table 1). Four genera are represented only by a single species: *Artacama* Malmgren, 1866; *Baffinia* Wesenberg-Lund, 1950; *Laphania* Malmgren, 1866; *Leaena* Malmgren, 1866 and *Stschapovella* Levenstein, 1957. Eleven of them are represented by two European species each: *Amphitritides* Augener, 1922; *Axionice* Malmgren, 1866; *Lanassa* Malmgren, 1866; *Lanice* Malmgren, 1866; *Loimia* Malmgren, 1866; *Nicolea* Malmgren, 1866; *Paramphitrite* Holthe, 1976; *Phisidia* Saint-Joseph, 1894; *Pistella* Hartmann-Schröder, 1996; *Proclea* Saint-Joseph, 1894 and *Terebella* Linnaeus, 1767 (Linnaeus 1767; Malmgren 1866; Saint-Joseph 1894; Augener 1922; Wesenberg-Lund 1950; Levenstein 1957; Holthe 1976; Hartmann-Schröder 1996; Lavesque *et al.* 2021). The genus *Eupolymnia* Verrill, 1900 is represented by four species and the two most diverse European genera are *Amphitrite* Müller, 1771, with ten species, and *Pista* Malmgren, 1866 with eleven (Müller 1771; Malmgren 1866; Verrill 1900; Lavesque *et al.* 2021). In our recent paper focusing on French Terebellidae *s.s.* we have confirmed the synonymy of *Neoamphitrite* with *Amphitrite*, as suggested by several authors (Jirkov 2020; Hutchings *et al.* 2021a). In contrast, we consider that *Amphitritides*, *Lanice Loimia* and *Paramphitrite* are still valid genera (Read & Fauchald 2021), contrary to what was proposed by Jirkov (2020) (see details in Lavesque *et al.* 2021).

Main morphological characters of European species

Branchiae. The number and shape of branchiae are very important to separate species of Terebellidae *s.s*. Typically, species 2–3 pairs of branchiae are present on SG II–III or II–IV, but members of some genera, as for Polycirridae, completely lack branchiae: *Baffinia*, *Lanassa*, *Laphania*, *Leaena*, *Phisidia* and *Proclea*. *Terebella banksyi* is characterised by having branchiae on discontinuous segments: SG II–III and V (Fig. 5D). Generally branchiae are branching (dichotomous or arborescent), originating dorso-laterally from a main stalk (Figs 5A–D; 6A–D) or a single point on body wall, but some species have multiple unbranching branchial filaments, like *Amphitrite cirrata* or *A. rzhavskyi*. The presence or absence and the size of the branchial stem is important, like in *Eupolymnia* (Figs 5A–B; 6D).

Lobes. Genera of Terebellidae *s.s.* are distinguished from each other by the presence (or absence) and morphology of anterior lobes, usually positioned laterally. These structures are flaps of tissues covering at least part of the preceding segment (Nogueira *et al.* 2010) (Figs 5B–C, 6A–D). They can be absent, as in *Nicolea* or *Terebella*, narrow, as in *Paramphitrite birulai*

or large, as in *Lanice* and *Eupolymnia* (Fig. 5 A–C) and they also vary significantly in morphology and position, from ventral to dorso-lateral (Figs 5B, C; 6A–D).

Nephridial and genital papillae. Terebellids are characterised by the presence of papillae situated close to the notopodia or between parapodial lobes. The nephridial papillae occur from SG III–IV, while genital papillae are present from SG VI onwards and are prominent only when the animals are mature (Fig. 5C–D; 6C). When they are visible, the morphology and the number of these papillae and their number permit the discrimination of species, as for *Amphitrite* or *Terebella* for example.

Notopodia and neuropodia. Terebellidae *s.s.* differ by the number of pairs of notopodia, the segment on which notopodia and neuropodia start and the morphology of both noto- and neurochaetae. Usually, notochaetae are present on 17 segments, beginning from SG IV, but several exceptions exist as for example for *Lanassa* (n<15) or *Terebella* (n>25, often present to the pygidium). Notochaetae of Terebellidae are divided in two types: distally smooth as in *Pista*, *Eupolymnia* or *Lanice*, or distally serrated as in *Amphitritides* or *Paramphitrite* (Fig. 5E), and each types are sub-divided in sub groups (see Table 4, Nogueira *et al.* 2010). Concerning the neurochaetae, each part of the uncinus (Fig. 1C–D) differ greatly among the genera of Terebellidae and their morphology should be examined in detail. For example, members of the genus *Pista* have long-handled uncini, with the handle originating from the heel (Fig. 1C), while uncini in most of the other genera have short-handles. Contrary to tendons which are soft and thin structures attached to uncini, handles are chitinous structures extended from the heel. Members of the genus *Loimia* are unique due to the presence of pectinate uncini, with teeth arranged vertically in a single row (Fig. 1D), while other species have multiple transverse rows of secondary teeth above the main fang (Fig. 6E–G). The dorsal button is generally well developed and situated about midway between the base of the main fang and the tip of the prow, but is inconspicuous in specimens of *Lanice* and can be closer to the tip of the prow, as in *Eupolymnia gili* or the base of the main fang, as for *Artacama proboscidea*. Finally, the prow and the heel vary in shape and can be distally rounded or pointed.

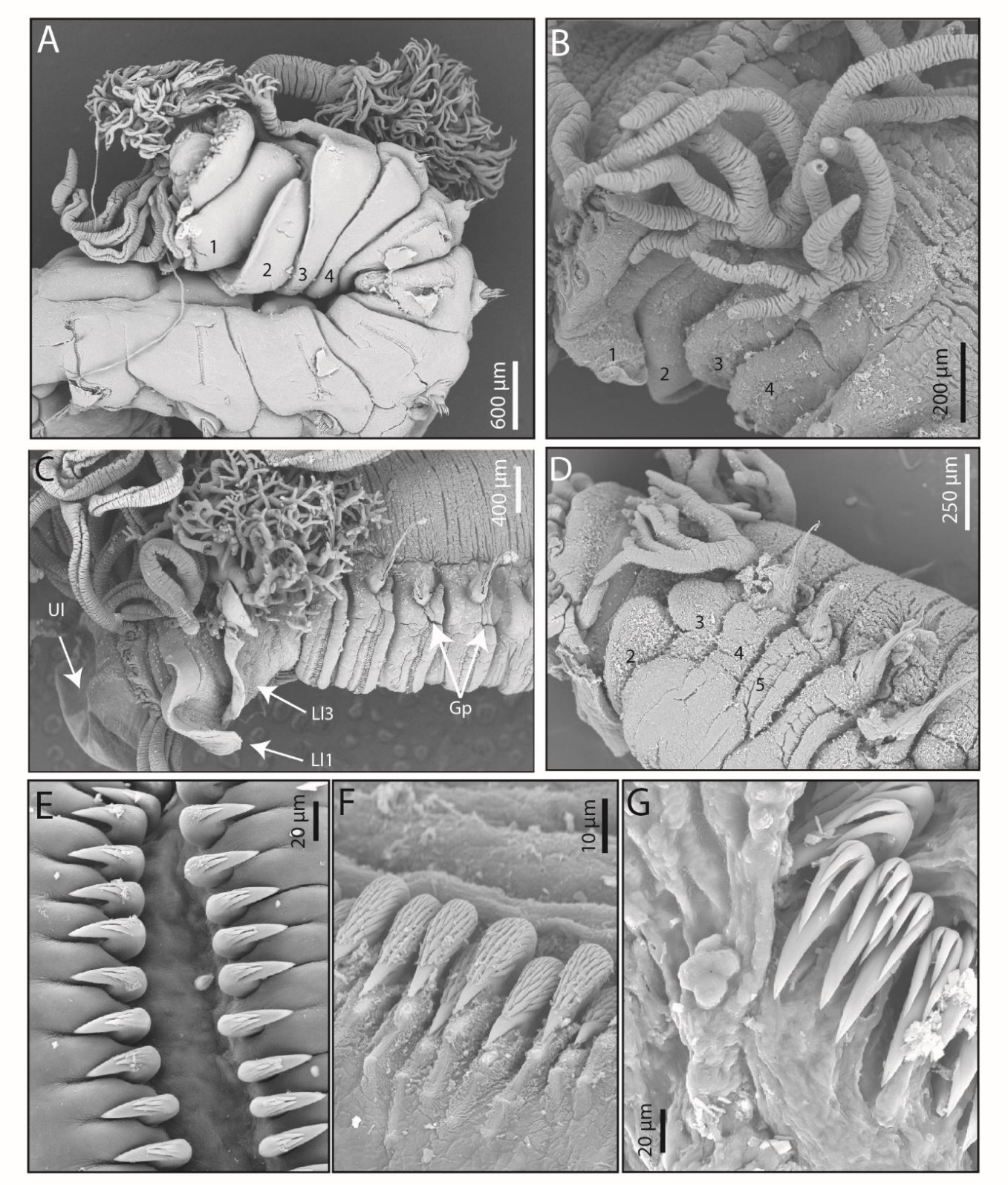

Fig. 6. Diversity of Terebellidae (*s.s.*), SEM. **A.** *Pista sauriaui*, anterior end, lateral view (paratype MNHN-IA-TYPE 2036). **B.** *Paramphitrite dragovabeci*, anterior end, lateral view (paratype MNHN-IA-TYPE 2030). **C.** *Lanice kellyslateri,* anterior end, lateral view **(**paratype MNHN-IA-TYPE 2028). **D.** *Eupolymnia meissnerae,* anterior end, ventro-lateral view (paratype MNHN-IA-TYPE 2025). **E.** *Lanice kellyslateri,* thoracic uncini **(**paratype MNHN-IA-TYPE 2028). **F.** *Paramphitrite dragovabeci*, uncini SG XIV (paratype MNHN-IA-TYPE 2030). **G.** *Eupolymnia meissnerae,* uncini SG VIII (paratype MNHN-IA-TYPE 2025). Abbreviations: Gp, genital papillae; Ll, lateral lobes; Ul, upper lip. Numbers referring to segments.

Key to European species of Terebellidae (*sensu stricto*) (after Lavesque *et al.* (2021)).

1A. Peristomium ventrally forming a large conical process…… ***Artacama proboscidea* Malmgren, 1866 (Malmgren 1866)**

1B. Absence of peristomial ventral process…… **2**

2A (1B). Notochaetae on more than 25 segments, body uniform throughout…… **3**
2B. Notochaetae on 25 or fewer segments, thorax and abdomen clearly defined…… **5**

3A (2A). Branchiae absent…….. ***Baffinia hesslei* (Annenkova, 1924) (Annenkova 1924)**
3B. Branchiae present…… **4 (*Terebella*)**

4A. Branchiae on SG II–IV, five pairs of nephridial and genital papillae……. ***Terebella lapidaria* Linnaeus, 1767 (Linnaeus 1767)**

4B. Branchiae on SG II–III and V, 12 pairs of nephridial and genital papillae…… ***Terebella banksyi* Lavesque, Daffe, Londoño-Mesa & Hutchings, 2021 (Lavesque *et al.* 2021)**

5A (2B). Absence of branchiae…… **6**
5B. Presence of branchiae…… **12**

6A (5A). Uncini from CH2…… **7**
6B. Uncini from CH3…… **11 (*Proclea*)**
6C. Uncini from CH7…… ***Laphania boecki* Malmgren, 1866 (Malmgren 1866)**

7A (6A). Notopodia with two types of notochaetae…… **8**
7B. Notopodia with one type of notochaetae only…… **10**

8A (7A). Notochaetae on 10 segments…… ***Leaena ebranchiata* (Sars, 1865) (Sars 1865)**
8B. Notochaetae on more than 13 segments…… **9 (*Phisidia*)**

9A (8B). Uncini in double rows on about 24 segments, eyespots present …… ***Phisidia oculata* (Langerhans, 1880) (Langerhans 1880)**

9B. Uncini in double rows on 9–10 segments, eyespots absent…… ***Phisidia aurea*** **Southward, 1956 (Southward, 1956)**

10A (7B). Notochaetae on 11 segments…… ***Lanassa venusta*** **(Malm, 1874) (Malm 1874)**
10B. Notochaetae on 15 segments…… ***Lanassa nordenskioldi*** **Malmgren, 1866 (Malmgren 1866)**
10 C. Notochaetae on 16 segments…… ***Stschapovella tatjanae*** **Levenstein, 1957 (Levenstein 1957)**

11A (6B). Ventral lobe of SG II smooth and moderately protruding…… ***Proclea graffii*** **(Langerhans, 1884) (Langerhans 1884)**

11B. Ventral lobe of SG II papillose and clearly protruding..... ***Proclea malmgreni*** **(Ssolowiew, 1899) (Ssolowiew 1899)**

12A (5B). All notochaetae subdistally denticulate…… **13**
12B. Notochaetae smooth…… **26**

13A (12A). Lateral lobes absent…… **14 (*Amphitritides*)**
13B. Lateral lobes present…… **15**

14A (13A). Notochaetae on 17–20 segments; 8 segments with nephridial and genital papillae…… ***Amphitritides gracilis*** **(Grube, 1860) (Grube 1860)**
14B. Notochaetae on 24 segments; 11–13 segments with nephridial and genital papillae…… ***Amphitritides kuehlmanni*** **Arvanitidis & Koukouras, 1995 (Arvanitidis & Koukouras 1995)**

15A (13B). Two pairs of arborescent branchiae, on SG II–III…… **16 (*Paramphitrite*)**
15B. Three pairs of unbranched branchiae, on SG II–IV…… **17 (*Amphitrite*)**

16A (15A). Branchiae separated by a wide dorsal gap, developed lateral lobes on SG II–IV, absence of nephridial papillae on SG IV…… ***Paramphitrite dragovabeci*** **Lavesque, Daffe, Londoño-Mesa & Hutchings, 2021 (Lavesque *et al.* 2021)**

16B. Branchiae without dorsal gap, small lateral lobes on SG II–IV, presence of nephridial papillae on SG IV…… ***Paramphitrite birulai*** **(Ssolowiew, 1899) (Ssolowiew 1899)**

17A (15B). Notopodia present on 17 chaetigers…… **18**
17B. Notopodia present on more than 17 chaetigers…… **23**

18A (17A). Branchiae with simple filaments…… **19**
18B. Branchiae dichotomous…… **21**

19A (18A). Seven pairs of nephridial and genital papillae (SG III and SG VI–XI)…… ***Amphitrite cirrata* Müller, 1771 (Müller 1771)**
19B. Four pairs of nephridial and genital papillae (SG III and SG VI–VIII)…… **20**

20A (19B). Branchiae arising from short stem or directly from body wall… ***Amphitrite fauveli* Jirkov, Ravara & Cunha, 2018 (Jirkov *et al.* 2018)**

20B. Branchiae arising from large and stout stem…… ***Amphitrite rzhavskyi* Jirkov, 2020 (Jirkov 2020)**

21A (18B). Nine pairs of nephridial and genital papillae, on SG III–XI…… ***Amphitrite edwardsi* (Quatrefages, 1866) (Quatrefages 1866)**

21B. Six pairs of nephridial and genital papillae, on SG III–VIII…… **22**

22A (21B). Branchiae with few ramifications, neuropodia of first abdominal segment less than half size of neuropodia of last thoracic segment…….. ***Amphitrite affinis* Malmgren, 1866 (Malmgren 1866)**

22B. Branchiae with many ramifications, neuropodia of first abdominal segment about same size as neuropodia of last thoracic segment…… ***Amphitrite variabilis* (Risso, 1826) (Risso 1826)**

23A (17B). Notopodia present on 19 chaetigers….. ***Amphitrite groenlandica* Malmgren, 1866 (Malmgren 1866)**

23B. Notopodia present on more than 19 chaetigers…… **24**

24A (23B). Notopodia present on 21 chaetigers, 9–10 pairs of nephridial and genital papillae…… ***Amphitrite grayi* Malmgren, 1866 (Malmgren 1866)**
24B. Notopodia present on more than 21 chaetigers, more than 10 pairs of nephridial and genital papillae…… **25**

25A (24B). Notopodia present on first 23–27 chaetigers, 16 pairs of nephridial and genital papillae, uncini in double rows on SGXI–XXV……. ***Amphitrite figulus*** **(Dalyell, 1853) (Dalyell 1853)**

25B. Notopodia present on first 22–24 chaetigers, 13–15 pairs of nephridial and genital papillae, uncini in double rows almost to end of abdomen……. ***Amphitrite rubra*** **(Risso, 1826) (Risso 1826)**

26A (12B). Absence of lateral lobes…… **27 (*Nicolea*)**
26B. Presence of lateral lobes…… **28**

27A (26A). Notochaetae on 15 segments, branchiae with short stems……. ***Nicolea zostericola*** **(Örsted, 1844) (Örsted 1844)**

27B. Notochaetae on 17–18 segments…… ***Nicolea venustula*** **(Montagu, 1819) (Montagu 1819)**

28A (26B). Double rows of uncini in a back to back arrangement …… **29**
28B. Double rows of uncini in a face-to-face or intercalated arrangement…… **32**

29A (28A). Uncini pectinate, with teeth in a single vertical row…… **30 (*Loimia*)**
29B. Uncini avicular, with several transverse rows of secondary teeth…… **31 (*Lanice*)**

30A (29A). Eyespots present, pygidium without distinct papillae, thoracic uncini with 4–5 rows of secondary teeth…… ***Loimia medusa*** **(Savigny, 1822) (Savigny 1822)***
30B. Eyespots absent, pygidium with 14 distinct papillae, thoracic uncini with 6 rows of secondary teeth …… ***Loimia ramzega*** **Lavesque, Bonifácio, Londoño-Mesa, Le Garrec & Grall, 2017 (Lavesque *et al.* 2017)**

31A (29B). Ventral shields fused on SGII–IV, notopodia short, neuropodia as low ridges, upper lip dorsally pigmented…… ***Lanice conchilega*** **(Pallas, 1766) (Pallas 1766)**
31B. Ventral shields well defined on SGIII–IV, notopodia well developed, neuropodia prominent, upper lip without pigmentation…… ***Lanice kellyslateri*** **Lavesque, Daffe, Londoño-Mesa & Hutchings, 2021 (Lavesque *et al.* 2021)**

32A (28B). Notopodia on 15–16 segments, a single pair of short dichotomously branchiae…… **33 (*Axionice*)**
32B. Notopodia on 17 segments…… **34**

33A (32A). Notopodia on 15 segments…… ***Axionice flexuosa*** **(Grube, 1860) (Grube 1860)**
33B. Notopodia on 16 segments…… ***Axionice maculata*** **(Dalyell, 1853) (Dalyell 1853)**

34A (32B). Short-handled avicular uncini throughout…… **35**
34B. Long-handled avicular uncini, at least on anterior neuropodia (i.e. SGV–VII)…… **40 (*Pista*)**

35A (34A). A single pair of plumose branchiae…… **36 (*Pistella*)**
35B. Three pairs of branching branchiae…… **37 (*Eupolymnia*)**

36A (35A). Branchial filaments arranged in distinct tiers, ventral shields on SG II–XV, dorsal crest on SG III…… ***Pistella rovignensis*** **Mikac & Hutchings, 2017 (Mikac & Hutchings 2017)**
36B. Branchial filaments arranged in spiral, ventral shields on SG VI–XX, dorsal crests on SG II–IV…… ***Pistella lornensis*** **(Pearson, 1969) (Pearson 1969)**

37A (35B). Branchiae with long stems…… **38**
37B. Branchial stems short or absent…… **39**

38A (37A). Abdominal neuropodia dorsally pointed, lateral lobes translucent…… ***Eupolymnia gili*** **Lavesque, Daffe, Londoño-Mesa & Hutchings, 2021 (Lavesque *et al.* 2021)**
38B. Abdominal neuropodia rounded, lateral lobes not translucent…… ***Eupolymnia lacazei*** **Lavesque, Daffe, Londoño-Mesa & Hutchings, 2021 (Lavesque *et al.* 2021)**

39A (37B). First pair of branchiae without stem, lateral lobes on SG III bilobed, lateral lobes of SG II small…… ***Eupolymnia nebulosa*** **(Montagu, 1819) (Montagu 1819)**
39B. First pair of branchiae with short stem, lateral lobes on SG III spherical, lateral lobes of SG II well-developed…… ***Eupolymnia meissnerae*** **Lavesque, Daffe, Londoño-Mesa & Hutchings, 2021 (Lavesque *et al.* 2021)**

40A (34B). A single branchia inserted mid-dorsally on SG II…… ***Pista labruneae*** **Lavesque, Daffe, Londoño-Mesa & Hutchings, 2021 (Lavesque *et al.* 2021)**
40B. All branchiae paired…… **41**

41A (40B). One or two pairs of branchiae…… **42**
41B. Three pairs of branchiae…… ***Pista cretacea*** **(Grube, 1860) (Grube 1860)**

42A (41A). One pair of branchiae……**43**
42B. Two pairs of branchiae…… **46**

43A (42A). Absence of lateral lobes on SG II…… ***Pista mirabilis*** **McIntosh, 1885 (McIntosh 1885)***
43B. Presence of lateral lobes on SG II…… **44**

44 (43B). Lateral lobes present on SG I–III, small on SG I and III…… ***Pista bansei*** **Saphronova, 1988 (Saphronova 1988)***
44B. Lateral lobes present on SG II–III, well developed on SG III…… **45**

45A (44B). Lateral lobes well developed on SG II, asymmetrical on SG III…… ***Pista colini*** **Labrune, Lavesque, Bonifácio & Hutchings, 2019 (Labrune *et al.* 2019)**
45B. Lateral lobes narrow on SG II, rectangular on SG III…… ***Pista adriatica*** **Mikac & Hutchings, 2017 (Mikac & Hutchings 2017)**

46A. (42B). Uncini of SG V very high, with a vertical prow…… ***Pista mediterranea*** **Gaillande, 1970 (Gaillande 1970)**
46B. Uncini of SG V with regular size…… **47**

47A (46B). Absence of long-handled uncini on SG X (CH5)…… **48**
47B. Presence of long-handled uncini on SG X…… **49**

48A (47A). Lateral lobes on SGI short, on SGIV long…… ***Pista cristata*** **(Müller, 1776) (Müller 1776)**
48B. Lateral lobes on SGI large, on SGIV very small…… ***Pista sauriaui*** **Lavesque, Daffe, Londoño-Mesa & Hutchings, 2021 (Lavesque *et al.* 2021)**

49A (47B). Lateral lobes on SG I small, on SG IV well developed, eyespots absent..... ***Pista wui*** **Saphronova, 1988 (Saphronova 1988)***
49B. Lateral lobes on SG I absent, on SG IV small, almost inconspicuous, eyespots present…… ***Pista miosseci*** **Lavesque, Daffe, Londoño-Mesa & Hutchings, 2021 (Lavesque *et al.* 2021)**

(*) doubtful record, probably a misidentification

Trichobranchidae Malmgren, 1866

Figs 1A, 7–8

Diagnosis (after Hutchings *et al.* 2021a, most important diagnostic characters highlighted in bold). Transverse prostomium attached to dorsal surface of upper lip; basal part as thick crest, eyespots sometimes present; distal part at base of upper lip or extending along lip. Buccal tentacles of two types, uniformly cylindrical and expanded at tips, spatulate. Peristomium forming lips, sometimes also a ventral lobe, as an extension of the lower lip; lips expanded, circular upper lip, distal margin folded or convoluted; lower lip button-like, usually continuing by ventral lobe, or expanded, forming large scoop-shaped process (Figs 7A–C; 8A, C–D). Segment I usually short, frequently only visible ventrally; anterior margin of anterior segments with lobes as low, even-length collars covering posterior margins of preceding segments, at least ventrally; ventro-lateral or lateral lobes on anterior segments sometimes present. Anterior segments poorly glandular ventrally, smooth, discrete shields absent; mid-ventral groove extending from posterior segments with notopodia. **Two to four pairs of branchiae**, beginning from SGII, each pair with single, thick and elongate, tapered or foliaceous filament, or two pairs fused in single four lobed structure originating mid-dorsally between SGII–III or II–IV (Figs 7C; 8C–D). Notopodia beginning from SGIII–VI, typically terminating at SGXX; short, conical notopodia, chaetae emerging from central core on top, distal lobes absent; narrowly-winged notochaetae in both rows throughout. Neuropodia beginning on same segment as notopodia or slightly posteriorly, rarely beginning before notopodia; sessile neuropodia until termination of notopodia, neurochaetae emerging directly from body wall, as rectangular to foliaceous pinnules after termination of notopodia; thoracic **neurochaetae as acicular uncini** (Figs 1A; 7D; 8F), sometimes with small hood or beard below main fang; avicular abdominal uncini, with secondary teeth in rows on top and laterally to main fang. Nephridial papillae on SGIII usually present, other papillae sometimes present on SGVI and SGVII, but reduced to inconspicuous in most taxa. Pygidium smooth to slightly crenulate, sometimes bilobed.

In the past, the family, the Trichobranchidae family was considered to be a subfamily of Terebellidae (Fauvel 1927, Day 1967, Garrafoni & Lana 2004), but recent phylogenetic analyses support the hypothesis of a valid family (Glasby *et al.* 2004; Nogueira *et al.* 2013). The family includes only three genera, i.e. *Octobranchus* Marion & Bobretzky, 1875,

Terebellides Sars, 1835, and *Trichobranchus* Malmgren, 1866 (Sars, 1835; Malmgren 1866; Marion & Bobretzky 1875). For *Trichobranchus* and *Octobranchus*, only three species of each occur in Europe. The genus *Terebellides* is very speciose and is represented in Europe by 19 species, 13 of them described in the last two years (Lavesque *et al.* 2019a; Parapar *et al.* 2020a) (Table 1).

Main morphological characters for European species

The number of branchiae is the best character to discriminate the different genera, with *Terebellides* having a single large branchia, *Trichobranchus* with two or three pairs of branchiae and finally *Octobranchus* with four pairs.

Trichobranchus species are easy to differentiate based on the number of branchiae (two vs three) (Figs 7C, 8C) and the absence or presence of eyespots. In *Octobranchus*, the species differ by the shape of the branchiae (Fig. 8D) and the number of secondary teeth above the main fang of the uncini. Regarding *Terebellides* species, recent studies highlighted that several characters are very important for identification to the species level (Lavesque *et al.* 2019a; Parapar *et al.* 2020a; 2020b). However, as many cryptic species occur at a small geographical scale (Nygren *et al.* 2018), which currently are confirmed only by molecular analyses (Parapar *et al.* 2020a) much more work needs to be done to resolve all the species present.

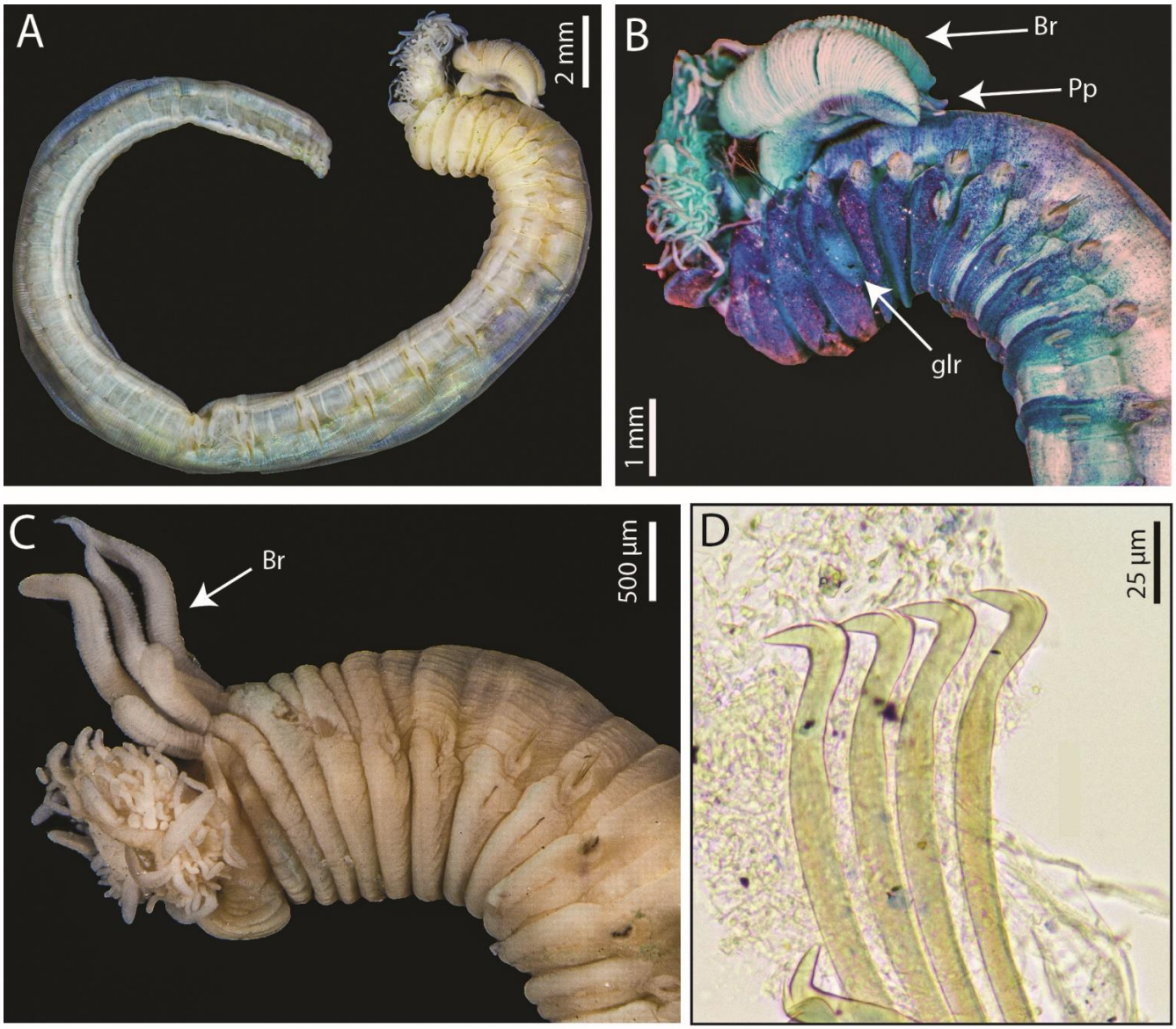

Fig. 7. Diversity of Trichobranchidae. **A.** *Terebellides lilasae*, entire specimen, lateral view (MNHN-IA-TYPE 1879). **B.** *Terebellides lilasae*, anterior end, lateral view, methyl green staining (MNHN-IA-TYPE 1879). **C.** *Trichobranchus glacialis*, anterior end, lateral view (MNHN-IA-PNT 96). **D.** *Terebellides* sp., thoracic acicular uncini (SMA-BR-Terebellides-KER1). Abbreviations: Br, Branchiae; glr, glandular region; Pp, Posterior process.

Branchiae. Even if *Terebellides* branchiae seem to be very similar within the genus (Figs 7A–B, 8A–B), several morphological characters permit the discrimination of species, such as the presence of a fifth anterior branchial lobe (e.g. *T. europaea*), the degree of fusion of both upper and lower lobes (e.g. not fused on *T. ceneresi*), the presence of long terminal filaments (e.g. in *T. shetlandica*) or short posterior processes (Fig. 7B), and finally the presence and the shape of papillae situated on the margins of the branchial lamellae (Fig. 8B) (e.g. *T. lilasae*).

Notochaetae from first chaetiger. The size of notochaetae of the first chaetiger varies between species. For most of the species, these chaetae are of a similar size compared to

those of the following chaetigers. However, they can be absent or much shorter (e.g. *T. ceneresi*) or much longer (e.g. *T. mediterranea*).

Presence of geniculate chaetae on one or two chaetigers. The geniculate chaetae are exclusive to members of *Terebellides* and they are typically present on CH6 (SG VIII) only (Fig. 8E), but in some species they are present on two chaetigers, as for example in *T. bigeniculatus*.

Uncini denticulation. The different types of uncini follow the classifications provided by Parapar *et al*. (2020b) for thoracic uncini (Fig. 8F) and Parapar *et al.* (2020a) for abdominal uncini. These classifications are based on the ratio between the length of the main fang (rostrum) and the crest of secondary teeth (capitium), and the size and number of the secondary teeth.

Thoracic ciliated papillae. Following the recent study of Parapar *et al.* (2020a), the absence or the presence of thoracic ciliated papillae allow for the discrimination of *Terebellides* species. These papillae are situated dorsally to the thoracic notopodia (see for example Parapar *et al.* 2020a, Fig. 7B).

Methyl green pattern. The colouration of *Terebellides* specimens prior to identification is essential. Indeed, MG staining highlights the presence and the shape of the glandular region of the third thoracic chaetiger (e.g. undulating glandular region present and in members of *T. gentili,* oval for *T. lilasae* Fig. 7B)) and the compact/striped pattern of the ventral part of anterior chaetigers (e.g. CH4 (SG VI) white in *T. ceneresi*).

Key to European species of Trichobranchidae (after Lavesque *et al.* (2019a) and Parapar *et al.* (2020a))

1A. One large branchia consisting of a stem and four lobes with transverse lamellae……..**5 (*Terebellides*)**
1B. Two or three pairs of branchiae……..**2 (*Trichobranchus*)**
1C. Four pairs of branchiae……..**4 (*Octobranchus*)**

2A (1B). Two pairs of branchiae……..**3**
2B. Three pairs of branchiae, eyespots present……..…***T. glacialis*** **Malmgren, 1866 (Malmgren 1866)**

3A (2A). Eyespots absent……***T. roseus*** **Malm, 1874**
3B. Eyespots present……***T. demontaudouini*** **Lavesque, Hutchings, Daffe, Nygren & Londoño-Mesa, 2019 (Lavesque *et al.* 2019a)**

4A (1C). Pairs of branchiae of different shapes; abdominal uncini with three rows of secondary teeth above the main fang …… ***O. floriceps*** **Kingston & Mackie, 1980 (Kingston & Mackie 1980)**
4B. All pairs of branchiae similar; abdominal uncini with two rows of secondary teeth above the main fang…… ***O. lingulatus*** **(Grube, 1863) (Grube 1863)**
4C. Bases of branchiae covered by dorso-lateral lobes, abdominal uncini with two rows of secondary teeth above the main fang…… ***O. sikorskii*** **(Leontovich & Jirkov 2001) (Leontovich & Jirkov in Jirkov 2001)**

5A (1A). Geniculate acicular chaetae on CH5 (SG VII) and CH6 (SG VIII)……..……***T. bigeniculatus*** **Parapar, Moreira & Helgason, 2011 (Parapar *et al.* 2011)**

5B. Geniculate acicular chaetae on CH6 (SG VI) only……..…..**6**

6A (5B). Branchial lamellae without marginal papillae……..…**7**
6B. Branchial lamellae with marginal papillae…….…… **15**

7A (6A). Lower branchial lobes with long filaments……..…… **8**
7B. Lower branchial lobes with or without short projections …… **9**

8A (7A). Glandular region on CH3 (SG V) present; branchial lamellae pointed; notochaetae from CH1 longer than following ones; dorsal papillae absent ……***T. parapari*** **Lavesque, Hutchings, Daffe, Nygren & Londoño-Mesa, 2019 (Lavesque *et al.* 2019a)**

8B. Glandular region on CH3 (SG V) absent; branchial lamellae rounded; all notochaetae equal-sized; dorsal papillae present……***T. shetlandica*** **Parapar, Moreira & O'Reilly, 2016 (Parapar *et al.* 2016)**

9A (7B). Ventral white band present on CH4 (SG VI) after MG staining ……**10**
9B. No distinct pattern on CH4 (SG VI) after MG staining……..…**11**

10A (9A). Large species (>30 mm); 5th branchial lobe present; notochaetae of CH1 (SG III) similar to following ones; main fang of thoracic uncini straight…***T. gracilis*** **Malm, 1874 (Malm 1874)**
10B. Small species (<20 mm); 5th branchial lobe absent; notochaetae of CH1 (SG III) absent or

shorter than following ones; main fang of thoracic uncini 'eagle head' (=curved) shaped……***T. ceneresi*** **Lavesque, Hutchings, Daffe, Nygren & Londoño-Mesa, 2019 (Lavesque *et al.* 2019a)**

11A (9B). First notopodia and notochaetae longer than following ones…… ***T. mediterranea*** **Parapar, Mikac & Fiege, 2013 (Parapar *et al.* 2013)**

11B. First notopodia and notochaetae similar or shorter than following ones……..…**12**

12A (11B). Large-sized species (>50 mm); dorsal rounded projections on CH1–CH5 conspicuous…… **13**
12B. Small-sized species (<20 mm); dorsal rounded projections on CH1– CH5 absent; main fang of thoracic uncini straight…… **14**

13A (12A). Abdominal uncini of type 1 (length of capitium about 0.7 length of the main fang, capitium simple consisting of a few, wide denticles)…… ***T. kongsrudi*** **Parapar, Capa, Nygren & Moreira, 2020 and *T. bakkeni* Parapar, Capa, Nygren & Moreira, 2020 complex (Parapar *et al.* 2020a)**

13B. Abdominal uncini of type 2 (capitium of about same length as main fang, capitium complex composed of a first row of 4(5) denticles and a variable number of teeth in two more rows)…….. ***T. stroemii*** **Sars, 1835 (Sars 1835)**

14A (12B). Glandular region on CH3 (SG V) and 5th branchial lobe both absent……***T. atlantis*** **Williams, 1984 (Williams, 1984) (Williams 1984)**

14B. Glandular region on CH3 (SG V) and 5th branchial lobe both present….***T. gralli*** **Lavesque, Hutchings, Daffe, Nygren & Londoño-Mesa, 2019 (Lavesque *et al.* 2019a)**

15A (6B). Glandular region on CH3 (SG V) rounded or oval……**16**
15B. Glandular region on CH3 (SG V) otherwise……..…**17**

16A (15A). Glandular region on CH3 (SG V) staining in white, branchial lamellae with rounded papillae, CH1–3 without conspicuous dorsal projection……***T. lilasae*** **Lavesque, Hutchings, Daffe, Nygren & Londoño-Mesa, 2019 (Lavesque *et al.* 2019a)**

16B. Glandular region on CH3 (SG V) staining in blue, branchial lamellae with conical papillae, CH1–3 with conspicuous dorsal projection……***T. bonifi*** **Lavesque, Hutchings, Daffe, Nygren & Londoño-Mesa, 2019 (Lavesque *et al.* 2019a)**

17A (15B). Most branchial lamellae with marginal papillae …… **18**
17B. Only anterior branchial lamellae with marginal papillae …… **19**

18A (17A). Branchial lamellae with digitiform papillae, upper lip elongated; MG staining pattern as compact bands from CH 1–5…… ***T. resomari*** **Lavesque, Hutchings, Daffe, Nygren & Londoño-Mesa, 2019 (Lavesque *et al.* 2019a)**

18B. Branchial lamellae with widely spaced, small and elongated digitiform papillae; MG staining pattern leaving white stripes from CH 1–5…… ***T. gentili*** **Lavesque, Hutchings, Daffe, Nygren & Londoño-Mesa, 2019 (Lavesque *et al.* 2019a)**

19A (17B). Thoracic uncini type 1 (main fang vs. capitium length ratio 2(3)/1; capitium with 2(3) large teeth, following ones much smaller)…… ***T. ronningae*** **Parapar, Capa, Nygren & Moreira, 2020 (Parapar *et al.* 2020a)**

19B. Thoracic uncini type 3 (main fang vs. capitium length ratio 1/1; capitium with 4(5) mid-sized teeth, following ones slightly smaller)…… **20**

20A (19A). Deep-water species, mostly found below 200 m deep……***T. norvegica*** **Parapar, Capa, Nygren & Moreira, 2020 (Parapar *et al.* 2020a)**

20B. Shallow-water species, mostly found above 100 m deep…… ***T. europaea*** **Lavesque, Hutchings, Daffe, Nygren & Londoño-Mesa, 2019 and *T. scotica* Parapar, Capa, Nygren & Moreira, 2020 complex (Lavesque *et al.* 2019a; Parapar *et al.* 2020a)**

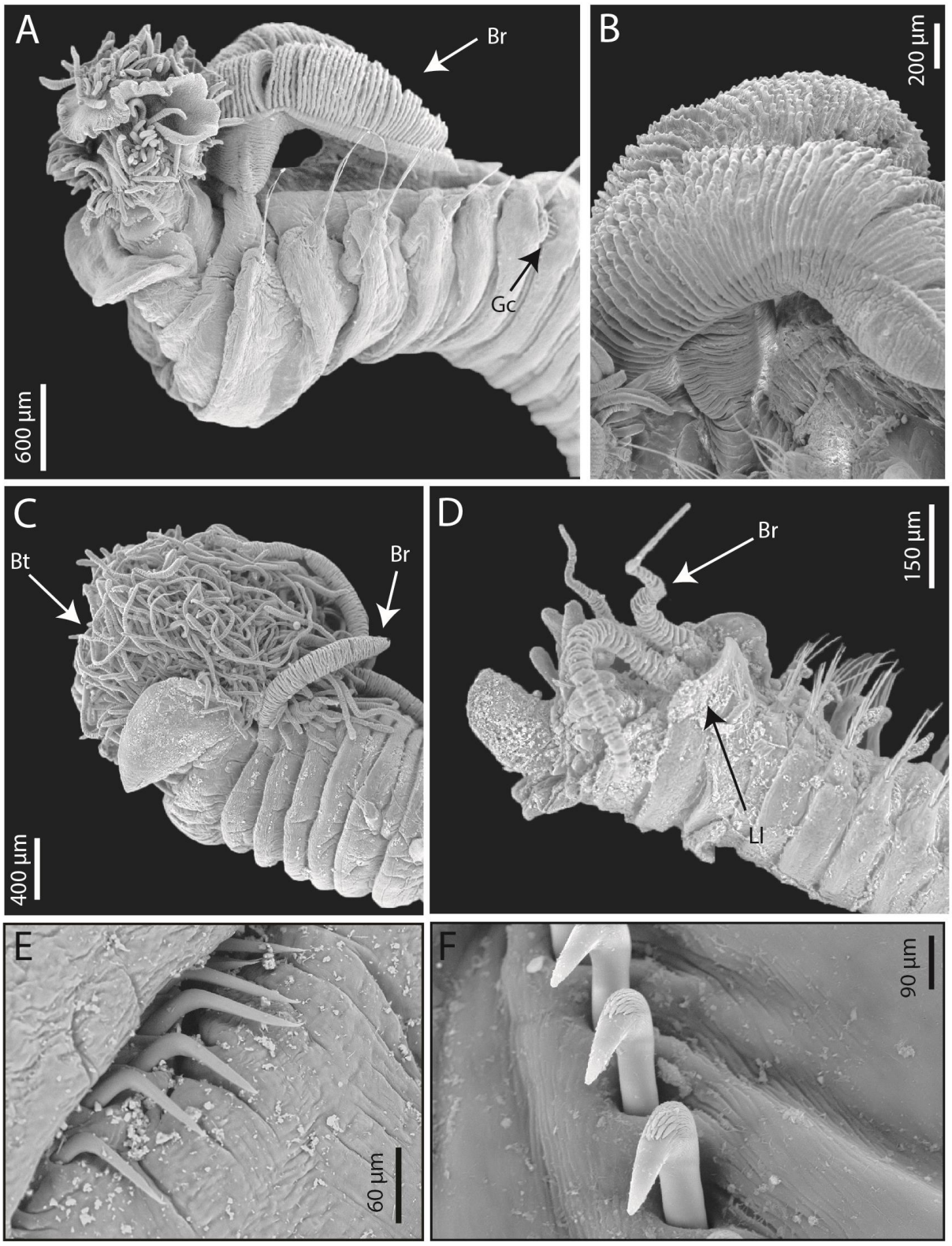

Fig. 8. Diversity of Trichobranchidae, SEM. **A.** *Terebellides gentili*, anterior end, lateral view (MNHN-IA-TYPE 1873). **B.** *Terebellides lilasae*, branchiae, lateral view (MNHN-IA-TYPE 1881). **C.** *Trichobranchus glacialis*, anterior end, lateral view (SMA-BR-Tricho-05). D. Octobranchus lingulatus, anterior end, lateral view (MNHN-IA-PNT 94). **E.** *Terebellides resomari*, geniculate chaetae (paratype MNHN-IA-TYPE 1892). **F.** *Terebellides lilasae*, thoracic uncini (SMA-ARC-Terebellides-VOG8-1). Abbreviations: Br, Branchiae; Bt, Buccal tentacles; Gc, Geniculate chaetae; Ll, Lateral lobes.

Discussion

Why have so many new species been discovered in such well-known waters?

In Europe (Greenland included), 109 valid species had been described since the first description of *Lanice conchilega* by Pallas (1766). Most of these species (i.e. 44) were described by early European taxonomists in the 18th and 19th century, and only a few during the 20th century (12 species). However, only five species were described before the start of this project from French waters: *Amphitrite edwardsii*, *Pista mediterranea*, *Polycirrus arenivorus*, *Polycirrus denticulatus* and *Thelepus setosus*. In addition, four species described from French waters are now considered as *nomen dubium*: *Lanassa proecox* (Saint-Joseph, 1899) which could be a postlarval stage of a known species (Saint-Joseph 1899; Fauvel 1927; Gil 2011), *Polycirrus haematodes* (Claparède, 1864) and *Polycirrus pallidus* (Claparède, 1864) for which no type material exists and the original descriptions are very brief (Claparède 1864; Glasby & Hutchings 2014), and finally *Amphitrite ramosa* Risso, 1826, stated to be indeterminable based on the original description (Risso 1826; Jirkov 2020). Since the start of the Spaghetti Project in 2018, more than 400 specimens were carefully examined and more than 100 molecular sequences obtained. In French coastal waters, 58 species occur, 31 of them described as new during this project. The first question we can ask ourselves is: why? Why have so many new species been discovered in such well-known waters?

How can we explain the quasi-absence of discovery of new species in France for over a century? The first reason is the difficulty to identify known European terebellids. Indeed, as commented on by Hutchings & Lavesque (2020), the lack of literature and type material are especially challenging for taxonomists. Most of the European species were described by earlier workers who failed to designate type specimens and to deposit them in an official collection, or when they did, material is often damaged and unusable (Lavesque *et al.* 2021). Moreover, they provided only approximate type localities and few details on habitat preferences. Thus, comparison between new material and type material is difficult. Referring to original descriptions is not helpful either; they are usually very brief with inadequate figures, and could correspond to several species because of the lack taxonomic details (Hutchings *et al.* 2021a, b).

The second reason, without any mystical connotation, is linked to the spectre of the priest Pierre Fauvel. Actually, the main reference work in polychaetes taxonomy literature is, without any doubt, his “Faune de France” (Fauvel 1923, 1927). These two books are widely

used by taxonomists, ecologists, students and private companies in France but also worldwide (Hutchings & Kupriyanova 2018; Hutchings & Lavesque 2020, Capa & Hutchings 2021). Fauvel was one of the most prolific authors in the history of polychaetes taxonomy with 141 accepted species described, ranking 16th polychaetologist in the world (Pamungkas *et al.* 2019). Surprisingly, he described only four species from French coastal waters as most of his works were focused on fauna from India (e.g. Fauvel 1932) or Africa (e.g. Fauvel 1918). He also described many deep sea species which are stored in the Musée Océanographique de Monaco and were sampled in the European Atlantic Ocean during the "Hirondelle" (1885-1888) and the "Princesse-Alice" (1894-1897) cruises by the Prince Albert 1st (e.g. Fauvel 1913). The specimens examined by Fauvel for his "Faune de France" were collected mainly at low tides or during dredging campaigns, while only some were received from a few colleagues (Fauvel 1923). In comparison, we had the opportunity to examine specimens from a greater variety of habitats, thanks to our RESOMAR colleagues working in eight coastal laboratories along the French coasts. With their help, we were able to compare material from a wide range of habitats, depths, and ecosystems. For example, 12 species were described from maerl (rhodolith) beds in Brittany (Lavesque *et al.* 2019a, 2020a, 2020b, 2021), confirming that this habitat is an important hotspot of biodiversity (Grall & Hall-Spencer 2003; Barbera *et al.* 2003). Moreover, our colleagues also undertook new sampling excursions to obtain fresh material so that we could undertake molecular analyses. These analyses, coupled with morphological observations, permitted us to confirm the existence of many cryptic species belonging to several species complexes such as the "*Terebellides stroemii* complex", "*Pista cristata* complex" or "*Eupolymnia nebulosa* complex" (Lavesque *et al.* 2019a, 2021). Even if, as taxonomists, we work in a similar way to Grube, Malmgren, McIntosh and other early scientists spending hours behind a stereomicroscope, we are fortunate to have access to advanced technologies like high resolution cameras, scanning electron microscopes, molecular laboratories and internet facilities. These technologies help us to find differences or characters that early taxonomists would have missed and easy access to all the available literature.

The third reason is the lack of accurate literature for European waters, which is intimately linked to Fauvel's work. His two volumes of the "Faune de France" were of an excellent standard for his time. But publication was time consuming and costly, and resources were lacking to update his work in subsequent decades. For a long time, to "correctly" identify a terebellid worm from French waters meant using either Fauvel's or Holthe's books. The

latter, more recent work (Holthe 1986) is based on accurate observations (type material when possible), but the diagnoses are very short and do not take into account recent valuable taxonomic characters. Moreover, this work was focused on Scandinavian waters, from Greenland to Great Britain, a large region which differs from French waters and other countries from southern Europe especially with regard to water temperatures. Fauvel's books were widely used for nearly a century in France, in Europe and also in the rest of the world. This wide use was not a big issue for decades as scientists, polychaetes taxonomists in particular, were convinced by the cosmopolitanism of marine worms (Hutchings & Kupriyanova 2018). Kristian Fauchald was the first one to suggest that polychaetes can show interesting biogeographical patterns when properly identified (Fauchald 1984). Recent studies clearly confirmed that species of polychaetes have restricted distributions and this is particularly true for terebellids. Focusing on the genus *Terebellides* in Northern European waters, Nygren *et al.* (2018) identified more than 25 species hidden within the so-called "cosmopolitan" species *Terebellides stroemii*. Most of these species occur only in a restricted area and specific habitat, and two species from Northern Europe are confirmed for French waters: *T. europaea* and *T. scotica* (Lavesque *et al.* 2019a; Parapar *et al.* 2020a).

The final explanation comes from the lack of taxonomic positions in France. This country is known for its famous early taxonomists such as Audouin, Gravier, Quatrefages, Saint-Joseph and Savigny, followed by few more recent ones like Bellan, Bhaud, Gillet, Laubier or Rullier. However, as many parts of the world, the number of taxonomists has dramatically declined in recent years, because taxonomy was not "sexy" or technology-focused enough to attract policy makers attention. As a result, French scientists were almost absent from the international worm community for the last few decades. Indeed, prior to 2016, almost no French taxonomists participated in the different International Polychaete Conferences, with the exception of the conference organized in Angers in 1992. The absence of French representatives on the council of the International Polychaetology Association meetings was also a reality for several years. Fortunately, French marine biologists are now included in the RESOMAR network, allowing for a new dynamic and the recruitment of several technicians and researchers specialised in identification of benthic fauna. The lack of experienced taxonomists acting as mentors in France was compensated by the motivation of these young scientists. During the past decade, they have published numerous papers on French polychaetes taxonomy (e.g. Blake & Lavesque 2017; Bonifácio *et al.* 2015; Jourde *et al.* 2015; Lavesque *et al.* 2015, 2020c; Le Garrec *et al.* 2017) with the fundamental help of international

experts such as Barnich, Blake, Glasby, Hutchings, Meißner, Londoño-Mesa and Parapar among others.

What are the consequences of this hidden biodiversity?

So what difference does it make to know that not only one, but two extremely similar species of *Lanice* exist? Does this hidden diversity really matters? Of course the answer is yes! Of course it is essential to use the appropriate name when identifying a species (Lavesque *et al.* 2019b; Hutchings & Lavesque 2020; Hutchings 2021). Specimens belonging to cryptic species are very similar and thus difficult for people, even for taxonomists, to distinguish. However, as most of these species evolve differently from a common ancestor, their life-traits and their ecological function may be different, or in the process of becoming different. Indeed, in his review on cryptic polychaetes diversity, Nygren (2014) shows that many cryptic species can be distinguished by a number of biological characteristics, such as reproductive biology, life history, feeding biology, salinity, habitat and depth preferences or anoxia and temperature tolerances. Each species has a unique set of micro-habitat requirements and functions with important ecological consequences. Misidentification or an underestimation of the diversity thus have a strong impact on ecological studies.

The sand mason worms, *Lanice conchilega*, is a perfect example to illustrate this point. By aggregating sand particles on its tube, this species acts as ecosystem engineer for forming reef-like structures (Rabaut *et al.* 2009; Hutchings *et al.* 2021b). The presence of these biogenic structures increase habitat quality and enhances local biodiversity by changing hydrodynamics and nature of the shore, increasing habitat stability and oxygen supply, and finally creating heterogeneity in a uniform environment (Van Hoey *et al.* 2008). This habitat is thus very attractive for predators like fishes and foraging waders, and due to its high functional value, this habitat also has high conservation value (Godet *et al.* 2008). By contrast, in Arcachon Bay, the very similar species *L. kellyslateri* has a scattered distributions with worms appearing solitary. Maybe this absence of a “reef structure” could be linked to a specificity of this new species or to the particular environment occurring in this lagoon. These worms from Arcachon Bay may not be attractive for birds and perhaps policy makers would be unlikely to protect this species and its habitat. As we can see, the stakes can be high when considering cryptic species individually.

Another example worth considering is the strawberry worm *Eupolymnia nebulosa*. Experiments conducted on specimens sampled in the Gulf of Lion (Mediterranean Sea) allowed for insights into its feeding mode and tube building (Grémare 1988; Grémare *et al.* 1989; Grémare & Amouroux 1990), its bioturbation activity (Maire *et al.* 2007) and development (Bhaud 1988; Bhaud & Grémare 1988). Another study by Grémare (1986) highlighted that two populations, one from Banyuls-sur-Mer (Gulf of Lion), the second from Dinard (English Channel) had different reproductive modes. However, Lavesque *et al*. (2021) have showed that specimens sampled from Banyuls-sur-Mer belonged to two new species: *E. lacazei* and *Eupolymnia* sp. C. Additionally, specimens from Normandy and Brittany (English Channel) belonged to a third new species: *E. gili*. All these specimens were previously identified as *E. nebulosa,* but clearly belong to three cryptic species. We can therefore observed that these differences in reproductive modes can be linked to different species rather than different populations, as previously suggested by Martin *et al.* (1996). Discovery of multiple species with restricted distributions has implications for conservation. For example, it may be assumed that isolated populations can easily recover from local disasters (oil spill for example) by recruitment from nearby populations. But if it turns out that a species previously thought to be widespread is really several different species, this may have implications for recovery from local perturbations.

Regarding non-indigeneous species (NIS), misidentifications can have a significant impact on the understanding of ecosystems, and cascading consequences for environmental management if they are detected too late. Frequently, exotic species are often morphologically very similar to native species. As they are not reported from European waters, they are absent from identification keys restricted to the local area. It is therefore essential that the most up-to-date and relevant literature is used to identify species for ecological monitoring studies. Even if this is time consuming and expensive, the species which are typically found in an ecosystem should be regularly checked in detail by using a complete diagnosis, and not just by means of outdated keys that will of course give a poor result. Particular attention should be paid to sensitive areas, where NIS are known to occur, such as harbours, marinas and oyster farms. For example to illustrate this problem, using the blood-worm *Marphysa sanguinea* (Montagu, 1813) (Montagu 1813) which was largely reported from Arcachon Bay for decades. However, after a thorough morphological and molecular analysis, a second species, new for science was found, i.e. *Marphysa victori* Lavesque, Daffe, Bonifácio & Hutchings, 2017 (Lavesque et al. 2017b). This discovery may seem anecdotal, but after

extensive investigations, we could confirmed that this species native to South East Asia was probably introduced into the bay via oyster transfers in the 1970's, after mass mortalities of Portuguese oysters (Lavesque *et al.* 2020c). Moreover, *M. victori* is an important economic resource as bait and collected both by recreational and professional fishermen, with about 1 million of worms traded per year (Lavesque *et al.* 2017b), most of them shipped live and sold in Western Mediterranean fishing shops in France (Lavesque *et al.* 2020c). Similarly, the presence of the Asiatic terebellid *Thelepus japonicus* was recently reported for the first time in Europe. Again, its presence in Arcachon Bay and in Normandy is linked to oyster farming with a probable introduction from Japan to Arcachon Bay via oyster transfers and a secondary introduction from Arcachon to Normandy by local transfers (Lavesque *et al.* 2020a). Prior to the Spaghetti project, this species was confused with *Thelepus setosus* originally described from France and therefore absent from European identification keys.

Finally, knowing the exact number of species within a region, or at least the number as close to reality as possible, is fundamental to understanding biodiversity issues. In the context of the extent of the biodiversity crisis, ignoring cryptic species leads to an underestimation of the species richness in the oceans (Bickford *et al.* 2007; Nygren 2014). Describing these cryptic diversity is absolutely fundamental in the context of the biodiversity crisis (Bickford *et al.* 2007). We cannot assess the loss of biodiversity in an anthropogenic context if we do not know how many species really occupy an area. Similarly, we cannot identify areas of endemism, and areas of biological interest, without knowledge of cryptic species. If we just take into account the results of this Spaghetti Project, the biodiversity of terebellids has exploded recently, with 31 new species for French waters. Of course, we know that all these new species are not really new but just overlooked for ages, representing a hidden biodiversity. The alarming message of how much biodiversity has been underestimated must be clearly conveyed to the public, the politicians and the managers. In the same way, we need to know exactly which species live in an ecosystem to evaluate the effects of global change. For example, recent studies tend to prove a "tropicalization" of the Bay of Biscay, with several species belonging to different biological groups (algae, fishes, decapods, molluscs or worms) shifting their northern distribution limit from tropical regions north to the southern part of the Bay of Biscay (Portugal, Spain and South of France) (Lima *et al.* 2007; Arias & Crocetta 2016; Encarnação *et al.* 2019; Schäfer *et al.* 2019). Among these species, at least one of them could become problematic. Indeed, the bearded fireworm *Hermodice carunculata* (Pallas, 1766) (Pallas 1766), originated from West Indies and recently observed in southwestern Iberian Peninsula

(Encarnação *et al.* 2019) can cause severe pain if its stinging chaetae come into contact with human skin.

What remains to be done with these Spaghetti worms?

We, as taxonomists, have the responsibility to share our studies and make sure that our work reaches a wide audience. Scientific papers and international conferences are not sufficient and we should use a variety of media (TV, newspapers, social media and blogs) to communicate our findings (Hutchings 2020). Biodiversity is not restricted to geeks of taxonomy and our mission is to help students, ecologists and other professionals to put the right name on the right animal (Hutchings & Lavesque 2020). We have also to explain to politicians why taxonomy is important to the economy and in biodiversity conservation, especially with regards to zoning plans for marine parks or management of marine pests (Hutchings 2020, 2021). We have to produce easy to use identification keys, which allows people to differentiate species from cryptic complexes if possible. Our keys should be web-based and thus widely available to the wider biological community (Hutchings *et al.* 2021b). We, as experts, should be available to help people to identify or confirm their identifications, especially if those seeking for help come from countries lacking taxonomists and/or accurate literature.

Even if our "Spaghetti Project" permitted the improvement of the knowledge of terebellids from French waters, there is still a lot to be done. Firstly, most of the specimens examined were collected in French coastal waters, with the exception of some worms sampled from the deep Capbreton canyon (Lavesque *et al.* 2019a). The exploration of off-shore deep sea areas should be enhanced in order to have a better understanding of the distribution of these species. Some regions, like the eastern part of the French Mediterranean Sea, were poorly surveyed due to absence of benthic ecologists and samples (i.e. Marseille and Villefranche-sur-mer). This project has highlighted the presence of at least another eight undescribed species in France, based on molecular results. These "orphan" sequences belonged to small or damaged specimens, which were not in good enough condition to be described morphologically. Nygren *et al.* (2018) obtained similar results while working on *Terebellides* from Northern Europe; they obtained sequences belonging to 14 still undescribed species (Parapar *et al.* 2020a). Many more new species probably occur in other parts of Europe where this group was not really studied in detail before, for example in the UK or Italy to name

but a few. As discussed before, due to species having restricted distributions (Nygren e*t al.* 2018), more local studies are needed to give us a better picture of the true biodiversity of the region. Globally, some regions like Australia and Brazil are relatively well studied, leading to descriptions of tens of species (Hutchings *et al.* 2021b), but several regions in the world represent a "taxonomic desert" for terebellids like African, Indian and polar regions (Hutchings *et al.* 2021b; Capa & Hutchings 2021). So this "Spaghetti Project" could provide a blue print for what is needed in other parts of the world.

For the stability of taxonomic nomenclature, it is important to erect neotypes for old European species described by early naturalists. Indeed, most of these species were only subsequently designated as type species of genera, and very often type specimens were not designated or do not exist anymore and original descriptions are very brief according to current standards. During this project, we highlighted this need for several species like *Trichobranchus glacialis* and *Octobranchus lingulatus*, both type species of their genera (Lavesque *et al.* 2019a), *Polycirrus denticulatus* (Lavesque *et al*. 2020b), *Amphitrite edwardsii* and *A. figulus*, *Eupolymnia nebulosa* and *E. nesidenis* (the type species of the genus), *Lanice conchilega* (the type species of the genus), and finally *Pista cristata* (the type species of the genus) which is currently being redescribed (Londoño-Mesa *et al. in prep.;*Lavesque *et al.* 2021) (Fig. 9; Table 1). Obtaining molecular sequences from neotypes is also crucial for future comparison and integrative taxonomy. This ensures that every species will have a modern description based on morphological and molecular tools. Undoubtedly, fixing neotypes will allow taxonomists to describe new species, as they will have a reference point for comparison. When Parapar & Hutchings (2014) designated a neotype for *T. stroemii*, they opened the door to the description of 13 new species of *Terebellides* from Europe, with most of these new species identified in the past as *T. stroemii* (Lavesque *et al*. 2019; Parapar *et al.* 2020a).

To conclude, the collaborative "Spaghetti Project", supported by numerous enthusiastic people was a real success story. We are aware that some areas and habitats along the French coast are under-represented in this study but nonetheless, we are sure that it will facilitate the discovery of additional undescribed species not only in our region, but also in the rest of Europe. This focus on the hidden biodiversity of terebellids can be translated to other parts of the world and also to other families, the estimated number of remaining new polychaetes species being greater than 20 000 (Pamungkas *et al.* 2019; Capa & Hutchings 2021; Magalhães *et al.* 2021). An interesting challenge will now be to develop online user-friendly tools, like the Delta (Coleman et al. 2010) or Xper (Ung et al. 2010) identification keys.

Fig. 9. Type localities of European species for which a neotype is required.

A new volume of the Fauna Iberica collection with a focus on terebellids is also in preparation and coordinated by Julio Parapar. Finally, a "European Terebellids Tour" to sample and erect neotypes of old species should be planned (Figure 9)!

Acknowledgments

We would like to thank the Resomar Benthic Team and all the people involved in the sampling campaigns, surveys and research programs for providing us with the specimens examined in this study. We are very grateful to Ruth Barnich and the second reviewer for their thorough and constructive reviews.

The study was partially funded by the Biodiversity Platform (EPOC laboratory, Arcachon) and generously supported by the Australian Museum, Sydney. Nicolas Lavesque and Guillemine Daffe have received financial support from the French State in the frame of the “Investments for the future” Programme IdEx Bordeaux, reference ANR-10-IDEX-03-02. JMMN receives a productivity grant from Conselho Nacional de Desenvolvimento Científico e Tecnológico (CNPq), level 2, Brazil.

References

Annenkova N.P. 1924. Neues über die Verbreitung einiger Arten der Polychaeten. *Comptes Rendus de l'Académie des Sciences de Russie, Leningrad* 1924 : 125–128.

Arias A. & Crocetta F. 2016. *Umbraculum umbraculum* (Gastropoda: Heterobranchia) spreading northwards: Additional evidence to the "tropicalization" of the Bay of Biscay. *Cahiers de Biologie Marine* 57: 285–206.

Arvanitidis C. & Koukouras A. 1995. *Amphitritides kuehlmanni* sp. nov. (Polychaeta, Terebellidae, Amphitritinae) from the Aegean Sea, with comments on the genus *Amphitritides* Augener. *Ophelia* 40(3): 219–227. https://dx.doi.org/10.1080/00785326.1995.10430587

Augener H. 1922. Über littorale Polychaeten von Westindien. *Sitzungsberichte der Gesellshaft naturforschender Freunde zur Berlin* 1922(3–5): 38–63.

Barbera C., Bordehore C., Borg J.A., Glemarec M., Grall J., Hall-Spencer J.M., De La Huz C., Lanfranco E., Lastra M., Moore P.G., Mora J., Pita M.E., Ramos-Espla A.A., Rizzo M., Sanchez-Mata A., Seva A., Schembri P.J., Valle C. 2003. Conservation and management of northeast Atlantic and Mediterranean maerl beds. *Aquatic Conservation Marine and Freshwater Ecosystems* 13: 65–76. https://doi.org/10.1002/aqc.569

Bhaud M. 1988. Experimental studies of influence of temperature and food available on development rate of *Eupolymnia nebulosa* (Polychaete, Terebellidae). *Journal of Experimental Marine Biology and Ecology* 118: 103–113.

Bhaud M. & Grémare A. 1988. Larval development of the Terebellid Polychaeta *Eupolymnia nebulosa*. *Zoological Scripta* 17: 347–356.

Bickford D., Lohman D.J., Sodhi N.S., Ng P.K.L., Meier R., Winker K., Ingram K.K. & Das I. 2007. Cryptic species as a window on diversity and conservation. *Trends in Ecology and Evolution*, 22: 148–155. https://doi.org/10.1016/j.tree.2006.11.004

Blake J.A. & Lavesque N. 2017. A new species of *Chaetozone* (Polychaeta, Cirratulidae) from the Bay of Biscay offshore France, together with a review of *Chaetozone* species from the North Atlantic and adjacent waters. *Zootaxa* 4312: 565–579. https://doi.org/10.11646/zootaxa.4312.3.10.

Bonifácio P., Lavesque N., Bachelet G. & Parapar J. 2015. *Anobothrus amourouxi* sp. nov., a new species of Ampharetidae (Polychaeta) from the Capbreton Canyon (Bay of Biscay, NE Atlantic Ocean). *Journal of the Marine Biological Association of the United Kingdom*: 961–969. doi:10.1017/S0025315414002094.

Capa M. & Hutchings P. 2021. Annelid Diversity: Historical Overview and Future Perspectives. *Diversity* 13: 129. https://doi.org/10.3390/d13030129.

Caullery M. 1915. Sur les Térébelliens de la sous-famille Polycirridae Malmgr. 1. Délimitation des genres. 11. *Polycirrus arenivorus* n.sp. *Société Zoologique de France Bulletin* 40: 239–248.

Cepeda D. & Lattig P. 2016. A new species of Polycirridae (Annelida: Terebellida) and three new reports for Cantabrian and Mediterranean Seas. *Cahiers de Biologie Marine* 57: 371–387. doi: 10.21411/CBM.A.AE1327D3

Claparède E. 1864. Glanures zootomiques parmi les annélides de Port-Vendres (Pyrénées Orientales). *Mémoires de la Société de Physique et d'Histoire Naturelle de Genève* 17(2): 463–60.

Claparède E. 1870. Les Annélides Chétopodes du Golfe De Naples. Supplément. *Mémoires de la Société de physique et d'histoire naturelle de Genève* 20(2): 365–542.

Coleman C.O., Lowry J.K. & Macfarlane T. 2010. DELTA for Beginners: an introduction into the taxonomy software package DELTA. *ZooKeys* 45: 1–75.

Dalyell J.G. 1853. *The Powers of the Creator displayed in the Creation: or, observations on life amidst the various forms of the humbler tribes of animated nature with practical comments and illustrations*, *volume 2*. John van Voorst. London. https://doi.org/10.5962/bhl.title.10022

Day J.H. 1967. *A monograph on the Polychaeta of Southern Africa. Part 2. Sedentaria*. Trustees of the British Museum (Natural History), London.

Eliason A. 1962. Die Polychaeten der Skagerak-Expedition 1933. *Zoologiska bidrag från Uppsala* 33: 207–293.

Encarnação J., Morais P., Baptista V., Cruz J. & Teodósio M.A. 2019. New Evidence of Marine Fauna Tropicalization off the Southwestern Iberian Peninsula (Southwest Europe). *Diversity* 2019, 11, 48. doi:10.3390/d11040048

Fabricius O. 1780. *Fauna Groenlandica, systematice sistens, Animalia Groenlandiae occidentalis hactenus indagata, quoad nomen specificum, triviale, vernaculumque synonyma auctorum plurium, descriptionem, locum, victum, generationem, mores, usum, capturamque singuli prout detegendi occasio fuit, maximaque parte secundum proprias observations*. Impensis Ioannis Gottlob Rothe, Hafniae (Copenhagen) et Lipsiae (Leipzig).

Fauchald K. 1984. Polychaete distribution patterns, or: can animals with Palaeozoic cousins show large-scale geographical patterns? *In:* Hutchings P. (ed.) *Proceedings of the First*

International Polychaete Conference', July 1983, Sydney, Australia: 1–6. The Linnean Society of New South Wales: Sydney.

Fauvel P. 1913. Quatrième note préliminaire sur les polychètes provenant des campagnes de l'Hirondelle et de la Princesse-Alice, ou déposées dans la Musée océanographique de Monaco. *Bulletin de l'Institut Océanographique* 270: 1–80.

Fauvel P. 1918. Annélides polychètes nouvelles de l'Afrique Orientale. *Bulletin du Muséum d'Histoire Naturelle* 24: 503–509.

Fauvel P. 1923. *Polychètes Errantes.* Faune de France 5, Lechevalier, Paris.

Fauvel P. 1927. *Polychètes Sédentaires. Addenda aux Errantes, Archiannélides, Myzostomaires*. Faune de France 16, Lechevalier, Paris.

Fauvel P. 1932. Annelida Polychaeta of the Indian Museum, Calcutta. *Memoirs of the Indian Museum* 12: 1–262.

Gaillande D. 1970. Une polychète Terebellidae nouvelle des côtes de Provence : *Pista mediterranea* n. sp. *Téthys* 2(2): 443–448.

Garraffoni A.R.S. & Lana P.C. 2004. Cladistic analysis of Trichobranchinae (Polychaeta; Terebellidae). *Journal of the Marine Biological Association of the United Kingdom* 84: 973–982.

Gil J.C. 2011. *The European Fauna of Annelida Polychaeta*. PhD Thesis. University of Lisbon, Portugal.

Glasby C.J. & Hutchings P. 2014. Revision of the taxonomy of *Polycirrus* Grube, 1850 (Annelida: Terebellida: Polycirridae). *Zootaxa* 3877: 1–117. https://doi.org/10.11646/zootaxa.3877.1.1

Glasby C.J., Hutchings P. & Hall K. 2004. Assessment of monophyly and taxon affinities within the polychaete clade Terebelliformia (Terebellida). *Journal of the Marine Biological Association of the United Kingdom* 84: 961–971.

Grall J. & Hall-Spencer J.M. 2003. Problems facing maerl conservation in Brittany. *Aquatic Conservation Marine and Freshwater Ecosystems* 13: 55–64. DOI: 10.1002/aqc.568.

Grémare A. 1986. A comparative study of the reproductive energetics of two populations of the terebellid polychaete *Eupolymnia nebulosa* (Montagu) with different reproductive modes. *Journal of Experimental Marine Biology and Ecology* 96: 287–302. https://doi.org/10.1016/0022-0981(86)90208-X

Grémare A. 1988. Feeding, tube-building and particle-size selection in the terebellid polychaete *Eupolymnia nebulosa*. *Marine Biology* 97: 243–252.

Grémare A. & Amouroux J.M. 1990. Feeding responses of the tentaculate deposit-feeder *Eupolymnia nebulosa* (Annelida: Polychaeta): Influence of sexual maturity. *Marine Biology* 107: 315–319.

Grémare A., Amouroux J.M. & Amouroux J. 1989. Modelling the ingestion and absorption in *Eupolymnia nebulosa* (Annelida: Polychaeta). *Marine Ecology Progress Series* 54: 239–248.

Grube A.E. 1850. Die Familien der Anneliden. *Archiv für Naturgeschichte Berlin* 1691: 249–364.

Grube A.E. 1855. Beschreibungen neuer oder wenig bekannter Anneliden. *Archiv für Naturgeschichte, Berlin* 21(1): 81–136.

Grube A.E. 1860. Beschreibung neuer oder wenig bekannter Anneliden. Beitrag: Zahlreiche Gattungen. *Archiv für Naturgeschichte Berlin* 26, 71–118.

Grube A.E. 1863. Beschreibung neuer oder wenig bekannter Anneliden. Sechster Beitrag. *Archiv für Naturgeschichte, Berlin* 29: 37–69.

Godet L., Toupoint N., Olivier F., Fournier J. & Retière C. 2008. Considering the Functional Value of Common Marine Species as a Conservation Stake: The Case of Sandmason Worm *Lanice conchilega* (Pallas 1766) (Annelida, Polychaeta) Beds. *AMBIO: A Journal of the Human Environment* 37: 347–355. DOI: 10.1579/07-A-317.1

Hartman O. 1959. Catalogue of the polychaetous annelids of the world. Part II. *Occasional Papers of the Allan Hancock Foundation*, 23: 355–628.

Hartmann-Schröder G. 1996. Annelida, Borstenwürmer, Polychaeta. *Die Tierwelt Deutschlands* 58: 1–648.

Hessle C. 1917. Zur Kenntnis der terebellomorphen Polychaeten. *Zoologiska bidrag från Uppsala* 5: 39–258.

Holthe T. 1976. *Paramphitrite tetrabranchia* gen. et sp. nov. a new terebellid polychaete from western Norway. *Sarsia* 60: 59–62. https://doi.org/10.1080/00364827.1976.10411303

Holthe T. 1986. *Polychaeta, Terebellomorpha*. Marine Invertebrates of Scandinavia 7, Norwegian University Press, Oslo.

Hutchings P. 2020. Major issues facing taxonomy – a personal perspective. *Megataxa* 1: 46–48. https://doi.org/10.11646/megataxa.1.1.9

Hutchings P. 2021. Potential loss of biodiversity and the critical importance of taxonomy- An Australian perspective. *Advances in Marine Biology* 88: 3–15. https://doi.org/10.1016/B978-0-12-824615-3.09986-8

Hutchings P. & Kupriyanova E. 2018. Cosmopolitan species, fact or fashion? A personal perspective. *Zoosymposia*, 19: 151–163. https://doi.org/10.11646/zoosymposia.19.1.16

Hutchings P. & Lavesque N. 2020. I know who you are, but do others know? Why correct scientific names are so important for the biological sciences. *Invertebrate Systematics* 32: 1–9. https://doi.org/10.1071/IS17035

Hutchings P., Nogueira J.M.N. & Carrerette O. 2021a. Terebellidae Johnston, 1846. *In:* Schmidt-Rhaesa A. Hr., Beutel R.G., Glaubrecht M., Kristensen N.P., Prendini L., Purschke G., Richter S., Westheide, W. & Leschen R.Z.E. (eds) *Handbook of Zoology. A Natural History of the Phyla of the Animal Kingdom* 1–64. Walter de Gruyter & Co, Berlin.

Hutchings P., Carrerette O., Nogueira J.M.N.N., Hourdez S. & Lavesque N. 2021b. The Terebelliformia- recent developments, future directions. *Diversity* 13: 60. https://doi.org/10.3390/d13020060

Jirkov I. 2018. Three new species of *Thelepus* Leuckart, 1849 from Europe and a re-description of *T. cincinnatus* (Fabricius, 1780) (Annelida, Terebellidae). *Zookeys* 759: 29–56.

Jirkov I. 2020. Review of the European *Amphitrite* (Polychaeta: Terebellidae) with description of two new species. *Invertebrate Zoology*, 17(4) 311–360. http://dx.doi.org/10.3853/j.0067-1975.40.1988.150

Jirkov I, Ravara A. & Cunha M.R. 2018; *Amphitrite fauveli* sp.n. (Polychaeta: Terebellidae) from the Bay of Biscay and the Gulf of Cadiz (NE Atlantic). *Invertebrate Zoology* 15(1): 85–91. https://doi.org/10.15298/invertzool.15.1.06

Johnston G. 1846. An index to the British Annelides. *Annals and Magazine of Natural History* 1(16): 433–462. https://doi.org/10.1080/037454809495980

Jourde J., Sampaio L., Barnich R., Bonifácio P., Labrune C., Quintino V., Sauriau P.G. 2015. *Malmgrenia louiseae* sp. nov., a new scale worm species (Polychaeta: Polynoidae) from southern Europe with a key to European *Malmgrenia* species *Journal of the Marine Biological Association of the UK* 95: 947–952. 10.1017/S0025315414001878.

Kingston P.F. & Mackie A.S.Y. 1980. *Octobranchus floriceps* sp. nov. (Polychaeta: Trichobranchidae) from the northern North Sea with a re-examination of *O. antarcticus* Monro. *Sarsia* 65: 249–254.

Labrune C., Lavesque N., Bonifácio P. & Hutchings P. 2019. A new species of *Pista* Malmgren, 1866 (Annelida, Terebellidae) from the Western Mediterranean Sea. *Zookeys* 838: 71–83. https:// doi.10.3897/zookeys.838.28634.

Langerhans P. 1880 Die Wurmfauna von Madeira. III. *Zeitschrift für wissenschaftliche Zoologie* 34(1) : 87–143.

Langerhans P. 1884. Die Wurmfauna von Madeira. IV. *Zeitschrift für wissenschaftliche Zoologie* 40 : 247–285.

Lavesque N., Bonifácio P., Meißner K., Blanchet H., Gouillieux B., Dubois S. & Bachelet G. 2015. New records of *Spio symphyta* and *Spio martinensis* ('Polychaeta': Canalipalpata: Spionidae) from Arcachon Bay (France), NE Atlantic. *Marine Biodiversity* 45: 77–86. DOI 10.1007/s12526-014-0230-7

Lavesque N., Bonifácio P., Londoño-Mesa M.H., Le Garrec V. & Grall J. 2017a. *Loimia ramzega* sp. nov., a new giant species of Terebellidae (Polychaeta) from French waters (Brittany,

English Channel). *Journal of the Marine Biological Association of the United Kingdom* 97 (5): 935–942. https://doi.org/10.1017/S0025315417000571

Lavesque N., Daffe G., Bonifácio P. & Hutchings P. 2017b. A new species of the *Marphysa sanguinea* complex from French waters (Bay of Biscay, NE Atlantic) (Annelida, Eunicidae). *ZooKeys* 716: 1–17. https://doi.org/10.3897/zookeys.716.14070

Lavesque N., Hutchings P., Daffe G., Nygren A. & Londoño-Mesa M.H. 2019a. A revision of the French Trichobranchidae (Polychaeta), with descriptions of nine new species. *Zootaxa* 4664 (2): 151–190. https://doi.org/10.11646/zootaxa.4664.2.1

Lavesque N., Daffe G., Grall J., Zanol J., Gouillieux B., Hutchings P. 2019b. Guess who? On the importance of using appropriate name: case study of *Marphysa sanguinea* (Montagu, 1813). *Zookeys* 859: 1–15. https://doi: 10.3897/zookeys.859.34117

Lavesque N., Londoño-Mesa M.H., Daffe G. &. Hutchings P. 2020a. A revision of the French Telothelepodidae and Thelepodidae (Annelida, Terebelliformia), with descriptions of three species and first European record of a non-indigenous species. *Zootaxa* 4810: 305–327. https://doi.org/10.11646/zootaxa.4810.2.4

Lavesque N., Hutchings P., Daffe G. & Londoño-Mesa M.H. 2020b. Revision of the French Polycirridae (Annelida, Terebelliformia), with descriptions of eight new species. *Zootaxa* 4869: 151–186. https://doi.org/10.11646/zootaxa.4869.2.1

Lavesque N., Hutchings P., Abe H., Daffe G., Gunton L.M. & Glasby C.J. 2020c. Confirmation of the exotic status of *Marphysa victori* Lavesque, Daffe, Bonifácio & Hutchings, 2017 (Annelida) in French waters and synonymy of *Marphysa bulla* Liu, Hutchings & Kupriyanova, 2018. *Aquatic Invasions* 15: 355–366.

Lavesque N., Daffe G., Londoño-Mesa M.H. & Hutchings P. (2021). Revision of the French Terebellidae sensu stricto (Annelida, Terebelliformia), with descriptions of nine species. *Zootaxa,* 5038: 1–63. https://doi.org/10.11646/zootaxa.5038.1.1

Le Garrec V., Grall J., Chevalier C., Guyonnet B., Jourde J., C., Lavesque N., Bonifácio P. & Blake J.A. 2017. *Chaetozone corona* (Polychaeta, Cirratulidae) in the Bay of Biscay: a new alien species for the North-east Atlantic waters? *Journal of the Marine Biological Association of the United Kingdom* 97: 433–445. doi:10.1017/S0025315416000540.

Leuckart R. 1849. Zur Kenntnis der Fauna von Island. *Archiv für Naturgeschichte*, *Berlin* 15 (1): 149–208.

Levinsen G.M.R. 1893. Annulata, Hydroidae, Anthozoa, Porifera. *Udbytte af Kanonbaaden "Hauche" togter i de Danske indenfor Skagen i Aarene* 1893: 321–464.

Lezzi M. & Giangrande A. 2019. New species of *Streblosoma* (Thelepodidae, Annelida) from the Mediterranean Sea: *S. pseudocomatus* sp. nov., *S. nogueirai* sp. nov. and *S. hutchingsae* sp. nov. *Journal of Natural History* 52(43-44): 2857–2873. DOI: 10.1080/00222933.2018.1556357.

Linnaeus C. 1767. *Systema Naturae per regna tria naturae, secundum classes, ordines, genera, species, cum characteribus, differentiis, synonymis, locis.* Editio duodecima reformata.

Lima F.P., Ribeiro P.A., Queiroz N., Hawkins S.J. & Santos A.M. 2007. Do distributional shifts of northern and southern species of algae match the warming pattern? *Global Change Biology* 13: 2592–2604. https://doi.org/10.1111/j.1365-2486.2007.01451.x.

Maire O., Duchêne J.C., Amouroux J.M. & Grémare A. 2007. Activity patterns in the terebellid polychaete *Eupolymnia nebulosa* assessed using a new image analysis system. *Marine Biology* 151: 737–749.

Magalhães W.F., Hutchings P., Oceguera-Figuero A., Martin P., Schmelz R.M, Wetzel M.J., Wiklund H., Macioloek N.J., Kawauchi G.Y. & Williams J.D. 2021. Segmented worms (Phylum Annelida): a celebration of twenty years of progress through *Zootaxa* and call for action on the taxonomic work that remains. *Zootaxa* 4979: 190–211. https://doi.org/10.11646/zootaxa.4979.1.18.

Malm A.W. 1874. Annulata i hafvet utmed Sveriges westkust och omkring Göteborg. Göteborgs Königlich vetenskaps - och vitterhetssamhälles handlingar. [Zoologiska observationer. VII.]. *Göteborgs Königlich vetenskaps - och vitterhetssamhälles handlingar* 14: 67–105.

Malmgren A.J. 1866. Nordiska Hafs-Annulater. *Öfversigt af Kongiliga Veteskaps-Akademiens Förhandlingar* 22: 355–410.

Marenzeller E. 1884. Südjapanische Anneliden. II. Ampharetea, Terebellacea, Sabellacea, Serpulacea. *Denkschriften der Akademie der Wissenschaften, Wien* 49 (2): 197–224.

Marion A.F. & Bobretzky N.V. 1875. Étude des Annélides du Golfe de Marseille. *Annales des Sciences Naturelles, Sixième Série* 2: 1–106.

Martin D., Cha J.H. & Bhaud M. 1996. Consequences of oocyte form modifications in *Eupolymnia nebulosa* (Annelida; Polychaeta). *Invertebrate Reproduction & Development* 29: 27–36. https://doi.org/10.1080/07924259.1996.9672492.

Marenzeller E. 1884. Südjapanische Anneliden. II. Ampharetea, Terebellacea, Sabellacea, Serpulacea. *Denkschriften der Akademie der Wissenschaften, Wien* 49: 197–224.

McIntosh W.C. 1869. On the structure of the British nemerteans, and some new British annelids. *Transactions Royal Society of Edinburgh* 25: 249–252.

McIntosh W.C. 1885. Report on the Annelida Polychaeta collected by H.M.S. Challenger during the years 1873-1876. *Report on the Scientific Results of the Voyage of H.M.S. Challenger during the years 1873–76*. *Zoology* 12: 1–554.

McIntosh W.C. 1915. Notes from the Gatty Marine Laboratory, St Andrews. *Annals and Magazine of Natural History Series* 8: 1–58.

Mikac B. & Hutchings P. 2017. One new species of *Pista* Malmgren, 1866 (Annelida: Terebellidae) and one new species of *Pistella* Hartmann-Schröder, 1996 (Annelida:

Terebellidae) from the Adriatic Sea (Mediterranean). *Journal of the Marine Biological Association of the United Kingdom* 97(05): 943–953. https://dx.doi.org/10.1017/s0025315417000868

Montagu G. 1813. Descriptions of several new or rare animals, principally marine, found on the south coast of Devonshire. *Transactions of the Linnean Society of London* 11: 18–21. https://doi.org/10.1111/j.1096-3642.1813.tb00035.x

Montagu G. 1819. Descriptions of five British species of the genus *Terebella*. *Transactions of the Linnean Society of London* 12 (2): 340–344. https://doi.org/10.1111/j.1095-8339.1817.tb00231.x

Müller O.F. 1771. *Von Würmern des süssen und salzigen Wassers*. Mumme & Faber, Copenhagen.

Müller O.F. 1776. *Zoologicae Danicae Prodromus, seu Animalium Daniae et Norvegiae indigenarum characteres, nomina et synonyma imprimis popularium*. Hallageriis. Havniae, Copenhagen.

Nogueira J.M.M. 2019. Redescriptions of *Streblosoma bairdi* (Malmgren, 1866) and *Thelepus cincinnatus* (Fabricius, 1780), based on types and material from type localities. *Zootaxa* 4544 (3): 419– 428. https://doi.org/10.11646/zootaxa.4544.3.7

Nogueira J.M.M., Hutchings P. & Fukuda M.V. 2010. Morphology of terebelliform polychaetes (Annelida: Polychaeta: Terebelliformia), with a focus on Terebellidae. *Zootaxa* 2460: 1–185.

Nogueira J.M.M., Fitzhugh K. & Hutchings P. 2013. The continuing challenge of phylogenetic relationships in Terebelliformia (Annelida: Polychaeta). *Invertebrate Systematics* 27: 186–238. https://doi.org/10.1071/IS12062.

Nogueira J.M.M., Carrerette O., Hutchings P. & Fitzhugh K. 2018. Systematic review of the species of the family Telothelepodidae Nogueira, Fitzhugh & Hutchings, 2013 (Annelida, Terebelliformia), with descriptions of three new species. *Marine Biology Research* 14: 217–257. https://doi.org/10.1080/17451000.2017.1401729.

Nygren A. 2014. Cryptic polychaete diversity: a review. *Zoologica Scripta* 43: 172–183. doi:10.1111/zsc.12044

Nygren A., Parapar J., Pons J., Meißner K., Bakken T., Kongsrud J.A., Oug E., Gaev D., Sikorski A., Johansen R.A., Hutchings P., Lavesque N. & Capa M. 2018. A megacryptic species complex hidden among one of the most common annelids in the North East Atlantic. *Plos One*. https://doi.org/10.1371/journal.pone.0198356.

Örsted A.S. 1844. Zur Classification der Annulaten mit Beschreibung einiger neuer oder unzulänglich bekannter Gattungen und Arten. *Archiv für Naturgeschichte, Berlin* 10(1): 99–112.

Pallas P.S. 1766. *Miscellanea Zoologica quibus novae imprimis atque obscurae animalium species describunture et observationibus iconibusque illustrantur*. Apud Petrum van Cleef, Hague Comitum, 224 pp. http://dx.doi.org/10.5962/bhl.title.69851

Pamungkas J., Glasby C.J., Read G.B. Wilson S.P. & Costello M.J. 2019. Progress and perspectives in the discovery of polychaete worms (Annelida) of the world. *Helgoland Marine Research* 73: 4. https://doi.org/10.1186/s10152-019-0524-z

Parapar J. & Hutchings P. 2014. Redescription of *Terebellides stroemii* (Polychaeta, Trichobranchidae) and designation of a neotype. *Journal of the Marine Biological Association of the United Kingdom* 95: 323–337. https://doi.org/10.1017/S0025315414000903

Parapar J., Moreira J. & Helgason G.V. 2011. Taxonomy and distribution of *Terebellides* (Polychaeta, Trichobranchidae) in Icelandic waters, with the description of a new species. *Zootaxa* 2983: 1–20. https://doi.org/10.11646/zootaxa.2983.1.1

Parapar J., Mikac B. & Fiege D. 2013. Diversity of the genus *Terebellides* (Polychaeta: Trichobranchidae) in the Adriatic Sea with the description of a new species. *Zootaxa* 3691: 333–350. https://doi.org/10.11646/zootaxa.3691.3.3

Parapar J., Moreira J. & O'Reilly M. 2016. A new species of *Terebellides* (Polychaeta: Trichobranchidae) from Scottish waters with an insight into branchial morphology. *Marine Biodiversity* 46 (3): 211–225. doi.org/10.1007/s12526-015-0353-5.

Parapar J., Capa M., Nygren A. & Moreira J. 2020a. To name but a few: descriptions of five new species of *Terebellides* (Annelida, Trichobranchidae) from the North East Atlantic. *Zookeys* 992: 1–58. https://doi: 10.3897/zookeys.992.55977.

Parapar J., Martin D. & Moreira J. 2020b. On the diversity of *Terebellides* (Annelida, Trichobranchidae) in West Africa, seven new species and the redescription of *T. africana* Augener, 1918 stat. prom. *Zootaxa* 4771(1): 1–61. https://doi.org/10.11646/zootaxa.4771.1.1.

Pearson T.H. 1969. *Scionella lornensis* sp. nov., a new terebellid (Polychaeta: Annelida) from the west coast of Scotland, with notes on the genus *Scionella* Moore, and a key to the genera of the Terebellidae recorded from European waters. *Journal of Natural History* 3(4): 509–516. https://doi.org/10.1080/00222936900770441

Polloni P.T., Rowe G.T. & Teal J.M. 1973. *Biremis blandi* (Polychaeta: Terebellidae), new genus, new species, caught by D.S.R.V. “Alvin” in the Tongue of the Ocean, New Providence, Bahamas. *Marine Biology* 20: 170–175.

Quatrefages A. de. 1866. Note sur la Classification des Annélides. *Annales des Sciences Naturelles* 5 : 253–296.

Rabaut M., Vincx M. & Degraer S. 2009. Do *Lanice conchilega* (sandmason) aggregations classify as reefs? Quantifying habitat modifying effects. *Helgoland Marine Research* 63: 37–46. DOI 10.1007/s10152-008-0137-4.

Read, G. & Fauchald, K. (Eds) (2021). World Polychaeta Database. Terebellidae Johnston, 1846. Available from: http://www.marinespecies.org/aphia.php?p=taxdetails&id=982 (accessed 06 October 2021)

Risso A. 1826. *Histoire naturelle des principales productions de l'Europe méridionale et particulièrement de celles des environs de Nice et des Alpes Maritimes*. Volume 4. Levrault, Paris. https://doi.org/10.5962/bhl.title.58984

Saint-Joseph A. 1894. Annélides Polychètes des côtes de Dinard. Troisième Partie. *Annales des Sciences naturelles Zoologie et Paléontologie* 17: 1–395.

Saint-Joseph A. 1899. Annélides polychètes de la rade de Brest et de Paimpol. *Annales des Sciences Naturelles, Zoologie et Paléontologie, Série 8* 10: 161–19 .

Saphronova M.A. 1988. On Cosmopolitan Distribution of *Pista cristata* (Polychaeta, Terebellidae). *Zoologicheskii zhurnal* 67(6) : 888–897.

Sars M. 1835. *Beskrivelser og Iagttagelser over nogle maerkelige eller nye i Havet ved den Bergenske Kyst Levende Dyr af Polypernes, Acalephernes, Radiaternes, Annelidernes og Molluskernes classer, med en kort Oversigt over de hidtil af Forfatteren sammesteds fundne Arter og deres Forekommen*. T. Hallager, Bergen.

Sars M. 1863. Geologiske og zoologiske lagttagelser, anstillede paa en Reise i en Deel af Trondhjems stift i Sommeren 1862. *Nyt magazin for naturvidenskaberne* 12: 253–340.

Sars M. 1865. Fortsatte Bidrag til Kundskaben om Norges Annelider. *Forhandlinger i Videnskabs-Selskabet i Christiania* 1864: 5–20.

Sars G.O. 1872. Diagnoser af nye Annelider fra Christianiaforden, efter Professor M. Sar's efterladte Manuskripter. *Forhandlinger i Videnskabs-Selskabet i Christiania* 1871: 406–417.

Savigny J.C. 1822. Système des annélides, principalement de celles des côtes de l'Égypte et de la Syrie, offrant les caractères tant distinctifs que naturels des Ordres, Familles et Genres, avec la Description des Espèces. *Description de l'Égypte ou Recueil des Observations et des Recherches qui ont été faites en Égypte pendant l'Expédition de l'Armée Française, publié par les Ordres de sa Majesté l'Empereur Napoléon le Grand, Histoire Naturelle, Paris* 1(3): 1–128. https://doi.org/10.5962/bhl.title.66284

Schäfer S., Monteiro J., Castro N., Rilov G. & Canning-Clode J. 2019. *Cronius ruber* (Lamarck, 1818) arrives to Madeira Island: a new indication of the ongoing tropicalization of the northeastern Atlantic. *Marine Biodiversity* 49: 2699–2707. https://doi.org/10.1007/s12526-019-00999-z

Southward E.C. 1956. On some Polychaeta of the Isle of Man. *Annals and Magazine of Natural History Series 12* 9(100): 257–270. https://doi.org/10.1080/00222935608655812

Ssolowiew M. 1899. Polychaeten-Studien I. Die Terebelliden des Weissen Meeres. *Annuaire du Musée Zoologique de l'Académie Impériale des Sciences de St. Pétersbourg* 4(2) : 179–220.

Ung V., Dubus G., Zaragüeta-Bagils R. & Vignes-Lebbe R. 2010. Xper2: introducing e-taxonomy. *Bioinformatics* 26: 703–704. https://doi.org/10.1093/bioinformatics/btp715.

Van Hoey G., Guilini K., Rabaut M., Vincx M. & Degraer S. 2008. Ecological implications of the presence of the tube-building polychaete *Lanice conchilega* on soft-bottom benthic ecosystems. *Marine Biology* 154: 1009–1019.

Verrill A.E. 1879. *Preliminary check-list of the marine invertebrate of the Atlantic coast, from Cape Cod to the Gulf of St. Lawrence*. Tuttle, Morehouse & Taylor, New Haven.

Verrill A.E. 1900. Additions to the Turbellaria, Nemertina, and Annelida of the Bermudas, with a revision of the New England genera and species. *Transactions of the Connecticut Academy of Arts and Sciences* 10: 595–671. https://doi.org/10.5962/bhl.part.7035

Wesenberg-Lund E. 1950. Polychaeta. *Danish Ingolf-Expedition* 4(14): 1–92.

Williams S.J. 1984. The status of *Terebellides stroemi* (Polychaeta; Trichobranchidae) as a cosmopolitan species, based on a worldwide morphological survey, including description of new species. In: Hutchings, P.A. (ed.) *Proceedings of the First International Polychaete Conference, Sydney, Australia, 1984,* 118–142. The Linnean Society of New South Wales, Sydney, Australia.

Wollebæk A. 1912. Nordeuropæiske Annulata Polychaeta 1. Ammocharidae, Amphictenidae, Ampharetidae, Terebellidae og Serpulidae. *Skrifter utgit av Videnskapsselskapet i Kristiana 1911.1. Mathematisk-naturvidenskabelig klasse* 1911 (18): 1–144.

Annexe 3.

Live (stained) benthic foraminifera from the West-Gironde Mud Patch (Bay of Biscay, NE Atlantic): Assessing the reliability of bio-indicators in a complex shelf sedimentary unit.

Fontanier* C.[1, 2, 3], Deflandre B.[1], Rigaud S.[4], Mamo B.[5], Dubosq N.[1], Lamarque B.[1], Langlet D.[6], Schmidt S.[1], Lebleu. P.[1†], Poirier D.[1], Cordier M.-A.[1], Grémare A.[1]

[1]Université de Bordeaux, UMR CNRS 5805 EPOC – OASU, Allée Geoffroy Saint-Hilaire, CS 50023, F-33615 Pessac, France.
[2]FORAM, Study Group, 9 rue des Fauvettes, F-49125 Tiercé, France.
[3]Université d'Angers, 4 boulevard Lavoisier, F-49000 Angers, France.
[4]Université de Nîmes, EA 7352 CHROME, rue du Dr Georges Salan, F-30021 Nîmes, France.
[5]Department of Biology, Macquarie University, North Ryde, NSW, 2109, Australia.
[6]Evolution, Cell Biology and Symbiosis Unit, Okinawa Institute of Science and Technology Graduate University, 1919-1 Tancha, Onna-son, Kunigami-gun, 904-0495, Japan.

**Corresponding author/ Tel: +33 (0)6 21 91 93 48, c.fontanier@foram.eu.com*
ORCID iD: 0000-0003-4849-6634

Article accepté en 2021 dans la revue *Continental Shelf Research*

Abstract

Live (Rose Bengal stained) shelf foraminiferal faunas have been studied at seven stations located along a shore-open ocean transect between 39–69-m depth in the West-Gironde Mud Patch (WGMP) (Bay of Biscay, NE Atlantic) to understand how complex environmental conditions (e.g., organic matter, oxygenation, sedimentary facies) control their ecological patterns (i.e., diversity, faunal composition, standing stock, and microhabitats). To do so, the WGMP was sampled in August 2017, at the end of the succession of phytoplankton blooms occurring in spring and summer. This morpho-sedimentary unit is bathed by well-oxygenated bottom waters and characterized by clay-silt facies containing variably degraded phytodetritus and traces of terrestrial organic matter. Oxygen penetration depth within the sediment is less than 7±3 mm, indicating efficient organic matter in-sediment mineralisation by aerobic respiration. Foraminiferal richness (S) presents relatively moderate values ranging between 15–35 taxa. According to Shannon Index H', foraminiferal diversity tends to increase with water depth. Accordingly, the relative contribution of *Eggerelloides scaber*, the dominant foraminiferal species at all stations, decreases with increased depth and decreased proximity to the coast. The shallowest station (Station 1, 39 m), closest to the shore, is characterised by *E. scaber*, *Quinqueloculina laevigata* and *Ammonia beccarii*, species typical of inner-shelf environments constrained by high-energy hydrodynamics and river discharge. Surficial sediments at Station 1 constitute of winnowed sands depleted in organic carbon. Towards the centre of the WGMP, where clay-silt facies contain variably degraded marine phytodetritus and terrestrial organic compounds, foraminiferal faunas are characterized by *Bulimina aculeata*, *Ammonia falsobeccarrii*, *Nouria polymorphinoides* and *Nonionoides turgidus*. Yet E. scaber remains the most dominant taxon. Deeper stations (>55 m depth) located at the distal part of the mud patch are dominated by *B. aculeata*, *A. falsobeccarrii*, *N. polymorphinoides* and *E. scaber*. Accompanying these taxa are *Bulimina marginata*, *Rectuvigerina phlegeri*, *Nonion faba* and *Paracassidulina neocarinata*, which are typical of mid- and outer-shelf ecosystems enriched in sedimentary organic matter.

Keywords: Benthic foraminifera; West-Gironde Mud Patch, Diversity, Organic matter, Sedimentary environment

1. Introduction

Continental shelves are areas of high primary production, playing a major role in the sequestration and mineralization of organic carbon (Walsh et al., 1981; Hargrave, 1985; Smith and MacKenzie, 1987; Walsh, 1988; Jahnke et al., 1990; Walsh, 1991; Wollast, 1991; Hedges and Keil, 1995; Bauer and Druffel, 1998). Indeed, biogeochemical cycles are exacerbated within the water column and sediments along the continental shelf where rivers deliver large quantities of dissolved nutrients and organic matter into coastal waters (Hedges et al., 1997). Among these nutrients, nitrate and phosphate stimulate the seasonal or perennial appearance of high primary production plumes along the continental shelf, leading to increased export of phytodetritus to the seafloor (Lohrenz et al., 1990; Lohrenz et al., 1997; Dagg and Breed, 2003). Rivers further release large quantities of particulate organic compounds from terrestrial sources and large quantities of freshwater phytoplankton onto continental shelves (Mopper and Degens, 1977; Eppley, 1984; Romankevich, 1984). When not degraded in the water column or exported laterally along continental slopes, this complex particulate organic matter (terrestrial organic matter and exported phytoplankton production) concentrates in muddy environments on continental shelves (e.g., mud belt, mud patch) where it is buried and then variably degraded by diagenetic processes (Froelich et al., 1979; Canfield et al., 1993). The efficiency of organic carbon burial and its final sequestration thus depends on (1) the deposition flux of organic matter at the sediment-water interface, (2) the rate of mineralization in surface sediments, and (3) the hydrosedimentary processes determining benthic biotope architecture (McKee et al., 2004).

The West-Gironde Mud Patch (WGMP) is a perfect example of a shelf environment where organic compounds from various sources (mainly marine phytodetritus) accumulate within fine sediments (Lamarque et al., 2021; Dubosq et al., in press; Dubosq et al., in prep). Together with the South-Gironde Mud Patch, the WGMP constitutes a particular set of morpho-sedimentary units that spread between 30–70 m water depth, covering the gravels and sands of the Northern Aquitaine continental shelf (Bay of Biscay, France) (Lesueur et al., 1996; 2002; Cirac et al., 2000). These muddy patches extend off the two main channels of the Gironde Estuary, the main source of the fine-grained sediments within the WGMP (Fig. 1) (Lesueur et al., 1996). The WGMP comprises of Gironde River silt deposited during flood events, and a smaller portion of inner continental shelf silts and fine sand deposited during periods of high energy (i.e., storms). Due to the complexity of its spatial structure, temporal dynamics and environmental characteristics, the WGMP has been the subject of intense

multidisciplinary investigation for more than ten years (e.g., the BIOMIN project between 2009–2013, the VOG project between 2018–2019, the JERICO-NEXT European project with this study). In combination with geochemical, geophysical, sedimentological and biological analyses, these projects have aimed to describe the mineralization processes of organic compounds in the mudflat, taking into account (1) the activity of the benthic organisms thriving there (e. g. bioturbation, aerobic/anaerobic respiration), by (2) integrating the hydrosedimentary dynamics structuring this morpho-sedimentary unit in space and time, and by (3) trying to define in fine, reliable bio-indicators of the mudflat in all its complexity (Lamarque et al., 2021; Dubosq et al., in press; Dubosq et al., in prep.). Benthic foraminifera constitute relevant proxies for studying present and past marine environments since their faunal communities (diversity, standing stock, microhabitat), their spatial distribution and their temporal dynamics are controlled by numerous physico-chemical parameters including exported organic matter flux, bottom- and pore-water oxygenation and sedimentary substrate (e.g., Gooday, 2003; Murray, 2006; Jorissen et al., 2007). The impact of seasonal phytodetritus input and the role of environmental oxygenation on benthic foraminiferal fauna has already been studied in “La Grande Vasière”, a mud belt located on the outer continental shelf (between 80–130 m deep) northwest of the WGMP (Duchemin et al., 2005; 2008) (Fig. 1). These works have shown that living benthic communities respond to episodic inputs of organic matter related to phytoplankton blooms from spring to autumn. Certain opportunistic species (i.e. *Nonionella iridea*, *Cassidulina carinata* according to the taxonomy of Duchemin et al., 2008) dominate the Grande Vasière mud belt fauna. Foraminiferal diversity, standing stock and vertical distribution within sediments shifts with water depth (Duchemin et al., 2005; 2008).

Following the Grande Vasière studies, the aim of our paper is to assess the relevance of using benthic foraminifera as bio-indicators of the various environmental conditions prevailing along the WGMP. To do so, we can draw on geochemical, geophysical and sedimentological data acquired during the 2017 oceanographic JERICOBENT-2 cruise (Deflandre, 2017; Dubosq et al., in prep; complementary sedimentological analysis presented in this paper). These data are compared to the faunal characteristics (diversity, standing stock, microhabitats) of the foraminiferal communities sampled at the seven stations ranging from 36–69 meters water depth (Fig. 1).

2. Material and Methods

2.1. Water parameters

This investigation is based on data obtained at seven stations sampled during the JERICOBENT-2 cruise in August 2017 (Fig. 1; Table 1) (Deflandre, 2017). Stations are organized according to a bathymetric gradient from the proximal part of the WGMP (Station 1, 39 m) to the distal (Station 4, 69 m) (Fig. 1; Table 1). Bottom water temperature (CTD measurements) decreases gradually from 14.6°C at station 1 (39 m) to 12.7°C at station 4 (69 m), whereas bottom water salinity (Conductivity-Temperature-Depth measurements) is constant (35.2) (Table 1). Bottom water oxygenation stays relatively high at all sites (between 184–197 µM) (Table 1), oxygen penetration depth (OPD) within the sediments is relatively limited (< 1 cm) indicating a relatively enhanced oxygen demand to degrade organic compounds compared to open-slope environments (Fontanier et al., 2002; Dubosq et al., in prep).

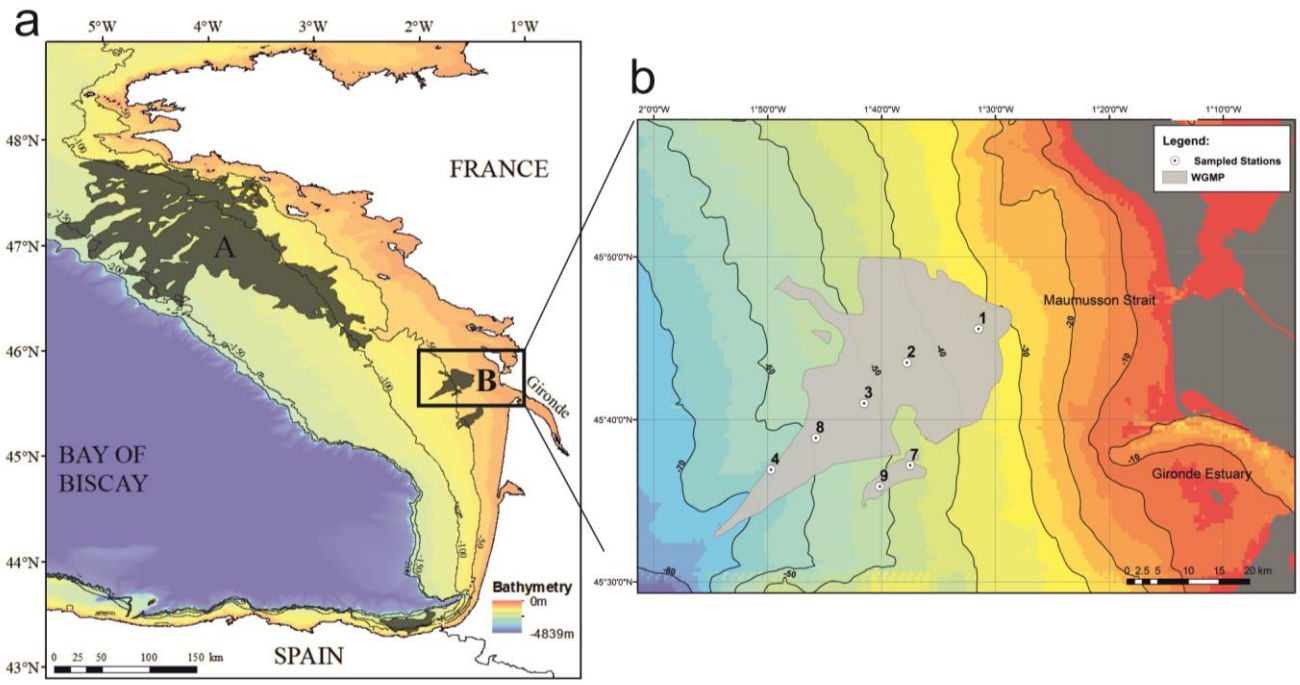

Figure 1. (a) Map of the Bay of Biscay continental shelf with the locations of mud belts and patches: A - La Grande Vasière Mud Patch and B - The Gironde Mud Patch (b) Map of the West Gironde Mud Patch showing the location of 7 sampling stations (white dots). The synoptic map of the WGMP has been determined during the JERICOBENT-5-TH cruise (Gillet and Deflandre, 2018)

Table 1. Location of the seven stations sampled during the JERICOBENT-2 cruise (August 2017) including station coordinates and depth. Physico-chemical parameters including BWT (bottom-water temperature in °C) and BWS (bottom-water salinity in psu) were extrapolated from CTD casts at each site. BWO_2 (bottom-water oxygen in µM) was measured in water overlying the sediment-water interface (SWI) of cores gathered during the JERICOBENT-2 cruise (Dubosq et al., in prep). Oxygen saturation (in %) of bottom water was also calculated (Dubosq et al., in prep). OPD (oxygen penetration depth in cm below the SWI) was determined after N in-situ measurements with a benthic profiler deployed at each station during the JERICOBENT-2 cruise.

Station	Sampling period	Depth (m)	Latitude	Longitude	BWT (°C)	BWS (psu)	BWO_2 (µM)	% Sat.	OPD (cm) (N)
1	August 2017	39	45°45.550'	1°31.335'	14.6	35.2	184.7	71.9	0.36 ± 0.16 (10)
2	August 2017	47	45°43.567'	1°37.657'	13.6	35.2	196.5	83.0	0.61 ± 0.32 (12)
7	August 2017	50	45°37.278'	1°37.544'	13.6	35.2	192.4	73.6	0.34 ± 0.07 (12)
9	August 2017	54	45°35.917'	1°40.062'	13.1	35.2	190.3	71.9	0.42 ± 0.04 (12)
3	August 2017	56	45°40.973'	1°41.762'	13.4	35.2	193.5	73.3	0.66 ± 0.25 (12)
8	August 2017	61	45°38.925'	1°45.825'	12.9	35.2	186.2	69.5	0.46 ± 0.12 (6)
4	August 2017	69	45°43.993'	1°37.427'	12.7	35.2	185.3	69.2	0.37 ± 0.08 (11)

2.2. Sediment sampling

Sediment samples were collected with a Barnett-type multiple corer equipped with Plexiglas tubes (9.6 mm internal diameter, surface area of 72 cm^2) (Barnett et al., 1984). The multi-corer allowed for sampling of the uppermost decimeters of the sediment column, the overlying bottom waters, and a comparatively undisturbed sediment-water interface. At each station, the multi-corer was deployed three to five times to get enough material for geochemical, sedimentological and biological investigations. Descriptors of sedimentary organic matter as well as the mineralization processes of organic compounds at and below the sediment-water interface are described in detail by Dubosq et al. (in press; in prep). We refer to a partial synthesis of their results in the discussion with data summarized in Tables 1 and 2.

2.3. Sedimentological analysis

At each station, one entire core was radiographed with a Scopix system, which consists of an X-Ray imaging system combined with image analysis software (Migeon et al., 1999) (Fig. 2). The aim of the X-ray radiography is to detect the presence of discrete sedimentary structures (e.g., erosional surfaces, burrows, coarse sedimentary layers). To visually evaluate changes, core photographs were also taken (Fig. 2). Particle grain sizes were measured with a Malvern Laser Diffraction Particle Sizer (type 2600). This technique was applied to sediment samples belonging to the previously radiographed and photographed core and allowed for the

calculation of grain size frequency D_{50}. To do so, each core was subsampled every 0.5 cm between 0–1 cm depth, every 1 cm between 1–4 cm depth, then every 2 cm between 4–22 cm depth, and with an adaptative resolution deeper downcore.

Table 2. Organic descriptors in the surface sediment (i.e. the 0–0.5 cm interval below the sediment-water interface) at the seven stations sampled during the JERICOBENT-2 cruise (August 2017) (Dubosq et al., in prep): Organic content (OC in % DW), Total nitrogen content (TN in % DW), C/N atomic ratio, Chlorophyllic pigment content (i.e. Chl-a, Chl-b and Phaeo-a) and their freshness index Chl-a/(Chl-a+Phaeo-a).

Station	OC		TN		C:N ratio		Chl-*a*	Chl-*b*	Phaeo-*a*	Chl-*a*/(Chl-*a* + Phaeo-*a*)	Pigments
	%DW	N	%DW	N		N	µg/g	µg/g	µg/g		N
1	0.30 ± 0.04	6	0.03 ± 0.00	5	12.11 ± 1.59	5	0.23 ± 0.09	<DL	1.46 ± 0.46	0.13 ± 0.02	3
2	0.89 ± 0.06	5	0.10 ± 0.01	5	10.07 ± 1.07	5	1.15 ± 0.20	0.10 ± 0.04	6.65 ± 0.88	0.15 ± 0.03	3
7	1.80 ± 0.13	5	0.20 ± 0.01	5	10.61 ± 0.59	5	1.82 ± 0.42	0.11 ± 0.06	13.55 ± 2.92	0.12 ± 0.00	3
9	1.38 ± 0.12	5	0.14 ± 0.02	5	11.99 ± 2.76	5	1.48 ± 0.71	0.15 ± 0.02	9.67 ± 3.71	0.13 ± 0.01	3
3	1.23 ± 0.12	5	0.13 ± 0.01	5	10.70 ± 0.68	5	0.87 ± 0.05	0.05 ± 0.02	6.07 ± 1.64	0.13 ± 0.03	3
8	1.21 ± 0.10	5	0.13 ± 0.01	5	11.13 ± 0.38	5	0.77 ± 0.29	0.07 ± 0.08	5.25 ± 0.57	0.13 ± 0.04	3
4	1.38 ± 0.05	5	0.14 ± 0.00	5	11.16 ± 0.29	5	0.91 ± 0.18	0.09 ± 0.07	6.90 ± 1.28	0.12 ± 0.04	3

2.4. Foraminiferal faunal analysis

Foraminiferal faunas were studied in a single core per station. Onboard, each core was sliced horizontally every 0.5 cm from the sediment-water interface to a depth of 2 cm, then every centimeter between 2–10 cm depth. Samples (12 slices per core) were transferred into 500 cm^3 bottles, which were filled with 95% ethanol containing 2 g/L Rose Bengal stain, commonly used to identify live foraminifera (Walton, 1952; Murray & Bowser, 2000).

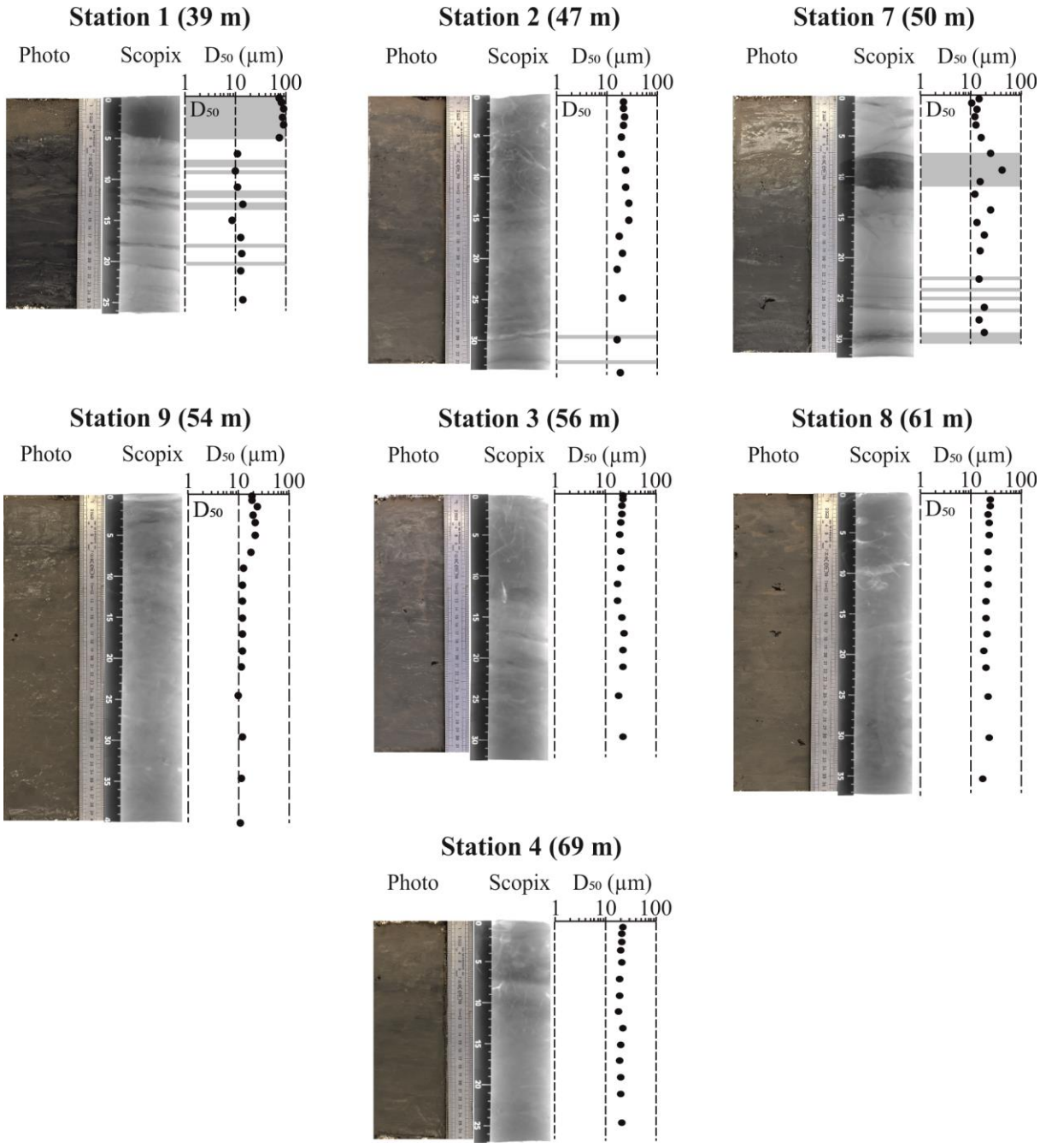

Figure 2. Photograph and X-Ray radiograph (Scopix) of split cores collected at the seven stations from the WGMP with grain size frequency D_{50}.

All samples were gently shaken for several minutes to obtain a homogeneous mixture. At the laboratory (one month after the cruise), samples were sieved through 150 µm mesh screens, and sieve residues were stored in 95% ethanol. Stained foraminifera belonging to the >150 µm fraction were sorted in wet samples and stored in Plummer slides. One concern with using Rose Bengal is that it may stain the protoplasm of dead foraminifera that may be relatively well-preserved for long time periods under the generally anoxic conditions prevailing in deep sediments (Corliss & Emerson, 1990; Bernhard, 2000). We therefore applied very strict staining criteria (i.e., all chambers, except the last chamber, stained in bright pink),

and compared doubtful individuals to perfectly stained specimens of the same species found in the superficial sediment layers. For miliolids, doubtful specimens were broken to inspect test interior. Most stained foraminifera were identified at species level and checked with the World Foraminifera Database (Hayward et al, 2021) for current taxonomic nomenclature (see Appendix A for taxonomical references and Appendix B for census data). Because samples were preserved and sorted in ethanol, many soft-shelled foraminiferal species may have shrunk and become unrecognizable during picking. Thus, our counts probably underestimate the soft-shelled foraminiferal abundance. We obtained digital photographs of major species using a scanning electron microscope at Angers University (Fig. 3). For each core, we calculated different indices to assess diversity. First, we calculated Species Richness (S) and then Shannon index, H' (log base *e*) as an information-statistic index as described in Murray (2006). We determined the Berger-Parker index, which represents the highest relative contribution (in %) calculated for the dominant taxon at each station. A Q-mode cluster analysis based on normalized relative abundances P_i values was applied for the seven stations and the 13 major species (≥2.5%), with P_i defined as:

$$P_i = Arc\sin(\sqrt{p_i})$$

in which "p_i" is the relative frequency of the "*i*th" species, and "P_i" is the normalized value of p_i (J. Hohenegger, personal communication). We constructed a tree diagram using Ward's method based on Euclidian distance. To do so, we used the PAST Software (Hammer et al., 2001).

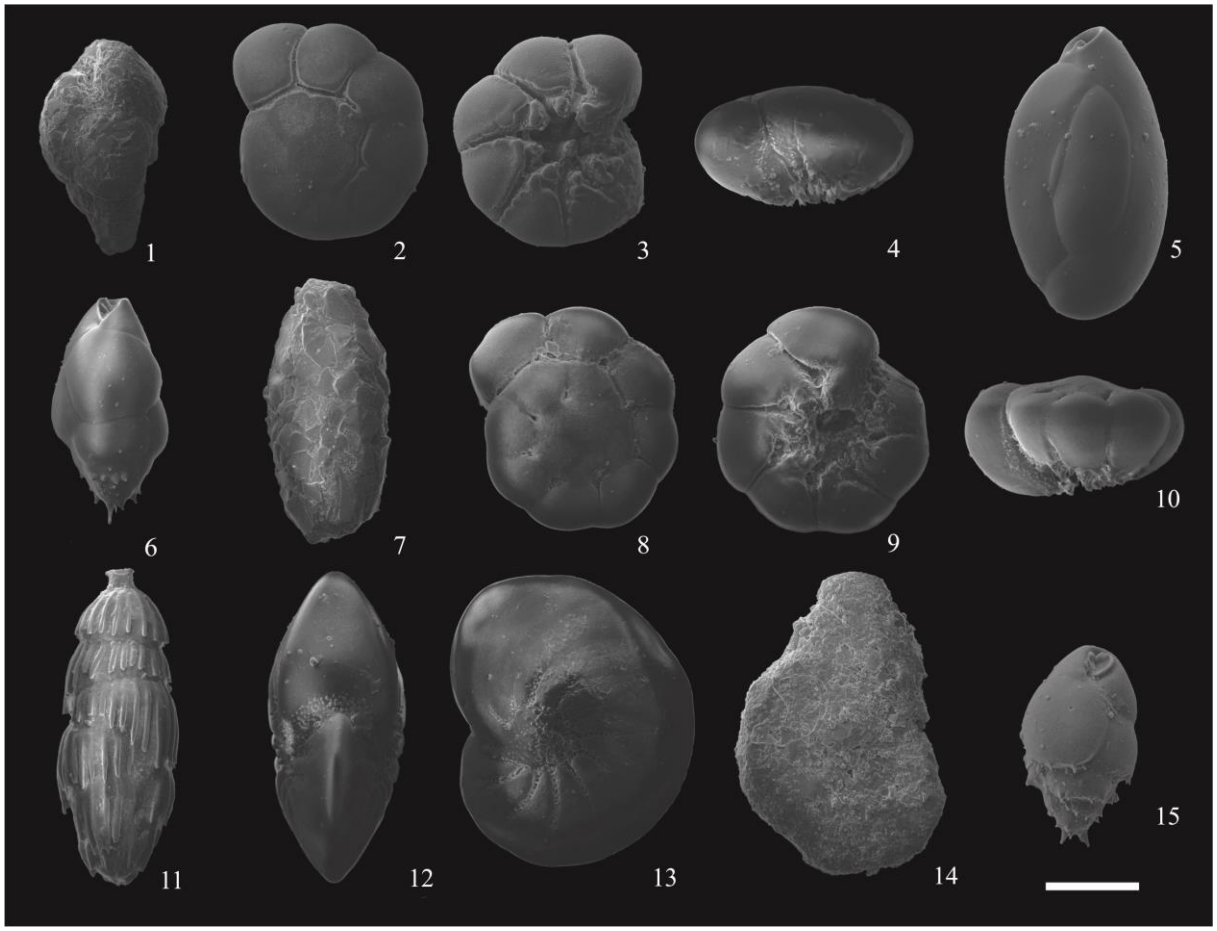

Figure 3. SEM photographs of some major foraminiferal taxa observed in our study area. 1 Eggerelloides scaber; 2, 3, 4 Ammonia beccarii (dorsal, umbilical and lateral views); 5 Quinqueloculina laevigata; 6 Bulimina aculeata; 7 Nouria polymorphinoides; 8, 9, 10 Ammonia falsobeccarii (dorsal, umbilical and lateral views); 11 Rectuvigerina phlegeri; 12, 13 Nonion faba (frontal and lateral views); 14 Ammoscalaria pseudospiralis; 15 Bulimina marginata. Scale bar represents 100 µm.

Using Q-mode cluster analysis, we applied the Indicator Value (IV) Method (Dufrêne and Legendre, 1997) with the 13 major species in order to determine indicative species in each cluster of stations. For this purpose, we used the following formula:

$$IV_{(i,\alpha)} = A_{(i,\alpha)} \times B_{(i,\alpha)} \times 100$$

$$A_{(i,\alpha)} = \frac{Nindividuals_{(i,\alpha)}}{Nindividuals_{(i)}}$$

$$B_{(i,\alpha)} = \frac{Nstations_{(i,\alpha)}}{Nstations_{(\alpha)}}$$

$Nindividuals_{(i,\alpha)}$ is the mean number of individuals belonging to the species *i* and present in the cluster α. $Nindividuals_{(i)}$ is the sum of the mean numbers of individuals of species *i* occurring in all clusters. $Nstations_{(i,\alpha)}$ is the number of stations in the cluster *α* where the species *i* is

present. $Nstations_{(\alpha)}$ is the total number of sites in the cluster α. P values were calculated based on 999 permutations using R package "*labdsv*" (Roberts 2019; R core team 2020).

2.5. Additional details

Our study concerns benthic foraminiferal faunas sampled at a specific time of the year and constitute an ecological snapshot and not a temporal survey. Our investigation into the seasonal dynamics of WGMP benthic fauna remains a work in progress and will be the subject of future publications. Therefore, in this paper, we have focused on benthic foraminiferal communities belonging to the >150-µm-size fraction as bio-indicators of average environmental conditions at each of our seven stations at the end of a sustained period of increased primary productivity. Seasonal monitoring incorporating smaller benthic foraminifera (e.g., belonging to the 63–150 µm-size fraction) will certainly provide valuable additional information on the temporal variability of ecological conditions in this mudflat. But this is not the goal of this study. Furthermore, our study is based on the analysis of a single core per station. Although it is recommended to study several replicates at each site to obtain a more robust, averaged view of foraminiferal faunas (Schönfeld et al., 2012), a lot of studies published for the last decades on the ecology of benthic foraminifera sampled in large study areas integrating various marine ecosystems does not follow this recommendation (e.g., Fontanier et al., 2002; Duchemin, 2005; 2008; Goineau et al., 2011; Dessandier et al., 2015; 2016). Conversely, environmental interpretations of modern foraminiferal faunas are mostly based on a single sample per site. We therefore consider in this study that even if small-scale (metric) spatial variability exists between benthic faunas living at the same station, this variability does not hide the faunal variability existing at the spatial scale of the WGMP, given that the seven sampled stations are several kilometres apart from each other. Finally, the many recent studies exclusively using >150 µm-sized benthic foraminifera living in the Bay of Biscay (e.g., Fontanier et al., 2002; Ersnt et al., 2005; Langezaal et al., 2006; Duchemin et al., 2005; 2008) sufficiently provide reliable information concerning what we might expect in terms of foraminiferal diversity, standing stock and distribution on the Aquitaine Shelf. Our study adds new and precious data about benthic environments from a river-dominated inner shelf.

3. Results

3.1. Sedimentary features

Station 1 (depth 39 m) is characterized by a 5 cm-thick surface layer made of very fine sand (D_{50} > 75 µm) (Fig. 2). Beneath this layer, dark grey sediments are made of highly compacted and sticky mud (D_{50} ~ 10 µm) within which some dense-material laminae are visible. Station 2 (depth 47 m) is characterized by a clay-silt facies (D_{50} ranging between 15–25 µm) throughout the sampled section. Horizontal, vertical and oblique biological structures (i.e. burrows) are abundant all along the core (Fig. 2). Station 7 (depth 50 m) constitutes a 4 cm-thick subsurface layer made of sandy silt (D_{50} reaching 50 µm) between 7–11 cm depth. Above and below this layer are sediments composed of fine particles (D_{50} < 27 µm). Millimetric laminae are visible between 20 and 30 cm depth (Fig. 2). Station 9 (54 m) is characterized by a silty layer (D_{50} ~20 µm) 7 cm thick overlying very fine sediments (D_{50} ~ 10 µm). Two gastropod shells of *Turritella communis* were found in the 10 first cm. Stations 3, 8 and 4 (between 56–69 m deep) present homogeneous facies made of clayey silt (D_{50} ranging between 15–25 µm). Biological structures (i.e., burrows) are abundant all along these three cores (Fig. 2).

3.2. Foraminiferal faunas (>150 µm)

3.2.1. Diversity Indices

Total foraminiferal standing stocks vary between 1,299 individuals/core at Station 7 (50 m) and 3,737 individuals/core at Station 9 (54 m) (Fig. 4a; Appendix B). There is no trend following water depth. Species richness S (/core) ranges between 18 at Station 7 and 31 taxa at the deepest Station 4 (69 m depth) (Fig. 4a; Appendix B). Excluding Station 1 (39 m), species richness S increases gradually with water depth along the WGMP. The H' (/core) is low (1.6) at Station 1 and increases with water depth to 2.4 at Station 4 (Fig. 4b). Berger-Parker index (/core) decreases with water depth between 0.24–0.55.

3.2.2 Foraminiferal Composition and Microhabitat

As a general trend, the relative abundance of rotaliid species in the total living fauna increases with water depth, from 25% of the total fauna at Station 1 (39 m) to 64% at Station 8 (60 m). Conversely, the relative abundance of textulariid taxa is relatively high at Stations 1, 2 and 7 (< 50 m) (% of the total fauna ranging between 60–70%) and reaches lower values at stations 3, 8 and 4 (< 56 m) (% ranging between 35–40%). Miliolids are only abundant at Station 1 (12% of the total fauna). At Station 1 (39 m), *Eggerelloides scaber* (55% of the total

fauna; Fig. 3[1]) is the dominant species (Fig. 5a). It presents an erratic down-core vertical distribution with no preferential microhabitat. *Quinqueloculina laevigata* (13% of the total fauna; Fig. 3[5]) and *Ammonia beccarii* (12% of the total fauna; Fig. 3[2–4]) are two other major calcareous species. Their abundances are greatest within the uppermost 0.5 cm of the sediment column. *Bulimina aculeata* (7% of the total fauna; Fig. 3[6]), a calcareous species, presents a plurimodal distribution with a density maximum in the 3–4 cm interval (Fig. 5a). The agglutinated *Nouria polymorphinoides* (4% of the total fauna; Fig. 3[7]) preferentially occupies the 0–0.5 cm interval (Fig. 5a). At Station 2 (47 m), *E. scaber* (50% of the total fauna) has a plurimodal distribution with a density maximum recorded in the 0–0.5 cm interval (Fig. 5b). *Bulimina aculeata* (15% of the total fauna) shows a bimodal distribution similar to Station 1. *Ammonia falsobeccarii* (9% of the total fauna) (Fig. 3[8–10]) and *A. beccarii* (10% of the total fauna) are secondary species. *Nouria polymorphinoides* (5% of the total fauna) preferentially occupies the 0–0.5-cm interval. At Station 7 (50 m) *E. scaber* (52% of the total fauna) shows a peculiar vertical distribution with two maxima recorded in the 0–0.5 cm and 9–10 cm intervals respectively (Fig. 5c). *Nouria polymorphinoides* (16% of the total fauna) and *A. falsobeccarii* (8% of the total fauna) show the same microhabitat pattern as *E. scaber. Nonionoides turgidus* (5% of the total fauna) and *B. aculeata* (5% of the total fauna) are subsidiary calcareous species. *Nonionoides turgidus* inhabits the subsurface sediments, 2–3 cm below the sediment-water interface. At Station 9 (54 m), *E. scaber* (44% of the total fauna) constitutes a bimodal distribution with maxima recorded in the 0–0.5 cm and 6–7 cm intervals (Fig. 5d). The secondary taxon *B. aculeata* (25% of the total fauna) follows an erratic vertical distribution with two peaks at the 0–0.5 cm and 9–10 cm intervals. Other major species, *A. falsobeccarii* (8% of the total fauna) and *N. polymorphinoides* (8% of the total fauna), are more abundant in the 0–0.5 cm interval. *Nonion faba* (4% of the total fauna) (Fig.3[12–13]) presents a density maximum recorded between 1.5–3 cm. *Nonionoides turgidus* (2.5% of the total fauna) is characterised by a density maximum recorded at the 3–4 cm interval. At Station 3 (56 m), *E. scaber* (30% of the total fauna) preferentially occupies the uppermost two centimeters of the sediment (Fig. 5e). *Bulimina aculeata* (23% of the total fauna), *A. falsobeccarii* (21% of the total fauna) and *Bulimina marginata* (11% of the total fauna) (Fig.3[15]) present erratic vertical distributions with density maxima recorded in the 0–0.5-cm interval. *Nouria polymorphinoides* (7% of the total fauna) preferentially occupies the 0–0.5-cm interval. At Station 8 (61 m), *E. scaber* (25% of the total fauna) comprises an erratic vertical distribution with a density maximum in the 2–3 cm interval (Fig. 5f). *Bulimina aculeata* (21% of the total fauna) has a plurimodal distribution with maxima recorded in the 0–0.5 cm, 4–3 cm and 6–7 cm intervals.

Ammonia falsobeccarii (20% of the total fauna) has two maxima in the 0–0.5 cm and 1.5–3 cm intervals. *Nonion faba* (11% of the total fauna) is most abundant between 1–3 cm. *Nouria polymorphinoides* (7% of the total fauna) and *B. marginata* (7% of the total fauna) are characterised by density maxima recorded in the uppermost centimeter of sediment. At Station 4 (69 m), *E. scaber* (25% of the total fauna) is still the dominant taxon presenting a plurimodal vertical distribution (Fig. 5g). *Ammonia falsobeccarii* (15% of the total fauna) is most abundant in the uppermost centimeter of sediment. *Nouria polymorphinoides* (13% of the total fauna) occupies the uppermost 2 cm of the sediment. *Nonion faba* (11% of the total fauna) is most abundant between 2–4 cm. It is worthy to note the occurrence of *Rectuvigerina phlegeri* (6% of the total fauna) (Fig.3[11]) and *Paracassidulina neocarinata* (4%) in the uppermost half centimeter of the sediment.

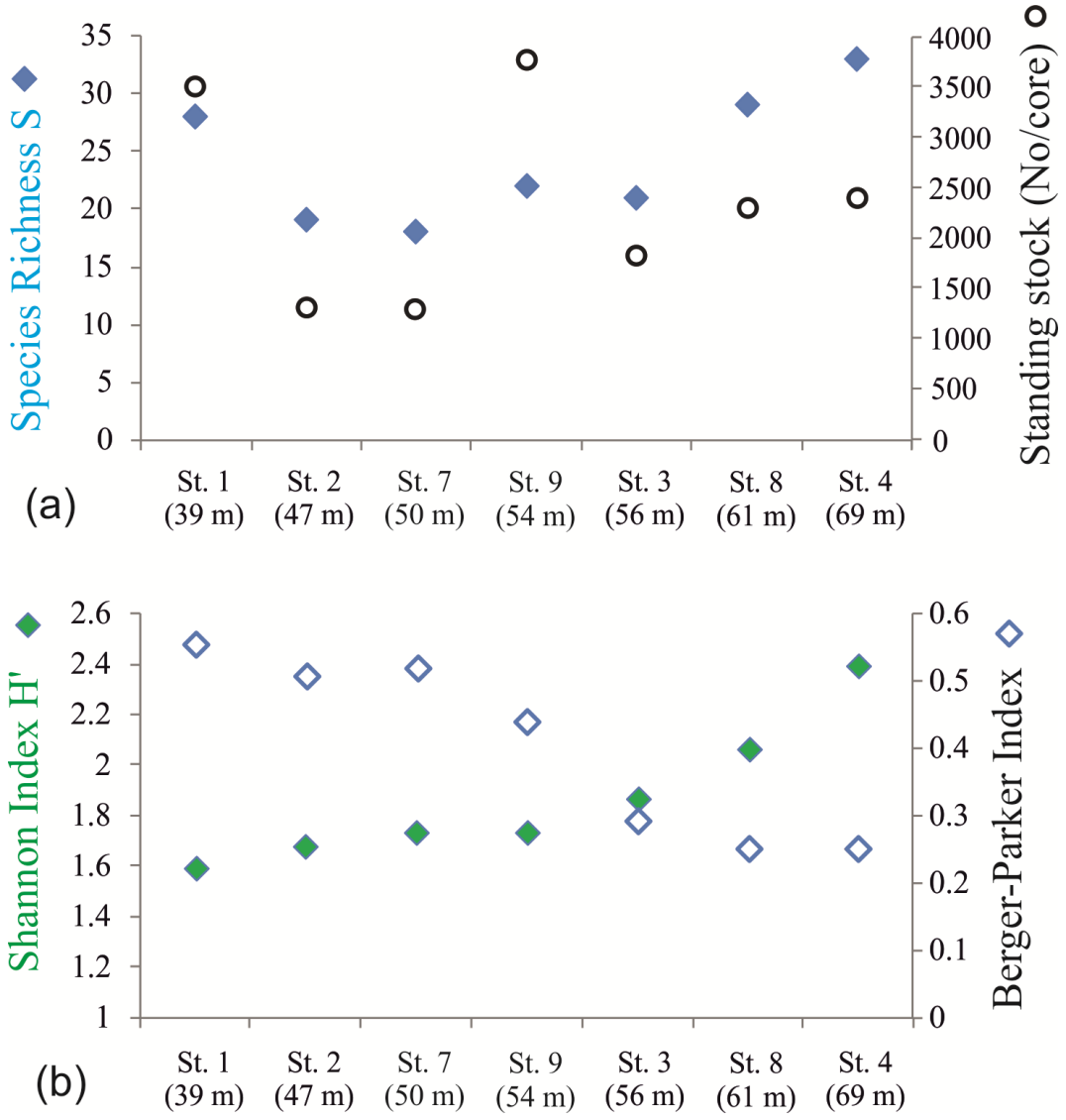

Figure 4. (a-b) Ecological indices describing foraminiferal faunas at the seven stations from the WGMP. (a) Species Richness (S) and foraminiferal standing stocks (no. individuals/core); (b) Shannon (H') and Berger-Parker indices.

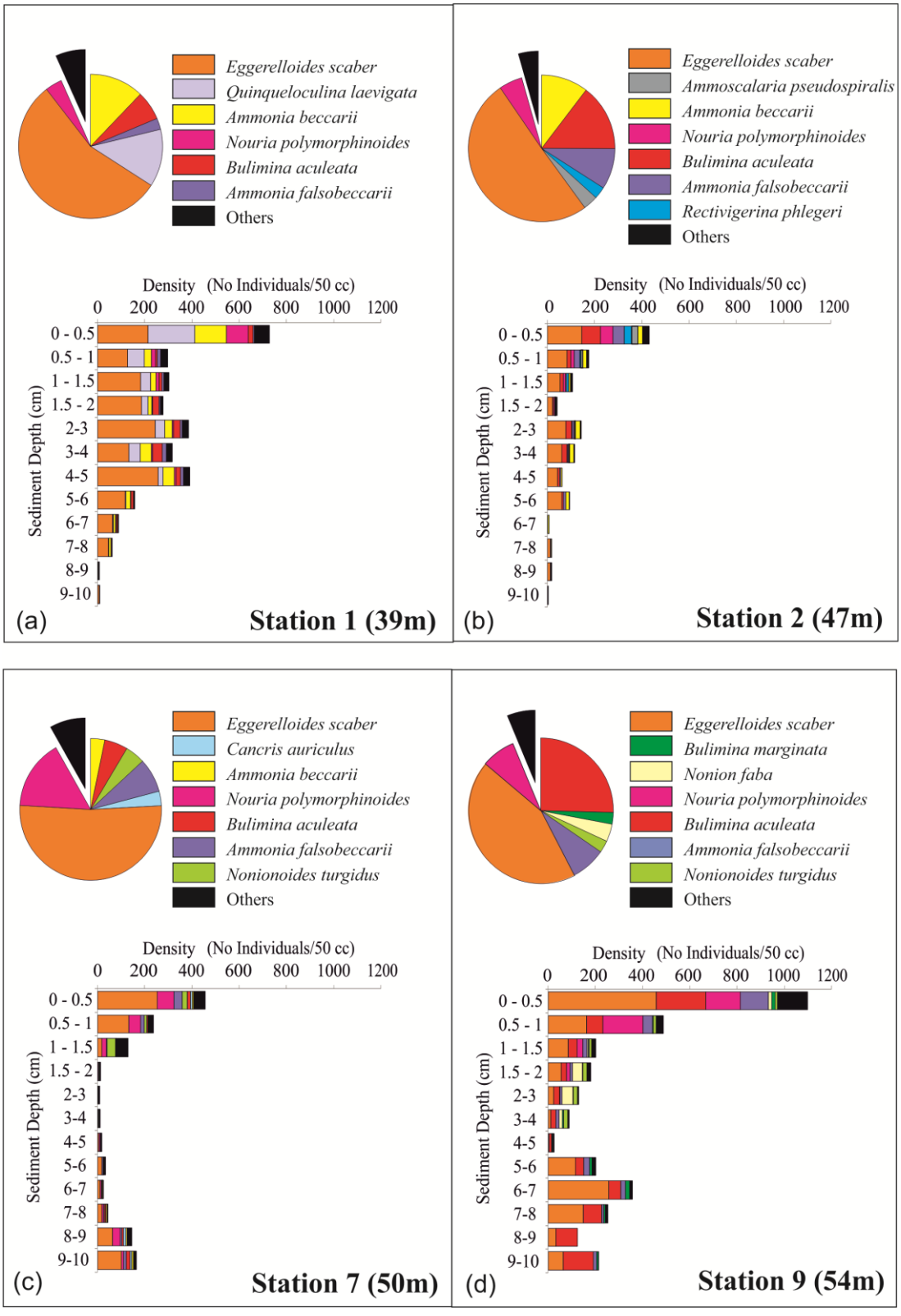

Figure 5. (a-g) Foraminiferal composition and down-core distribution of live benthic foraminifera in the seven cores gathered in the WGMP. Pie charts represent the composition of live benthic foraminiferal faunas (composition in % of total fauna). The number of individuals belonging to the >150 µm-size fraction found in each level is standardized for a 50 cm³ sediment volume. In both pie charts and core distribution, only taxa with relative abundances >2.5% are pictured.

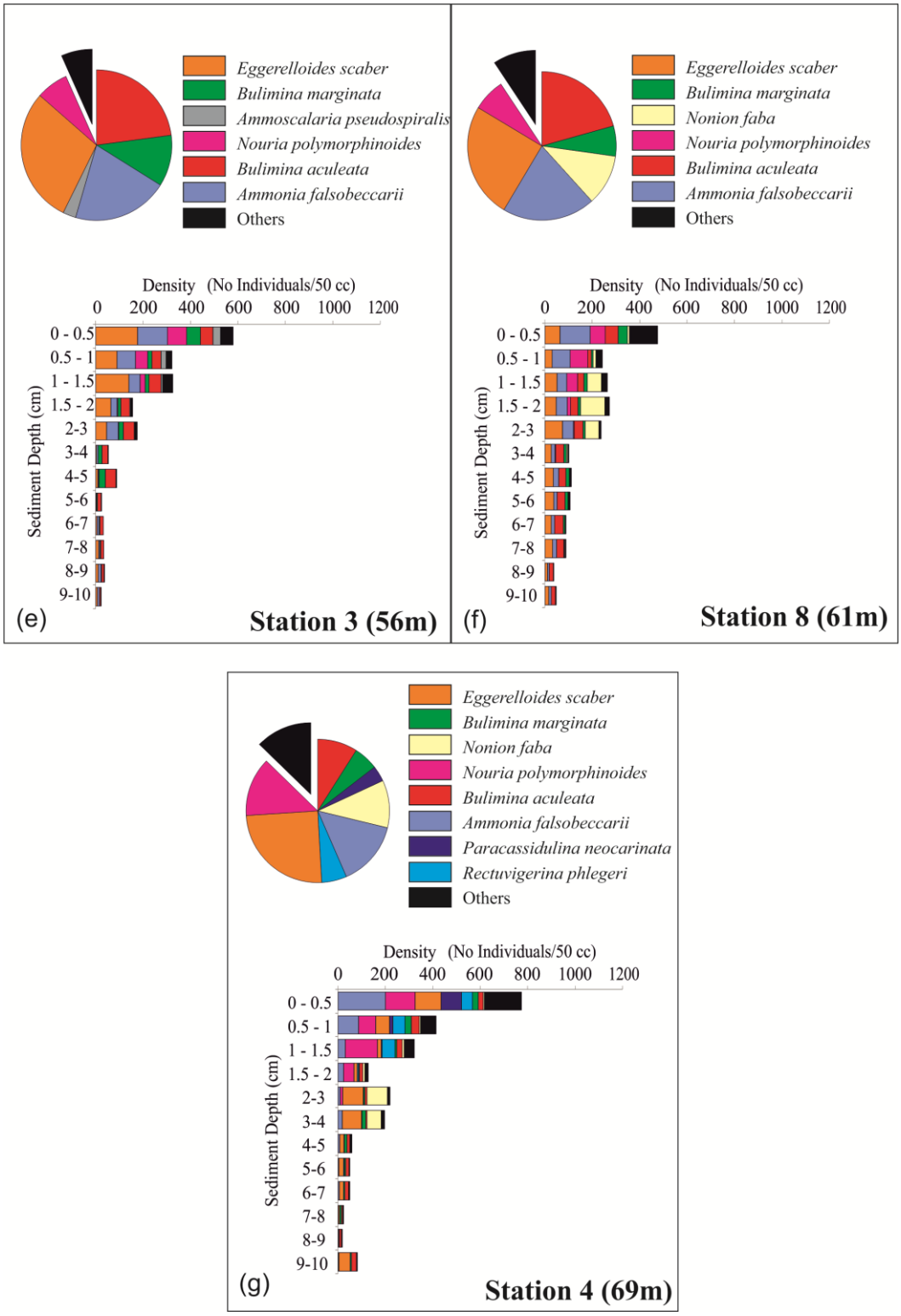

Figure 5. (a-g) Foraminiferal composition and down-core distribution of live benthic foraminifera in the seven cores gathered in the WGMP. Pie charts represent the composition of live benthic foraminiferal faunas (composition in % of total fauna). The number of individuals belonging to the >150 µm-size fraction found in each level is standardized for a 50 cm^3 sediment volume. In both pie charts and core distribution, only taxa with relative abundances >2.5% are pictured.

3.2.3. Q-mode clustering and Indicative Values (IV)

Based on faunal content, Q-mode cluster analysis of the seven stations reveals two groups of three stations and one isolated site (Fig. 6). The calculation of Indicative Values (IV) for the 13 major species of our study area shows a marked spatial variability for some taxa as well as species common to certain areas (Table 3). Station 1 (39 m), which is isolated by cluster analysis, is characterized by *Q. laevigata* (IV = 84%), *A. beccarii* (IV = 69%), and *E. scaber* (IV = 42%). Cluster 1 consisting of Stations 2, 7 and 9 (water depth comprised between 47–54 m), is characterized by *N. turgidus* (IV = 77%), *Cancris auriculus* (IV = 46%), *N. polymorphinoides* (IV = 43%). Cluster 2 includes Stations 3, 8 and 4 (all deeper than 56 m) and is characterized by *P. neocarinata* (IV = 98%), *N. faba* (IV = 80%), *B. marginata* (IV = 79%), *A. falsobeccarii* (IV = 63%), *Ammoscalaria pseudospiralis* (IV = 48%), *B. aculeata* (IV = 45%) and *R. phlegeri* (IV = 44%). Permutation test based on 999 iterations reveals that *N. turgidus* can be considered as a robust indicator (p-value < 0.05) for Cluster 1 whereas *N. faba, B. marginata* and *A. falsobeccarii* are significantly indicative of Cluster 2.

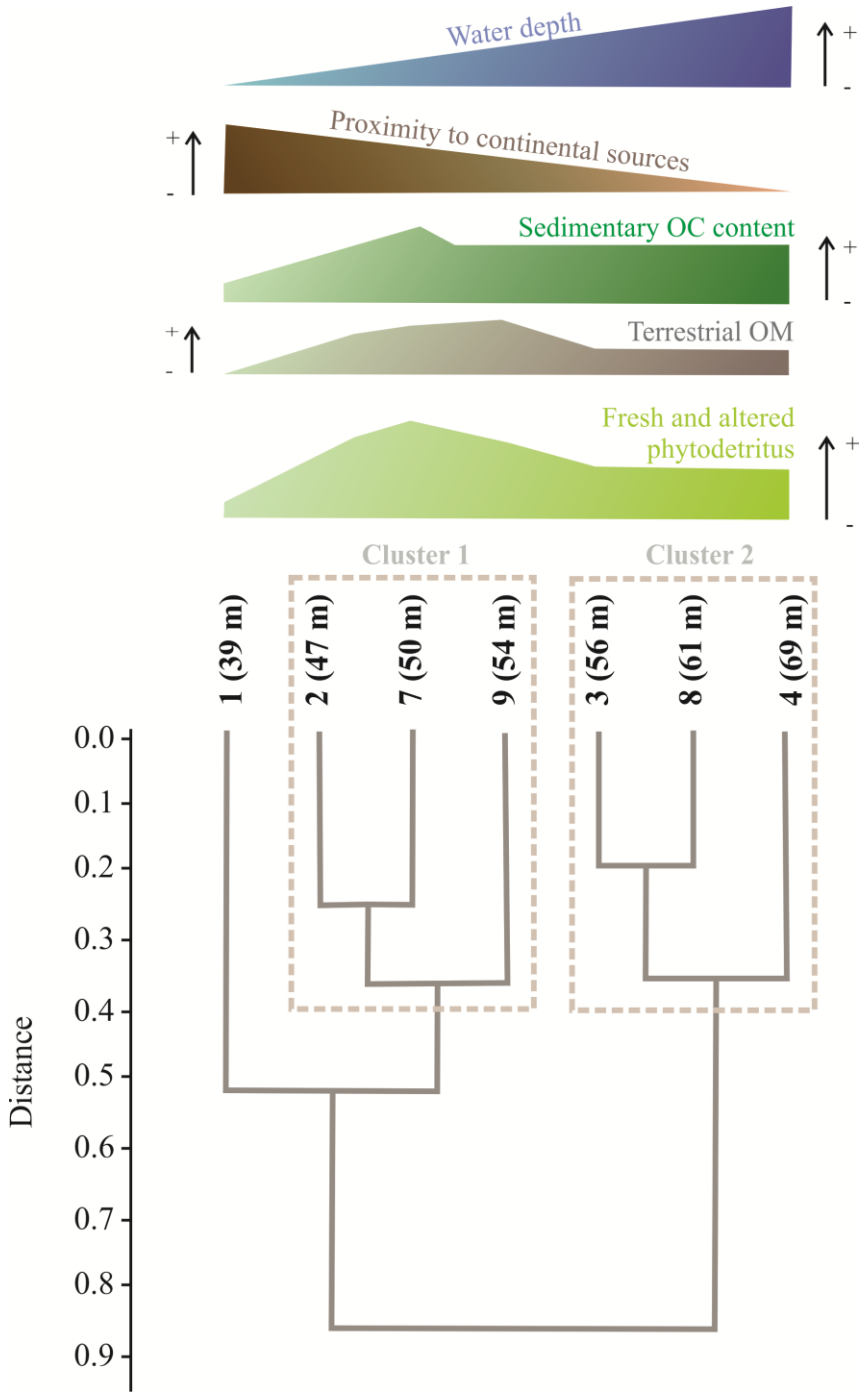

Figure 6. Q-mode cluster analysis of the seven stations following the Ward's method based on transformed percentages Pi of major foraminiferal species (>2.5%). Environmental trends (station water depth, proximity to continental sources, sedimentary organic matter content, terrestrial organic matter, fresh and degraded phytodetritus) are pictured. Dotted boxes correspond to groups identified by Q-mode cluster analysis (Clusters 1 and 2).

Table 3. Indicator values (IndVal – IV in %) of the major station species of the groups defined by Q-mode cluster analysis. Indicator values are calculated according to Dufrêne and Legendre (1997) (see Material and Methods). For each species, IV are indicated by red shading, and the maximum IV by bold numbers. Underlined IV are significant with a p-value < 0.05.

IndVal (IV)	Station 1 (39 m)	Cluster 1	Cluster 2
Ammonia beccarii	**69**	29	2
Ammonia falsobeccarii	9	28	**63**
Bulimina aculeata	17	39	**45**
Bulimina marginata	5	16	**79**
Cancris auriculus	17	**46**	37
Nonion faba	1	18	**80**
Nonionoides turgidus	3	**77**	21
Paracassidulina neocarinata	0	6	**98**
Rectuvigerina phlegeri	23	32	**44**
Quinqueloculina laevigata	**84**	5	11
Ammoscalaria pseudospiralis	7	44	**48**
Eggerelloides scaber	**42**	37	20
Nouria polymorphinoides	17	**43**	41

4. Discussion

4.1. Environmental features of the West-Gironde Mud Patch in August 2017

Sedimentological studies carried out over the last three decades on the WGMP have shown that this seafloor feature is difficult to isolate, define and categorise (e.g., Lesueur et al., 1991; 1996; 2002; Cirac et al., 2016) (Fig. 1). The boundaries between the muddy WGMP facies (silt-clay) and the sands of the surrounding Aquitaine Shelf are hard to define as episodic inputs of suspended matter from the Gironde River associated with storm-induced bottom currents cause these facies to migrate several hundred metres from their source (Cirac et al., 2000; Lesueur et al., 2002). Figure 2 shows that Stations 1 and 7, located at the edge of the WGMP (presumably within the zone of shifting boundaries), present complex sedimentary facies where sandy layers are intercalated in finer sediments. Such sedimentary patterns were also documented in core samples collected in Autumn 2016 and in June 2018 during the JERICOBENT-1 and JERICOBENT-5 cruises (Deflandre, 2016; Gilet and Deflandre, 2018; Lamarque et al., 2021; Dubosq et al., in press). Whereas Station 1 is, due to its coastal proximity, impacted by episodic high-energy hydrodynamics causing low sediment deposition, massive but sporadic sedimentary deposits characterize Station 7 (Dubosq et al., in press). All other stations from within the WGMP present relatively continuous sediment accumulation with rates ranging between 0.3–0.5 cm yr^{-1} (Dubosq et al., in press). This lateral and vertical

heterogeneity in the sedimentary architecture of the WGMP influences the geochemical processes at the sediment-water interface (Dubosq et al, in press; in prep.). In August 2017, at Station 1 (39 m), the sandy surface, assumedly winnowed, is depleted in organic matter (<0.3% DW), fresh ([Chl-*a*] = 0.23 µg/g) and degraded ([Phaeo-*a*] = 1.46 µg/g) pigment compounds (Table 2). Conversely, at Station 7 (50 m) where the surface sediments are the most fine and clayey of the seven stations, the organic carbon (1.8% DW) and fresh ([Chl-*a*] = 1.82 µg/g) and degraded ([Phaeo-*a*] = 13.55 µg/g) chlorophyll pigment contents are the highest in our study area (Table 2). As a possible consequence of an efficient aerobic mineralization of labile organic compounds, oxygen penetration at Station 7 is the shallowest of our seven-stations transect (OPD ~ 0.34 cm: Table 1). Stations 9 (54 m) and 4 (69 m), also located close to the limits of the WGMP, present relatively homogeneous silt-clay facies where organic compounds accumulate in relatively high quantities (OC = 1.4% DW) (Table 2). There, oxygen penetration enables efficient organic matter degradation via aerobic respiration below the sediment-water interface (< 0.42 cm). Finally, Stations 2 (47 m), 3 (56 m) and 8 (61 m) located along the central axis of the WGMP show muddy facies moderately enriched in organic compounds (OC between 0.9–1.2% DW) and moderate OPD (0.46 – 0.66 cm) (Table 1). In our study area, late summer corresponds to the end of a long sequence of enhanced phytoplankton production initiated in late winter/early spring (Fig. 7). Lampert (2001) has studied phytoplankton successions on the inner shelf facing the Gironde River estuary. Other studies have also briefly described the seasonal evolution of primary production in the Bay of Biscay using satellite images (SeaWIFS/NASA data) to interpret chlorophyll-a pigment concentration in surface waters (Lampert et al., 2002; Fontanier et al., 2003; Duchemin et al., 2008). Both offshore and on the shelf, diatoms and coccolithophores bloom during the boreal spring (April–May) (Lampert, 2001; Fontanier et al., 2003; Duchemin et al., 2008) (Fig. 8). Thereafter, autotrophic marine dinoflagellates and cyanobacteria form a Deep Chlorophyll Maximum during the summer stratification of surface waters (Lampert, 2001). Phototrophic productivity in the coastal zone close to the Gironde estuary is particularly intense (Lampert, 2001). Therefore, the export of marine phytodetritus between spring and late summer due to the phytoplankton bloom may explain the relatively high content of both degraded and fresh chlorophyll *a* (i.e., phytodetritus) in the surface sediments of our study area, especially in the central and distal areas of the WGMP (Stations 2, 9, 7, 3, 4 and 8) where hydrodynamic energy remodelling the sea floor is weaker compared to sandy Station 1 (Table 1). The presence of fresh chlorophyll *b* pigment ([Chl-*b*] >0.10 µg/g), which originates from land plants, demonstrates that terrestrial organic compounds have recently accumulated in the mud

patch. This continental imprint is relatively well marked in the central WGMP (Stations 2, 9 and 7; [Chl-*b*] >0.10µg/g) (Table 2).

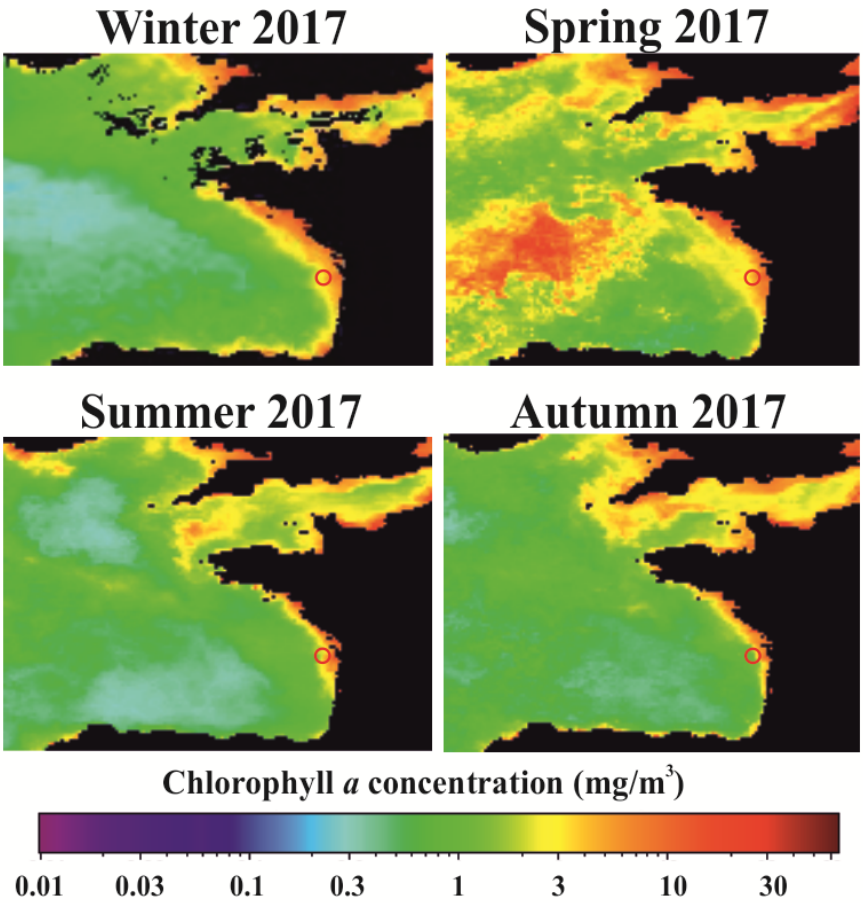

Figure 7. Synthetic seasonal maps of Chlorophyll *a* concentration in surface waters of the Bay of Biscay in 2017. Maps are based on MODIS satellite images (SNPP VIIRS Chlorophyll Concentration, OC3 Algorithm – Seasonal winter, spring, summer and autumn 2017 - https://oceancolor.gsfc.nasa.gov/). Red circles indicate our study area.

4.2. Benthic foraminifera biofacies and environmental implications

By the Q-mode clustering of the seven stations and by the IndVal calculation of our 13 most abundant species, benthic foraminifera living in the West-Gironde Mud Patch can be grouped into three main biofacies (Table 3, Fig. 5a–g). These can be further correlated with a clear bathymetric gradient and gradual changes of sedimentary and geochemical parameters (Fig. 6). The shallowest Station 1 (39 m), characterized by sandy sediments and low organic matter content, is dominated by *E. scaber* (55%), *A. beccarii* (12%) and *Q. laevigata* (13%) (Fig. 5a). At the other six stations characterized by clay-silt facies and variably enriched in organic carbon, foraminiferal diversity (i.e. Shannon index and simple diversity) increases and the cumulative contribution of *E. scaber, A. beccarii* and *Q. laevigata* decreases strongly with increasing water depth. Our observations at Station 1 are in agreement with many publications where both *E. scaber, A. beccarii* and *Quinqueloculina* spp. are described in inner-

shelf, either prodeltaic or estuarine environments, near river mouths (e.g., Barmawidjaja et al., 1992; Debenay and Redois, 1997; Diz et al., 2006; Diz and Francés, 2008; Goineau et al, 2011; Mendes et al., 2012; Dessandier et al., 2015; 2016). For instance, Dessandier et al. (2016) documented a strong contribution of both *E. scaber* and *A. beccarii* at the shallower sites (< 50 m depth) of a bathymetric transect in front of the Tagus River (Portugal, NE Atlantic). Like Station 1, those inner-shelf environments were characterized by sandy sediments (Q_{50} > 100 µm) and very low organic carbon content (< 0.05 % DW). Goineau et al. (2011) similarly described a strong contribution of *E. scaber* (*Eggerella scabra* in their study), *A. beccarii* (*Ammonia beccarii* f. *beccarii* in their study) and *Quinqueloculina* spp. at stations sampled in inner-shelf environments from the Gulf of Lions (France, Western Mediterranean Sea). Those stations were located between 15–37 m depth on a relict prodeltaic lobe, adjacent to the Grand Rhône River and were subject to high-energy hydrodynamics. They were characterized by sandy sediments with low organic matter comprised of continental and degraded compounds (OC content < 1.1 % DW, C:N ratio ranging between 11.5–17.7). It seems that *E. scaber*, *A. beccarii* and *Q. laevigata* thrive preferentially in shallow-water environments where hydro-sedimentary constraints (i.e., sedimentary reworking, winnowing and erosion by strong bottom currents) are enhanced. It is noteworthy that the erratic vertical distribution of *E. scaber* within anoxic sediments of all our stations underline its capacity to thrive under low oxygenation without any preference for fresh food (Diz et al., 2006; Langlet et al., 2014). Such patterns have also been documented in laboratory experiments simulating hypoxia and/or organic supply with sediment material sampled in the Bay of Biscay (Ernst et al., 2005).

Q-mode analysis Cluster 1 groups stations located in the central part of the WGMP (between 47–54 m water depth). There, organic compounds (OC content between 0.9–1.8 % DW) with fresh and degraded marine phytodetritus ([Chl-*a*] >1.15 µg/g; [Phaeo-*a*] > 6.65 µg/g)) and terrestrial organic matter ([Chl-*b*] > 0.10 µg/g) focus in muddy sediments (Table 2; Fig. 6). Foraminiferal faunas are characterized by a relatively high contribution of *B. aculeata, A. falsobeccarrii, N. polymorphinoides* and, to a lesser degree, *N. turgidus* (Fig. 5b-d). *Cancris auriculus* and *A. pseudospiralis* are both complementary and indicative (IV>44) species (Table 3). *Eggerelloides scaber* is still the dominant species of all stations grouped in this cluster. *Bulimina aculeata* was described in the Gulf of Cadiz (SW Iberian Peninsula) between water depths of 30–100 m by Mendes et al. (2012). This species occurs in muds associated with weak hydrodynamics, in-sediment enhanced hypoxia and high organic matter content. *Nouria polymorphinoides* with *C. auriculus* and *A. pseudospiralis* were documented in shelf environments between depths of 27–75 m in the Gulf of Guinea due to the high primary

productivity and fresh organic matter found in the sediments along the Ivory Coast and near the Volta Delta (Altenbach et al., 2003). Debenay and Redois (1997) described live and dead *A. falsobeccarii* (*Eponides falsobeccarii* in their study), *C. auriculus* and *A. pseudospiralis* (*Ammobacculites pseudospirale* in their study) on the shelf off Senegal (NW Africa), at the mouth of the Senegal River. Goineau et al. (2011) have also documented the dominance of both living *E. scaber* (*Eggerella scabra* in their study) and *N. turgidus* (*Nonionella turgida* in their study) at depths ranging between 47–62 m close to the Rhône River mouth. There, both species take advantage of terrestrial and marine organic compounds buried within the sediments (Goineau et al., 2011). *Nonionoides turgidus* is often considered an opportunistic and stress-tolerant taxon thriving in hypoxic and eutrophic conditions (Duchemin et al., 2008; Goineau et al., 2011). Its relatively deep infaunal microhabitat (> 2 cm depth) in our study area confirms both trophic and metabolic strategies.

Cluster 2 groups stations with silt-clay facies located between 56–60 m depth in the distal section of the WGMP. There, sedimentary organic carbon content is moderate with values ranging between 1.2–1.4% DW (Table 2). Fresh and degraded phytodetritus are available in a lesser quantity compared to the central area of the WGMP (Fig. 5e–g). *Paracassidulina neocarinata, N. faba, B. marginata, A. falsobeccarrii, B. aculeata* and *R. phlegeri* are the most indicative species of this 'outer-WGMP' cluster (Table 3). Those taxa are all commonly recorded in mid- to outer-shelf environments (e.g., Debenay and Redois, 1997; Fontanier et al., 2002; Langezaal et al., 2006; Duchemin.et al., 2005; 2008; Goineau et al., 2011; Dessandier et al., 2015; 2016). For example*, N. faba, B. marginata* and *P. neocarinata* dominate the >150 µm-sized faunas sampled between 80–140 m depth in La Grande Vasière mud belt in the Bay of Biscay (NE Atlantic) (Duchemin et al., 2005; 2008). In Goineau et al. (2011), *P. neocarinata* (*Cassidulina carinata* in their study)*, N. faba* (*Nonion fabum* in their study), and *R. phlegeri* statistically clustered together and were indicative of benthic ecosystems located between 44–86 m depth under the influence of the Rhône River plume. These species thrived in very fine sediments (D_{50} ~10 µm) with moderate organic carbon content (OC between ~1.1–1.3% DW). These environmental conditions are close to those found at the distal end of the WGMP. In Dessandier et al. (2016), *P. neocarinata* (*Cassidulina carinata* in their study)*, R. phlegeri* and *N. faba* (*Nonion scaphum* in their study) were documented between 50–100 m depth in mid- and outer-shelf environments characterized by silt to fine-sand facies supporting moderate quantities of organic compounds. In all studies comparable to our study area, *P. neocarinata* and *R. phlegeri*, present a shallow infaunal microhabitat typical of species feeding preferentially on labile organic compounds available in

the most oxygenated sediments. *Paracassidulina neocarinata* behave as an opportunistic species relying on freshly deposited phytodetritus produced during spring to early summer blooms (Fontanier et al., 2003; Duchemin et al., 2008). In our study area, *N. faba* inhabits an intermediate infaunal distribution traversing the dysoxic and the anoxic sediments (Fig. 5f–g). This pattern agrees with all other publications where this outer-shelf species is documented (e.g., Fontanier et al., 2002, Langezaal et al., 2006; Goineau et al., 2011; Dessandier et al., 2016). Though *N. faba*'s putative abilities such as denitrifying metabolism or endosymbiosis with procaryotes are still debated. In subsurface sediment layers, *N. faba* can rely on fresh or degraded organic compounds actively buried in deeper sediments (Fontanier et al., 2002; Duchemin et al., 2008). Alternatively, this species may migrate toward the sediment surface to gather fresher phytodetritus (Langezaal et al., 2006).

4.3. An ecological continuum through the muddy environments of the Bay of Biscay

Our investigation allows us to appreciate the faunal continuum existing in the Bay of Biscay from the WGMP (40–70 m) (our study area) to the Grande Vasière located between 80–130 m depth on the outer continental shelf (Duchemin et al., 2005; 2008). Although geographically disconnected (Fig. 1), these two muddy environments have dominant foraminiferal species that appear clearly organized along a range of correlated environmental gradients. *Nonion faba, B. marginata* and *P. neocarinata,* typical of the deepest part of the WGMP, are all dominant in the Grande Vasière (Duchemin et al., 2008). These species can be considered specialists preferentially living in fine sediments from open-ocean environments and relying on marine phytodetritus derived from median and outer shelf primary production (i.e., diatoms and coccolithophore blooms in spring). In contrast, other species, although dominant in the distal WGMP, are absent from the outer continental shelf. This is notable in regard to *A. falsobeccarrii, B. aculeata* and *R. phlegeri* which seem restricted to the WGMP potentially due to trophic preferences (i.e., phytodetritus associated with coastal primary production, terrestrial organic compounds) or a higher competitive ability compared to taxa living in deeper ecosystems. Other species which are clearly dominant in the proximal part of the WGMP (*E. scaber*, *Q. laevigata*, *A. beccarii*) are extremely rare or even absent in the Grande Vasière (Duchemin et al., 2008). As explained previously, these species are considered to be generalists with the ability to proliferate in hydrodynamically-impacted costal ecosystems where hydro-sedimentary pressure and food availability represent major ecological constraints. To summarize, our Bay of Biscay study illustrates the utility of using foraminiferal faunas with muddy environmental preferences to discriminate well-oxygenated

biotopes and how they are variably impacted by spatially disparate hydrodynamics and their correlated deposition of organic compounds. Due to their propensity to be readily preserved in the fossil record, the calcareous benthic foraminifera of the WGMP and Grand Vasière could be successfully used in sedimentary records to rebuild precisely how muddy sedimentary units developed in the Bay of Biscay during the Late Holocene.

5. Conclusions

Live (Rose-Bengal stained) shelf foraminiferal faunas have been studied at seven stations between 39–69-m depth in the West-Gironde Mud Patch (WGMP) (Bay of Biscay, NE Atlantic) to understand how complex environmental conditions (e.g., organic matter, oxygenation, sedimentary facies) control foraminiferal ecological patterns (i.e., diversity, faunal composition, standing stock, and microhabitats). The main conclusions of this work are:

(1) In the WGMP, foraminiferal simple diversity (S) presents relatively moderate values ranging between 15–35 taxa. According to Shannon Index H', foraminiferal diversity tends to increase with water depth. The relative contribution of *Eggerelloides scaber,* the dominant foraminiferal species at all stations, decreases with decreased proximity to the coast and increased depth in the WGMP.

(2) The shallowest station (Station 1, 39 m) proximal to the WGMP is characterized by the relatively important contribution of *Eggerelloides scaber, Quinqueloculina laevigata* and *Ammonia beccarii,* which are all typical of inner-shelf environments constrained by high-energy hydrodynamics and river discharge. There, surface sediments are comprised of winnowed sand strongly depleted in organic matter.

(3) In the central part of the WGMP where variably degraded marine phytodetritus and terrestrial organic compounds are concentrated within clay-silt facies, foraminiferal faunas are characterized by a relatively high contribution of *Bulimina aculeata, Ammonia falsobeccarrii, Nouria polymorphinoides* and *Nonionoides turgidus*. The agglutinated *Eggerelloides scaber* is still the most important taxon.

(4) The deeper stations (>55 m depth) located distally within the mud patch are characterised by the high contribution of *B. aculeata, A. falsobeccarrii* and *N. polymorphinoides.* But they are accompanied by *Bulimina marginata, Rectuvigerina phlegeri*, *Nonion faba* and *Paracassidulina neocarinata*, typical of mid- and outer-shelf ecosystems where fine sediments and organic compounds accumulate.

Finally, our unique study underlines the foraminiferal continuum existing through the muddy environments of the Bay of Biscay, between the WGMP and the Grande Vasière.

Acknowledgement

We would like to thank the crews and the captain of the Côte de la Manche (CNRS-INSU) during the JERICOBENT-2 cruise. We have special thoughts for all scientific members who participated to this scientific mission. This work was supported by: (1) the JERICO-NEXT project (European Union's Horizon 2020 Research and Innovation program under grant agreement no. 654410), (2) the VOG project (LEFE-CYBER and EC2CO-PNEC), and (3) the MAGMA project (COTE cluster of Excellence ANR-10-LABX-45). NASA is acknowledged as a source of MODIS Satellite images (https://modis.gsfc.nasa.gov/). Finally, we thank both reviewers who have provided very useful comments to improve the overall quality of this paper.

References

Barmawidjaja, D.M., Jorissen, F.J., Puskaric, S. and Van Der Zwaan, G.J., 1992. Microhabitat selection by benthic foraminifera in the northern Adriatic Sea. Journal of Foraminiferal Research. 22(4), 297-317.

Barnett, P.R.O., Watson, J. and Connely, D., 1984. A multiple corer for taking virtually undisturbed sample from shelf, bathyal and abyssal sediments. Oceanologica Acta. 7, 399-408.

Bauer, J.E. and Druffel, E.R.M., 1998. Ocean margins as a significant source of organic matter to the deep open ocean. Nature 392, 482-485.

Bernhard, J.M., 2000. Distinguishing live from dead foraminifera: Methods review and proper applications. Micropaleontology 46(1), 38-46.

Berthois, L. and Le Calvez, Y., 1959. Deuxième contribution à l'étude de la sédimentation dans le golfe de Gascogne. Revue des Travaux de l'Institut des Pêches Maritimes. vol. 23 n° 3: 323-375.

Canfield, D.E., Jørgensen, B.B., Fossing, H., Glud, R., Gundersen, J., Ramsing, N.B., Thamdrup, B., Hansen, J.W., Nielsen, L.P. and Hall P.O.J., 1993. Pathways of organic carbon oxidation in three continental margin sediments. Marine Geology. 113, 27-40.

Cirac, P., Berné, S., Castaing, P. and Weber, O., 2000. Processus de mise en place et d'évolution de la couverture sédimentaire superficielle de la plate-forme nord-aquitaine. Oceanologica Acta. 23/6, 663-686.

Cirac, P., Hervé, G., Mazières, A. and Simplet, L., 2016. Carte des formations superficielles du plateau aquitain (2016). EPOC-Université de Bordeaux. https://doi.org/10.12770/602a30c5-c338-4e75-a591-baccb8ba1f79.

Corliss, B.H. and Emerson, S., 1990. Distribution of Rose Bengal stained deep-sea benthic foraminifera from the Nova Scotia continental margin and Gulf of Maine. Deep-sea Research. 37, 381-400.

Cushman, J.A., 1931. The Foraminifera of the Atlantic Ocean. Part 8. Rotaliidae, Amphisteginidae, Calcarinidae, Cymbaloporettidae, Globorotaliidae, Anomalinidae, Planorbulinidae, Rupertiidae and Homotremidae. Bull. U.S. Natl. Mus. 104.

Dagg, M.J. and Breed, G.A., 2003. Biological effects of Mississippi River nitrogen on the northern gulf of Mexico--a review and synthesis. Journal of Marine Systems. 43(3-4), 133-152.

Debenay, J.P. and Redois, F., 1997. Distribution of the twenty seven dominant species of shelf benthic foraminifers on the continental shelf, north of Dakar (Senegal). Marine Micropaleontology. 29(3-4), 237-255.

Deflandre, B., 2016. JERICOBENT-1 cruise, Côtes De La Manche R/V. https://doi.org/10.17600/16010400

Deflandre, B., 2017. JERICOBENT-2 cruise, Côtes De La Manche R/V. https://doi.org/10.17600/17011000

Dessandier, P.-A., Bonnin, J., Kim J.-H., Bichon, S., Grémare, A., Deflandre, B., de Stigter, H. and Malaizé, B., 2015. Lateral and vertical distributions of living benthic foraminifera off the Douro River (western Iberian margin): Impact of the organic matter quality. Marine Micropaleontology, 120, 31–45.

Dessandier, P.-A., Bonnin, J., Kim J.-H., Bichon, S., Deflandre, B., Grémare, A. and Sinninghe Damsté, J. S., 2016. Impact of organic matter source and quality on living benthic foraminiferal distribution on a river-dominated continental margin: A study of the Portuguese margin. Journal of Geophysical Research: Biogeosciences, 121, 1689–1714, doi:10.1002/2015JG003231

Diz, P., Francés, G. and Roson, G., 2006. Effects of contrasting upwelling-downwelling on benthic foraminiferal distribution in the Ria de Vigo (NW Spain). Journal of Marine Systems. 60, 1-18.

Diz, P. and Francés, G., 2008. Distribution of live benthic foraminifera in the Ría de Vigo (NW Spain). Marine Micropaleontology. 66(3-4), 165-191.

Dubosq, N, Schmidt, S, Walsh, J. P., Grémare, A., Gilet, H., Lebleu, P., Poirier, D, Perello, M.-C., Lamarque, B. and Deflandre, B. (in press). A first assessment of organic carbon burial in the West Gironde Mud Patch (Bay of Biscay). Submitted in Continental Shelf Research.

Duchemin, G., Jorissen, F.J., Le Loc'h, F., Andrieux-Loyer, F., Hily, C. and Thouzeau, G., 2008. Seasonal variability of living benthic foraminifera from the outer continental shelf of the Bay of Biscay. Journal of Sea Research. 59(4), 297-319.

Duchemin, G., Jorissen, F.J., Andrieux-Loyer, F., Le Loc'h, F., Hily, C. and Philippon, X., 2005. Living benthic foraminifera from "La Grande Vasière", French Atlantic continental shelf: faunal composition and microhabitats. Journal of Foraminiferal Research. 35, 198-218.

Dufrêne, M. and Legendre, P., 1997. Species assemblages and indicator species: The need for a flexible asymmetrical approach. Ecological Monographs. 67(3), 345-366.

Eppley, R.W., 1984. Relations between primary production and ocean chlorophyll determined by satellite. In: Global Ocean Flux Study. Natl. Acad. Press, Washington, DC, pp 85-102.

Ernst, S., Duijnstee, I., Fontanier, C., Jorissen, F.J. and Van der Zwaan, B., 2005. A comparison of foraminiferal infaunal distributions in field and experimental samples from 550-m depth in the Bay of Biscay. Deep Sea Research Part I: Oceanographic Research Papers. 55 (4), 498-518

Fontanier, C., Jorissen, F.J., Chaillou, G., David, C., Anschutz, P. and Lafon, V., 2003. Seasonal and interannual variability of benthic foraminiferal faunas at 550 m depth in the Bay of Biscay. Deep Sea Research Part I: Oceanographic Research Papers. 50(4), 457-494.

Fontanier, C., Jorissen, F.J., Licari, L., Alexandre, A., Anschutz, P. and Carbonal, P., 2002. Live benthic foraminiferal faunas from the Bay of Biscay: faunal density, composition, and microhabitats. Deep Sea Research Part I: Oceanographic Research Papers. 49(4), 751-785.

Froelich, P.N. et al., 1979. Early oxidation of organic matter in pelagic sediments of the eastern equatorial Atlantic: suboxic diagenesis. Geochimica, Cosmochimica Acta. 43, 1075-1090.

Gillet, H., Deflandre, B., 2018. JERICOBENT-5-TH cruise, Thalia R/V. https://doi.org/10.17600/18000425

Glud, R.N., Gundersen, J.K., Jorgensen, B.B., Revsbech, N.P. and Schulz, H.D., 1994. Diffusive and total oxygen uptake of deep-sea sediments in the eastern South Atlantic Ocean: In situ and laboratory measurements. Deep-Sea Research Part I: Oceanographic Research Papers. 41(11 /12), 1767-1788.

Goineau, A., Fontanier, C., Jorissen, F.J., Lansard, B., Buscail, R., Mouret, A., Kerhervé, P., Zaragosi, S., Ernoult, E. and Artéro, C., 2011. Live (stained) benthic foraminifera from the Rhône prodelta (Gulf of Lion, NW Mediterranean): Environmental controls on a river-dominated shelf. Journal of Sea Research. 65, 58–75.

Gooday, A.J., 2003. Benthic Foraminifera (Protista) as tools in Deep-water Palaeoceanography: Environmental Influences on Faunal Characteristics. Advances in Marine Biology. 46, 1-90.

Hammer, Ø., Harper, D.A.T., Ryan, P.D., 2001. Past: Paleontological Statistics Software Package for Education and Data Analysis. Palaeontologia Electronica, vol. 4, issue 1, art. 4: 9pp., 178kb.

Hargrave, B.T., 1985. Particle sedimentation in the ocean. Ecological Modelling. 30, 229-246.

Hayward, B.W.; Le Coze, F.; Vachard, D.; Gross, O. 2021. World Foraminifera Database. Accessed at http://www.marinespecies.org/foraminifera on 2021-03-12. doi:10.14284/305

Hedges, J.I. and Keil, R.G., 1995. Sedimentary organic matter preservation: an assessment and speculative synthesis. Marine Chemistry. 49(2-3), 81-115.

Hedges, J.I., Keil, R.G. and Benner, R., 1997. What happens to terrestrial organic matter in the ocean? Organic Geochemistry. 27(5-6), 195-212.

Heron-Allen, E. and Earland, A., 1914. The Foraminifera of the Kerimba Archipelago (Portuguese East Africa) -Part I. Transactions of the Zoological Society of London. 20(12): 363-390.

Jones, R.W., 1994. The Challenger Foraminifera. Oxford Science Publications - The Natural History Museum, 149 pp.

Jorissen, F.J., Fontanier, C., Thomas, E. and Claude Hillaire-Marcel and de Vernal, A., 2007. Chapter Seven Paleoceanographical Proxies Based on Deep-Sea Benthic Foraminiferal Assemblage Characteristics, Developments in Marine Geology. Elsevier, pp. 263-325.

Lamarque, B., Deflandre, B., Galindo Dalto, A., Schmidt, S., Romero-Ramirez, A., Garabetian, F., Dubosq, N., Diaz, M., Grasso, F., Sottolichio, A., Bernard, G., Gillet, H., Cordier, M.-A., Poirier, D., Lebleu, P., Deriennic, H., Danilo, M., Murilo Barboza Tenório, M. and Grémare, A., submitted. Spatial distributions of surface sediment and Sediment Profile Image characteristics in a high energy temperate marine RiOMar: the West Gironde Mud Patch. Submitted in Journal of Marine Science and Engeneering.

Lampert, L., Queguiner, B., Labasque, T., Pichon, A. and Lebreton, N., 2002. Spatial variability of phytoplankton composition and biomass on the eastern continental shelf of the Bay of Biscay (north-east Atlantic Ocean). Evidence for a bloom of Emiliania huxleyi (Prymnesiophyceae) in spring 1998. Continental Shelf Research. 22, 1225–1247.

Lampert, L., 2001. Dynamique saisonnière et variabilité pigmentaire des populations phytoplanctoniques dans l'atlantique nord (Golfe de Gascogne). Thèse d'Etat, Université de Bretagne Occidentale, 340 p.

Langezaal, A.M., Jorissen, F.J., Brauna, B., Chailloud, G., Fontanier, C., Anschutz, P. and van der Zwaan G.J. 2006. The influence of seasonal processes on geochemical profiles and foraminiferal assemblages on the outer shelf of the Bay of Biscay. Continental Shelf Research. 26(15), 1730-1755.

Langlet, D., Baal, C., Geslin, E., Metzger, E., Zuschin, M., Riedel, B., Risgaard-Petersen, N., Stachowitsch, M., and Jorissen, F. J., 2014. Foraminiferal species responses to in situ,

experimentally induced anoxia in the Adriatic Sea, Biogeosciences, 11, 1775–1797, https://doi.org/10.5194/bg-11-1775-2014, 2014.

Lesueur, P., Tastet, J.P. and Marambat, L., 1996. Shelf mud fields formation within historical times: examples from offshore the Gironde estuary, France. Continental Shelf Research. 16, 1849–1870.

Lesueur, P., Tastet, J.P. and Weber, O., 2002. Origin and morphosedimentary evolution of fine grained modern continental shelf deposits: the Gironde mud fields (Bay of Biscay, France). Sedimentology 49, 1299–1320.

Lohrenz, S.E., Dagg, M.J. and Whitledge, T.E., 1990. Enhanced primary production at the plume/oceanic interface of the Mississippi River. Continental Shelf Research. 10(7), 639-664.

Lohrenz, S.E. Fahnenstiel, G. L., Redalje, D. G., Lang, G. A., Chen, X., and Dagg, M. J., 1997. Variations in primary production of northern Gulf of Mexico continental shelf waters linked to nutrient inputs from the Mississippi River. Marine Ecology Progress Series. 155, 45-54.

McKee, B.A., Aller, R.C., Allison, M.A., Bianchi, T.S. and Kineke, G.C., 2004. Transport and transformation of dissolved and particulate materials on continental margins influenced by major rivers: benthic boundary layer and seabed processes. Continental Shelf Research. 24(7-8), 899-926.

Mendes, I., Dias, J. A., Schönfeld, J. and Ferreira, Ó., 2012. Distribution of living benthic foraminifera on the northern Gulf of Cadiz continental shelf. Journal of Foraminiferal Research. 42, 18–38

Mopper, K. and Degens, E.T., 1977. Organic carbon in the ocean: nature and cycling. In: The Global Carbon Cycle. Wiley, Chichester, pp 293-316.

Murray, J.W., 2006. Ecology and Applications of Benthic Foraminifera. Cambridge University Press, pp 426.

Murray, J.W. and Bowser, S.S., 2000. Mortality, protoplasm decay rate, and reliability of staining techniques to recognize 'living' foraminifera: a review. Journal of Foraminiferal Research. 30, 66-70.

Orbigny, A. D. d'., 1826. Tableau méthodique de la classe des Céphalopodes. Annales des Sciences Naturelles. vol. 7: 96-169, 245-314.

Orbigny, A. D. d'., 1839. Foraminifères des îles Canaries. Histoire naturelle des Iles Canaries. 2(2): 120-146.

R Core Team, 2020. R: A language and environment for statistical computing. R Foundation for Statistical Computing, Vienna, Austria. URL https://www.R-project.org/.

Roberts, D. W., 2019. Labdsv: Ordination and Multivariate Analysis for Ecology. R package version 2.0-1.

Romankevich, E.A., 1984. Geochemistry of Organic Matter in the Ocean. Springer, Berlin, 334 pp.

Smith, S. and MacKenzie, F., 1987. The ocean as a net heterotrophic system: implications for the carbon biogeochemical cycle. Global Biogeochemical Cycles. 1, 187-198.

Stevenson, F.J. and Cheng, C.N., 1970. Amino acids in sediments: Recovery by acid hydrolysis and quantitative estimation by a colorimetric procedure. Geochimica et Cosmochimica Acta. 34, 77-88.

Walsh, J.J., 1988. On the nature of continental shelves. Academic Press Inc., New York, 520 pp.

Walsh, J.J., 1991. Importance of continental margins in the marine biogeochemical cycling of carbon and nitrogen. Nature 350, 53-55.

Walsh, J.J., Rowe, G., Iverson, R. and McRoy, C., 1981. Biological export of shelf carbon is a sink of the global CO2 cycle. Nature. 292, 196-201.

Walton, W.R., 1952. Techniques for recognition of living Foraminifera. Contributions from the Cushman Foundation for Foraminiferal Research. 3, 56-60.

Wollast, R., 1991. The coastal organic carbon cycle: fluxes, sources and sinks. In: Ocean Margin Processes in Global Change. Wiley, New York, pp 365-381.

Appendix captions

Appendix A

Major foraminiferal species (≥ 5%) identified in the West-Gironde Mud Patch, with reference to plates and figures in the literature. Supplementary data associated with this article can be consulted in the online version at xxxx.

Appendix B

Census data for live (stained) benthic foraminifera in the >150 µm fraction for the seven stations sampled in the West-Gironde Mud Patch. N.B. Numbers are not standardized for sediment volume. Supplementary data associated with this article can be consulted in the online version at xxxx.